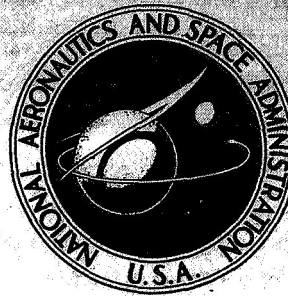


**NASA TECHNICAL
MEMORANDUM**



N73-33475
THRU
N73-33489
NASA TM X-2720

NASA TM X-2720

**CASE FILE
COPY**

**SYMPOSIUM ON REUSABLE SURFACE
INSULATION FOR SPACE SHUTTLE**

Volume II - Environmental Testing

Held at
Ames Research Center
Moffett Field, Calif.
November 1-3, 1972

NATIONAL AERONAUTICS AND SPACE ADMINISTRATION • WASHINGTON, D. C. • SEPTEMBER 1973

1. Report No. NASA TM X-2720	2. Government Accession No.	3. Recipient's Catalog No.	
4. Title and Subtitle Symposium on Reusable Surface Insulation for Space Shuttle, Volume II - Environmental Testing		5. Report Date September 1973	
		6. Performing Organization Code	
7. Author(s)		8. Performing Organization Report No. A-4725	
9. Performing Organization Name and Address NASA Ames Research Center Moffett Field, Calif. 94035		10. Work Unit No. 502-37-02	
		11. Contract or Grant No.	
12. Sponsoring Agency Name and Address National Aeronautics and Space Administration Washington, D. C. 20546		13. Type of Report and Period Covered Technical Memorandum	
		14. Sponsoring Agency Code	
15. Supplementary Notes Held at NASA Ames Research Center, November 1-3, 1972.			
16. Abstract The conference encompasses three technology efforts, each published as a separate volume. Volume I - RSI Fabrication, Improvement, Morphology and Properties (NASA TM X-2719) Volume II - Environmental Testing (NASA TM X-2720) Volume III - Thermal Protection System Design and Optimization (NASA TM X-2721)			
17. Key Words (Suggested by Author(s)) Thermal Protection System Reusable Surface Insulation Space Shuttle		18. Distribution Statement Unclassified - Unlimited	
19. Security Classif. (of this report) Unclassified	20. Security Classif. (of this page) Unclassified	21. No. of Pages 574	22. Price* \$6.00

FOREWORD

Howard K. Larson

One of the critical technology needs of the Space Shuttle is development of a reusable thermal protection system (TPS). The baseline material for a large part of the shuttle TPS is now reusable surface insulation (RSI). Because of the rapid progress which has occurred in this development effort during FY'72-'73, it was deemed appropriate to review the state of RSI technology at this time. Therefore, Ames Research Center, under the auspices of the Shuttle Thermal Protection Systems and Materials Technology Working Group, hosted a three-day symposium on Reusable Surface Insulation for Thermal Protection of the Space Shuttle on November 1-3, 1972.

The objective of this symposium was to define the state-of-the-art for RSI materials. The meeting was divided into five sequential half-day sessions; each session addressing a specific technology area.

The first session "RSI Fabrication and Improvement" was chaired by Howard E. Goldstein of NASA-Ames, and included papers discussing the development of silica, mullite and alumino-silicate RSI materials. Rigid and flexible RSI materials were described. The results reported showed that mullite, silica and alumino-silicate rigid fibrous RSI materials could be fabricated reproducibly. One paper described a somewhat different RSI concept, a rigid closed pore alumino-silicate insulation having good physical stability. Also described was a silica non-rigid insulation which offers the possibility of minimizing strain compatibility problems with the structure. While substantial improvements have been made in the past two years, it was pointed out by many of the papers that much effort is still required to optimize the RSI materials. Substantial improvement in physical properties and thermal stability should be expected with continued research.

The second session "RSI Morphology and Properties" was chaired by Salvatore J. Grisaffe, NASA-Lewis, and included papers describing the detailed mechanical and thermophysical properties of the rigid fibrous RSI materials and their coatings. The mechanical properties as a function of temperature for REI mullite and LI-1500 were presented. One paper described a comparison of the mechanical and thermophysical properties of HCF, REI mullite, and LI-1500. Radiant energy transmission through mullite RSI was discussed in one paper and the high temperature surface optical properties of all the RSIs were discussed in another paper. The final paper described the microstructure of mullite fibers. This session demonstrated that the mechanical properties of the RSI materials are reasonably well understood, though the precision of the reported values is still in doubt. Thermal conductivity, particularly radiant heat transfer effects, are not well defined for the fibrous mullite materials. Emittances of the surface coatings of all the RSI materials are still questionable and require further study.

The third session "Environmental Testing I" was chaired by David H. Greenshields, NASA-MSC, and described the results of arc-plasma testing of the RSI materials. Most of these papers were concerned with both techniques for proper convective heating environment simulation and the response of the materials to the environment. Two papers described thermal response in gaps due to laminar and turbulent heating, respectively. In both studies, large panels simulating shuttle heat shield configurations were used. Other papers described the internal thermal response, catalytic wall effects and material response to cyclic heating. These studies were carried out on small models in uniform stagnation region heating regimes. Significantly higher thermal efficiency was reported for silica RSI compared with mullite RSI. Silica RSI coatings were also shown to be more chemically stable and less subject to cracking due to thermal shock.

The fourth session "Environmental Testing II" was chaired by John D. Buckley, NASA-Langley, and included papers that discussed the results of several diverse environmental testing programs. There were papers on the response of the RSI coatings in both convective and radiative heating environments. In these papers, emphasis was placed on the chemical and morphological changes that occur due to each heating environment. Significant differences were shown between the effects of radiant and convective heating. Convective heating was shown to have more severe effects. Other papers in the session described the effects of combined salt spray and cyclic radiant heating. It was shown that salt spray is more deleterious for silica than for mullite. Cold soak, acoustical rain erosion, and meteoroid impact tests were also described. The results of large panel tests in radiant heating and acoustic environments showed the silica RSI to be more stable. Mullite materials experienced thermostructural failures in these tests.

The fifth session "Thermal Protection System Design and Optimization" was chaired by George Strouhal, NASA-MSC, and included papers describing a number of specific design problems. Among these problems were the adhesive cold soak, the effect of optical properties on thermal design and techniques for mechanical attachment of RSI to the structure. The design concept of a non-rigid silica heat shield was described. Papers on mullite and silica RSI, respectively, contrasted the design philosophies and development maturities of the respective systems. Finally, a paper on thermostructural analysis of RSI application showed that mullite was much more subject to thermal stress failure than silica.

In conclusion, it is felt that the Symposium fulfilled its intended purpose in providing an "open forum" for Industry and Government to present, receive, and discuss the most recent results of a young, intensive technology program. NASA needed the results of this RSI technology program in order to make important decisions as to which of the RSI materials to choose for the shuttle heat shield. Early in 1973, NASA made the announcement that silica was chosen for the base material and that a coating with a ratio of solar absorbance to room temperature emittance of 1.0 would be baselined.

CONTENTS

SYMPOSIUM CO-CHAIRMEN: Howard K. Larson,
Ames Research Center
David H. Greenshields,
Manned Spacecraft Center

VOLUME I. - RSI FABRICATION, IMPROVEMENT, MORPHOLOGY, AND PROPERTIES

Session I - RSI Fabrication and Improvement
Chairman: Howard E. Goldstein
Ames Research Center

1. FABRICATION AND IMPROVEMENT OF LMSC'S ALL-SILICA RSI 1
R. M. Beasley, Y. D. Izu, H. N. Nakano, A. A. Ozolin, and
A. Pechman
Lockheed Missiles & Space Company
2. PROCESSING OF RIGIDIZED REI-MULLITE INSULATIVE COMPOSITES 17
J. J. Gebhardt, P. D. Gorsuch, and M. A. Braun
General Electric Company
3. DEVELOPMENT AND CHARACTERIZATION OF CPI SURFACE INSULATION 61
A. Tobin, C. Feldman, J. Reichman, M. Russak, and A. Varisco
Grumman Aerospace Corporation
4. FUSED SILICA SURFACE COATING FOR A FLEXIBLE SILICA MAT
INSULATION SYSTEM 87
W. H. Rhodes
AVCO Systems Division
5. MAR-SI, MARTIN SURFACE INSULATION 107
P. Paul Plank, Arthur Feldman, William C. Miiller,
John F. Creedon, and Joseph M. Toth, Jr.
Martin Marietta Corporation

Session II - RSI Morphology and Properties
Chairman: Salvatore J. Grisaffe
Lewis Research Center

6. SILICA REUSABLE SURFACE INSULATION IMPROVEMENT RESEARCH 155
H. E. Goldstein, M. Smith, D. Leiser, V. Katvala, and D. Stewart
Ames Research Center
7. RADIANT HEAT TRANSFER IN REUSABLE SURFACE INSULATION 197
T. A. Hughes, R. M. F. Linford, R. J. Schmitt, and
H. E. Christensen
McDonnell Douglas Astronautics Company-East

8.	OPTIMIZATION OF REI-MULLITE PHYSICAL PROPERTIES	227
	R. A. Tanzilli, S. M. Musikant, P. N. Bolinger, and J. P. Brazel General Electric Company	
9.	SILICA RSI MORPHOLOGY AND PROPERTIES	261
	R. M. Beasley and J. C. Robinson Lockheed Missiles & Space Company	
10.	EVALUATIONS OF RSI MATERIALS	275
	C. W. Kistler, D. E. Niesz, and E. L. Foster Battelle, Columbus Laboratories	
11.	PORE STRUCTURE ANALYSIS OF RSI TILE	311
	O. J. Whittemore, Jr. and L. W. Smiser University of Washington	
12.	SPECTRAL AND TOTAL NORMAL EMITTANCE OF REUSABLE SURFACE INSULATION MATERIALS	327
	Andronicos G. Kantsios, S. Franklin Edwards, and Dennis L. Dicus Langley Research Center	
13.	AN EXPLORATORY STUDY OF THE MICROSTRUCTURE OF MULLITE FIBERS.	349
	G. Santoro, H. B. Probst and B. Buzek Lewis Research Center	

VOLUME II. - ENVIRONMENTAL TESTING

Session III - Environmental Testing I

Chairman: David H. Greenshields
Manned Spacecraft Center

14.	AERODYNAMIC SIMULATION TESTS OF RSI PANELS	371
	F. J. Centolanzi, N. B. Zimmerman, M. A. Covington, and F. H. Nichols Ames Research Center	
15.	CONVECTIVE HEATING TESTS OF REUSABLE SURFACE INSULATION JOINTS AND GAPS	425
	H. E. Christensen and D. A. Osborne McDonnell Douglas Astronautics Company-East	
16.	ENTRY ENVIRONMENTAL SIMULATION TESTING OF REI-MULLITE TPS	485
	D. E. Florence, R. A. Brewer, and T. E. Hess General Electric Company	
17.	PLASMA ARC TESTING TECHNIQUES FOR SPACE SHUTTLE REUSABLE SURFACE INSULATION (RSI)	525
	Ira M. Grinberg and Ross G. Luce Battelle, Columbus Laboratories	

18. CYCLIC ARC PLASMA TESTS OF RSI MATERIALS USING A PREHEATER . . . 559
D. A. Stewart
Ames Research Center

19. ARC JET TESTS OF RSI MATERIALS - SCREENING AND COMPARATIVE
EVALUATION 591
John W. Schaefer, Aerotherm Division, Acurex Corporation
Nick S. Vojvodich, Ames Research Center

20. SILICA RSI ENTRY SIMULATION TESTS 623
R. P. Banas, J. O. Donaldson, and J. Jue
Lockheed Missiles & Space Company

- Session IV - Environmental Testing II
Chairman: John D. Buckley
Langley Research Center

21. ENVIRONMENTAL TESTING OF REI-MULLITE THERMAL PROTECTION SYSTEM
FOR THE SPACE SHUTTLE ORBITER 667
R. Gluck, R. Romano, and H. Thibault
General Electric Company

22. ENVIRONMENTAL COMPATIBILITY OF THE ALL-SILICA RIGID SURFACE
INSULATION 709
S. J. Houston, J. A. De Runtz, and D. R. Elgin
Lockheed Missiles & Space Company

23. SIMULATED METEOROID PENETRATION OF REUSABLE SURFACE INSULATION . . 731
J. K. Lehman and H. E. Christensen
McDonnell Douglas Astronautics Company-East

24. EFFECTS OF SEA SALTS ON THE PHYSICAL CHARACTERISTICS OF
REUSABLE SURFACE INSULATION 765
Philip O. Ransone and Dennis L. Dicus
Langley Research Center

25. CHARACTERIZATION OF RSI COATINGS 793
A. D. Miller, S. H. Garofalini, L. W. Smiser, and J. I. Mueller
University of Washington

26. CHEMICAL AND MORPHOLOGICAL CHANGES OF REUSABLE SURFACE INSULATION
COATINGS AS A FUNCTION OF CONVECTIVELY HEATED CYCLIC TESTING . . 851
D. B. Leiser, D. A. Stewart, and H. E. Goldstein
Ames Research Center

27. REUSABLE SURFACE INSULATION THERMAL PROTECTION SYSTEMS
TEST EVALUATION STATUS 895
George Strouhal and Donald J. Tillian
Manned Spacecraft Center, Houston

VOLUME III. - THERMAL PROTECTION SYSTEM DESIGN AND OPTIMIZATION

Session V - Thermal Protection System Design and Optimization

Chairman: George Strouhal

Manned Spacecraft Center

28. CHARACTERIZATION OF ADHESIVES FOR ATTACHING REUSABLE SURFACE
INSULATION ON SPACE SHUTTLE VEHICLES 935
H. P. Owen and M. T. Carroll
General Dynamics
29. EFFECT OF OPTICAL PROPERTIES ON THERMAL DESIGN 965
C. L. Statham and R. T. Tsutsui
North American Rockwell
30. CLOSED-PORE INSULATION THERMAL PROTECTION SYSTEM DESIGN
CONCEPT DEVELOPMENT 981
A. Varisco and H. G. Harris
Grumman Aerospace Corporation
31. MECHANICAL ATTACHMENT OF REUSABLE SURFACE INSULATION TO SPACE
SHUTTLE PRIMARY STRUCTURE 1029
R. W. Fleck and J. K. Lehman
McDonnell Douglas Astronautics Company-East
32. OPTIMUM TPS DESIGN WITH REI-MULLITE 1063
T. E. Hess, R. J. Michalak, and R. A. Brewer
General Electric Company
33. SILICA RSI FOR APPLICATION TO THE SHUTTLE ORBITER 1121
K. J. Forsberg, J. Jue, M. H. Kural, and F. A. Velligan
Lockheed Missiles & Space Company
34. A NON-RIGID REUSABLE SURFACE INSULATION CONCEPT FOR THE SPACE
SHUTTLE THERMAL PROTECTION SYSTEM 1185
J. G. Alexander
Avco Systems
35. RESULTS OF RSI THERMAL-STRUCTURE ANALYSIS 1227
O. E. Pigg
Manned Spacecraft Center, Houston

The following papers were not presented at the Symposium
but are included as part of these proceedings:

36. INTERFERENCE HEATING TO CAVITIES BETWEEN SIMULATED RSI TILES . . 1269
Charles B. Johnson
Langley Research Center

37. EFFECT OF CRISTOBALITE ON THE MECHANICAL PROPERTIES OF
SILICA RSI MATERIALS 1277
Pramod K. Khandelwal and William D. Scott
University of Washington
38. EMITTANCE OF RSI COATINGS DETERMINED FROM RADIATION
MEASUREMENTS IN ARC JET TESTS 1291
R. M. Wakefield and D. A. Stewart
Ames Research Center

AERODYNAMIC SIMULATION TESTS OF RSI PANELS

F.J. Centolanzi, N.B. Zimmerman, M.A. Covington, and F.H. Nichols

Ames Research Center
Moffett Field, California

INTRODUCTION

During the past several years the concept of protecting the space shuttle vehicle with reusable surface insulation (RSI) has received considerable attention. Most emphasis has been placed on two different fiber systems--mullite and silica. Since convective heating plays such an important role in the thermal response of these materials, many tests have been conducted in arc-heated facilities in an attempt to simulate the space shuttle environment. It became readily apparent that no existing ground-based facility could simultaneously duplicate the correct combinations of scale, enthalpy, pressure, and air chemistry encountered by the shuttle during its entry into the atmosphere. Some tests have been conducted with relatively small samples in laminar, stagnation flows to assess hypervelocity effects on coating response, emissivity changes, and surface catalytic effects. Since it is a well-known fact that the aerodynamic boundary layer affects the heating rate in the vicinity of gaps and steps, this problem has received some attention for laminar flows. Because the boundary-layer flow over a large percentage of the vehicle surface is likely to be turbulent and supersonic, it was apparent that this facet also needed to be simulated.

In order to accomplish this objective, an arc-heated, supersonic turbulent-flow duct facility was developed at the Ames Research Center. This duct, with an internal cross section of 5.08 x 22.9 cm (2 x 9 inches), can accommodate test panels up to 20 x 51 cm (8 x 20 inches) in planform. The first RSI panels to be tested in this facility were obtained through the NASA-Manned Spacecraft Center from three RSI contractors; Lockheed Missiles and Space Company, General Electric Company, and McDonnell Douglas Astronautics. This paper describes the facility and presents the results of preliminary tests performed on 20 x 25.4 cm (8 x 10 inch) panels--the first TPS tests to be performed in this facility.

SCHEMATIC OF AMES 2 X 9 INCH TURBULENT FLOW DUCT FACILITY

(Figure 1)

A schematic of the Ames 2 x 9 Inch Turbulent Flow Duct Facility for evaluating space shuttle TPS is shown in figure 1. This facility consists of a Linde N-15000 arc heater coupled to a water cooled nozzle and test section (Mach Number 3.5). Panel sizes 20.3 x 25.4 cm (8 x 10 inches) and 20.3 x 50.8 cm (8 x 20 inches) can be accommodated in one wall of the test section as shown in the figure. Calorimeters and pressure orifices are located on the opposite wall. Individual calorimeters may be removed and replaced with small, optical ports for viewing the test specimen with an optical pyrometer. In order to reduce the thermal shock associated with starting and stopping the arc-heater, argon is used as a test gas at the beginning and end of each run. This technique is discussed in more detail in figure 3.

SCHEMATIC OF AMES 2x9 INCH TURBULENT FLOW DUCT FACILITY

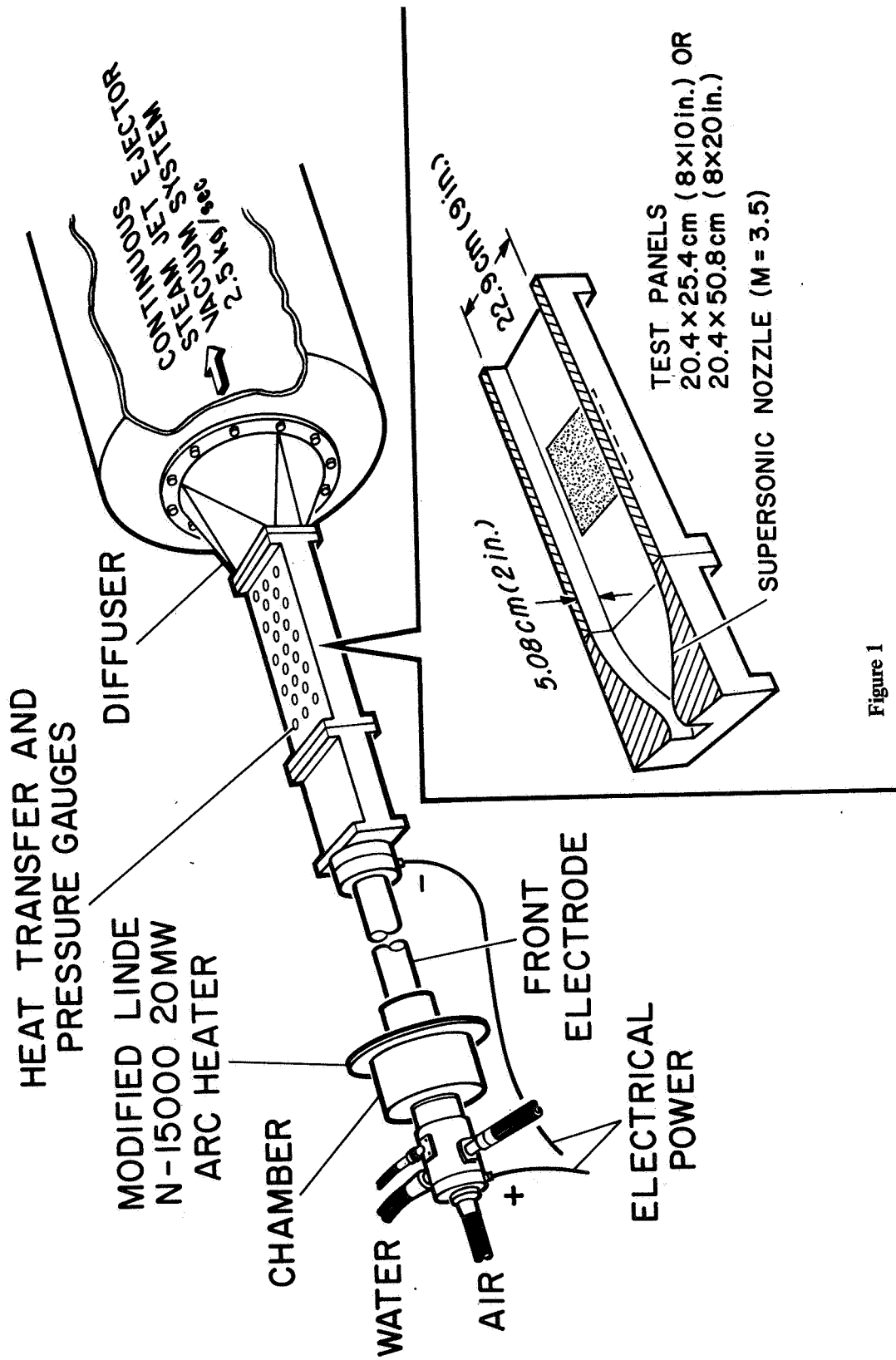


Figure 1

PHOTOGRAPH OF AMES 2 X 9 INCH TURBULENT FLOW DUCT FACILITY

(Figure 2)

A photograph of the facility is shown in this figure. This photograph illustrates the relative scale of the facility and the general arrangement of the associated apparatus and equipment.

PHOTOGRAPH OF AMES 2 x 9 INCH TURBULENT FLOW
DUCT FACILITY

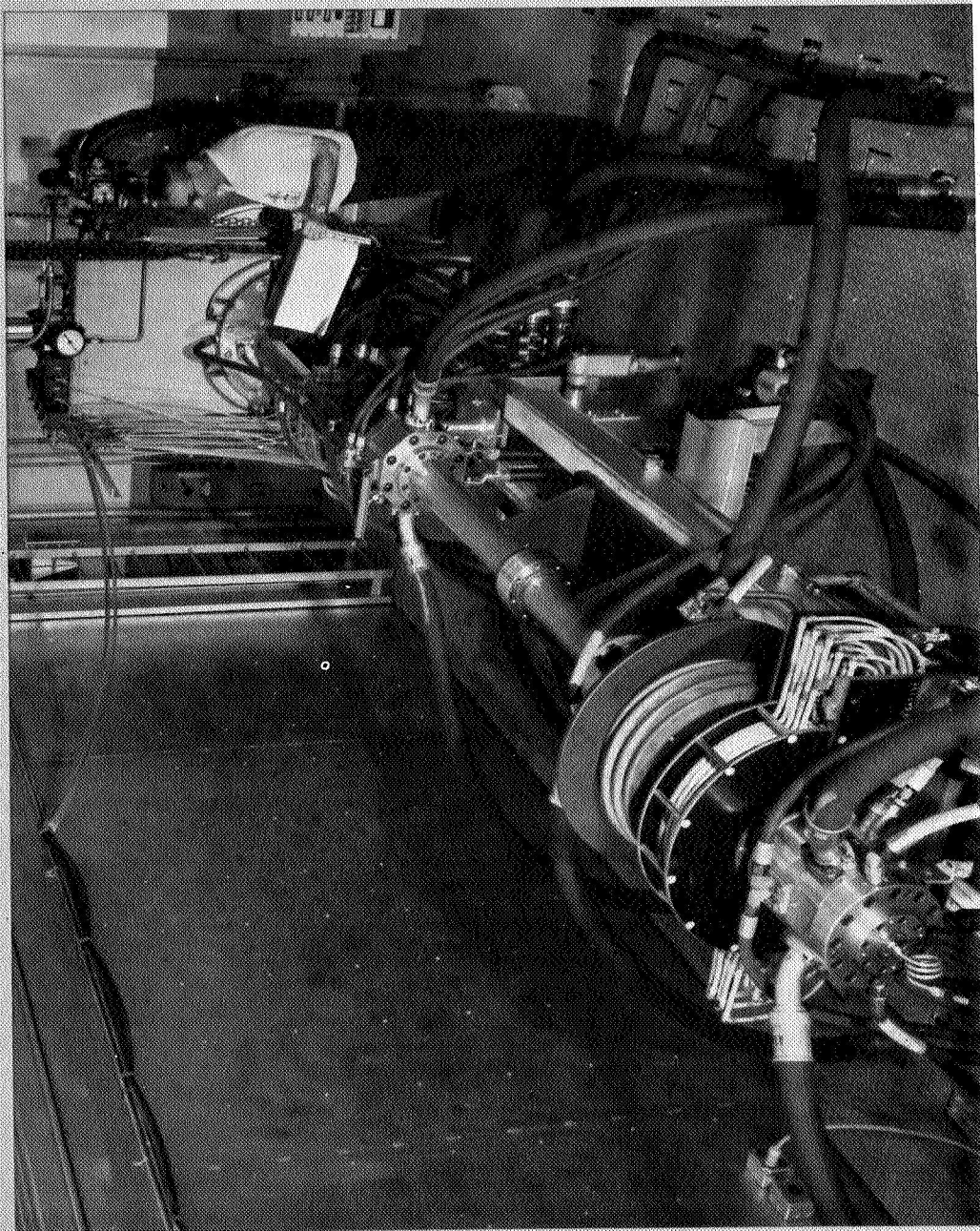


Figure 2

COMPARISON OF HEATING RATES USING AIR ONLY WITH ARGON + AIR MIXTURE

(Figure 3)

When using air as a test gas, there is a minimum heating rate at which an arc-heated facility can be operated. In addition, a spike in the heating rate occurs at the start of the run as shown in this figure. Argon, because of its lower ionization potential, provides a much lower minimum heating rate while also avoiding the undesirable spike at the start of the run. Shown in this figure are the measured cold wall heating rates during simulation of the Space Shuttle Area 2 heating trajectory using air only compared with a similar run where argon and air are used. The simulation of temperatures and pressures is shown in figure 4.

COMPARISON OF HEATING RATES USING AIR ONLY WITH ARGON + AIR MIXTURE

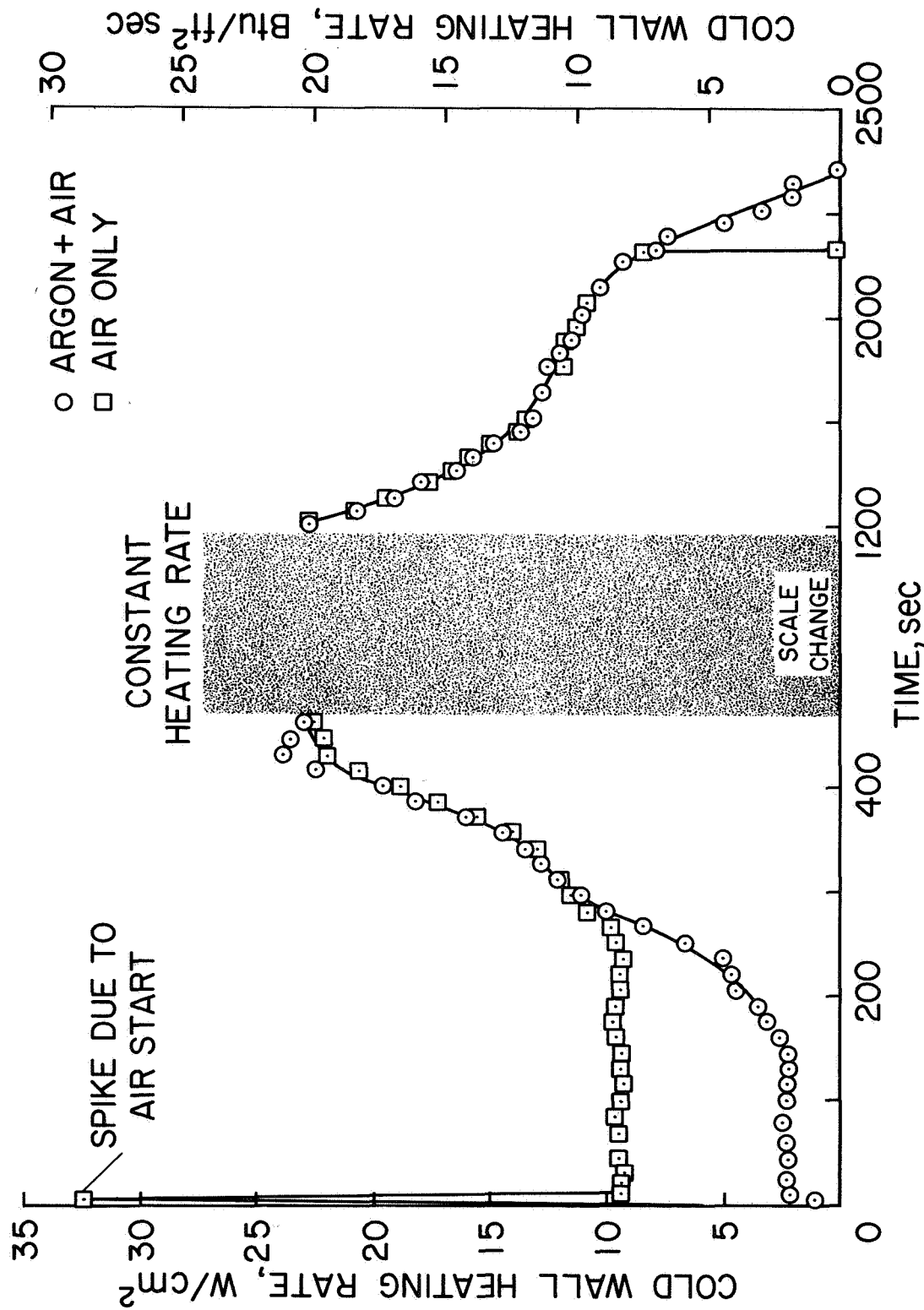


Figure 3

SIMULATION OF SPACE SHUTTLE AREA 2 TRAJECTORY
LOCKHEED LI-1542 PANEL

(Figure 4)

The measured temperatures and pressures for two separate tests of the Lockheed LI-1542 panel are shown in this figure and compared with those specified for the NASA-MSC Area 2 trajectory. At the start of the tests, nearly pure argon is used to avoid the high heating rate associated with starts using air. The maximum rate of change of temperature with time (\dot{T}) occurred at the start and was measured to be 17°K/sec (30°F/sec). Air is then introduced and the air/argon ratio is increased. Finally, the arc heater is operating on air alone. Variation of arc current and pressure provide the necessary control of heating rate and temperature during the high heating part of the trajectory and argon is reintroduced to realistically produce the lower heating completion of the trajectory. The simulation of temperature during the runs is good. The simulation of pressure is high in the early part of the trajectory and low in the later part. The test enthalpy at the peak temperature of simulation is 6.2 MJ/gm (2700 Btu/lb). At the end of the simulation, the arc heater is turned off and the ambient pressure is held at a low level (about 1000 N/m^2 or 0.01 atm). The test panels are allowed to cool by radiation, internal conduction, and the small amount of free convection that exists at the low ambient pressures.

SIMULATION OF SPACE SHUTTLE AREA 2 TRAJECTORY LOCKHEED L1-1542 PANEL

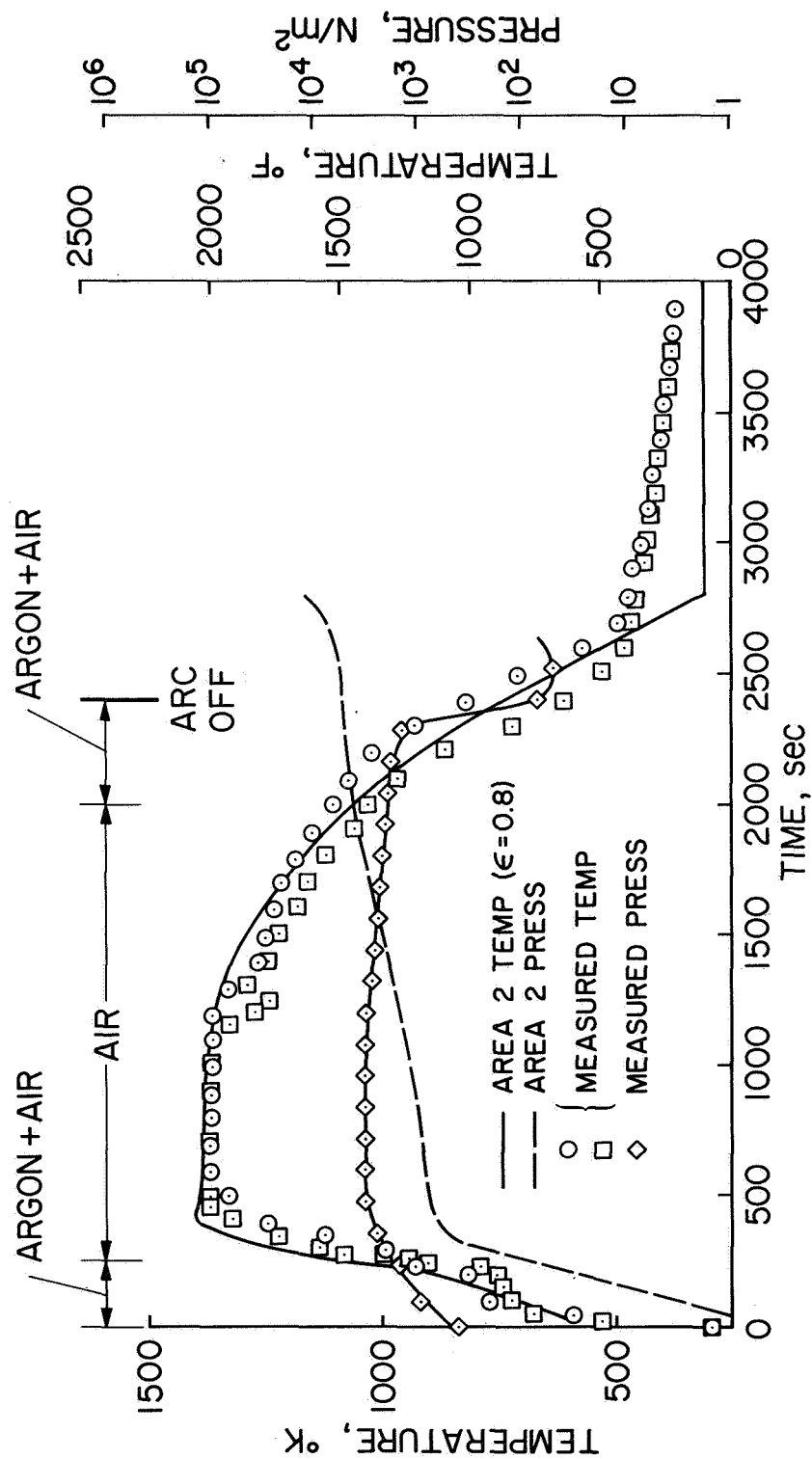


Figure 4

TYPICAL 2 X 9 INCH DUCT TURBULENT BOUNDARY LAYER PROFILES

(Figure 5)

Total pressure surveys were made in the 2 x 9 Inch Duct to characterize the boundary layer flows over the RSI test panels. Results of a typical survey are shown on the left of figure 5 for a total enthalpy of 3.7 MJ/kg (1600 Btu/lb) and a static pressure of $3.5 \times 10^3 \text{ N/m}^2$ (0.035 atm). Although this stream enthalpy level was lower than that during the panel tests, the measured boundary layer characteristics are probably typical of those occurring at the test conditions. A tantalum-tipped, water-cooled probe moved by a remote controlled traversing mechanism was used to obtain the survey data. No boundary layer temperature profiles were measured because of the high stream temperatures, and the Crocco relationship between total temperature and velocity was assumed in deriving the typical velocity profile shown on the right side of the figure. The momentum thickness and the displacement thickness are seen to be about 2 mm and 5 mm, respectively, while the total boundary layer thickness is about 20 mm. Also indicated on the figure are the maximum gap width and step height dimensions for the RSI panels, and they are seen to be comparable to the momentum thickness.

TYPICAL 2x9 INCH DUCT TURBULENT BOUNDARY LAYER PROFILES

$\bar{H}_e = 3.7 \text{ MJ/kg}$ $q_{cw} = 16 \text{ W/cm}^2$ ASSUMED $T_{\text{WALL}} = 400 \text{ }^\circ\text{K}$

PITOT PRESSURE SURVEY

CALCULATED VELOCITY PROFILE

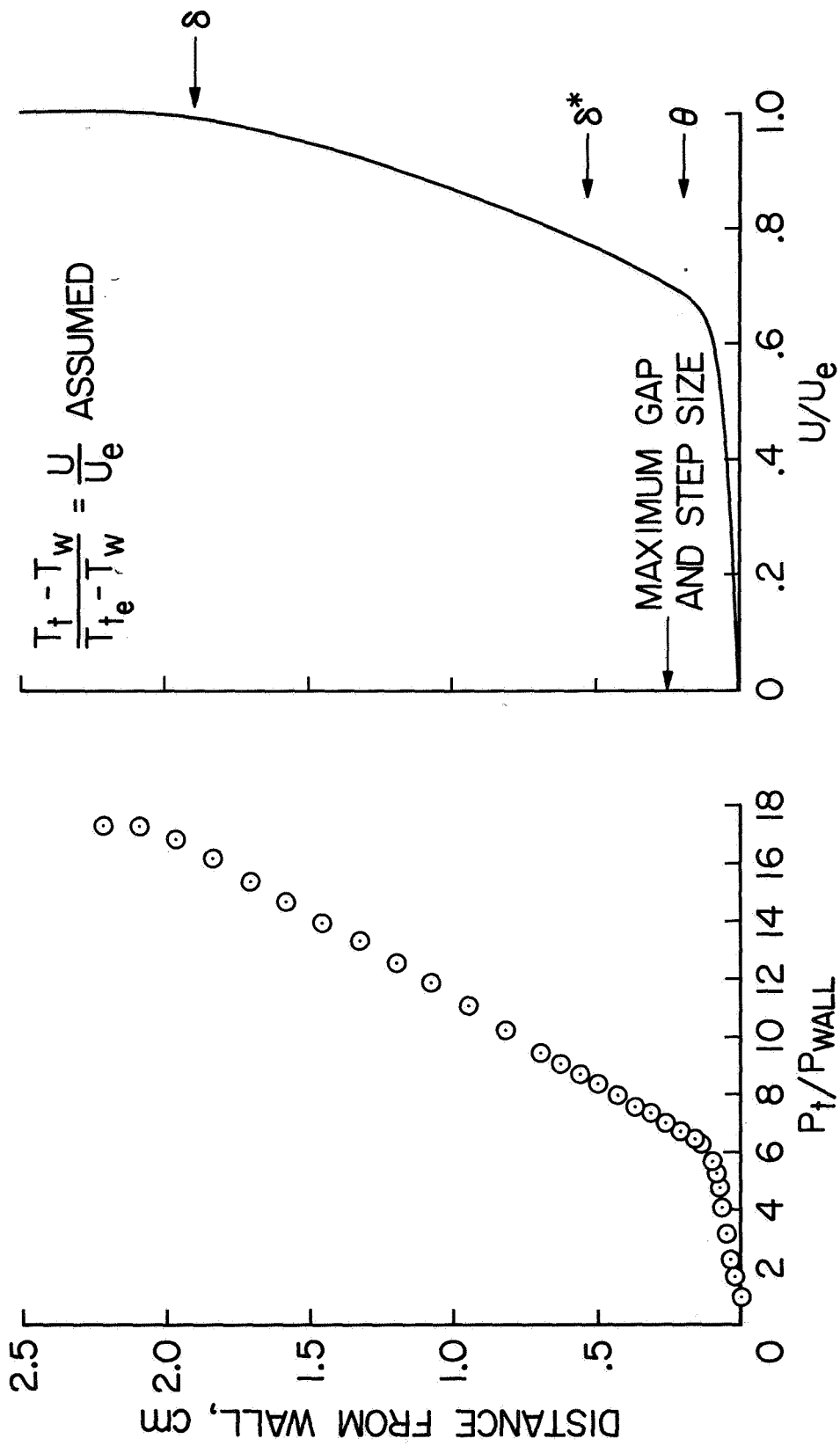


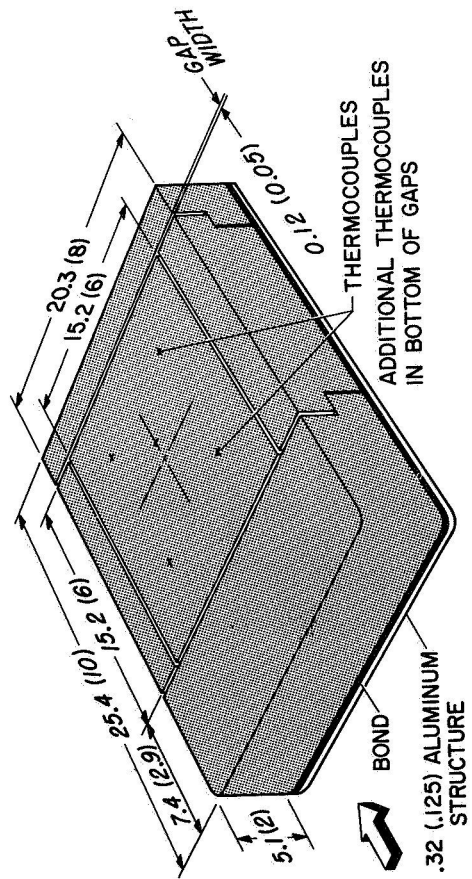
Figure 5

LOCKHEED LI-1542 PANEL

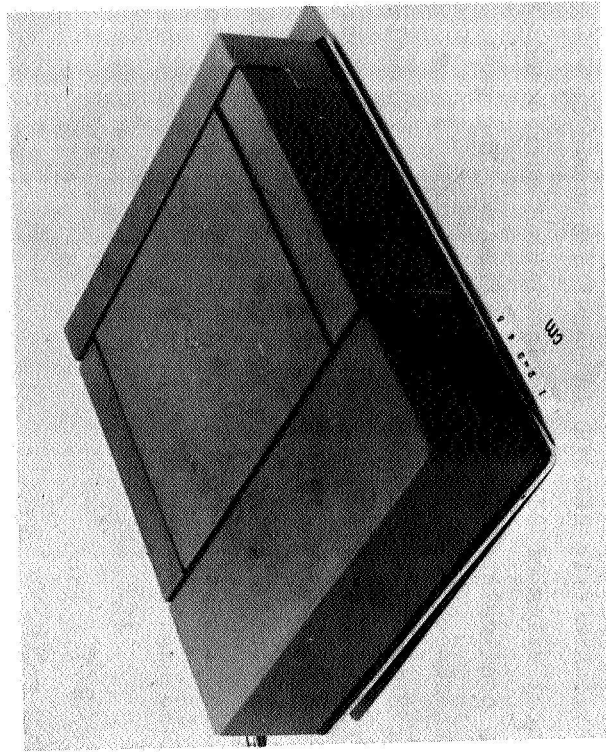
(Figure 6)

An illustration and pre-test photograph of the Lockheed LI-1542 panel are shown in figure 6. The panel consisted of a 15.2 x 15.2 cm (6 x 6 inch) tile of LI-1542 insulation surrounded by smaller tile segments of the same material. The gaps were nominally .13 cm (.050 inch), but varied somewhat with depth and location on the panel. The tiles were bonded to a .32 cm (.125 inch) aluminum plate with RTV 560 adhesive 0.23 cm (.090 inch) thick. There were five platinum-platinum/13 percent rhodium thermocouples located on the surface of the 15.2 x 15.2 cm (6 x 6 inch) tile. Near the center of tile there were three chromel-alumel thermocouples located 1.27 cm (0.50 inch), 2.54 cm (1.0 inch), and 3.81 cm (1.50 inch) below the surface to provide in-depth thermal response measurements. Additional chromel-alumel thermocouples were located at the bottom of the gaps, in the RTV bond, and in the aluminum plate.

LOCKHEED LI-1542 PANEL



a) ILLUSTRATION



b) PRE-TEST PHOTOGRAPH

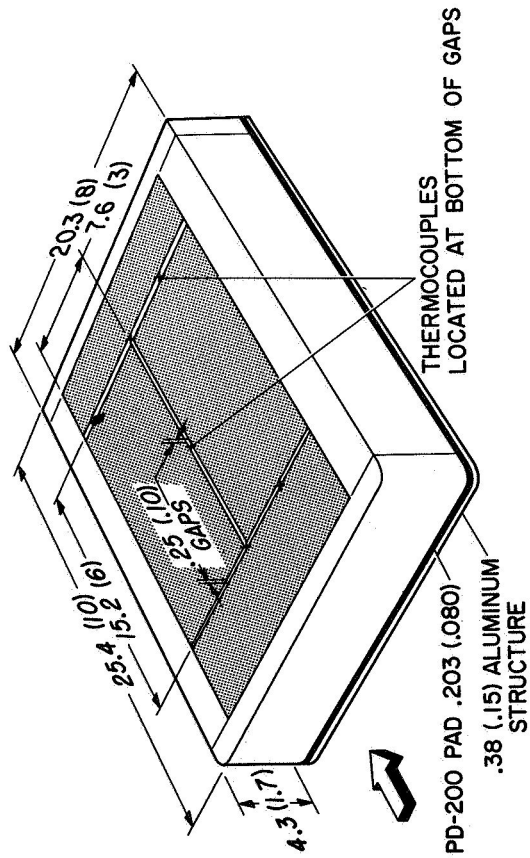
Figure 6

GENERAL ELECTRIC REI-MOD 1A PANEL

(Figure 7)

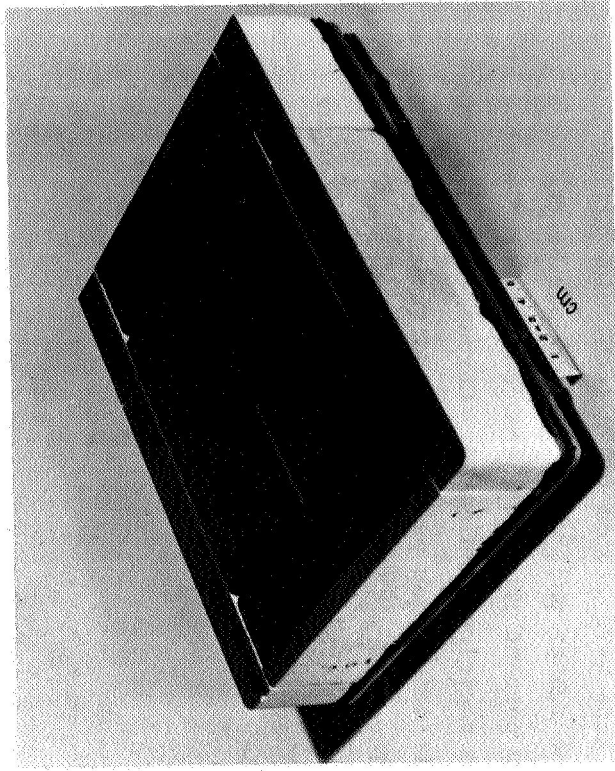
An illustration and pre-test photograph of the General Electric REI-MOD 1A panel are shown in figure 7. The panel consisted of two 7.6 x 15.2 cm (3 x 6 inch) tiles of REI-MOD 1A insulation surrounded by smaller tile segments of the same material to form the gap configuration shown in the figure. The gaps were .25 cm (.100 inch) wide and of depth equal to the tile thickness. The tiles were bonded to a .20 cm (.080 inch) PD-200 foam pad which was, in turn, bonded to a .38 cm (.15 inch) aluminum plate. Five chromel-alumel thermocouples were located at the bottom of the gaps in the positions shown in the figure. Additional thermocouples were located at the backface of the tiles and on the aluminum plate. The General Electric Company supplied two similar panels for this investigation, one with unfilled gaps and the other filled with a silica omniweave gasket material. At the time of this writing the panel with the filled gaps had not been tested; therefore, only the results for the panel with unfilled gaps are reported.

GENERAL ELECTRIC REI-MOD 1A PANEL



ALL DIMENSIONS
ARE IN cm (in.)

a) ILLUSTRATION



b) PRE-TEST PHOTOGRAPH

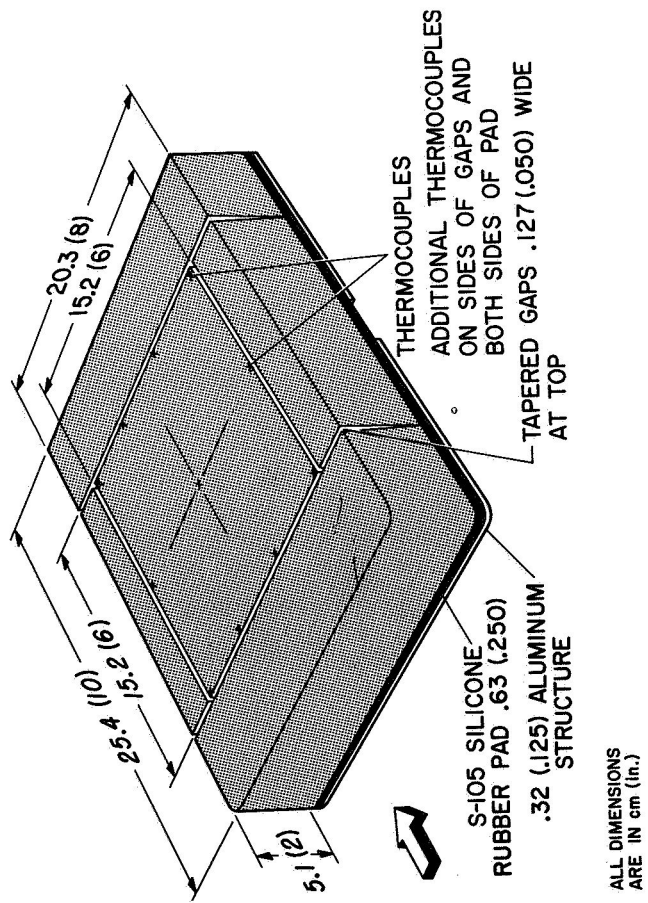
Figure 7

MCDONNELL DOUGLAS HCF-MOD III PANEL

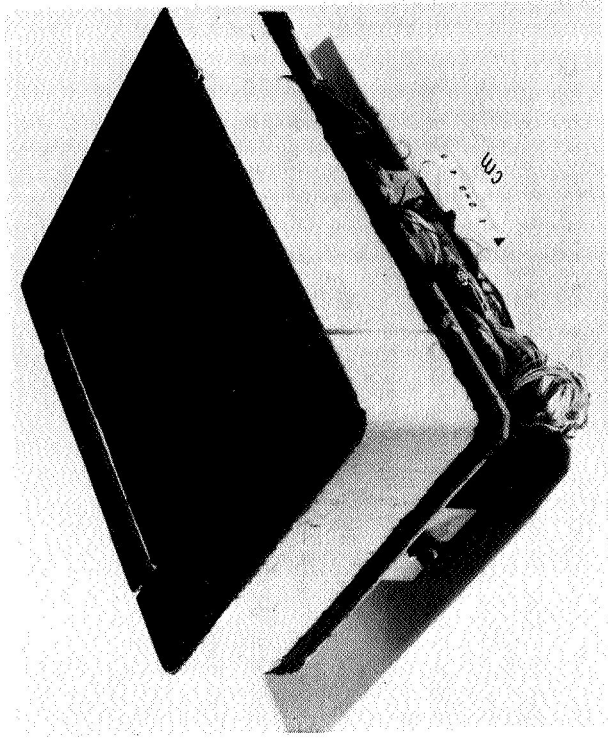
(Figure 8)

An illustration and pre-test photograph of the McDonnell Douglas HCF-MOD III panel are shown in the accompanying figure. This panel consisted of a 15.2 x 15.2 cm (6 x 6 inch) HCF MOD-III tile surrounded by smaller tile segments of the same material. The tapered gaps were .13 cm (.050 inch) wide at the top. The tiles were bonded to a 0.63 cm (.250 inch) S-105 silicone rubber pad, which in turn was bonded to a .32 cm (.125 inch) aluminum plate. Ten platinum-platinum/10 percent rhodium thermocouples were located at the top edges of the 15.2 x 15.2 cm (6 x 6 inch) tile in the positions indicated. Chromel-alumel thermocouples were also located along the vertical wall of the tile at one gap position. Additional thermocouples were located in the rubber pad and on the aluminum panel. The McDonnell Douglas Company supplied two similar panels for this investigation, one having tiles 5.1 cm (2.0 inch) thick and the other 7.6 cm (3.0 inch) thick. At the time of this writing, the 7.6 cm thick panel had not been tested; therefore, only the results for the 5.1 cm thick panel are presented.

MCDONNELL DOUGLAS HCF-MOD III PANEL



(a) ILLUSTRATION



(b) PRE-TEST PHOTOGRAPH

Figure 8

LOCKHEED LI-1542 PANEL AFTER 6 CYCLES

(Figure 9)

A photograph taken of the Lockheed LI-1542 panel after six simulations is shown in figure 9. The air flow over the panel was from left to right as viewed in the photograph. Because of manufacturing and assembly tolerances, this panel had two forward facing steps on the outer windward edges of the rear tile segment. The largest of these steps was .13 cm (.050 inch). The higher heating which results from interaction with the relatively thin turbulent boundary layer resulted in local softening of the coating and substrate and is apparent to some extent in this figure. This local heating appeared to be self-aggravating because softening and resulting coating flow caused the step height to increase. The loss of coating exposed the low emittance tile material resulting in higher local temperatures and shrinkage which resulted in a small cavity. The inability of this cavity to radiate effectively caused more shrinkage and the tests were terminated after ten cycles. A photograph of the panel taken after ten cycles is shown in the next figure.

LOCKHEED LI-1542 PANEL
AFTER 6 CYCLES

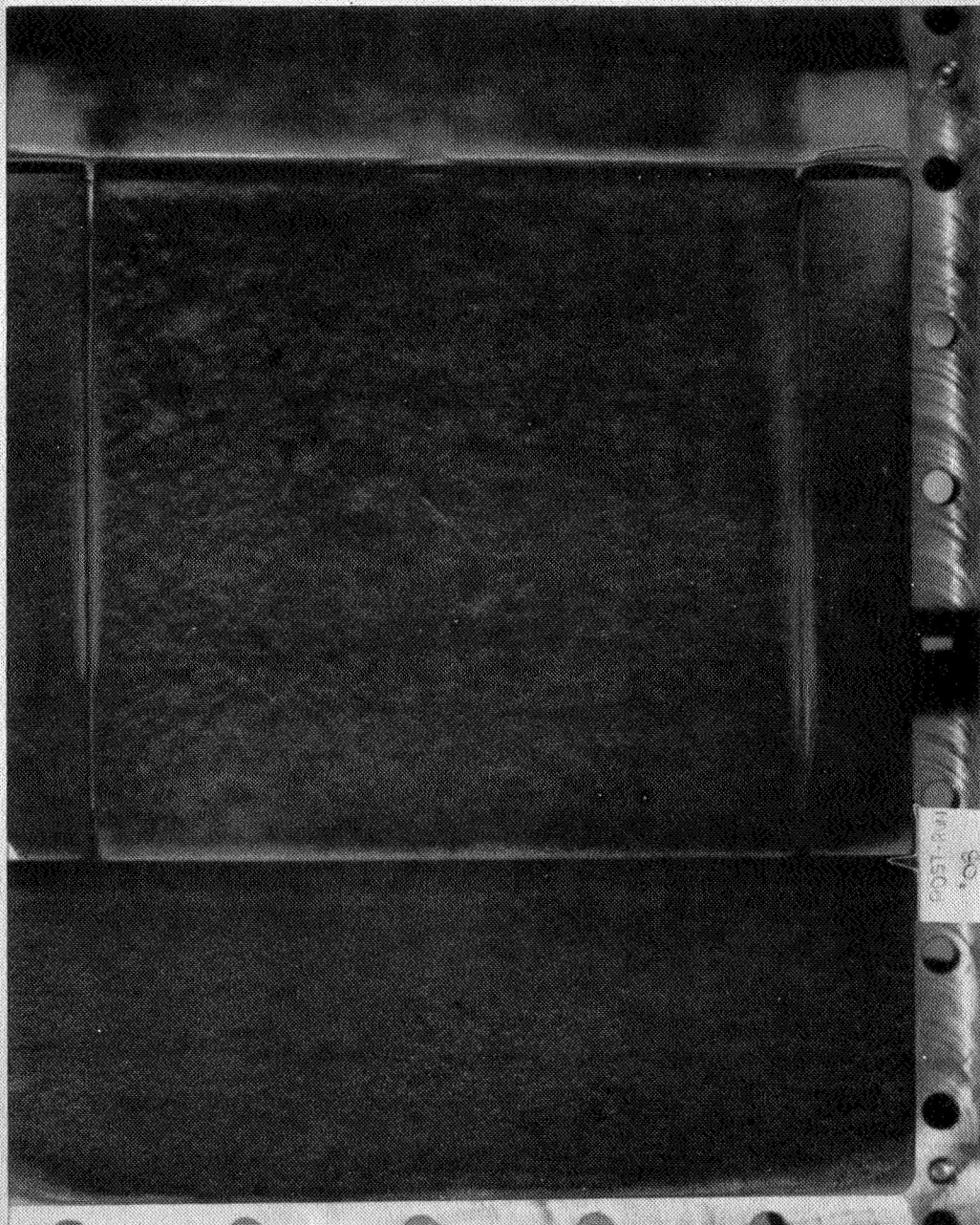


Figure 9

LOCKHEED LI-1542 PANEL AFTER 10 CYCLES

(Figure 10)

This figure presents the photograph of the Lockheed LI-1542 test panel after the 10 cycles of testing. The final result of the aggravated heating due to the forward facing steps is apparent in this figure.

LOCKHEED LI-1542 PANEL AFTER 10 CYCLES

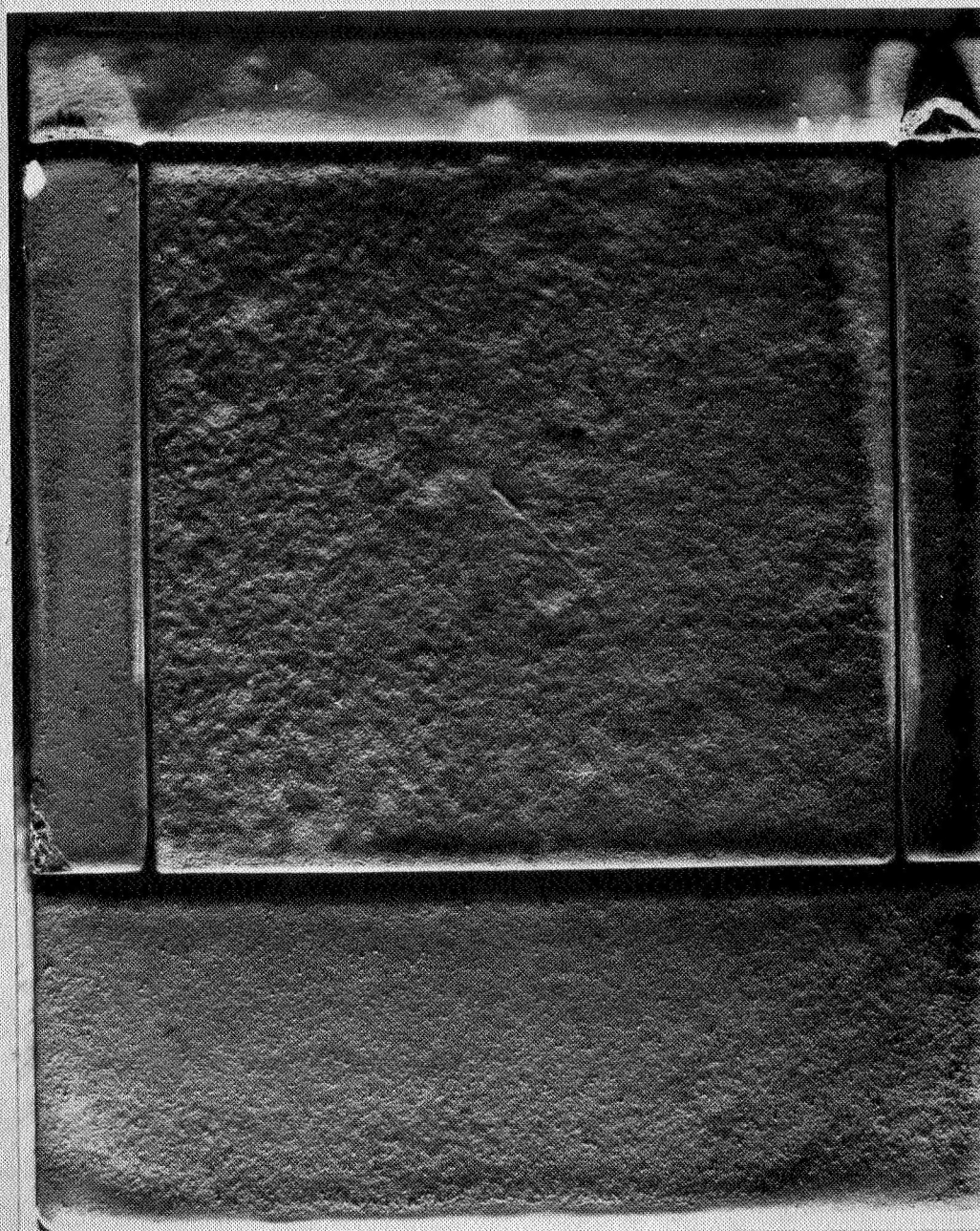


Figure 10

LOCKHEED LI-1542 REAR GUARD TILE AFTER 10 CYCLES

(Figure 11)

A close-up photograph of the area that was overheated due to the presence of the step is presented in this figure. A saw cut taken through the damaged section showed an oblong cavity of about 1.3 x 2.5 cm (1/2 x 1 inch) of inside dimension.

The temperature in the area that failed is estimated to be about 1920°K (3000°F), the softening point of silica glass. This implies a factor of about three increase in the cold wall heating rate in the vicinity of the step. Whether or not this could present a problem on the vehicle, because of its thicker boundary layer, is not clear. It is clear, however, that this is a potential mode of failure. The maximum size of steps permissible on the vehicle must be determined by more experimentation to determine the boundary layer thickness parameter that governs the heating.

LOCKHEED LI-1542 REAR GUARD
TILE AFTER 10 CYCLES

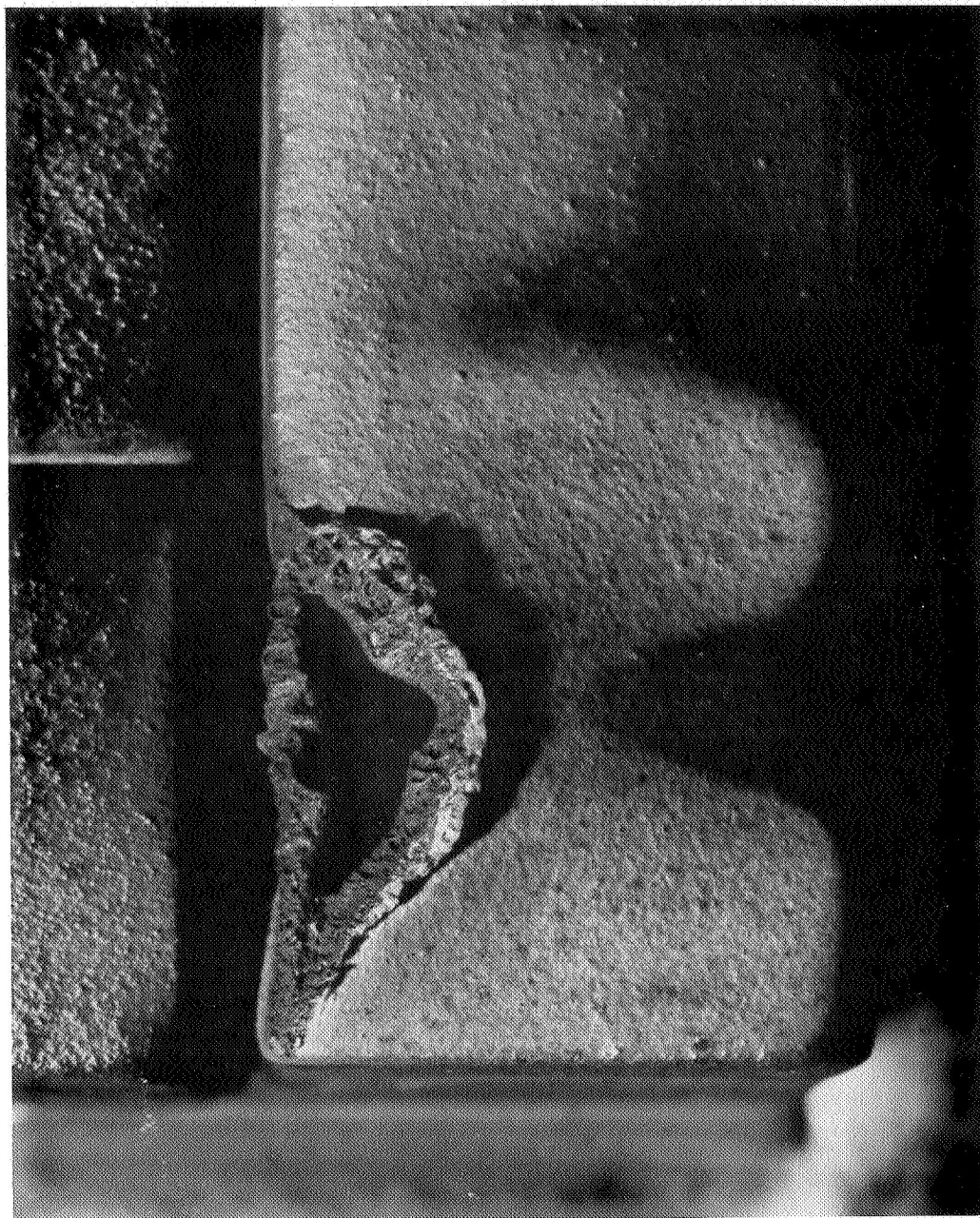


Figure 11

GENERAL ELECTRIC REI-MOD 1A PANEL AFTER 13 CYCLES

(Figure 12)

A photograph of the General Electric REI-MOD 1A panel after 13 simulations is shown in figure 12. At the leading edge of the lower 7.6 x 15.2 cm (3 x 6 inch) tile is an area which has a "paint peel" texture. This area, which could be interpreted as a failure of one or more layers of coating appeared very early in the tests but did not seem to worsen. Another area, near the leading edge of the upper 7.6 x 15.2 cm (3 x 6 inch) tile of the figure showed visible signs of cracking. This will be shown in more detail in the section on nondestructive testing. Visual inspection of the silicone rubber, which can be seen at the bottoms of the gaps after the test, showed no apparent signs of deterioration. A small area, on the thin strip at the trailing edge of the panel, lost its coating due to handling during the course of the tests but no adverse effect was observed.

GENERAL ELECTRIC REI-MOD IA PANEL
AFTER 13 CYCLES

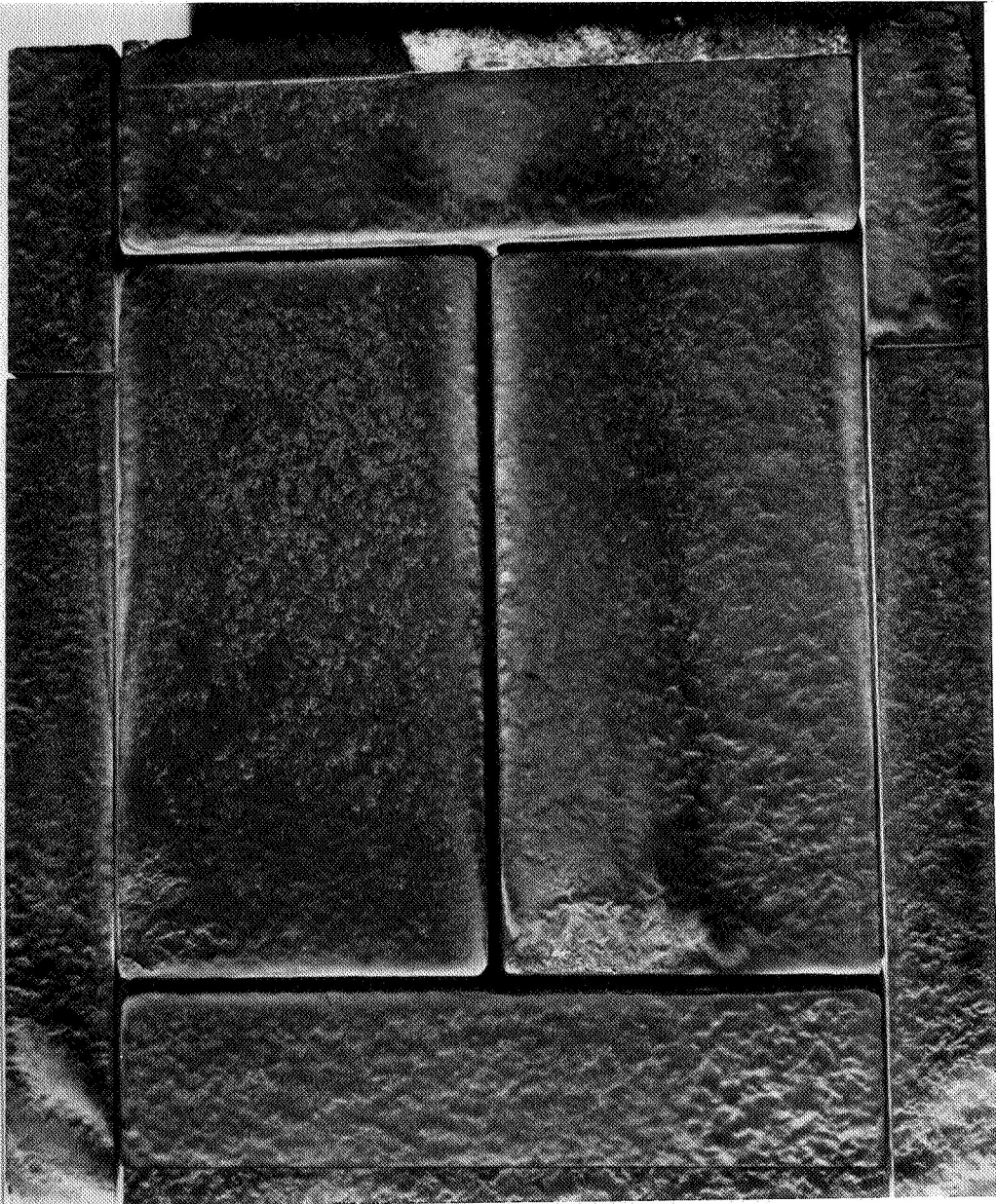


Figure 12

MCDONNELL DOUGLAS HCF-MOD III PANEL AFTER 14 CYCLES

(Figure 13)

A photograph of the McDonnell Douglas HCF-MOD III panel after 14 simulations is shown in this figure. Cracks in the 15.2 x 15.2 cm (6 x 6 inch) tile are clearly visible in the photograph taken after removal from the facility. The cause of the color gradations in the vicinity of the cracked area is not known. Cracking in this panel was detected by visual inspection after the first exposure. Despite the presence of cracks, the tests were continued for another 13 cycles with only a small amount of additional cracking noted.

MCDONNELL DOUGLAS HCF - MOD III PANEL
AFTER 14 CYCLES



Figure 13

TEMPERATURE HISTORIES AT BOTTOM OF GAPS
LOCKHEED LI-1542 PANEL

(Figure 14)

The temperatures measured at the bottom of two streamwise and two spanwise gaps for the Lockheed panel are shown in this figure. The results are compared with a reference temperature measured at the center of the tile at the same depth and which is unaffected by gap heating. The differences between the measured gap temperatures and the reference temperature provide a measure of the heating due to the presence of the gap. The temperatures measured in the two spanwise gaps are slightly higher than the reference temperature. The temperature in one of the streamwise gaps is as much as 111°K (200°F) lower than the reference temperature. The temperature in the other streamwise gap in the region of the forward facing step is considerably higher than the reference temperature because of the aggravated heating in this area. In the absence of steps, no excessive heating problems are evident in this gap design.

TEMPERATURE HISTORIES AT BOTTOM OF GAPS

LOCKHEED LI-1542 PANEL

Y = 2.54 cm

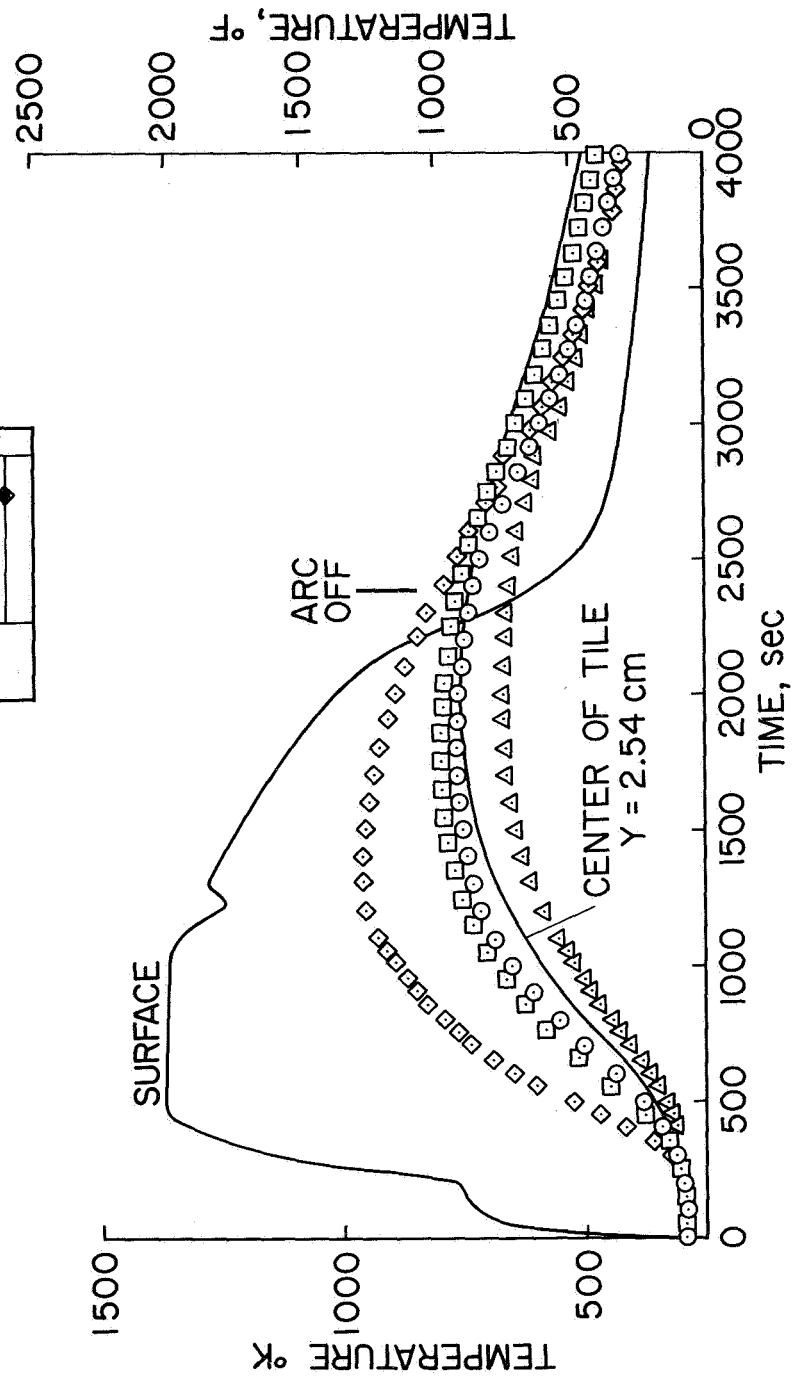
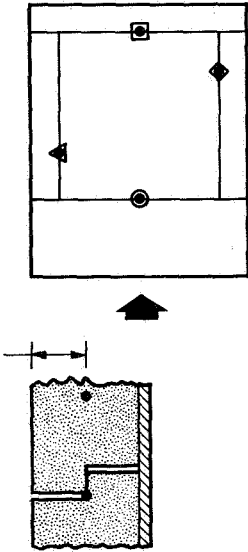


Figure 14

MEASURED AND PREDICTED TEMPERATURE HISTORIES
LOCKHEED LI-1542 PANEL

(Figure 15)

The surface and in-depth temperature response for the Lockheed LI-1542 panel is shown in this figure. The results are compared with predictions made using a one-dimensional heat transfer program that accounts for thermophysical property variations with temperature and pressure. The predictions account for the nonadiabatic conditions at the rear of the aluminum support plate. The calculations tend to overpredict the in-depth temperatures but, in general, are in good agreement. The properties used in the calculations were obtained from the Midterm Review, Space Shuttle Thermal Protection System Development (LMSC-A995708, SS-1135). Thermal conductivities for a pressure of 100 N/m² (.001 atm) were used in the calculations. The comparison between the measurements and predictions lead to the conclusion that the values of density, specific heat, and pressure-dependent thermal conductivity as published in the above document tend to give somewhat conservative results.

MEASURED AND PREDICTED TEMPERATURE HISTORIES LOCKHEED L1-1542 PANEL

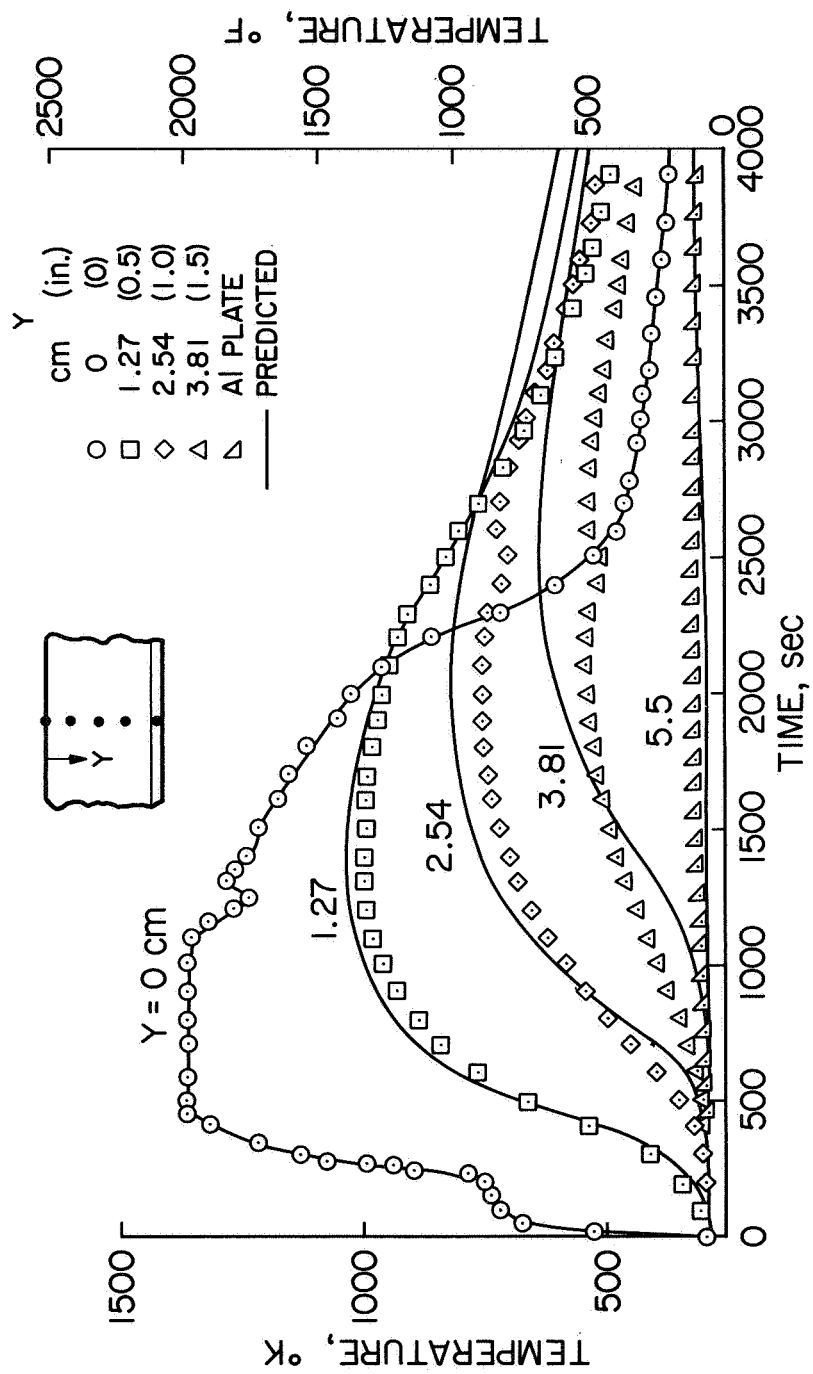


Figure 15

TEMPERATURE HISTORIES
GENERAL ELECTRIC REI-MOD 1A PANEL

(Figure 16)

The measured temperature histories for the General Electric REI-MOD 1A panel are shown in the accompanying figure. Optical pyrometer measurements (solid circular symbols) were made on the rear tile segment (see sketch) using an Infrared Industries TD-9 optical pyrometer with emissivity set at 0.8. The spacing of the observation ports (7.6 cm or 3.0 inch) precluded measurements being made on the larger 7.6 x 15.2 cm (3 x 6 inch) tiles. A measure of the heating at the bottom of the gaps can be made by comparing these temperatures with a reference temperature at the same depth that is unaffected by gap heating. It can be seen that the temperatures at the bottom of the gaps are as much as 167°K (300°F) higher than the reference temperature. The area most affected appears to be at the upstream end of the gap. It is also noteworthy that the maximum temperature at one point reached 590°K (600°F), the maximum use temperature for the adhesive used to bond these tiles to the substrate.

TEMPERATURE HISTORIES GENERAL ELECTRIC REI-MOD 1A PANEL

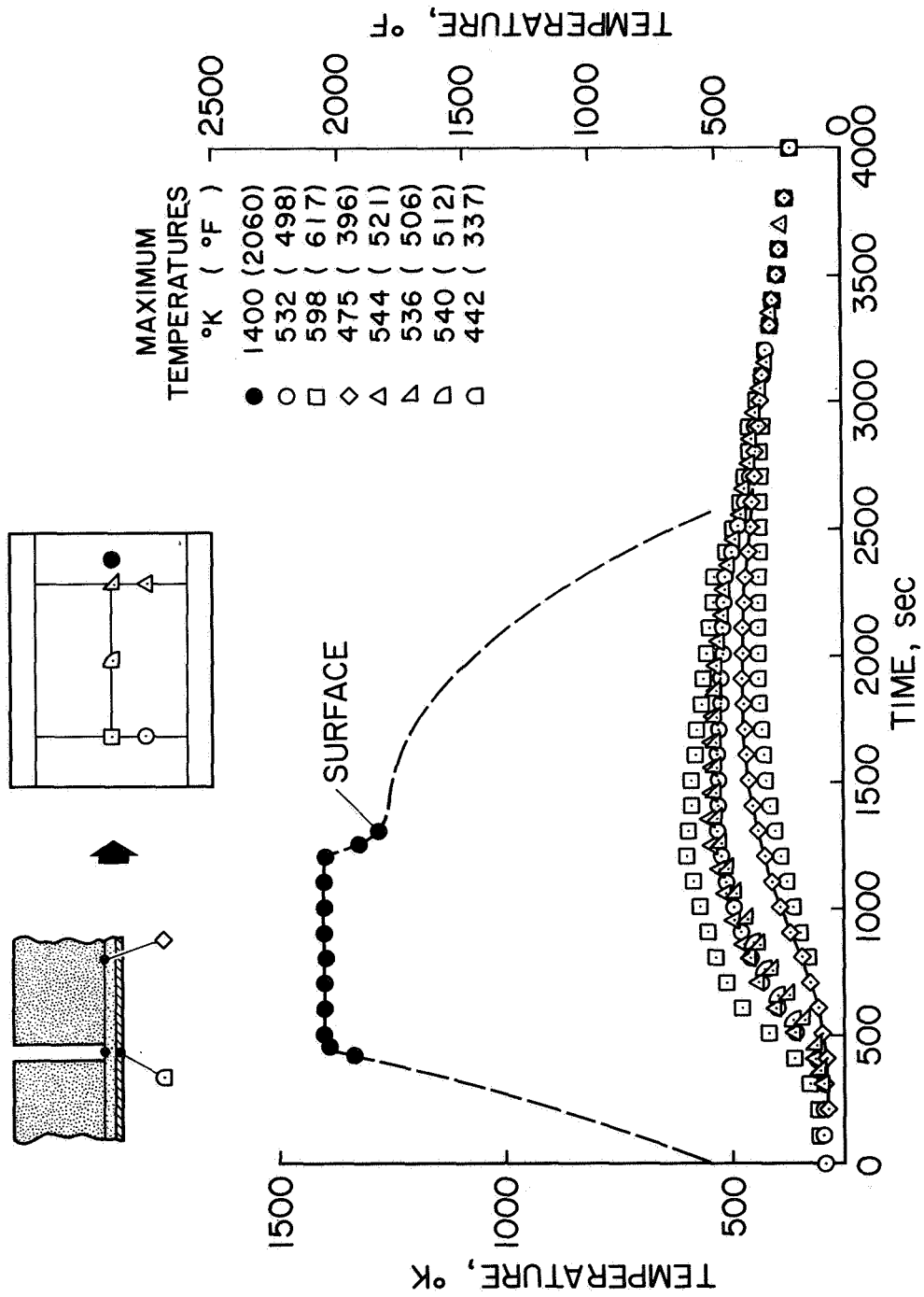


Figure 16

TEMPERATURE HISTORIES

MCDONNELL DOUGLAS HCF-MOD III PANEL

(Figure 17)

The measured temperatures along the top edges of the 15.2 x 15.2 cm (6 x 6 inch) tile and at the bottom of the gap of the McDonnell Douglas HCF-MOD III panel are shown in the accompanying figure. The temperatures at the edges of the tile that form streamwise and spanwise gaps can be compared with a reference temperature unaffected by gap heating measured at the center of the top surface of the tile (solid circular symbols) using an optical pyrometer (Infrared Industries TD-9 with emissivity set at 0.8). In general, the temperatures at the downstream side of spanwise gaps are higher than the reference temperature, while the temperatures at the upstream side of spanwise gaps are lower than the reference temperature. The temperatures at the top edges of gaps aligned with the stream are also lower than the reference temperature. A measure of the heating at the bottom of the gap can be made by comparing this temperature with a reference temperature at the same depth in an area unaffected by the gap. In general, the temperature at the bottom of the gap is as much as 56°K (100°F) higher than this reference temperature. The maximum temperature at the bottom of the gap was 530°K (490°F), about 56°K (100°F) lower than the maximum use temperature of the adhesive used to bond these tiles to the substrate.

TEMPERATURE HISTORIES

MCDONNELL DOUGLAS HCF-MOD III PANEL

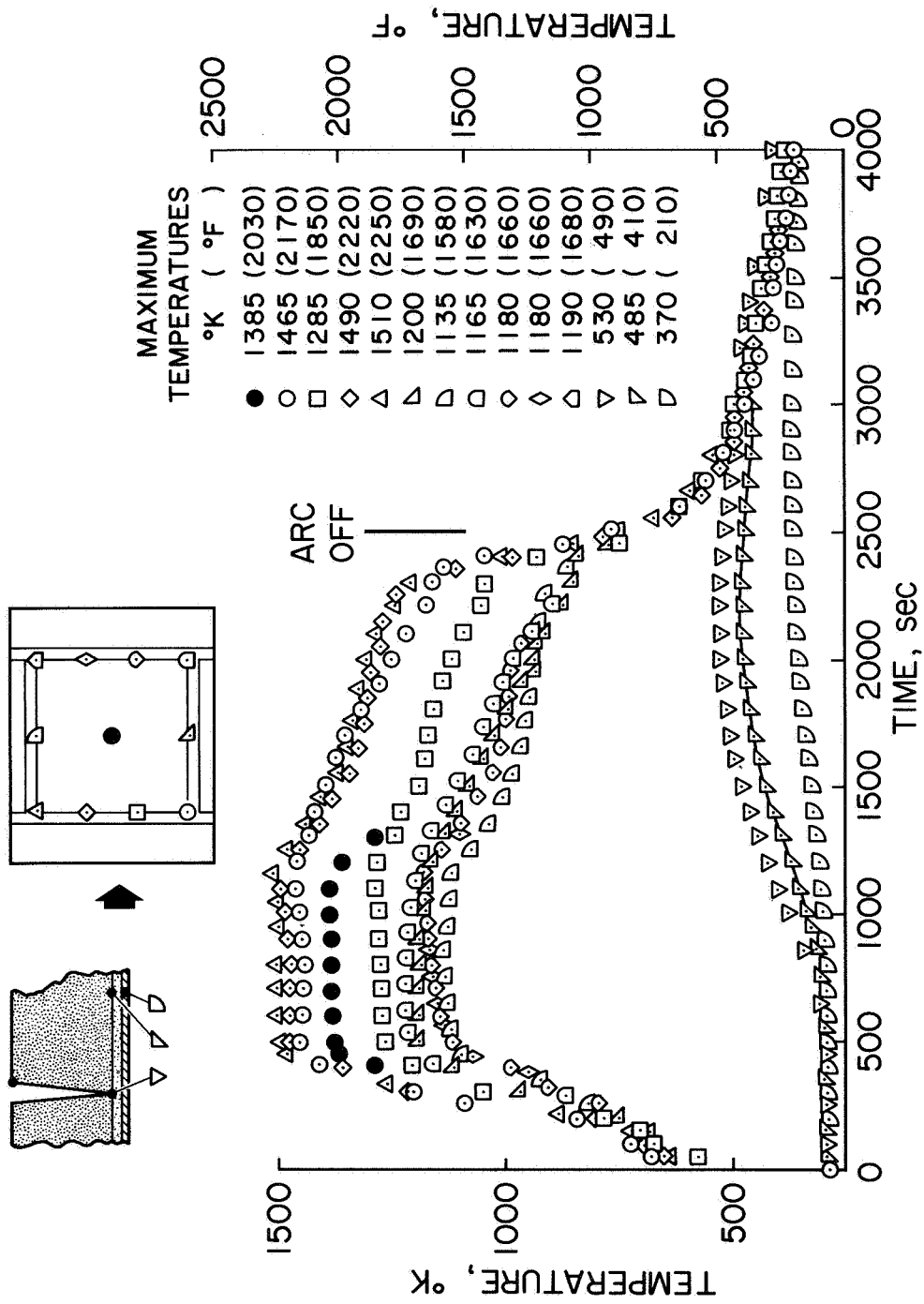


Figure 17

TEMPERATURE HISTORIES ALONG GAP WALL
MCDONNELL DOUGLAS HCF-MOD III PANEL

(Figure 18)

The temperature histories along the vertical gap wall of the McDonnell Douglas HCF-MOD III panel at a point along the leading edge of the 15.2 x 15.2 cm (6 x 6 inch) tile are shown in this figure. (See sketch for location of thermocouples.) For purposes of comparison, the temperatures measured using the TD-9 optical pyrometer are also shown (solid circular symbols).

TEMPERATURE HISTORIES ALONG GAP WALL MCDONNELL DOUGLAS HCF-MOD III PANEL

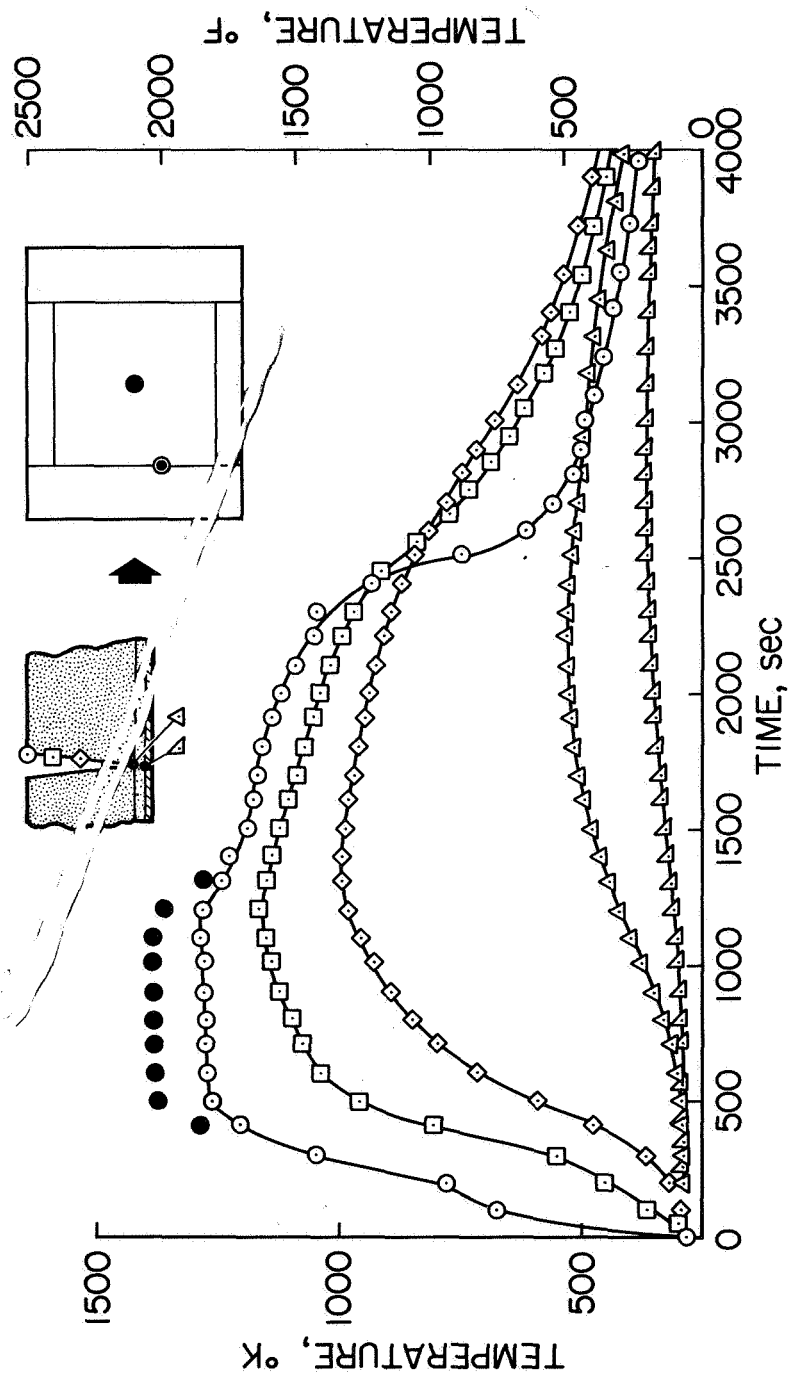


Figure 18

NONDESTRUCTIVE CRACK DETECTION
GENERAL ELECTRIC PANEL

(Figure 19)

The next four figures illustrate the results of surface crack detection using the technique developed at NASA-Manned Spacecraft Center. This technique consists of applying highly volatile acetaldehyde to the surfaces of the tiles. Some of this liquid penetrates the cracks (if any) while the remainder volatilizes. After waiting an appropriate time, chemically sensitized paper is placed over the tile. Vapor emanating from the cracks causes the paper to turn blue. This technique determines the presence of surface cracks or porosity. The depth of the cracks must be determined by other means, such as X-ray methods.

The cracks detected in the General Electric REI-MOD 1A panel after 13 simulations are depicted in figure 19. No cracking was observed in the lower tile. However, an area near the leading edge of this tile reacted strongly to the acetaldehyde test indicating possibly many microcracks or porosity of the coating. It should be emphasized that these 7.6 x 15.2 cm (3 x 6 inch) tiles were the smallest in this test series. Cracking due to thermal stresses is highly size dependent.

NONDESTRUCTIVE CRACK DETECTION GENERAL ELECTRIC PANEL

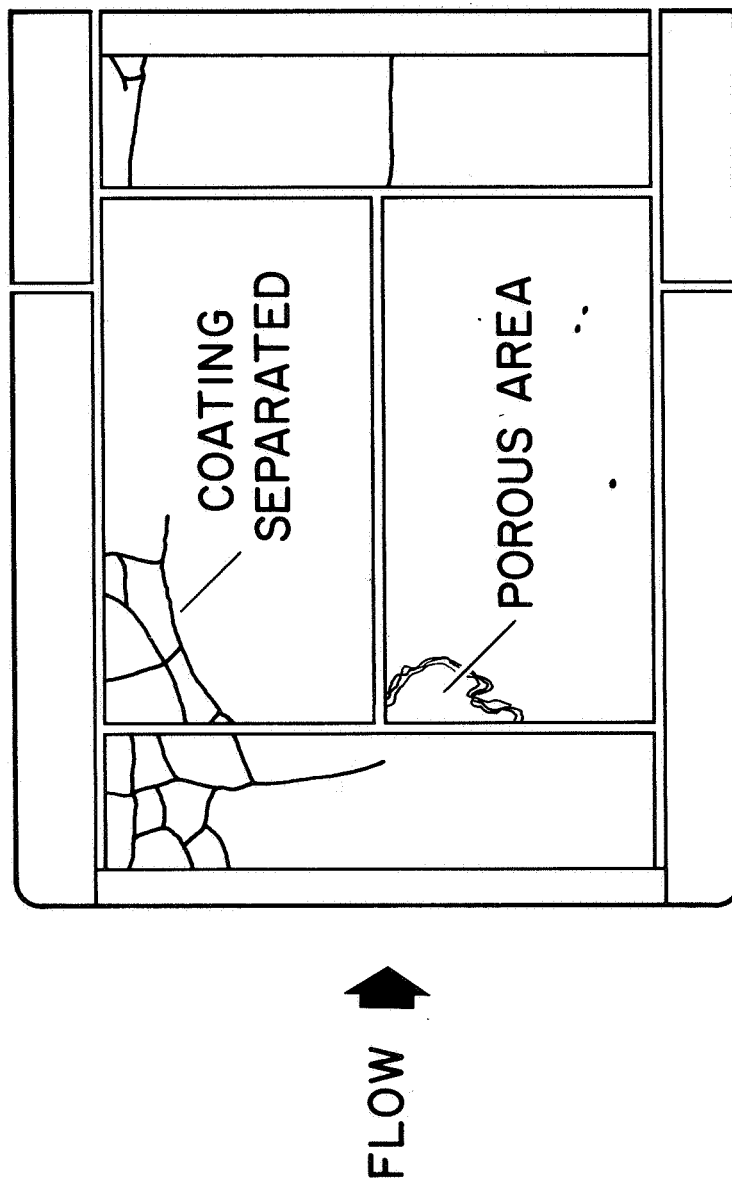


Figure 19

NONDESTRUCTIVE CRACK DETECTION
MCDONNELL DOUGLAS PANEL

(Figure 20)

The cracks detected in the McDonnell Douglas HCF-MOD III panel after 13 simulations are depicted in figure 20. Most of this cracking was visually detected after the first arc-jet simulation.

NONDESTRUCTIVE CRACK DETECTION MCDONNELL DOUGLAS PANEL

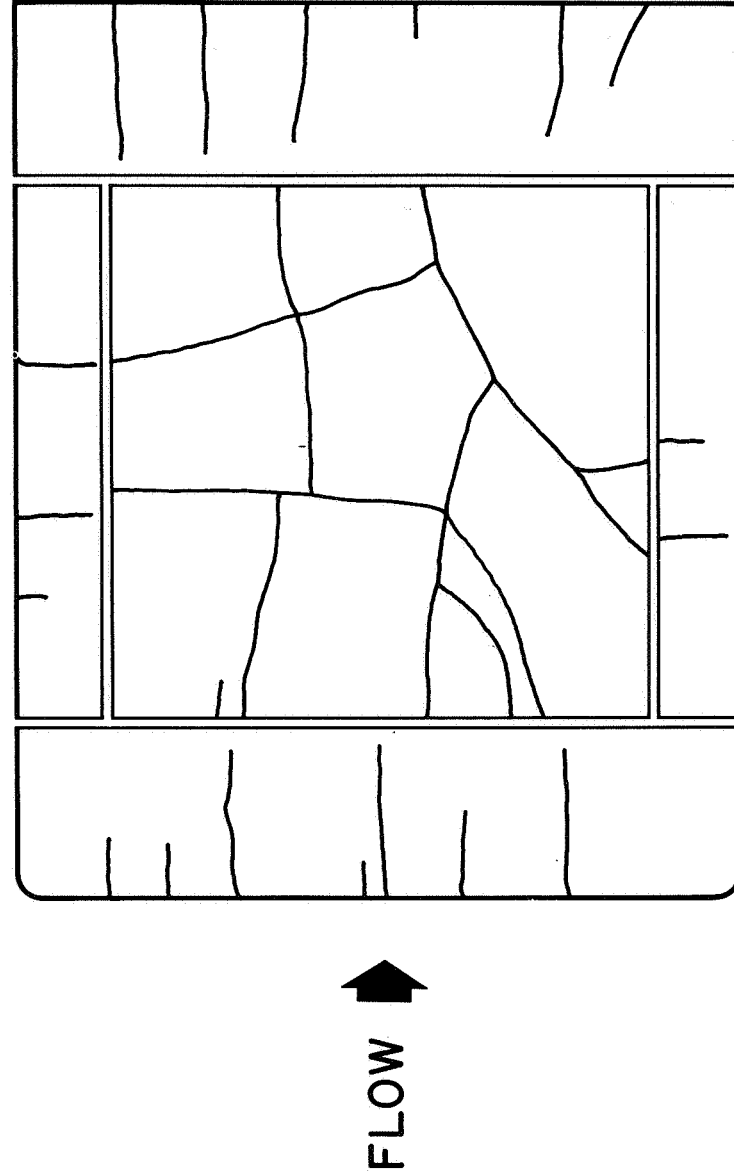


Figure 20

NONDESTRUCTIVE CRACK DETECTION
LOCKHEED PANEL

(Figure 21)

The cracks detected on the Lockheed LI-1542 panel using the acetaldehyde technique are depicted in this figure. The majority of these cracks are in the vicinity of the surface thermocouples. However, immediately after application of the acetaldehyde, small cracks could be seen visually that were not detectable on the sensitized paper.

NONDESTRUCTIVE CRACK DETECTION LOCKHEED PANEL

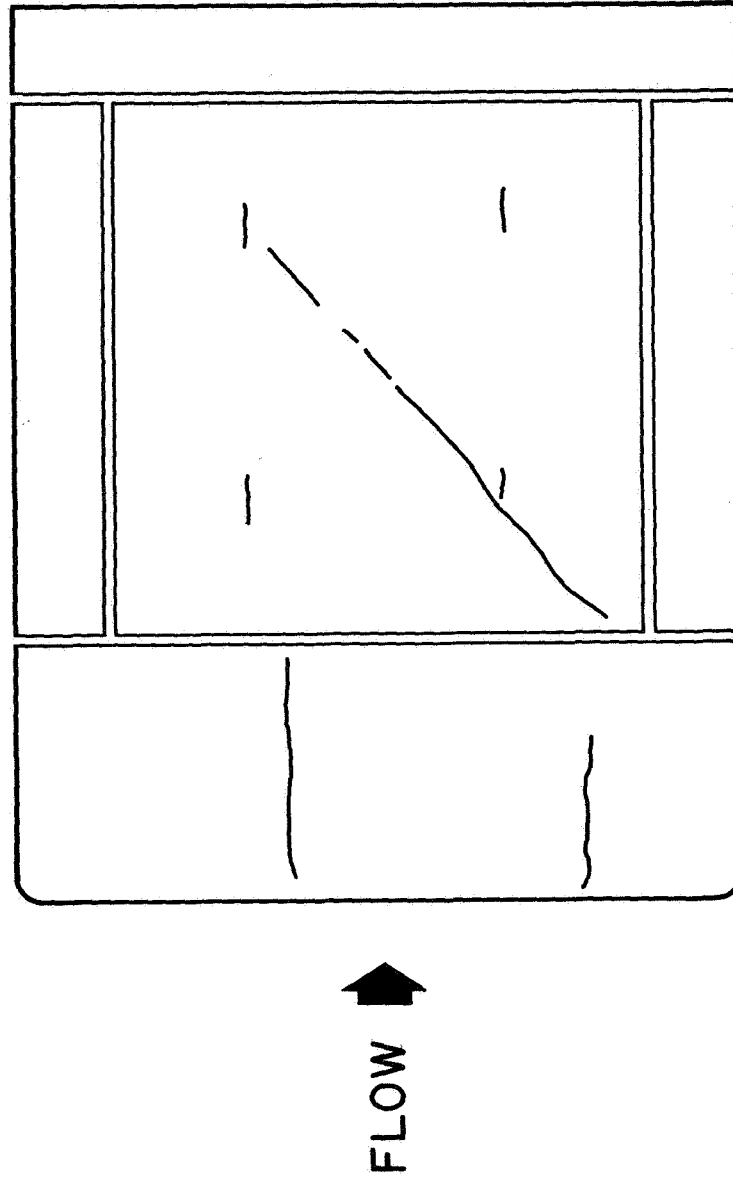


Figure 21

NONDESTRUCTIVE CRACK DETECTION OF LOCKHEED PANEL
AFTER APPLICATION OF ACETALDEHYDE

(Figure 22)

This figure presents a photograph of the Lockheed LI-1542 panel where the cracks that were not detectable on the sensitized paper are clearly evident. However, it should be emphasized that, at the time of these experiments, Ames Research Center had a minimum of experience using this technique. These small cracks might have easily been detected by the more experienced experimenters at the Manned Spacecraft Center where the technique was developed.

NONDESTRUCTIVE CRACK DETECTION
LOCKHEED PANEL AFTER APPLICATION OF ACETALDEHYDE

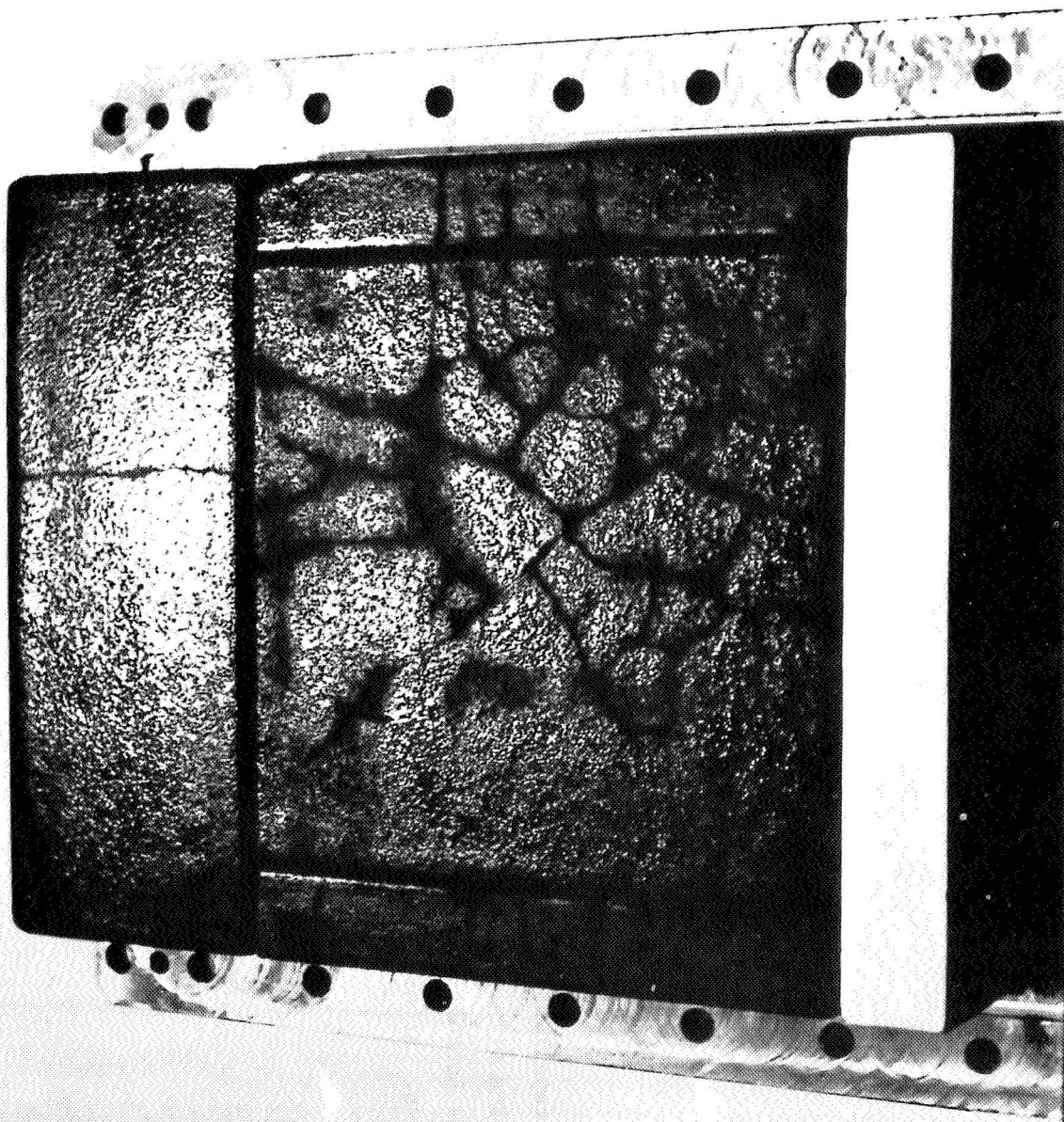


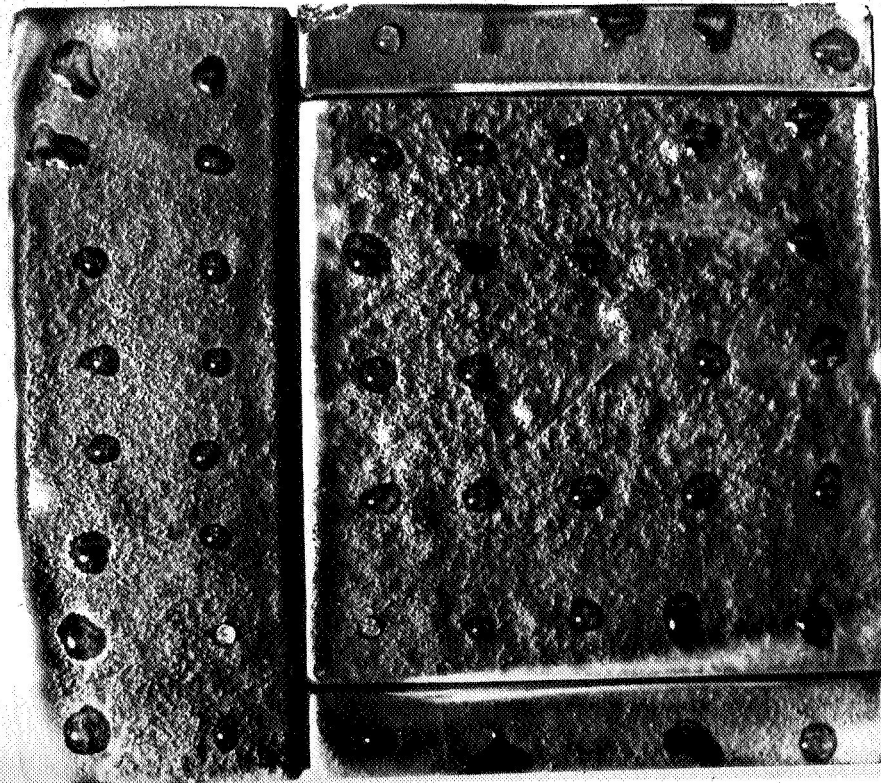
Figure 22

WATER REPELLENCY TEST OF LOCKHEED PANEL

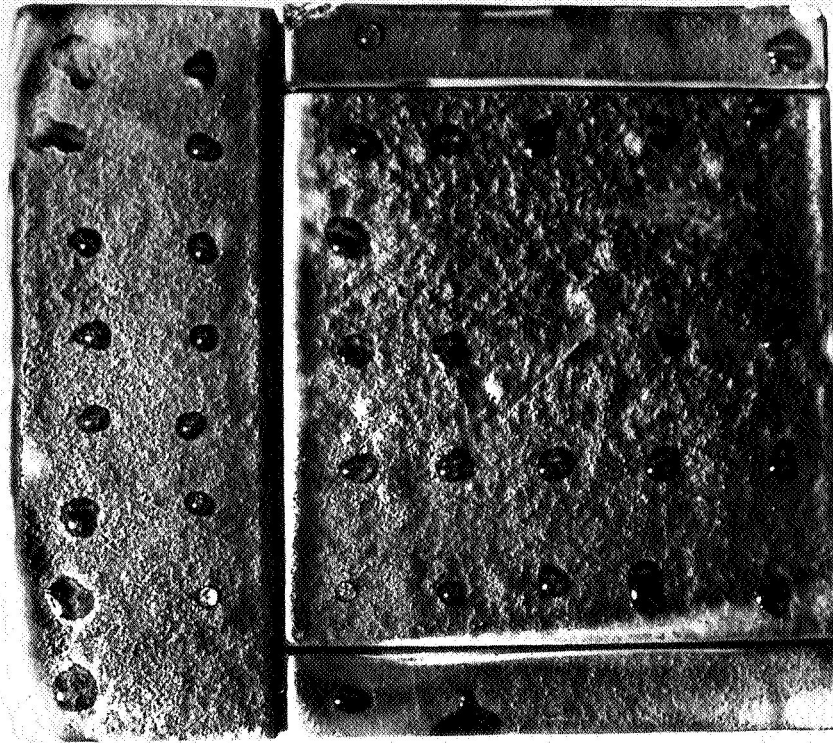
(Figure 23)

Water repellency tests of the panels after arc-jet exposure are shown in the next three figures. This test consisted simply of applying drops of distilled water at various locations and observing the results. For the Lockheed LI-1542 panel shown in figure 23 there was water absorption at four locations after five minutes. After 25 minutes there was indication of water absorption at a total of about 12 locations.

WATER REPELLENCY TEST OF LOCKHEED PANEL



5 min



25 min

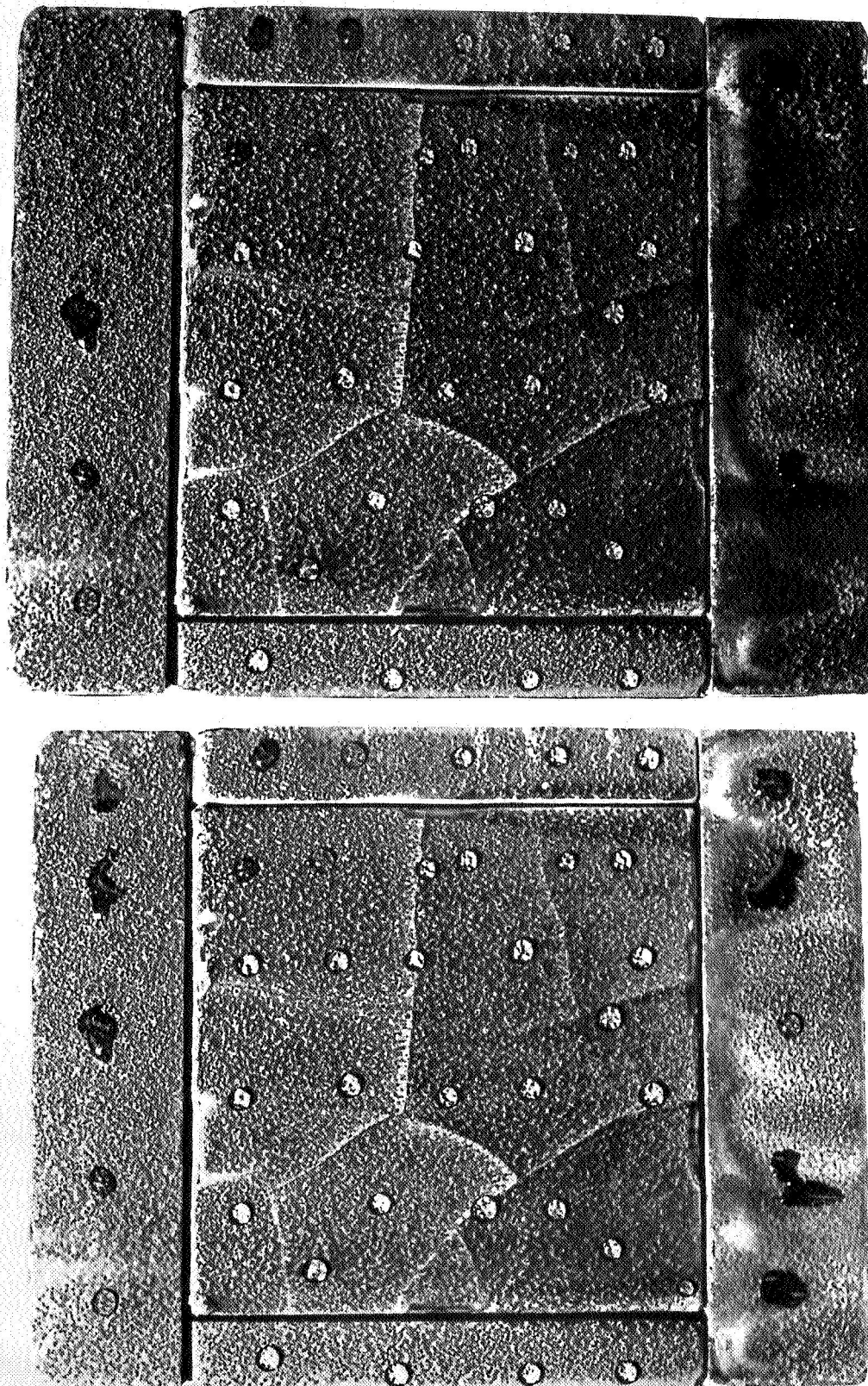
Figure 23

WATER REPELLENCY TEST OF MCDONNELL DOUGLAS PANEL

(Figure 24)

The McDonnell Douglas HCF MOD-III panel shown in this figure showed no signs of absorbing water, even when the droplets were placed over visible cracks.

WATER REPELLENCY TEST OF McDONNELL DOUGLAS PANEL



25 min

0 min

Figure 24

WATER REPELLENCY TEST OF GENERAL ELECTRIC PANEL

(Figure 25)

The General Electric REI MOD-1A panel shown in this figure also showed no signs of absorbing water, even when droplets were placed on the area which had lost the surface coating. In some cases, water droplets would not penetrate the uncoated edges of panels prior to arc-jet exposure.

This simple test may not be good measure of waterproofness; however, based on the observations, some comments are in order. First, if water droplets penetrate easily, the coating is certainly not waterproof. Second, if the droplets wet the coating and spread out evenly, the results are difficult to interpret. Third, the lack of penetration in cracks and even in uncoated areas is somewhat inconclusive. One possible interpretation of this lack of penetration, even in uncoated areas, is the presence of silicone oil at these sites. A possible source of silicone, if not present prior to the test, is volatilization from the bond area, which had been heated to several hundred degrees during the tests. Another possible reason is the condensation of stream impurities on the tile surfaces.

WATER REPELLENCY TEST OF GENERAL ELECTRIC PANEL

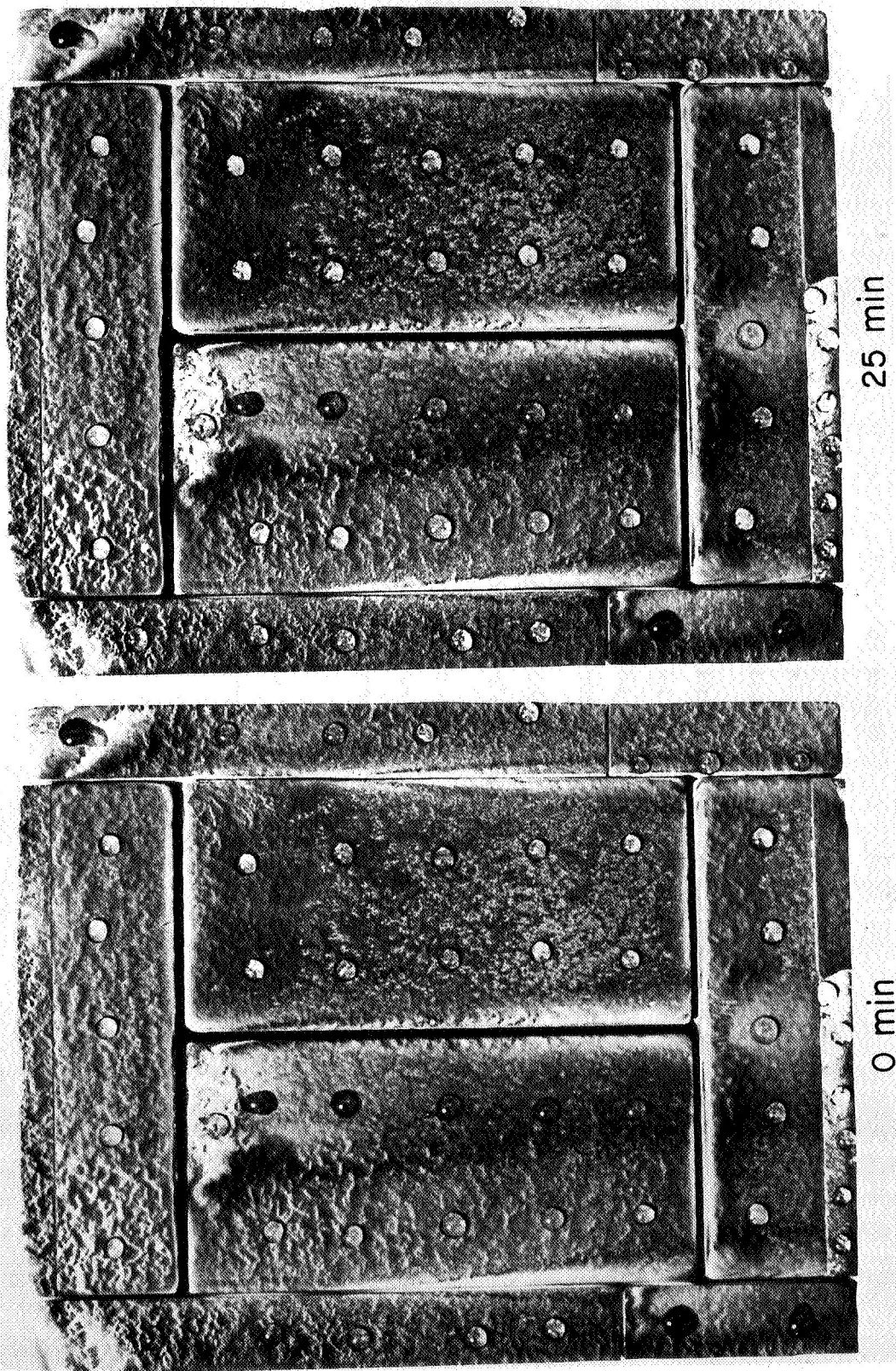


Figure 25

CONCLUSIONS

(Figure 26)

1. Using the technique of mixing argon with air it is possible to closely simulate the temperature-time trajectory experienced by the Space Shuttle Vehicle in facilities of this type.
2. Gap heating appears to be highly dependent upon gap design. It is relatively low for the interlocking Lockheed design and tapered design of McDonnell Douglas. It is significantly higher for the wider, unfilled gap design of General Electric. While the filled gap design was not tested in this investigation, it is expected that the heating will be reduced significantly.
3. The heating rate appears to be significantly higher at the windward facing edges of flush tiles, while at the same time, being lower at the leeward and streamwise edges.
4. The heating rate is aggravated at forward facing steps. This heating, however, is highly dependent on step heights relative to some characteristic thickness of the boundary layer. Further tests are required to identify the magnitude of this heating as it relates to the Space Shuttle Vehicle and its boundary layer characteristics.
5. Cracking of varying degrees was observed on all the RSI panels tested. These ranged from numerous fine cracks on the Lockheed panel to numerous larger cracks on the McDonnell Douglas panel.

CONCLUSIONS

- GOOD TRAJECTORY TEMPERATURE -TIME SIMULATION ACHIEVED USING ARGON - AIR TECHNIQUE
- GAP HEATING HIGHLY DEPENDENT UPON GAP GEOMETRY
- HEATING SIGNIFICANTLY HIGHER AT WINDWARD FACING EDGES OF FLUSH TILES
- HEATING AGGRAVATED AT FORWARD FACING STEPS - FURTHER TESTS ARE REQUIRED TO ESTABLISH DESIGN CRITERIA
- CRACKING OF VARYING DEGREES OBSERVED ON ALL PANELS

Figure 26

CONVECTIVE HEATING TESTS OF REUSABLE SURFACE INSULATION JOINTS AND GAPS

H. E. (Ned) Christensen and D. A. Osborne

McDonnell Douglas Astronautics Company - East
St. Louis, Missouri

INTRODUCTION

One of the most important areas needing characterization for the Shuttle TPS and other entry vehicles is the effect of additional convective heating in gaps and joints. The size of the gap and the joint design are hallmark variables as well as boundary layer flow conditions. The gap-joint problem has many facets, and this paper addresses the study of experimental measurement of heating in gaps, effects on the mission and adequacy of several theories. This paper does not address the required gap size as affected by: tile size, tolerances associated with fabricating a tile and the assembly of the TPS, the dimensional changes in the structure due to temperatures and loads, or the manufacturing and refurbishment problems associated with the TPS. These other facets are important and also affect the TPS design.

The scope of this investigation and tests are given below. The information presented herein only scratches the surface of the gap-joint iceberg and additional investigations are warranted.

Scope

- Obtain comparative effects of gap width on the convective heating in RSI joints
- Compare thermal performance of candidate joint designs
- Effects of steps
- Derive heating distributions in the joints and then compare with theory

Completed Tests

- Wedge flow in the NASA-MSC 10-MW Arc Tunnel

Scheduled Testing

- Channel nozzle at NASA-MSC
- Thick boundary layer using tunnel wall in Langley's CPHT
- Arc tunnel tests of large RSI panel in Wright Field's 50-MW facility (tentative)

This work was sponsored by NASA-MSC as part of contracts NAS9-12082 and NAD9-12854, Development and Design Application of Rigidized Reusable Surface Insulation Thermal Protection System.

HEATING RATE RATIO IN LONGITUDINAL SLOT AS FUNCTION OF ANGLE OF ATTACK

(Figure 1)

Previous investigations have dealt with shallow gaps, such as shown in figure 1, but the RSI-TPS will have relatively deep gaps due to tile thickness requirements. As shown in the figure, heating on the windward and leeward edges of the slot diverges with angle of attack and shows an increase in heating over the heating on a smooth surface. The experimental portion of the present investigation consisted of fabricating a series of joint models for a wedge and performing a series of comparative tests in the NASA-MSX 10 MW Arc Tunnel.

HEATING RATE RATIO IN LONGITUDINAL SLOT AS FUNCTION OF ANGLE OF ATTACK

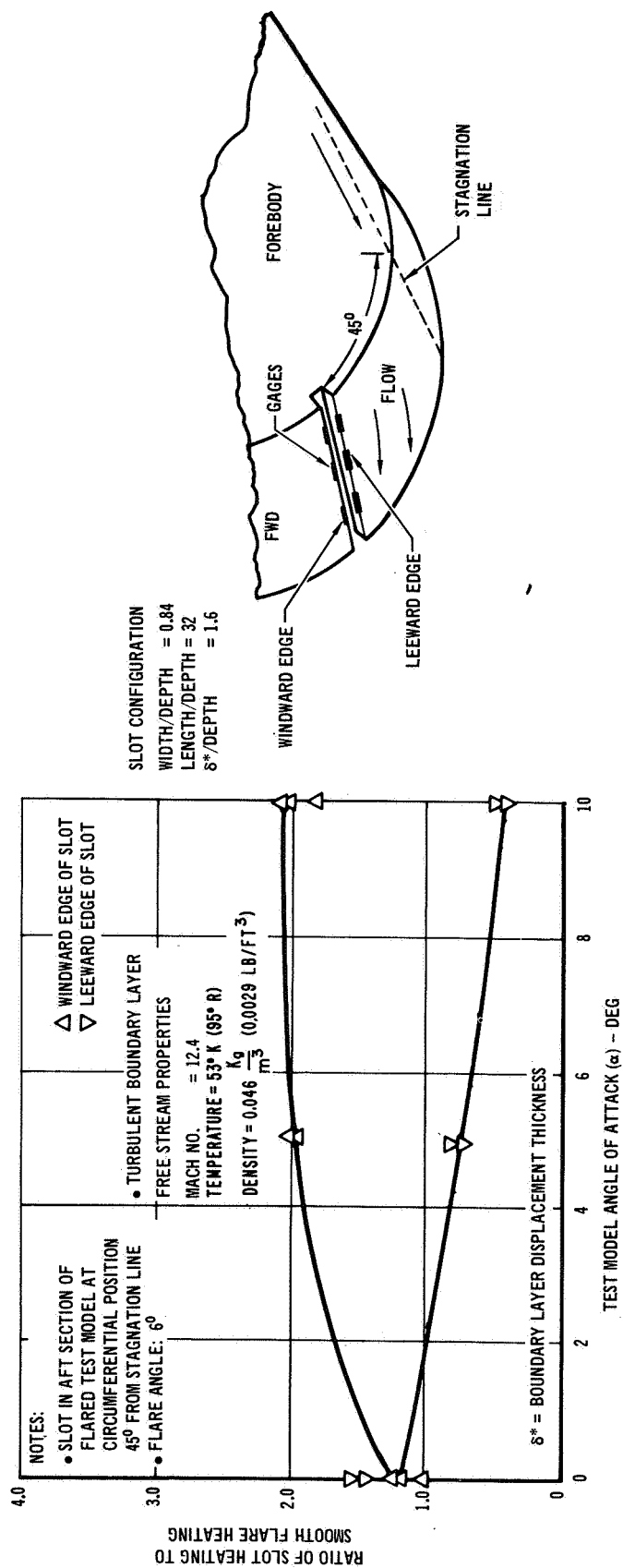


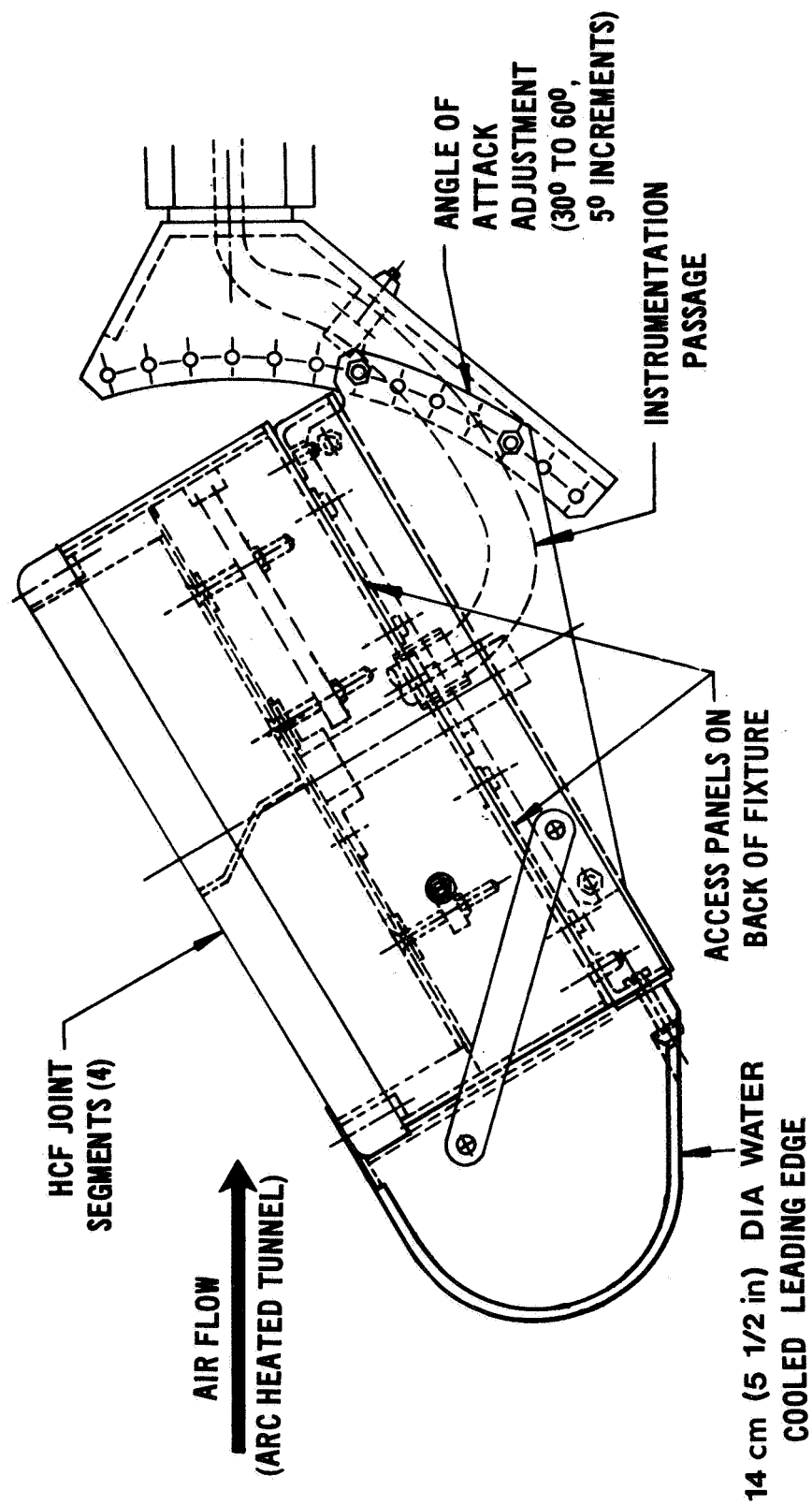
Figure 1

PLASMA WEDGE TEST FIXTURE FOR EVALUATING JOINTS, GAPS, AND STEPS

(Figure 2)

Sets of four tiles were designed to be interchangeable within a test fixture containing a gap setting mechanism. The fixture was designed so that the gaps would be reset between tunnel runs without removing the wedge from the Arc tunnel facility. The test fixture also contained a set of HCF guards around the tiles, and the test fixture (box) fits into a wedge with a 14 cm (5-1/2 inch) diameter leading edge (water cooled).

PLASMA WEDGE TEST FIXTURE FOR EVALUATING JOINTS, GAPS AND STEPS



*BASIC TEST FIXTURE ALSO FABRICATED BY MDAC (SSTP)

Figure 2

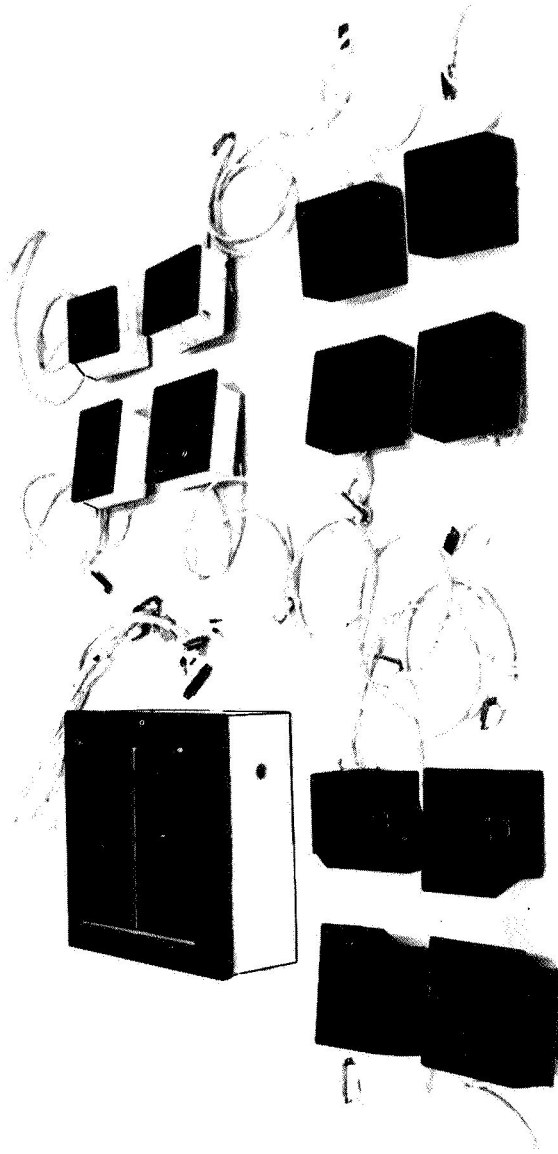
MODELS FOR ARC TUNNEL TESTS OF JOINTS AND GAPS

(Figure 3)

Twelve sets of joint models have been fabricated as shown in figure 3. Results for the contoured, butt, and butt step model are contained in this paper. The models are heavily instrumented, and the features of the model design are listed in the figure.

MODELS FOR ARC TUNNEL TESTS OF JOINTS AND GAPS

(30.5 x 30.5 CM TEST FIXTURE)



JOINT	TILE THICKNESS			
	INCH	1.25	2.00	2.50
	CM	3.17	5.08	6.35
CONTOURED BUTT	✓	✓	✓	✓
BUTT STEP	✓	✓	✓*	✓
OVERLAP BLOCK			±0.15	
INCLINED TAPERED			✓	✓

*(INCH)

37 THERMOCOUPLES 4 SURFACE
16 JOINT
6 IN-DEPTH

- MSC 10 MW ARC HEATED TUNNEL
- WEDGE OR CHANNEL NOZZLE
- GAP SETTINGS EASILY ADJUSTED
- QUICK DISCONNECTS FOR INSTRUMENTATION
- FIBROUS INSERTS—STUDY EFFECTS OF ROVING

Figure 3

NASA-MSC 10 MW ARC TUNNEL

(Figure 4)

The tests performed to date were performed in the NASA-MSC 10 MW Arc Tunnel shown in figure 4. This view of the facility not only shows the sting for the wedge but also the channel nozzle to be used in the upcoming test series.

NASA-MSC 10 MW ARC TUNNEL

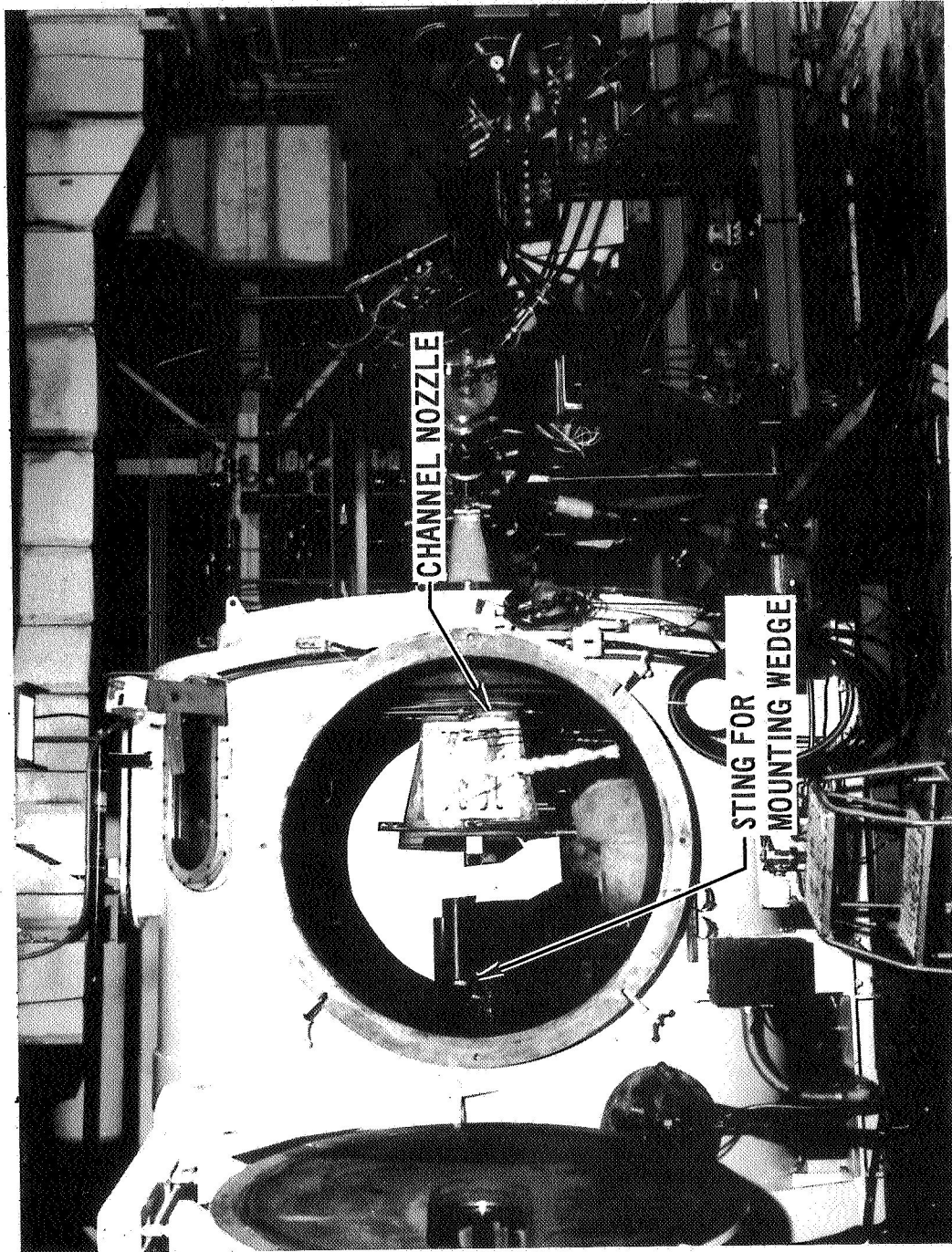


Figure 4

INSTALLATION OF HCF JOINT MODEL IN NASA-MSC 10 MW ARC TUNNEL

(Figure 5)

Figure 5 is a view of the wedge test fixture installed on the sting of the tunnel. The wedge is positioned over the radiant preheater for simulating the portion of the entry heat pulse below 1200°K (1700°F). When the surface thermocouples indicate 1200°K (1700°F), the model is swung into the flow stream of the tunnel.

INSTALLATION OF HCF JOINT MODEL IN NASA-MSC 10 MW ARC TUNNEL

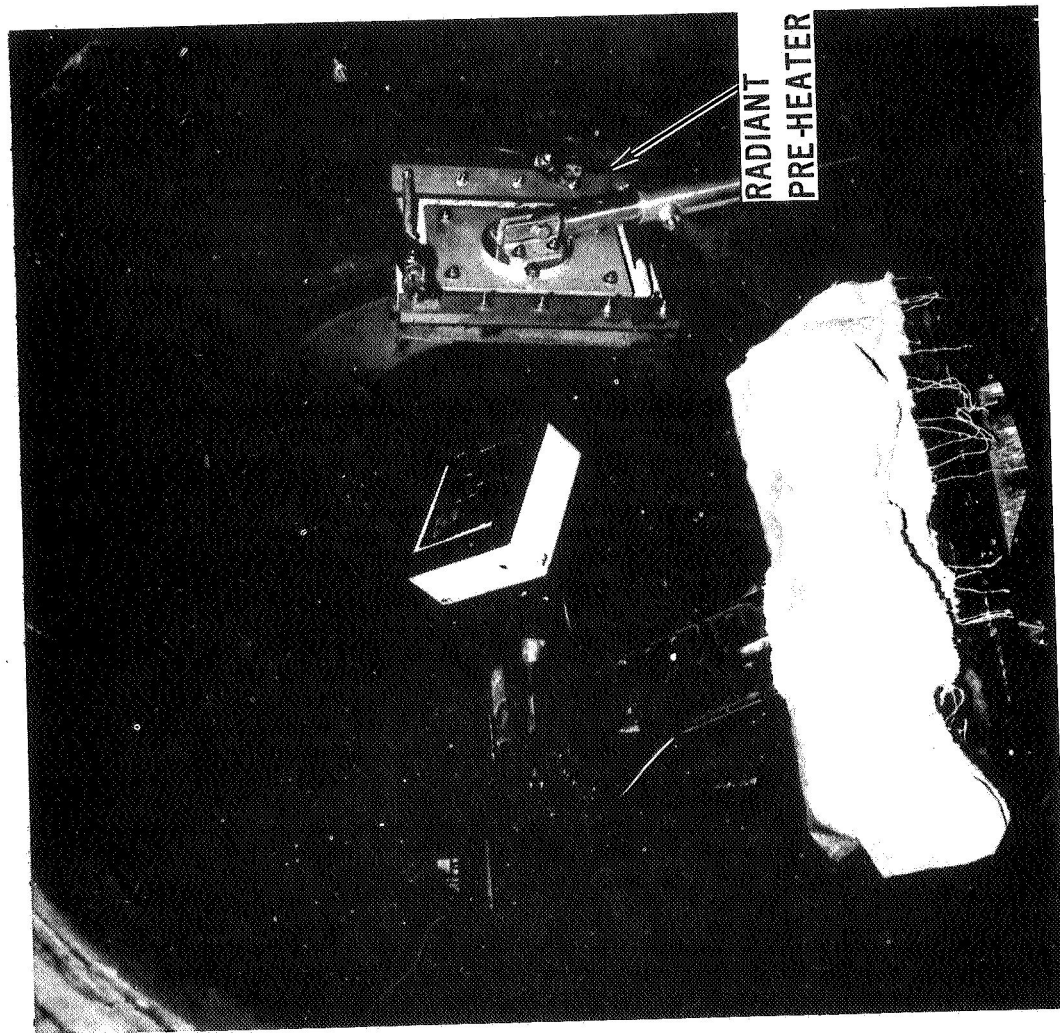


Figure 5

TESTING OF HCF JOINT MODEL IN NASA-MSC 10 MW ARC TUNNEL

(Figure 6)

A side view of the joint model during testing is shown in this figure.

TESTING OF HCF JOINT MODEL IN NASA-MSC 10 MW ARC TUNNEL



Figure 6

TESTING CONTOURED JOINT IN THE NASA-MSC 10 MW ARC TUNNEL

(Figure 7)

As can be seen in figure 7, the heating in the gaps was very high.

TESTING CONTOURED JOINT IN THE NASA-MSC 10 MW ARC TUNNEL

0.76 cm (0.30 INCH) GAP

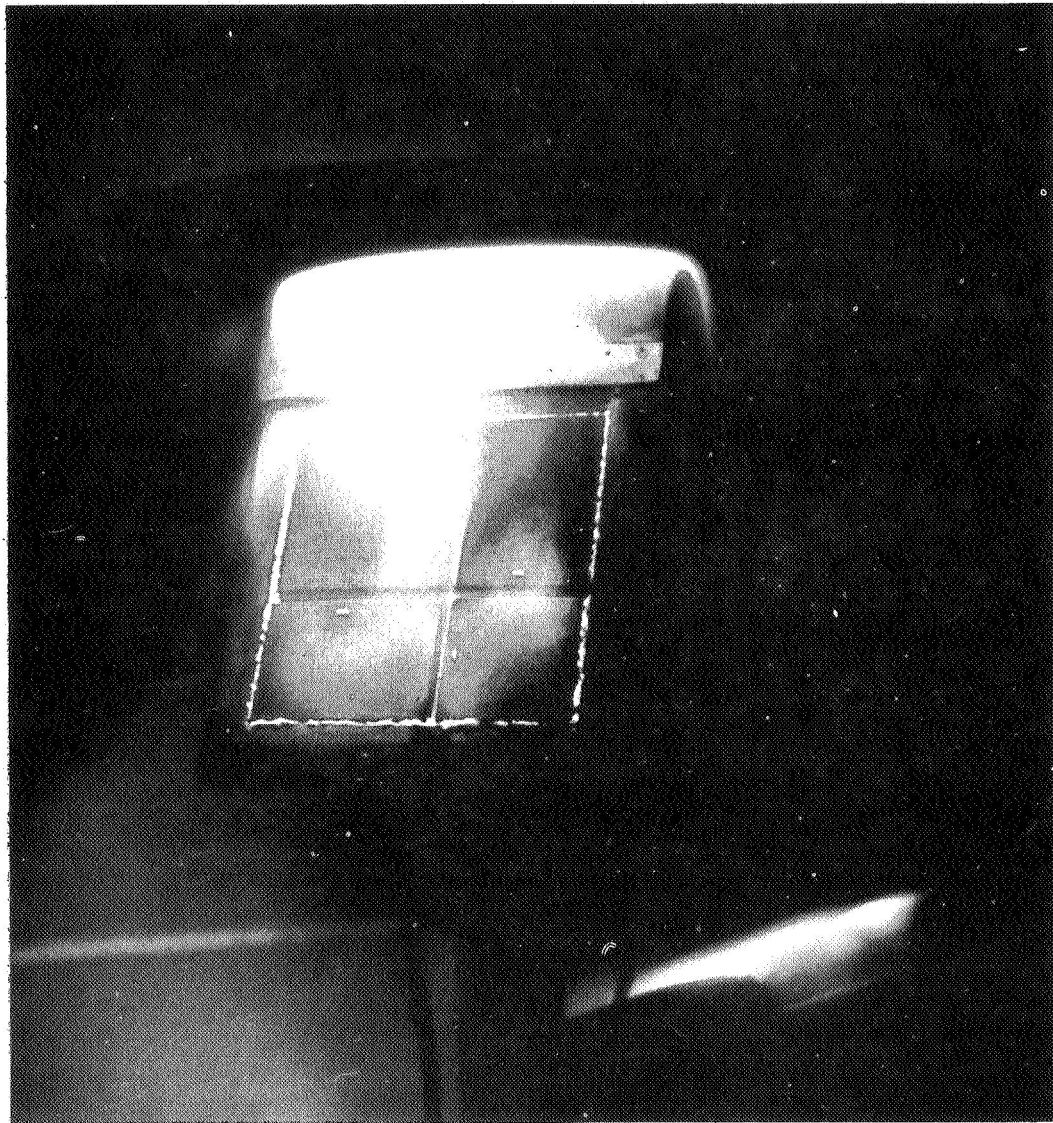


Figure 7

MEASURED TEMPERATURE OF HCF/JOINT MODEL IN MSC
10 MW ARC TUNNEL

(Figure.8)

The next four figures present temperature response data for some of the models tested. The temperature history of the tile surface and bondline, and the temperature distribution down the gap are shown in figure 8 for a typical model. The radiant heating and convective heating portions of the tests are also shown. It is interesting to note the increase in temperature and hence heating across the transverse gap (locations C and A). The shape of the temperature distribution down the faces of the gap is as expected.

MEASURED TEMPERATURE OF HCF/JOINT MODEL IN MSC 10 MW ARC TUNNEL

0.127 cm (0.050 in.) Ti MOUNTING AND BASE PLATES

CONTOURED GAP CONFIGURATIONS
5.1 cm (2.0 in.) THICK TILE
0.127 cm (0.050 in.) GAP SETTING

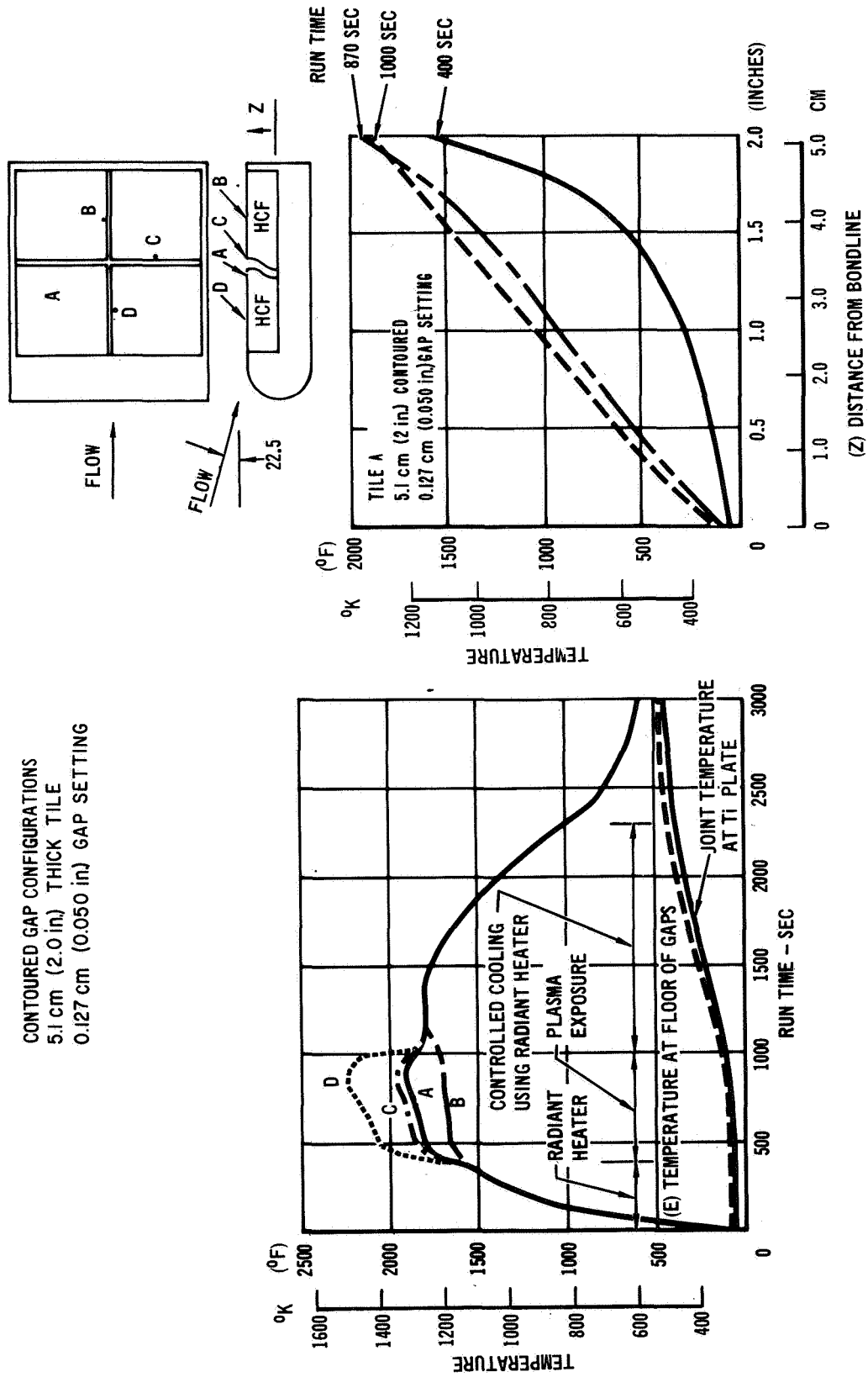


Figure 8

BONDLINE THERMAL RESPONSE AT INTERSECTION OF TILES
WITH A FORWARD FACING STEP

(Figure 9)

The heat-up rate measured by the thermocouples at the bottom of the gap where the four tiles intersect experienced almost a linear increase in heat-up as the transverse gap was opened. Tests were performed at gap widths of 0.127, 0.381, and 0.762 cm (0.05, 0.15, and 0.30 inch) in order to obtain heating trends over a range of gap widths that might be contemplated for the TPS.

It can also be noted from these data that a 0.381 cm (0.15 inch) forward step did not result in an increase in heating at the downstream intersection of the tiles at the bottom of the gap. The reason most likely for this is that the parallel gap is small (held constant at 0.127 cm (0.05 inch) and minimal lateral outflow was present.

To get a feel for the magnitude of a tolerable heat-up rate, consider a temperature increase rate of 0.14°K (0.25°F)/sec acting for 800 seconds at peak heating conditions would produce a bondline temperature increase of 112°K (200°F). This added to a 311°K (100°F) initial temperature and a bondline temperature increase of 112°K (200°F) for the remainder of the trajectory produces a final bondline temperature of 534°K (500°F). Most adhesives/sponge attachments have approximately a 534°K (500°F) reuse limit. For a TPS attached to aluminum primary structure the aluminum is limited to approximately 450°K (350°F). Hence, a 0.14°K (0.25°F)/sec heat-up rate is most likely high.

BONDLINE THERMAL RESPONSE AT INTERSECTION OF TILES

WITH A FORWARD FACING STEP

- 5.1 cm (2.0 in) HCF TILES
- BUTT JOINT
- FORWARD FACING STEP (H) IS 0.381 cm (0.15 in)
- PARALLEL GAP IS A CONSTANT 0.127 cm (0.05 in) (G)
- MSC 10 MW ARC TUNNEL
- HCR ORBITER AREA 2P PEAK HEATING ENVIRONMENT

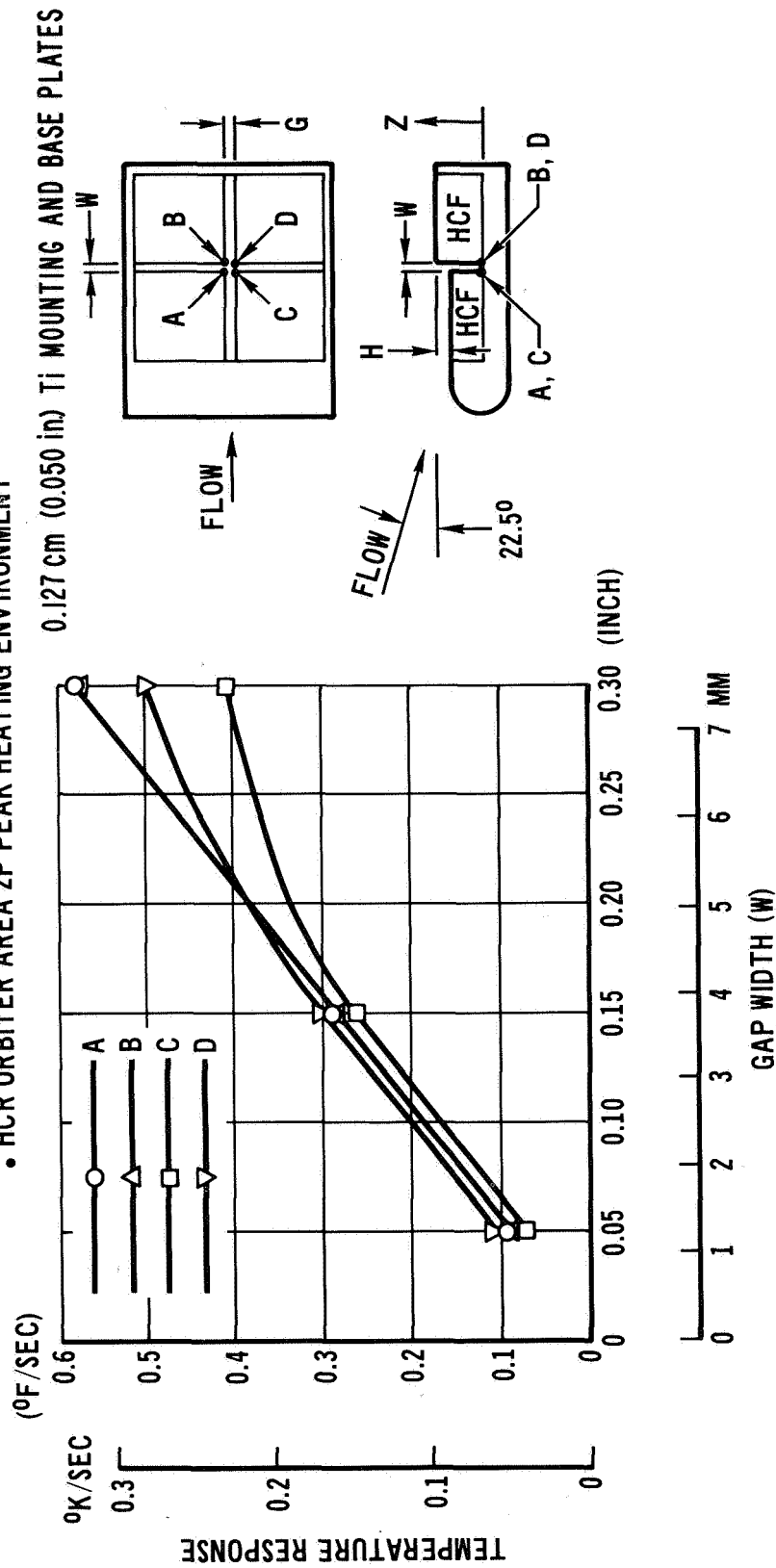


Figure 9

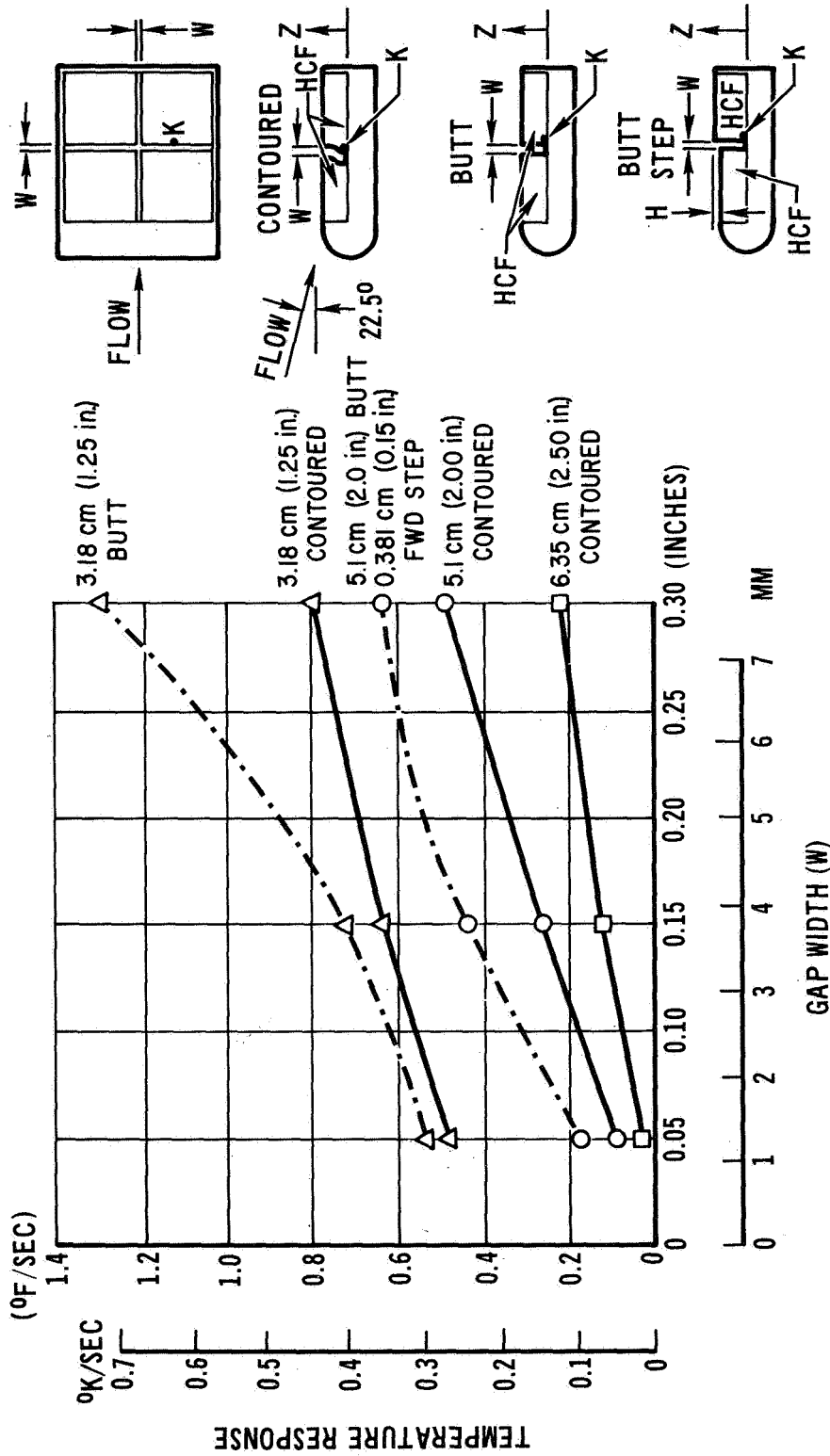
BONDLINE HEAT-UP IN TRANSVERSE GAPS (LOCATION K)

(Figure 10)

The effect of tile thickness on bondline heat-up for the transverse gap is shown in figure 10. As can be seen by examining the contoured joint data, a significant improvement in heat protection is provided by the thicker tiles. A comparison can be made between butt and contoured joints. The heat-up rate for the butt joint is more severe, especially for wider gaps.

BONDLINE HEAT-UP IN TRANSVERSE GAPS (LOCATION K)

(CONTOURED, BUTT, BUTT-STEP JOINTS)



- MSC 10 MW ARC TUNNEL
 - HCR ORBITER AREA 2P HEATING ENVIRONMENT
 - TEMPERATURE MEASURED AT BONDLINE
 - 0.127 cm (0.050 in) Ti MOUNTING AND BASE PLATES
- H = 0.381 cm (0.15 in)
PARALLEL GAP = 0.127 cm (0.05 in)

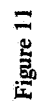
Figure 10

TEMPERATURE RESPONSE IN PARALLEL GAP OF 3.18 CM (1.25 INCH)
BUTT AND CONTOURED JOINTS

(Figure 11)

The same trend holds for the parallel gap--for large gaps the contoured gap provides improved heat protection over a butt joint. Another conclusion that can be drawn from these data is that small gaps are necessary to limit convective heating in the gaps.

TEMPERATURE RESPONSE

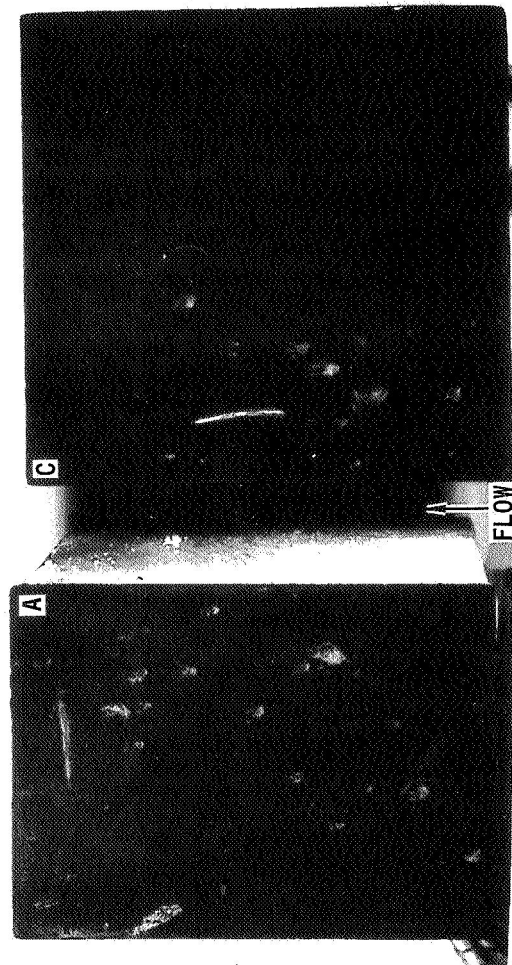
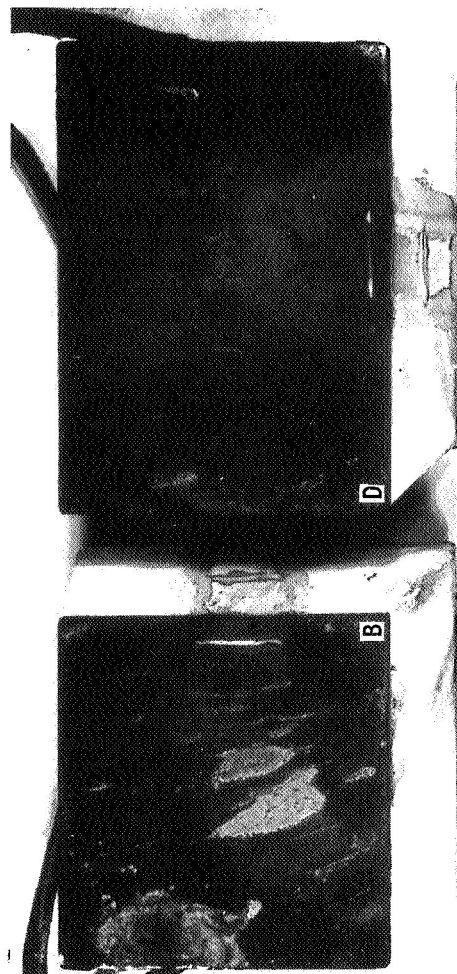


PLASMA WEDGE SPECIMENS - CONTOURED JOINT

(Figure 12)

Photographs of the joint models are very valuable in understanding the flow in the gaps. Residue from the Arc tunnel flow field deposited on the tiles and provides a visual picture of the flow in the gap and across the surface of the wedge. It appears that flow in the transverse gap emanates from the intersection of the tiles and that there was a slight diverging of the flow over the wedge.

PLASMA WEDGE SPECIMENS - CONTOURED JOINT (HCF JOINT TESTING)



5.08 cm (2.00 in.) TILE THICKNESS

SCHEMATIC OF FLOW WITHIN CONTOURED JOINT

(Figure 13)

The flow field within the RSI joint, especially at the intersection of tiles, is complex. As depicted in figure 13, boundary layer flow tends to penetrate the parallel gap, setting up recirculation patterns. At the tile intersection, flow in the transverse gap is initiated, adding to the recirculation in the transverse gap. The gas outflow in the transverse gap is also caused by the diverging flow over the wedge. The test configuration is also representative of the staggered tile pattern in that the ends of the gaps are blocked.

SCHEMATIC OF FLOW WITHIN CONTOURED JOINT

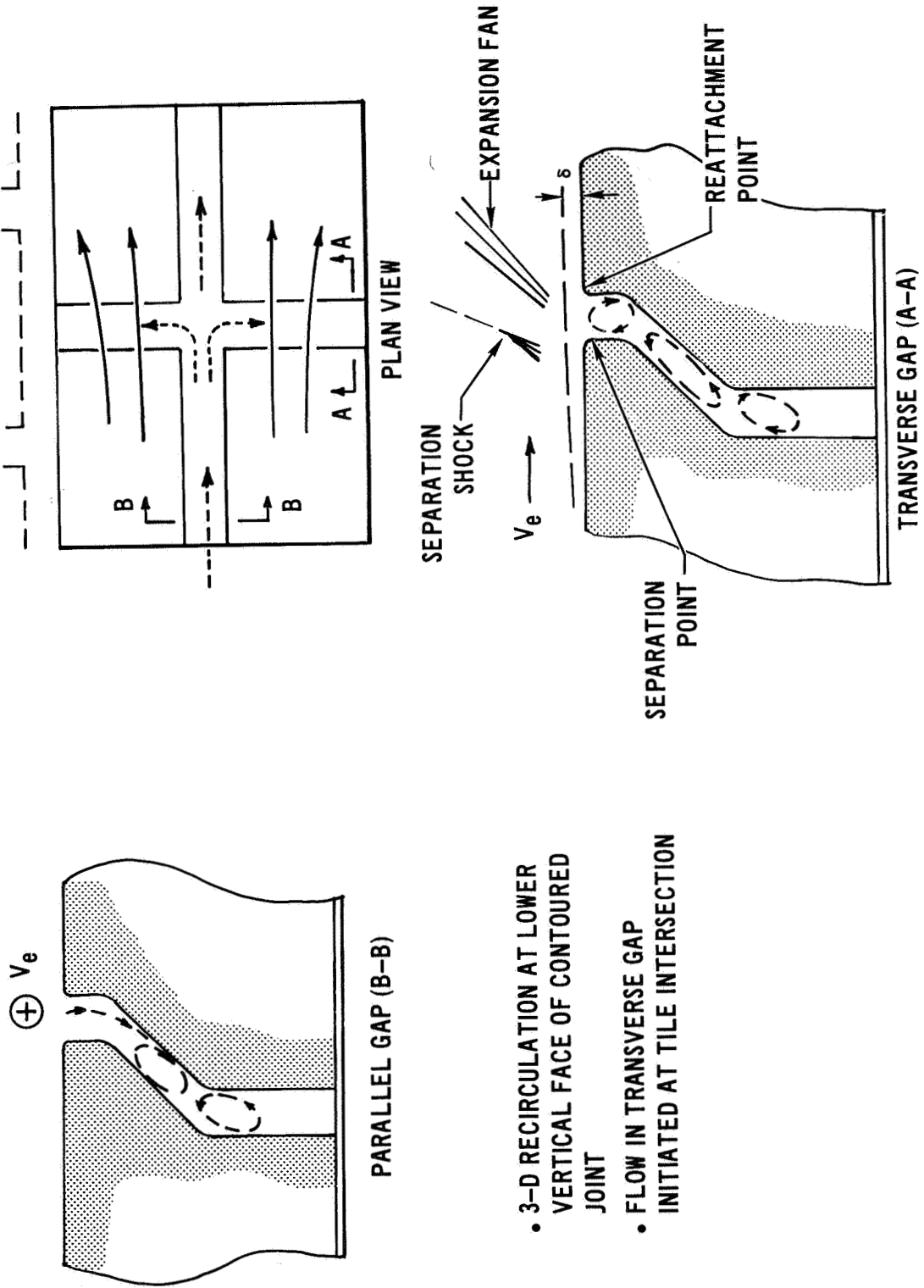


Figure 13

- 3-D RECIRCULATION AT LOWER VERTICAL FACE OF CONTOURED JOINT
- FLOW IN TRANSVERSE GAP INITIATED AT TILE INTERSECTION

ANALYSIS OF GAP HEATING TESTS

(Figure 14)

Convective heating rates down the sides of the tiles were derived by constructing thermal models of the joint and feeding the measured temperature responses into the MDAC-E General Heat Transfer computer program. The inorganic coating on the HCF, the HCF, adhesive and carrier plate for opposing tiles were divided into thermal nodes. Heat storage and conduction links were defined for each node. In addition to radiative exchange with space, an automated view factor calculation was used to describe radiative exchange between tiles. Temperature responses of each thermocouple were recorded on magnetic tape during the tests at MSC and then fed directly into our computer for the heating calculation. Heating distributions have been calculated for the contoured, butt, and butt step joints and will be discussed in the next several figures. The effect of these heating distributions in upstream parallel gaps, downstream parallel gaps, and transverse gaps is assessed next, followed by a comparison with several analytical prediction methods.

ANALYSIS OF GAP HEATING TESTS

- THERMAL MODEL OF JOINT (2-D)
 - 84 NODE FINITE ELEMENT
 - THERMAL CONDUCTION AND HEAT STORAGE
 - RADIATION EXCHANGE BETWEEN FACES OF JOINT AND TO SPACE
 - AUTOMATICALLY PROCESSED MEASURED TEMPERATURES FROM MAGNETIC TAPE INTO TRANSIENT COMPUTER PROGRAM
 - INVERSE SOLUTION TO OBTAIN HEATING RATES ON FACES OF TILES
- DATA ANALYZED
 - 5.1 cm (2.0 in.) CONTOURED JOINT
 - THREE GAP SETTINGS
 - GAP PARALLEL TO FLOW – UPSTREAM
 - GAP PARALLEL TO FLOW – DOWNSTREAM
 - TRANSVERSE GAP
 - 3.18 cm (1.25 in.) BUTT AND 5.1 cm (2.0 in.) BUTT WITH FWD STEP
- COMPARISON OF DERIVED HEATING DISTRIBUTION WITH SEVERAL THEORIES

Figure 14

CONVECTIVE HEATING IN UPSTREAM GAP

(Figure 15)

The heating distribution in the upstream parallel gap is presented in figure 15.

At location E, the heating distribution for gap settings of 0.127, 0.381, and 0.762 cm (0.05, 0.15, and 0.30 inch) gaps are shown. There is a considerable difference in heating in the first half inch down into the gap for the various gaps tested. The heating deep into the gap is very low and indicates a recirculating flow field.

CONVECTIVE HEATING IN UPSTREAM GAP

(LOCATION E)

- 5 CM (2.0 IN.) CONTOURED HCF JOINT
- 10 MW ARC TUNNEL, HCR ORBITER PEAK HEATING CONDITIONS
- GAP ANALYZED: PARALLEL TO FLOW AT LOCATION E

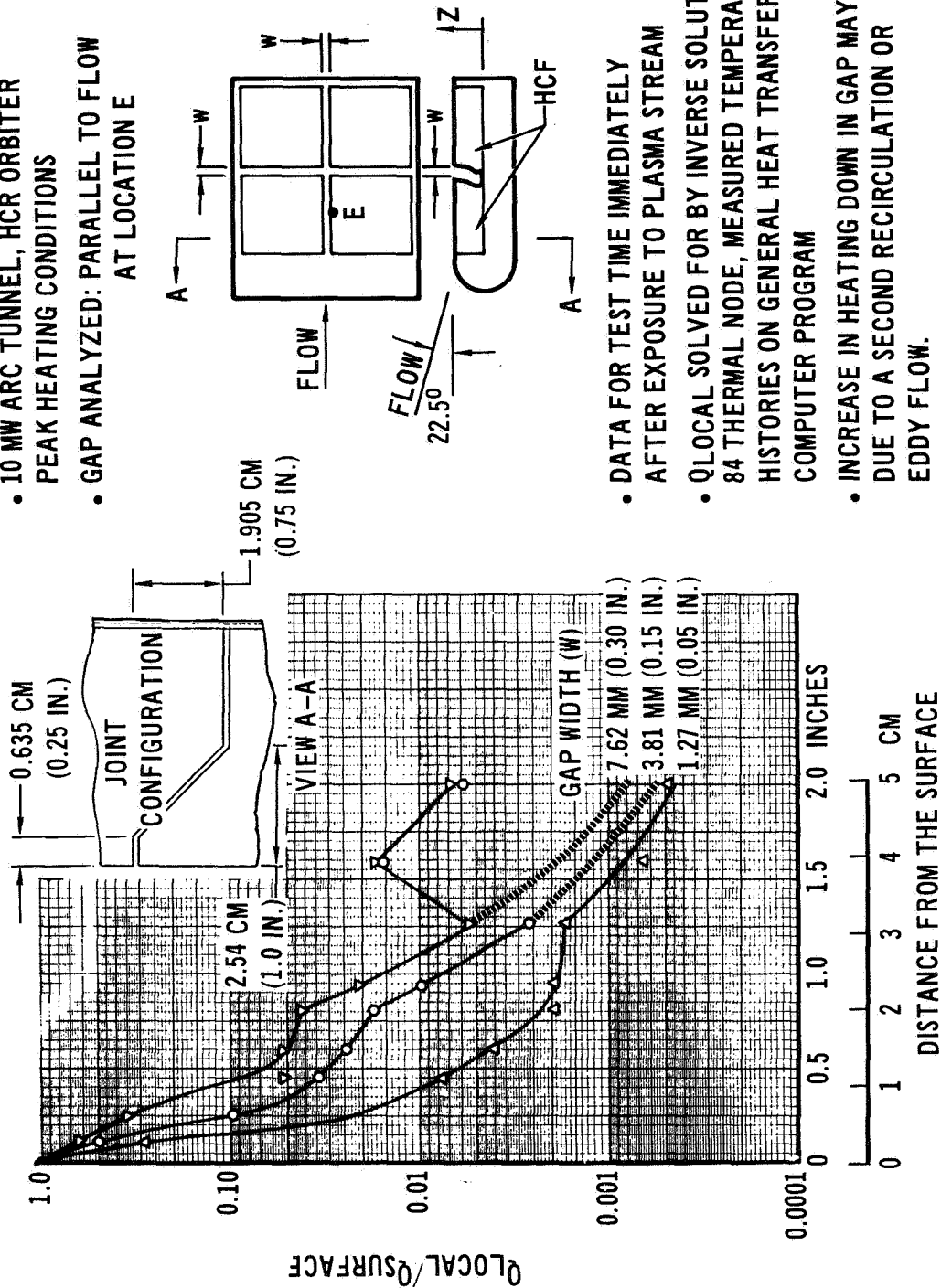


Figure 15

CONVECTIVE HEATING IN DOWNSTREAM GAP

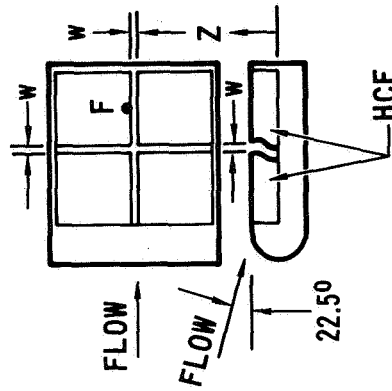
(Figure 16)

The heating distributions in the downstream parallel gap are similar to the upstream gap but drop off more sharply. This may be due to the slowing of the flow because of the close-out of the cavity downstream and the diverting of flow into the transverse gap. These heating distributions also show the effects of recirculation.

CONVECTIVE HEATING IN DOWNSTREAM GAP

(LOCATION F)

- 5.1 cm (2.0 in.) CONTOURED HCF JOINT
- 10 MW ARC TUNNEL, HCR ORBITER
- PEAK HEATING CONDITIONS
- GAP ANALYZED: PARALLEL TO FLOW AT LOCATION F



- Q_{LOCAL} SOLVED FOR BY INVERSE SOLUTION, 84 THERMAL NODE, MEASURED TEMPERATURE HISTORIES ON GENERAL HEAT TRANSFER COMPUTER PROGRAM.

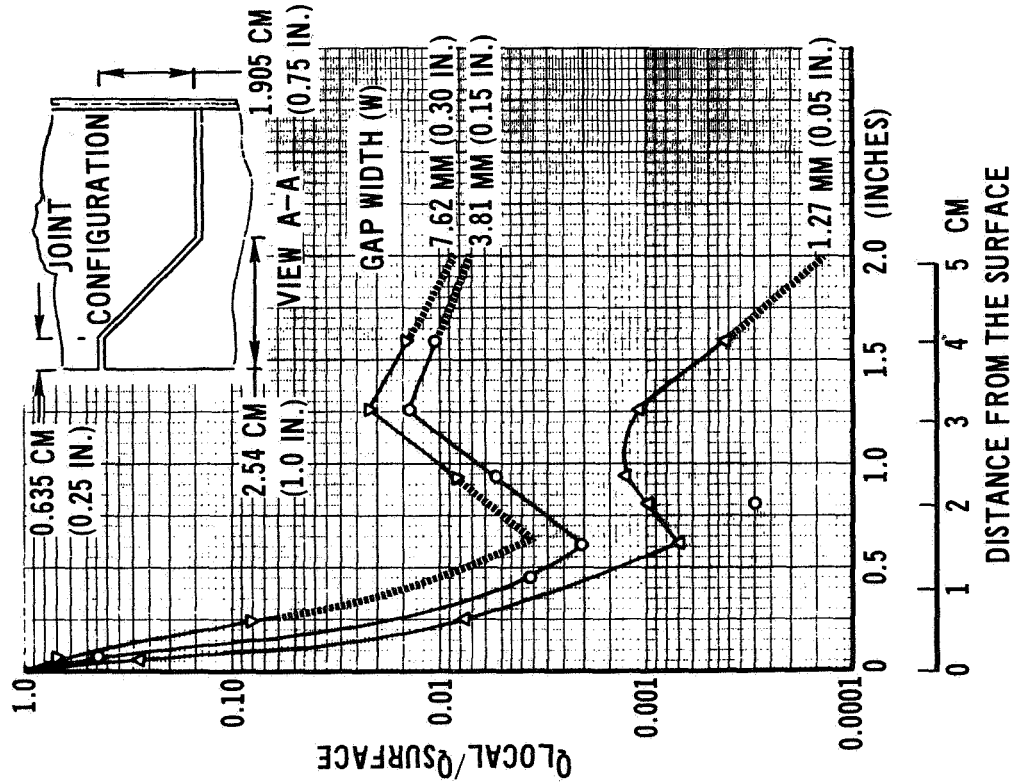


Figure 16

CONVECTIVE HEATING IN TRANSVERSE GAP

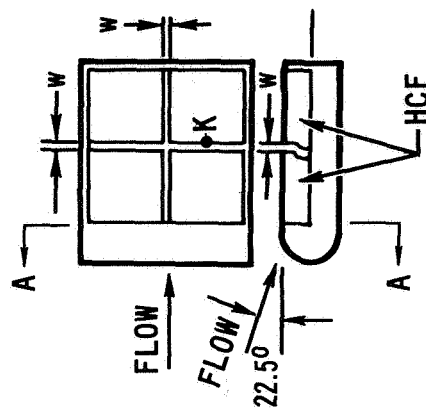
(Figure 17)

In the transverse gap, recirculation is also evident and the heating is only lower for the thin gaps 0.127 and 0.381 cm (0.05 and 0.15 inch) as compared with the parallel gap.

CONVECTIVE HEATING IN TRANSVERSE GAP

(LOCATION K)

- 5 CM (2.0 IN.) CONTOURED HCF JOINT
- 10 MW ARC TUNNEL, HCR ORBITER
- PEAK HEATING CONDITIONS
- GAP ANALYZED: TRANSVERSE TO FLOW AT LOCATION K



- DATA FOR TEST TIME IMMEDIATELY AFTER EXPOSURE TO PLASMA STREAM
- Q_{LOCAL} SOLVED FOR BY INVERSE SOLUTION, 84 THERMAL NODE, MEASURED TEMPERATURE HISTORIES ON GENERAL HEAT TRANSFER COMPUTER PROGRAM.

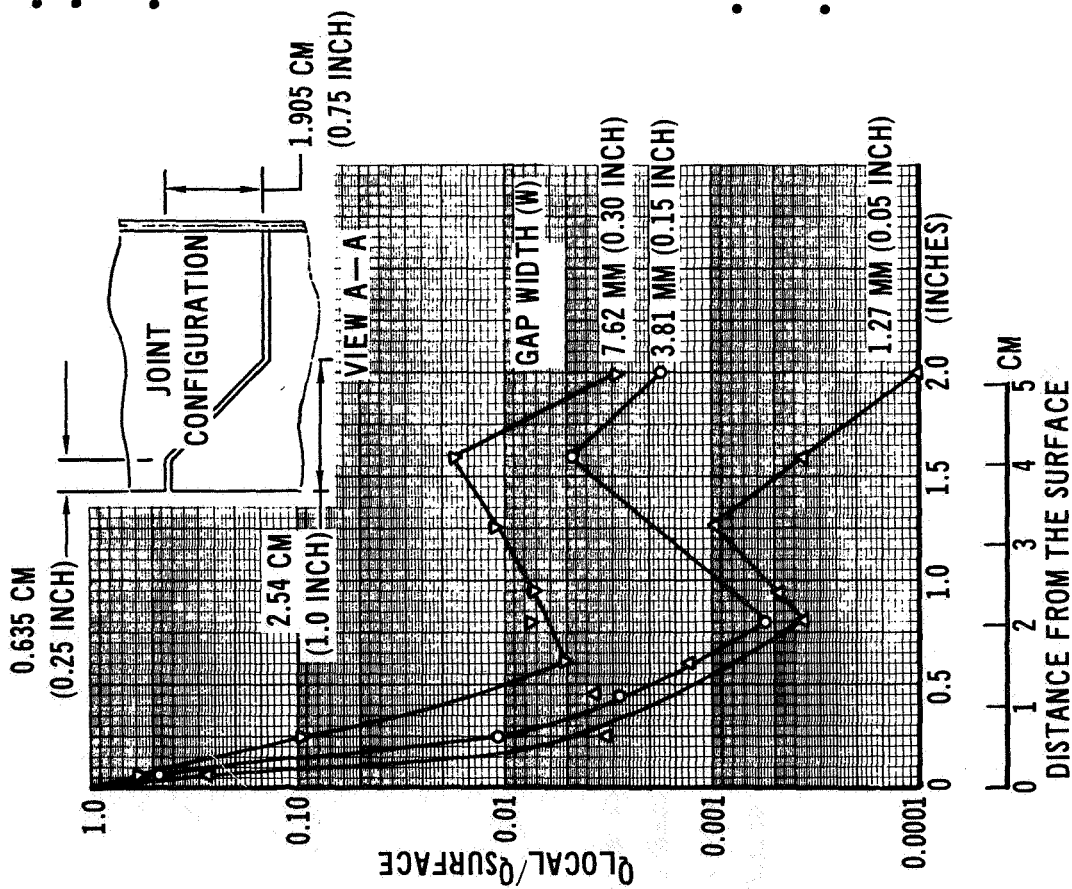


Figure 17

CONVECTIVE HEATING DISTRIBUTIONS IN TRANSVERSE
GAPS OF 3.18 CM (1.25 INCH) BUTT JOINT MODEL

(Figure 18)

The heating distributions for the butt and butt with a forward facing step are shown in figures 18 and 19. These heating distributions do not indicate as strong a recirculation effect as for the contoured joint. The heating distribution for the upstream and downstream faces of the transverse gap are quite similar. It should be noted that these data are for 3.18 cm (1.25 inch) thick tiles.

CONVECTIVE HEATING DISTRIBUTIONS IN TRANSVERSE GAP OF 3.18cm (1.25 in.) BUTT JOINT MODEL

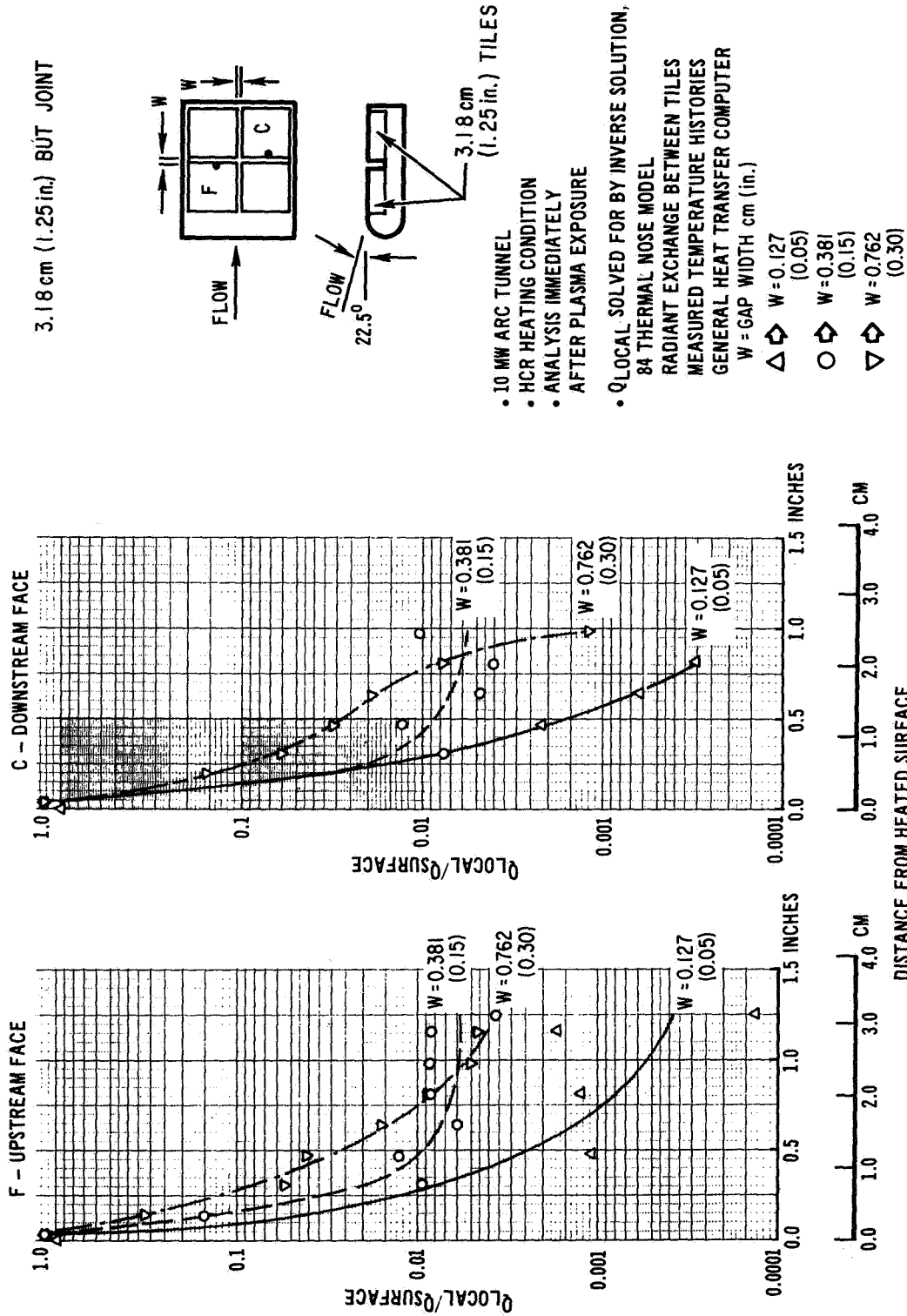


Figure 18

CONVECTIVE HEATING DISTRIBUTIONS IN TRANSVERSE GAP OF BUTT-STEP MODEL

(Figure 19)

The effect of a forward facing step on the heating distribution in the transverse gap are shown in figure 19. The model tested was a 5.1 cm (2.00 inch) tile with a 0.381 cm (0.15 inch) forward facing step. The parallel gap was held at a constant 0.127 cm (0.05 inch) on this model. The heating on the downstream face was slightly higher than on the upstream (or shadowed) face of the joint. The heat distributions deep within the gap show a slight upturn and this may or may not be a real effect. The drop-off in heating rate in the gap has somewhat of a similar shape as hypothesized for a 2-D recirculation pattern.

Sensitivity studies were performed on the heating calculations to determine the effect of thermocouple location and changes in HCF thermal conductivity. A random 0.076 cm (± 0.03 inch) relocation of thermocouples and a $\pm 5\%$ change in HCF conductivity caused less than a 10% shift in heating near the surface and less than 50% shift deep within the joint. This magnitude of accuracy on heating rates is well within normal experienced tolerances.

CONVECTIVE HEATING DISTRIBUTIONS IN TRANSVERSE GAP OF BUTT-STEP MODEL

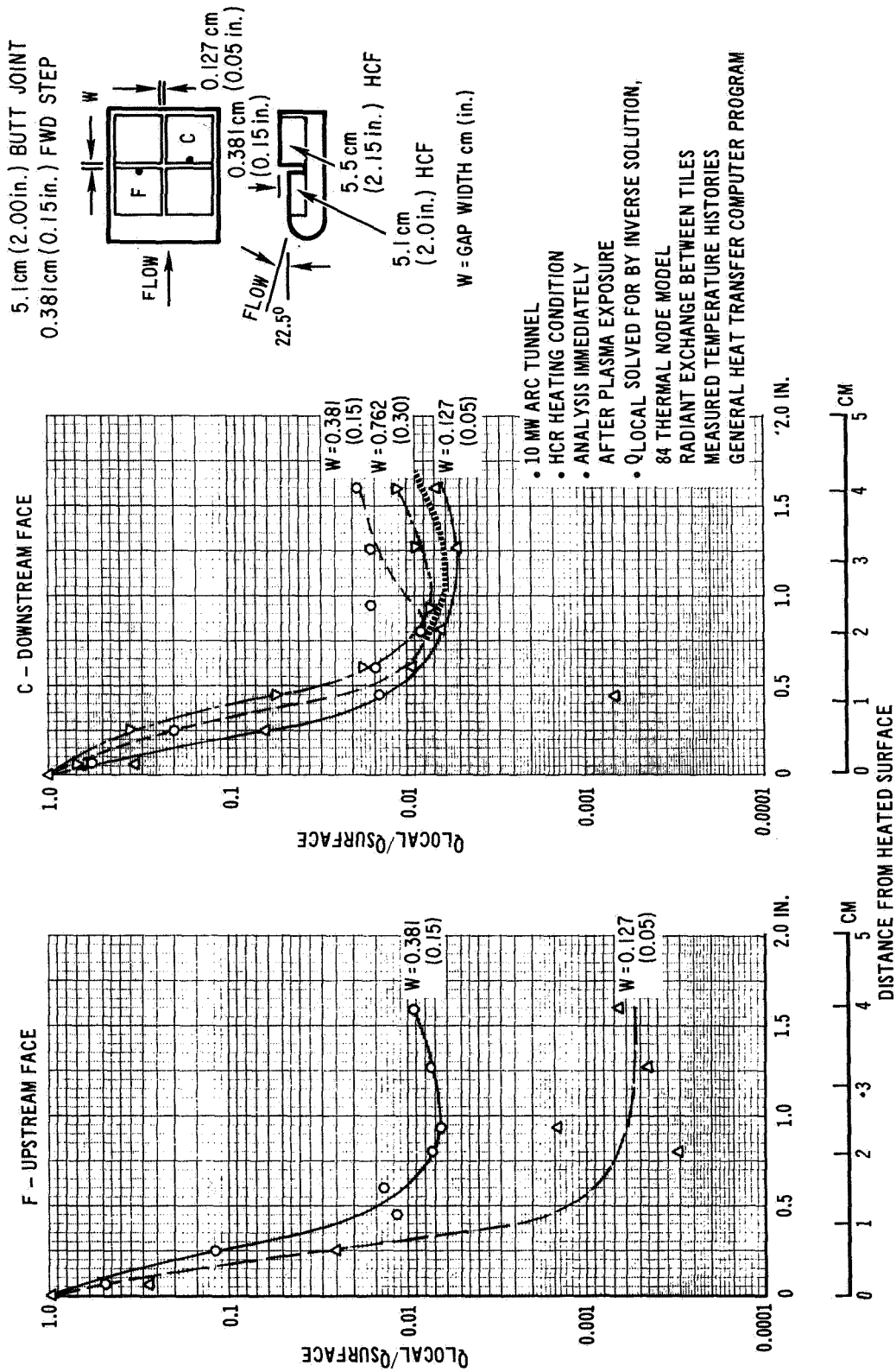


Figure 19

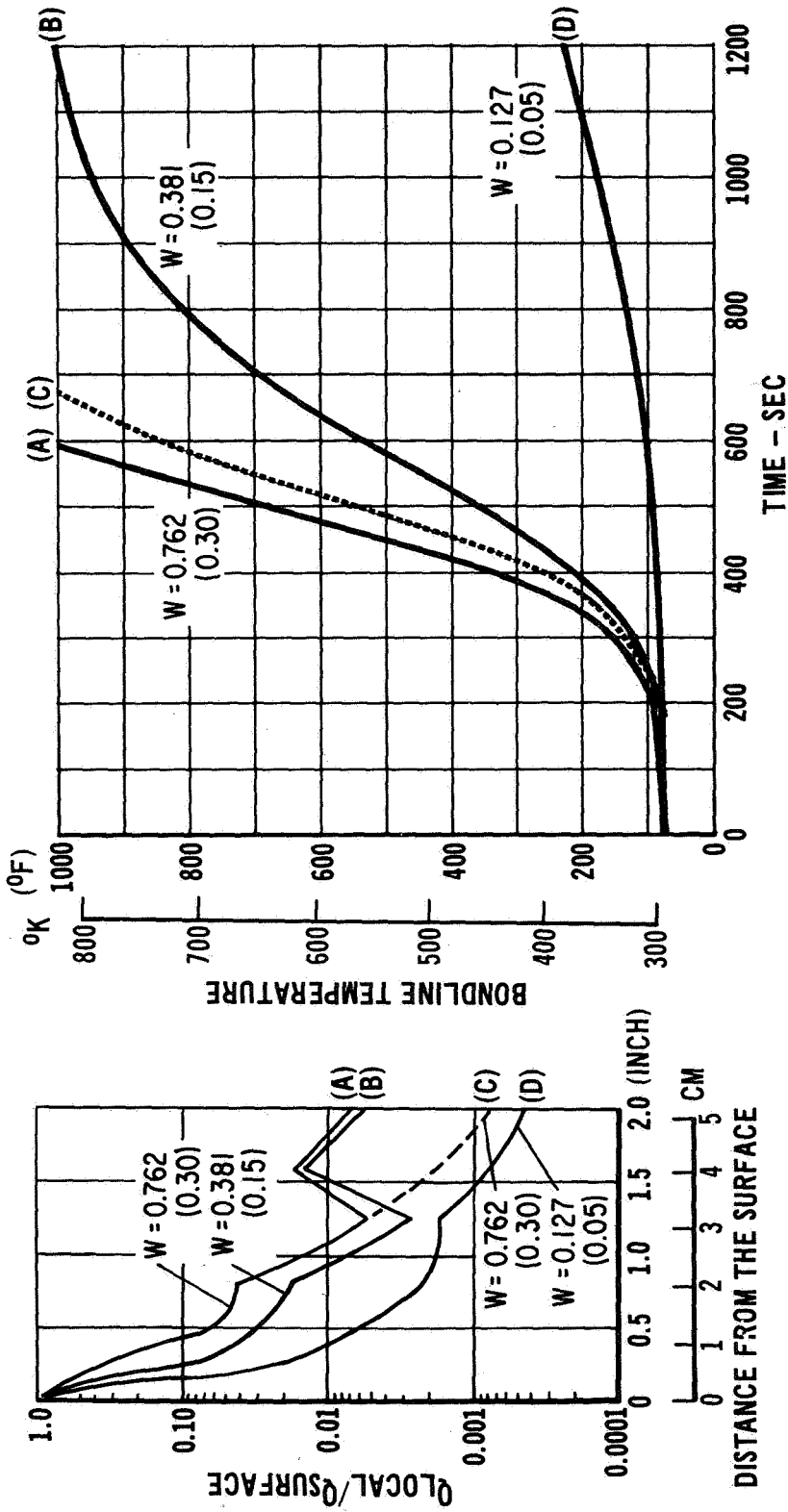
SENSITIVITY OF TPS HEAT-UP TO GAP HEATING DISTRIBUTIONS
DERIVED FROM ARC TUNNEL TESTS

(Figure 20)

The data in figure 20 were computed to obtain a feel for the effects of the derived heating distributions on bondline temperature response for an orbiter entry. The high cross range 2P-1530°K (2300°F) maximum surface heat pulse was applied to the thermal model of a 5.1 cm (2.0 inch) HCF-TPS with a contoured joint with the heating distributions we have derived. As can be seen for the 0.127 cm (0.05 inch) gap heating distribution, the bondline at the base of the joint did not experience an excessive temperature rise. The 0.381 cm (0.15 inch) gap resulted in a very hot condition and the 0.762 cm (0.3 inch) gap was catastrophic. The differences in the heating magnitudes within the first 1.27 cm (0.5 inch) down the gap attributes to the difference in bondline response. The effect of the recirculation deep within the joint is minimal as can be seen by comparing temperatures for curves (A) and (C).

It should be noted that the temperature response shown in figure 20 is a result of radiation transport from the faces of the tiles to the bottom of the gap as well as convective heating.

SENSITIVITY OF TPS HEAT-UP TO GAP HEATING DISTRIBUTIONS DERIVED FROM ARC TUNNEL TESTS



W = GAP WIDTH cm (in.)

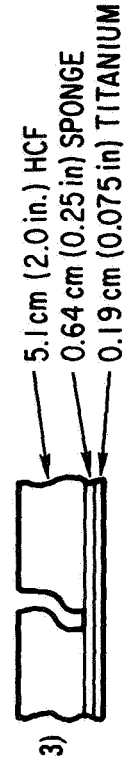


Figure 20

- 1) HEATING DISTRIBUION OBTAINED FROM 5.1cm (2.0 in.) CONTOURED HCF TILE TESTS
- 2) AREA 2P - 1530°K (2300°F) HEAT PULSE

COMPARISON OF DERIVED HEATING DISTRIBUTIONS WITH SEVERAL THEORIES

(Figure 21)

Four analytical methods for predicting heating within the gap (primarily the transverse gap) were applied to the Arc tunnel test conditions.

The method by Hanmer¹ as we applied it considers gap width to depth ratio and the effects of boundary displacement thickness. The computed heating rate in the gap is also only applied one gap width down into the gap. The Hanmer predictions tend to be greater than a heating ratio of unity.

The method by Hodgson² is for a laminar boundary layer and involves reattachment lengths as well as velocity distributions and a derived Stanton Number-Reynolds Number heating distribution. The calculations using the method of Hodgson produced a heating distribution in the gap but the heating did not drop off as rapidly as was measured.

The method by Brewer et al.³ considers the energy flux across the gap opening as compared with energy flux for attached flow and the gap width to height ratio to obtain heating at the bottom of the gap.

Burggraf's⁴ method was also examined but it is only applicable for high Reynolds Number, according to Burggraf.

From these comparisons, it is evident that a refined prediction procedure is needed.

COMPARISON OF DERIVED HEATING DISTRIBUTIONS WITH SEVERAL THEORIES

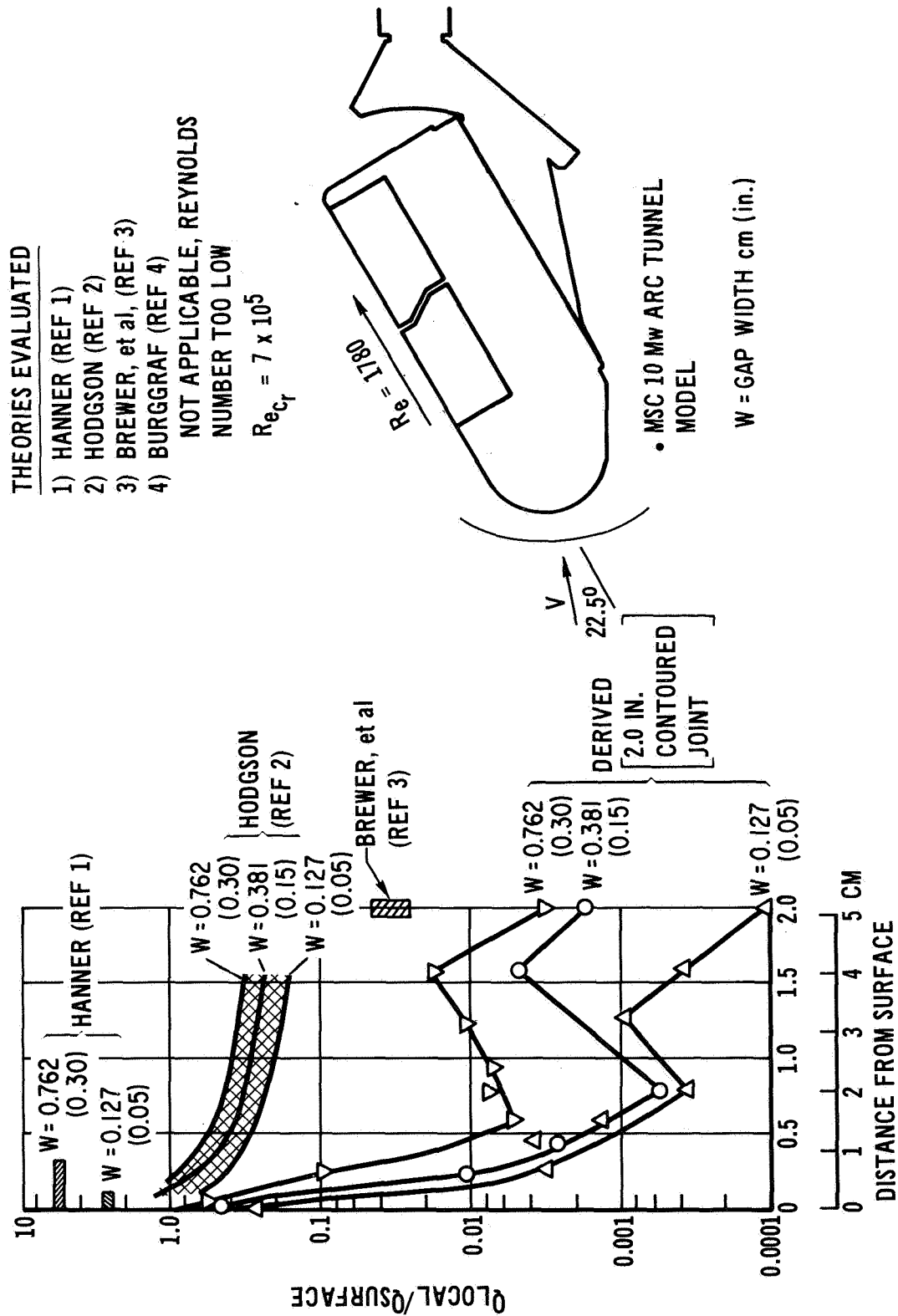


Figure 21

SIDE VIEW OF MSC CHANNEL NOZZLE WITH MDAC-E RSI JOINT
CONTAINER AND ADAPTER

(Figure 22)

In the next series of Arc tunnel tests at NASA-MSC, the channel nozzle will be used because it produces a more uniform heating distribution on the panel than can be obtained with a wedge. The channel nozzle produces a Mach 4 laminar flow with an approximate 0.64 cm (1/4 inch) thick boundary layer. An adapter was fabricated for the nozzle to house the joint test container used in the wedge test setup. The adapter has quick disconnects for thermocouples and pressure transducers (for measuring pressure gradients at the bottom of the joint). Air lines are provided to cool the model to room temperatures between tunnel runs which reduces dead time.

The adapter also contains access ports for setting the gaps between tunnel runs. This also improves test efficiency.

SIDE VIEW OF MSC CHANNEL NOZZLE WITH MDAC-E RSI JOINT CONTAINER AND ADAPT R

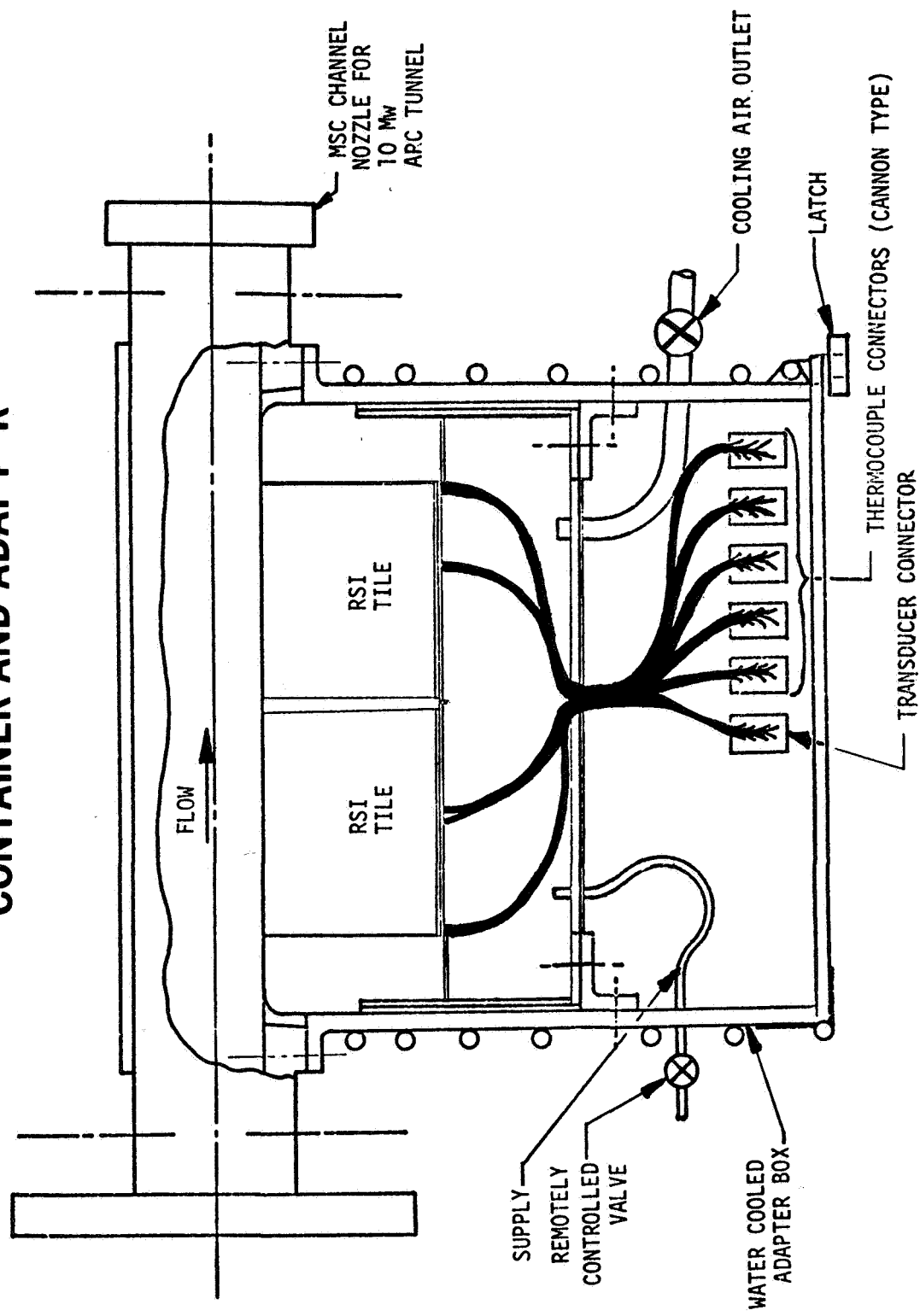


Figure 22

ADAPTER FIXTURE FOR MSC 10 MW CHANNEL NOZZLE

(Figure 23)

The adapter also contains accessports for setting the gaps between tunnel runs. This also improves test efficiency.

ADAPTER FIXTURE FOR MSC 10 MW CHANNEL NOZZLE

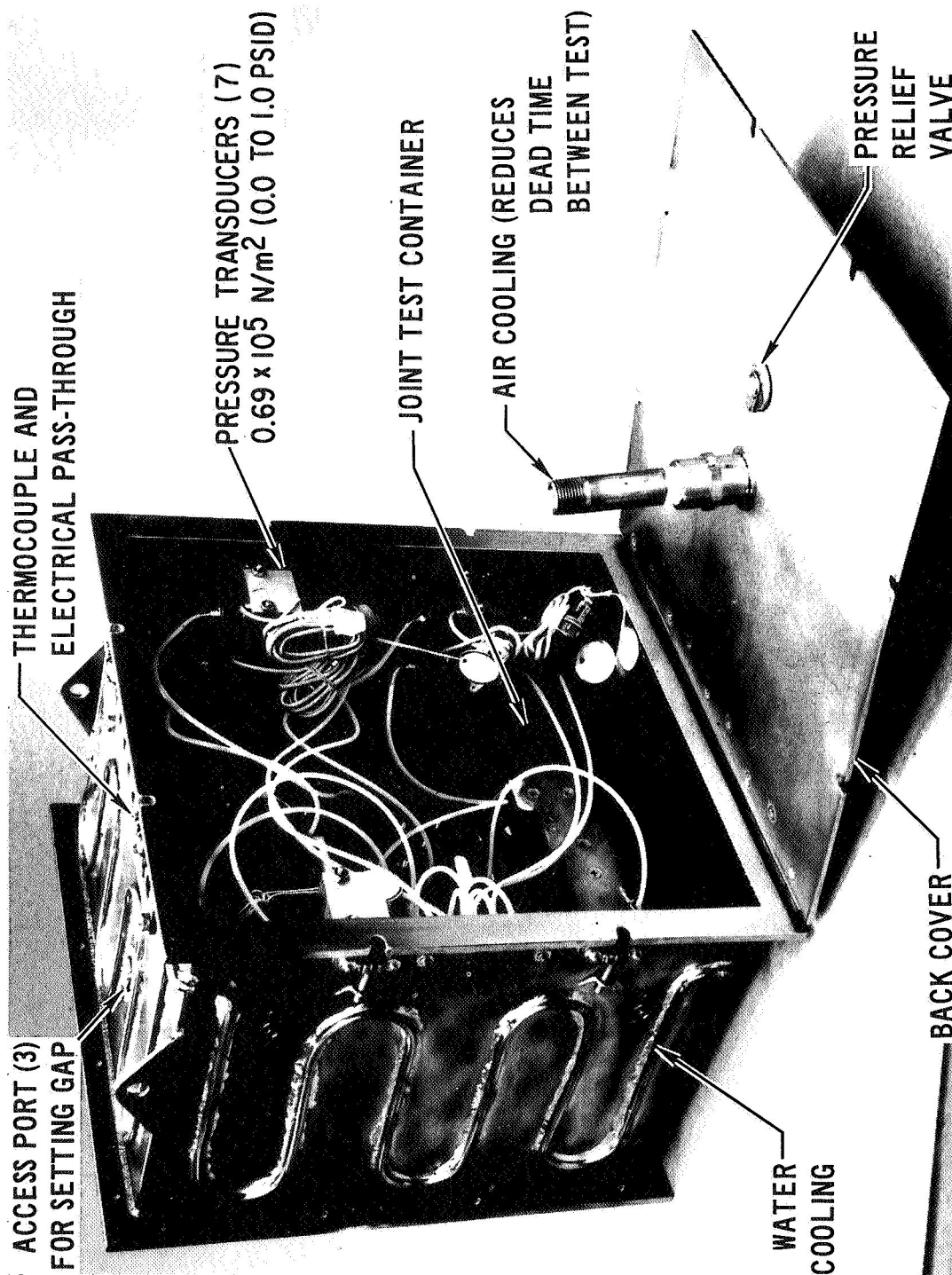


Figure 23

ADAPTER, HCF GUARDS, AND TILE SET (11) FOR MSC 10 MW ARC TUNNEL TESTS

(Figure 24)

Figure 24 is a view of the adapter as would be seen "so to speak" by the flow in the channel nozzle. There are four guards surrounding a tile set and as with the previous test configurations the tile sets are interchangeable.

ADAPTER, HCF GUARDS, AND TILE SET (11) FOR MSC 10 MW ARC TUNNEL TESTS

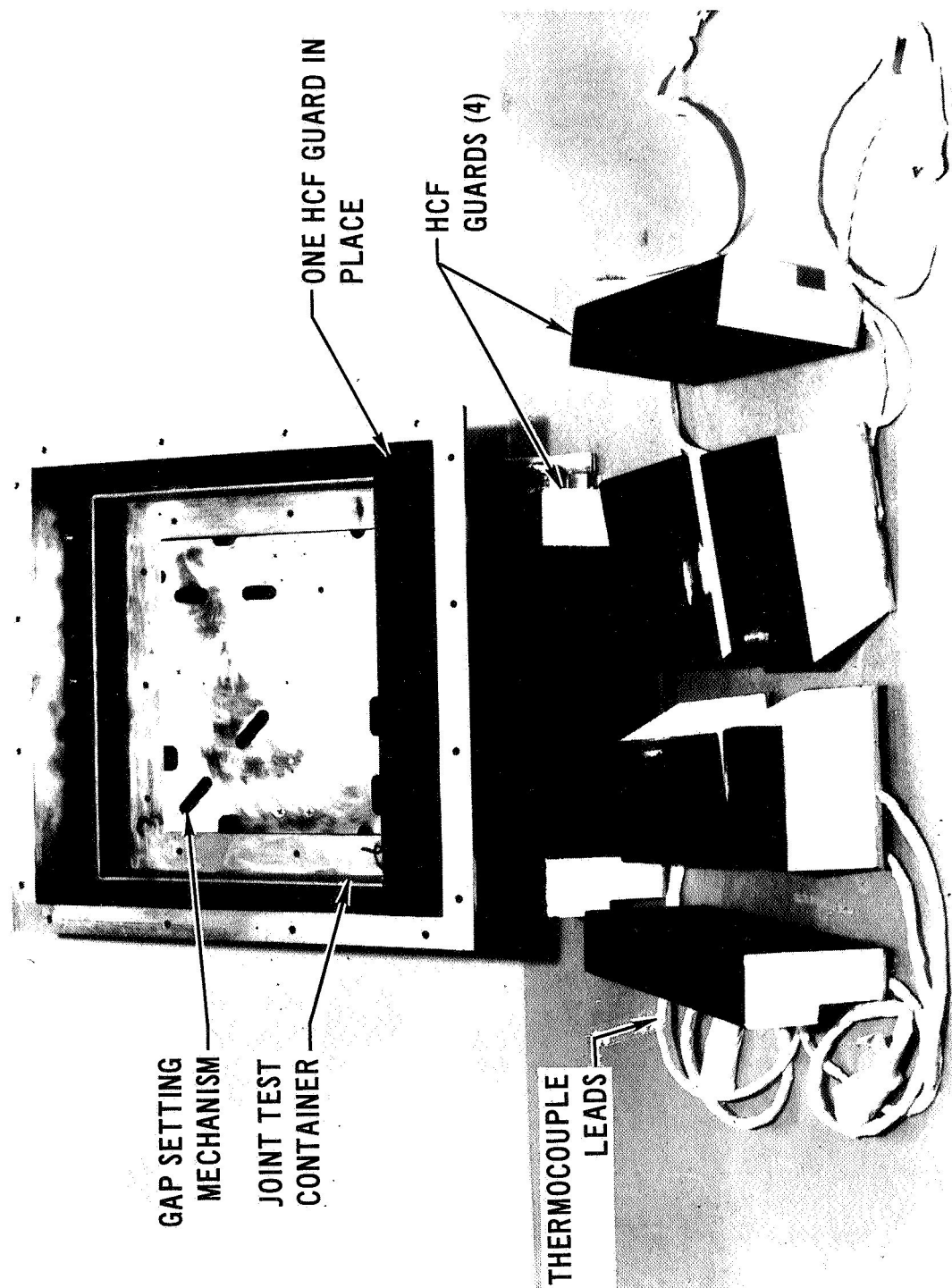


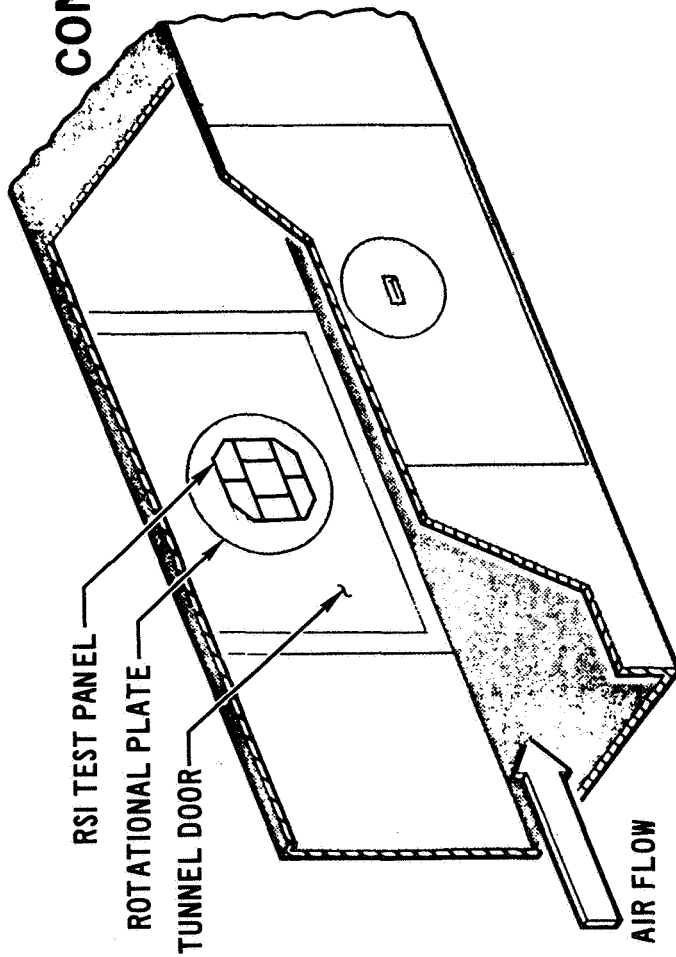
Figure 24

RSI-TPS WIND TUNNEL CONFIGURATION (CFHT AT LaRC)

(Figure 25)

To complement the Arc tunnel data, a wind tunnel test program will be conducted in Langley's CFHT Mach 10 facility. The purpose of these tests is to study the heating on the faces of a tile for a thick boundary layer as a function of gap width, tile mismatch, and flow orientation. The center tile is a heavily instrumented thin skin model being fabricated at LaRC. Tests will be performed on the side wall of the tunnel which has a boundary layer thickness of 5.1 to 10.2 cm (2 to 4 inches). The panel can also be tested in the Unitary Plan tunnel at LaRC providing an adapter to one of their tunnel doors can be made available. Testing in the Unitary tunnel would provide data at lower Mach numbers and variation in Reynolds number.

RSI-TPS WIND TUNNEL CONFIGURATION (CFHT AT LaRC)



- ADJUSTABLE GAP
- SHIMS FOR STUDYING MISMATCH
- 0 TO $\pm 45^\circ$ ORIENTATION

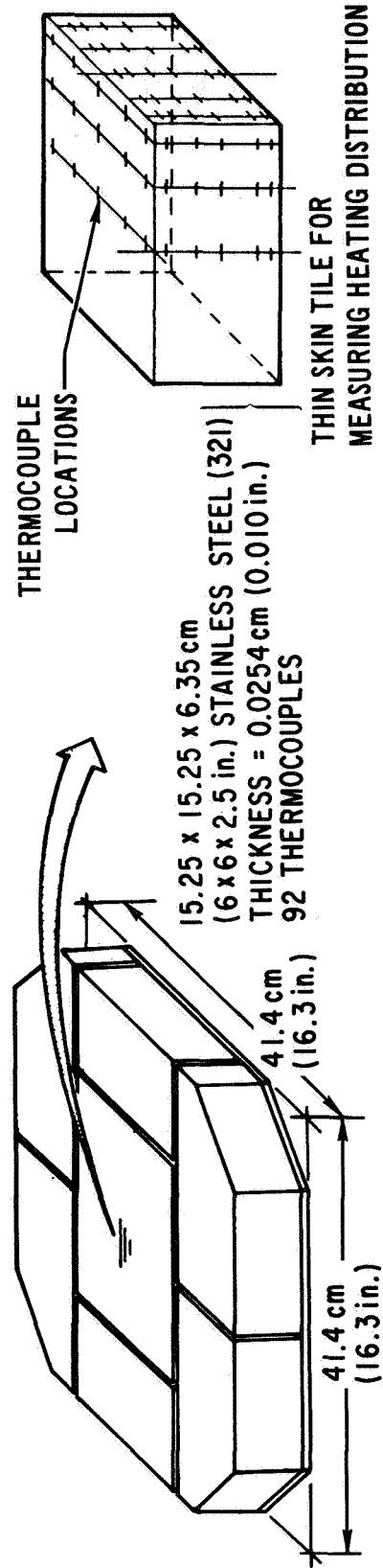


Figure 25

METALLIC COMPONENTS FOR THE WIND TUNNEL TESTS OF RSI-TPS

(Figure 26)

The metallic components (minus the thin skin tile) are shown in figure 26. Tile height adjustment is accomplished by shims and each tile is mechanically attached to the adapter. Spacers for the edge of the adapter are used to maintain uniform gap over the entire panel. Tests will be performed at four gap settings.

METALLIC COMPONENTS FOR THE WIND TUNNEL TESTS OF RSI-TPS

(MACH 10 CONTINUOUS FLOW HYPERSONIC TUNNEL)

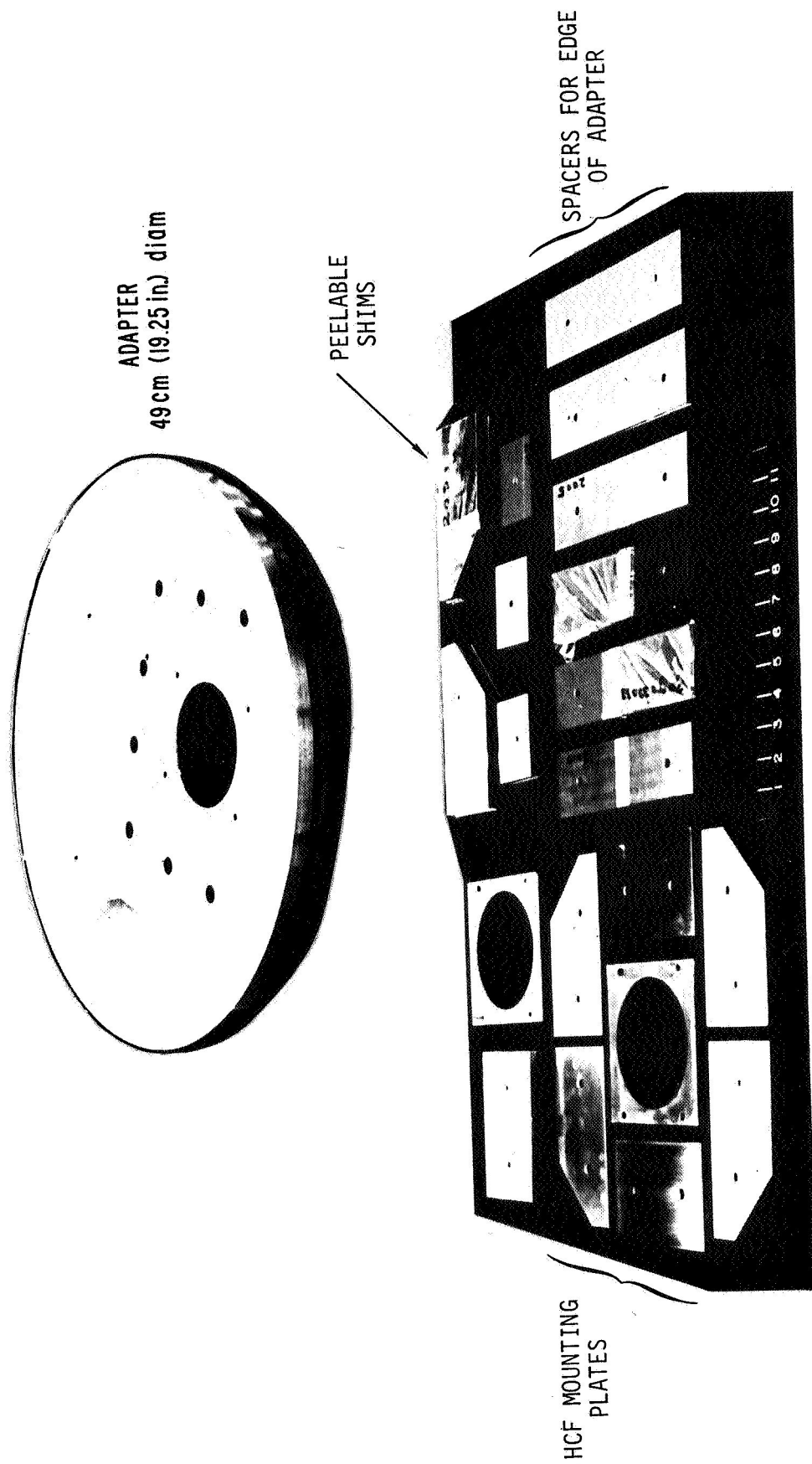


Figure 26

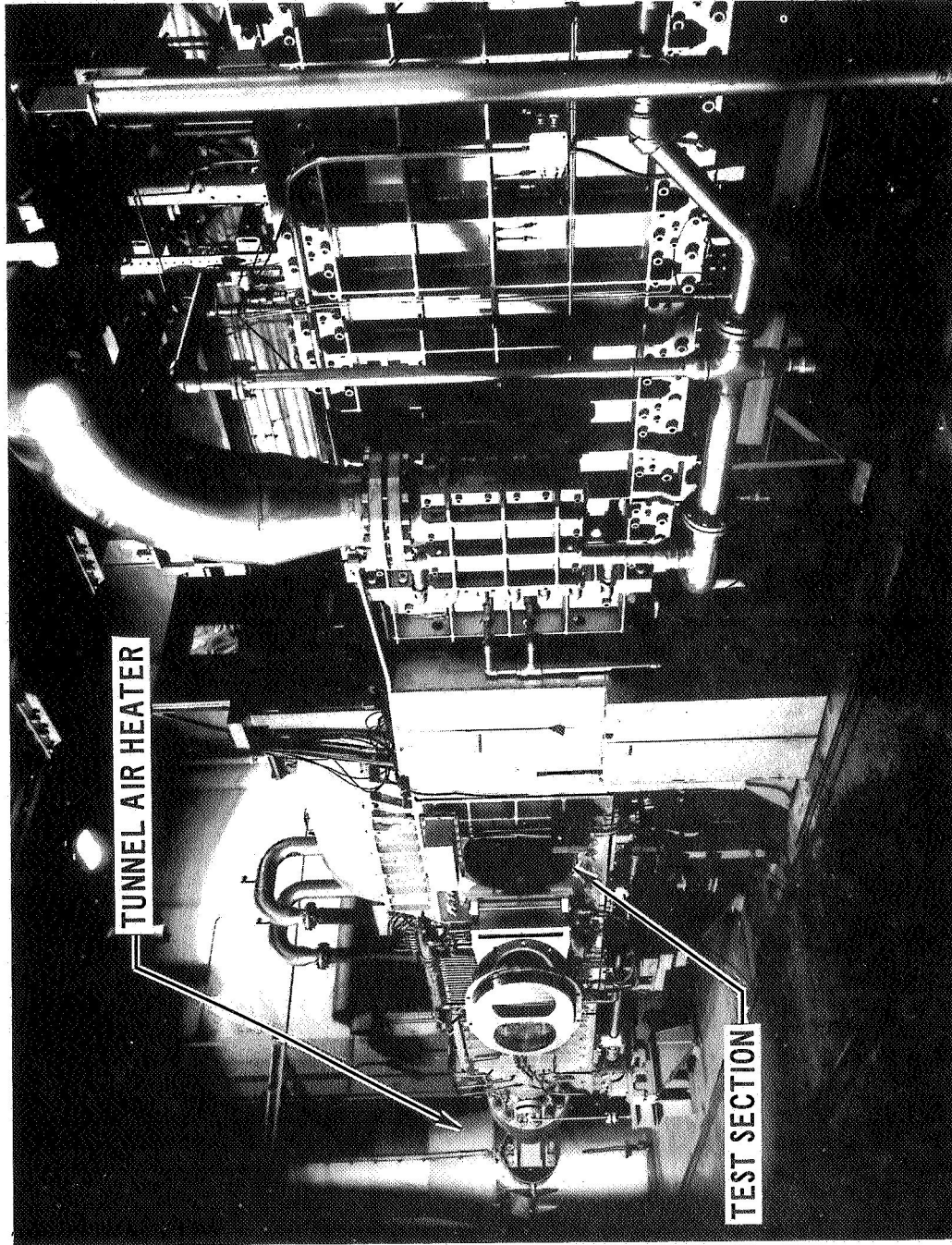
• CONTINUOUS FLOW HYPERSONIC TUNNEL (CFHT) NASA-LaRC

(Figure 27)

Testing of the panel will be performed in the CFHT and the heating measurements will be made by injecting the panel to the test position and recording thermocouple responses for the thin skin tile. This is a normal operation procedure for testing wind tunnel models.

CONTINUOUS FLOW HYPERSONIC TUNNEL (CFHT) NASA - LaRC

(MACH 10)



FLOW IS FROM LEFT TO RIGHT

Figure 27

ARC TUNNEL TESTS AT 50 MW (WRIGHT FIELD)

(Figure 28)

Tentative plans are being formulated to perform tests in the 50 MW Arc tunnel at Wright Field using a larger [45.7 x 45.7 x 6.35 cm (18 x 18 x 2.5 inch)] HCF panel to study the heating in the gaps. The panel design is similar to that of the other panels used to study gap heating. This panel will be used to perform tests corresponding to MSC's arc tunnel tests and to tests in the wind tunnel. Hopefully, this will provide a basis for correlating results for all three test programs.

ARC TUNNEL TESTS AT 50 Mw (WRIGHT FIELD)

(TENTATIVE)

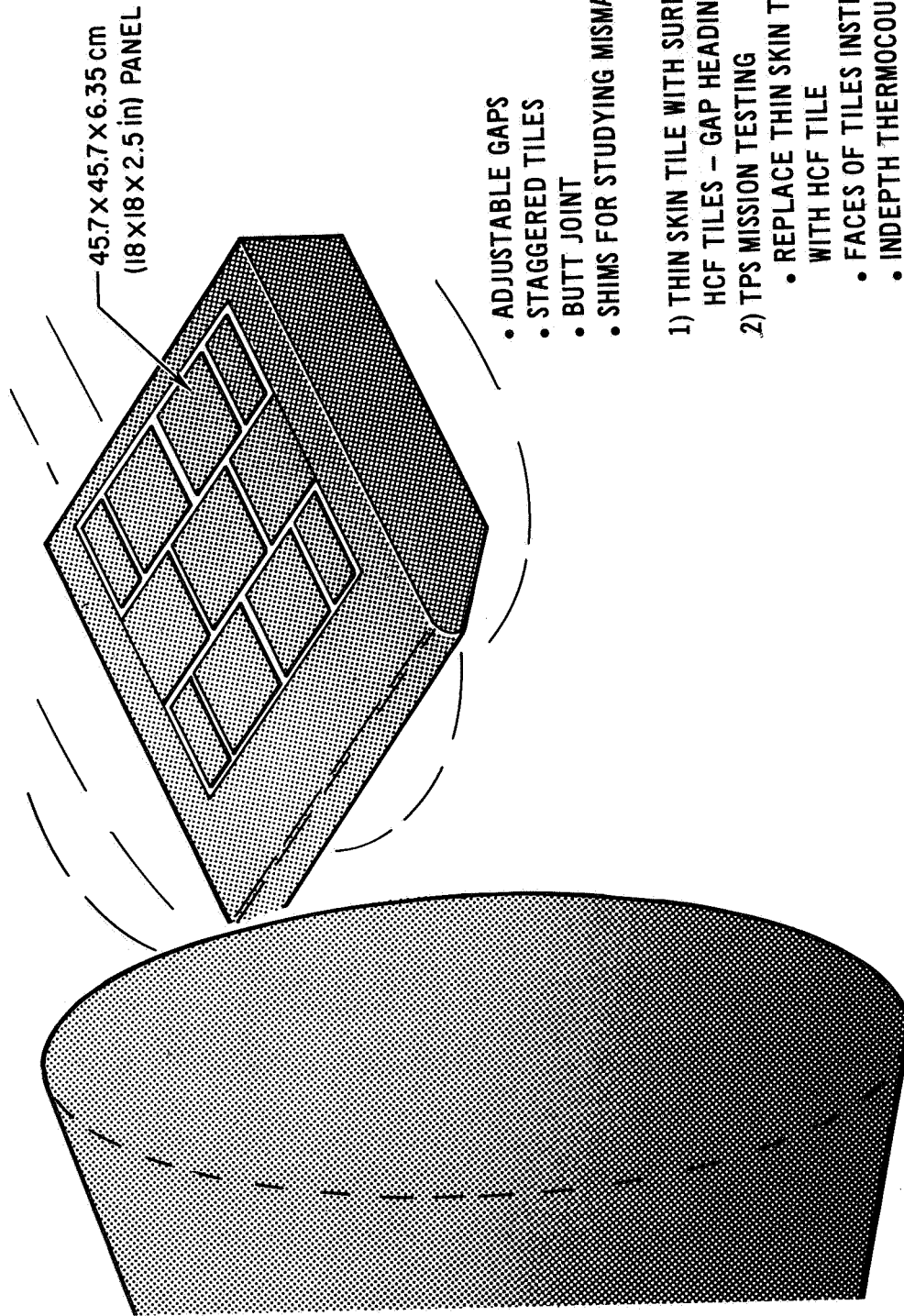


Figure 28

CONCLUSIONS

ARC TUNNEL FINDINGS

- EXCESSIVELY WIDE GAPS EXPERIENCE SIGNIFICANT CONVECTIVE HEATING AND MAY RESULT IN A BONDLINE OVERHEAT
- INCREASED HEAT PROTECTION IS AFFORDED BY CONTOURED JOINT AS COMPARED TO A BUTT JOINT
- 3-D RECIRCULATION EVIDENT AT INTERSECTION OF RSI TILES
 - OUT FLOW EMANATES FROM TILE INTERSECTION
- HEATING DISTRIBUTIONS IN GAPS WERE OBTAINED
 - CONTOURED JOINT
 - BUTT JOINT
 - BUTT/STEP MODEL
- ANALYTICAL MODEL FOR HEATING IN GAPS NEEDS TO BE DEVELOPED

ADDITIONAL TESTING

- ARC TUNNEL – USING CHANNEL NOZZLE, NASA MSC
- THICK BOUNDARY LAYER EFFECTS – LANGLEY'S CFHT
- WEDGE 45.7 X 45.7 cm (18 X 18 in) TEST – WRIGHT FIELD'S 50 MW (TENTATIVE)

REFERENCES

1. Hanner, O.M., Jr., "Aerodynamic, Gap Heating for Booster Entry, " SSD-71-247, March 1971.
2. Hodgson, J.W., "Heat Transfer in Separated Laminar Hypersonic Flow," AIAA J. Vol. 8, No. 12, December 1970.
3. Brewer, R.A.; Saydah, A.R.; Nestler, D.E.; and Florence, D.E., "Thermal Performance Evaluation of REI Panel Steps and Gaps for Space Shuttle Thermal Protection System," AIAA Paper No. 72-388, April 10, 1972.
4. Odus, R. Burggraf, "A Model of Steady Separated Flow in Rectangular Cavities at High Reynolds Number," Proceedings of the 1965 Heat Transfer and Fluid Mechanics Institute, Andrew F. Charwatt ed Stanford University Press, 1965, pp. 190-229.

**ENTRY ENVIRONMENTAL SIMULATION TESTING OF
REI-MULLITE TPS**

BY

D. E. FLORENCE, R. A. BREWER, T. E. HESS

**GENERAL ELECTRIC COMPANY
RE-ENTRY AND ENVIRONMENTAL SYSTEMS DIVISION
PHILADELPHIA, PENNSYLVANIA**

INTRODUCTION

(Figure 1)

During the development of REI-Mullite for use in a multimission thermal protection system (TPS) with a 1644° K (2500° F) temperature capability, the General Electric Company's Re-entry and Environmental Systems Division (GE-RES-D) has developed and used several specialized tests. These tests were used to obtain material response characteristics and to confirm the applicability of thermophysical properties obtained in laboratory experiments for design purposes. Specifically these studies have included: (1) determination of the melting temperature, noncatalytic nature and variation of total hemispherical emittance with temperature for the SR-2 family of coating materials; (2) evaluation of the adequacy of an analytical modeling approach for predicting thermal responses that uses laboratory measured values of thermal conductivity; and (3) derivation of an analytical modeling approach for routine shuttle orbiter TPS analyses that includes in-depth radiation transport on the insulative composites. The results of these studies are summarized in this paper.

High temperature surface emittance was obtained for coated Mod 1A REI-Mullite by exposing models in the GE-RES-D and NASA-Ames plasma arcs until the surface temperatures stabilized, and measuring the incident heat fluxes and the resultant surface temperatures. The heat flux level to the model was increased in steps until there was evidence of coating melting and flowing. The coating emittance was then determined by a surface heat balance. The data obtained in the GE-RES-D plasma arc compared favorably with laboratory measurements. However, SR-2 coated Mod 1A REI-Mullite tiles displayed totally noncatalytic surface characteristics in the lower pressure tests reported by NASA-Ames.

Evaluation of the adequacy of the model for predicting the thermal response of REI-Mullite revealed some discrepancies in the accuracy of the prediction for the transient response, although the maximum structure temperatures were reasonably well predicted. Evaluation of spectral transmittance data indicated another heat transfer mechanism operative in the model, namely, a radiation shine in effect. The impact of the shine in effect on the bond-structure temperature response was found to be both surface temperature and REI thickness dependent. Shine-in coefficients have been derived from a steady state thermal soak test in a radiantly heated entry simulator. These coefficients, when used in conjunction with the guarded hotplate measured Mod 1A REI-Mullite thermal conductivity data, produce excellent agreement between measured and predicted temperature response for both transient and steady state conditions.

The need for consideration of the real backside boundary conditions rather than the assumption of adiabatic conditions was shown to be important as a result of the analyses conducted relative to the NASA-MSC prototype panel test results.

INTRODUCTION

- **OVERTEMPERATURE AND HIGH TEMPERATURE EMITTANCE EVALUATION**
 - **MELT TEMPERATURE**
 - **NONCATALYTIC SURFACE EFFECTS**
 - **SURFACE EMITTANCE**
- **THERMAL MODEL VERIFICATION**
 - **USE OF LABORATORY MEASURED THERMAL CONDUCTIVITY**
 - **INCLUSION OF RADIATION TRANSPORT**
 - **SENSITIVITY TO BACKSIDE BOUNDARY CONDITIONS**

Figure 1

HIGH TEMPERATURE EVALUATION OF COATED REI-MULLITE

(Figure 2)

For a man-rated vehicle the coated REI-TPS must exhibit capability to survive off-nominal entry heating conditions, such as might occur in an aborted mission. It is necessary to know the surface temperature at which the coated REI starts to melt, and more important, the heat flux necessary to produce surface melting. Thus, the primary objective of this specific test program was to determine the heat flux and surface temperature required to melt the coating materials. Melting in this case is defined as the time at which material is visually flowing from the model. Secondary objectives were to determine the high temperature emissivity values and the catalytic nature of the coating.

These tests were conducted in the GE-RES-D Hyperthermal Arc Facility using the tunnel mode of operation. In this mode, flow is delivered to the model at a low supersonic Mach number with a stagnation pressure of about 4137 N/m² (0.6 psia). Total enthalpy for these runs was nominally 1.64×10^7 J/Kg (7100 Btu/lb).

Heat flux was varied by moving the model closer to the nozzle during the run. Sting positioning was remotely controlled from the control room. All models were instrumented with Pt/Pt-10% Rh thermocouples located in the coating for recording the approximate surface temperatures. The test procedure was to incrementally increase the heat transfer rate in gradual steps up to the melt temperature. Prior to each increase the model was retracted for two to three seconds while a calorimeter was inserted to measure the heat flux.

A calorimeter coated with 1 mil of teflon gave a heat flux reading only 7 to 13 percent lower than an uncoated calorimeter. This indicated that, in the GE-RES-D facility, there would be no difference observed between the temperature response of a fully noncatalytic or fully catalytic coating.

HIGH TEMPERATURE EVALUATION OF COATED REI-MULLITE

PRIMARY OBJECTIVE:

DETERMINE HEAT FLUX AND SURFACE TEMPERATURE TO MELT COATING

SECONDARY OBJECTIVES:

**DETERMINE HIGH TEMPERATURE EMISSIVITY VALUES OF COATING
DETERMINE CATALYTIC NATURE OF COATING**

VARIABLES:

**HIGH TEMPERATURE EMITTANCE OF COATING
CATALYTIC RECOMBINATION RATE COEFFICIENT OF COATING
MELTING AND/OR SUBLIMATION THRESHOLD OF COATED REI**

TEST CONFIGURATION AT GE HYPERTHERMAL ARC:

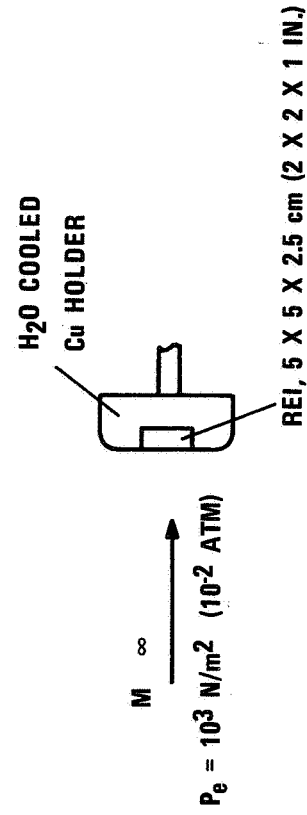


Figure 2

PLASMA ARC TEST RESULTS

(Figure 3)

The SR-2 coating system remained shape stable until a temperature of 1967°K (3080°F) was reached. At that time the change in flow field appearance indicated products were being removed or vaporized from the coating. A heat flux of about 44 w/cm^2 ($39\text{ BTU/ft}^2\text{ sec}$) was required to reach this surface temperature.

Data comparing the variation of surface temperatures with hot wall heat fluxes in the GE-RES and NASA-Ames* test facility are presented in this figure. It is seen that the SR-2 coating exhibits totally noncatalytic surface characteristics for the combinations of test conditions used at NASA-Ames and fully catalytic characteristics for the GE-RES test conditions.

*Reported in the April 1972 Monthly Status Report for NASA Space Shuttle Structures and Technology Working Group

PLASMA ARC TEST RESULTS

SYMBOL	FACILITY	HEATING RATE		PRESSURE		RECOVERY ENTHALPY	
		BTU/FT ² SEC	W/cm ²	ATM	N/m ²	BTU/LB	MJ/Kg
△	GE 5MW	ALL	ALL	4 X 10 ⁻²	4 X 10 ³	7100	1.65
○	NASA-AMES	20	18	7.5 X 10 ⁻³	7.5 X 10 ²	3510	0.82
○	NASA-AMES	30	27	7.5 X 10 ⁻³	7.5 X 10 ²	4189	0.97
○	NASA-AMES	40	35	7.5 X 10 ⁻³	7.5 X 10 ²	5800	1.35

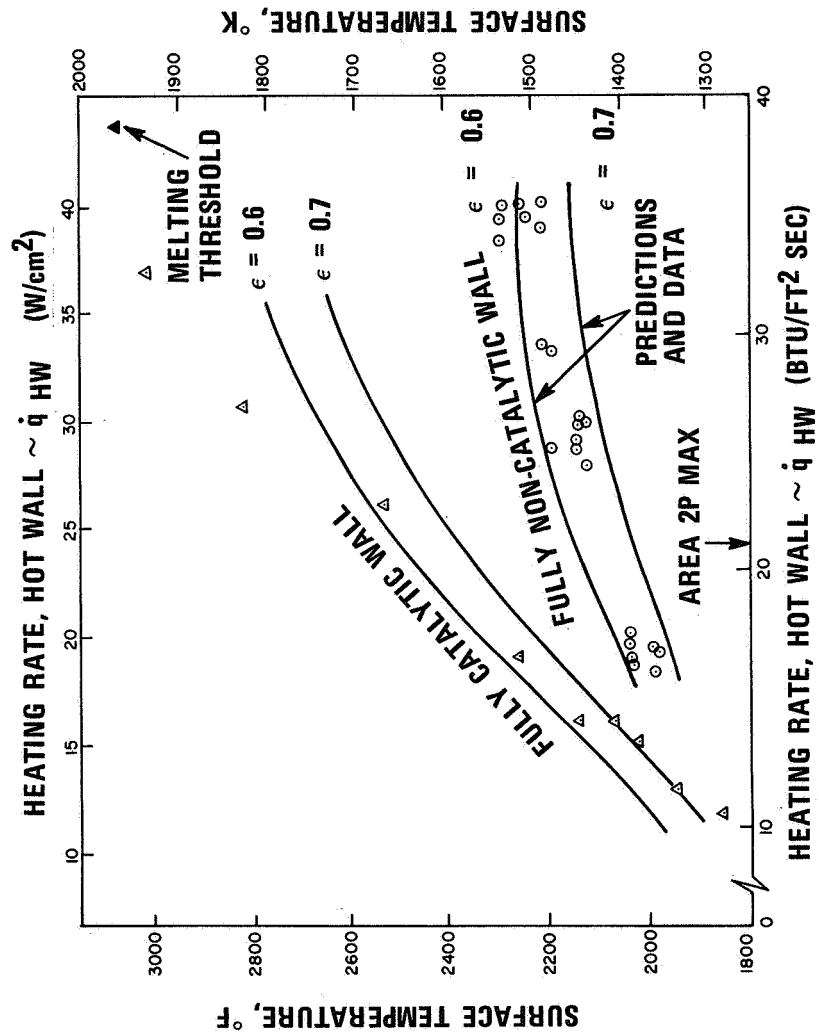


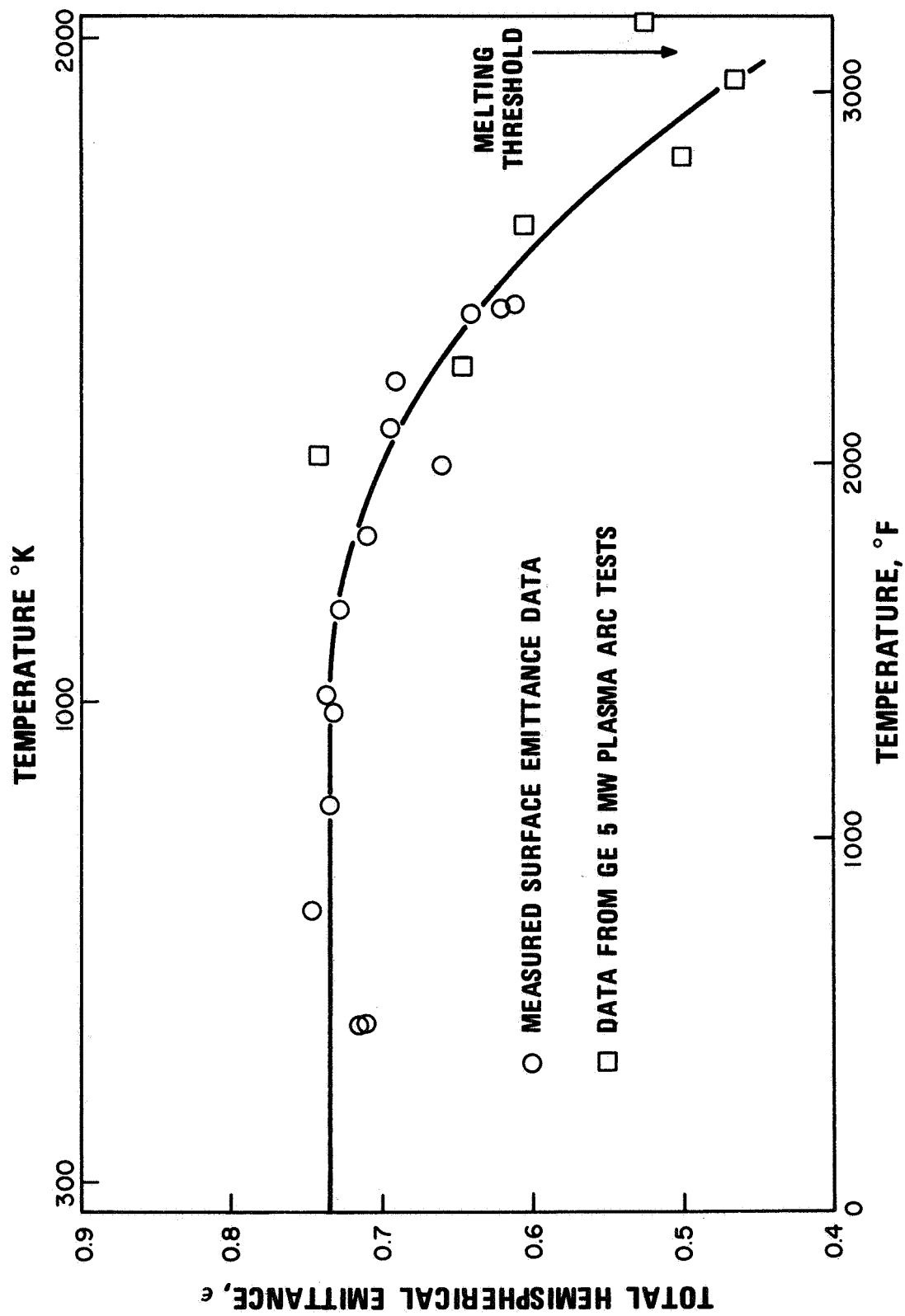
Figure 3

SR-2 COATING SURFACE EMITTANCE

(Figure 4)

The emittance data deduced from the overtemperature assessment tests are compared with data measured calorimetrically on the SR-2 coating. It can be seen that the two independent sets of results compare favorably. The dimensional stability of the SR-2 coating up to 1967° K (3080° F) is excellent.

SR-2 COATING SURFACE EMITTANCE



SUMMARY OF HIGH TEMPERATURE CHARACTERISTICS OF COATED MOD IA REI-MULLITE

(Figure 5)

The melting temperature of the SR-2 coated Mod IA REI-Mullite has been established as about 1967° K (3080° F). This results in a large overtemperature capability for the material in relation to surviving off-nominal entry heating conditions.

The coating emittance determined from arc tests agree with that measured calorimetrically and has a value of 0.73 to 1100° K (1600° F) where it tends to decrease to a small extent with increasing temperature.

The SR-2 coating system exhibited totally noncatalytic surface characteristics in the tests conducted at NASA Ames where flow conditions were conducive to measuring differences in net convective heat flux to catalytic and non-catalytic surfaces. Thus for the shuttle orbiter TPS, if flow conditions are such that during any portion of the entry, a significant portion of the total heat transfer is due to atomic recombination at the surfaces, the SR-2 coated Mod IA REI-Mullite will exhibit a fully noncatalytic response and run at significantly cooler surface temperatures.

SUMMARY OF HIGH TEMPERATURE CHARACTERISTICS OF COATED MOD IA REI-MULLITE

- **MELTING TEMPERATURE ~ 1967° K (3080° F)**
- **COATING EMITTANCE ~ 0.73 TO 1100° K (1600° F)**
- **SR-2 COATING IS NONCATALYTIC**

Figure 5

THERMAL DESIGN MODEL VERIFICATION

(Figure 6)

To verify the validity of the thermal design model used for Space Shuttle TPS design, high temperature thermal response tests were conducted on a 15 x 20 cm (6 in. x 8 in.) sample of coated REI-Mullite bonded to an aluminum backplate. The data have been used to determine the validity of the current thermal design model, both for the transient and steady state conditions of the tests. The tests were run at ambient pressure and at 10^3 N/m^2 (10^{-2} ATM) pressure. Steady state conditions were achieved on the 5 cm (2 in.) thick model by heating the surface at constant temperatures of 1370°K (2000°F) and 1644°K (2500°F) and by providing cooling water at the aluminum backplate to maintain its temperature at about 311°K (100°F). Steady state conditions were obtained after 40-55 minutes for the two tests.

The test facility consists of eight silicon carbide heaters spaced on 2.5 cm (1 in.) centers, enclosed in a foam quartz holder with water cooled terminal ends. The test samples are held with their backplates in contact with a water cooled copper plate. The test facility is operated within a vacuum chamber, with water cooled walls wherein the vacuum is maintained during the run. Tests were also run at ambient pressure.

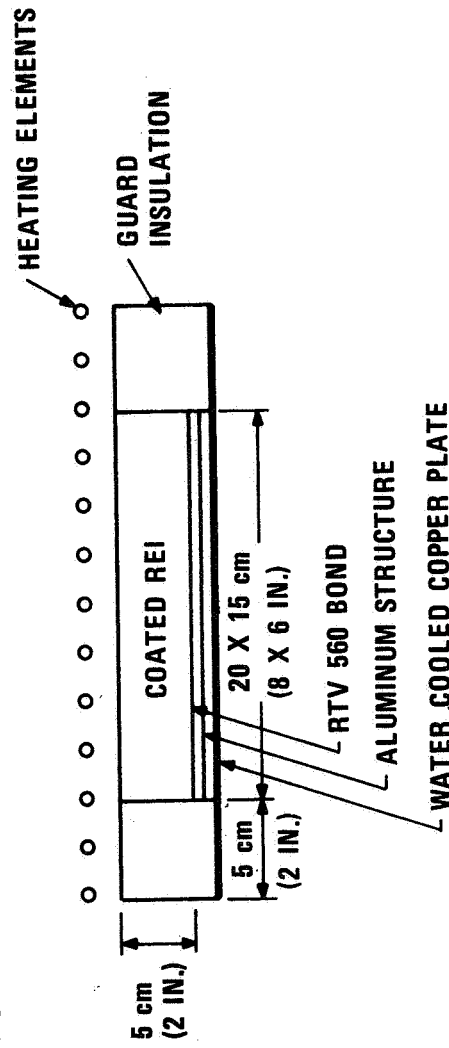
Control instrumentation in the coating consisted of platinum 10 percent rhodium/platinum (Type "S") thermocouples. Also recorded were in-depth REI, bond-line and backplate temperatures, using chromel-alumel thermocouples. The in-depth instrumentation was installed using a thermocouple plug. Exact locations of thermocouples were determined from x-ray photographs. Test surface temperature was controlled by one surface thermocouple and recorded with the other. Gaps between the model and the foamed quartz were stuffed with mullite fibers.

THERMAL DESIGN MODEL VERIFICATION

- **PRIMARY OBJECTIVE:**

VERIFY VALIDITY OF THERMAL DESIGN MODEL EMPLOYED FOR
MOD IA REI-MULLITE

- **CONFIGURATION**



- **THERMOCOUPLES IN THE COATING AND THROUGH THE THICKNESS**

- **TEST CONDITIONS:**

- **SURFACE TEMPERATURE** ~ 1370°K (2000°F) AND 1644°K (2500°F)
- **LOCAL PRESSURE** ~ 10^3 N/m^2 (10^{-2} ATM) AND 10^5 N/m^2 (1 ATM)

Figure 6

REI-MULLITE THERMAL RESPONSE AT 1 ATM TEST PRESSURE

(Figure 7)

The measured transient temperature responses for the ambient pressure test are shown. The surface temperature was driven to 1370° K (2000° F) in about 10 minutes and was increased to 1644° K (2500° F) after a time period of 25 minutes at 1370° K (2000° F). Analytical predictions were made using the surface and backplate temperature histories as boundary conditions in the one-dimensional thermal analysis using the Reaction Kinetics Ablation Program (REKAP). The predictions were made using the 10^5 N/m^2 (1 ATM) thermal conductivity design curve shown on Figure 9. As can be seen, there is reasonable agreement between the test data and the analytical predictions.

REI-MULLITE THERMAL RESPONSE AT 1 ATM TEST PRESSURE

MOD 1A REI-MULLITE
PRESSURE = 10^5 N/m^2 (1 ATM)

MOD 1A REI-MULLITE
PRESSURE = 10^5 N/m^2 (1 ATM)
TIME = 55 MINUTES

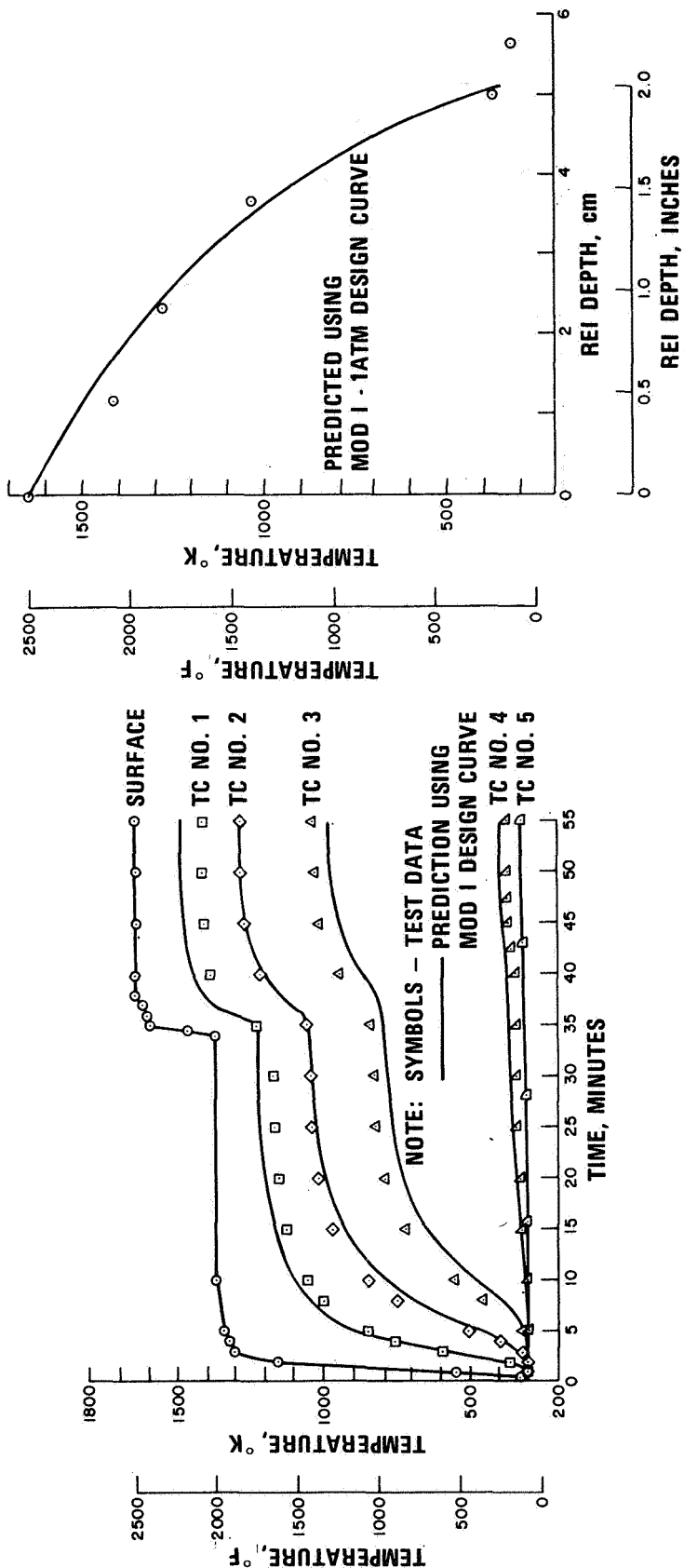


Figure 7

REI-MULLITE THERMAL RESPONSE AT 10⁻² ATM TEST PRESSURE

(Figure 8)

The measured transient temperature response from the 10³ N/m² (10⁻² ATM) test is shown compared with predictions using REKAP and the design thermal conductivity curve shown on Figure 9 for 10³ N/m² (10⁻² ATM) pressure. Again the overall comparison is reasonably good, but the in-depth predicted transient response is lagging behind the data.

It is interesting to note that the steady state in-depth temperatures for the 10⁵ N/m² (1 ATM) pressure tests are lower than for the 10³ N/m² (10⁻² ATM) pressure test. This is also predicted with REKAP and the reason is that for the 10⁵ N/m² (1 ATM) pressure test more heat is flowing through the sample and being removed through the backplate into the cooling water than for the reduced pressure test.

REI-MULLITE THERMAL RESPONSE AT 10⁻² ATM TEST PRESSURE

TRANSIENT RESPONSE

STEADY-STATE RESPONSE

PRESSURE = 10³ N/m² (10⁻² ATM)

MOD 1A REI-MULLITE

NOTE: SYMBOLS — TEST DATA
—— PREDICTION USING
MOD 1 DESIGN CURVE

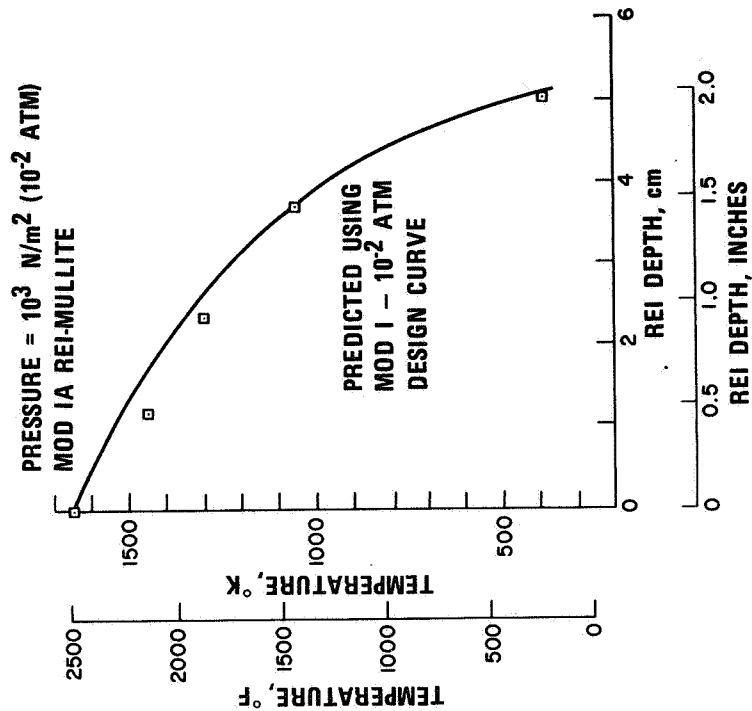
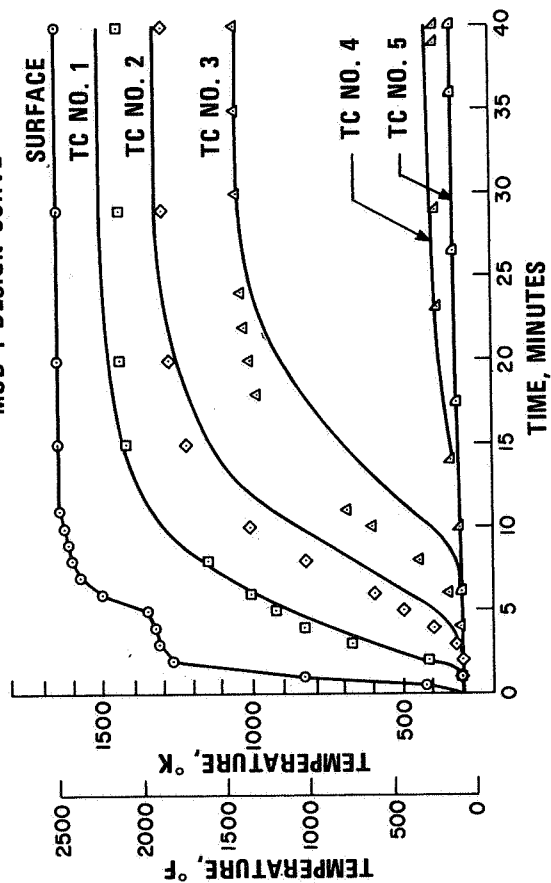


Figure 8

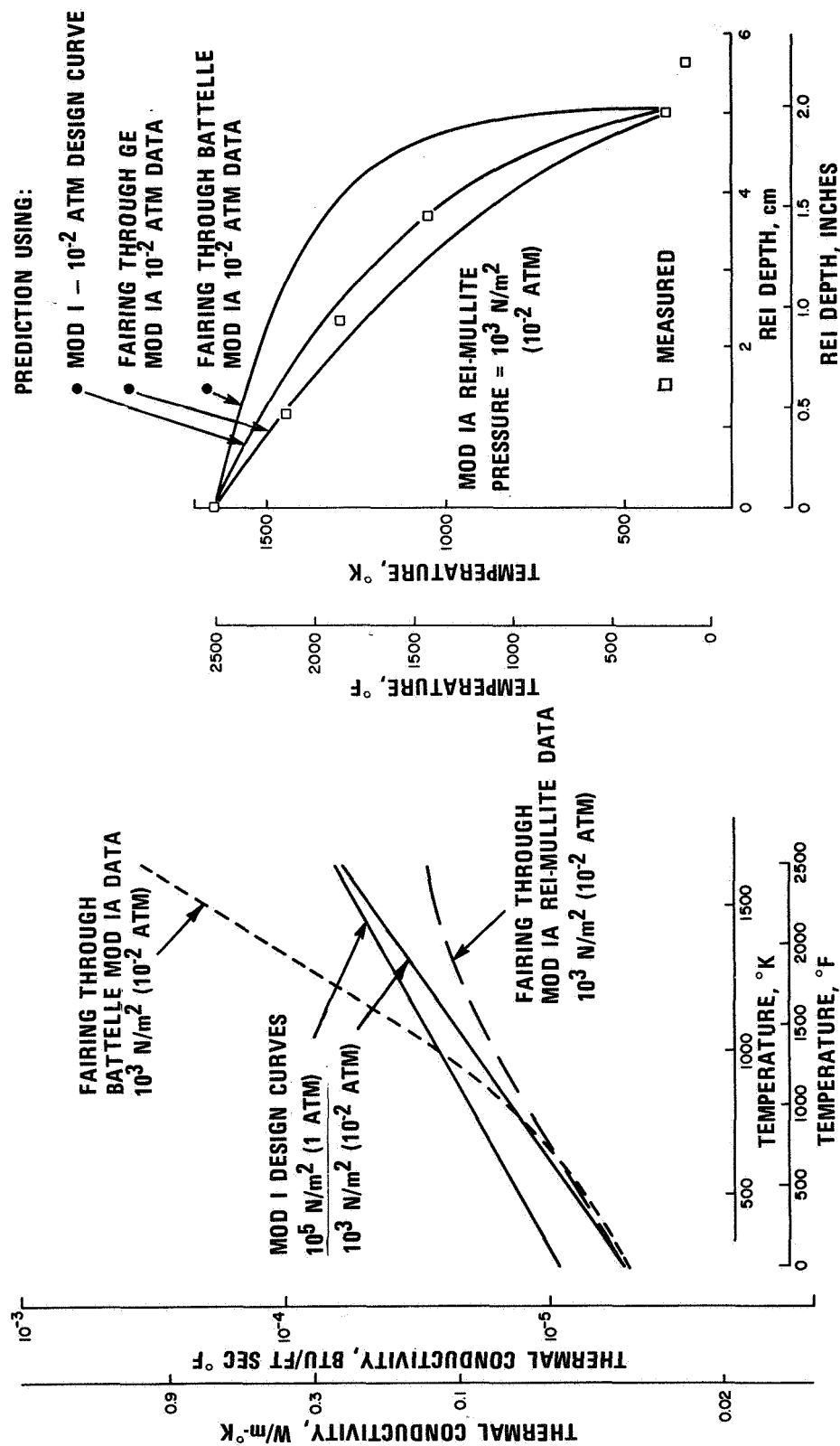
ESTABLISHMENT OF REI-MULLITE THERMAL DESIGN MODEL

(Figure 9)

Additional predictions are shown based on the thermal conductivity reported by Reference 1, and a fairing through the guarded hotplate Mod 1A REI-Mullite measured data. The prediction based on the Battelle Memorial Institute data shows extremely high temperatures compared to the data. Also shown is a fairing through the Mod 1A data, which underpredicts the in-depth data. A comparison of all thermal conductivity values used in the analysis is shown.

The data show the Mod I REI-Mullite design curve provides reasonable agreement with test results, but requires modification above about 1255°K (1800°F).

ESTABLISHMENT OF REI-MULLITE THERMAL DESIGN MODEL



THERMAL CONDUCTIVITY DESIGN CURVES

COMPARISON OF STEADY STATE THERMAL PREDICTIONS

Figure 9

SUMMARY OF THERMAL DESIGN MODEL VERIFICATION ANALYSES

(Figure 10)

The following conclusions can be drawn from the thermal design verification studies and analyses. They are:

1. Use of Mod I REI-Mullite thermal conductivity design curves provides reasonable agreement with test results but requires modification above about 1255° K (1800° F).
2. Use of GE-RESO measured guarded hot plate thermal conductivity data for Mod IA REI-Mullite does not improve the modeling accuracy.
3. Use of Battelle Memorial Institute measured thermal conductivity data provides poor agreement with test results.

SUMMARY OF THERMAL DESIGN MODEL VERIFICATION ANALYSES

- **MOD I REI-MULLITE THERMAL CONDUCTIVITY DATA DESIGN CURVES PROVIDE REASONABLE AGREEMENT WITH TEST RESULTS BUT REQUIRE MODIFICATION AT HIGH TEMPERATURES**
- **MOD IA REI-MULLITE THERMAL CONDUCTIVITY DATA DOES NOT IMPROVE MODELLING ACCURACY**
- **BATTELLE MEASURED THERMAL CONDUCTIVITY DATA FOR MOD IA REI-MULLITE PROVIDE POOR AGREEMENT WITH TEST RESULTS**

Figure 10

REI-MULLITE TRANSMITTANCE

(Figure 11)

An evaluation was performed to determine if other modes of heat transfer might be present that, if properly accounted for, could improve the accuracy of the predictions. As a result, transmittance measurements for three different thicknesses of 181 Kg/m³ (11.3 pcf) density Mod IA REI-Mullite were performed utilizing the Gier-Dunkle integrating sphere reflectometer. The measurements are a normal incidence/hemispherical exit transmittance type that collects all the energy transmitted by the specimen. The results are compared to those reported in Reference 2 for the MOD III HCF.

REI-MULLITE TRANSMITTANCE

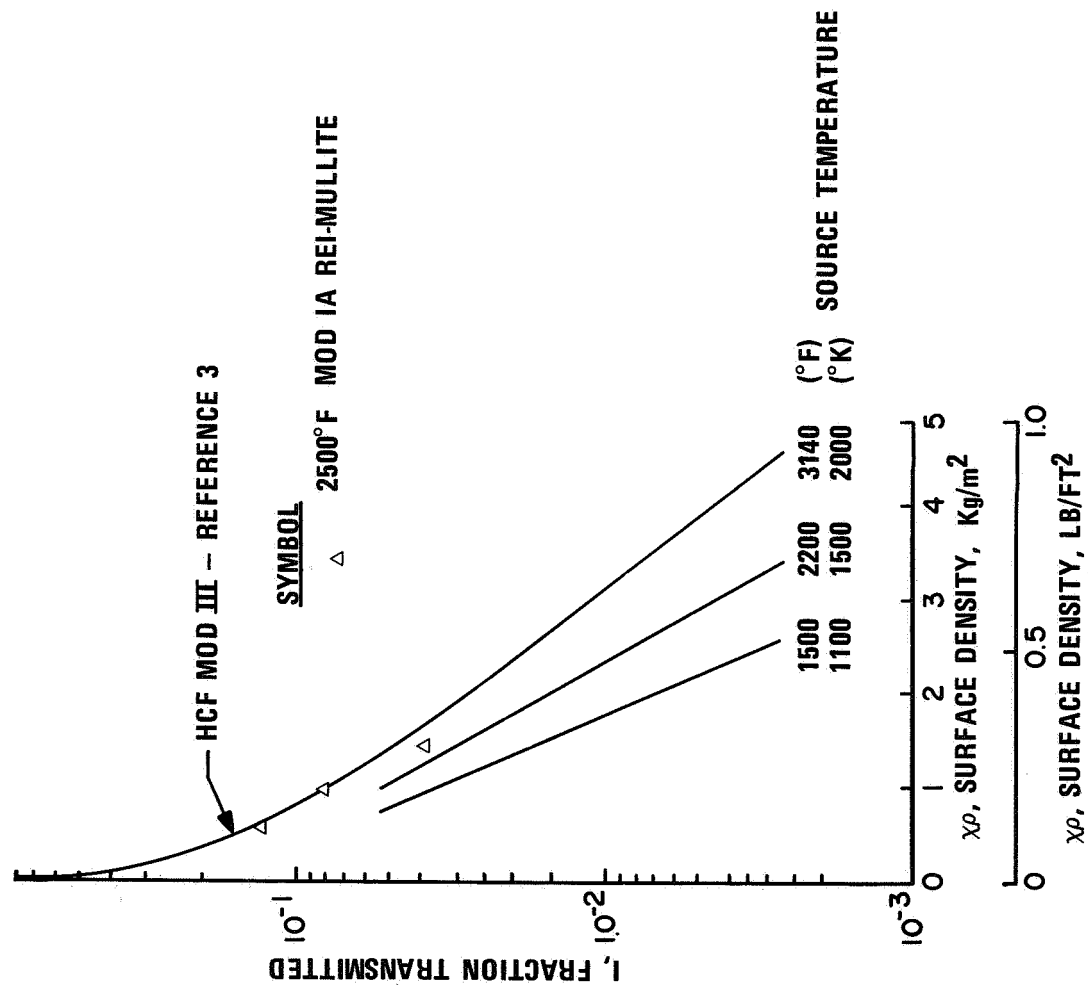


Figure 11

SHINE-IN PENETRATION DEPTH FOR AREA 2P PROTOTYPE PANEL TEST*

(Figure 12)

The quantity of heat conducted into the REI-Mullite is small during the major portion of the heating period. The transmittance data indicate an additional heat input is incurred in the outer 1.25 cm (1/2 in.) of the REI due to shine in from the backside of the coating. These shine in depths were computed as the depth where the heat input due to shine in had decreased to 10% of the heat conducted into the REI surface. It is seen that the shine-in effect is dominant only in the outer 1.25 cm (1/2 in.) of the REI-Mullite.

*Details of design of NASA-MSC Area 2P prototype panels are discussed in GE-RES final report on Contract No. NAS 9-12084 dated May 1972.

SHINE-IN PENETRATION DEPTH FOR AREA 2P PROTOTYPE PANEL TEST

MODULATED PRESSURE

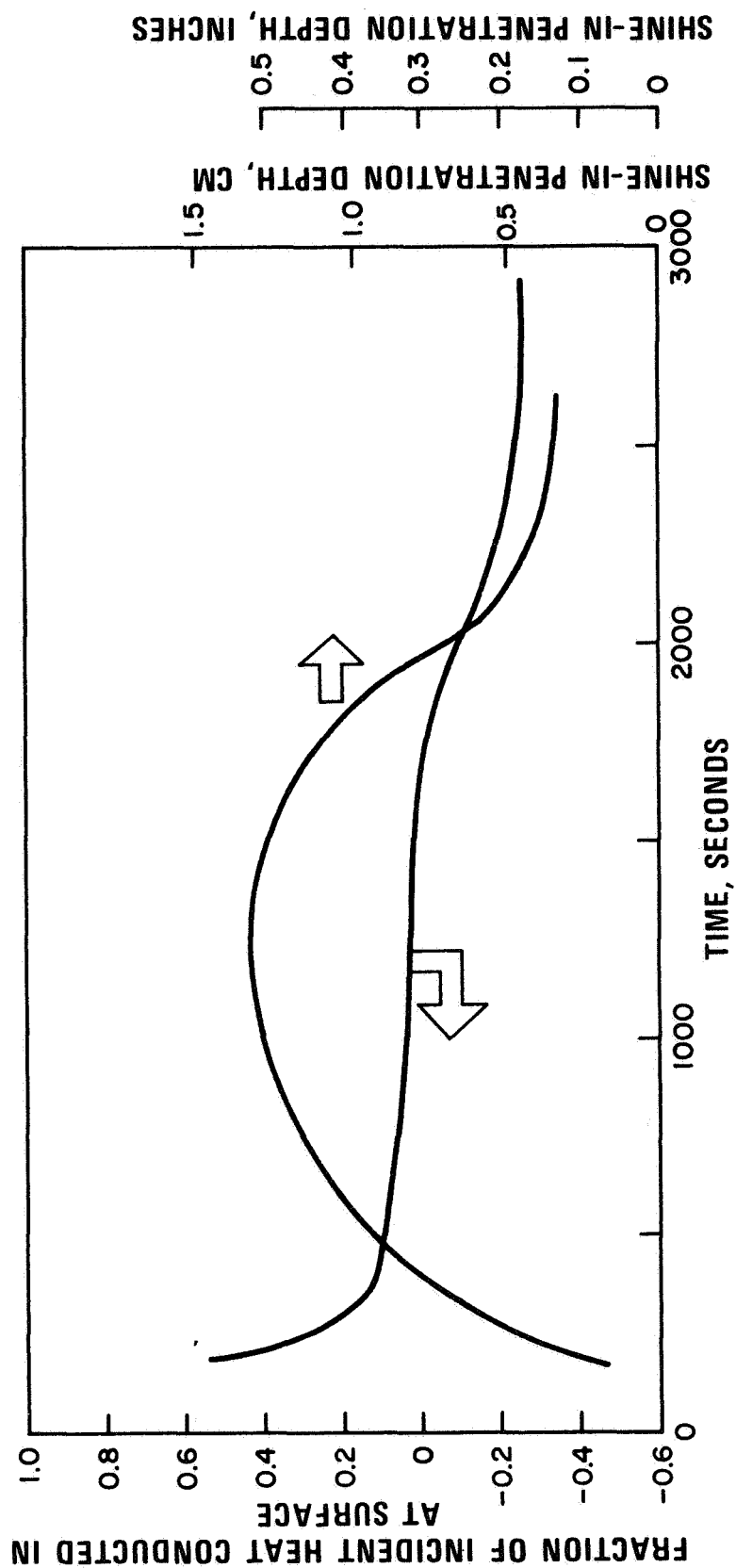


Figure 12

SHINE-IN CORRECTION EFFECTS ON THERMAL DESIGN MODEL

(Figure 13)

To properly handle this shine in mode of heat transfer analytically, one must resort to a computerized solution of the governing heat transfer differential equations. These equations must include the radiant heat transmitted, absorbed, and backscattered through each element of the material. However, such programs are not now in operation, and it is necessary to use an approximate technique for routine design work.

Consideration of the transmittance characteristics of the Mod IA REI-Mullite indicates that the total effect of shine in on bond and structure temperature response is both surface temperature and REI-Mullite thickness dependent. For the steady-state tests conducted on the 5 cm (2 in.) thick model with surface temperature at 1370° K (2000° F) and 1644° K (2500° F), shine in coefficients have been derived. These coefficients have been employed in combination with the Mod IA REI-Mullite thermal conductivity data to predict the steady state response of the 5 cm (2 in.) thick REI model.

SHINE-IN CORRECTION EFFECTS ON THERMAL DESIGN MODEL

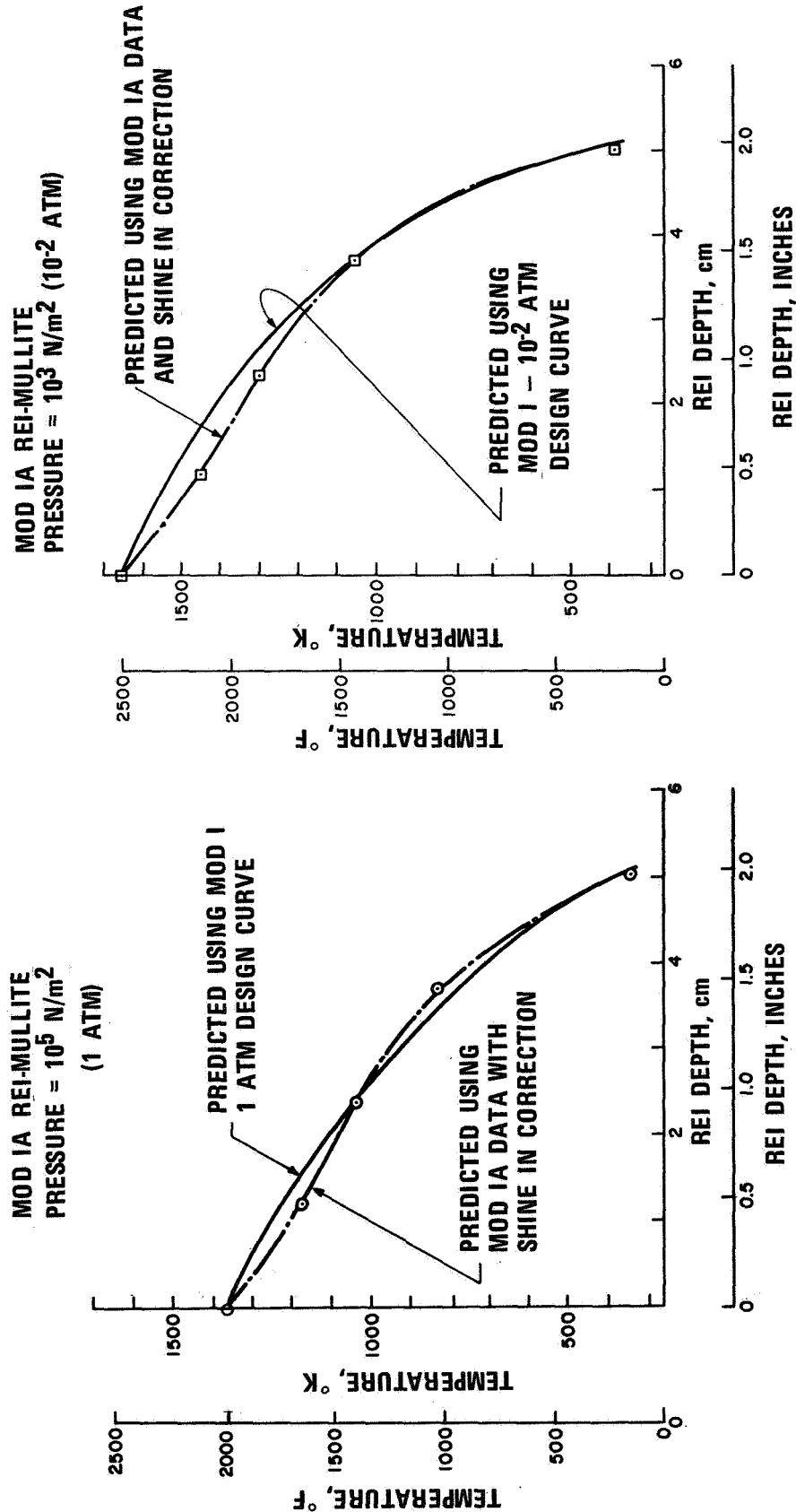


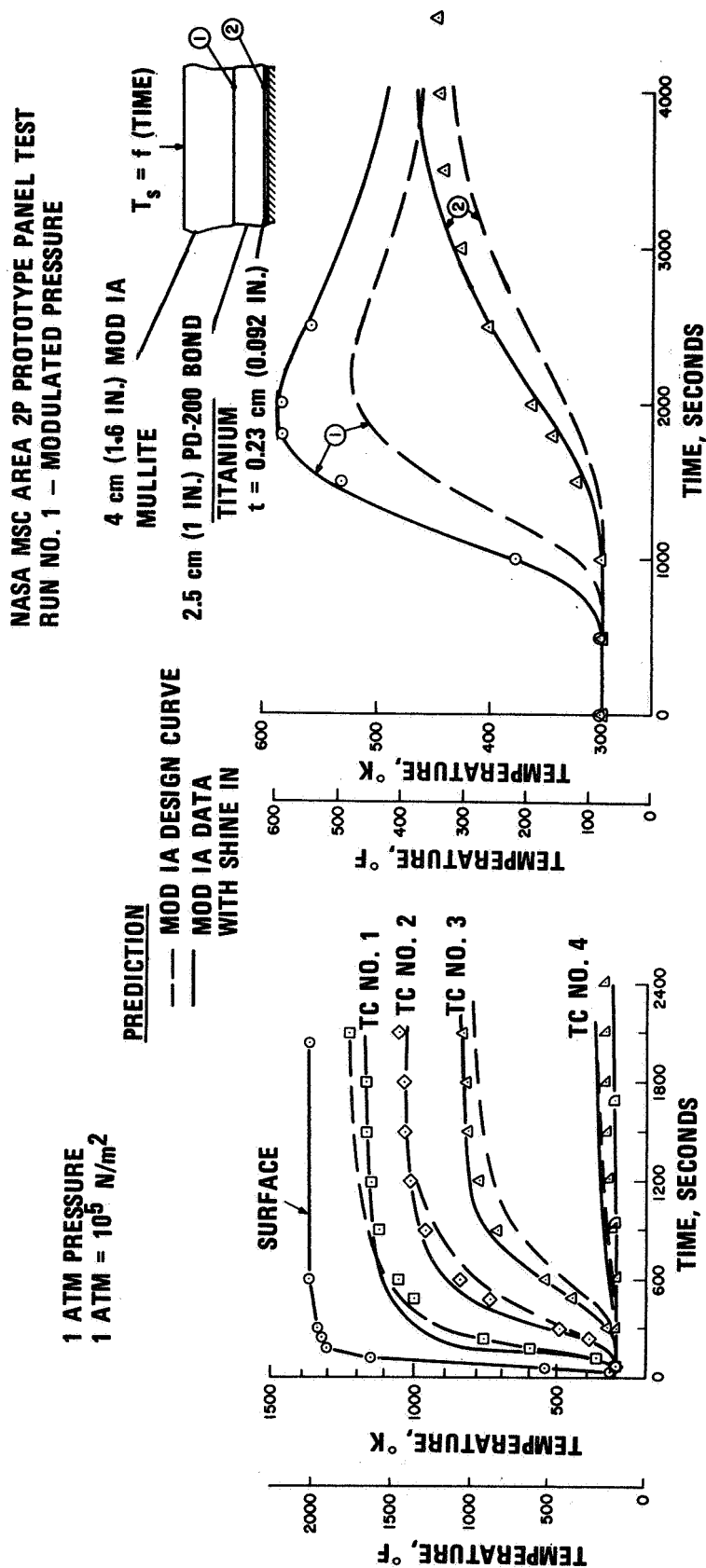
Figure 13

COMPARISON OF REI-MULLITE TRANSIENT TEMPERATURE RESPONSE WITH PREDICTIONS MADE WITH AND WITHOUT SHINE-IN CORRECTIONS

(Figure 14)

Employing the shine in coefficients derived from the steady state tests and fairings through the Mod IA REI-Mullite thermal conductivity data, predictions of the transient response have been made and compared to predictions made employing the Mod I REI-Mullite thermal conductivity design curves. These comparisons have been made for several different tests run both at GE-RESO and NASA-MSC. It can be seen that consideration of all the heat transfer mechanisms, including both conduction and in-depth shine in from the coating backside, is necessary to accurately predict the transient temperature response.

COMPARISON OF REI-MULLITE TRANSIENT TEMPERATURE RESPONSE WITH PREDICTIONS MADE WITH AND WITHOUT SHINE-IN CORRECTIONS



IN-DEPTH TRANSIENT RESPONSE
OF MOD IA REI-MULLITE
FROM GE-RESO TESTS

REI/BOND AND BOND/STRUCTURE
TRANSIENT RESPONSE FOR NASA-MSC
AREA 2P PROTOTYPE PANEL

Figure 14

COMPARISON OF REI-MULLITE TRANSIENT TEMPERATURE RESPONSE WITH PREDICTIONS

(Figure 15)

Employing the thermal model derived from the steady-state tests, predictions of the transient response have been made with and without proper thermal modeling of the backside boundary conditions. These comparisons have been made for a test run at NASA-MSC. It is seen that the impact of proper treatment of this boundary condition on the predicted structure response is about 16°K (30°F).

COMPARISON OF REI-MULLITE TRANSIENT TEMPERATURE RESPONSE WITH PREDICTIONS

NASA MSC AREA 2P PROTOTYPE PANEL TEST
RUN NO. 1

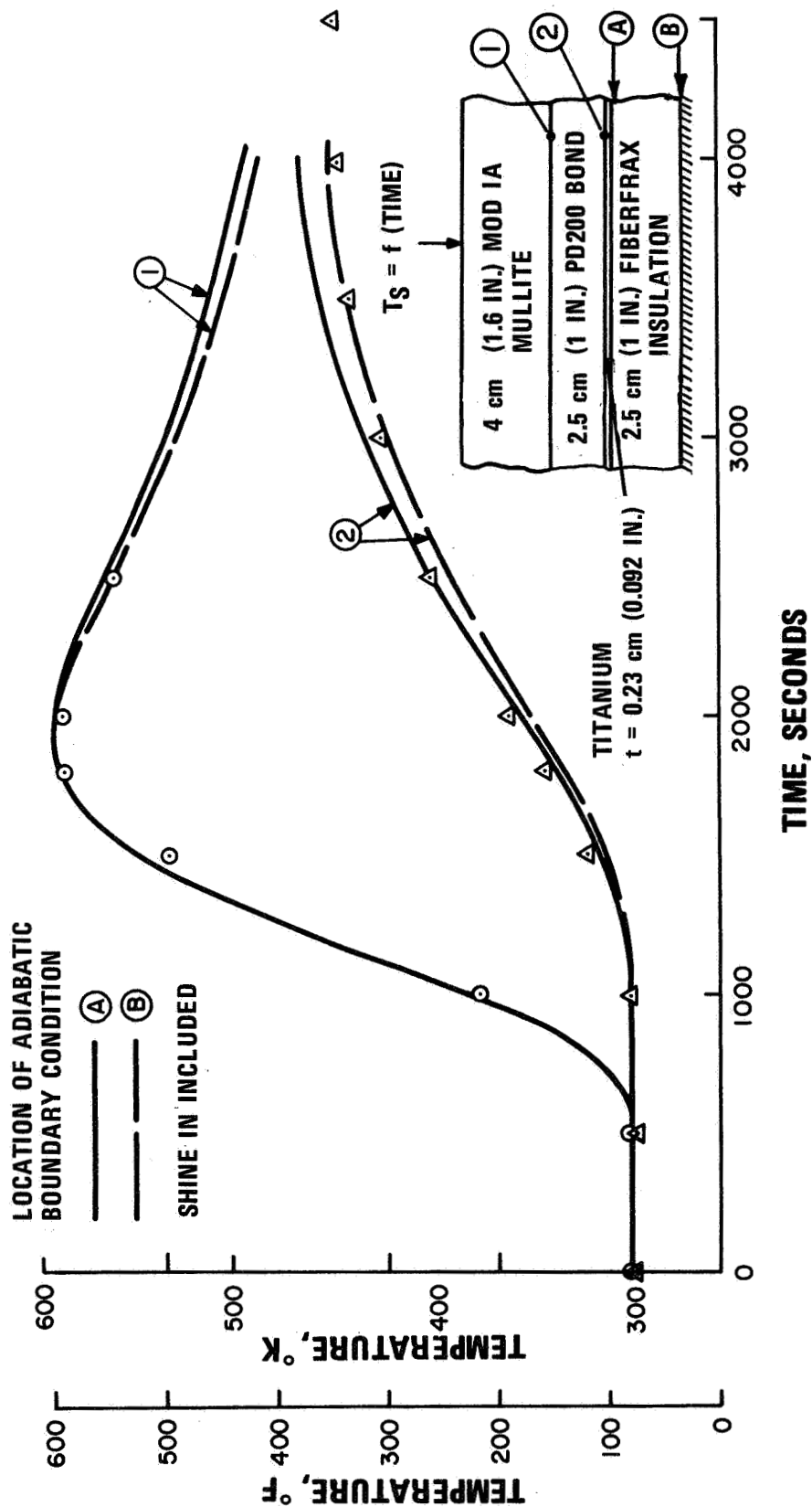


Figure 15

FUNCTIONAL DEPENDENCE OF SHINE-IN COEFFICIENTS

(Figure 16)

The functional dependence of the shine-in coefficients employed in these analyses is illustrated in this figure. For a constant model thickness, the integrated through-the-model-thickness effect of these shine-in coefficients is seen to diminish rapidly with reduced surface temperatures.

Shine-in effects for REI-Mullite results from the fact that the voids between fibers are relatively large compared to the wavelength of the radiation producing the thermal energy transfer. The shine-in phenomenon will be minimized or eliminated when the smaller diameter ($1.7\text{ }\mu\text{m}$) mullite fibers now under development by B&W become available and are utilized in the insulation composites.

FUNCTIONAL DEPENDENCE OF SHINE-IN COEFFICIENTS

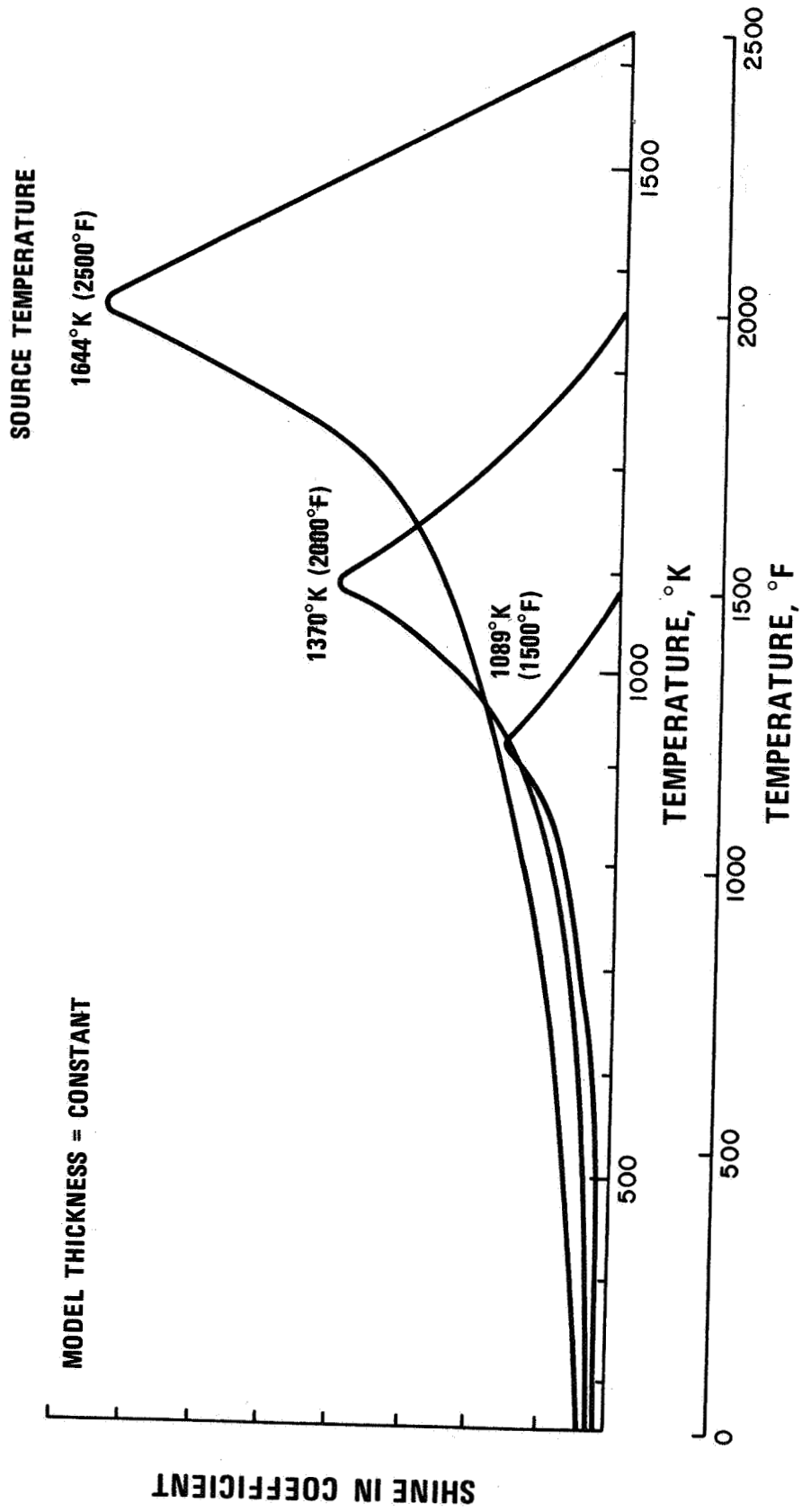


Figure 16

THERMAL MODEL VERIFICATION SUMMARY

(Figure 17)

Prediction of through the thickness temperature gradients and maximum soak out temperatures is improved through use of an approximate thermal model that includes all of the heat transfer modes and an accurate definition of the structural backside thermal boundary condition. Predicted maximum structure temperature increases 16°K (30°F) for the 1530°K (2300°F) (Area 2P) maximum surface temperature environment, but it is not expected to change for the 980°K (1300°F) (Area 1) maximum surface temperature environment.

THERMAL MODEL VERIFICATION SUMMARY

- **INCLUSION OF SHINE-IN EFFECTS IMPROVES ACCURACY OF TRANSIENT TEMPERATURE PREDICTIONS.**
- **INCLUSION OF PROPER STRUCTURE THERMAL BOUNDARY CONDITION IS NECESSARY TO ADEQUATELY PREDICT STRUCTURE TEMPERATURE RESPONSE.**

THERMAL STRESS IMPLICATIONS OF SHINE-IN GRADIENT

(Figure 18)

The effect of shine-in gradients on thermal stress is shown at critical times during heat up for an Area 2P environment. Note that there is negligible difference at this time when the thermal stresses are computed to be maximum. The small increase required in REI-Mullite thickness for this case has no effect on the critical stress/strain parameters.

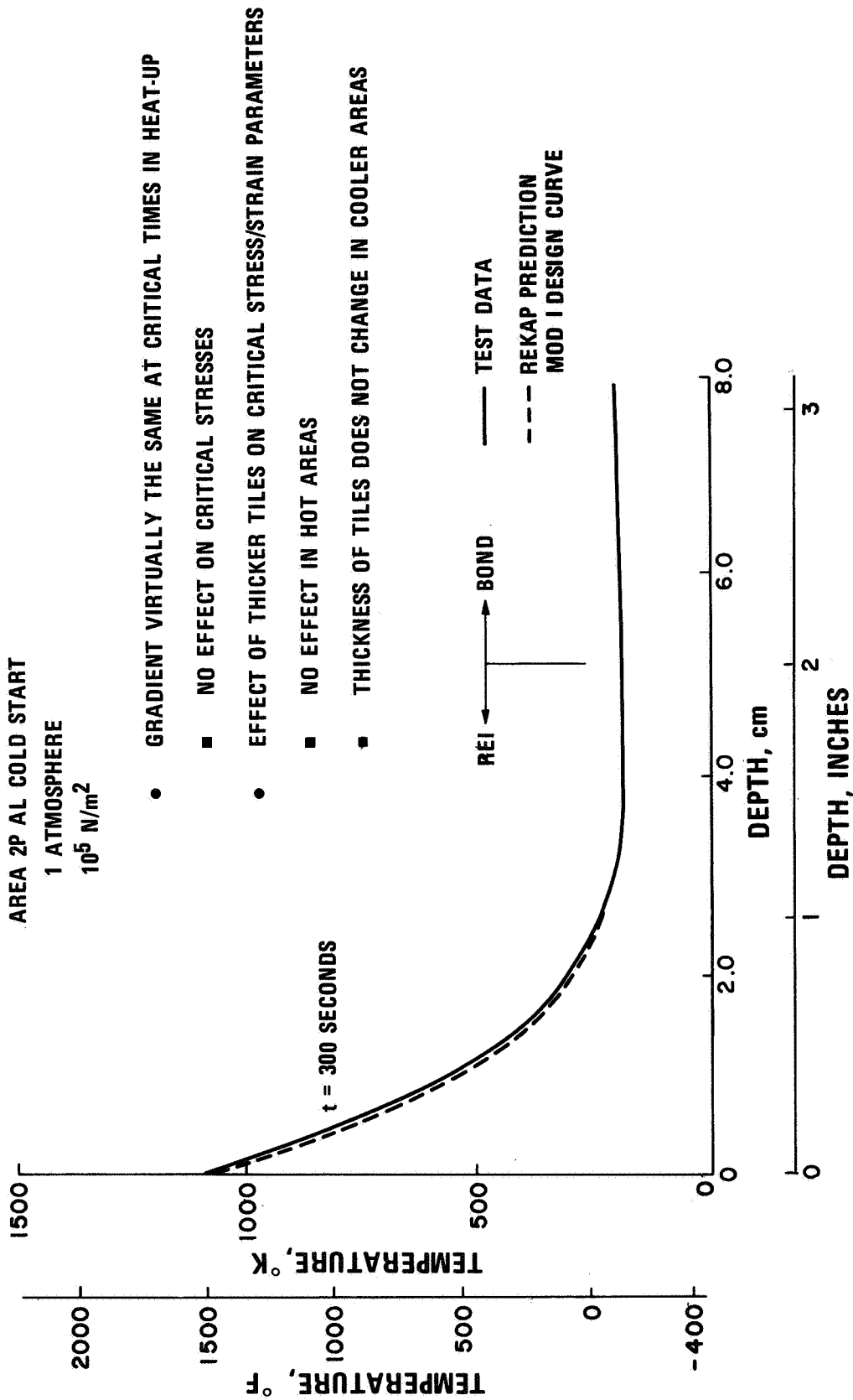
THERMAL STRESS IMPLICATIONS OF SHINE-IN GRADIENT

NASA-MSC PROTOTYPE PANEL TEST

AREA 2P AL COLD START

1 ATMOSPHERE

10^5 N/m^2



- GRADIENT VIRTUALLY THE SAME AT CRITICAL TIMES IN HEAT-UP
- NO EFFECT ON CRITICAL STRESSES
- EFFECT OF THICKER TILES ON CRITICAL STRESS/STRAIN PARAMETERS
- NO EFFECT IN HOT AREAS
- THICKNESS OF TILES DOES NOT CHANGE IN COOLER AREAS

Figure 18

SUMMARY

(Figure 19)

The GE-RES-D SR-2 coating exhibits totally noncatalytic surface characteristics in those tests where flow conditions are conducive to measuring differences in net convective heat flux to catalytic and noncatalytic surfaces.

The Mod I thermal conductivity design curves and the Mod IA REI-Mullite thermal conductivity data yield much better agreement between predicted and measured in-depth temperature response than do the Battelle Memorial Institute data.

Prediction of through-the-thickness temperature gradients is greatly improved by inclusion of shine-in effects. Inclusion of these shine-in effects has only a limited impact on the severity of predicted thermal stresses, structure temperatures, and TPS system weights (when compared to the weights previously generated employing the Mod I design curves).

SUMMARY

- SR-2 COATING SYSTEM EXHIBITS NONCATALYTIC SURFACE CHARACTERISTICS WHICH LIMIT SURFACE TEMPERATURE RISE UNDER CERTAIN CONVECTIVE HEAT FLUX CONDITIONS.
- GE-RESO MOD I REI-MULLITE THERMAL CONDUCTIVITY DESIGN CURVES PROVIDE MUCH BETTER AGREEMENT WITH TEST RESULTS THAN DOES BATTELLE MEMORIAL INSTITUTE DATA.
- INCLUSION OF SHINE-IN EFFECTS RESULTS IN IMPROVED ACCURACY OF TRANSIENT TEMPERATURE GRADIENT PREDICTIONS.
- SHINE-IN EFFECTS HAVE LIMITED IMPACT ON SEVERITY OF THERMAL STRESSES, PREDICTED STRUCTURE TEMPERATURE OR TPS SYSTEM WEIGHT.

Figure 19

REFERENCES

1. Kissler, C. W., et al., "Evaluation of Non-Metallic Thermal Protection Materials for the Manned Space Shuttle," Battelle Columbus Laboratories, Columbus, Ohio, Contract NAS 9-10853 Final Report, Volume V, 1 June 1972.
2. Hughes, T. A., "High Temperature Insulation Materials for Radioactive Thermal Protection Systems," Report No. MDC E0666, 19 July 1972.

PLASMA ARC TESTING TECHNIQUES FOR SPACE SHUTTLE
REUSABLE SURFACE INSULATION (RSI)

Ira M. Grinberg and Ross G. Luce
BATTELLE
Columbus Laboratories

INTRODUCTION

Reusable Surface Insulation (RSI) is considered a prime candidate for thermal protection of large areas of the space shuttle orbiter vehicle. As part of a program supported by NASA, Manned Spacecraft Center, on assessment of technical risks associated with the development and/or use of nonmetallic materials for the reusable orbiter, Battelle-Columbus recently completed a task to provide screening data on thermal and mechanical properties of RSI materials. Results of mechanical property evaluations of three candidate RSI materials are presented in the paper by Kistler, et al, in Volume I of these Proceedings. Within this task, dynamic, multicycle, plasma arc exposures of the RSI materials were conducted in the Battelle Aerothermal Research Facility. The techniques used to characterize material response during plasma arc exposures are described in this paper.

AEROTHERMAL RESEARCH FACILITY

(Figure 1)

Plasma arc exposures of three RSI materials were conducted in the BCL Aerothermal Research Facility. General Electric's REI, Lockheed's LI-1500, and McDonnell Douglas' HCF (January 1972) were tested in multicycle exposures. The GE material was mullite fiber insulation, bulk density of 200 to 210 kg/m³ including the coating, with SR2-55A1 (brown over green, fibrous intermediate zone) and SR2-XSR2 (brown) coatings. The Lockheed material was the silica insulation, bulk density of 260 to 290 kg/m³ including the coating, with an 0042 coating (bluish-gray). The McDonnell Douglas material was the mullite HCF, bulk density of 270 to 280 kg/m³ including the coating, with an M5₂₃A7P700 coating (black).

The facility consists of two separate wind tunnel legs, each of which includes a continuous-flow arc heater, a conical convergent-divergent nozzle, a free-jet cabin, and a conical convergent-divergent diffuser. Each leg exhausts to the pressure recovery system, which consists of a five-stage steam ejector. Electrical power for both legs is supplied by a 1.5 saturable reactor. For these exposures, the nontoxic, nonradioactive leg of the facility was used with the high-enthalpy arc heater. A nozzle with a 2.54-cm (1-inch)-diameter throat and a 12.7-cm (5-inch)-diameter exit was used.

AEROTHERMAL RESEARCH FACILITY

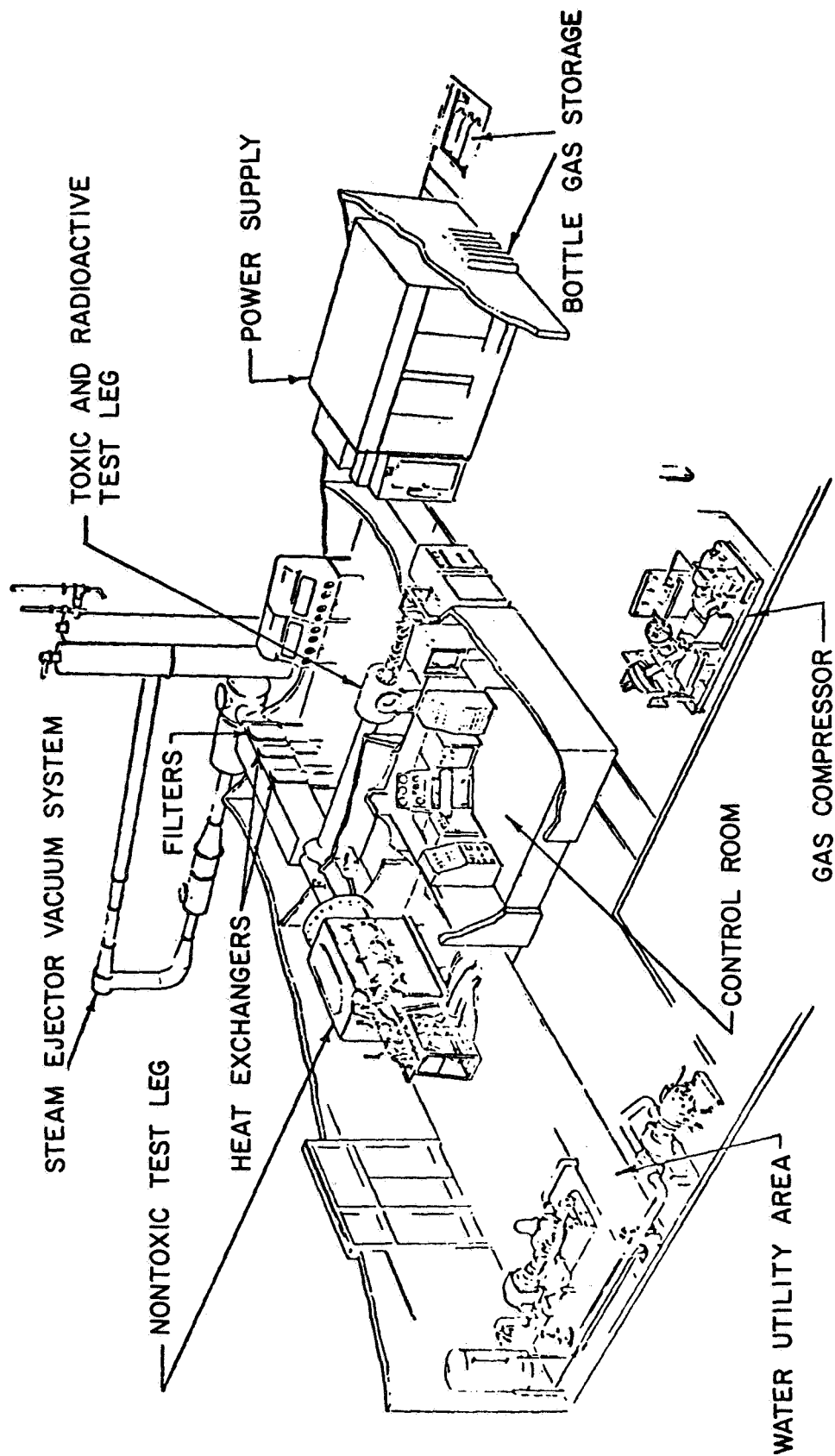


Figure 1

NOMINAL SURFACE TEMPERATURE HISTORY DURING ARC-PLASMA EVALUATIONS

(Figure 2)

One dynamic reentry profiling condition was used for the RSI specimens. The nominal surface-temperature profiling condition for the materials is shown in figure 2 along with a reentry surface-temperature history representative of a high cross-range orbiter (Area 2 on lower surface of the vehicle at 50-percent length location). In order to avoid rapid expansion of the coating relative to the insulation material and thermal-stress failure of the insulation material due to the high temperature gradients that would result from insertion of "cold" specimens into the heated test stream, electric radiant heaters were used to preheat the specimens prior to initiating the arc.

The surface of the specimens was heated to 1032-1089°K (1400-1500°F) using the radiant heaters. Two radiant heaters were mounted on a traversing mechanism in the test cabin so they could be moved away from the RSI specimens just prior to the arc heater start. The radiant heaters were positioned such that there was a narrow gap between them through which a pyrometer sighted on one of the specimens.

Limited experiments were conducted on the coating/insulator systems prior to the arc exposures to determine if cracks would develop in the coating materials as a result of the preheat thermal cycle (identical preheat cycle used as part of the arc exposures). Visual examinations of the specimens exposed to the heating cycle indicated no such failures.

When the specimen surface temperature reached the desired level, the radiant heaters were moved out of the way and the arc heater was started. Power to the radiant heaters was left on during the first five seconds in which the heaters were being moved in order to minimize cooldown of the specimens prior to convective heating from the arc-heated gas. The time interval between first movement of the radiant heaters and initiation of the arc was approximately eight seconds. The specimens were then convectively heated by the arc-heated gas for approximately 20 minutes following the surface temperature history shown in figure 2. At approximately 30 minutes into the cycle, the power and gas flow to the arc heater was terminated, and the specimens were allowed to cool until the temperature of the coating was 422°K (300°F) or less. The cooling water to the holder in which the specimens were mounted was also turned off when the arc-heater power was terminated. This procedure was repeated so that each pair of specimens received four such cycles.

NOMINAL SURFACE TEMPERATURE HISTORY DURING ARC-PLASMA EVALUATIONS

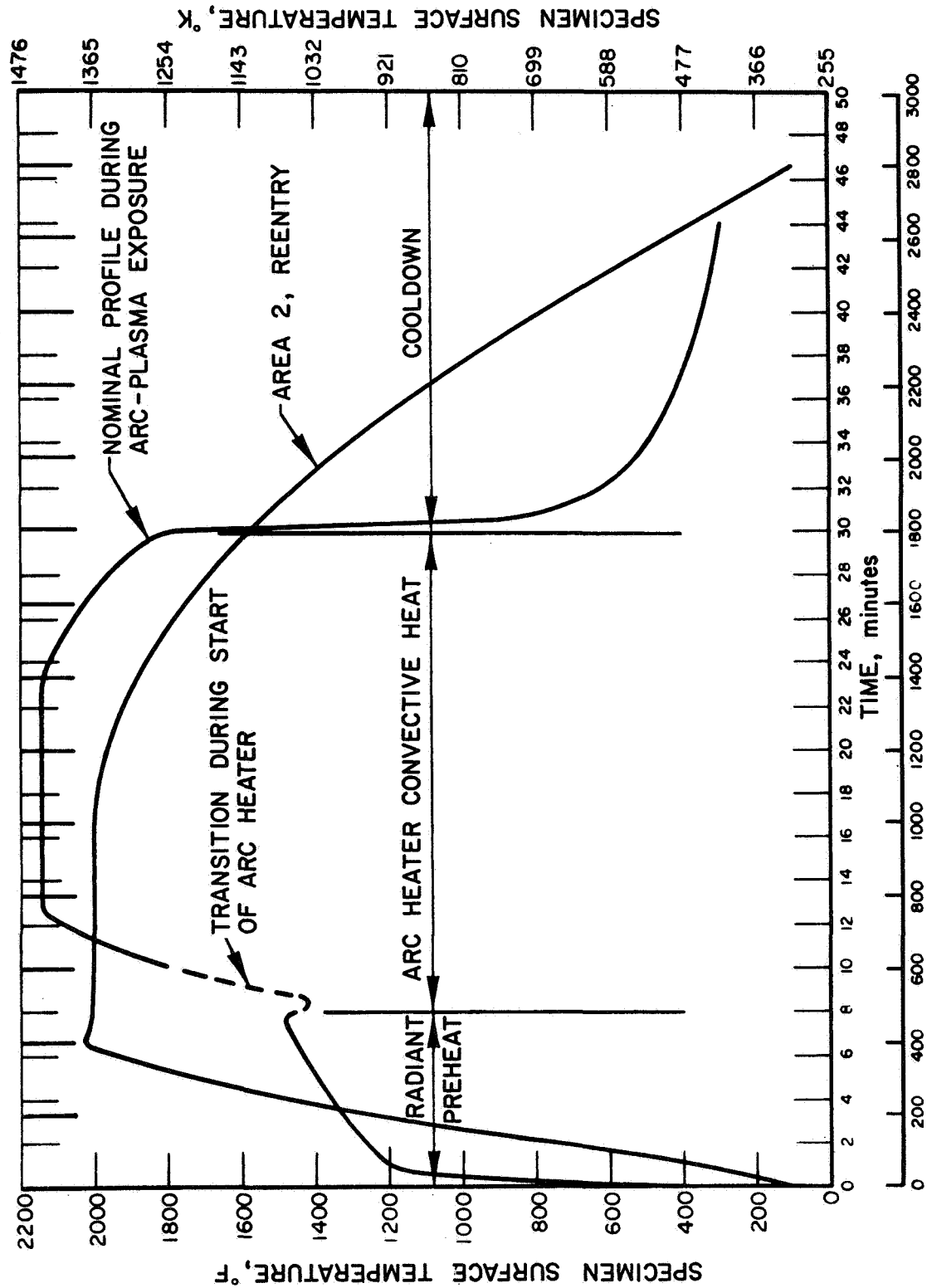


Figure 2

DETAILS OF RSI SPECIMEN HOLDER USED IN PLASMA-ARC EXPOSURES

(Figure 3)

RSI specimens having nominal dimensions of 2.54 x 2.54 x 14.99 cm were tested. Two specimens were tested simultaneously so that the specimen surface area exposed to the test gas was nominally 5.08 x 14.99 cm. In each run, specimens supplied from only one contractor were mounted and exposed. The specimens were paired so that geometric discontinuities at the specimen-to-specimen interface were minimized in order to avoid large temperature nonuniformities at the interface.

The specimens were mounted in a copper model holder 1.9 cm thick with machined passages for water cooling. Overall dimensions of the water-cooled holder are 13.9 cm wide and 26 cm long (gas flow direction). A cutout was provided in the holder for the specimens, which were seated on a 0.62 cm thick aluminum plate located below the water-cooled model holder. The specimens were not bonded to the aluminum plate. The cutout was nominally 5.88 x 15.7 cm and was centered with respect to the width of the holder. The cutout extended from 8.9 cm to 24.7 cm from the leading edge of the holder in the flow direction.

The specimens protruded approximately 0.62 cm below the bottom surface of the water-cooled holder. The aluminum plate, on which the specimens were seated, was fastened to the water-cooled holder. The position of the 0.62 cm thick plate could be readily varied by adjustment of the fastening screws to provide the proper specimen height and orientation relative to the water-cooled holder. Cerafelt insulation, 192 kg/m³ (12 pcf), was placed around the portion of the specimens protruding below the water-cooled holder. This material served to maintain low heat losses from the specimens to the enclosed surroundings beneath the water-cooled model holder.

Zircar insulation was placed between the sides and ends of the specimens and the water-cooled copper to reduce heat losses from the specimens and to minimize stresses induced in the specimens by fastening.

The water-cooled holder was set at an angle of attack of 18 degrees with respect to the test gas stream. This angle was previously used in exposures of metallic space-shuttle candidate TPS materials.

DETAILS OF RSI SPECIMEN HOLDER USED IN PLASMA-ARC EXPOSURES

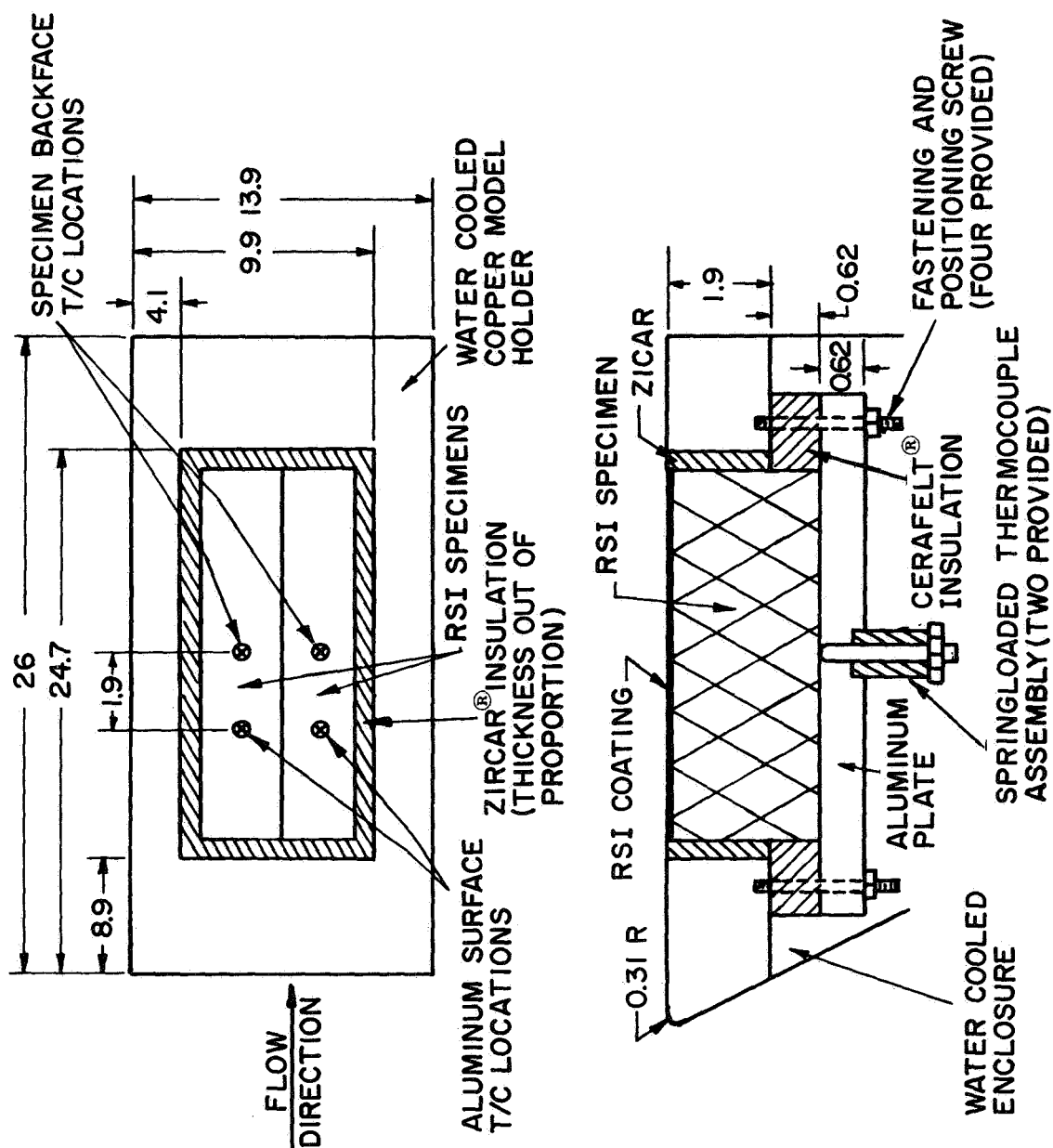


Figure 3

INSTRUMENTATION USED DURING PLASMA-ARC EXPOSURES

(Figure 4)

A spring-loaded, 28-gauge, chromel-alumel thermocouple was used to determine the backface temperature of each specimen during exposure. A light spring was used to avoid penetration of the thermocouple bead into the RSI material.

Two infrared pyrometers were used to measure the surface temperature of the specimens. One pyrometer (Thermodot TD-9) has a centerband sensing wavelength of $0.8\text{ }\mu\text{m}$ and the other pyrometer, manufactured by Ircon, Inc. (Model 300), senses in the wavelength range of 2.0 to $2.6\text{ }\mu\text{m}$ with a peak response of $2.3\text{ }\mu\text{m}$. The response of the TD-9 is relatively insensitive to the surface emittance, whereas accurate knowledge of the surface emittance is necessary to obtain accurate specimen surface temperatures using the Model 300. The TD-9 pyrometer was sighted at the center of one of the specimens (with respect to length and width) and was used for arc-heater control of the gas enthalpy and specimen surface temperature with time. The Model 300 pyrometer was sighted at a location adjacent to the TD-9 site. The Model 300 pyrometer, which is suitable for measuring temperatures as low as 366°K (200°F), was used to obtain specimen surface temperature during preheat and cooldown before and after the arc-plasma exposures. This pyrometer was also used during the time when the arc heater was in operation, although not for control purposes. Also, because the pyrometers were mounted on top of the test cabin, it was necessary to connect the signals for radiation attenuation due to the test cabin window.

Black-and-white infrared photographs were taken during the nominal temperature exposure portion of the cycles to determine the temperature gradients over the entire exposed surface area of the specimens. Kodak HIE 35-mm infrared film was used for these pictures with an 87C filter over the camera lens.

A Spatial Data Datacolor System was used to convert the shades of gray in the infrared photographs to a spectrum of colors. In this technique, the surface temperature variation is displayed by a series of colors.

INSTRUMENTATION USED DURING PLASMA-ARC EXPOSURES

- **BACKFACE THERMOCOUPLES**
- **INFRARED PYROMETRY**

		EMITTANCE SETTINGS		
		MDAC (HCF)	LMSC (LI)	GE (REI)
THERMODOT TD-9	0.8 μ M	0.915	0.84	0.65
IRCON	300 2.3 μ M	0.85	0.9	0.6

- **INFRARED PHOTOGRAPHY**
BLACK AND WHITE 35 MM
COLOR ANALYZER

Figure 4

ENVIRONMENTAL CONDITIONS FOR COATED RSI PLASMA-ARC EXPOSURES

(Figure 5)

Environmental conditions for the RSI materials are summarized in figure 5. The arc heater reservoir pressure was measured experimentally using a pressure transducer and the bulk gas enthalpy was calculated using the energy balance technique. Surface pressures were measured using water-cooled blocks that fit into the water-cooled copper model holder. Surface shear stresses were calculated using a technique described by Harney and Petrie⁽²⁾.

Heat transfer rates were measured at arc heater conditions identical to those needed to obtain the nominal temperature levels for the LMSC and MDAC and GE specimens.⁽¹⁾ Heat-flux calorimeters were positioned in a water-cooled block located in the water-cooled plate in place of the RSI materials. The heat-flux calorimeters were located at approximately 2.29 and 5.33 cm from the leading edge of the cutout in the water-cooled plate. Measured cold wall heat transfer rates for the MDAC/GE arc heater condition are 38 and $32 \times 10^4 \text{ W/m}^2$ for the front and rear calorimeters, respectively. The measured heat transfer rates for the LMSC arc heater condition are 60 and $51 \times 10^4 \text{ W/m}^2$ for the front and rear calorimeters, respectively. Calculated cold-wall heat-transfer rates using the method of Reference 2 are 37 and $33 \times 10^4 \text{ W/m}^2$ for the MDAC/GE condition and 62 and $51 \times 10^4 \text{ W/m}^2$ for the LMSC condition.

ENVIRONMENTAL CONDITIONS FOR COATED RSI
PLASMA-ARC EXPOSURES

SPECIMEN TYPE	SURFACE TEMPERATURE		RESERVOIR PRESSURE ²		GAS TOTAL ENTHALPY		SURFACE PRESSURE ^(a)		AVERAGE SURFACE SHEAR STRESS ²	
	°F	°K	ATM	KN/M	BTU/LB	MJ/KG	Torr	KN/M	PSF	N/M
GE	2135	1440	1.1	112	3500-4300	7.1-10.0	12.5	1.7	2.0	96
LSMC	2135	1440	1.3	132	5800-6600	13.5-15.3	16	2.1	2.1	101
MDAC	2135	1440	1.1	112	3500-4100	7.1- 9.5	12.5	1.7	2.1	101

(a) Based on average of six pressure measurements obtained at one run condition.

Figure 5

COMPARISON OF SPECIMEN SURFACE TEMPERATURES OBTAINED FROM PYROMETERS

(Figure 6)

Specimen temperatures obtained from the pyrometers during the nominal temperature portion of the cycle are compared in figure 6. For the emittance settings used, a maximum temperature difference of approximately 75°K (135°F) is indicated at the two wavelengths. Potential sources of error contributing to the differences in indicated temperatures by the pyrometers are (1) calibration inaccuracies of the pyrometers (calibration accuracies are 33.3°K (60°F) for the Model 300 pyrometer and 15°K (27°F) for the TD-9; (2) arc radiation reflected from the specimen surfaces (e.g., Land has found that the background radiant flux from an arc heater was highest at a wavelength of about 0.5 μm , with a lower peak at a wavelength of 0.8 μm , and a decreasing intensity with increasing wavelength⁽³⁾); (3) differences in infrared transmission of the coatings (limited data published by Lockheed indicate that coating transmission is 0.1 percent or less in the wavelength range of 1.5 to 2.0 μm ⁽⁴⁾); and (4) incorrect values for the coating emittances at the sensing wavelengths of the two pyrometers (relatively little data have been published on the variation of coating emittance with wavelength). On the balance, it appears that the nominal coating temperatures obtained from the pyrometers are in reasonably good agreement.

During the specimen exposures, attempts were made to see if a gray body emittance could be determined by varying the pyrometer emittance settings until the indicated temperatures were identical. However, due to errors associated with arc reflected radiation, nongrayness of the coatings, and inaccuracies associated with the pyrometer calibrations, the resulting emittance values were unrealistic in comparison to published data⁽⁴⁻⁶⁾.

**COMPARISON OF SPECIMEN SURFACE TEMPERATURES
OBTAINED FROM PYROMETERS**

WAVELENGTH μm	μIN.	EMITTANCE SETTING			INDICATED SPECIMEN TEMPERATURE, °K (°F)		
		MDAC	LMSC	GE	MDAC	LMSC	GE
0.8	32	0.915	0.84	0.65	1440 (2135)	1440 (2135)	1440 (2135)
2.0	79	0.85	0.9	0.6	1495 (2230)	1367 (2000)	1367 (2000)

Figure 6

NOMINAL SPECIMEN SURFACE TEMPERATURE VARIATION IN FLOW DIRECTION

(Figure 7)

Nominal leading edge to trailing edge temperature gradients obtained during the nominal temperature portion of the exposures are shown in figure 7. Values of the ratio of the leading-edge-to-trailing-edge temperatures can be compared to a value of 1.14 which was obtained on the basis of laminar convective heat-transfer-rate distribution (fully catalytic wall), negligible axial conduction in the RSI material, and a reradiation-equilibrium exposed-surface boundary condition. The specimen surface temperatures at a distance of 7.6 cm from the leading edge were obtained from the TD-9 pyrometer output at the emittance settings shown in figure 6. Temperatures at 7.6 and 14.2 cm from the leading edge were obtained from (1) a calibration of the infrared film density with relative film energy level, (2) a calculated relationship between the surface temperature and the radiant energy, and (3) a known specimen surface temperature (from the pyrometer) and the corresponding film density.* Thus, although the absolute temperatures may be in error due to errors associated with temperature measurement with the pyrometer, the differences in surface temperature (axial gradient) should be accurate.

538

It can be seen that the highest surface temperature gradients were obtained for the MDAC specimens. A check of the infrared photographs for all of the specimen exposures revealed consistently higher surface temperature gradients for the MDAC specimens than for the GE and LMSC specimens. These high apparent temperature gradients could be due to (1) nonuniform, elevated temperature, coating emittance characteristics at a wavelength of approximately $0.8\text{ }\mu\text{m}$; (2) significantly different coating surface characteristics in terms of reflection of arc radiation as compared with the GE and LMSC coatings; or (3) possible degradation of the coating during elevated temperature exposure, which could change the surface emittance characteristics. Although there was some flow of the MDAC coating as a result of the plasma-arc exposures, this degradation should not have resulted in higher gradients on both the front and rear portions of the specimens.

* See reference (7) for detailed discussion on calibration of infrared film and application of infrared photographic techniques to plasma arc testing.

NOMINAL SPECIMEN SURFACE TEMPERATURE VARIATION IN FLOW DIRECTION			
MATERIAL	DISTANCE FROM LEADING EDGE OF SPECIMEN, CM (INCH)	SPECIMEN SURFACE TEMPERATURE, °K (°F)	RATIO OF LEADING EDGE TO TRAILING EDGE TEMPERATURE
GE	0.76 (0.3)	1460 (2173)	1.09
	7.6 (3.0)	1440 (2135)	
	14.2 (5.6)	1340 (1949)	
LMSC	0.76 (0.3)	1494 (2232)	1.11
	7.6 (3.0)	1440 (2135)	
	14.2 (5.6)	1343 (1954)	
MDAC	0.76 (0.3)	1520 (2273)	1.2
	7.6 (3.0)	1440 (2135)	
	14.2 (5.6)	1266 (1819)	

Figure 7

INFRARED PHOTOGRAPH OF GE SPECIMENS DURING PLASMA-ARC EXPOSURE

(Figure 8)

An infrared photograph of two GE specimens taken during plasma-arc exposure is shown in figure 8. Actually, the photographs of figures 8-10 are negatives so that the hotter leading portions of the specimens appear as dark regions whereas the cooler portions appear as lighter regions.

In spite of the efforts to minimize physical discontinuities at the specimen-to-specimen interface, it can be seen that there is a temperature gradient across the interface. The surface temperatures shown in the figure are those listed previously in figure 7 and were obtained as described in the discussion of that figure. A more comprehensive mapping of the surface temperature distribution can be obtained by recording the photographic density of the transparency according to a fixed grid system. In this way, isotherms of the surface can be displayed such that temperature increments as small as 5°K can be resolved.

**INFRARED PHOTOGRAPH OF GE SPECIMENS DURING PLASMA-ARC
EXPOSURE**

Note: Arc-heated gas flow is from left to right.

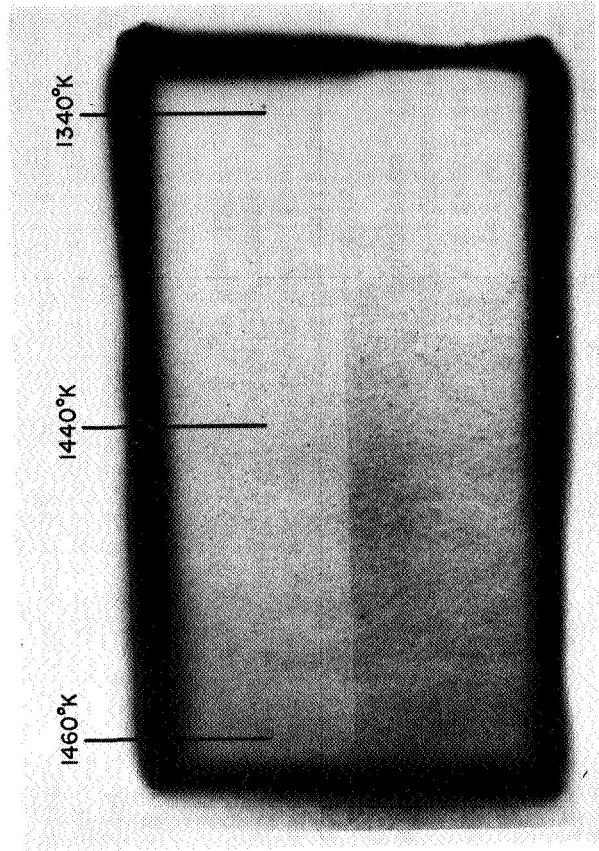


Figure 8

INFRARED PHOTOGRAPH OF LMSC SPECIMENS DURING PLASMA-ARC EXPOSURE

(Figure 9)

An infrared photograph (negative) of two LMSC specimens taken during plasma-arc exposure is shown in Figure 9. It can be seen that the region in which the surface temperature is 1440°K appears darker (hotter) than the corresponding region for the GE specimens (Figure 8). This is due to the higher emissivity of the LMSC coating as compared to the emissivity of the GE coating.

During the plasma-arc exposures, it was necessary to operate the arc heater at higher input power levels in order to achieve the desired nominal maximum surface temperature (1440°K) for the LMSC specimens. Operation at a higher arc-heater power results in a higher gas enthalpy and a correspondingly higher convective heat-transfer rate to the specimens. Several possible explanations for this phenomenon include (1) differences in heat-transfer conduction losses, (2) incorrect (too high) emittance settings on the pyrometers, (3) differences in reflective and transmission properties of the coating, and (4) differences in surface catalytic efficiencies. A check of the reported thermal conductivities and thermal diffusivities of the three insulation materials indicates comparable values with no significant differences among the materials. Also, during the plasma-arc exposures, the LMSC specimens exhibited the lowest backface temperature rise of the three RSI materials.

Pyrometer emittance settings higher than the actual coating emittance would require increased power levels (and gas enthalpies) to obtain the desired nominal surface temperature as indicated by the pyrometer output signal. However, the output of the TD-9 control pyrometer is relatively insensitive to emittance setting, and it is believed that the value used for the LMSC coating surface emittance is reasonably accurate.

Differences in reflective properties of the coatings could also affect the power level needed to achieve the nominal surface temperature. Factors that contribute to this include radiation characteristics of the arc, optical properties of the coating at temperature (transmissivity, emissivity, reflectivity), and topographic properties of the coating. Unfortunately, there is relatively little property information available for the RSI coating systems so that an accurate assessment of their effects cannot be made. However, it is believed that differences in the reflective properties of the coatings would not result in the need to operate at significantly higher power levels for the LMSC specimens.

Differing surface catalytic efficiencies could necessitate operation at different power levels to achieve the same surface temperature. In the plasma-arc exposures, most of the oxygen was dissociated (as compared with a sizable but smaller portion during shuttle entry), and little nitrogen is dissociated. It is possible that differences in surface catalytic efficiencies of the LMSC material as compared with the GE and MDAC materials could have resulted in the need for significantly higher gas enthalpies in order to achieve the same surface temperature.

INFRARED PHOTOGRAPH OF LMSC SPECIMENS DURING PLASMA-ARC
EXPOSURE

Note: Arc-heated gas flow is from left to right.

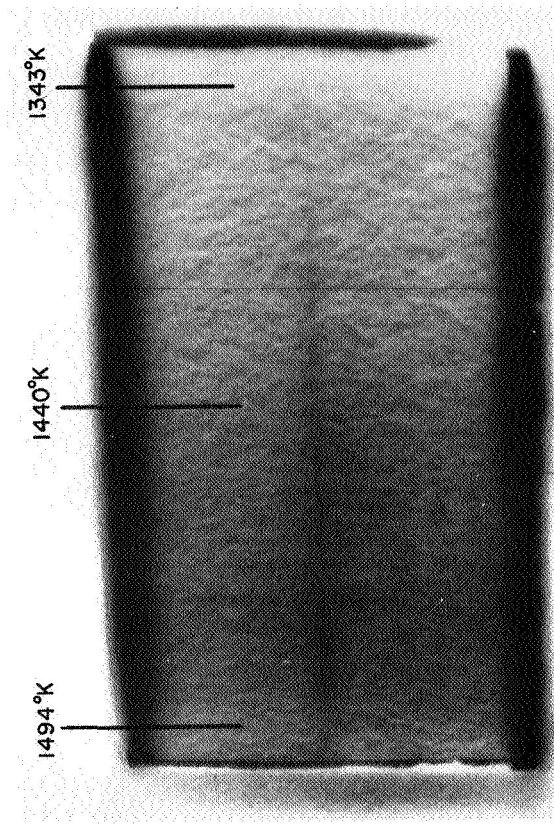


Figure 9

INFRARED PHOTOGRAPH OF MDAC SPECIMENS DURING PLASMA-ARC EXPOSURE

(Figure 10)

An infrared photograph (negative) of two MDAC specimens taken during plasma-arc exposure is shown in figure 10. The region in which the surface temperature is 1440°K is darker than the corresponding region for the GE specimen and lighter than the corresponding region for the LMSC specimen. This is consistent with the relative emittance values of the three coating systems, i.e., LMSC, MDAC, and GE, in decreasing value of coating emittance.

**INFRARED PHOTOGRAPH OF MDAC SPECIMENS DURING PLASMA-ARC
EXPOSURE**

Note: Arc-heated gas flow is from left to right.

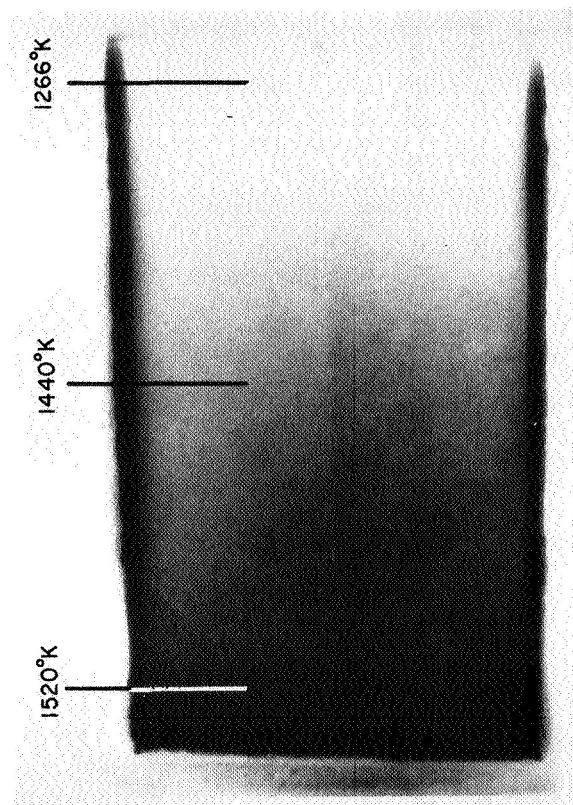


Figure 10

ISODENSITY CONTOURS OF INFRARED PHOTOGRAPH - GE SPECIMENS

(Figure 11)

A color enhanced (reproduced here in black and white) picture of the infrared photograph of the GE specimens is shown in figure 11. In the original, each color represents a photographic density interval considered to be a region of constant temperature. For the Spatial Data Data-color System used to obtain this image enhanced photograph, the number of colors can be varied by altering the density interval to a maximum of 32 colors. In this figure these colors appear as various shades of gray. For a fixed, preselected photographic density interval, the number of colors on the photograph is proportional to the surface temperature gradient.

The temperature discontinuity previously identified in the infrared photograph of figure 8 at the specimen-to-specimen interface can be clearly seen in figure 11. The central portions of the specimens can be characterized as regions of relatively uniform temperature distribution.

ISODENSITY CONTOURS OF INFRARED PHOTOGRAPH - GE SPECIMENS

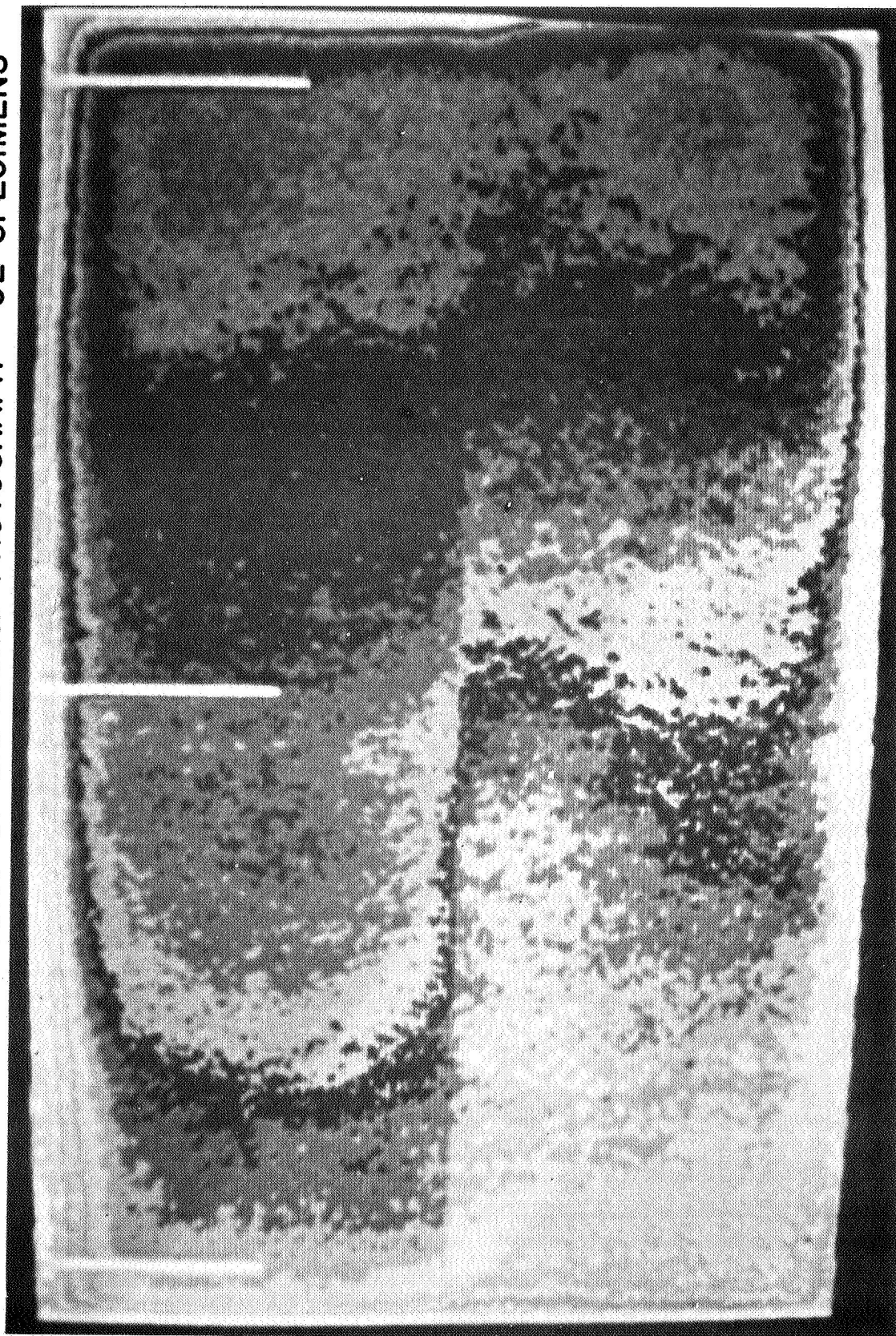


Figure 11

ISODENSITY CONTOURS OF INFRARED PHOTOGRAPH - LMSC SPECIMENS

(Figure 12)

A color enhanced picture of the infrared photograph of the LMSC specimens is shown in figure 12. The density interval used in this photograph is identical to that used in figure 11. It can be seen that the temperature distribution in the central region of the specimens is relatively uniform. The broad light band running from the bottom center to the upper left of the photograph is due to extraneous light present when the photograph of the image enhanced black and white infrared photograph was made.

ISODENSITY CONTOURS OF INFRARED PHOTOGRAPH - LMSC SPECIMENS

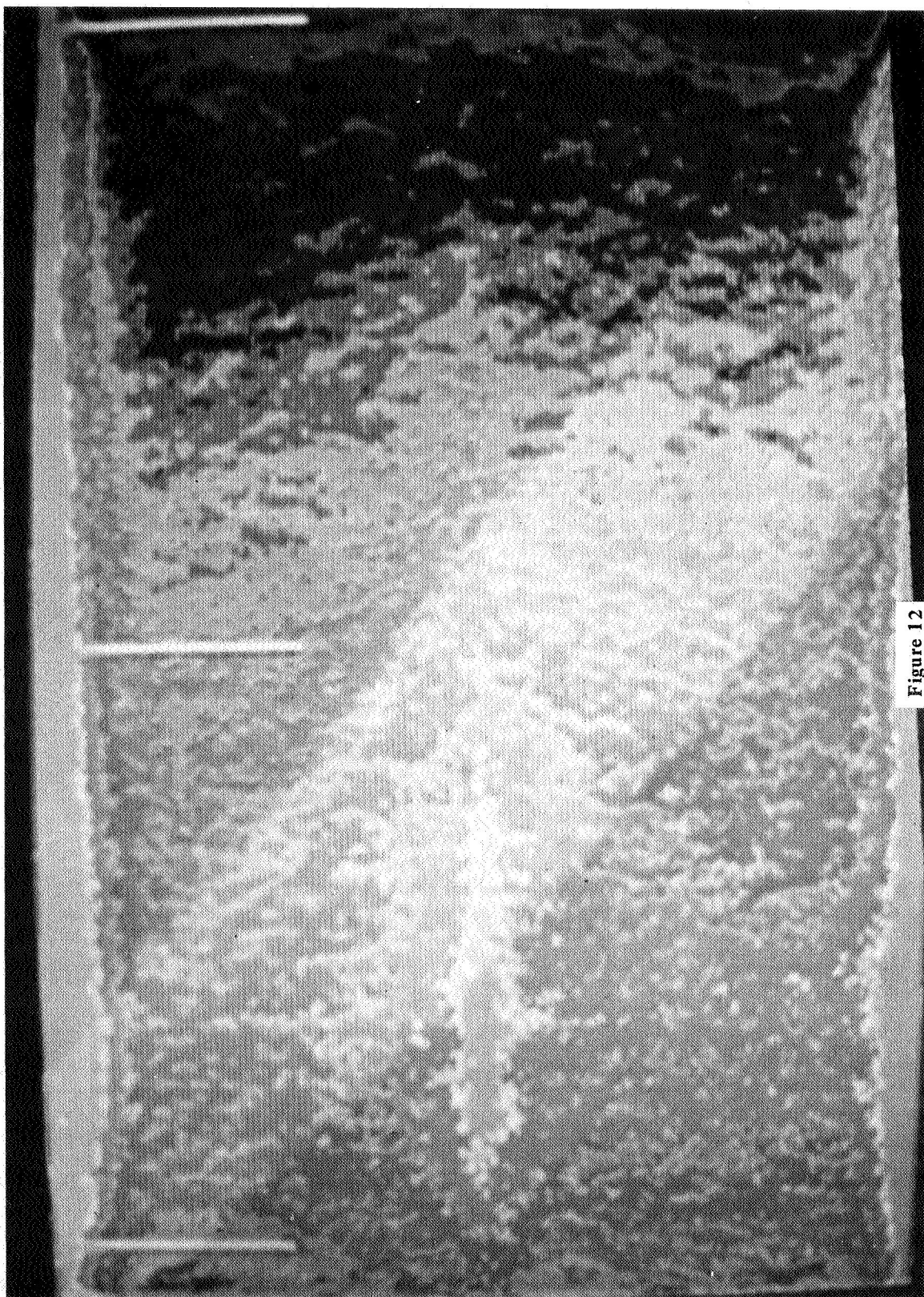


Figure 12

ISODENSITY CONTOURS OF INFRARED PHOTOGRAPH - MDAC SPECIMENS

(Figure 13)

A color enhanced picture of the infrared photograph of the MDAC specimens is shown in figure 13. The relatively high temperature gradients in the central portion of the specimens can be ascertained from the large number of color bands in this region. An identical density increment was used for this photograph as was used for figures 11 and 12.

The temperature range represented by each color in figures 11-13 is approximately 20°K. A finer increment of temperature per color can be achieved by selecting a finer density interval on the Data-color System. This would result in a greater number of constant density intervals for the density range of the photograph.

ISODENSITY CONTOURS OF INFRARED PHOTOGRAPH - MDAC SPECIMENS

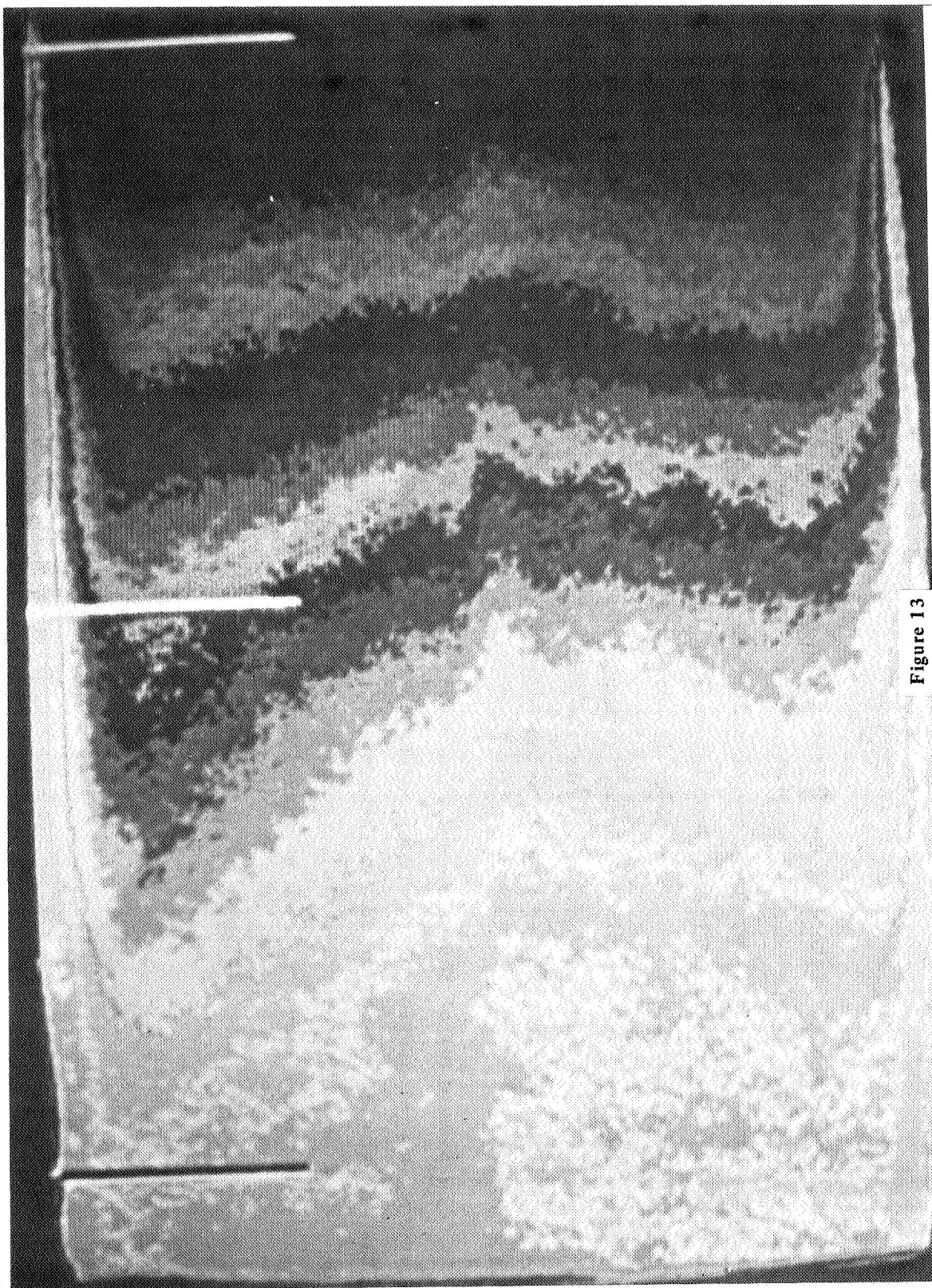


Figure 13

ISODENSITY CONTOURS AND DENSITY PROFILE - MDAC SPECIMENS

(Figure 14)

A color enhanced picture of the infrared photograph of the MDAC specimens is shown in figure 14 along with a plot of the local density value for a section through the RSI material. The density interval used in this picture is one-half that used in figure 13. Thus, there are twice as many color contours for a given temperature interval in this figure as there are in figure 13. The temperature range represented by each color is approximately 10°K.

The amplitude of the plotted curve (as measured from the abscissa through the specimen) at any axial location on the specimen represents the local density or surface temperature. From this plot, the axial surface temperature gradients can be readily determined by direct measurement from the abscissa.

51
52

The percentage of the surface area at any specified temperature level can be automatically obtained by integration of the color bands representing the desired temperature level or increment. This integration is performed electronically within the Datacolor System and the result is displayed on a digital voltmeter. With this technique, it is possible to determine the percentage of the specimen surface above or below specified temperatures.

ISODENSITY CONTOURS AND DENSITY PROFILE - MDAC SPECIMENS

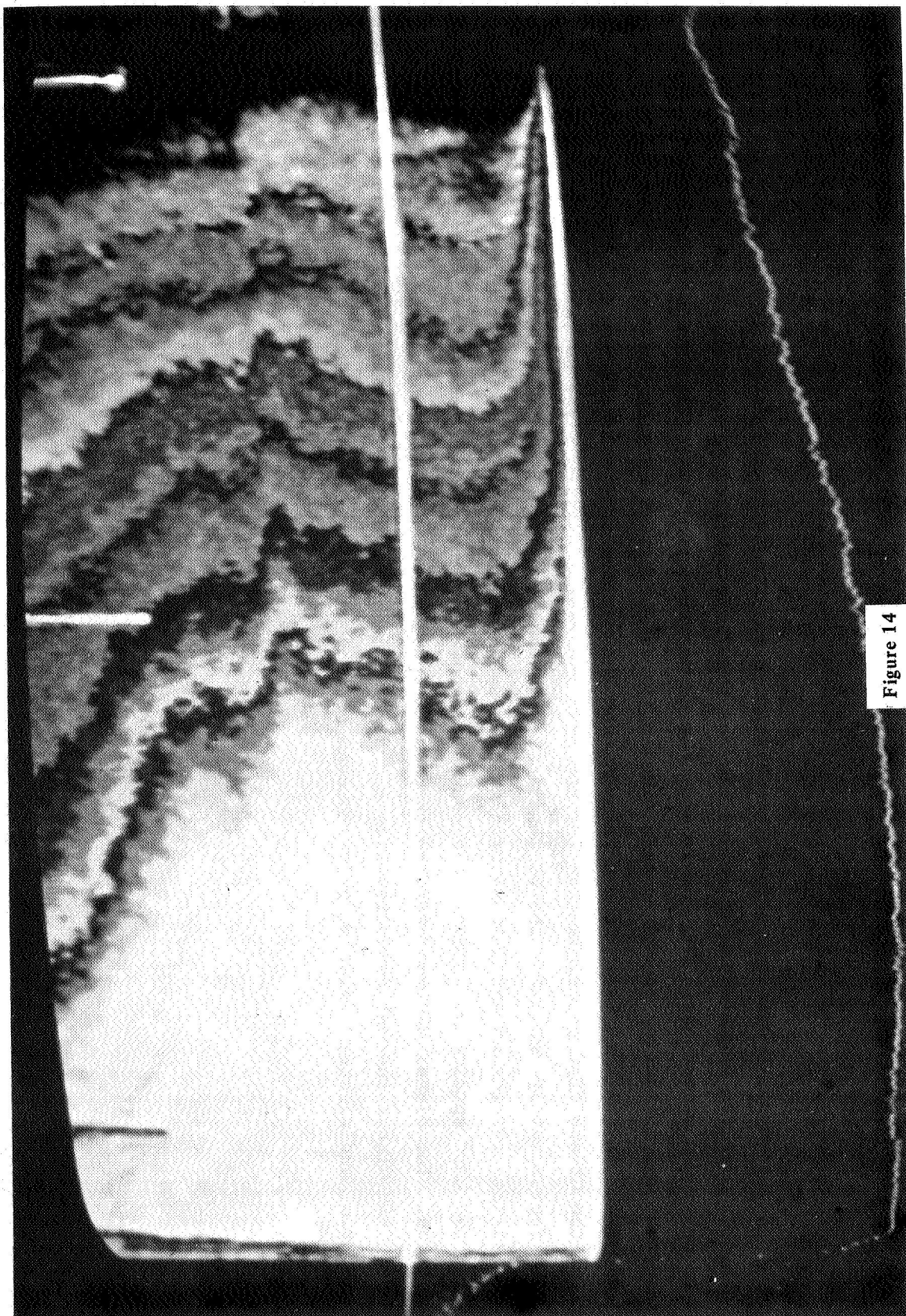


Figure 14

SPECIMEN BACKFACE TEMPERATURES DURING PLASMA-ARC EXPOSURES

(Figure 15)

Representative backface temperature histories for the three RSI materials are shown in figure 15. In each case the temperature histories are for the first cycle of the multicycle test. Also, in order to provide a common basis for comparison, the temperature-time histories have been shifted horizontally so that arc initiation occurs at zero time. This was necessary because the preheat time varied depending on RSI material. It can be seen that the maximum specimen backface temperatures are higher for the GE and MDAC materials than for the LMSC material. Maximum first cycle backface temperatures are approximately 380°K for the GE material, 370°K for the MDAC material, and 320°K for the LMSC material. For the GE and MDAC materials these peaks occurred just prior to termination of the arc. For the LMSC specimens, however, the peak backface temperatures occurred slightly following arc termination. The higher maximum backface temperatures for the GE and MDAC specimens are probably due to slightly higher thermal conductivities and diffusivities of these materials in comparison to the LMSC material and greater radiation shine-through for the larger diameter, mullite fiber materials.

SPECIMEN BACKFACE TEMPERATURES DURING PLASMA-ARC EXPOSURES

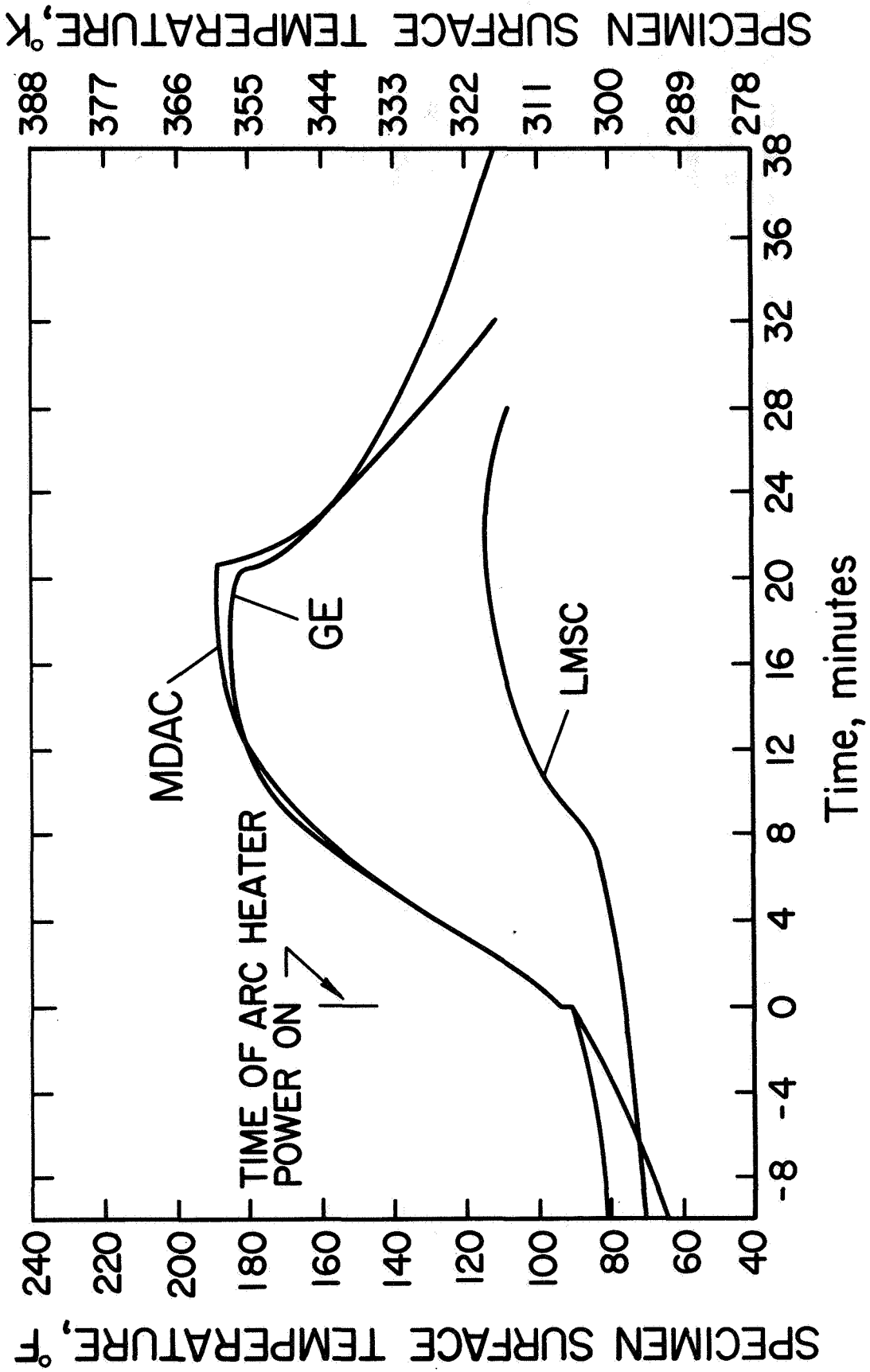


Figure 15

CONCLUDING REMARKS

Relatively accurate surface temperature characterization of RSI materials can be obtained during plasma arc exposures. Infrared pyrometry, infrared photography, and color image enhancement are useful techniques that can be used in arc-heated wind tunnel environments to measure surface temperature levels and degree of temperature uniformity. Variation in surface temperatures as small as 5 to 10°K can be distinguished with the infrared and color enhancement techniques.

Accurate information on specimen emittance and emittance change in a dynamic, plasma-arc environment is difficult to obtain because of pyrometer calibration inaccuracies, arc-reflected radiation, and nongrayness of the surface.

Higher arc-heater power levels are required to heat the LMSC RSI to the nominal surface temperature as compared to power levels needed to achieve the nominal surface temperatures for the GE and MDAC materials. Differences in surface catalytic efficiencies of the coatings are probably responsible for the higher required power levels.

Higher backface temperatures are experienced for the GE and MDAC specimens than for the LMSC specimens.

REFERENCES

1. Bartlett, E.S., et al, "Degradation and Reuse of Radiative-Thermal-Protection-System Materials for the Space Shuttle", Final Report, Battelle Columbus Laboratories, Columbus, Ohio, October 25, 1972, Contract NAS8-26205.
2. Harney, D.J. and Petrie, S.L., "Hypersonic Surface Pressure and Heat Transfer on Slender Bodies in Variable Composition and Nonequilibrium Atmospheres", AFFDL-TR-70-31 (April 1970), 42 pp.
3. Land, D.W., "Superalloy Material Tests in a Plasma Arc Tunnel", Space Simulation, NASA SP-298, May 1972, Paper No. 64, pp. 703-721.
4. "Space Shuttle Thermal Protection System Development", Volume I, Final Report, Lockheed Missiles and Space Company, Inc., LMSC-D152738, January 17, 1972, Contract NAS9-12083.
5. "Reusable Surface Insulation (RSI) Thermal Protection Development for Shuttle", Volume I, Final Report, McDonnell Douglas Astronautics Company-East, MDC EO-557, March 21, 1972, Contract NAS9-12082.
6. "Reusable Surface Insulation Thermal Protection System Development Program", Final Report, General Electric Company, GE-EYP-012, May 1972, Contract NAS9-12084.
7. Kistler, C.W., et al, "Evaluation of Nonmetallic Thermal Protection Materials for the Manned Space Shuttle", Volume V, Final Report, Battelle Columbus Laboratories, Columbus, Ohio, NASA CR-115667, June 1, 1972.

D. A. Stewart
 Ames Research Center
 Moffett Field, California

ABSTRACT

This paper describes the results of a test program in which a preheater was used with an arc plasma stream to study the thermal response of samples of candidate reusable surface insulation (RSI) materials for space shuttle. The convective laminar heating environments simulated include both the shuttle Area 2 and 2P surface temperature and pressure histories as defined by NASA-MSC, while giving a uniform heating rate over the sample surface. A test cycle was composed of 35 minutes of radiant heating and 10 or 15 minutes of convective heating. The preheater was used to simulate the shuttle temperature history during the first and last portions of the test cycle, which could not be simulated by the air arc plasma flow. This investigation was conducted over a convective heating rate range from 225 to 450 kw/m^2 (20 to 40 $\text{Btu/ft}^2\text{sec}$) and at a surface pressure of approximately 810 N/m^2 (0.008 atm). The materials tested included LI-1542 (LMSC), HCF-MOD I and HCF-MOD III (MDAC), and REI-MOD I and REI-MOD 1A (GE). All materials had approximately a 240 kg/m^3 (15 lb/ft^3) density except the REI-MOD 1A, which had a 192 kg/m^3 (12 lb/ft^3) density. The LI-1542 is a high-purity silica rigidized fibrous material and the other materials are basically mullite fibrous materials rigidized with silica or mixed glass binders. The test samples were 10 cm (4 in) diameter cylinders. The cylinder thicknesses were 3.8 cm (1-1/4 in) and 4.8 cm (1-7/8 in). Test samples were mounted on a support consisting of a 0.15 cm (1/16 in) thick aluminum plate bonded to a fiberglass honeycomb and an aluminum baseplate 0.95 cm (3/8 in) thick. Thermocouples were installed within the RSI materials; the output of these and backplate temperature histories were recorded during each test cycle. Pre- and post-test data taken for each of the materials included magnified views, optical properties, and chemical analyses. The test results show that no catastrophic failure occurred during convective heating of the RSI materials tested; however, one of the coatings did fail, and this failure is discussed here. The test results also indicate that the HCF samples experience higher surface temperatures than the other materials at heating rates greater than $\dot{q} = 225 \text{ kw/m}^2$ (20 $\text{Btu/ft}^2\text{sec}$). The REI and LI-1542 coatings show noncatalytic wall behavior. Internal temperature response data for the materials are compared and are correlated with analytical predictions.

PROGRAM GOALS

(Figure 1)

This paper describes the results of a test program that uses an arc plasma stream to evaluate samples of reusable surface insulation (RSI) materials for space shuttle application. Arc plasma evaluations of these materials (silica and mullite) have been conducted by NASA and its contractors for approximately two years using stagnation-region and wedge-mounted samples with essentially an isothermal backwall (refs 1-4). In general, the procedure used in those tests was to insert the test sample directly into the arc plasma stream. In many cases, this resulted in the cracking of the mullite materials due to thermal stresses considerably in excess of those expected in the shuttle environment. A preheater was used in this study to more closely simulate the reentry temperature environment on the shuttle, thereby reducing the thermal stresses to more realistic values.

The primary program goals were to evaluate changes in morphology, optical properties, and chemical composition of the RSI coatings after cyclic arc plasma exposure. The secondary program goals were to evaluate thermal response and surface temperature of the RSI materials during arc plasma exposures. The RSI materials were tested using nearly adiabatic backface model configurations. The investigation was conducted in two parts using second and third generation RSI materials supplied through the Manned Spacecraft Center, RSI contracts, and in-house programs by General Electric, Lockheed, and McDonnell Douglas. The first part of the investigation dealing with coating morphology changes, thermal response, surface temperature, and variation of optical properties of the coatings are discussed in this paper. The second part of the investigation dealing with coating morphology and chemistry changes is reported in another paper in this volume entitled, "Chemical and Morphological Change of Reusable Surface Insulation Coatings as a Function of Convectively Heated Cyclic Testing," by D.B. Leiser, D.A. Stewart, and H.E. Goldstein.

PROGRAM GOALS

EVALUATE:

- CHANGES OF COATING MORPHOLOGY AND CHEMISTRY
- THERMAL RESPONSE OF RSI TILES
- SURFACE TEMPERATURE - CATALYTIC WALL ACTIVITY
- OPTICAL PROPERTIES

Figure 1

MODEL CONFIGURATION

(Figure 2)

The model configurations shown in figures 2 and 3 are 10 cm (4 in) diameter by 3.8 cm (1-1/2 in) thick disks made from RSI materials. The disks are mounted to a 0.15 cm (1/16 in) thick aluminum plate. An adiabatic backwall condition was approximated by using a 1.3 cm (1/2 in) thick fiberglass honeycomb material as insulation between the aluminum backplate and the mounting plate. The first model configuration is shown in figure 2. This configuration consisted of a single RSI sample secured to the backplate with 0.013 cm (.005 in.) thick RTV adhesive.

Chromel-alumel thermocouples were installed through the center of the RSI material at depths of 0.31, 0.64, 1.3, and 3.2 cm (1/8, 1/4, 1/2, and 1-1/4 in.) from the coated surface. Two additional thermocouples were installed at the center and at 3.8 cm (1-1/2 in.) from the center in the 0.15 cm (1/16 in) aluminum backplate. Surface morphology changes, thermal response, and surface temperature data were obtained using this model configuration.

MODEL CONFIGURATION

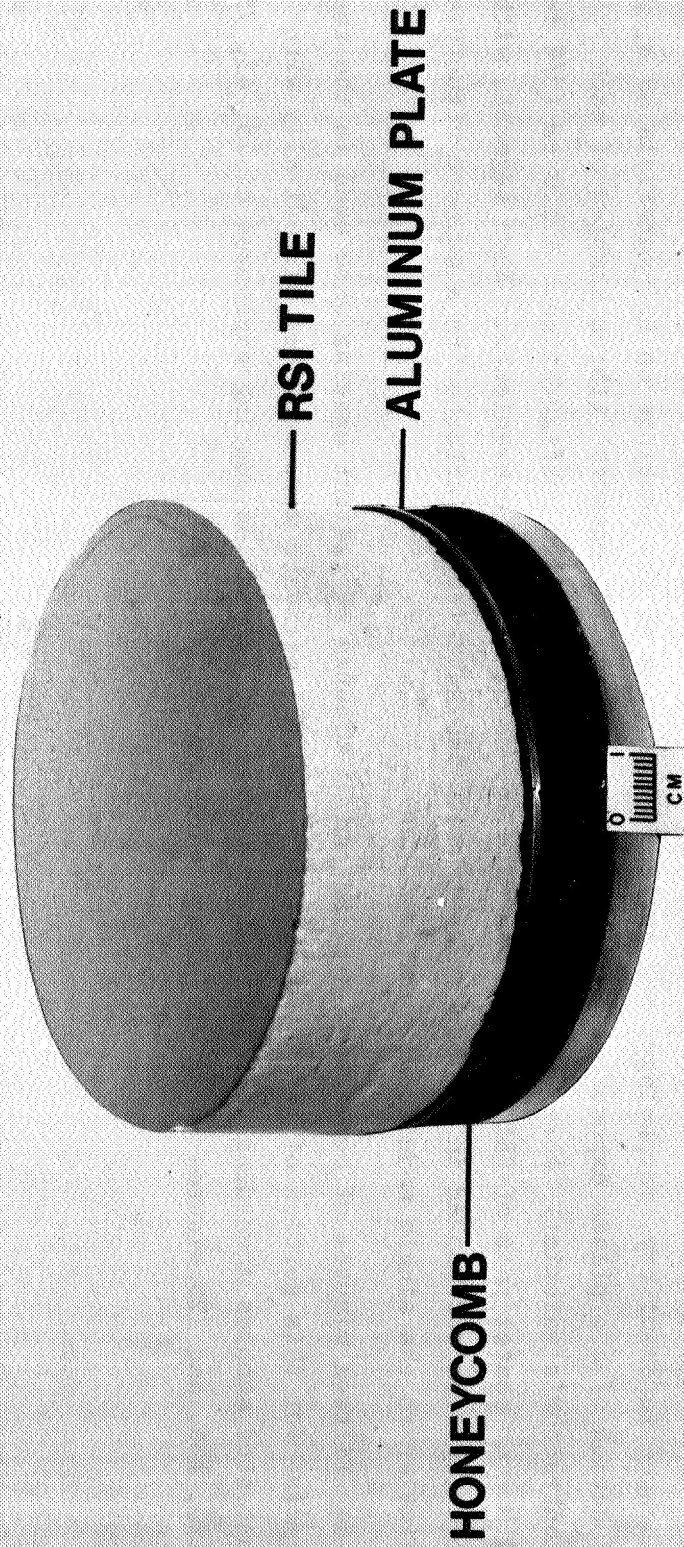


Figure 2

MULTIPLE SAMPLE CONFIGURATION

(Figure 3)

The second model configuration, shown in figure 3, was designed specifically to study the changes in chemistry, morphology, and optical properties of the coatings on RSI materials as a function of arc plasma exposure time. Nine 40° wedge-shaped segments (three samples of each contractor's material) were used to make up the multiple-sample configuration. A 1.0 cm (3/8 in.) diameter center post of RSI material was used for model assembly convenience. Each segment, with two brass screws bonded in the backside with RTV 560 adhesive, is attached to a support structure similar to the single model configuration.

Fifteen minutes of convective heating and 35 minutes of radiant heating were used in the test cycles for this portion of the investigation. The RSI segments were replaced periodically with untested samples according to a test matrix worked out to provide coating exposures of 15, 45, 75, 120, 135, and 225 minutes to an arc plasma environment.

MULTIPLE SAMPLE CONFIGURATION

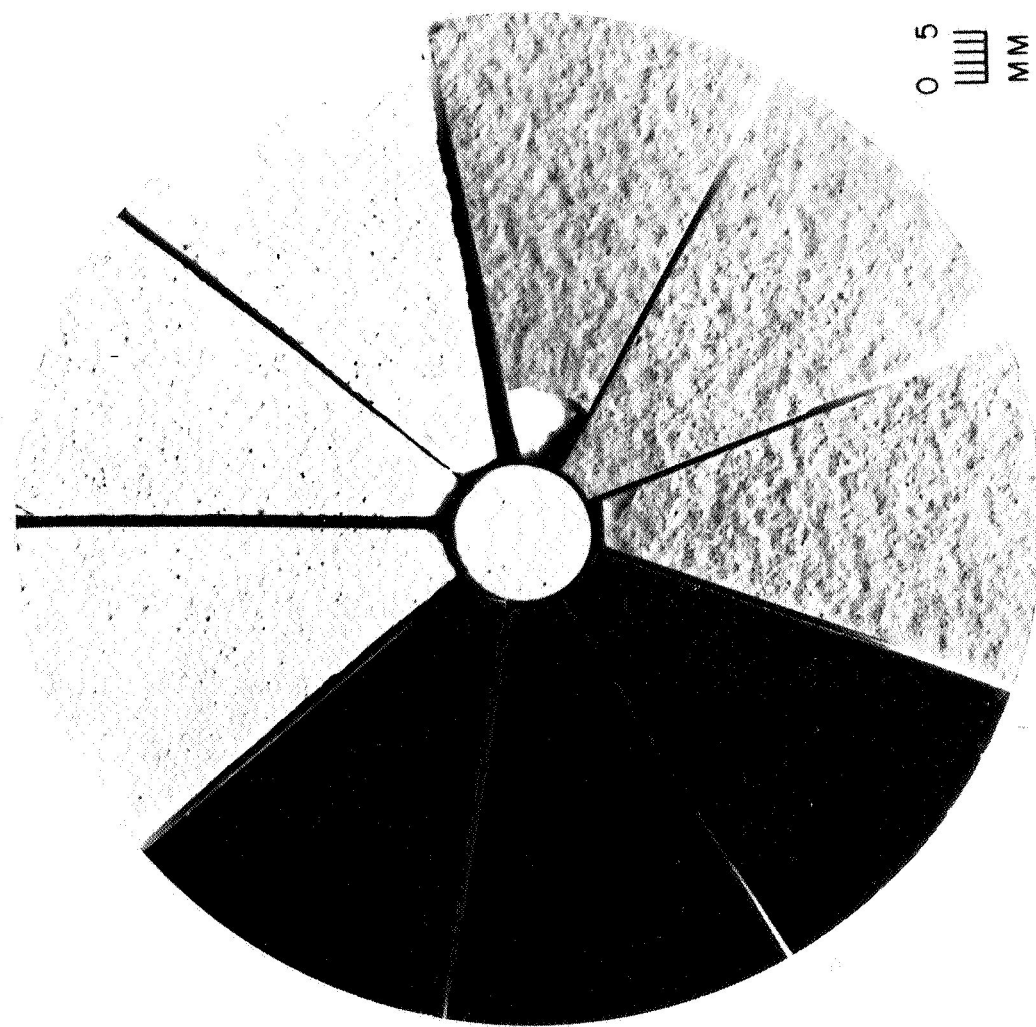


Figure 3

TRAJECTORY SIMULATION USING ARC PLASMA FACILITY AND PREHEATER

(Figure 4)

The model configuration was mounted in the center of a 20 cm (8.0 in) diameter flat-face water cooled copper cylindrical sample holder. The sample holder also contained a calorimeter and two 0.1 cm (0.040 in) diameter pressure orifices located 90° apart and circumferentially on a radius of 6.3 cm (2-1/2 in). A radiant preheater, consisting of a Kanthal-1A wire coil positioned in a spherical cavity in the base of a 60° blunted cone, is shown in front of the sample holder. The blunted cone was made from high purity silica, coated with an emittance agent of silica bonded chromium oxide, and attached to a water-cooled movable support.

Comparisons of the shuttle temperature and pressure reentry simulations with the NASA Area 2P trajectory are shown to the right of this figure. The preheater was used for the initial and final portions of the simulation, and an arc plasma stream was used for the high temperature portion (600 to 1200 seconds) of the simulation. The preheater heated the sample surface to 1367°K (2000°F) at which time the preheater and sample holder were both translated into the arc plasma flow exiting from a 61 cm (24 in) diameter nozzle. The preheater was then removed from the arc plasma stream and the sample was exposed to the arc plasma flow. The reverse procedure was used with the preheater during the cool-down portion of the simulation. During the cool-down (1200 to 3000 seconds) portion of the surface temperature simulation, the arc plasma stream was turned off and the test chamber pressure was increased to simulate the surface pressure history during the later phase of reentry.

Sample surface environmental conditions were determined using measurements from an impact-pressure probe and a 3.2 cm (1-1/4 in) diameter hemispherical calorimeter probe located on the swing-in arm and assuming an equilibrium boundary-layer edge condition. In addition, the stagnation point heating rate to the sample was obtained by correcting the calorimeter measurement taken from the sample holder and using the convective heating rate distribution theory of Lees (refs. 5-6). A more detailed description of the facility is given in reference 7.

TRAJECTORY SIMULATION USING ARC PLASMA FACILITY AND PREHEATER

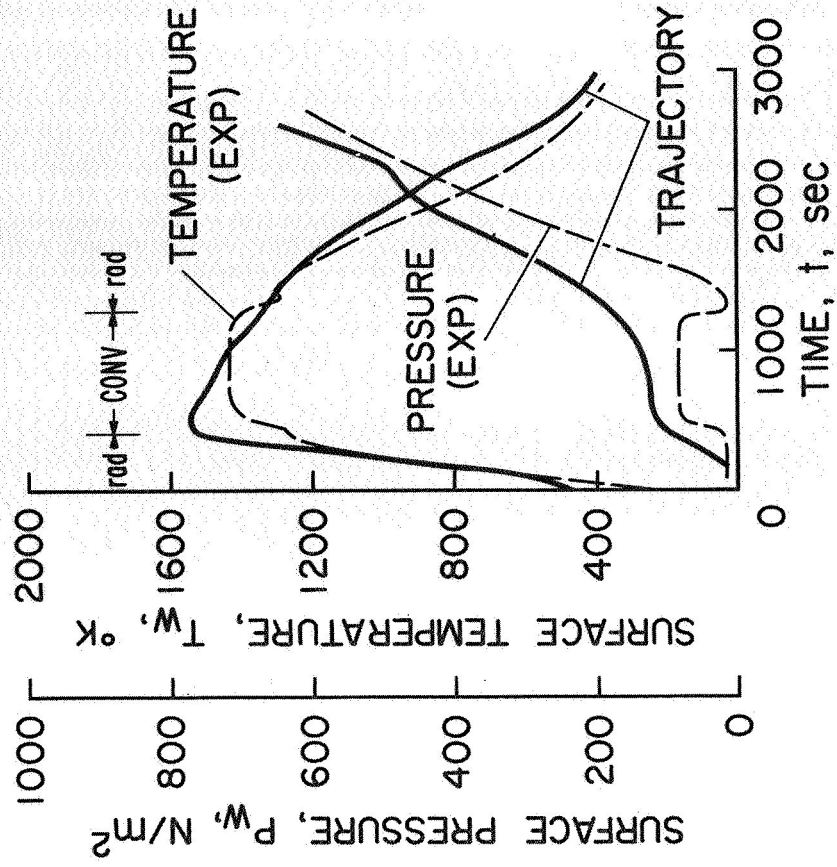
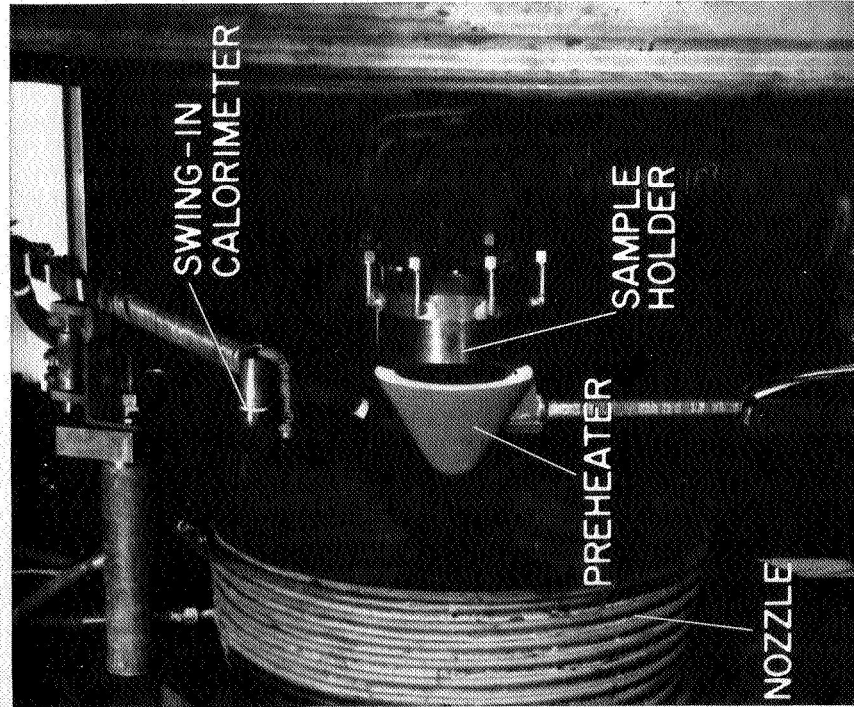


Figure 4

SUMMARY OF ARC PLASMA/RADIANT HEATED TEST RESULTS ON RSI CANDIDATE MATERIALS

$$D = 10 \text{ cm}, P_s = 810 \text{ N/m}^2$$

(Figure 5)

This figure summarizes the tests performed on the RSI candidate materials using the single 10 cm (4.0 in) diameter model configuration. The total number of test cycles for each material given is for more than one RSI sample of LI-1542, HCF-MOD III, and REI-MOD IA. One hundred and seventy test cycles, consisting of 35 minutes of radiant heating and 10 minutes of convective heating were conducted on these materials. Each RSI material was exposed to test conditions of cold-wall stagnation point heating rates (\dot{q}) from 225 kw/m² (20 Btu/ft²sec) to 450 kw/m² (40 Btu/ft²sec) with a surface pressure (P_s) of approximately 810 N/m² (0.008 atm). The surface temperature (T_w) varied from 1311°K (1900°F) to 1627°K (2469°F) on these RSI coatings. The largest variation of the surface temperature 1367°K (2000°F) to 1627°K (2469°F) was observed on the HCF-MOD III coatings. The smallest variation in surface temperature, 1367°K (2000°F) to 1478°K (2200°F), was observed on the LI-1542 coatings. The backplate temperatures (TBP) for the various RSI materials tested are included in the figure. Although these measurements are not directly applicable to the shuttle, they do illustrate the difference in thermal conductivity of the various RSI materials tested.

Two LI-1542 samples were tested. The first sample was tested for 20 cycles at heating rates from $\dot{q} = 225 \text{ kw/m}^2$ (20 Btu/ft²sec) to $\dot{q} = 340 \text{ kw/m}^2$ (30 Btu/ft²sec). The coating on this sample became contaminated during the 20th test cycle due to the failure of a waterline on the model support system. The surface temperature data from these tests at $\dot{q} = 225 \text{ kw/m}^2$ (20 Btu/ft²sec) are used in the catalytic wall activity results. A second LI-1542 sample was then tested for 22 cycles at heating rates from $\dot{q} = 340 \text{ kw/m}^2$ (30 Btu/ft²sec) to $\dot{q} = 450 \text{ kw/m}^2$ (40 Btu/ft²sec).

Three HCF samples were tested. The first was an HCF-MOD I and the other two were HCF-MOD III samples. The HCF-MOD I sample was tested for 30 cycles at heating rates from $\dot{q} = 225 \text{ kw/m}^2$ (20 Btu/ft²sec) to $\dot{q} = 450 \text{ kw/m}^2$ (40 Btu/ft²sec). Repeat cycles at heating rates of $\dot{q} = 340 \text{ kw/m}^2$ (30 Btu/ft²sec) and $\dot{q} = 225 \text{ kw/m}^2$ (20 Btu/ft²sec) were also conducted to check for possible changes in catalytic activity of the coating. The second HCF sample, made from HCF-MOD III material was tested for 28 cycles at heating rates from $\dot{q} = 225 \text{ kw/m}^2$ (20 Btu/ft²sec) to $\dot{q} = 450 \text{ kw/m}^2$ (40 Btu/ft²sec). The third HCF sample tested, also made from HCF-MOD III material, had in-depth thermocouples installed at a radius of 3.8 cm (1-1/2 in) and through the center of the sample ($R = 0$). This sample was tested at heating rates from $\dot{q} = 260 \text{ kw/m}^2$ (23 Btu/ft²sec) to $\dot{q} = 450 \text{ kw/m}^2$ (40 Btu/ft²sec) to determine the relative change in thermal response through a mullite tile as a function of radial position and heating rate.

Four REI samples were tested. First, an REI-MOD I material was tested 33 cycles at heating rates from $\dot{q} = 225 \text{ kw/m}^2$ ($20 \text{ Btu/ft}^2\text{sec}$) to $\dot{q} = 450 \text{ kw/m}^2$ ($40 \text{ Btu/ft}^2\text{sec}$). Next, three samples made from REI-MOD 1A material having a density of 192 kg/m^3 (12 lb/ft^3) were tested. The first of these samples, identified with an asterisk, had a thickness of 4.8 cm ($1\text{-}7/8 \text{ in.}$). This REI-MOD 1A sample was tested at $\dot{q} = 340 \text{ kw/m}^2$ ($30 \text{ Btu/ft}^2\text{sec}$) to provide temperature distribution data for comparison with the other REI materials on an equivalent section weight basis. The second of these REI samples, having a thickness of 3.8 cm ($1\text{-}1/2 \text{ in.}$), was tested at $\dot{q} = 275 \text{ kw/m}^2$ ($24 \text{ Btu/ft}^2\text{sec}$). After severe cracking near the edge of the coating occurred on both of these REI-MOD 1A samples, a third sample, which had a 7.6 cm (3.0 in.) diameter, was tested. This latter REI-MOD 1A sample was tested for 22 cycles at heating rates from $\dot{q} = 340 \text{ kw/m}^2$ ($30 \text{ Btu/ft}^2\text{sec}$) to $\dot{q} = 450 \text{ kw/m}^2$ ($40 \text{ Btu/ft}^2\text{sec}$).

Figures 6 through 9 show the general morphology characteristics of representative LI-1542, HCF-MOD III, and REI-MOD 1A materials after various arc plasma cyclic exposures.

SUMMARY OF ARC PLASMA/RADIANT HEATED TEST RESULTS ON RSI CANDIDATE MATERIALS

D = 10 cm, $P_s = 810 \text{ N/m}^2$

MATERIAL	SAMPLE NUMBER	TOTAL TEST CYCLES	\dot{q} kW/m ²	Heo MJ/kg	T _W °K	T _{BP} °K	REMARKS
LI-1542	1	20	225-340	8.3-11.0	1367-1430	333-335	CONTAMINATED NO CRACKS
	2	22	225-450	8.3-13.8	1367-1478	333-341	
HCF-MOD I MOD III MOD III	1	32	225-450	8.5-13.6	1311-1575	374-421	NO CRACKS CRACK-RAISED AREA NO CRACK
	2	28	225-450	8.8-14.8	1367-1627	372-422	
	3	4	260-450	10.0-13.3	1483-1622	387-410	
REI-MOD I *MOD IA MOD IA MOD IA	1	33	225-450	8.4-13.8	1381-1509	377-406	SMALL EDGE CRACK SEVERE CRACKS SEVERE CRACKS NO CRACKS
	2	3	340	11.0	1456	344	
	3	6	275	9.4	1413	377	
	4	22	225-450	8.4-13.2	1381-1502	377-434	

*4.8 CENTIMETER THICK SAMPLE

Figure 5

LI-1542 TEST SAMPLE

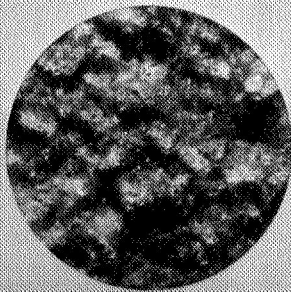
(Figure 6)

A front surface view of the LI-1542 sample after 22 cycles is shown in the center of this figure. This sample was tested for ten cycles at $\dot{q} = 340 \text{ kw/m}^2$ (30 Btu/ft²sec), ten cycles at $\dot{q} = 450 \text{ kw/m}^2$ (40 Btu/ft²sec), a repeat cycle at $\dot{q} = 340 \text{ kw/m}^2$ (30 Btu/ft²sec), and one cycle at $\dot{q} = 225 \text{ kw/m}^2$ (20 Btu/ft²sec). Pre- and post-test magnified views of a 0.30 cm (1/8 in) diameter area at the center and near the edge of the coating were taken at a magnification of 27X with a Macro-Dia apparatus. Some variation in the appearance of the magnified views are apparently due to slightly different angles of the incident light used to illuminate the surface of the sample.

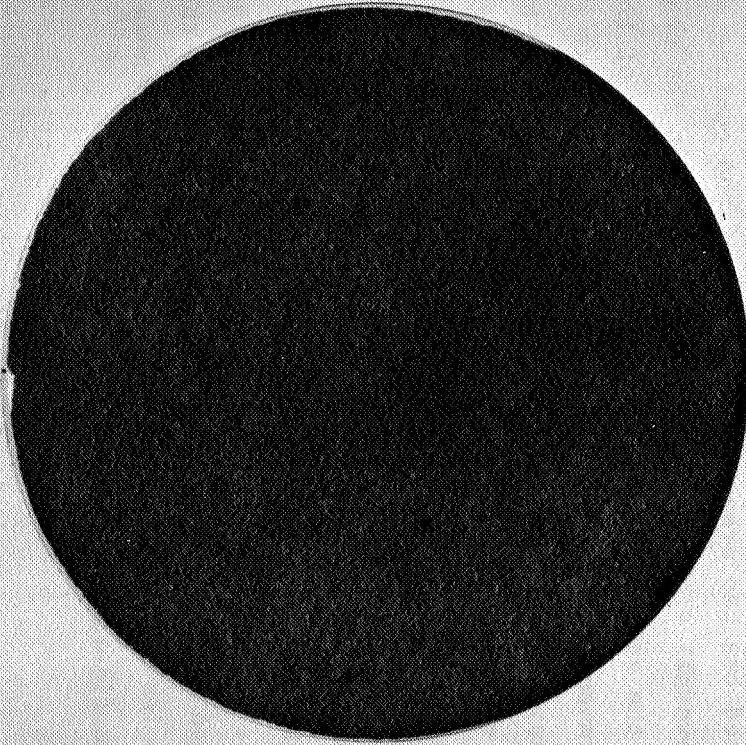
A pre-test magnified view of the coating is shown in the upper left corner of the figure. A magnified view near the edge of the coating after ten cycles at a heating rate of $\dot{q} = 340 \text{ kw/m}^2$ (30 Btu/ft²sec) is shown in the upper right corner. Post-test magnified views are shown in the bottom half of the figure. The left view was taken at the center and the right view was taken near the edge of the sample. The figure shows the morphology changes of the LI-1542 coating are minimal after 22 test cycles at heating rates from $\dot{q} = 225 \text{ kw/m}^2$ (20 Btu/ft²sec) to $\dot{q} = 450 \text{ kw/m}^2$ (40 Btu/ft²sec).

LI1542 TEST SAMPLE

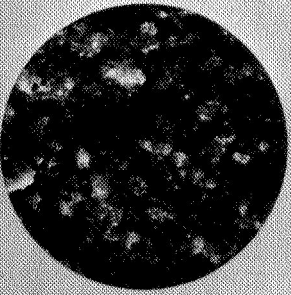
CENTER



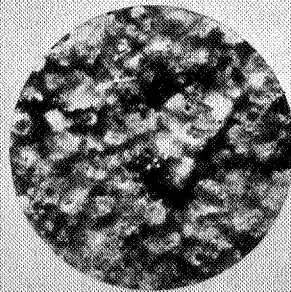
22 CYCLES



EDGE



PRETEST



10 CYCLES

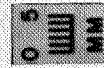
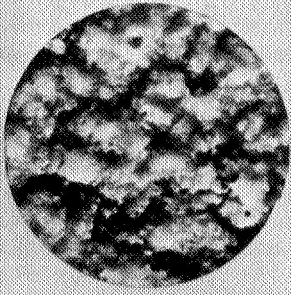


Figure 6

HCF-MOD III

(Figure 7)

The second HCF sample tested is shown in this figure. This sample, HCF-MOD III, is shown after ten cycles at $\dot{q} = 225 \text{ kw/m}^2$ (20 Btu/ft²sec), ten cycles at $\dot{q} = 340 \text{ kw/m}^2$ (30 Btu/ft²sec), and eight cycles at $\dot{q} = 450 \text{ kw/m}^2$ (40 Btu/ft²sec). Due to the failure of a number of in-depth thermocouples and the appearance of a raised cracked area at the center of the coating after 28 cycles the tests were terminated. An overall view of the coating is shown in the center of the figure. The white area at the center of the sample surface is the raised portion of the coating caused by the mechanical failure of a thermocouple just under it. A magnified view of this area of the coating is shown in the lower left corner of the figure. Note the crack (indicated by the shaded area in the lower part of the magnified view) and the advanced state of the foaming of the borosilicate glass in the sublayer of the coating. Again, a pre-test photograph of the coating taken at a magnification of 27X is shown in the upper left corner of the figure. The magnified view in the upper right corner of the figure was taken after ten test cycles each at $\dot{q} = 225 \text{ kw/m}^2$ (20 Btu/ft²sec) and $\dot{q} = 340 \text{ kw/m}^2$ (30 Btu/ft²sec). Note the apparent removal of the potassium silicate sealer coating, microcracks in the remainder of the coating, and forming of the sublayer borosilicate glass after 20 cycles. The coating has become rougher and the foaming of the borosilicate glass in the sublayer has increased after an additional eight cycles at $\dot{q} = 450 \text{ kw/m}^2$ (40 Btu/ft²sec), as shown by the magnified view in the lower right corner of the figure.

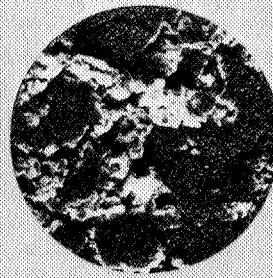
HCF-MOD III

28 CYCLES

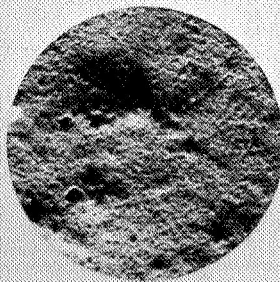
EDGE



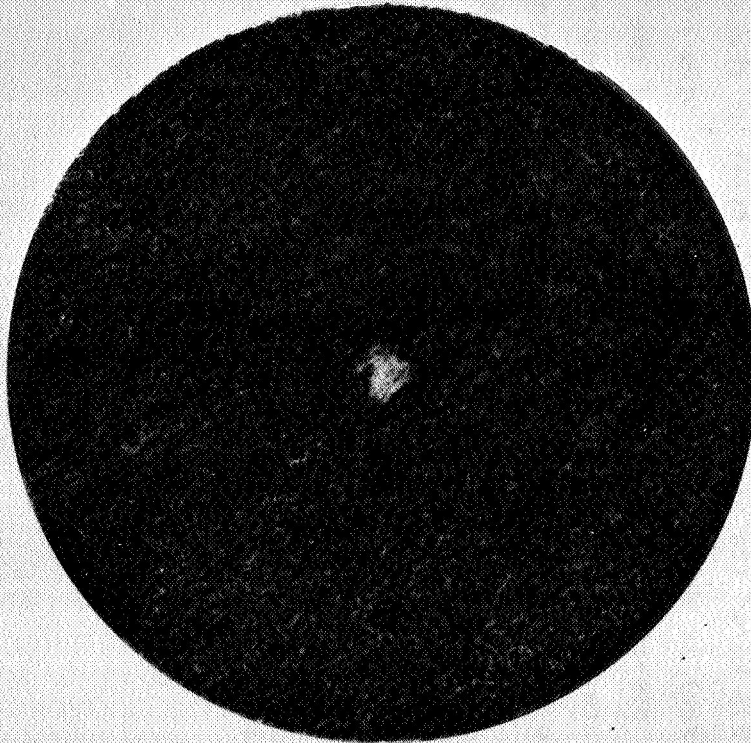
20 CYCLES



CENTER



PRETEST



0 5
MM

Figure 7

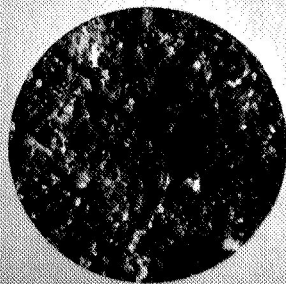
REI-MOD 1A
(Figure 8)

As mentioned earlier, the coating on the two REI-MOD 1A 10 cm (4.0 in) diameter samples cracked severely near the edge. The coating on one sample cracked after three cycles at a heating rate of $\dot{q} = 340 \text{ kw/m}^2$ (30 Btu/ft²sec) and the coating on the other sample cracked after six cycles at a reduced heating rate of $\dot{q} = 275 \text{ kw/m}^2$ (24 Btu/ft²sec). The first of these samples, which was tested at $\dot{q} = 340 \text{ kw/m}^2$ (30 Btu/ft²sec), is shown in this figure. A front view of the sample is shown in the center of the figure. A pre-test magnified view of the center of the coating is shown in the upper left corner of the figure. A post-test magnified view of the center of the coating is shown in the lower left corner and the RSI substrate material just under the coating near the edge of the sample is shown in the lower right corner of the figure. Apparent foaming of the low viscosity glass in this coating is indicated by the post-test magnified view of the center of the coating and explains the color change of the coating from a brownish-green to a gray after exposure to the arc plasma stream. Examination of the coating pieces after the tests indicated that the coating failed at the substrate coating interface. The coating failure is attributed to high thermal stresses caused by either high temperature gradients or a large change in the thermal expansion coefficient of the coating material.

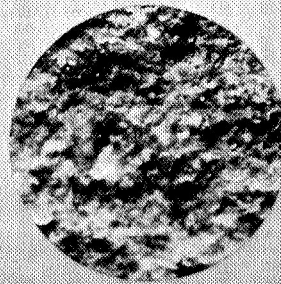
REI - MOD 1A

3 CYCLES

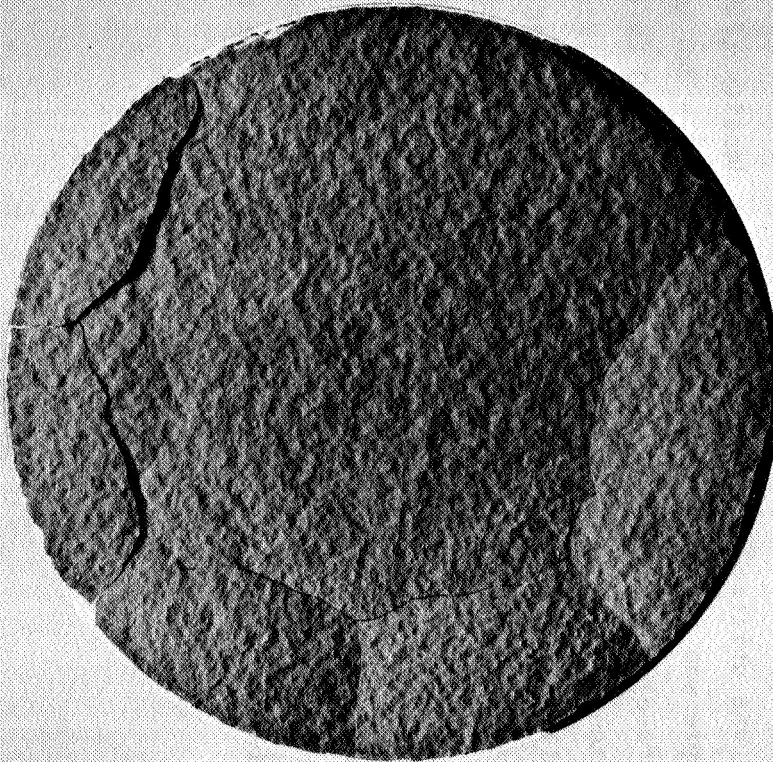
CENTER



PRETEST



EDGE



0 5
MM

Figure 8

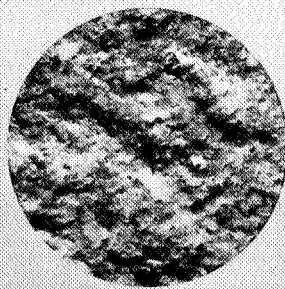
REI-MOD 1A
(Figure 9)

The model configuration used to reduce the thermal stresses near the edge of the REI-MOD 1A sample is shown in this figure after 22 test cycles. The configuration consisted of a 7.6 cm (3.0 in.) diameter REI-MOD 1A sample surrounded with a 1.2 cm (1/2 in.) wide annulus of HCF-MOD III material. The HCF material was utilized because of its higher density (240 kg/m^3 , 15 lb/ft^3) and availability. This REI sample was tested for ten cycles each at $\dot{q} = 340 \text{ kw/m}^2$ ($30 \text{ Btu/ft}^2\text{sec}$) and at $\dot{q} = 450 \text{ kw/m}^2$ ($40 \text{ Btu/ft}^2\text{sec}$). A repeat cycle was taken at $\dot{q} = 340 \text{ kw/m}^2$ ($30 \text{ Btu/ft}^2\text{sec}$), and one additional cycle was taken at $\dot{q} = 225 \text{ kw/m}^2$ ($20 \text{ Btu/ft}^2\text{sec}$) to determine the effect of arc plasma testing on the catalytic wall activity and total emissivity of the coating. The coating did not crack during these tests based on visual observations. Pre-test and post-test magnified views of the center and near the edge of the coating are shown in the figure. These views, as previously mentioned, represent a spot on the coating surface having a 0.3 cm (1/8 in) diameter. A pre-test magnified view is shown in the upper left corner of the figure. Two post-test magnified views taken after 22 cycles are shown in the lower half of the figure. Again, foaming of the low viscosity glass in the coating is apparent from the magnified views and explains the color change of the coating from a brownish-green to a gray.

REI - MOD 1A

22 CYCLES

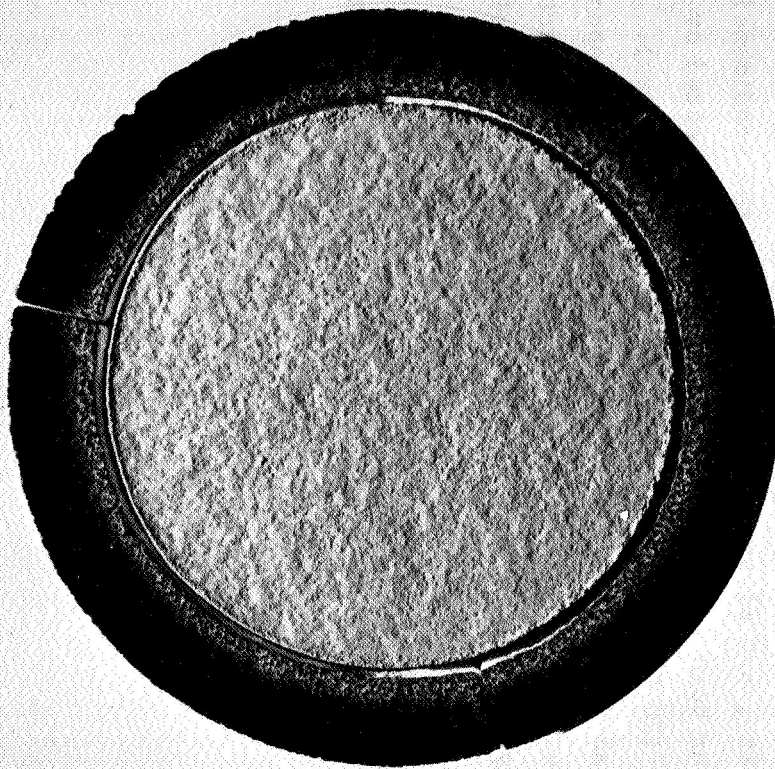
CENTER



PRETEST



EDGE



0 5
MM

Figure 9

TEMPERATURE DISTRIBUTION OF MULLITE AND SILICA AT
1200 SEC AS A FUNCTION OF HEATING RATE

Density = 240 kg/m^3

(Figure 10)

The temperature distributions through a mullite (HCF-MOD III) sample and a silica (LI-1542) sample having the same density, are plotted as a function of the nondimensional RSI thickness. The temperature distributions for both materials were relatively unaffected by increasing the stagnation heating rate from 225 kw/m^2 ($20 \text{ Btu/ft}^2\text{-sec}$) to 450 kw/m^2 ($40 \text{ Btu/ft}^2\text{-sec}$). A one dimensional heat transfer computer program was used to calculate the in-depth thermal response using the measured surface temperatures and thermal conductivity data supplied by the contractors. The prediction for HCF-MOD III and LI-1542 temperature distributions at 1200 seconds into a simulated shuttle Area 2 surface temperature history are compared with experiment at a heating rate of $\dot{q} = 225 \text{ kw/m}^2$ ($20 \text{ Btu/ft}^2\text{-sec}$). The calculations agree reasonably well with the HCF-MOD III data. For the LI-1542 sample, the calculations over-predict the in-depth temperature data for values of $X/L < 0.5$ and agree well for values of $X/L > 0.5$.

TEMPERATURE DISTRIBUTION OF MULLITE AND SILICA AT
1200sec AS A FUNCTION OF HEATING RATE

DENSITY = 240 kg/m³

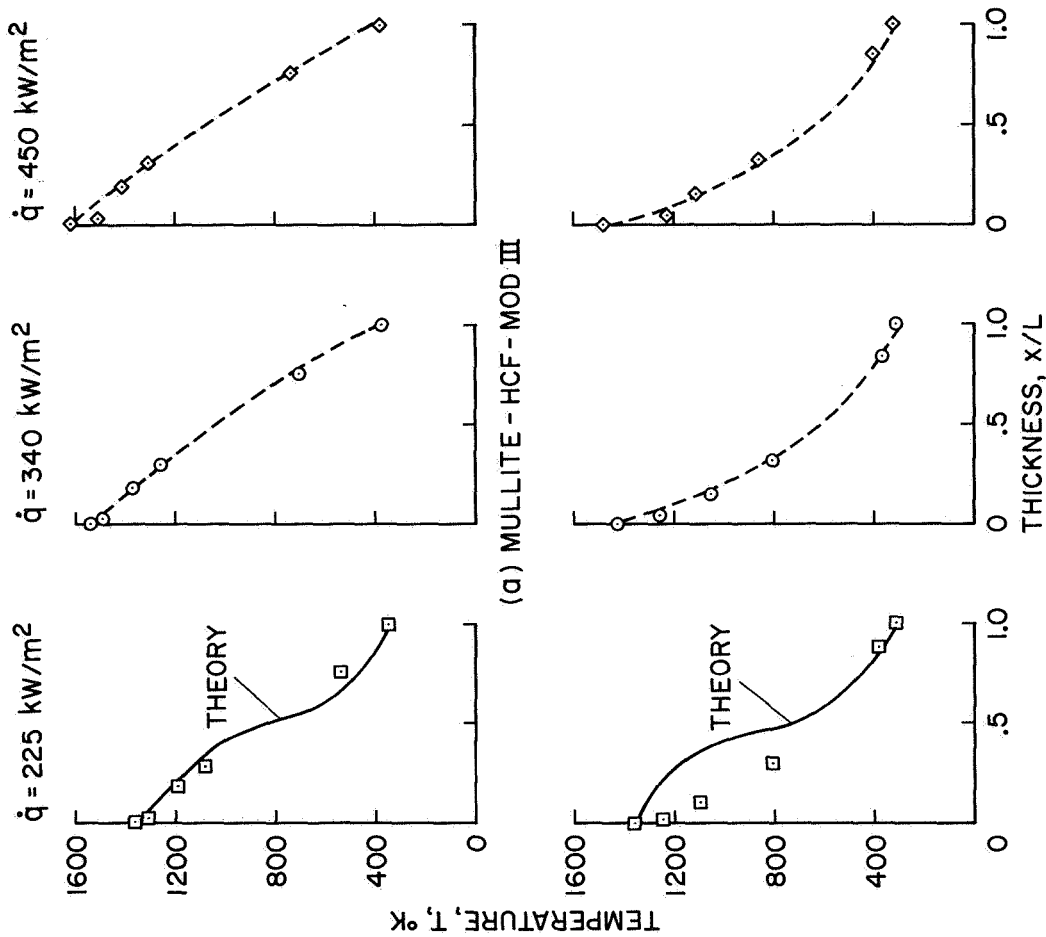


Figure 10

COMPARISON OF RSI TEMPERATURE DISTRIBUTION AT
1200 SEC ON EQUIVALENT SECTION WEIGHT BASIS

(Figure 11)

In this figure the measured internal temperature distributions for the RSI materials in a convective heating environment are compared on an equivalent section weight basis. The temperature distributions through the RSI materials at 1200 seconds into a temperature history simulation using $\dot{q} = 225 \text{ kw/m}^2$ (20 Btu/ft²sec) and $\dot{q} = 340 \text{ kw/m}^2$ (30 Btu/ft²sec) heating rates are plotted as a function of the nondimensional thickness. Starting at the left of the figure, the first comparison was made at $\dot{q} = 225 \text{ kw/m}^2$ (20 Btu/ft²sec) for two 240 kg/m³ (15 lb/ft³) density mullite materials (REI-MOD I and HCF-MOD III). A close similarity between the temperature distribution data for the two materials is shown. The second comparison was made at $\dot{q} = 340 \text{ kw/m}^2$ (30 Btu/ft²sec) between two mullite materials made by General Electric (REI-MOD I and REI-MOD 1A) having densities of approximately 240 kg/m³ (15 lb/ft³) and 192 kg/m³ (12 lb/ft³), respectively. Here the temperature distributions are different. The thermal diffusivity of the REI-MOD I material is greater than the thermal diffusivity of the REI-MOD 1A. The last comparison was also made at $\dot{q} = 340 \text{ kw/m}^2$ (30 Btu/ft²sec) and presents temperature distribution data through a silica (LI-1542) and a mullite (REI-MOD 1A) material having densities of approximately 240 kg/m³ (15 lb/ft³) and 192 kg/m³ (12 lb/ft³), respectively. The temperature distributions through the two materials indicate that the silica material has a lower thermal diffusivity.

COMPARISON OF RSI TEMPERATURE DISTRIBUTION AT 1200 sec ON EQUIVALENT SECTION WEIGHT BASIS

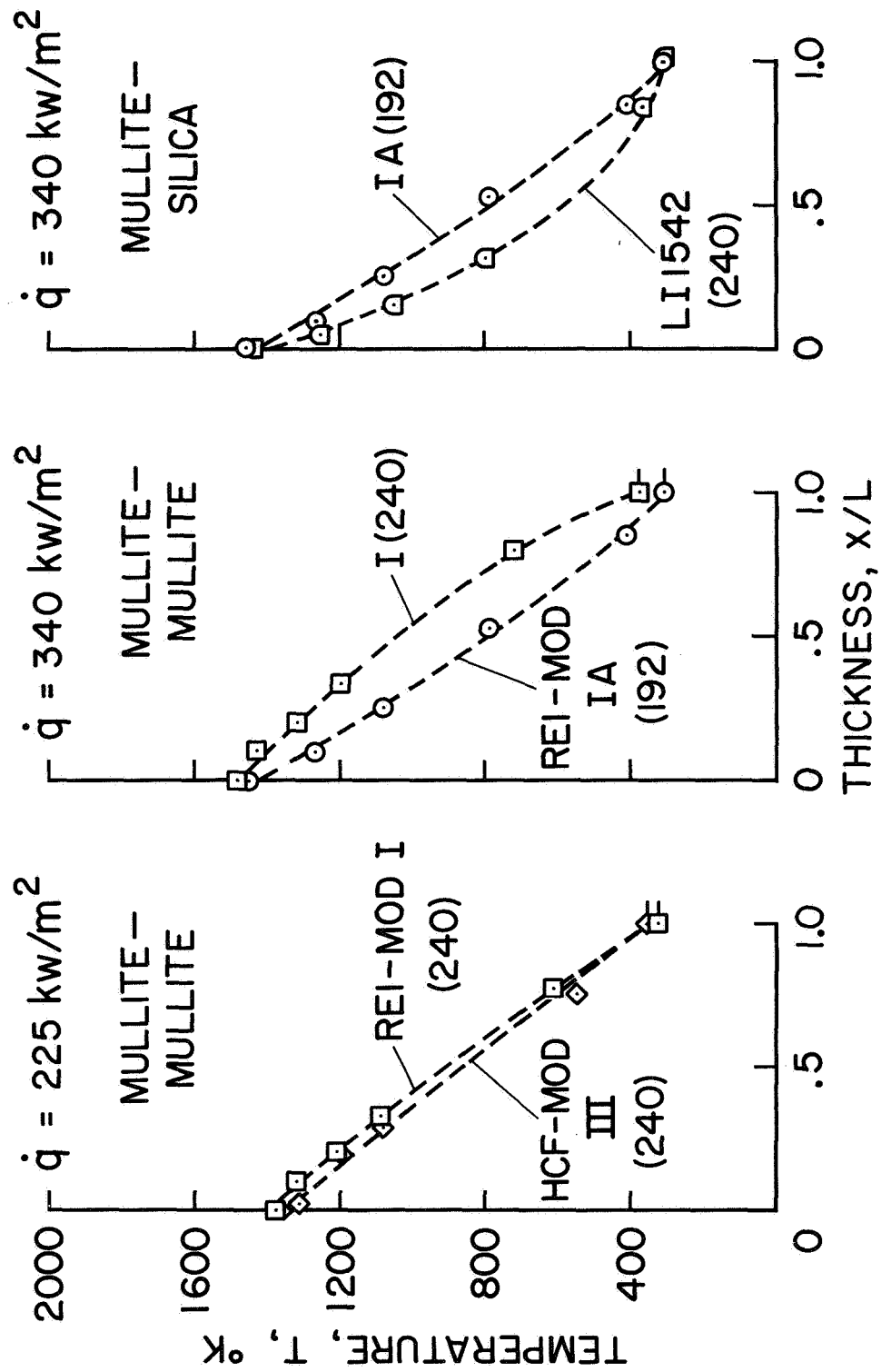


Figure 11

EFFECT OF SURFACE CATALYTIC WALL ACTIVITY ON SURFACE
TEMPERATURE OF RSI COATING

(Figure 12)

The surface temperature of a coating at a given convective heating rate depends on both emissivity and its catalytic efficiency in relation to recombination of atomic oxygen and nitrogen species present in the boundary layer. Surface temperature data (utilizing TD-9 and micro optical pyrometers) are plotted as a function of heating rate for the RSI materials. In order to interpret these data, calculated surface temperatures for fully catalytic and fully noncatalytic surfaces (refs 8-9), using pre-test measured total normal emissivity values at $T_w = 1367^\circ\text{K}$ (2000°F), are included in the plots. These data show the HCF-MOD III with a M5₂₃A7P₇₀₀ coating was most catalytic and the HCF-MOD I with a M5A7 coating was a little less catalytic. The coatings on the LI-1542, REI-MOD I (SR-2), and REI-MOD 1A (SR-2/XSR-2) were essentially noncatalytic over the range of the heating rates investigated. However, the coating on the LI-1542 sample had a fully catalytic surface at the lowest heating rate $\dot{q}_{\text{HW}} = 200 \text{ kw/m}^2$ ($17.6 \text{ Btu/ft}^2\text{-sec}$). Using bulk and surface chemical analyses it was determined that the LI-1542 coating was impervious and the HCF and REI coatings were permeable to copper and silver vapor contaminants in the arc plasma stream and resulted in copper deposition on the surface of the LI-1542 but not on the others. At heating rates above $\dot{q}_{\text{HW}} = 200 \text{ kw/m}^2$ ($17.6 \text{ Btu/ft}^2\text{-sec}$) the surface temperature on the LI-1542 coating was high enough to prevent the deposition of copper and silver.

In summary, the HCF-MOD III exhibits the largest spread in surface temperature data [1367°K to 1627°K (2000°F to 2470°F)] and the LI-1542 the smallest spread in surface temperature [1367°K to 1467°K (2000°F to 2181°F)] because of the catalytic wall activity. The importance of catalytic wall behavior is realized in the interpretation of arc plasma test results, but has yet to be determined in the design weight of a shuttle heat shield.

EFFECT OF SURFACE CATALYTIC WALL ACTIVITY ON SURFACE TEMPERATURE OF RSI COATING

$$P_S = 810 \text{ N/m}^2$$

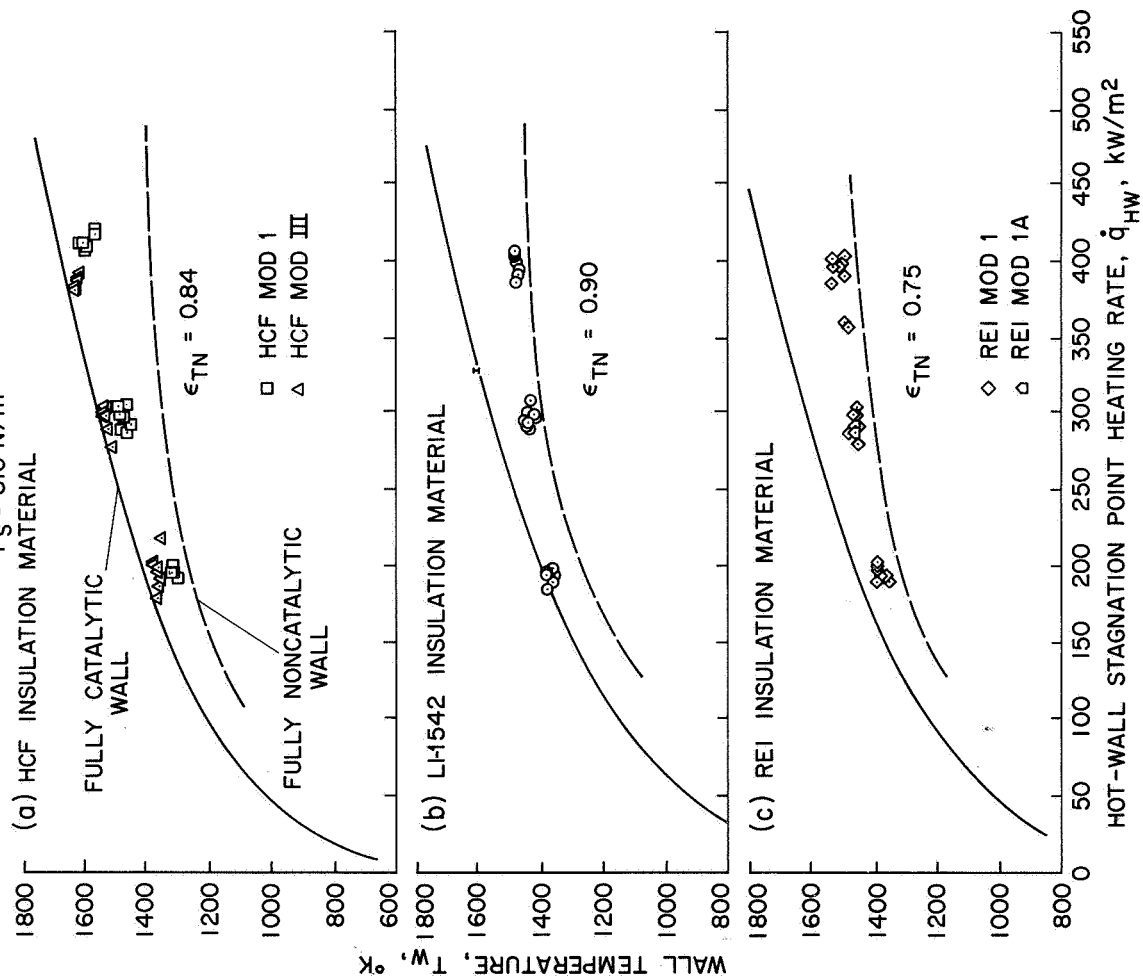


Figure 12

VARIATION OF OPTICAL PROPERTIES OF RSI COATINGS

AFTER ARC PLASMA TESTING

$$q = 340 \text{ kw/m}^2$$

(Figure 13)

The variation of the total hemispherical emittance and the solar absorption coefficient are shown in this figure as a function of arc plasma exposure time at a stagnation point heating rate of $q = 340 \text{ kw/m}^2$ (30 Btu/ft²-sec). Included at the bottom of the figure is the ratio of the two optical properties, α_s/ϵ_{TH} , an important parameter for thermal control of an orbiting space shuttle. The samples from which the optical properties data were obtained were tested at Ames (square symbols), as well as at Aerotherm (circular symbols) (refs. 2-3). The values of the total hemispherical emittance, and the solar absorption coefficients are calculated from room temperature measurements of spectral hemispherical reflectance and spectral normal reflectance obtained using both a Willey 318 (wavelength range of 2.0 to 15.0 microns) and a Beckman DK1A (wavelength range of 0.3 to 2.3 microns) spectrophotometer. The total 15 micron wavelength limitation of the Willey 318 spectrophotometer (ref. 10). However, calculations of the total hemispherical emittance as a function of temperature show the emittance values at $T_w = 1360^\circ\text{K}$ (2000°F) and $T_w = 300^\circ\text{K}$ (80°F) are within 10 percent of the data shown (ref. 2). It is, therefore, believed that the total hemispherical emittance and the ratio, α_s/ϵ_{TH} , are reasonable first approximations for the two above surface temperatures.

The total hemispherical emittance calculated for the HCF-MOD I and HCF-MOD III coatings were in close agreement for arc plasma exposure times greater than 15 minutes. The results for the REI-MOD I and REI-MOD 1A coatings were also similar to each other. Therefore, the data are plotted using only HCF and REI to identify these coatings in the figure. The total hemispherical emittance calculated for the HCF and REI coatings approach constant values of $\epsilon_{TH} = 0.79$ and $\epsilon_{TH} = 0.70$, respectively, after roughly 100 minutes of arc plasma exposure time. The emittance value calculated for the LI-1542 coating was relatively unchanged with arc plasma exposure time. Substantial changes in the calculated total hemispherical emittance occurred for both the HCF and REI coatings during early arc plasma exposure times. These changes in emittance have been correlated with surface chemistry changes as discussed by Leiser, et al., in the second part of this study. A 44°K (80°F) increase in the Area 2 surface temperature on the shuttle during peak heating would result from these variations in the total hemispherical emittance of the coatings. The solar absorption coefficients are plotted at the center of the figure. Considerably less change in the solar absorption coefficient occurred for the LI-1542 compared to the HCF and REI coatings. The variation in the solar absorption coefficient appears to depend on the amount of foaming of the low viscosity glass in the RSI coatings. The coefficient decreases with increasing amounts of foaming of the glass as noted from magnified views of the coatings. At the bottom of the figure the ratio α_s/ϵ_{TH} is plotted. The results show that the effect of convective heating on this parameter is large for the HCF and REI coatings compared to the LI-1542 coating. In addition, the results show that the variation in total hemispherical emittance during the early arc plasma exposure times has a 10 percent effect on α_s/ϵ_{TH} for the HCF coating.

VARIATION OF OPTICAL PROPERTIES OF RSI COATINGS AFTER ARC PLASMA TESTING

$\dot{q} = 340 \text{ kw/m}^2$

□ AMES
○ AEROTHERM

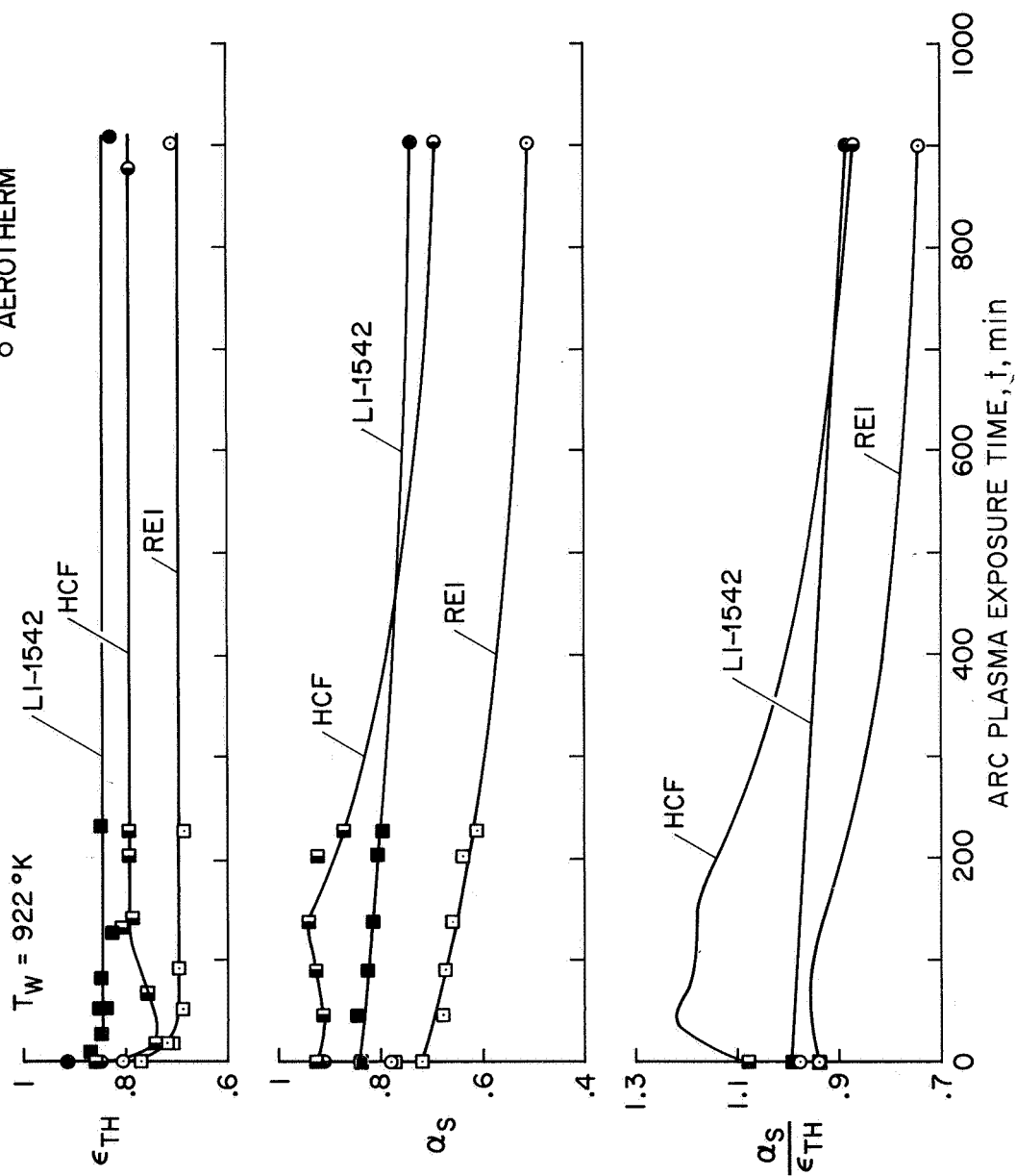


Figure 13

CONCLUSIONS

(Figure 14)

This paper has presented results from tests conducted on RSI materials using a preheater in conjunction with an arc plasma stream to simulate shuttle Area 2 and 2P temperature histories. The following observations are noted:

1. Large changes in coating morphology occur on coatings using low viscosity glasses on mullite tiles with glass foaming resulting in decreases in α_s/ϵ_{TH} after several entry simulations.
2. The HCF-MOD III coating (M523A7P700), a multiple layer coating, lost its potassium-silicate sealer coating early in the testing and had a nearly fully catalytic surface. The LI-1542 and both REI coatings, basically single layer coatings of pigmented glasses, had nearly fully noncatalytic surfaces.
3. The thermal diffusivity of the 240 kg/m³ (15 lb/ft³) density silica material was less than the 192 kg/m³ (12 lb/ft³) density mullite material compared on an equivalent section weight basis. In addition, these data show that the thermal diffusivity of the 240 kg/m³ (15 lb/ft³) density mullite was greater than that of the 192 kg/m³ (12 lb/ft³) density mullite, as would be expected.
4. Large variations in emittance and absorptance were observed on HCF and REI coatings compared to the LI-1542 coating after cyclic arc plasma exposure at a stagnation point heating rate of $\dot{q} = 340$ kw/m² (30 Btu/ft²-sec). The changes in α_s/ϵ_{TH} are attributed to both surface chemistry changes and forming of the low viscosity glasses in the coatings caused by the boundary layer convective heating and low surface pressure.
5. From these data it is apparent that the LI-1542 coating was the most stable and the HCF-MOD III the least stable of the coatings based on changes in surface morphology and optical properties.

REFERENCES

1. Goldstein, H.E. and Stewart, D.A.: "Cyclical Arc Jet Tests of Low Density Refractory Surface Insulation Materials." Space Shuttle Materials National Sample Tech. Conference, Society of Aerospace Materials and Process Engineering, Vol. 3, October 5-7, 1971.
2. Goldstein, H.E., Buckley, J.D., King, H.M. Probst, H.B. and Spiker, I.K.: "Reusable Surface Insulation (RSI) Materials Research and Development." NASA TM X-2570, May 30, 1972.
3. Schaefer, J.W. and Vojvodich, N.S.: "Test Program for Thermal Screening of Candidate Shuttle Vehicle TPS Materials." Final Oral Report, NASA, ARC, Contract NAS2-6445, June 1972.
4. Rinehart, W.A. and Painter, J.H.: "Cyclical Tests of Selected Space Shuttle TPS Materials in a Plasma Arc Tunnel." Technical Monitor Vojvodich, N.S., Contract NAS2-6601, Final Review for NASA, ARC, June 14, 1972.
5. Marvin, J.G. and Sinclair, R.A.: "Convective Heating in Regions of Large Favorable Pressure Gradient." AIAA Journal, Vol. 5, No. 11, November 1967.
6. Stewart, D.A. and Marvin, J.G.: "Convective Heat-Transfer Rates on Large-Angle Conical Bodies at Hypersonic Speeds." NASA TN D-5526, 1969.
7. Centolanzi, F.J., Probst, H.B., Lowell, C.E. and Zimmerman, N.B.: "Arc Jet Tests of Metallic TPS Materials." NASA TM X-62092.
8. Marvin, J.G. and Akin, C.M.: "Pressure and Convective Heat-Transfer Measurements in a Shock Tunnel Using Several Test Gases." NASA TN D-3017, 1965.
9. Pope, R.B.: "Stagnation-point Convective Heat Transfer in Frozen Boundary Layers." AIAA Journal, Vol. 6, No. 4, 1968, pp 619-626.
10. Holman, J.P.: "Heat Transfer," McGraw-Hill Book Company, New York, Chapter 8, 1968, pp 211-264.

$\psi\omega_0$

ARC JET TESTS OF RSI MATERIALS - [†]
SCREENING AND COMPARATIVE EVALUATION[†]

John W. Schaefer*

Aerotherm Division, Acurex Corporation
Mountain View, California

Nick S. Vojvodich**
NASA Ames Research Center
Moffett Field, California

[†]Work presented here was performed under Contracts NAS2-6445 and NAS2-6600.

* Assistant Manager.

** Research Scientist.

CONTRACT TEST PROGRAM OBJECTIVES (NAS2-6445)

(Figure 1)

An extensive screening test program including a comparative evaluation of candidate RSI materials was performed under cyclic convective heating conditions (ref. 1).* The RSI materials evaluated were LI-1500, HCF, REI, and silicon carbide foam. The test samples were nominally exposed to 30 half hour cycles at conditions that covered the spectrum of surface temperature and heat flux appropriate to the application of RSI materials to the shuttle orbiter vehicle.

The test configurations and procedures maximized efficiency and minimized cost by utilizing multiple (up to six) test samples in each test model, and by employing continuous testing of two models, which were alternately exposed to the test stream. The test model and test sample designs allowed a quick change of test samples, which employed common instrumentation, to minimize turnaround time between each series of cyclic tests.

Measurements were made during each cycle and nominally after every six cycles to define thermal response in terms of surface and in-depth temperatures, mass loss and surface recession, surface properties in terms of emissivity and catalycity, failure modes, and operating limits. A calibration test series was also performed to measure the distribution of properties across the test stream and across the model face, and to measure surface catalycity effects.

* Metallics, carbon-carbon composites, and ablators were also evaluated under the program.

CONTRACT TEST PROGRAM OBJECTIVES (NAS2-6445)

- PROVIDE A TEST STREAM WHICH SIMULATES THE EXPECTED SHUTTLE ORBITER REENTRY ENVIRONMENT (HEATING, ENTHALPY, PRESSURE)
- DESIGN AND FABRICATE A TEST SAMPLE AND MODEL CONFIGURATION WHICH MAXIMIZES DATA AND MINIMIZES ASSOCIATED TEST COSTS
- CONDUCT CYCLIC SCREENING TESTS OF ALL TPS CANDIDATES WITH SUFFICIENT INSTRUMENTATION TO PROVIDE THE FOLLOWING COMPARATIVE INFORMATION:
 - SURFACE AND IN-DEPTH TEMPERATURE RESPONSE CHARACTERISTICS
 - SURFACE PROPERTIES (EMITTANCE AND SURFACE CATALYTICITY)
 - MASS LOSS AND SURFACE RECESSION
 - RESPONSE CHARACTERISTICS AND FAILURE MODES

SCOPE AND COST OF TESTS

(Figure 2)

The total facility test time for all material types - metallics, RSI, carbon-carbon composites, and ablators - was 271-1/3 hours and the total sample exposure time was 870 hours. For the RSI tests, the facility time was 131-1/2 hours and the sample exposure time was 288 hours.

At maximum testing efficiency the demonstrated test cost was as low as \$70 per hour of exposure, which, with a six sample model configuration, resulted in a cost of roughly \$12 per sample hour.

SCOPE AND COST OF TESTS

	FACILITY HOURS	SAMPLE HOURS
● METALLICS	82-1/4	487-1/2
● SURFACE INSULATORS (RSI)	131-1/2	288
● CARBON-CARBON COMPOSITES	54-1/4	91
● ABLATORS	3-1/3	3-1/3
●	COST PER FACILITY HOUR = \$70 MINIMUM	
●	COST PER SAMPLE HOUR = \$12 MINIMUM	

Figure 2

DESCRIPTION OF RSI MATERIALS TEST

(Figure 3)

The types of RSI materials tested were LI-1500, with five different coating versions; HCF, with three different coating versions; REI; and silicon carbide foam. The most extensive testing was performed on the LI-1500 and HCF versions. Direct comparative performance results were obtained for LI-1500, HCF, and REI (two sets of three 120° samples) for a total of 30 sample hours on each material.

DESCRIPTION OF RSI MATERIALS TEST

MATERIAL	FABRICATOR	NUMBER OF DIFFERENT COATINGS	BASIC MATERIAL SYSTEM	SAMPLE HOURS
LI-1500	LMSC	5	SILICA	104
HCF	MDAC	3	MULLITE	102
REI	GE	1	MULLITE	30
SIC FOAM	LMSC	-	SILICON CARBIDE	51

TEST SETUP

(Figure 4)

The test program was performed in the Aerotherm 1.5 MW arc plasma facility, and the hyperthermal test stream was generated by the Aerotherm 300 kW constrictor arc heater. The test gases were nitrogen and oxygen in proper proportion to yield the composition of air. A conventional convergent/divergent nozzle with a 0.025-meter (one-inch) throat diameter and 0.203-meter (eight-inch) exit diameter was employed. The test model configuration was a flat-face stagnation point model which was 0.121-meters (4-3/4 inches) in diameter.

TEST SETUP

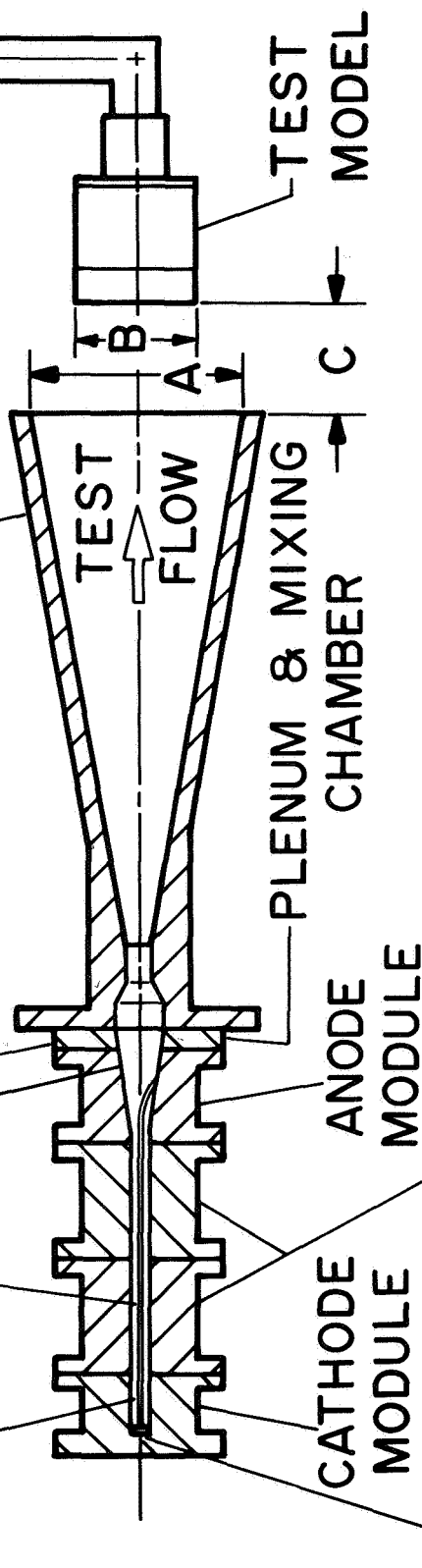
ALTERNATE OXYGEN
INJECTION

COPPER ANODE

OXYGEN
INJECTION

AXISYMMETRIC
NOZZLE

NITROGEN
INJECTION



DIMENSION	METERS	INCHES
A	.203	8.00
B	.121	4.75
C	.102	4.00

Figure 4

MODEL CONFIGURATION

(Figure 5)

The flat-face model configuration was chosen for convenience in test sample fabrication, and was 0.121 meters (4-3/4 inches) in diameter with a 3.2 mm (1/8-inch) corner radius. This model body diameter allowed the maximum practical test sample size consistent with uniform property distributions across the test samples for the 0.203 m (8 in) dia. test stream and the projected test conditions. The test models were made of copper and were water cooled. They included a centerpost containing a calorimeter and pressure tap for continuously monitoring conditions throughout each test. A peripheral copper ring was employed to ensure that the test samples were not exposed to any unusual thermal or aerodynamic edge effects.

The RSI test samples were 120° (as illustrated) or 180° pie-shaped configurations which were 0.025 meters (one-inch) thick. The test samples and models incorporated the necessary quick-change capability for optimum testing efficiency. The test samples were removed simply by removing the retention pins in the peripheral ring. Spring-loaded thermocouples were used throughout to eliminate the requirement for disconnecting instrumentation leads. These thermocouples were located at 60° intervals in a circular pattern through the central region of the test samples.

Surface temperature was measured with an infrared optical pyrometer (TD-9 or TD-7). The pyrometer was mounted on an oscillating mechanism, which indexed the pyrometer in 60° increments in the same circular pattern defined by the spring-loaded thermocouples. Surface recession was measured with a microscope micrometer (no surface contact), mass loss was measured with an analytic balance, and qualitative documentation of the sample response was performed through post-test 35 mm color still photography.

MODEL CONFIGURATION

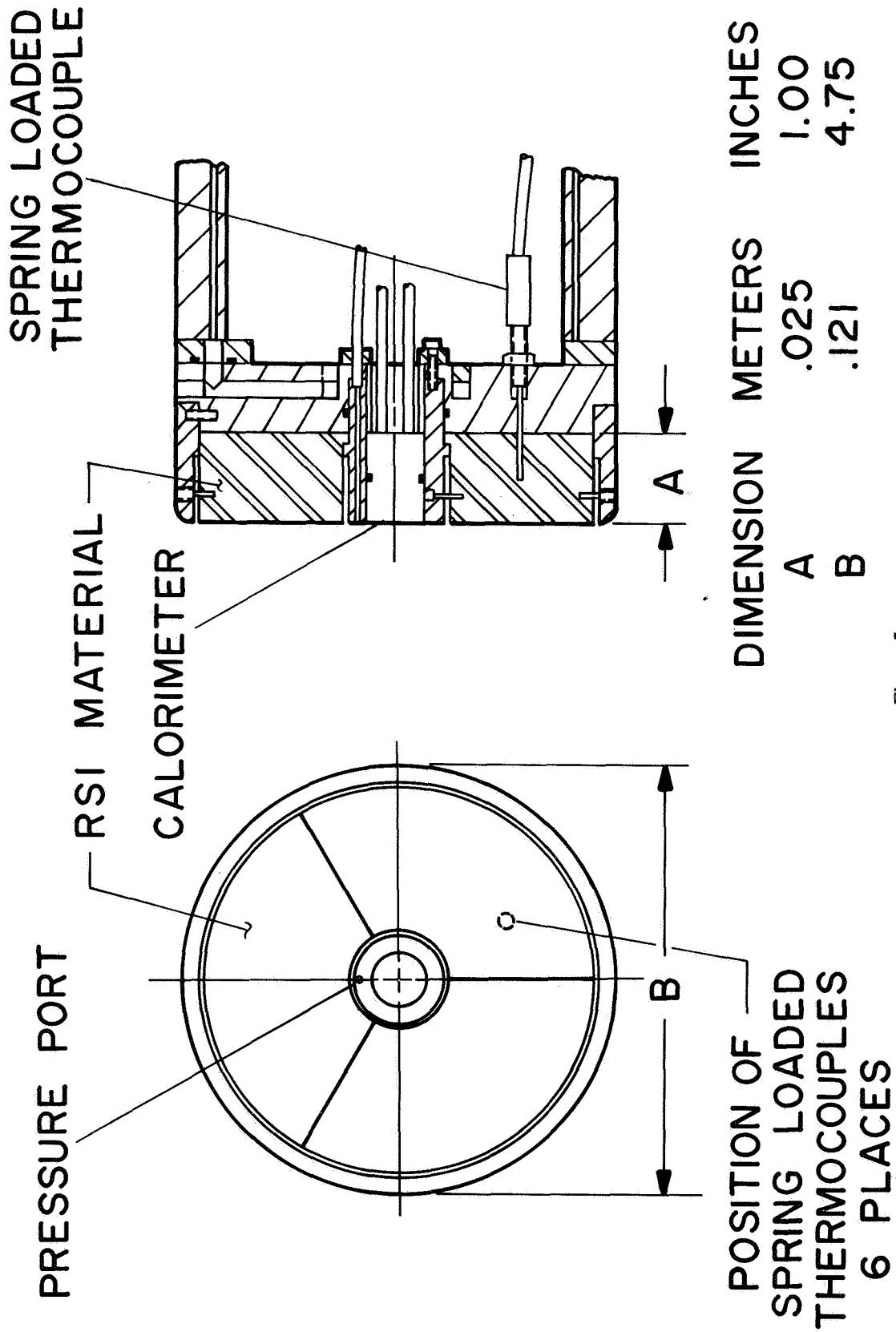


Figure 5

NOMINAL TEST CONDITIONS

(Figure 6)

Tests were run over a range of heat flux primarily at a single stagnation pressure, 6.08×10^2 N/m² (0.006 atm), and therefore single heat transfer coefficient, 0.019 kg/m²sec (0.0038 lb/ft²sec). One test series was run at the nominal baseline heat flux of 3.4×10^5 W/m² (30 Btu/ft²sec) but at a higher stagnation pressure, 14.2×10^2 N/m² (0.014 atm), and heat transfer coefficient, 0.028 kg/m²sec (0.0058 lb/ft²sec), to check the effect of these variables.

Testing was nominally performed in blocks of six 30-minute cycles on each of two test models. The models were alternately exposed to the test stream for the required 30 minute intervals. Between each model change, a calibration model of the same configuration as the test sample models and containing six calorimeters and six pressure taps was also exposed to the test stream for a test condition check and reference. The facility therefore was run for approximately 6-1/2 hours continuously--3 hours (6 cycles) on each of the two test sample models and approximately 1/2 hour on the calibration model. In an 8-hour shift, the remaining 1-1/2 hours were occupied by test sample changes and measurements. Much of the program was performed on a two-shift basis, resulting in facility operation of over 65 hours a week.

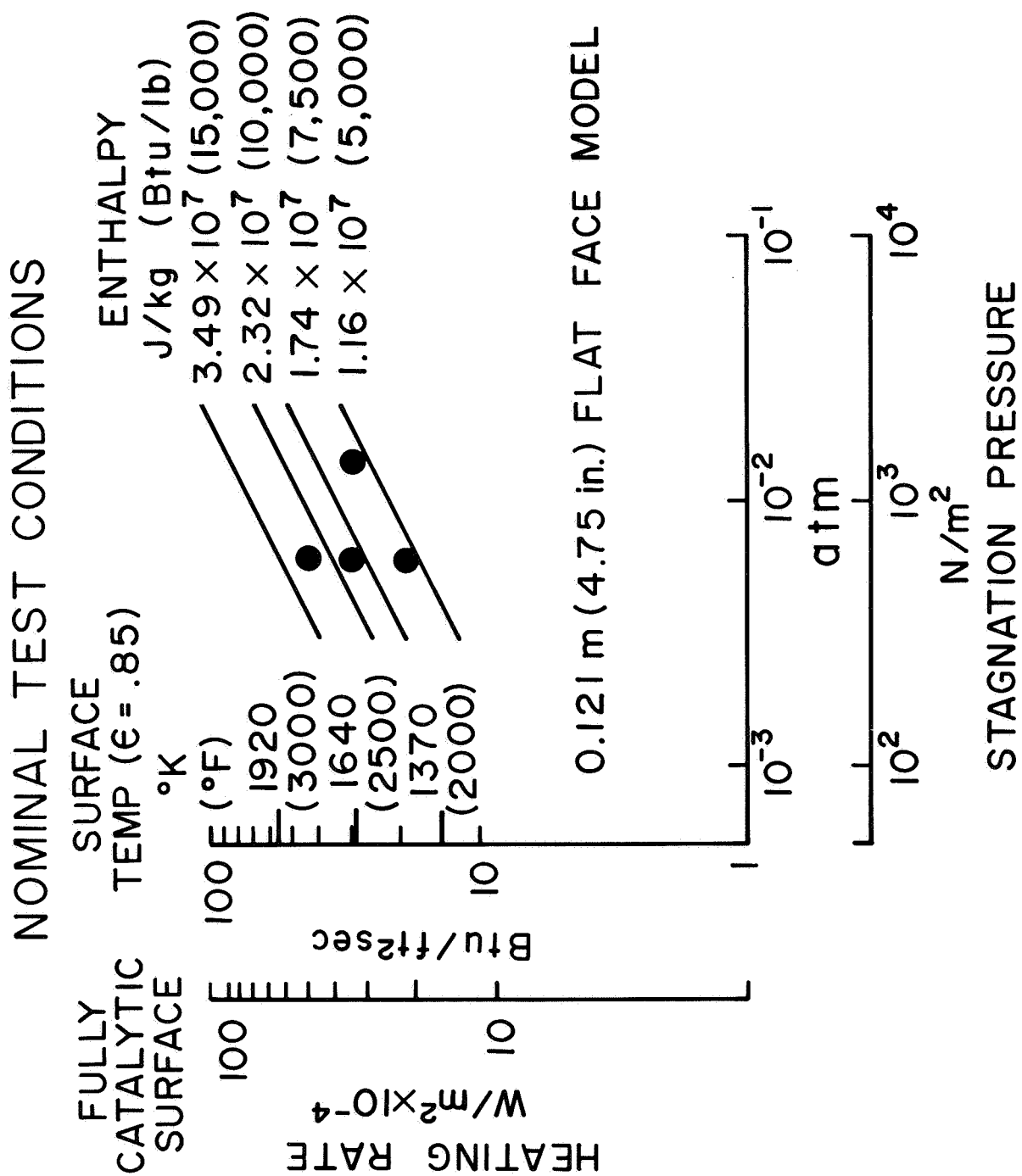


Figure 6

MODEL AND TEST STREAM CALIBRATION RESULTS

(Figure 7)

A detailed calibration test series was performed prior to the start of testing to define:

- Distribution of properties across the test stream (heat flux, stagnation pressure, enthalpy)
- Distribution of properties across the model face (heat flux, pressure)
- Surface catalycity potential as defined by a catalytic wall calorimeter (polished copper) and a noncatalytic wall calorimeter (coated teflon)

Typical model distribution results exhibit a uniform variation in pressure but some scatter in heat flux.* This scatter in the heat flux measurements is felt to be due to scatter in the calorimeter performance and not an indication of the actual distribution on the model. For all RSI conditions, the distributions across the test stream in the model region and the distributions across the model face were relatively flat.

The surface catalycity calibration results are presented in a following plot.

* The flagged symbols in the plot denote measurement locations 90° either side of the primary locations.

MODEL AND TEST STREAM CALIBRATION RESULTS TYPICAL MODEL PROPERTIES DISTRIBUTION

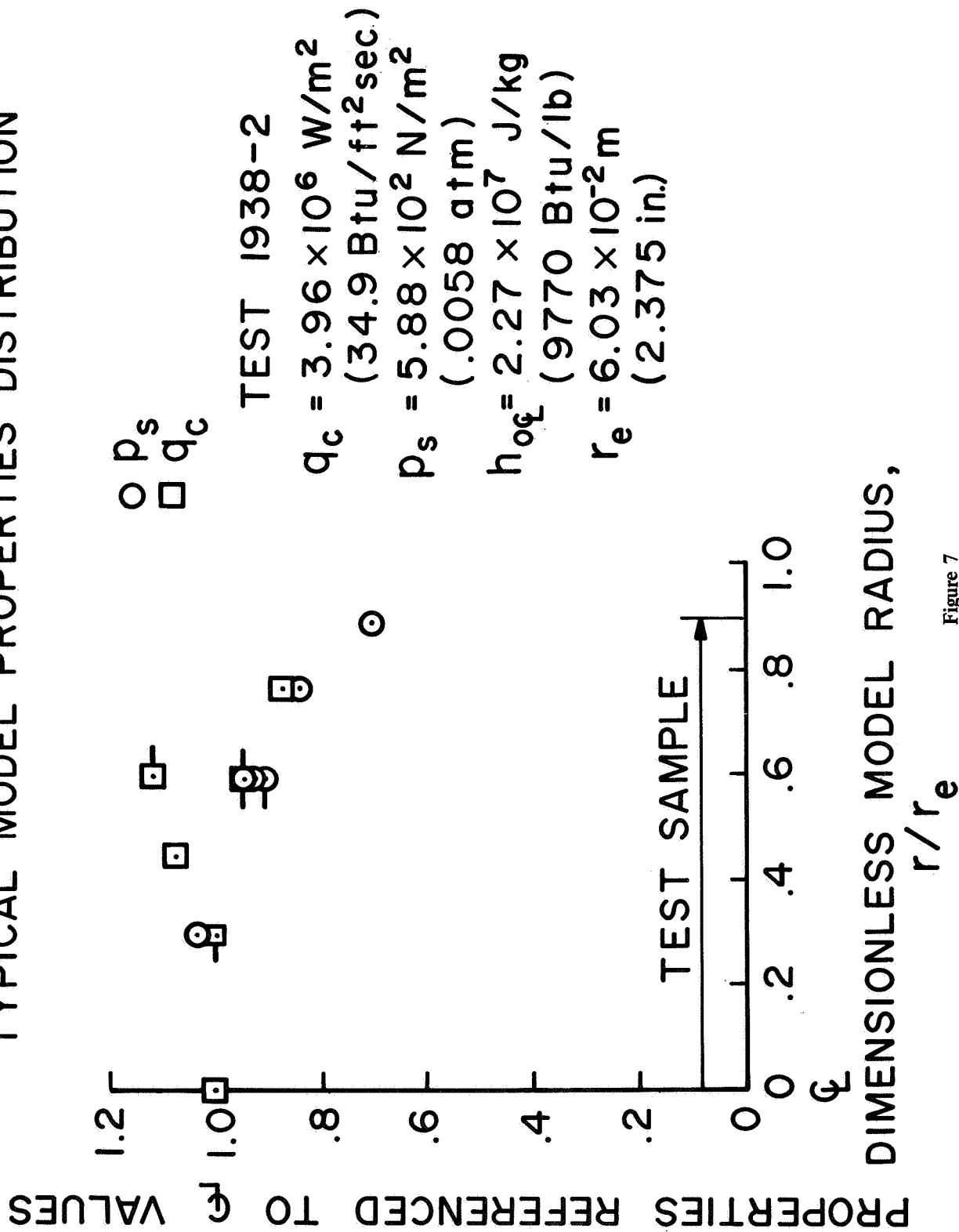


Figure 7

NOMINAL TEST MATRIX AND FAILURE MODES

(Figure 8)

The nominal and actual test matrix for the RSI materials is presented in figure 8.

The lines \longleftrightarrow indicate the nominal test program, and in the absence of any other symbols the actual test program as well. The symbol \blacktriangle indicates termination of testing on the particular sample due to a sample failure and the symbol \blacklozenge indicates termination of testing on the particular sample due to insufficient companion samples. In the case of a sample failure, testing was continued whenever possible by replacing the failed sample with another to-be-tested sample

The sample failures indicated in the test matrix were not necessarily indicative of the material performance capabilities. The initial emissivity data available and used for LI-1500 was incorrect and resulted in unexpectedly high surface temperatures, the radial split line between samples resulted in a singularity region that promoted failure, and the retention pins could have promoted the SiC foam failure (cracks).

The specific failures in the order presented in the text matrix are defined below:

<u>RSI Type</u>	<u>Reason for Failure</u>
LI-1500	Actual emissivity lower than used for surface temperature control
LI-1500	As above
SiC	Severe cracking
LI-1500	Subsurface removal along radial split line
LI-1500	As above
LI-1500	As above
HCF	Severe coating cracking
HCF	As above
HCF	As above
HCF	As above
HCF	As above

TEST MATRIX AND FAILURE MODES

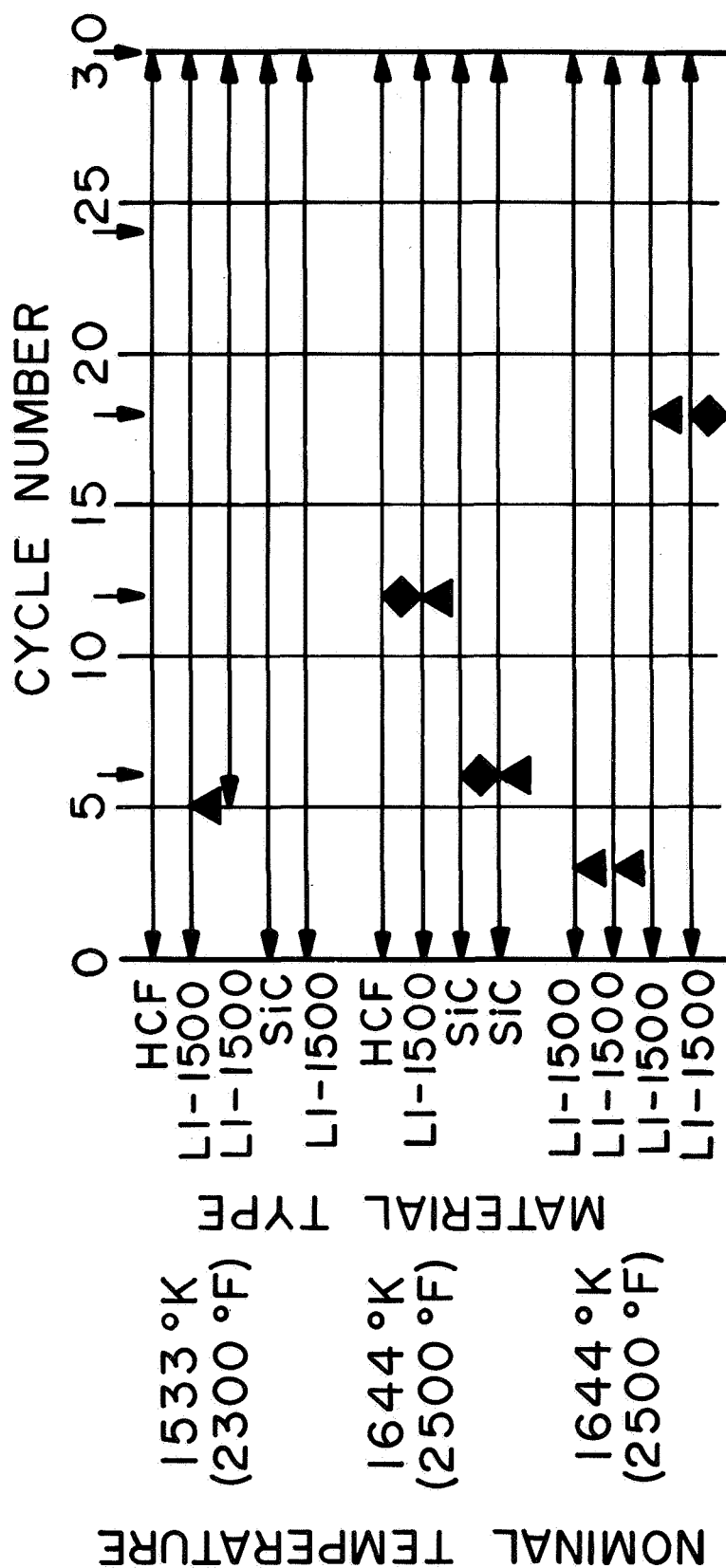


Figure 8

NOMINAL TEMPERATURE	
1533°K (2300 °F)	Hi P
1478°K (2200 °F)	TYPE
MATERIAL	
1644°K (2500 °F)	
1644°K (2500 °F)	



TYPICAL SURFACE AND IN-DEPTH TEMPERATURE RESPONSE

(Figure 9)

In the presentation of the RSI test results, emphasis is placed on the test series that employed the 120° test samples of REI, HCF, and LI-1500 (the last series in the test matrix) since it provided complete comparative data.

Surface and in-depth temperature results are presented for the twelfth cycle in the 30 cycle series. The results for REI and LI-1500 are typical for the entire 30 cycles. The HCF sample, however, started out at a surface temperature of about 1672°K (2550°F), and this temperature continuously decreased with increased cycling to a stable temperature of about 1478°K (2200°F) after about the fifteenth cycle. There was a visible change in the surface condition during this period, this change resulting in a change in surface catalytic activity from nearly fully catalytic to noncatalytic.

The different insulative performance of the three materials is apparent from the spring-loaded thermocouple measurements. As expected the silica system material is a better insulator than the two mullite system materials.

TYPICAL SURFACE AND IN-DEPTH TEMPERATURE RESPONSE TEST 1984 MODEL 2 CYCLE 12

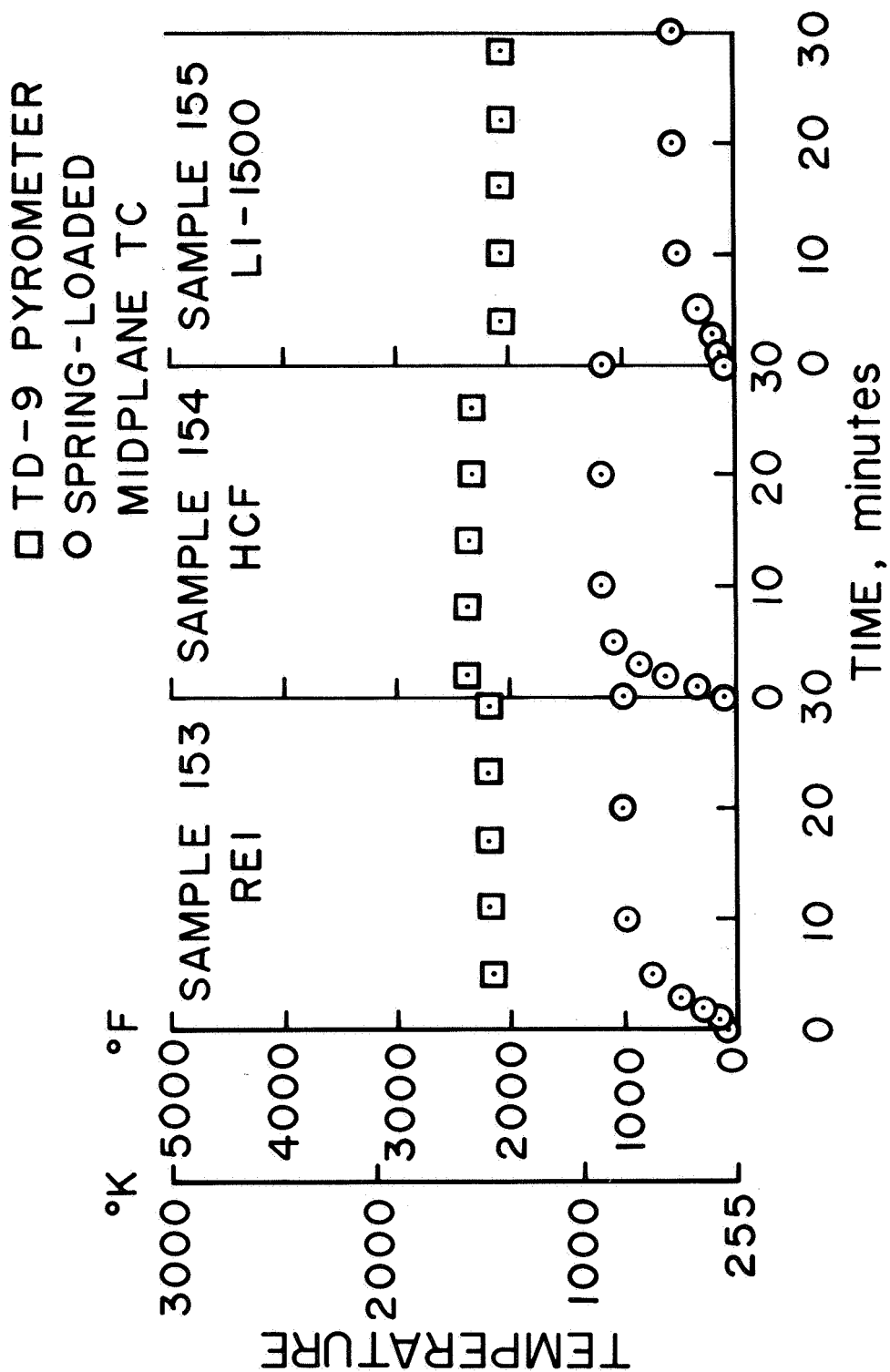


Figure 9

TYPICAL MASS LOSS RESULTS

(Figure 10)

The same set of three RSI test samples (REI, HCF, and LI-1500) exposed at constant heat flux exhibited average loss rates over 30 cycles as follows:

<u>RSI Type</u>	<u>Average Loss Rate Over 30 Cycles</u>
REI	1.2×10^{-6} kg/m ² sec (0.00086 lb/ft ² hr)
HCF	3.4×10^{-6} kg/m ² sec (0.00250 lb/ft ² hr)
LI-1500	0.7×10^{-6} kg/m ² sec (0.00050 lb/ft ² hr)

Note that the high average rate for HCF is due to the very high rate during the first few cycles (during which the surface temperature was also high due to the catalytic surface condition mentioned earlier).

TYPICAL MASS LOSS RESULTS TESTS 1983-1987

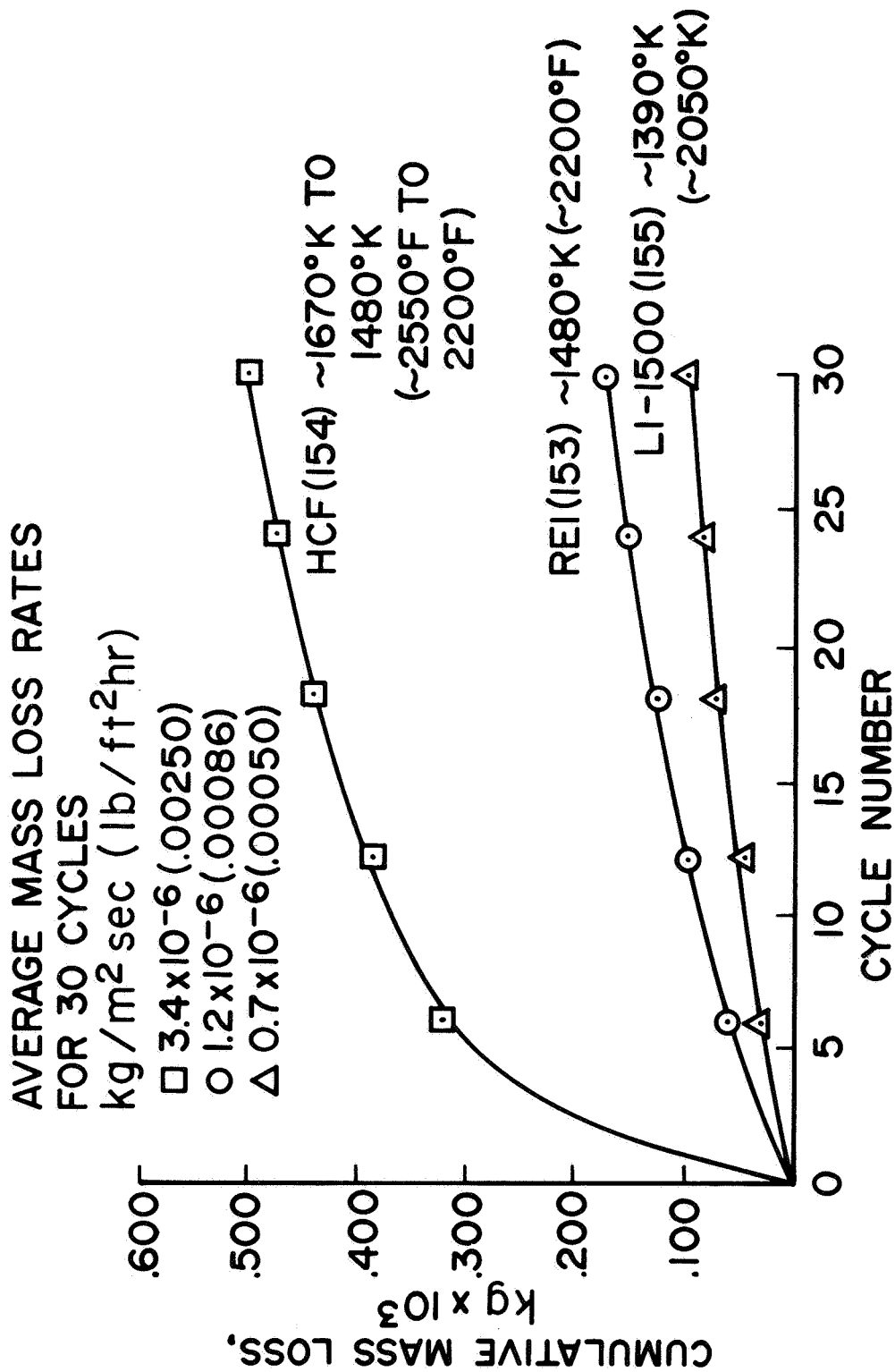


Figure 10

SURFACE CATALYCITY RESULTS
HCF FOR A RANGE OF HEAT FLUX
(Figure 11)

During one cycle on each of two models, the test conditions were varied in steps to define the surface catalycity effect over a flux range from about 28×10^4 to 57×10^4 W/m² (25 to 50 Btu/ft²sec). These results were obtained on one of the HCF versions. The solid line is the calculated fully catalytic wall variation of heat flux with surface temperature. The dotted line is a fit of the catalycity calibration results mentioned previously. This version of HCF is seen to have a noncatalytic surface at approximately the heat flux ratio defined from the calibration tests.

SURFACE CATALYCITY RESULTS HCF FOR A RANGE OF HEAT FLUX

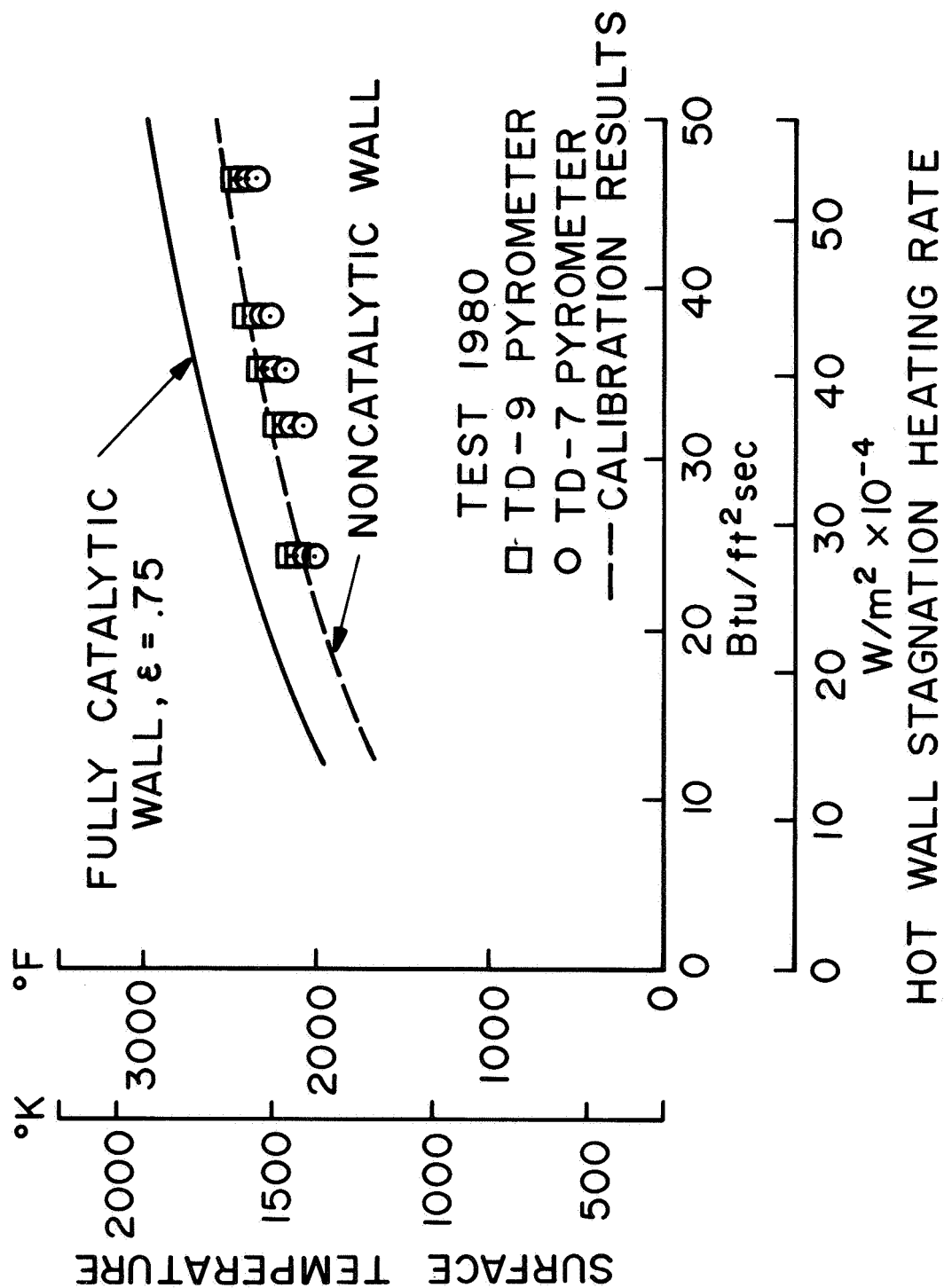


Figure 11

SURFACE CATALYTICITY RESULTS

(Figure 12)

The RSI materials and coating variations tested exhibited a wide range of surface catalyticity--- from essentially fully catalytic to fully noncatalytic. This catalyticity varied with the material and the coating and also varied with exposure time. For example (and as presented previously), at 2.3×10^7 J/kg (10,000 Btu/lb) enthalpy, one version of HCF exhibited an essentially fully catalytic surface for the first several cycles but became noncatalytic such that the ratio of radiation equilibrium heat flux to fully catalytic wall heat flux was about 0.70 after 30 cycles. The same flux ratio at the same enthalpy for the other three materials (LI-1500, REI, and SiC foam) was about 0.60 independent of exposure time. Tests on another version of HCF (as presented previously) over a broad enthalpy and flux range, 28×10^4 to 57×10^4 W/m² (25 to 50 Btu/ft²sec), also exhibited this same 0.60 ratio independent of flux (enthalpy) level.

Surface emissivity exhibited wide variations from about 0.3 to 0.9; the former value corresponded to an early version of LI-1500 in the wavelength band 1.7 to 2.6 microns, and the latter value was typical of SiC foam independent of wavelength.

SURFACE CATALYCITY RESULTS

ALL MATERIALS AT NOMINAL 2.3×10^7 J/KG (10,000 BTU/LB) AND
 3.4×10^5 W/M² (30 BTU/FT² SEC)

MATERIAL	$\frac{Q_{\text{NONCAT}}}{Q_{\text{CAT}}}$
LI-1500	0.60
HCF	0.95 to 0.60
REI	0.60
SiC FOAM	0.60

Figure 12

CONCLUSIONS

(Figure 13)

The conclusions shown in this figure are based on the 288 sample hours of testing as exemplified by the results presented in the preceding figures.

CONCLUSIONS

RSI MATERIALS EXHIBIT A WIDE RANGE OF SURFACE EMITTANCE AND CATALYTIC ACTIVITY DEPENDING ON THE SURFACE COATING

RSI COATINGS (OR SURFACES) EXHIBIT A SIGNIFICANT NONCATALYTICITY; THE POTENTIAL IMPACT IN TPS DESIGN FOR THE ORBITER VEHICLE IS ALSO SIGNIFICANT

THE INTERPRETATION OF TEST RESULTS RELATIVE TO SURFACE CATALYTICITY FOR APPLICATION TO FLIGHT CONDITIONS REQUIRES AN ACCURATE KNOWLEDGE OF THE BOUNDARY LAYER CHARACTERISTICS

COATINGS CAN HAVE A SIGNIFICANT EFFECT ON THE OVERALL RSI RESPONSE

DUE TO DIFFERENCES IN SURFACE CATALYTICITY AND EMITTANCE, TESTS AND COMPARISONS OF MATERIALS SHOULD BE MADE AT COMMON LEVELS OF HEATING RATE, NOT SURFACE TEMPERATURE

TEST MODEL SINGULARITY REGIONS WHICH MAY INFLUENCE MATERIAL RESPONSE AND WHICH ARE NOT TYPICAL OF THE FLIGHT APPLICATION SHOULD BE AVOIDED.

Figure 13

PHASE II CONTRACT TEST PROGRAM (NAS2-6600)

(Figure 14)

Material testing in the Phase II contract test program is starting in November 1972 and will emphasize RSI materials and carbon-carbon composites. The list of RSI materials and the test conditions are still subject to additions and revisions at this date.

PHASE II CONTRACT TEST PROGRAM (NAS2-6600)

- MATERIALS
 - RSI
 - LI-1500
 - HCF
 - REI
 - CPI
 - SiC LAMINATE
 - SiC FOAM
 - MAR-SI
- CARBON-CARBON COMPOSITES
 - LTV
 - CONVAIR
- METALLICS
 - COATED COLUMBIUM
- MODEL AND SAMPLE CONFIGURATIONS
 - SAME AS PHASE I EXCEPT NO MODEL CENTERPOST IN MOST TESTS
- TEST CONDITIONS
 - HEAT FLUX FROM 4.5×10^5 TO 11.0×10^5 W/M² (40 TO 95 BTU/FT² SEC)
 - STAGNATION PRESSURE OF 1.2×10^3 N/M² (0.012 ATM)
 - ENTHALPY FROM 1.7×10^7 TO 4.4×10^7 J/KG (7500 TO 19,000 BTU/LB)
- TEST PROCEDURE
 - SAME AS PHASE I EXCEPT 10 OR 15 MINUTE CYCLES

Figure 14

REFERENCE

1. Schaefer, John W., "Thermal Screening of Shuttle Orbiter Vehicle TPS Materials Under Convective Heating Conditions," Aerotherm Division, Acurex Corporation, Mountain View, California, Aerotherm Report No. 72-56, August 24, 1972, NASA CR (to be published).

SILICA RSI ENTRY SIMULATION TESTS

R. P. Banas, J. O. Donaldson, and J. Jue
LOCKHEED MISSILES & SPACE COMPANY, INC.

SYMBOLS

C_2	Constant in Plank's Law, 1.4387 cm deg Kelvin
H_t	Total enthalpy, joules per kilogram
K	Apparent thermal conductivity, watts per meter degree Kelvin
P_t	Total pressure behind normal shock, Newtons per meter ²
T	Temperature, degrees Kelvin
q or q_{cw}	Cold wall heat rate, watts per meter ²
V_∞	Indicates flow direction
ϵ	Spectral normal emittance
μ	Micron, 10 ⁻⁶ meter
ρ	Spectral normal reflectance
Subscripts:	
λ	At a specified wavelength

RESULTS OF DEVELOPMENT TESTING LMSC SILICA RSI

(Figure 1)

Silica RSI has been under development at LMSC for the past several years. Extensive test experience has resulted, but only those more significant tests accomplished the past year are reported here. In summarizing these tests, the presentation is divided in two parts. The simulated reentry testing is presented here; the more specialized environmental testing is presented in Volume II of these Proceedings in the paper by S. J. Houston.

RESULTS OF DEVELOPMENT TESTING OF LMSC SILICA RSI

SIMULATED REENTRY TESTING

- TESTS BY LMSC, NASA/MSC, NASA/ARC
- MULTICYCLE – RADIANT AND CONVECTIVE
- ACCUMULATED TEST EXPOSURE TO DEMONSTRATE PERFORMANCE AND STABILITY

SPECIALIZED ENVIRONMENTAL TESTING

- LAUNCH CONDITIONS
- ORBIT CONDITIONS
- REENTRY – SPECIALIZED CONDITIONS

Figure 1

LI-1500/0042 COATING 100-CYCLE TEST PROGRAM

(Figure 2)

One of the primary requirements of the orbiter TPS is that of reuse for 100 missions. In October of 1971, LMSC conducted a 100-cycle radiant heat test on six 10 x 10 x 6.3 cm (4 x 4 x 2.5 in.) LI-1500 specimens selected from the numerous coatings being evaluated under the Material Improvement Contract (NAS 9-12137), Ref. 1. As a result of these tests a new coating was baselined for the silica RSI. This coating, designated 0042, consists of a silicon carbide emittance agent in a borosilicate matrix. This coating system proved so successful that it has been used exclusively on the LMSC silica RSI since October 1971.

As shown, the imposed heat pulse (controlled by thermocouples installed directly below the coating) dwelled at 1648°K (2500°F) for 2.5 minutes per cycle. The total time at 1648°K (2500°F) was 4 hours with 14 hours at temperatures greater than 1533°K (2300°F). The time above 1533°K (2300°F) is equivalent to 336 missions when compared to the reference heat pulse (Area 2P). It should be noted that the total heat load resulting from this heat pulse greatly exceeds that of the reentry trajectories currently being considered for the orbiter. These tests were performed at LMSC under NAS 9-12083, Ref. 2.

LI-1500/0042 COATING 100 CYCLE TEST PROGRAM

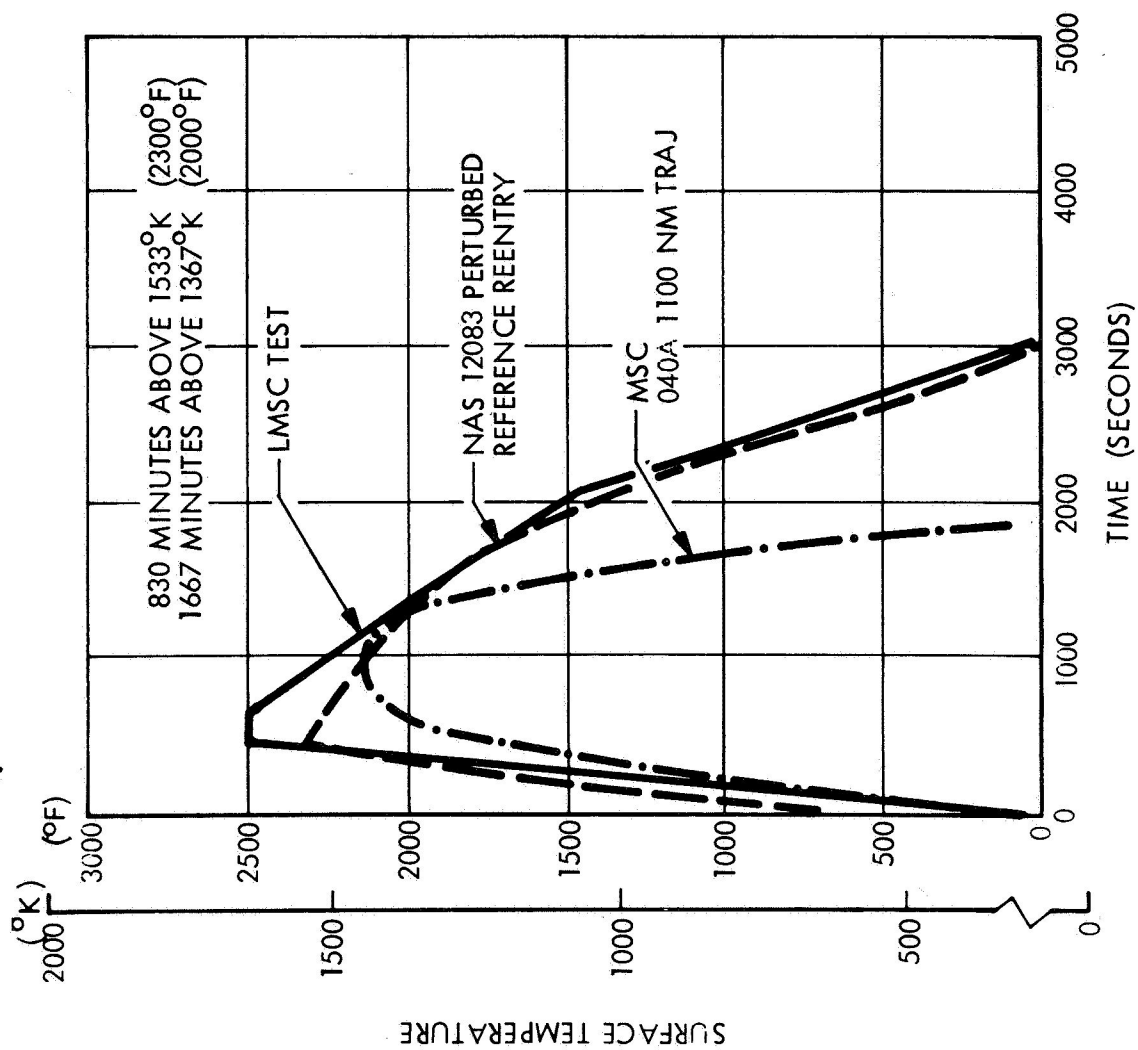


Figure 2

TEMPERATURE HISTORIES FOR SPECIMEN TT42-6

100-CYCLE TESTS

(Figure 3)

The test samples discussed in the previous chart were also instrumented with thermocouples both in depth and on the aluminum substrates. Thermal predictions are shown along with measured temperatures for two representative cycles. The predictions are based on a one-dimensional thermal model and utilize the LI-1500 thermal conductivity and specific heat design values developed in late 1970 and reported in the Phase I Final Report (Ref. 3). The maximum in-depth temperatures compare closely with predictions and were repeatable throughout the tests. It is interesting to note that the calculated temperature variations with time were also closely predicted. The tests were performed at atmospheric pressure, and this agreement verifies the thermal conductivity design values for this pressure.

TEMPERATURE HISTORIES FOR SPECIMEN TT 42-6

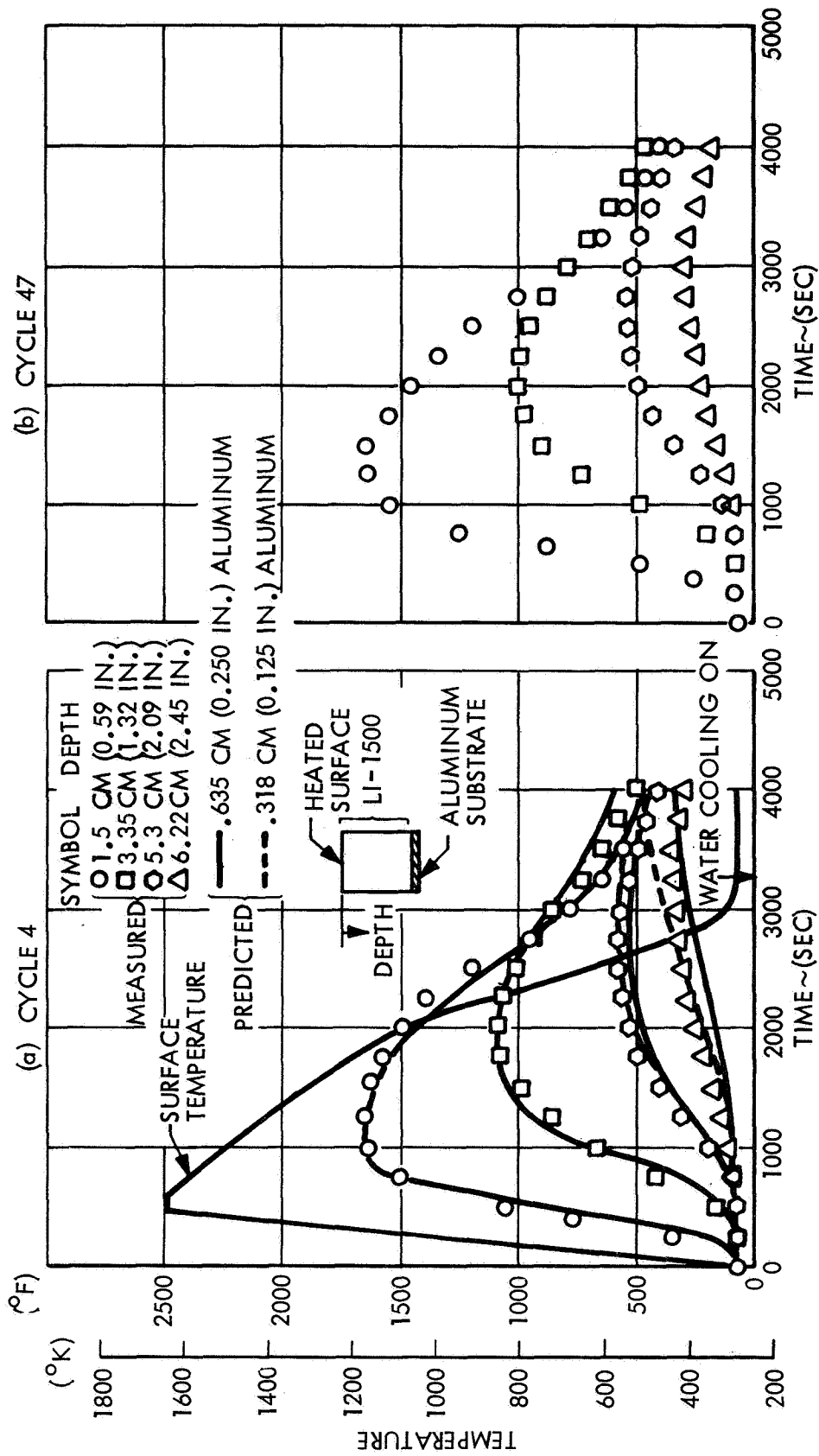


Figure 3

COMPARISON OF MEASURED AND PREDICTED PEAK TEMPERATURES

100-CYCLE TESTS - SPECIMEN TT 42-6

(Figure 4)

Variation of in-depth measured temperatures for the entire 100 cycles is compared with the predicted thermal gradient. At all locations the measured values are less than predictions, illustrating that the LI-1500 conductivity is conservative. Thermal and dimensional stability of the LI-1500 were also demonstrated for the severe thermal conditions of this test. The change in pre- and post-test length and width was less than 0.05 percent, which is well within the accuracy of the measuring device, 0.005 out of 9.9 cm (0.002 in. out of 3.900 in.).

COMPARISON OF MEASURED AND PREDICTED PEAK TEMPERATURES

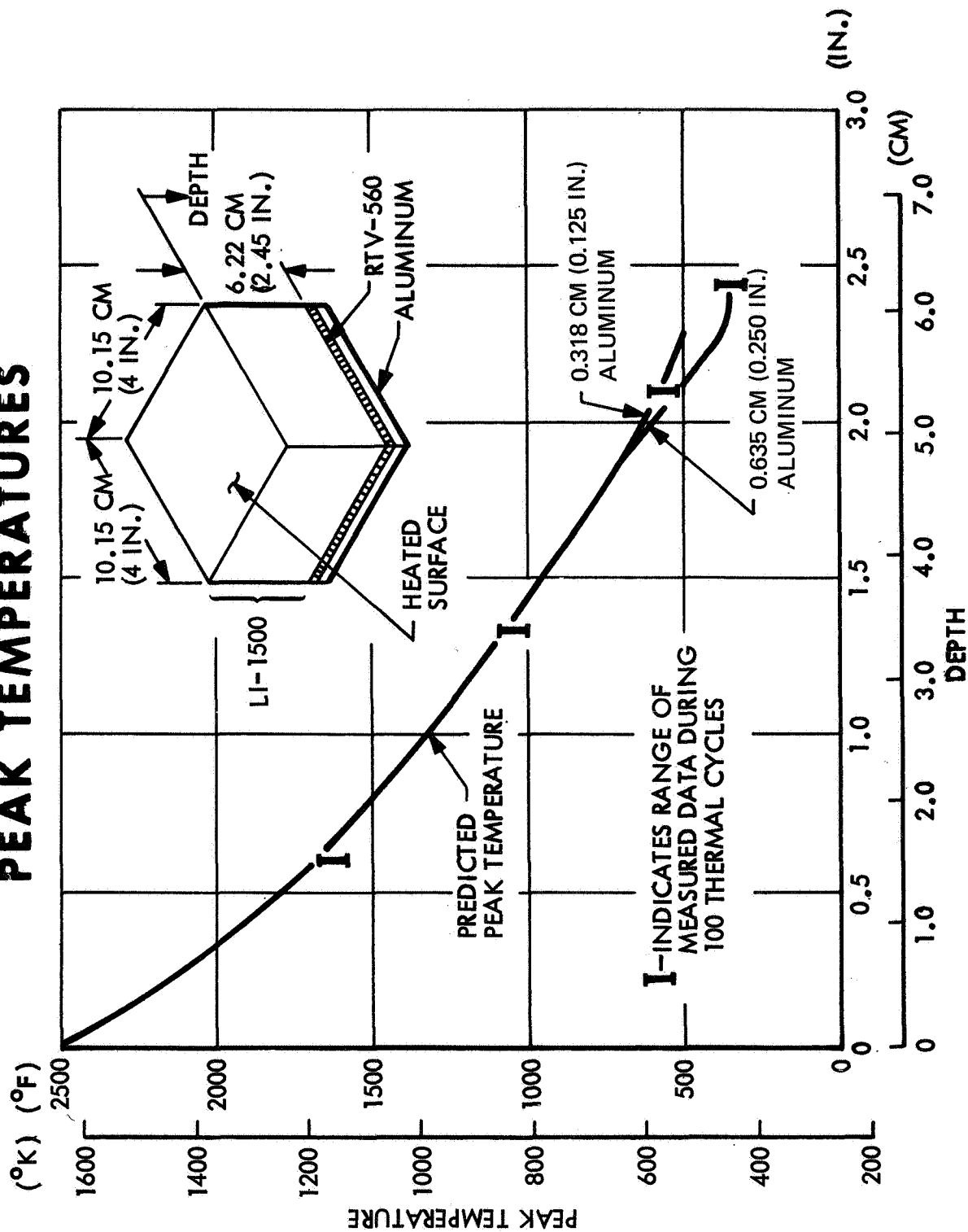


Figure 4

DESIGN CURVES SHOWING VARIATION OF LI-1500 THERMAL CONDUCTIVITY WITH TEMPERATURE AND PRESSURE

(Figure 5)

LI-1500 thermal conductivity interim design curves developed in late 1970 and reported in Ref. 3 are shown. The rapid increase in thermal conductivity at about 10 mm Hg is attributed to the increasing significance of the gaseous conduction portion of the apparent thermal conductivity. The use of an apparent thermal conductivity, which includes the effects of conduction along fibers, gaseous convection between fibers, and radiation between fibers, is justified for materials like silica, which have a very small fiber diameter (about 0.5 to 1.5 μ) and a corresponding large value for the scattering coefficient. This simplified approach allows use of the Fourier heat conduction law, which can be easily used with finite difference solutions to size the TPS and predict structural thermal response.

These thermal conductivity design curves were utilized along with the specific heat values listed in Ref. 3, Vol. I, for the temperature predictions shown in succeeding charts.

DESIGN CURVES SHOWING VARIATION OF LI-1500 THERMAL CONDUCTIVITY WITH TEMPERATURE AND PRESSURE

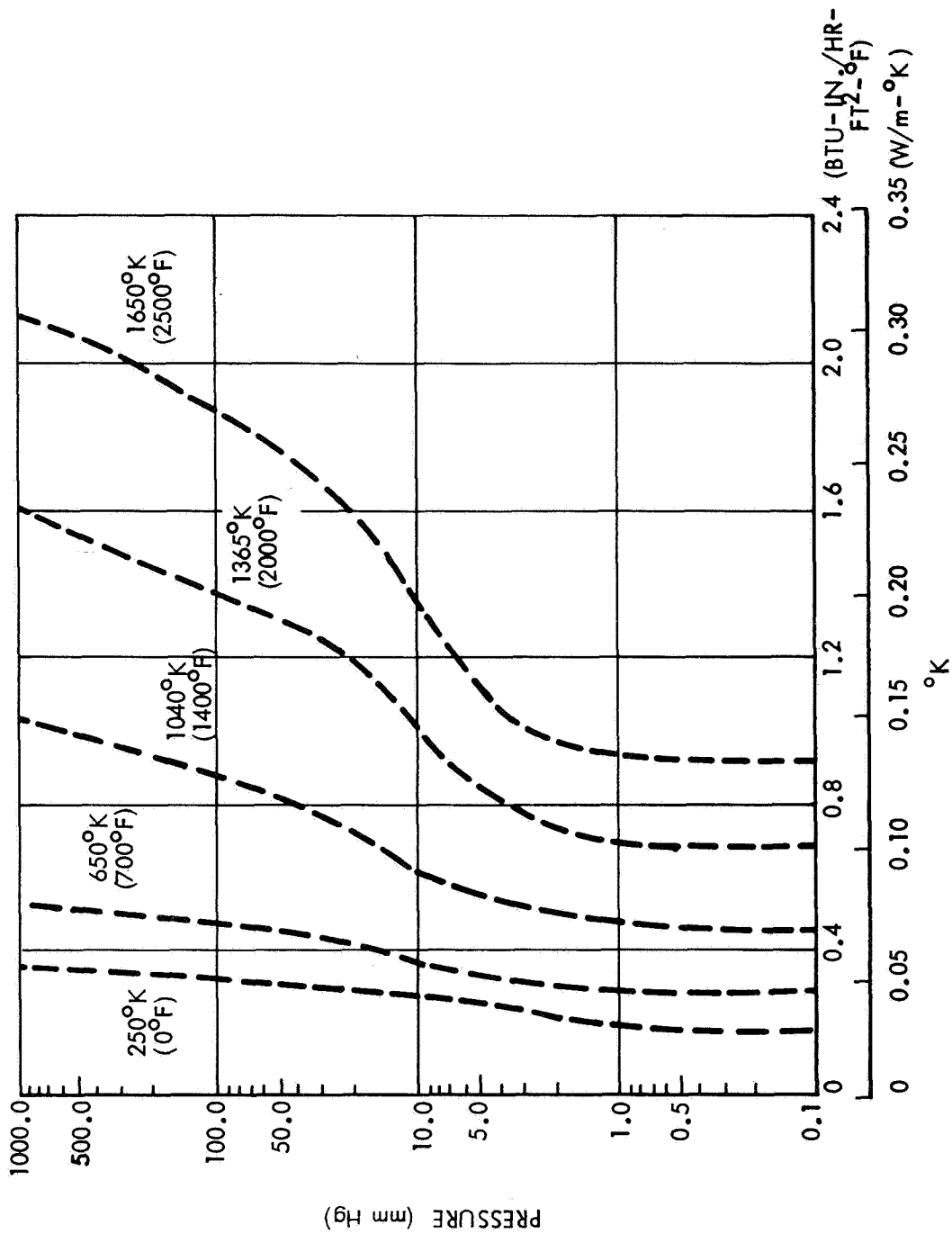


Figure 5

100-CYCLE TESTS

(Figure 6)

LMSC has been experimentally and analytically evaluating reduced density silica RSI (i.e., less than 240 kg/m^3 (15 lb/ft^3)) for several years. This work led to the introduction of LI-900, with a density of 144 kg/m^3 (9 lb/ft^3) during the recently completed Material Improvement Contract (NAS 9-12137).

The current Phase III Development Contract (NAS 9-12856) is providing more detailed characterization of this material.

To demonstrate reuse capability, two LI-900 samples with two LI-1500 standards were subjected to a 100-cycle test sequence at LMSC in October 1972. The samples were $12.7 \times 12.7 \times 5 \text{ cm}$ ($5 \times 5 \times 2 \text{ in.}$) bonded with 0.0254 cm (0.010 in.) of RTV 560 to an 0.0203 cm (0.080 in.) thick RL1973 foam pad, which was subsequently bonded with 0.0254 cm (0.010 in.) of RTV 560 to 0.317 cm (0.125 in.) to aluminum plates. All samples were coated on the top and 4.44 cm (1.75 in.) down the sides with the 0042 coating. The NAS 9-12856 reference heat pulse (Area 2P) was used for the test cycles.

100-CYCLE TESTS

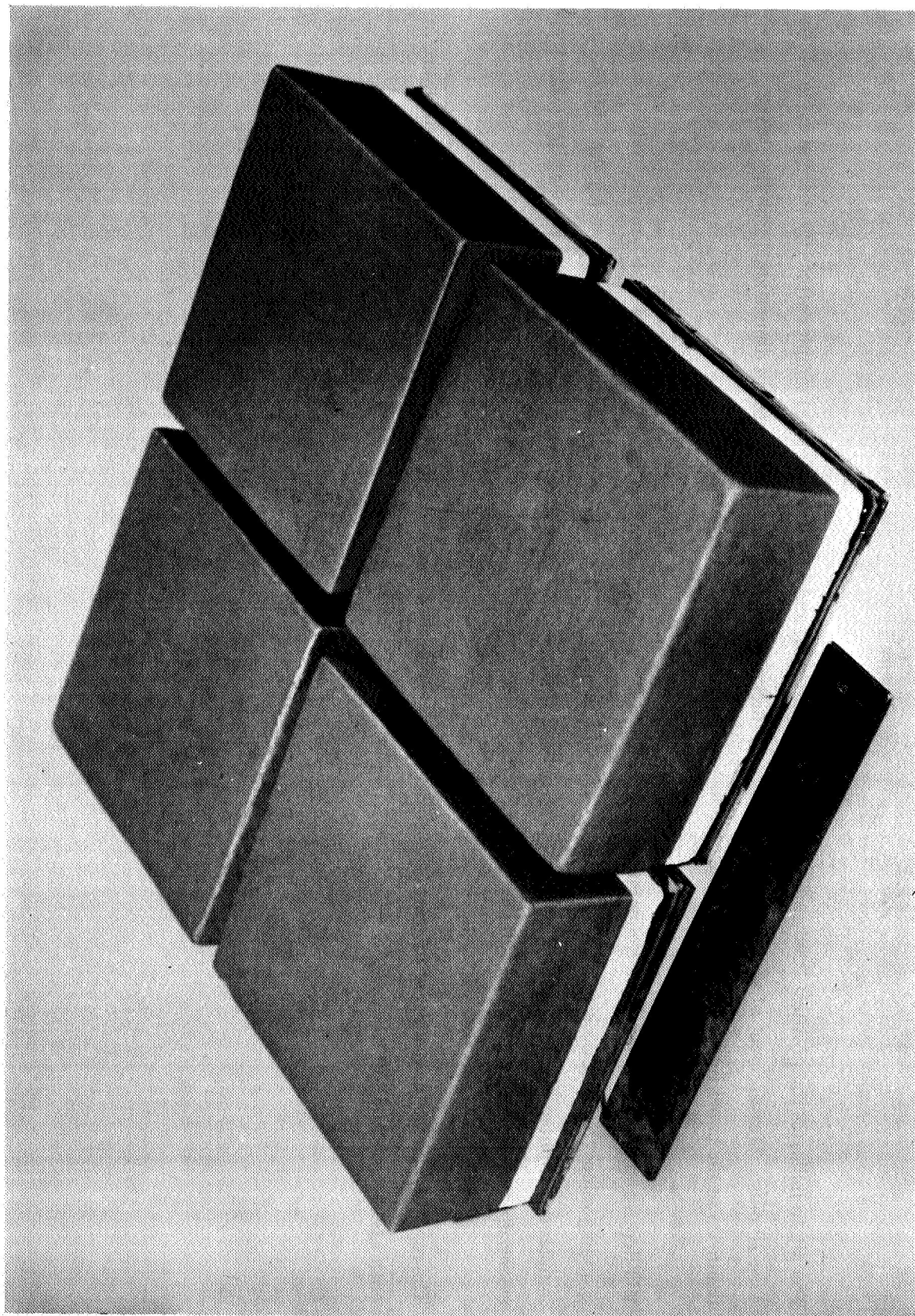


Figure 6

POST-TEST PHOTO OF LI-1500 AND LI-900

(Figure 7)

The photo indicates the post-test condition of the LI-900 (right side) and LI-1500 (left side) samples after 100 thermal cycle of the Area 2P pulse. Measurement of sample length, width, and thickness for tiles indicated excellent dimensional stability. (See

Figure 25 in the paper by K. J. Forsberg presented in Volume III of these Proceedings.)

Mid-depth and backface maximum temperatures for the LI-900 were 1015°K (1370°F) and 489°K (420°F), respectively. Corresponding values for LI-1500 were 921°K (1200°F) and 472°K (390°F). The moderate increase in temperature for the LI-900 samples is attributed primarily to the lower heat capacity of this material, since the thermal conductivity up to 1143°K (1600°F) is essentially the same as that of LI-1500 (see Figure 8).

The repeatability of the measured temperatures over the 100 cycles demonstrates the consistent thermal performance capability of both LI-900 and LI-1500.

POST-TEST PHOTO OF LI-1500 AND LI-900

(100 CYCLES AT AREA 2 P HEATING - OCTOBER 1972)

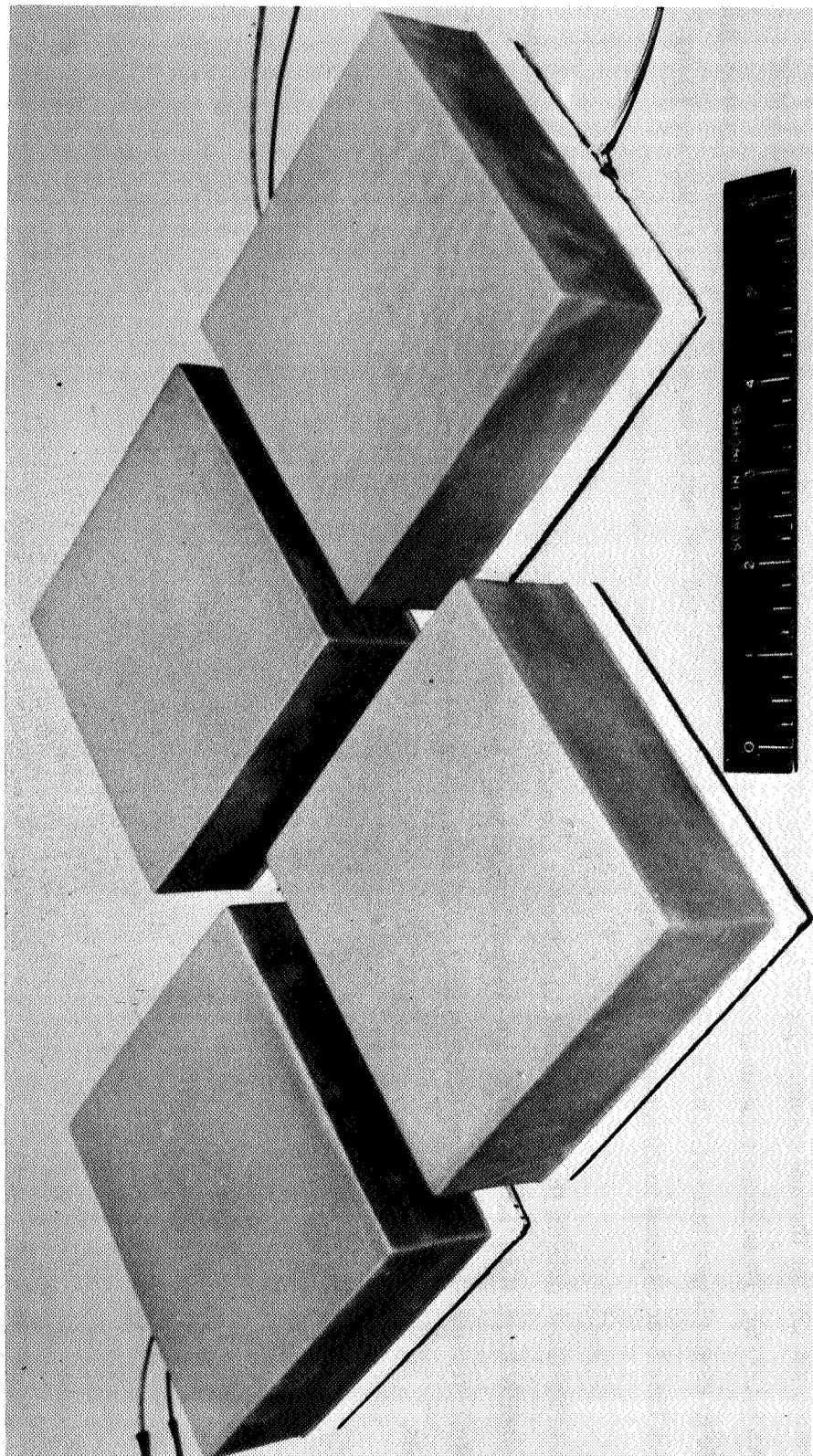


Figure 7

LI-900 CONDUCTIVITY DATA

(Figure 8)

Measurements of the thermal conductivity of LI-900 are being performed under the Phase III TPS Contract from NASA/MSFC (NAS 9-12856). These measurements are currently being performed using a Dynatech 17.8 and 20.3 cm (7 and 8 in.) guarded hot plate to mean temperatures of 1367°K (2000°F) and pressures of 1, 10, 50, and 760 mm Hg on as-fabricated LI-900 and LI-900, which have been exposed to 20 thermal cycles of the Area 2P temperature and pressure histories.

Measurements to date on the as-fabricated LI-900 when compared to the LI-1500 design curves (Ref. 3) indicate the LI-900 values are slightly lower than the LI-1500 design curve at low pressures and slightly higher than LI-1500 design curve at 760 mm Hg (1 atm) pressure. The differences between the LI-900 data and the LI-1500 design curves are within the uncertainty of the measurements.

LI-900 CONDUCTIVITY DATA

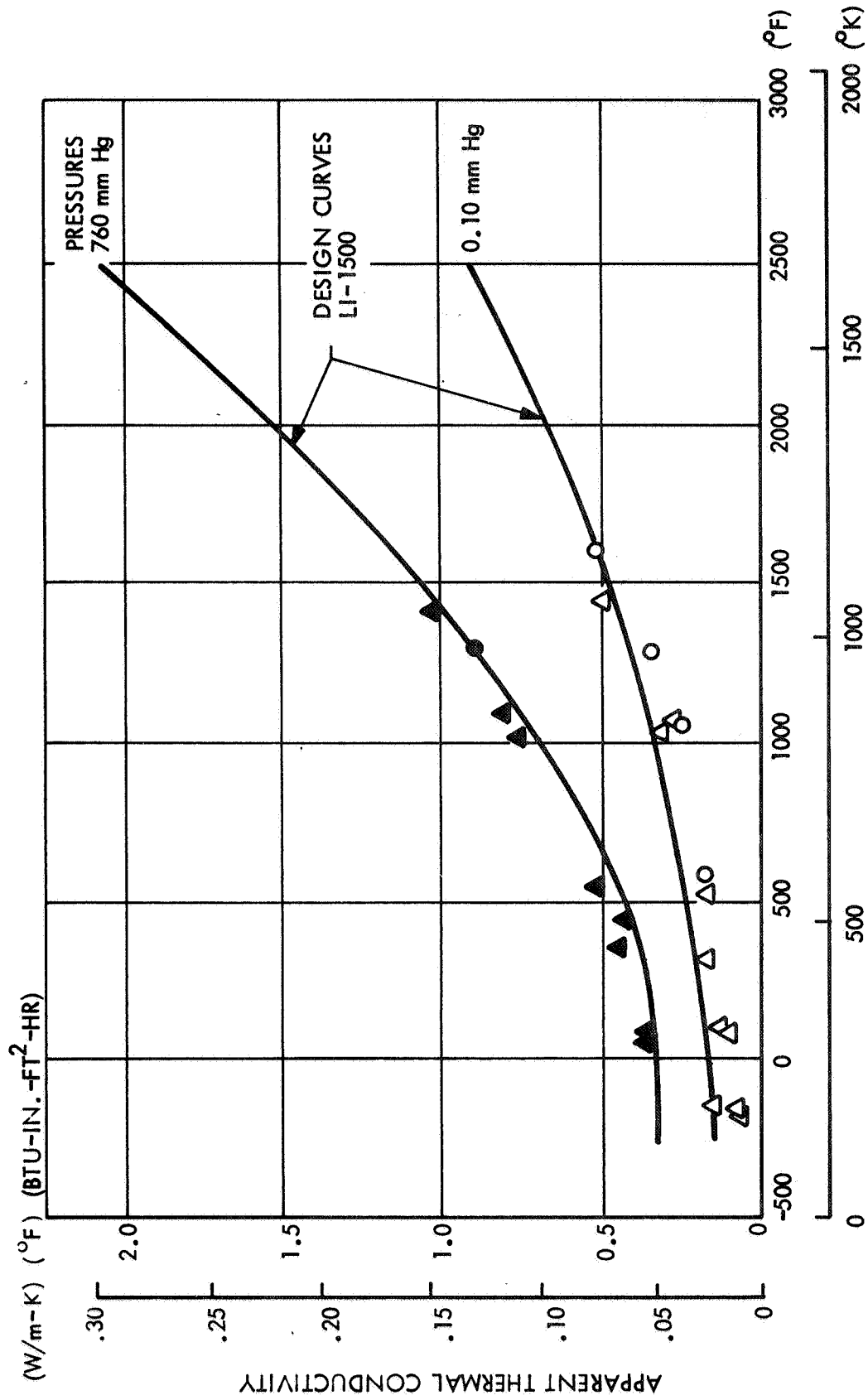


Figure 8

PREDICTABLE THERMAL PERFORMANCE

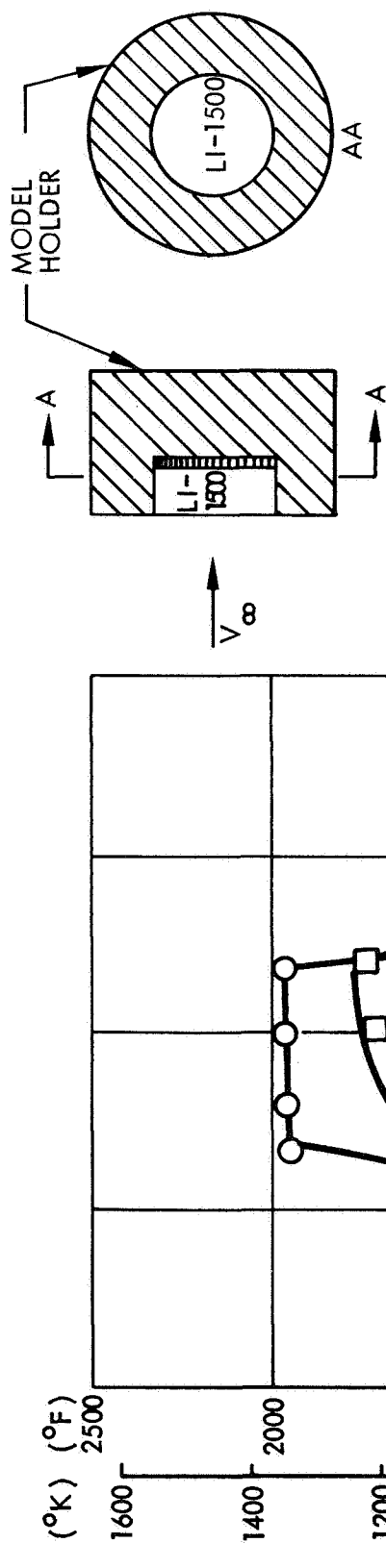
(Figure 9)

A realistic weight for the Orbiter TPS must be known as early as possible in the Shuttle Program, since it affects both program cost and orbiter weight growth. TPS weight is a direct function of the assumed variation of thermal conductivity with both pressure and temperature. The test results presented in this chart were performed by NASA/ARC personnel in their 2-MW arc-plasma facility with LI-1500 specimens supplied under the Phase II TPS development contract. A 10 cm dia. x 5 cm (4 in. dia. x 2 in.) thick LI-1500 sample (cut from the TT 70-3) coated on the top with 0042 coating was placed in a 20.3 cm (8 in.) dia flat face cylindrical model holder. The test procedure and results are discussed in the paper by D. A. Stewart also presented in this Volume of the Proceedings.

The predictions were based on a one-dimensional thermal model and an adiabatic backface, as will be all predictions shown in succeeding charts. Good agreement between predicted and measured temperature is shown and indicates that the low pressure LI-1500 thermal conductivity design values are slightly conservative but sufficient for TPS sizing purposes.

PREDICTABLE THERMAL PERFORMANCE

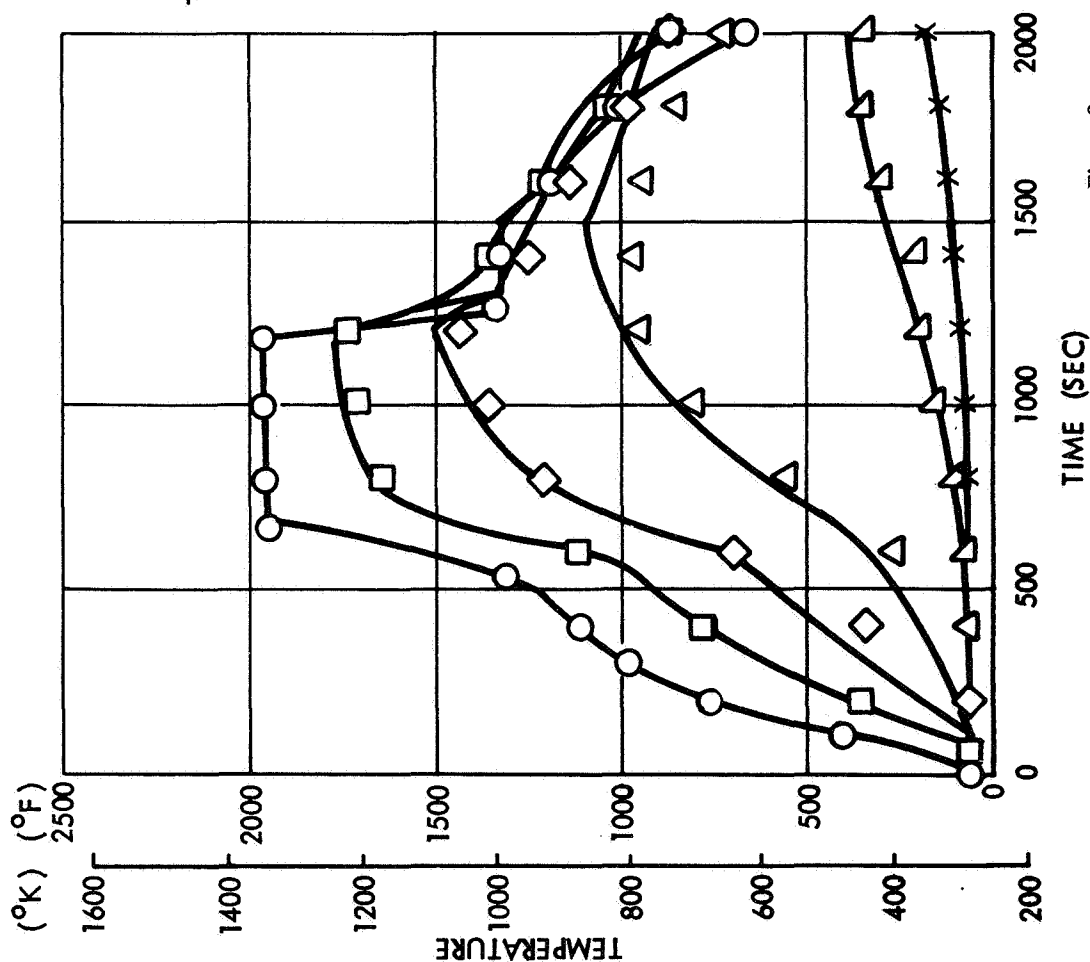
TEST PERFORMED IN NASA/ARC ARC-PLASMA FACILITY - RUN 16



$$\dot{q} = 230 \text{ KW/m}^2 \text{ (20.3 BTU/FT}^2\text{-SEC)}$$

$$H_t = 7710 \text{ J/g (3307 BTU/LB)}$$

$$P_t = 4.5 \text{ mm Hg}$$



MEASURED TEMP	PREDICTED TEMPERATURE	THERMOCOUPLE DEPTH
○	—	SURFACE
□	—	0.33 CM (0.13 IN.)
◇	—	0.79 CM (0.31 IN.)
△	—	1.17 CM (0.46 IN.)
△	—	3.17 CM (1.25 IN.)
X	—	3.96 CM (1.56 IN.)

Figure 9

0042 COATING IS WATERPROOF AFTER NASA-ARC TESTS

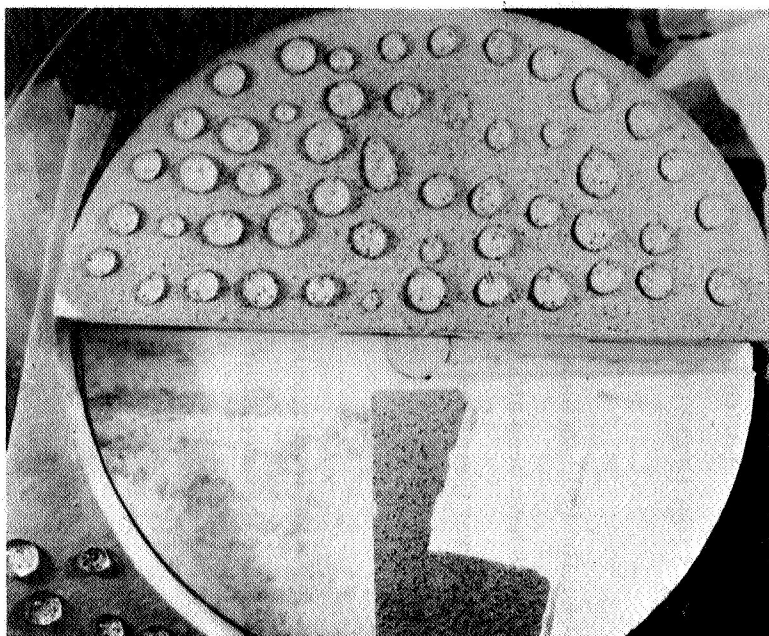
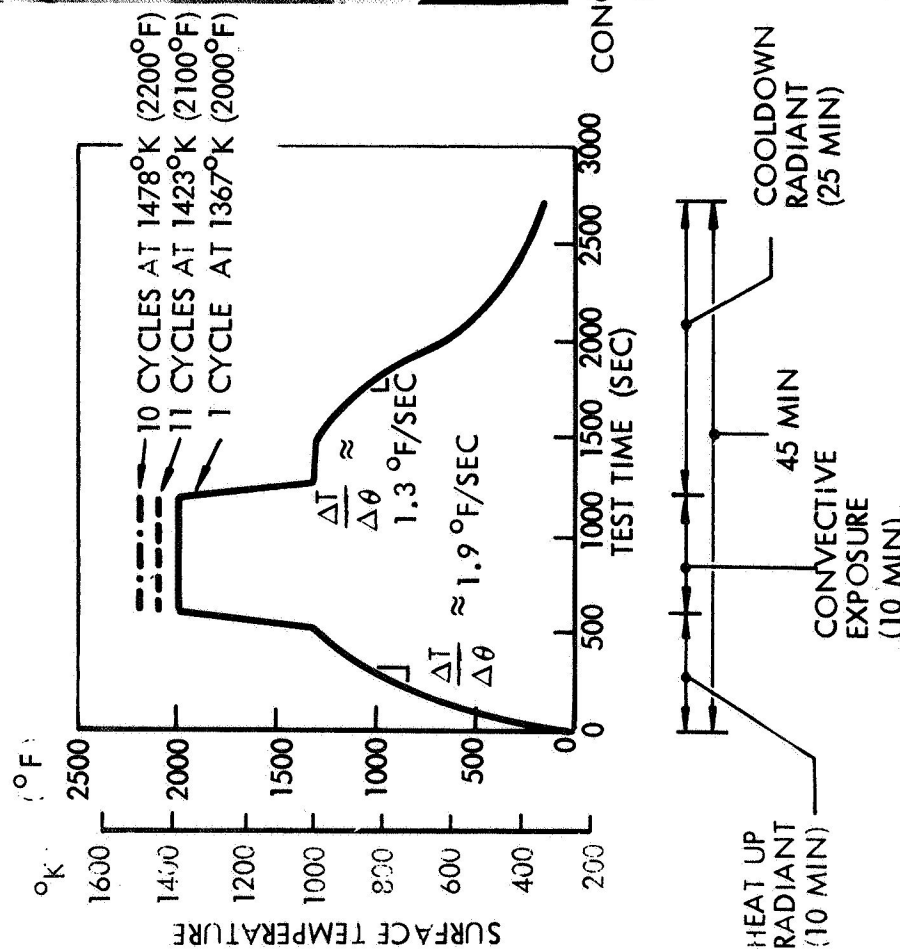
(Figure 10)

The surface temperature history for the previous chart is depicted here along with a photo of the LI-1500 sample after it was exposed to a total of 22 cycles in the NASA-ARC 2-MW facility. As shown, the test consisted of both radiant and convective heating to simulate an Area 2 entry heat pulse. The heatup rate of 1.05°K/sec (1.9°F/sec) and cooldown rate of 6.5°K/sec (1.3°F) are listed for comparison purposes with the Area 2 rates, which were 2.5°K/sec (4.5°F) for heatup and about 1.05°K/sec for cooldown. Further tests in both arc-plasma and radiant facilities should attempt to bound the thermal shock parameter to determine the thermal shock sensitivity of all RSI candidate materials. This can be accomplished by exposing RSI samples to a range of heatup rates that are representative of entries from all anticipated shuttle orbits. Preliminary estimates indicate that these heatup rates, which depend on initial entry angle, entry angle of attack, boundary layer transition criteria, and turbulent heat transfer method, range from about 1.67°K/sec (3°F) to 3.9°K/sec (7°F) for a 185 km (100 nm) orbit to $5.5 - 8.3^{\circ}\text{K/sec}$ ($10 - 15^{\circ}\text{F}$) for a 310 or 580 km (270 or 500 nm) orbit.

A water drop test (where drops of tap water are placed on the 0042 surface coating for 45 minutes) was used to determine if the 0042 coating was waterproof. The results, as illustrated by the beaded water in the photo, indicate no surface cracks or water absorption after 22 thermal cycles. In terms of time at peak temperature for an Area 2 type entry pulse these tests were equivalent to 50 to 55 entries from 185 km (100 nm) orbits.

0042 COATING IS WATERPROOF AFTER NASA-ARC TESTS

DATA SOURCE: NASA-ARC 2.0 MW FACILITY
F. J. DeMERITTE STATUS REPORT 23 MAY 1972



CONCLUSION:

0042 COATING IS WATERPROOF AND DOES NOT CRACK AFTER;

1.83 HR AT $T_{SUR} = 1423^\circ\text{K}$ (2100°F) OR

1.67 HR AT $T_{SUR} = 1478^\circ\text{K}$ (2200°F)

50-55 EQUIVALENT FLIGHTS TO AREA 2 HEATING

Figure 10

RSI MATERIAL THERMAL PERFORMANCE

(Figure 11)

This figure presents the temperature distribution through samples of LI-1500, G.E. Mullite (MOD I), and MDAC HCF to illustrate the difference in thermal performance between Mullite and Silica. All materials were supplied to NASA/MSC under parallel Phase II RSI development contracts, which ended in January 1972. The samples are the same thickness and the data were taken from tests performed at NASA/ARC, Mountain View, California, in January 1972 and informally reported in the Space Shuttle Structures and Materials Working Group Monthly Status Report for February (15 Jan 1972 to 15 Feb 1972) 1972.

A comparison of measured and predicted temperatures for all materials is shown for 1000 seconds into the test. The shape of the temperature distribution through the Mullite indicates that steady-state conditions have been attained. The non-linear-temperature variation for LI-1500 (Silica) indicates a non-steady-state condition and hence a lower thermal conductivity. All predictions are based on the same boundary conditions and a one-dimensional thermal model.

The comparisons indicate that the LI-1500 design thermal conductivity (Ref. 2 or 3) at low pressure is conservative, while the Mullite thermal conductivity design values (Ref. 4 and 5) are overly optimistic since the calculations predict lower temperatures than the measured data.

RSI MATERIAL THERMAL PERFORMANCE

COMPARISON OF MEASURED AND PREDICTED TEMPERATURES DURING PLASMA ARC TESTS

TESTS WERE PERFORMED IN NASA AMES RESEARCH CENTER 3 MW PLASMA ARC FACILITY

REFERENCE: MONTHLY STATUS REPORT FOR FEBRUARY (15 JAN 1972 TO 15 FEB 1972),
3 APRIL 1972, OAST SPACE SHUTTLE STRUCTURES AND MATERIALS
TECHNOLOGY WORKING GROUP

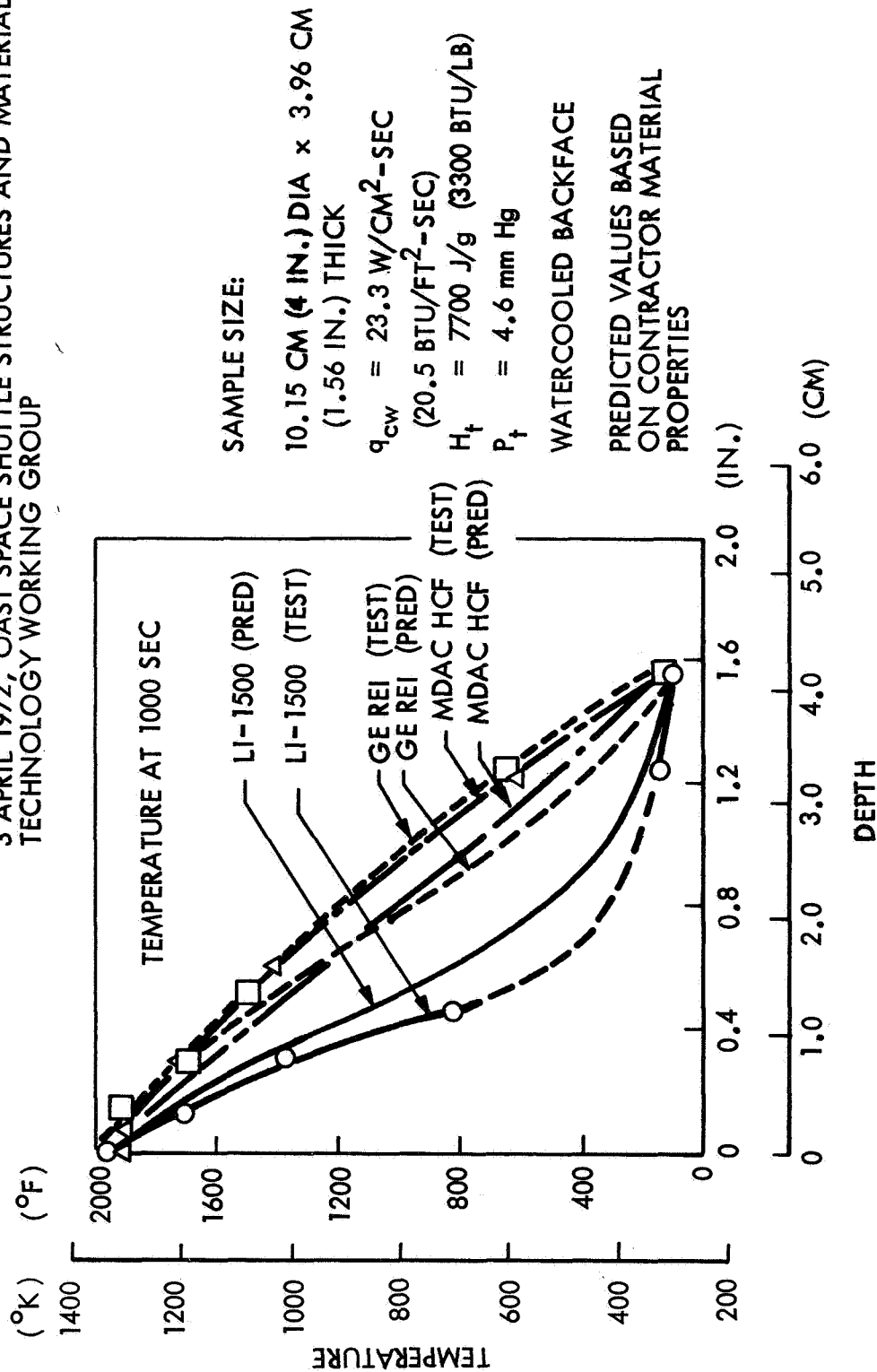


Figure 11

042 COATING IS WATERPROOF AFTER NASA-MSC TESTS

(Figure 12)

Arc-plasma tests were also performed by NASA/MSC on LI-1500 samples delivered under the Phase II Development Contract (Ref. 2). These tests were performed in their 1.5-MW facility in May through June 1972 (Personal communication with D. J. Tillian discussing an internal NASA/MSC Memo by R. E. Vale). The 10 cm (4 in.) diameter sample was placed in a 12.7 cm (5 in.) diameter water-cooled copper holder and tested in a stagnation flow attitude to a heat rate 25 W/cm^2 ($22 \text{ Btu/ft}^2 \text{ -sec}$), and a surface pressure of about 1.6 mm Hg. The sample (TT67-2A) was exposed to a pulse consisting of both radiant and convective heating to simulate Area 2P heating. The sample was precooled to 116°K (-250°F) with LN_2 and then exposed to peak surface temperature of about 1553°K (2340°F) over a 50 min interval. The sample was exposed to 35 cycles of the pulse shown in the chart. After exposure the sample was cut into three segments with the one shown here provided to LMSC for post test analysis.

A simple water drop test was used to determine the waterproof nature of the coating after the test. While the water wetted the surface in some areas and beaded (water drops) in others, it did not work into the material. Hence, the coating was considered waterproof with no apparent cracks after 35 thermal cycles..

Similar results were reported by Battelle (Ref. 6), where they indicated the LMSC, MDAC, and GE surface coatings spread water easily after exposure to heat treatment but it did not work into the surface coatings. However, the mullite material after heat treatment rapidly absorbed water while the silica material resisted water absorption.

In terms of time at peak temperature (11.6 cumulative hours at 1553°K (2340°F), the 35 test cycles correspond to 336 equivalent entries from a 100 nm orbit using an Area 2P peak temperature of 1533°K (2300°F).

0042 COATING IS WATERPROOF AFTER NASA-MSC TESTS

DATA SOURCE:

NASA-MSC 1.5 MW FACILITY
R. E. VALE MEMO 27 JUL 1972

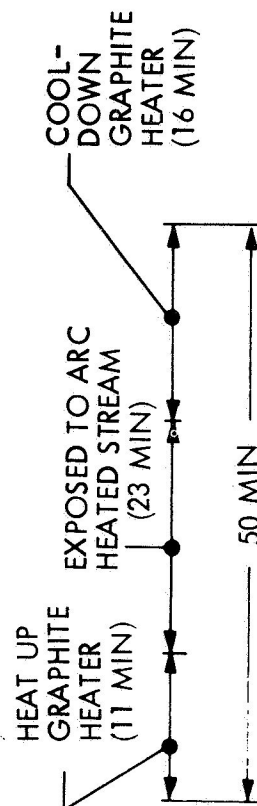
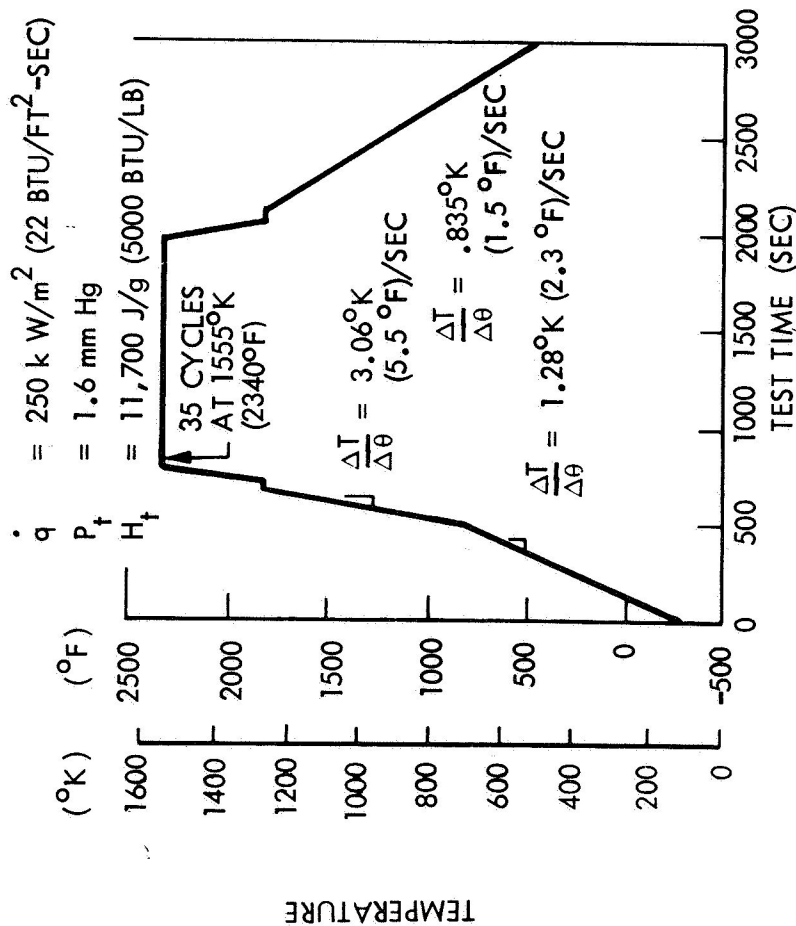
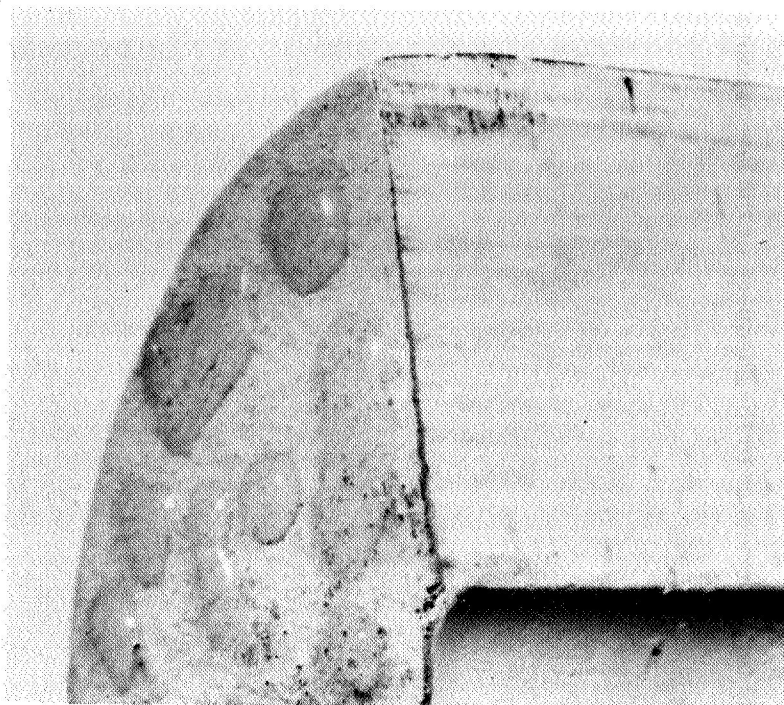


Figure 12



CONCLUSION:

0042 COATING IS WATERPROOF AND DOES NOT CRACK AFTER,

11.6 HR AT $T_{\text{SUR}} = 1555^\circ\text{K (} 2340^\circ\text{F)}$

OR

350 EQUIVALENT FLIGHTS TO AREA 2P HEATING

PREDICTABLE THERMAL RESPONSE

(Figure 13)

This chart presents a comparison of predicted and measured temperature for one cycle of the 35 cycles in Figure 12. The LI-1500 sample 10 cm dia x 5 cm thick (4 in. x 2 in.) was instrumented in-depth with 10 thermocouples, six on the centerline and four 3.17 cm (1.25 in.) off the centerline. The six centerline thermocouples were used for this comparison. A one-dimensional thermal model was used for the predictions, with the first in-depth thermocouple as the driving temperature and an adiabatic backface. Comparisons of the predicted and measured data indicate good agreement and supply further evidence to the adequacy of the low-pressure thermal conductivity design values discussed earlier.

PREDICTABLE THERMAL RESPONSE

TEST PERFORMED BY NASA/AARC IN 5.08 x 20.32 CM (2 x 8 IN.) TURBULENT DUCT — RUN 11

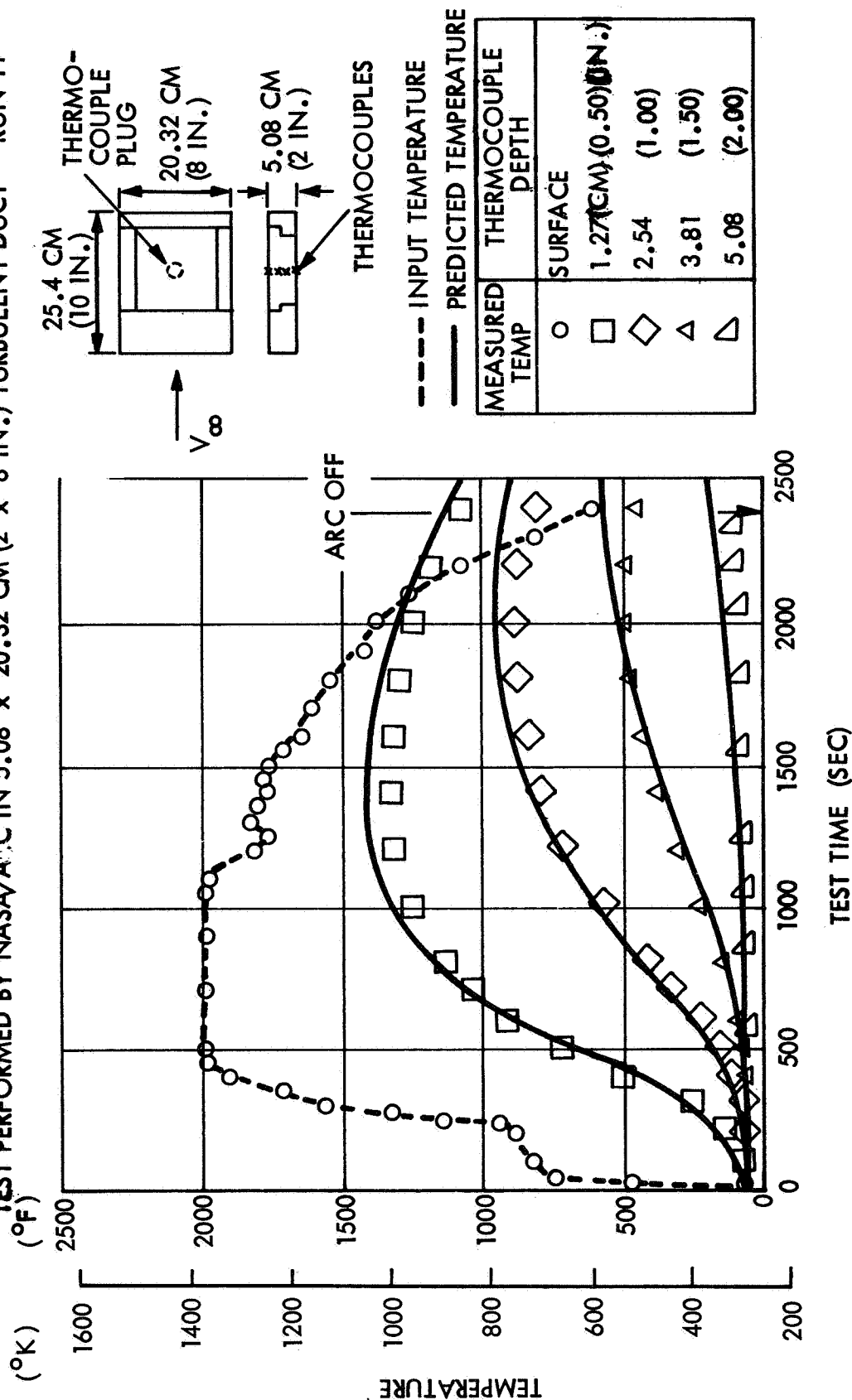


Figure 13

PREDICTABLE THERMAL RESPONSE

(Figure 14)

In addition to the stagnation flow tests of LI-1500 performed at NASA/ARC and NASA/MSC, F. J. Centalanzi et al. (Section 14 of this Volume) discussed results obtained when 20.3 x 25.4 cm (8 x 10 in.) RSI models consisting of a 15.2 x 15.2 x 5 cm (6 x 6 x 2 in.) tiles surrounded by various guard tiles were exposed to a high energy 11,700 J/g (5000 Btu/lb) high shear 13,790 N/m² (~2 psi) turbulent boundary layer. A test of this type is more representative of Shuttle Orbiter conditions during entry, since most of the heating may occur in a turbulent boundary layer.

The LI-1500 model (a deliverable discussed in Ref. 2) was instrumented in the gaps between tiles and in the center of the 15.2 x 15.2 x 5 cm (6 x 6 x 2 in.) tile. This run simulated an Area 2 heat pulse with a peak surface temperature of 1367°K (2000°F). The surface pressure varied from 6 to 55 mm Hg. The prediction used bivariate interpolation to determine the appropriate thermal conductivity values as a function of pressure and temperature. The pressure within the LI-1500 was assumed equal to the surface pressure.

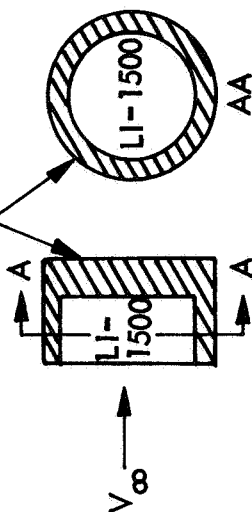
The predicted and measured data show good agreement and indicate that the LI-1500 design values are conservative and resulting weight predictions using these values for the Shuttle Orbiter may be slightly high.

These tests also provided some unanticipated gap/step heating results in that local melting of a downstream LI-1500 closure strip occurred in the vicinity of a tee-slot. The closure strip resulted in a 50-mil forward facing step. Based on correlations of wind tunnel and flight heating data, the closure strip experienced a peak heating rate of at least 3.5 times the undisturbed value, which produced a temperature greater than 1925°K (3000°F). This situation is not expected to occur in flight because of constraints on the allowable forward facing steps and larger turbulent boundary layer thicknesses.

PREDICTABLE THERMAL RESPONSE

TEST PERFORMED BY NASA/MSC IN 1.5 MW ARC TUNNEL FACILITY - RUN 703

MODEL HOLDER



$$q = 25 \text{ W/CM}^2\text{-SEC}$$

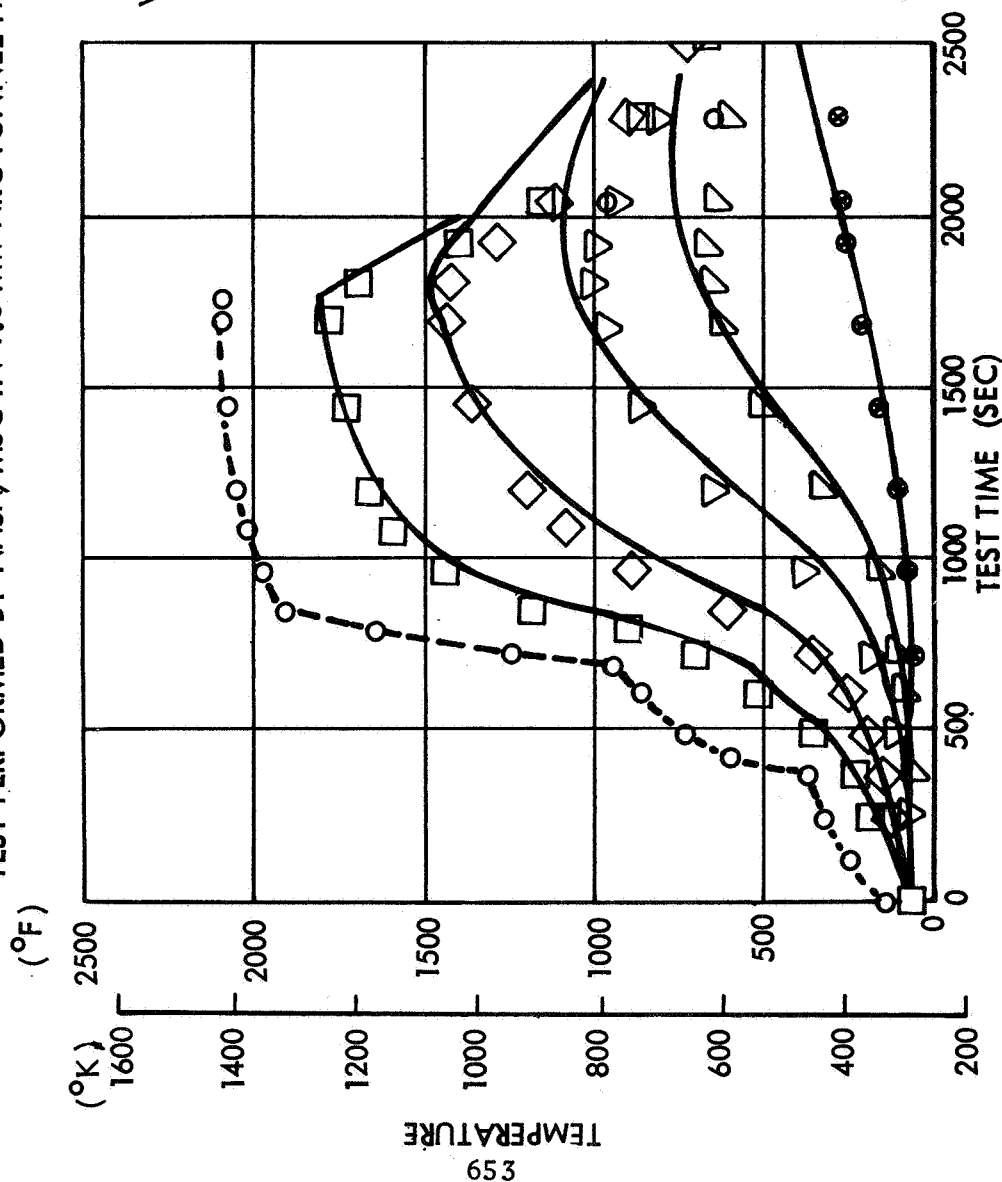
$$(22 \text{ BTU/FT}^2\text{-SEC})$$

$$H_t = 11,7000 \text{ J/g}$$

$$(5,000 \text{ BTU/LB})$$

$$P_t = 1.6 \text{ mm Hg}$$

--- INPUT TEMPERATURE
— PREDICTED TEMPERATURE



MEASURED TEMP	THERMOCOUPLE DEPTH (CM)	THERMOCOUPLE DEPTH (IN.)
○	0.254	(0.10)
□	0.762	(0.30)
◇	0.127	(0.50)
△	1.805	(0.75)
●	2.54	(1.00)
●	3.81	(1.50)

Figure 14

PROTOTYPE PANEL THERMAL RESPONSE

(Figure 15)

To verify the adequacy of various competitor RSI designs for the Shuttle Orbiter, NASA/MSC under the Phase II contracts had GE, LMSC, and MDAC supply full-scale prototype panels with RSI attached. The panels were 60.8 x 60.8 cm (2 x 2 ft) and had a sufficient amount of RSI material to limit the maximum panel temperature to 420°F (300°F) during exposure to a simulated Area 2P entry temperature and pressure history. G. Strouhal and D. J. Tillian (Section 27 of these Proceedings) present a more thorough history of the RSI development contracts and NASA requirements for the Orbiter Thermal Protection System.

The results discussed here are for LMSC Area 2P Aluminum Panel (TT62). The panel contained 24 LI-1500 tiles bonded with about 0.24 to 0.40 cm of RTV-560 adhesive to the aluminum. All tiles were 6.4 cm thick, 8 had surface dimensions of 15 x 15 cm, 8 were about 10 x 15 cm and 8 were about 5 x 15 cm. The panel was instrumented with 22 thermocouples — 4 below the surface of the 0042 coating, 3 in depth, and 15 on the aluminum panel. The gaps between tiles, which represent the LMSC joint filler strip design for the orbiter, were between 0.127 to 0.254 cm. The panel was tested in NASA/MSC radiant/vacuum facility.

As of November 1972, this panel has gone through 25 cycles of a simulated Area 2P environment. The thermal performance, as measured by the thermocouples, was repeatable within the uncertainty of the measurements. The panel has gone through 4 acoustic tests in NASA/MSC progressive wave facility of the Component Acoustic Laboratory. Each acoustic test had a duration of 150 sec, which is equivalent to 5 Shuttle liftoffs. An acoustic test was performed prior to thermal cycling, and after 5, 15, and 25 cycles. Although no visible damage was noted on the 0042 surface coating or the LI-1500 and no tiles were separated or fell off the panel, NDEs with acetaldehyde performed prior to and after the acoustic tests indicated various micro-cracks in the 0042 coating (see Section 24 of these Proceedings). Hence, even though these microcracks were present, and in some cases propagated either during or subsequent to the thermal or acoustic cycles, the LI-1500 system performed satisfactorily in that no tiles were fractured.

Comparison of the predicted and measured temperature histories indicates that the LI-1500 design thermal conductivity curves are sufficient for TPS sizing where the pressure varies from 10^3 to 10^5 N/m² (10^{-2} to 1.0 atm) and the temperature varies from room temperature to 1535°K (2300°F). The temperature predictions were included in the Phase II final report (Ref. 2) dated 2 Jan 1972 and were verified by these test results in October through November 1972.

Additional thermal and acoustic tests were performed by NASA/MSC on a LMSCI titanium panel (TT69) with sixteen 15 x 15 x 3.4 cm (6 x 6 x 1.35 in.) LI-1500 tiles bonded with 0.24 to 0.40 cm (0.090 to 0.160 in.) of RTV-560 to the titanium. A total of ten Area 2P entry cycles and three acoustic tests were performed successfully on this panel. The temperature data were predictable and repeatable and no tiles were lost in the acoustic tests.

PROTOTYPE PANEL THERMAL RESPONSE

TESTS PERFORMED BY NASA/MSC IN RADIANT HEAT/VACUUM TEST FACILITY

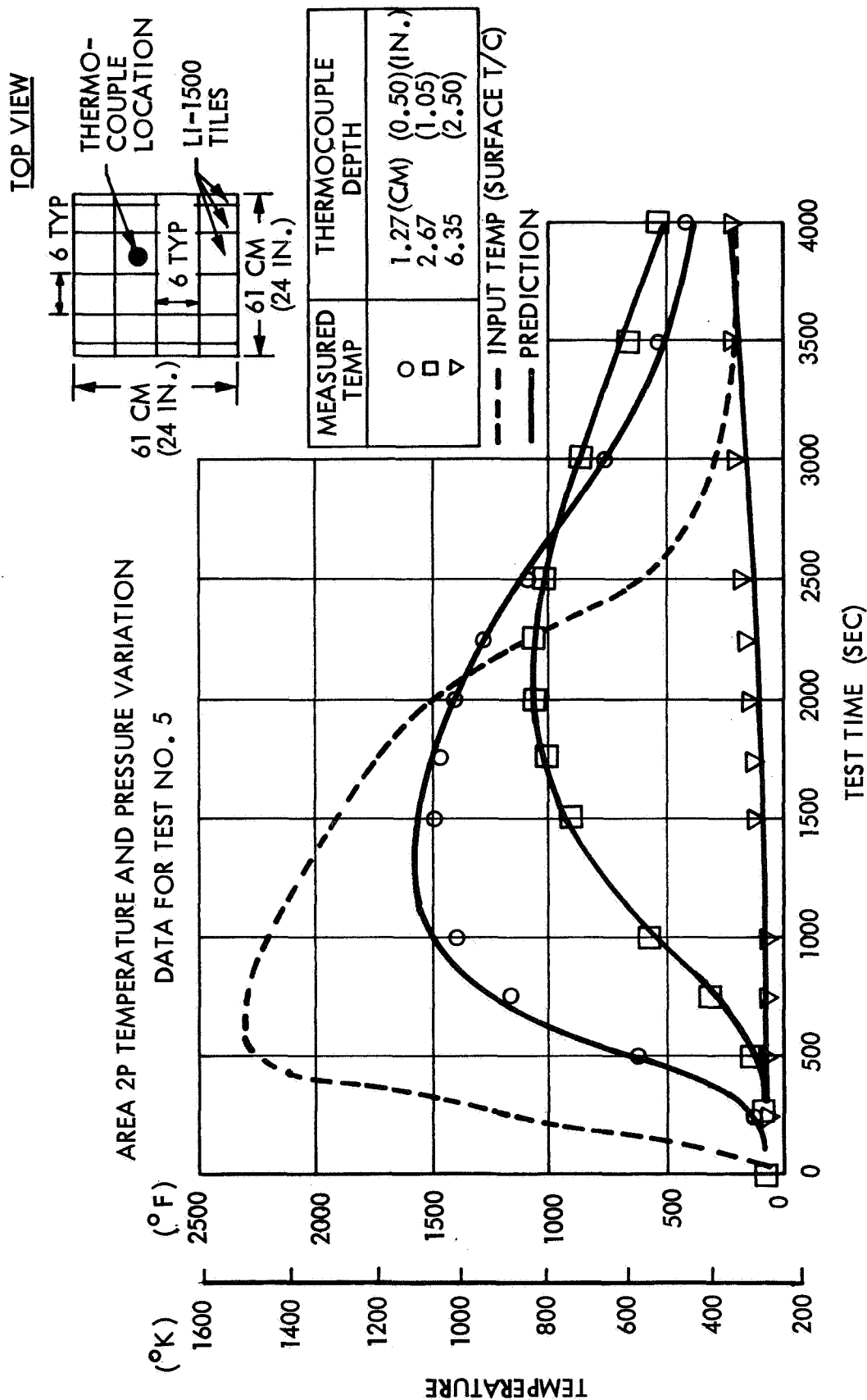


Figure 15

LI-1500 THERMAL CONDUCTIVITY COMPARISON

(Figure 16)

Comparisons of the LI-1500 design thermal conductivity at a pressure of 1.0 and 760 mm Hg are shown with conductivity values obtained by Dr. D. Curry of NASA/MSC. Dr. Curry and S. Williams in Ref. 7 discuss a nonlinear least-squares technique of "backing-out" thermal conductivity curves from transient test data. Data shown were taken from Ref. 7 and were obtained on LI-1500 samples manufactured in 1970 and tested at low pressure in NASA/MSC 1.5 MW plasma arc facility. One atmosphere pressure data were obtained from an LI-1500 sample (TT5C) tested at LMSC in November 1970. Additional thermal conductivity data, using the nonlinear least-squares technique, were obtained from the LI-1500 measured temperature data presented in Figure 13 (Personal communication with D. M. Curry on September 11, 1972).

At low pressure the conductivity values from the least-squares method are slightly lower than the LI-1500 design curves (Figure 5). At atmospheric pressure the values from the least squares method are higher than the design curve at low temperatures [73 percent at 255°K (0°F)] and slightly lower at high temperature [10 percent at 1366°K (2000°F)]. The high least-squares values from 255 to 978°K (0 to 1300°F) are questionable due to the good agreement with the aluminum panel measured temperature shown in Figure 15 and the titanium panel (TT69) and other comparisons for 10^5 N/m² (1 atm) pressure tests performed at NASA/MSC and LMSC. The comparisons between the least-squares values and the guarded hot plate values lend credibility to the nonlinear least-squares method of obtaining thermal conductivity from transient test data.

LI-1500 THERMAL CONDUCTIVITY COMPARISON

NONLINEAR LEAST SQUARES METHOD

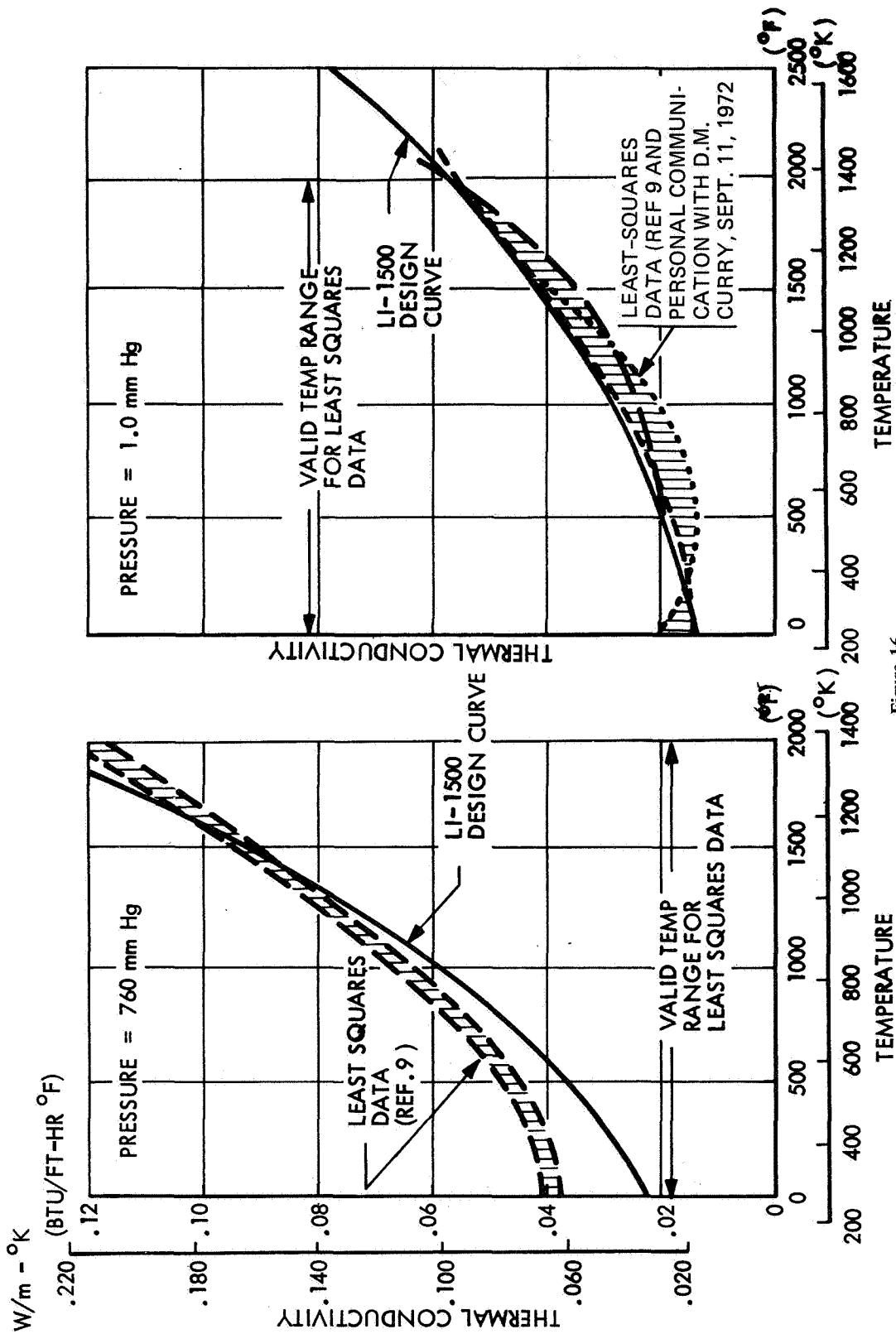


Figure 16

COMPARISON OF 0042 EMITTANCE DATA

(Figure 17)

Values for the total normal emittance of the 0042 coating from various sources computed from spectral reflectance data and emittance data are shown. The data exhibit a wide disparity in total normal emittance (values for total hemispherical emittance can be obtained from sources such as Jakob, Ref. 8). For a heat rate of 25 W/cm^2 ($22 \text{ Btu/ft}^2\text{-sec}$), an emittance of 0.9 yields a surface temperature of about 1490°K (2220°F), using an emittance of 0.6, corresponding to the NASA/LaRC data, would yield a temperature of about 1640°K (2500°F). Hence a surface temperature difference of about 411°K (280°F) could exist if the uncertainty in coating emittance is similar to that shown on the chart.

The integrated LMSC and TRW spectral data yield a total emittance that varies little with temperature. The Langley data show total emittance decreasing with increasing temperature and with lower absolute values. Battelle data, based on a total radiometric measurement, are in reasonable agreement with the Langley data, and the Ames data fall in between. From the comments made in

Figure 18 regarding temperature measurement, the Battelle and Langley data may both be in error for this coating because of true surface temperature measurement inaccuracies.

COMPARISON OF 0042 EMITTANCE DATA

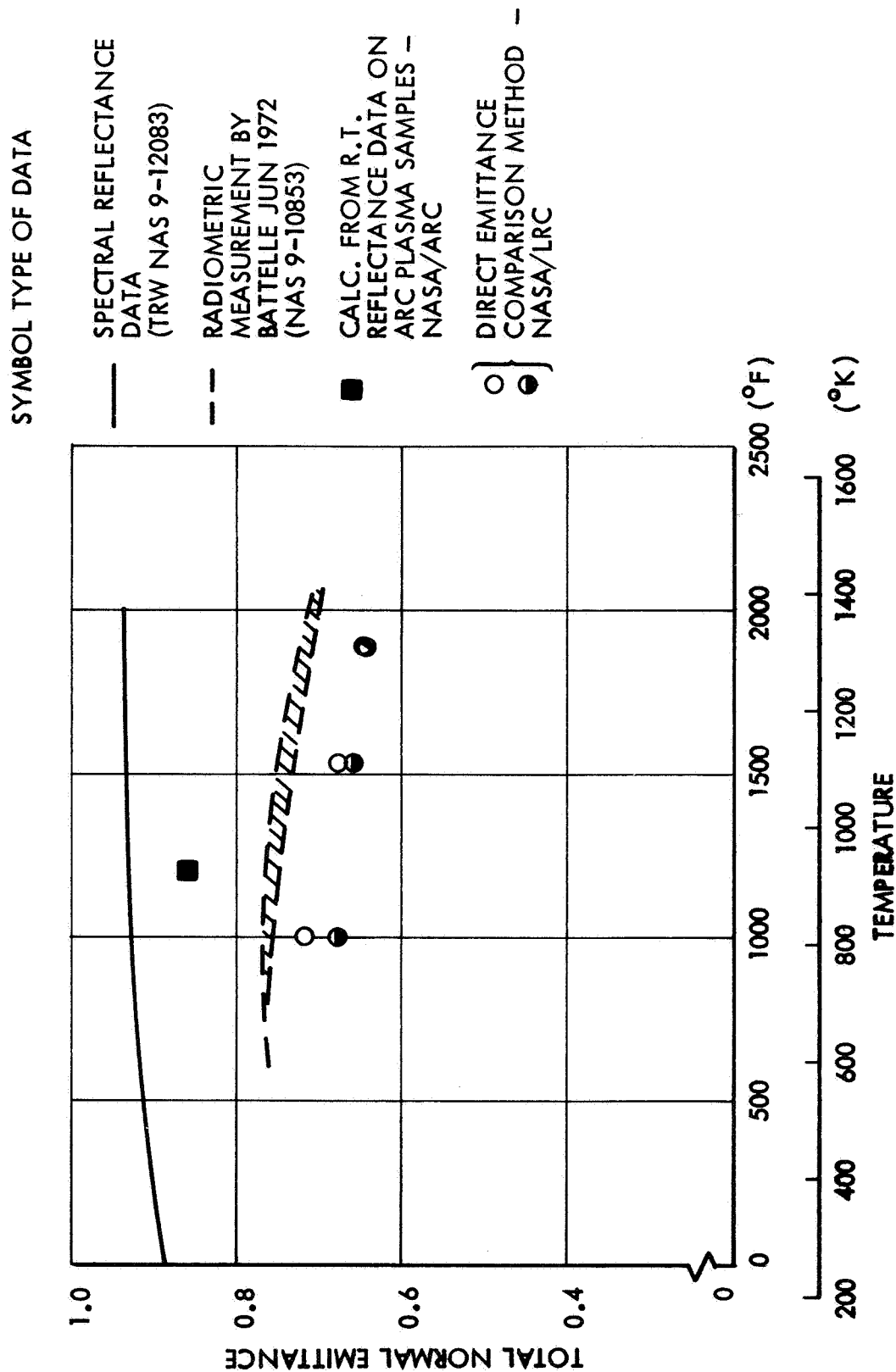


Figure 17

COMPARISON OF SPECTRAL NORMAL EMITTANCE

(Figure 18)

Spectral emittance data (in air) for the 0042 coating from several sources are shown. Direct measurements of spectral emittance were made by Langley using a comparison of radiances from the coating and a reference (standard or cavity) by the Furnace Enclosed Sample/Reference method (Ref. 9). Spectral emittance values are also shown that were computed from spectral reflectance measurements at LMSC and TRW. Emittance is inferred from reflectance data using the relationship $\epsilon_\lambda = (1 - \rho_\lambda)$ assuming the coating is opaque. This assumption was verified by the TRW measurements by using both a low reflectance oxidized metal (Inconel) and a high reflectance platinum strip to back the sample. Measurements made at 1, 2.2, and 5 μ with both backing surfaces were within 0.01 verifying that transparency is not a significant source of error in using the reflectance-emittance relationship.

The large discrepancies between the two sets of data can be attributed to (1) specimen differences, (2) measurement errors, or (3) a combination of both. As the LMSC data (reflectance) on the Langley specimen (sent to LMSC in July 1972) after emittance testing are essentially in agreement with both earlier LMSC measurements and the TRW data (Ref. 2, Vol. I, pp. 4-33), the specimen-to-specimen differences are considered to be minimal. Concerning measurement error, the coating was found to be opaque so the reflectance-emittance relationship is valid.

Sample emission is not a primary source of error in the TRW measurement method since for reflectance measurements temperature determination does not enter into the method other than to assign a temperature at which reflectance is measured. A primary source of measurement error for the direct emittance data (NASA/LRC) lies in the temperature measurement since the accuracy is strongly dependent on the accuracy to which surface temperature is known.

Using Planck's law the spectral emittance error can be expressed as:

$$\frac{\Delta\epsilon_\lambda}{\epsilon_\lambda} = \frac{C_2/\lambda T}{T} \left(e^{\frac{C_2}{\lambda T}} - 1 \right)^{-1} \frac{C_2}{\lambda T} \frac{\Delta T}{T}$$

An estimate was made of the potential for surface temperature error in the Langley data by comparing their spectral data with the TRW data, and computing the temperature difference that would be required for both sets of data to agree. The following results show the magnitude of this temperature difference (ΔT) for two measurement temperatures.

ϵ_{λ} (μ)	T ($^{\circ}\text{K}$)	ΔT ($^{\circ}\text{K}$)	T ($^{\circ}\text{K}$)	ΔT ($^{\circ}\text{K}$)
3.5	1307	106	813	59
5.0	1307	110	813	56
8.0	1307	107	813	63
12.0	1307	93	813	68

From these consistent temperature differences at several wavelengths it appears that the actual surface temperatures for the Langley data are lower than their indicated temperatures, and it is suggested that they reevaluate the measurement procedure for surfaces placed on very low thermal diffusivity substrates.

COMPARISON OF SPECTRAL NORMAL EMITTANCE

LMSC-0042 COATING

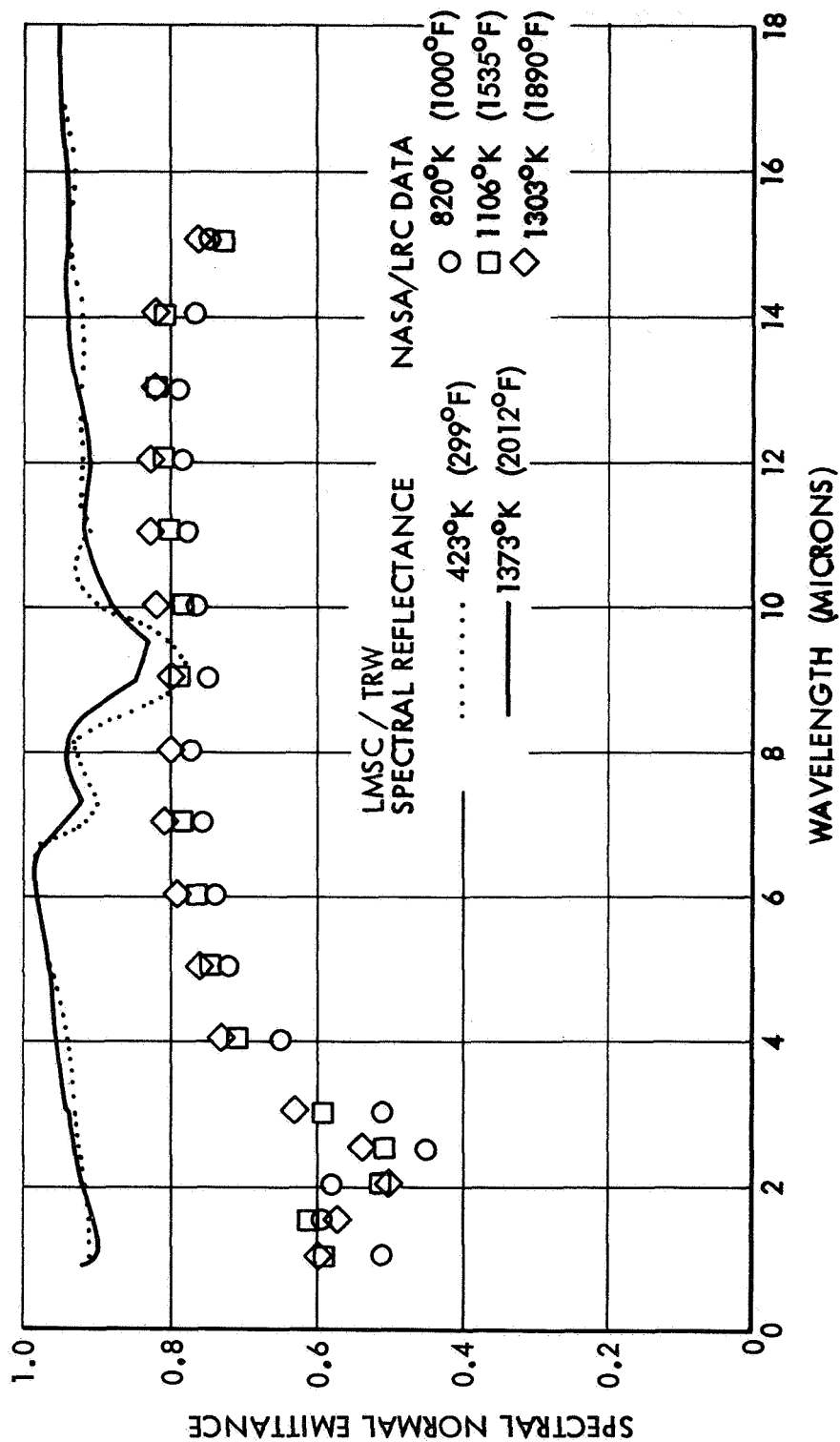


Figure 18

CONCLUSIONS – LMSC SILICA

(Figure 19)

Simulated reentry heating of the all-silica RSI under a variety of conditions including arc-jet and radiant lamp facilities for up to 100 simulated flight cycles has demonstrated consistent thermal performance capability. This consistency has been evident in testing of this material from 1967 to the present. Additionally, LMSC has successfully predicted (pre-test) this performance since 1967 on the basis of both LMSC and NASA-generated thermophysical material property data. This consistent predictability, along with the demonstrated coating integrity and dimensional stability to 1645° K (2500°F), serves to validate the earlier LMSC selection of the all-silica material for the RSI application.

This consistent predictable performance provides the confidence base for designing an Orbiter Thermal Protection System with the all-silica RSI.

CONCLUSIONS – LMSC SILICA

MULTICYCLE REENTRY HEATING TESTS HAVE DEMONSTRATED:

- CONSISTENT THERMAL PERFORMANCE CAPABILITY
- PREDICTABLE THERMAL PERFORMANCE BASED ON NASA GENERATED DATA
- COATING INTEGRITY
- DIMENSIONAL STABILITY TO 1648⁰K (2500⁰F)

Figure 19

REFERENCES

1. Beasley, R. M., Izu, Y. D., et al: Improvement of Reusable Surface Insulation Material. Final Report NAS 9-12137, LMSC-D166104, Lockheed Missiles & Space Company, Inc., Mar 1, 1972
2. Buttram, R. D., Banas, R. P., DeRuntz, J. A., Kural, M. H., et al: Space Shuttle Thermal Protection System Development. Vols. I and II, Final Report, NAS 9-12083, LMSC-D152738, Lockheed Missiles & Space Company, Inc., Jan 17, 1972
3. Buttram, R. D., Beasley, R. M., et al: Development of a Rigidized, Surface Insulative Thermal Protection System for Shuttle Orbiter. Final Report, NAS 9-11222, LMSC-A984200, Lockheed Missiles & Space Company, Inc., Feb 16, 1971
4. Michalak, R. J., Hess, T. E., et al: Reusable Surface Insulation Thermal Protection System Development Program, Final Report, NAS 9-12084, GE-EYP-012, Reentry and Environmental System Division-General Electric, May 1972
5. Ruset, E. L., Christensen, H. E., et al: Reusable Surface Insulation (RSI) Thermal Protection Development for Shuttle, Addendum to Final Report MDC E0557, NAS 9-12082, McDonnell Douglas Astronautics Co., — East, June 23, 1972
6. Kistler, C. W., et al: Evaluation of Nonmetallic Thermal Protection Materials for Manned Space Shuttle, Vol. V (Phase II, Task 3 and Phase III, Task 1), NAS 9-10853, Battelle; Columbus, Ohio, June 1, 1972
7. Curry, D. M. and Williams, S. D.: Nonlinear Least Squares — An Aid to Thermal Property Determination, NASA TMX-58092, June 1972
8. Jakob, Max: Heat Transfer, Vol. I, pg 43, John Wiley & Sons, Inc., New York, 1949
9. Slomp, W. S. and Wade, W. R.: A Method for Measuring the Spectral Normal Emittance in Air of a Variety of Materials Having Stable Emittance Characteristics, p 433, Paper No. 43 — Measurement of Thermal Radiation Properties of Solids, NASA SP31, 1963

**ENVIRONMENTAL TESTING OF REI-MULLITE
THERMAL PROTECTION SYSTEM FOR THE
SPACE SHUTTLE ORBITER**

BY

R. GLUCK, R. ROMANO, H. THIBAUT

**GENERAL ELECTRIC COMPANY
RE-ENTRY & ENVIRONMENTAL SYSTEMS DIVISION
PHILADELPHIA, PENNSYLVANIA**

INTRODUCTION
TPS DESIGN ENVIRONMENTS
(Figure 1)

The Space Shuttle Orbiter has as its requirements a 10-year lifetime with 100 or more mission reuse capability to re-entry surface temperatures of 1644° K (2500° F). To meet these requirements, the thermal protection system (TPS) for the Orbiter must, in addition to surviving the thermostructural environments of entry into the earth's atmosphere, have all-weather capability similar to current aircraft operations, resistance to vacuum/temperature exposure in space, and resistance to the structural fatigue environments of aircraft mode operations.

The objectives of this paper are to discuss and present results of special environmental tests performed on the General Electric Company's Re-entry and Environmental Systems Division (GE-RES) Reusable Surface Insulation System, REI-Mullite. These environmental tests make up the mission environments that affect the design and reliability of the Orbiter TPS, and include salt spray, humidity, rain erosion, acoustics, orbital vacuum, hot and cold orbital soak conditions, re-entry heat, and structural loads.

Discussions are first presented on individual test series to evaluate the natural environments of salt spray, humidity, rain and vacuum followed by a discussion of the results of the Structures Test Program (STP) performed for North American Rockwell/Space Division (NR/SD) to evaluate the performance of the REI-Mullite TPS for induced multiple cycle environments of acoustics, orbital temperature, re-entry heat, and structural loadings.

TPS DESIGN ENVIRONMENTS

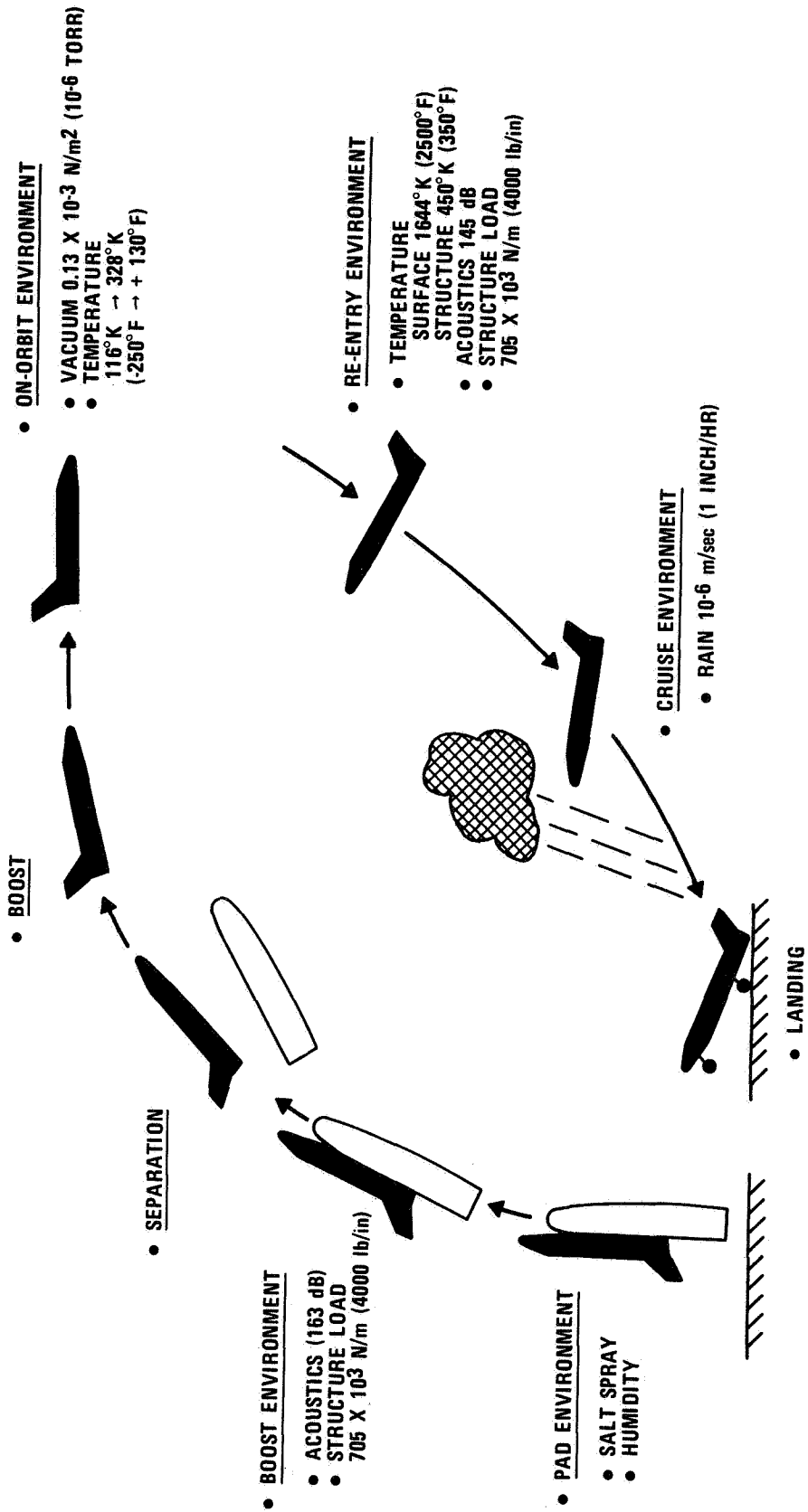


Figure 1

REI-MULLITE TPS INSTALLATION

(Figure 2)

The General Electric Company's RSI Thermal Protection System consists of REI-Mullite coated on five sides with a thin ceramic base material, SR-2, bonded with PD200 foamed elastomeric pads to an aluminum primary skin structure. The REI-Mullite is a low density, 192 kg/m³ (12 lb/ft³) rigidized fibrous material that provides the insulative characteristics necessary to protect the aluminum structure to its maximum operating temperature of 450° K (350° F). The ceramic coating provides a hard waterproof surface for resistance to rain erosion and handling damage. This coating, being the outer surface of the vehicle, must also have proper high temperature emissivity characteristics, $\epsilon > 0.8$, to maximize re-entry heat rejection by reradiation and proper optical property characteristics, $\alpha/\epsilon \approx 0.4$ to 0.5, to limit on-orbit temperature extremes.

Differences in thermal expansion coefficient between the insulation and structure and deformations of approximately 0.5 percent strain require, for structural margin considerations, that interaction between the structure and the TPS be minimized. This strain isolation is accomplished by means of a foamed silicone elastomeric pad, PD-200, bonded in place between the insulation and the structure.

The insulation tiles are provided with a vent to allow depressurization of the material during ascent.

REI-MULLITE TPS INSTALLATION

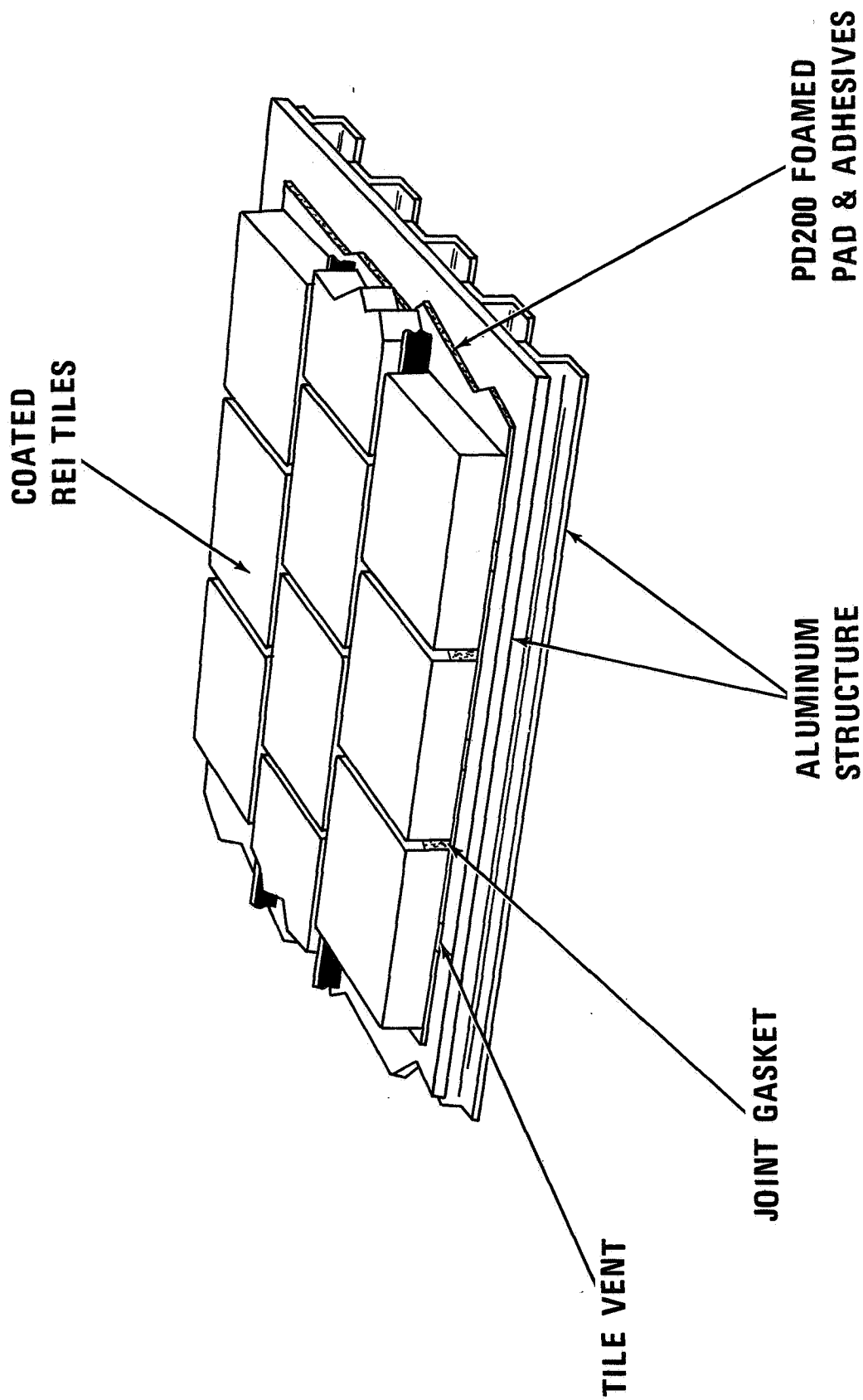


Figure 2

VACUUM VENT TESTING

(Figure 3)

The REI-Mullite TPS panel must be vented to allow decompression during boost and repressurization during re-entry while preventing boundary layer flow through from surface pressure gradients and water and moisture injection. A test series⁽¹⁾ was performed in which coated REI-Mullite tiles bonded to aluminum plates were subjected to boost depressurization and boost heating, orbital vacuum, and re-entry heating. The specimens were $0.1 \times 0.2 \times 0.038$ m ($4 \times 8 \times 1.5$ in.) with a pressure tap located in the center of the REI-Mullite tile. The vent for the tile is located on the aft facing tile side and consists of a 0.8×10^{-4} square meter (0.125 square inch) vent hole in the PD-200. The vented REI-Mullite surface is coated with PD-200 primer to provide waterproofness to the tile.

Tests were run on both dry and wet specimens because it was determined that the case of absorbed moisture in a damaged tile that had escaped detection during nondestructive evaluation (NDE) would be the critical design condition. One test was performed with 30 percent H₂O by weight in the tile with the vent sealed to determine the failure mode.

VACUUM VENT TESTING MATRIX

MODEL NO.	TEST NO.	CONDITIONS	FACILITY	OBJECTIVE
1	1	COATED REI-MULLITE SPECIMEN WITH VENT HOLE	VACUUM SYSTEM TO SIMULATE VENT PRESSURE HISTORY	DEMONSTRATE ADEQUACY FOR DEPRESSURIZATION OF DRY REI-MULLITE
	2	COATED REI-MULLITE SPECIMEN WITH VENT HOLE	VACUUM SYSTEM COUPLED WITH RE-ENTRY SIMULATOR	DETERMINE EFFECT OF BOOST THERMAL ENVIRONMENT ON VENTING REQUIREMENTS
	3	COATED REI-MULLITE SAMPLE WITH VENT HOLE (10% H ₂ O BY WEIGHT)	VACUUM SYSTEM TO SIMULATE VENT PRESSURE HISTORY	DEMONSTRATE ADEQUACY OF VENTING AREA FOR WATER/AIR MIXTURE IN REI-MULLITE
	4	COATED REI-MULLITE SAMPLE WITH VENT HOLE (10% H ₂ O BY WEIGHT)	VACUUM SYSTEM COUPLED WITH RE-ENTRY SIMULATOR	SHOW THAT VENTING AREA IS SUFFICIENT TO PREVENT PRESSURE BUILD UP IN REI-MULLITE FOR WATER/AIR MIXTURE
	5	COATED REI-MULLITE SAMPLE WITH VENT SEALED (30% H ₂ O BY WEIGHT)	RE-ENTRY SIMULATOR	DEMONSTRATE ACCEPTABLE SINGLE MISSION CAPABILITY FOR WATER IMPREGNATED REI-MULLITE
2	1	COATED REI-MULLITE SAMPLE WITH VENT HOLE (5% H ₂ O BY WEIGHT ON 3rd CYCLE)	VACUUM SYSTEM COUPLED WITH RE-ENTRY SIMULATOR	DEMONSTRATE ADEQUACY OF VENTED REI-MULLITE DESIGN FOR MULTIPLE (3) MISSION CYCLES OF BOOST DEPRESSURATION AND HEAT, ORBITAL VACUUM AND COLD SOAK, AND RE-ENTRY HEATING

Figure 3

VACUUM VENTING TEST RESULTS

(Figure 4)

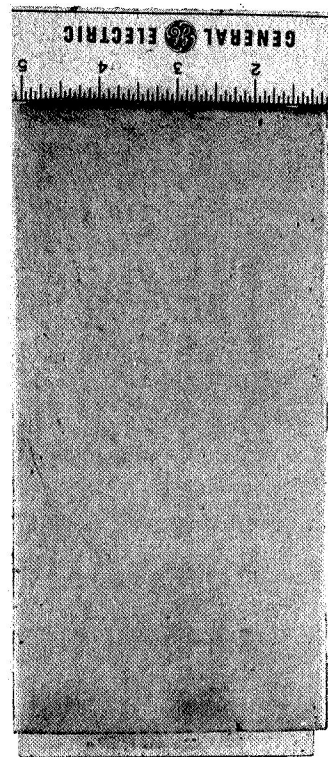
Results of this test series showed the proposed vent design would provide adequate venting of a coated REI-Mullite panel without impairing the waterproof characteristics of the design. Model pressures tracked the vacuum chamber pressures to within 667 N/m^2 (5 mm Hg) for up to 10 percent of H_2O by weight in the specimen even with boost heating applied.

Eighty-five to ninety-nine percent of the initial H_2O in the specimens was lost during the boost depressurization and heating cycles.

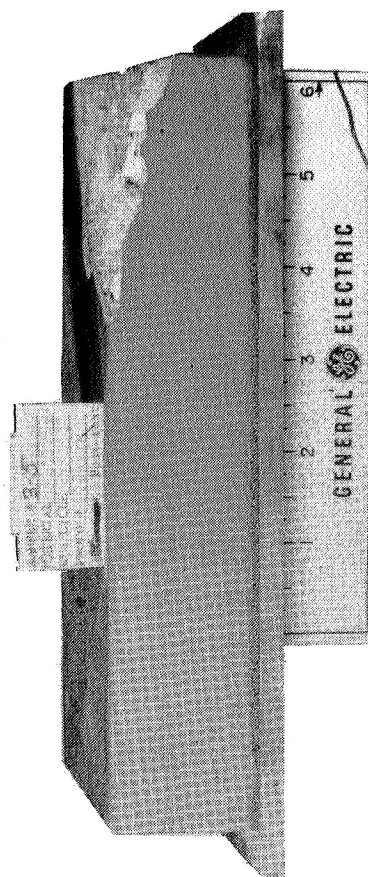
Pressure levels in the specimen of less than 10^3 N/m^2 (10^{-2} atm) were measured after a period of 94 minutes. This represents a launch orbit cycle, confirming the use of 10^3 N/m^2 (10^{-2} atm) conductivity data for TPS design.

The failure mode for a tile that had 30 percent H_2O and a sealed vent was found to be that of surface coating failure. The tile remained intact, still capable of providing thermal protection for one re-entry condition, demonstrating the fail safe characteristics of the system for water injection. A ΔP of $16.5 \times 10^3 \text{ N/m}^2$ (2.4 psi) was developed across the coating prior to failure.

675



**VENTING TEST — MODEL 1, TEST NO. 4, AIR/WATER
(10 PERCENT H₂O)**



**VENTING TEST – MODEL 1, TEST NO. 5, SEALED MODEL
(30 PERCENT WATER)**

Figure 4

SALT SPRAY AND HUMIDITY TESTING

(Figure 5)

Salt spray and humidity tests were performed to evaluate the performance of the REI-Mullite TPS. Specimen geometry consisted of $0.1 \times 0.2 \times 0.038$ m ($4 \times 8 \times 1.5$ inch) coated tiles bonded to aluminum plates with 0.008 m (0.3 inch) thick PD-200. The REI-Mullite tiles were vented with the design previously discussed. Three specimens were subjected to the salt spray and humidity environment. The salt spray environment consisted of a forty-eight hour exposure to a 5 percent salt spray at 308° K (95° F). Following salt spray, the specimens were exposed to seven twenty-four hour humidity cycles. Each cycle consisted of an increase to $95 \text{ percent} \pm 5 \text{ percent}$ relative humidity and 308° K $\pm 3^\circ$ (95° F $\pm 5^\circ$) in two hours, a six hour hold at 95 percent R.H. and 308° K, and a reduction to 85 percent R.H. and 294° K (70° F) in sixteen hours. Following salt spray and humidity exposure two specimens, along with an identical specimen that had not been exposed, were subjected to a re-entry temperature simulation cycle where the surface temperature of the panels were maintained at 1478° K (2200° F) for a period of eighteen hours at 10^3 N/m^2 (10^{-2} atm). This represents the equivalent time at temperature of 100 missions. The specimens were actively cooled on the backface to maintain the REI/PD-200 interface to below 616° K (650° F).

Specimens were evaluated by means of coating bending test specimens and scanning electron micrographs (SEM's) to assess the material behavior as a function of exposure environment.

SALT SPRAY & HUMIDITY TEST PROGRAM

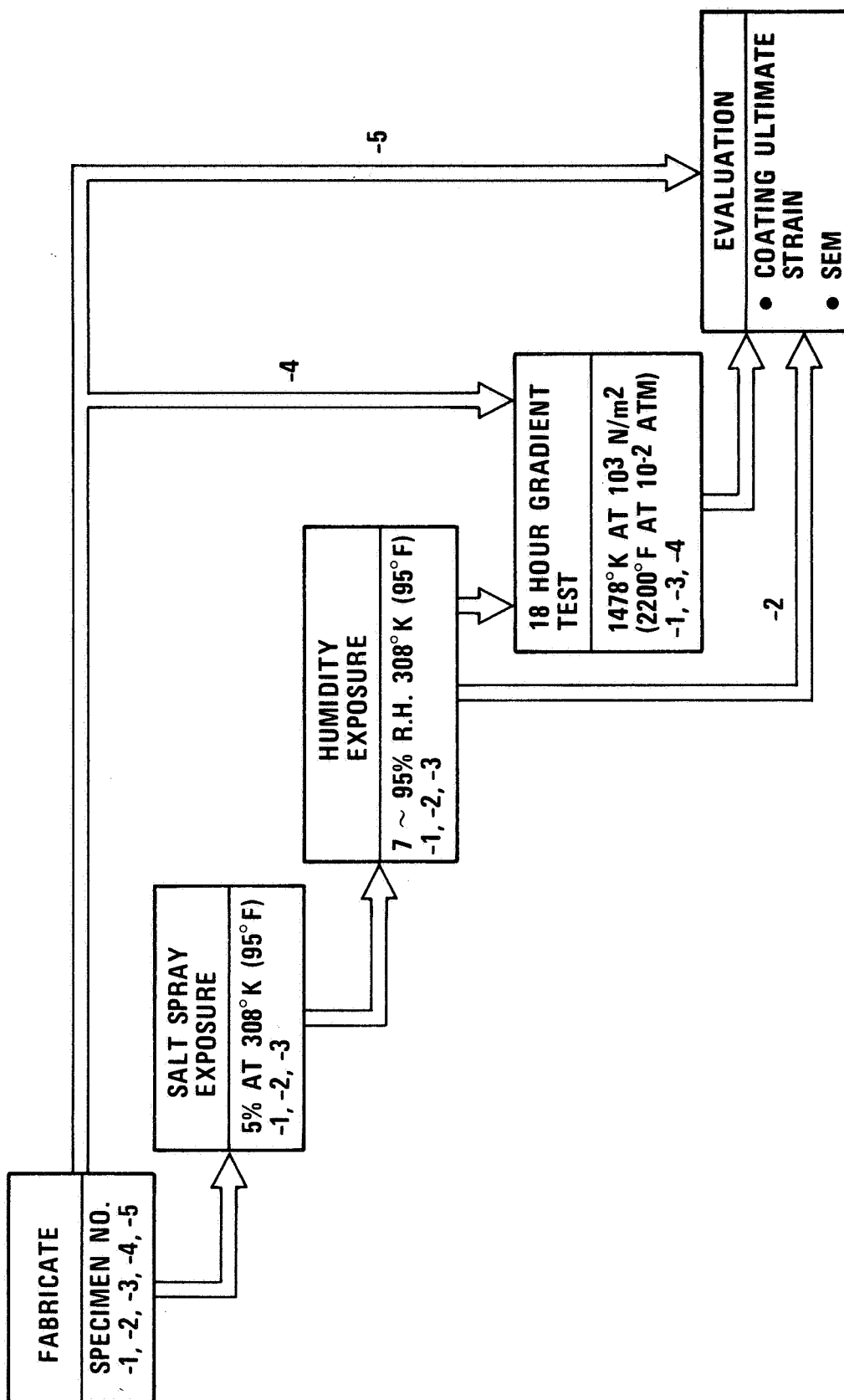


Figure 5

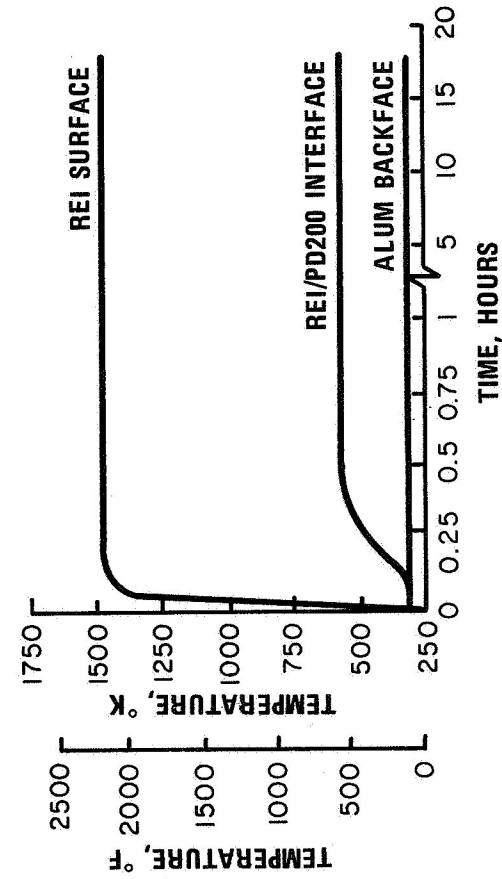
SALT SPRAY AND HUMIDITY TEST RESULTS (Figure 6)

Specimens were weighed before and after exposure to salt spray and humidity. One specimen showed a slight increase in weight during salt spray and remained stable during the humidity testing. The other two specimens were unchanged throughout the test cycles. Initial plans were to run the 18 hour gradient test at 1644° K (2500° F) surface temperature; however, the maximum temperature limit of 616° K (650° F) was exceeded and caused bond decomposition on one specimen. Remaining specimens were tested at 1478° K (2200° F) surface temperature. Maximum surface temperature was achieved in approximately eight minutes and held constant for 18 hours. The REI-Mullite/PD-200 interface reached a maximum temperature of 566° K (560° F) after approximately 1/2 hour and remained constant for the remainder of the test indicating no change in thermal conductivity after long exposure at temperature. No degradation of performance was determined as a result of exposure to salt spray and humidity.

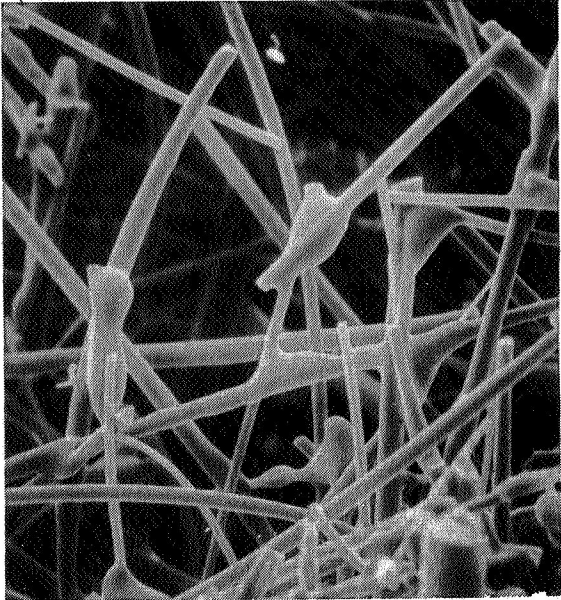
Tensile failure strain of the SR-2 coating of each specimen was obtained after testing. 0.0127 m (1/2 inch) square cross-section beams with the coating on the tensile face were machined from the specimens and loaded by four point bending. Failure strains were determined by strain gage measurements. Comparison with virgin coating data indicates that the exposure conditions did not have a detrimental effect on coating structural capability.

SEM's were obtained from coupons cut from the front and back face of the specimens. Visual scanning and photographs showed no damage to the fibers or deterioration of the binder fillets between fibers confirming that exposure to salt spray, humidity and thermal gradient, or salt spray and humidity only, has no harmful effects on the REI-Mullite. These conclusions were confirmed by NASA tests.⁽²⁾

SALT SPRAY & HUMIDITY TEST RESULTS



SPECIMEN NO.	WEIGHT (GRAMS)		
	AS FABRICATED	AFTER SALT SPRAY	AFTER HUMIDITY
-1	595	595.5	595.5
-2	577	590	589
-3	600	601	601



SEM AFTER SALT SPRAY, HUMIDITY AND 18 HOUR GRADIENT TEST

COATING FAILURE STRAIN (%)				
	AFTER SALT AND HUMIDITY	AFTER SALT, HUMIDITY AND GRADIENT	AFTER 18 HOUR GRADIENT	AS FABRICATED
ϵ	0.016	0.067	0.030	0.015
RANGE	0.012 0.022	0.058 0.082	0.012 0.052	0.014 0.015
N	3	3	3	2
				PRIOR DATA
				0.026 0.013 0.034 25

Figure 6

FREEZE/THAW TESTING

(Figure 7)

The results of the vacuum vent test program showed that moisture can be retained in the REI-Mullite tile after the boost cycle. Hence, two specimens, a coated specimen and an uncoated REI-Mullite specimen were impregnated with 30 and 43 percent H₂O by weight and subjected to a freeze thaw cycle. The specimens were cooled with LN₂ to 166° K (-160° F) and held for a period of four hours. The specimens were then warmed to room temperature. No degradation of the coating or REI-Mullite was observed.

FREEZE/THAW TEST RESULTS

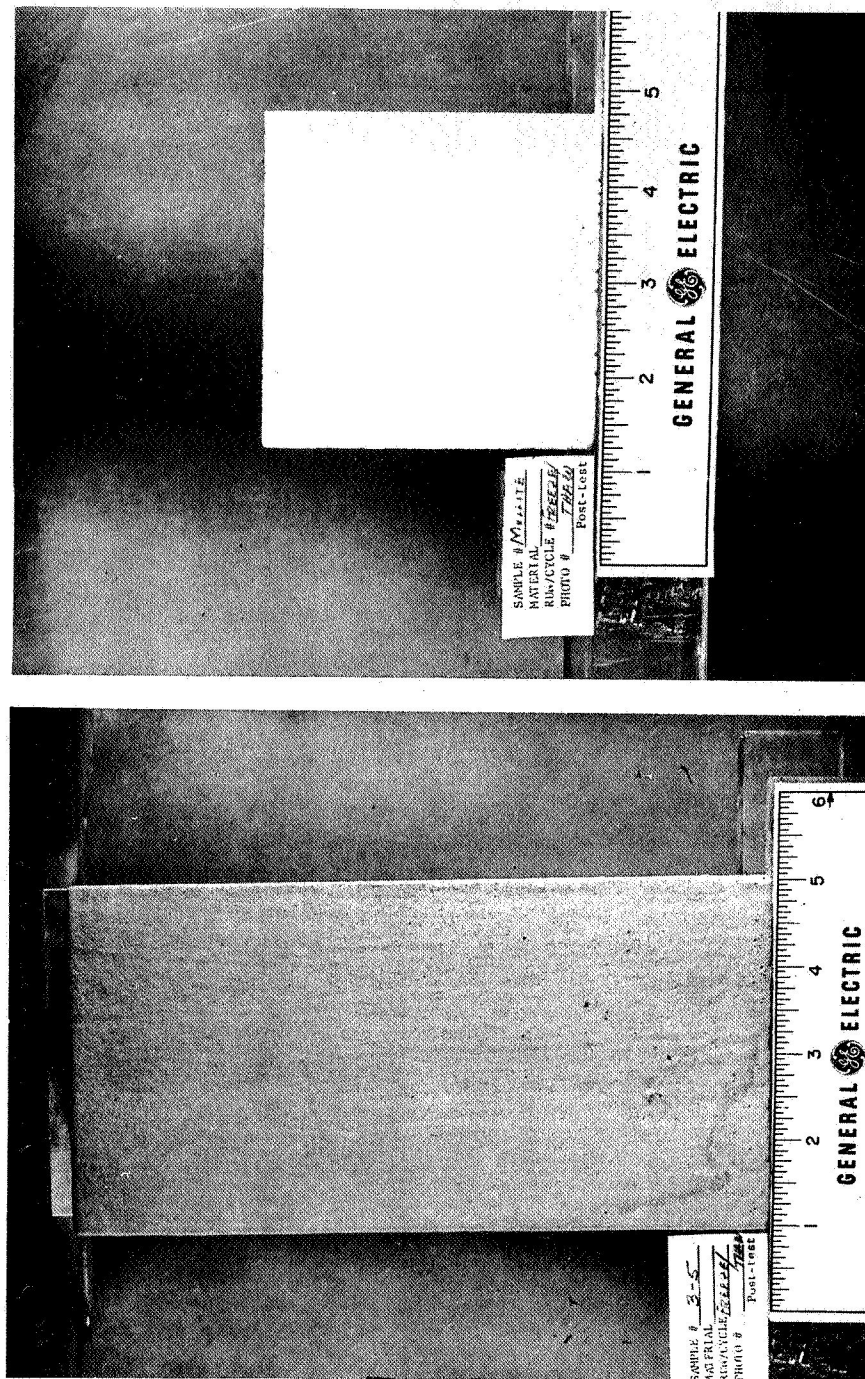


Figure 7

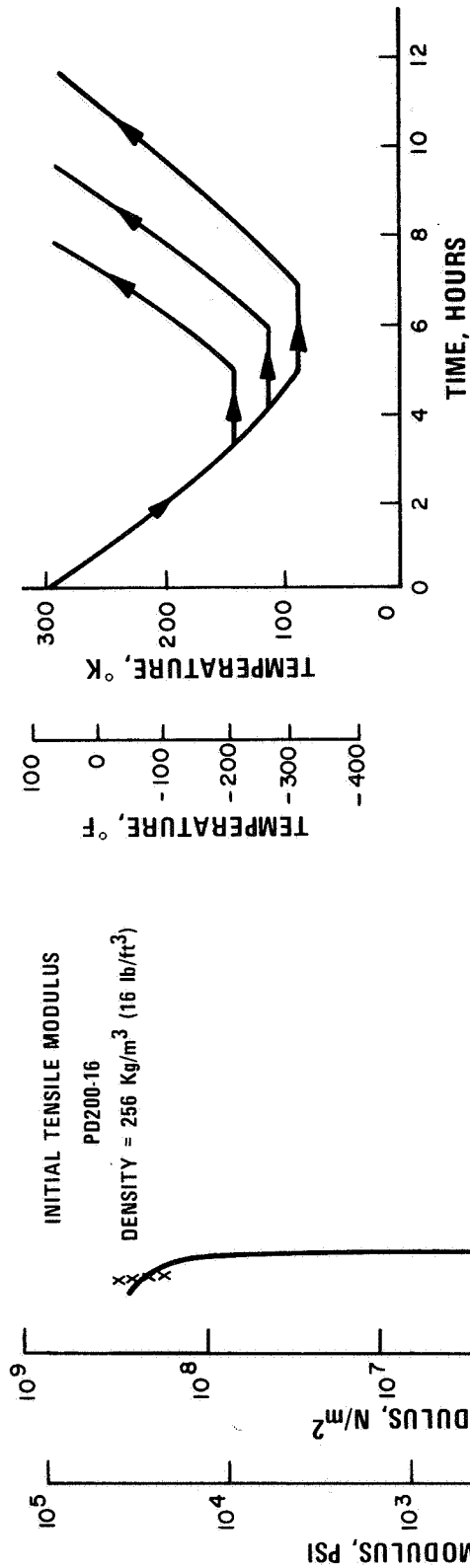
COLD SOAK TESTS

(Figure 8)

The orbital phase of the mission results in a cold environment of 116°K (-250°F). This temperature is significantly below the glass transition temperature of the PD200 strain isolator system. High tensile and shear stress are developed at the REI-Mullite/PD200 and PD200/Aluminum interface as the temperature is lowered below glass transition. Cold soak tests on representative REI-Mullite/PD200/structure composites were conducted. The tests consisted of a controlled cool-down to the desired temperature, a hold at temperature, and a controlled warm-up to room conditions. Tests were conducted to temperatures as low as 89°K (-300°F) to empirically demonstrate a 50% margin of safety on the ΔT below the glass transition temperature.

Results showed that PD 200-28, 448 kg/m^3 (28 lb/ft^3) density material, could not provide a satisfactory margin for the 116°K (-250°F) environment. Subsequent tests showed that PD200-16, 256 kg/m^3 (16 lb/ft^3) was completely compatible for the cold soak condition.

COLD SOAK TESTS



TEST TEMP °K (°F)	PD200-28		PD200-16	
	THICKNESS m (IN)	RESULTS	THICKNESS m (IN)	RESULTS
144 (-200)	7.6 x 10 ⁻³ (0.3)	NO FAILURES	6.3 x 10 ⁻³ (0.25)	NO FAILURES
116 (-250)	7.6 x 10 ⁻³ (0.3)	NO FAILURE	6.3 x 10 ⁻³ (0.25)	NO FAILURES
89 (-300)	7.6 x 10 ⁻³ (0.3)	REIMULLITE COATING CRACKED	6.3 x 10 ⁻³ (0.25)	NO FAILURES

Figure 8

RAIN EROSION TESTING

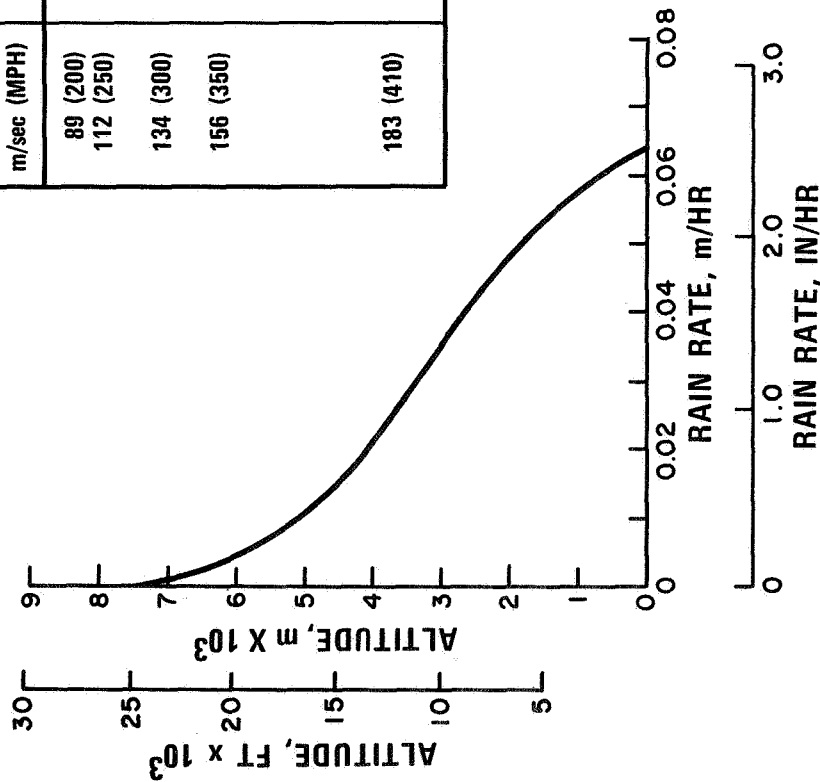
(Figure 9)

Rain erosion tests⁽³⁾⁽⁴⁾ were performed in the AFML-Bell rotating arm rain and sand erosion test apparatus on REI-Mullite coated with SR-2. Tests were conducted at 0.175, 0.35, and 0.7 rad (10, 20, and 40 degree) incidence angles and velocities ranging from 89 m/sec (200 mph) to 183 m/sec (410 mph). Rain rates were limited to a maximum of 0.025 m/hr (1 in/hr), which is representative of subsonic cruise above 3,500 m (11,500 ft). Test data showed no erosion of the SR-2 coating. Impact damage to the coating was observed and found to be time dependent. After initial impact damage, coating removal was evident. In evaluating this failure mode it was determined that rain rates were constant at 0.025 m/hr (1 in/hr). Lower rain rates were achieved by intermittently subjecting the specimens to the 0.025 m/hr (1 in/hr) rate. These conditions result in constant droplet mass, frequency and distribution with exposure time the only variable.

Two possible reasons exist for the time dependent failure mode. The first is the statistical probability of a droplet impacting a weak spot in the coating. The second is the possibility of cumulative damage to the coating by multiple impacts. Improvements to the damage threshold of the SR-2 coating are readily achievable by increased coating thickness and more uniform application.

RAIN EROSION TESTING

SUMMARY OF RAIN DAMAGE THRESHOLD			
VELOCITY m/sec (MPH)	INCIDENCE ANGLE RAD (DEG)	RAIN RATE m/hr (in/hr)	DAMAGE THRESHOLD
89 (200)	0.35 (20)	0.025 (1)	NO DAMAGE AFTER 60 MINUTES
112 (250)	0.175 (10)	0.025 (1)	NO DAMAGE AFTER 30 MINUTES
	0.35 (20)	0.025 (1)	DAMAGE STARTS AFTER 20 MINUTES
134 (300)	0.175 (10)	0.025 (1)	NO DAMAGE AFTER 20 MINUTES
	0.35 (20)	0.025 (1)	NO DAMAGE AFTER 10 MINUTES
156 (350)	0.175 (10)	0.012 (.5)	DAMAGE STARTS AFTER 18.5 MINUTES
		0.025 (1)	DAMAGE STARTS AFTER 5 MINUTES
	0.35 (20)	0.006 (.25)	DAMAGE STARTS AFTER 3 MINUTES
		0.012 (.5)	DAMAGE STARTS AFTER 1.7 MINUTES
	0.70 (40)	0.025 (1)	DAMAGE STARTS AFTER 1.3 MINUTES
183 (410)	0.175 (10)	0.006 (.25)	DAMAGE STARTS AFTER .25 MINUTES
		0.025 (1)	NO DAMAGE AFTER 5 MINUTES
	0.35 (20)	0.006 (.25)	DAMAGE STARTS AFTER 2 MINUTES



RAINFALL RATE FOR
0.0635 m/hr (2.5 in/hr) THUNDERSTORM
REF.: TMX53872 & 64589

Figure 9

STRUCTURES TEST PROGRAM

(Figure 10)

A Structural Test Program (STP) was performed by GE-RESO for NR/SD. Under this program, a series of mission environmental simulation tests was performed to establish multimission capability of REI-Mullite. Testing was performed on specimens that realistically simulated panels of the TPS for both hot windward, maximum surface temperature of 1644° K (2500° F), and cool windward, maximum surface temperature of 978° K (1300° F). Mission simulations included twenty-five cycles of boost acoustics and one-hundred cycles of re-entry heat simulation with interspersed orbital-cold and orbital-hot vacuum soaks and structural loadings. In order to demonstrate the multimission capability, the following test objectives were established:

- Determination of ultimate load capability on representative primary airframe structure
- Determination of effects of acoustics, orbital soak, and re-entry cycling on failure mode and load
- Evaluation of coating, attachment, and REI overall performance after simulated environmental cycling

Four phases of tests on the hot windward specimens to determine one, 10, 25, and 100 mission cycle performance and two phases of tests on the cool windward specimens to determine one and 25 mission cycle performance were conducted.

```

graph TD
    Fabricate[FABRICATE NO. 1-18] --> NDE1((NDE))
    NDE1 --> BoostAc[1 ~ BOOST ACOUSTICS NO. 3-8, 15-18]
    BoostAc --> NDE2((NDE))
    NDE2 --> ColdSoak1[166°K (-160°F) COLD SOAK NO. 3-8, 15-18]
    ColdSoak1 --> NDE3((NDE))
    NDE3 --> EntryHeat1[1 ~ ENTRY HEAT Tj = 172°K (-150°F) NO. 3-8, 15-18]
    EntryHeat1 --> NDE4((NDE))
    NDE4 --> Reject[REJECT NO. 6 & NO. 8]
    NDE4 --> UltimateTensile1[ULTIMATE TENSILE LINE LOAD @ 450°K (350°F) NO. 3, 4, 15, 16]
    UltimateTensile1 --> Fabricate2[FABRICATE NO. 1R, 2R]
    Fabricate2 --> UltimateTensile2[ULTIMATE TENSILE LINE LOAD @ 450°K (350°F) NO. 1, 2, 13, 14]
    UltimateTensile2 --> LimitTensile1[LIMIT TENSILE LINE LOAD @ 450°K (350°F) NO. 5, NO. 7]
    LimitTensile1 --> NDE5((NDE))
    NDE5 --> BoostAc2[9 ~ BOOST ACOUSTICS NO. 5, 1R, 7, 2R  
24 ~ BOOST ACOUSTICS NO. 17, NO. 18]
    BoostAc2 --> NDE6((NDE))
    NDE6 --> ColdSoak2[328°K @ 1.33 x 10^-5 N/m^2 (130°F @ 10^-5 TORR) HOT SOAK NO. 1R, NO. 2R]
    ColdSoak2 --> NDE7((NDE))
    NDE7 --> ColdSoak3[166°K (-160°F) COLD SOAK NO. 5, 1R, 7, 17, 18]
    ColdSoak3 --> EntryHeat2[ENTRY HEAT Tj = 172°K (-150°F) Tj = 311°K (100°F) NO. 5, 1R, 7, 2R, 17, 18]
    EntryHeat2 --> NDE8((NDE))
    NDE8 --> LimitTensile2[LIMIT TENSILE LINE LOAD @ 450°K (350°F) NO. 7, NO. 2R]
    LimitTensile2 --> NDE9((NDE))
    NDE9 --> UltimateTensile3[ULTIMATE TENSILE LINE LOAD @ 450°K (350°F) NO. 5, NO. 1R]
    UltimateTensile3 --> BoostAc3[15 ~ BOOST ACOUSTICS NO. 7, NO. 2R]
    BoostAc3 --> NDE10((NDE))
    NDE10 --> ColdSoak4[166°K (-160°F) COLD SOAK NO. 7, 2R, 17, 18]
    ColdSoak4 --> EntryHeat3[ENTRY HEAT Tj = 172°K (-150°F) Tj = 311°K (100°F) NO. 7, NO. 2R]
    EntryHeat3 --> NDE11((NDE))
    NDE11 --> UltimateTensile4[ULTIMATE TENSILE LINE LOAD @ 450°K (350°F) NO. 7, 2R, 17, 18]
    UltimateTensile4 --> NDE12((NDE))
    NDE12 --> Fabricate3[FABRICATE NO. 1R, 2R]
    
```

687

STP TEST MATRIX AND SPECIMEN CONFIGURATION
(Figure 11)

The specimens tested represented the baseline REI-Mullite system proposed for the Phase C/D Space Shuttle Orbiter and considered two vehicle configurations:

- Hot windward conditions for an all-bonded system
- Cold windward conditions for an all-bonded system

The materials utilized were the REI-Mullite coated on five sides with PD-200-28 foam pads for attachment to the aluminum substrates. Mission simulation tests were performed in a sequential fashion to evaluate the thermal-structural capability of the REI-Mullite TPS to the critical design environments.

The aluminum structures were designed and provided by NR/SD. The REI-Mullite and foam pad thicknesses were sized for heating environments and test conditions established to subject the hot windward specimen to 1644° K (2500° F) surface temperature and the cold windward specimen to 978° K (1300° F) surface temperature without exceeding an aluminum substrate temperature of 450° K (350° F).

The designs were configured to simulate the thermal, structural, and dynamic response characteristics of an aluminum primary airframe structure protected by REI-Mullite. The configurations were:

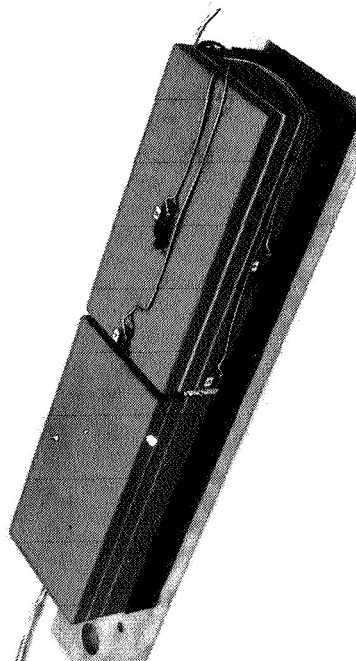
- Hot windward area simulation consisting of 0.048 m (1.9 inch) thick REI-Mullite bonded with 0.028 m (1.1 inch) thick PD-200 foam pads.
- Cold windward area simulation consisting of 0.043 m (1.7 inch) thick REI-Mullite bonded with 0.008 m (0.3 inch) thick PD-200 foam pads.

The specimens incorporated all the features of the proposed flight design except the final design solution for the tile sidewall coating. Analyses predicted that fully coated tile sidewalls would develop cracks normal to the vehicle outer moldline from the re-entry heating gradient. At the time of this test program, a design configuration was not sufficiently developed to prevent this problem and specimens were tested with uncoated grooves in the sidewall that provided some degree of stress relief. This problem is under intensive investigation. Sidewall designs utilizing coated grooves configured to provide increased flexibility have been successfully tested.

STP TEST MATRIX AND SPECIMEN CONFIGURATION

DESIGN CONFIGURATION	SPECIMEN NUMBER	ACOUSTIC CYCLES	ENTRY HEAT CYCLES	COLD SOAK CYCLES	HOT SOAK CYCLES	LIMIT LOAD CYCLES	ULTIMATE LOAD CYCLE
HOT WINDWARD ALL BONDED 0.048 m REI/0.028 m PD200 (1.9 IN. REI/1.1 IN. PD200)	1	-	-	-	-	-	1
	2	-	-	-	-	-	1
	3	1	1	1	-	-	1
	4	1	1	1	-	-	1
	5	10	10	2	-	1	1
	6 (1R)*	1 (9)	1 (9)	1 (1)	1	-	(1)
	7	25	100	3	-	2	1
	8 (2R)*	1 (24)	1 (98)	1 (2)	1	(1)	(1)
COLD WINDWARD ALL BONDED 0.043 m REI/0.008 m PD200 (1.7 IN. REI/0.3 IN. PD200)	13	-	-	-	-	-	1
	14	-	-	-	-	-	1
	15	1	1	1	-	-	1
	16	1	1	1	-	-	1
	17	25	25	3	-	-	1
	18	25	25	3	-	-	1

*SPECIMENS NO. 6 & NO. 8 REPLACED AFTER 1st ENTRY HEAT CYCLE



STP TEST SPECIMEN

Figure 11

ACOUSTIC TESTING

(Figure 12)

Acoustic tests were performed on the STP program to assess the TPS design when subjected to the dynamic environment associated with the lift-off and boost acoustics. The tests were performed in the progressive wave acoustic facility of Wyle Laboratories, Huntsville, Alabama. The tests were performed in three phases to comply with the STP Test Flow. Each test cycle was 2 minutes in duration, the equivalent of one boost cycle, at a sound pressure level (SPL) of 163 dB. The test specimens were mounted so that the flow was parallel with the panel length. Radius blocks were used at the mounting points to give simple support conditions. Test instrumentation included four microphones to monitor the acoustic environment as well as accelerometers mounted to the backface of the substrate at the midspan to record structural response. Prior to mounting the specimens in the test chamber, the acoustic spectrum was shaped, resulting in an overall SPL of 161.5 dB. During actual test runs, processed microphone data revealed overall SPL's of as high as 164 dB.

The hot windward specimens were tested in three phases to accumulate 25 simulated mission cycles. The first phase subjected specimens not having been exposed to prior cyclic environments to the equivalent of one boost acoustic cycle. The second phase subjected specimens that had been exposed before testing to one-entry heat and one-limit tensile load cycle to an accumulation of 10 boost acoustic cycles. The third phase subjected specimens that had prior exposure to 10-entry heat and two limit load cycles to an accumulation of 25 boost acoustic cycles. Similarly, cold windward specimens were subjected to one boost acoustic cycle without prior environmental cycles and to an accumulation of 25 boost acoustic cycles after prior exposure to 10 entry heat and two limit load cycles.

ACOUSTIC TESTING

MODEL CONFIGURATION	MODEL NO.	NO. OF 2-MINUTE CYCLES		
		1st PHASE	2nd PHASE	3rd PHASE
HOT WINDWARD	3	1		
	4	1		
	5	1	9	
	6 (1R)	1	(10)	
	7	1	9	15
	8 (2R)	1	(10)	(15)
	15	1		
	16	1		
COLD WINDWARD	17	1		24
	18	1		24

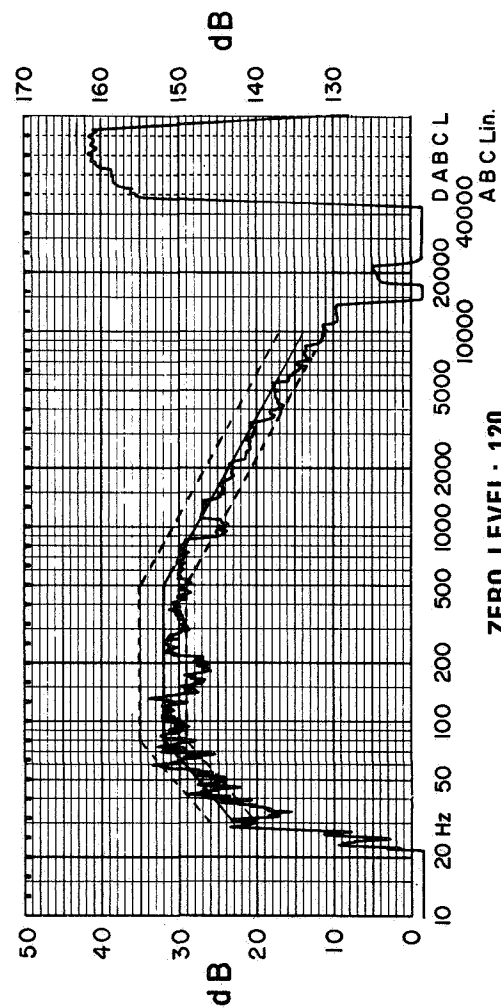


Figure 12

ACOUSTIC TEST PSD ACCELERATION (Figure 13)

Substructure accelerometer data for the hot windward specimens showed the performance of the REI-Mullite system to be predictable. The initial response peak between 150 and 200 Hz is associated with a series of modes where the REI-Mullite is "bouncing" on the PD-200 with some substrate bending motion. The second response peak between 300 and 400 Hz is associated with a mode where the REI-Mullite and substrate are moving in opposite directions. The power spectral density (PSD) plots for the acoustic test sequence are all very similar and show that:

- There is no structural deterioration of the REI-Mullite system from long term exposure to the boost acoustic environment.
- There is no structural deterioration of the REI-Mullite system from prior entry heat and limit load applications.

The PSD plots were evaluated to determine 'g' rms levels. These ranged from a low of 10 to a high of 28, the range being attributable to differences in input acoustic spectrum for each acoustic cycle and location of specimen within the facility. This corresponds to a peak acceleration response of 84 g's.

The data from the cold windward specimens showed a slightly different spectrum shape, resulting primarily from the decreased thickness of PD-200. The 'g' rms values ranged from 8 to 26. On one specimen during test the 'g' rms value increased from 26 during the initial cycles to 42 on the twenty-fifth cycle.

Non-destructive evaluation (NDE) was performed after each test phase. The acoustic testing caused minor side coating cracks on two specimens, which are attributable to the uncoated grooves. The specimens whose response increased to 42 g rms showed partial delamination of the PD-200 foam pad from the aluminum structure after 25 accumulated cycles. This failure was diagnosed as an adhesive failure resulting from inadequate loading during bonding.

ACOUSTIC TEST PSD ACCELERATION

HOT WINDWARD ACOUSTIC TEST
CYCLE NO. 1

HOT WINDWARD ACOUSTIC TEST
CYCLE NO. 25

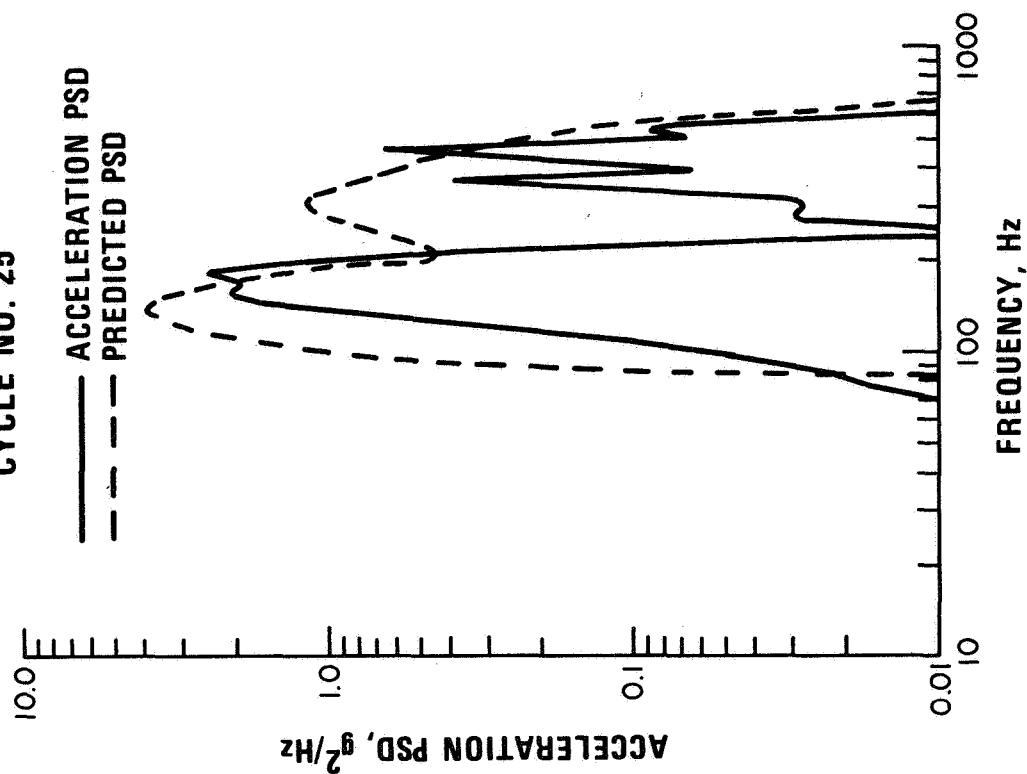
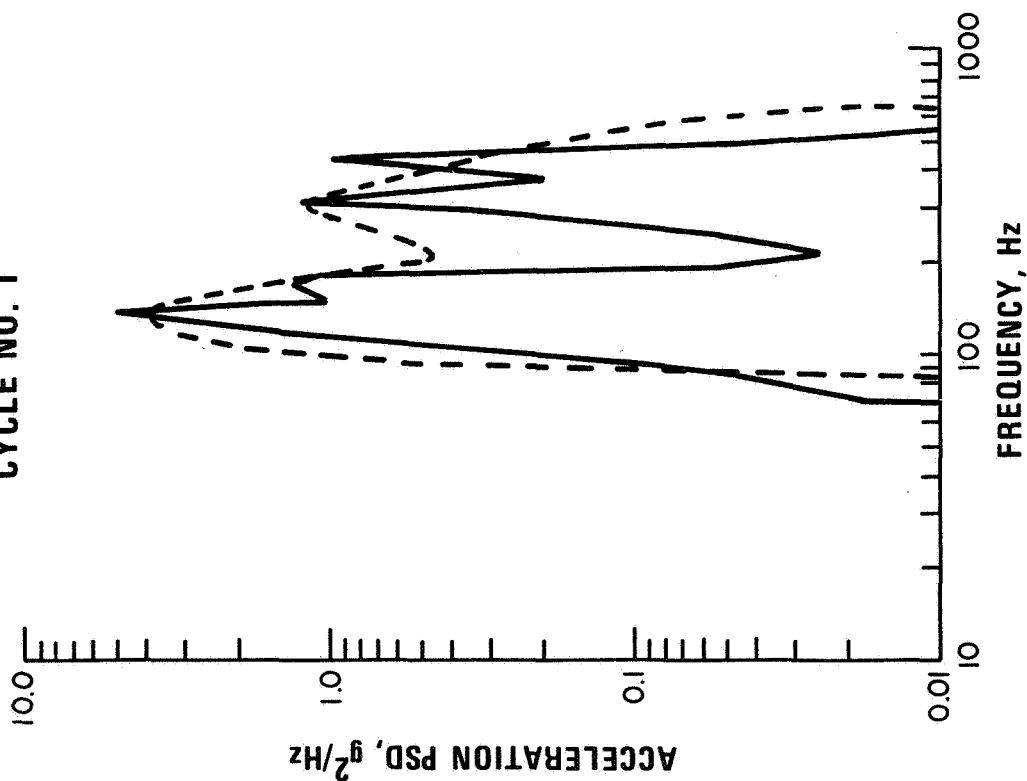


Figure 13

RE-ENTRY HEAT SIMULATION

(Figure 14)

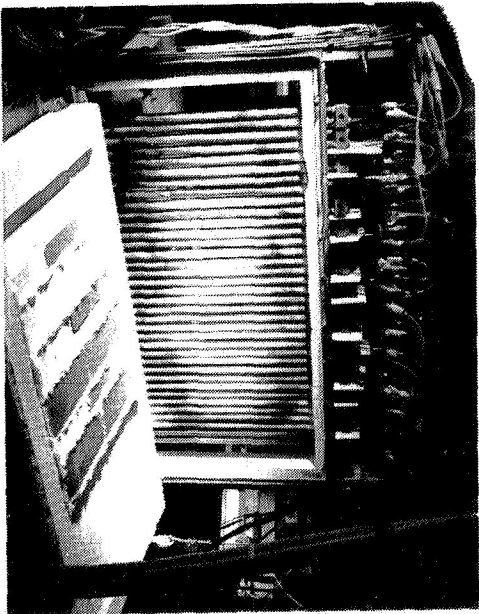
Re-entry heating simulation was performed in the 3 meter (10 foot) diameter vacuum chamber at the GE-RESO facility. The chamber is capable of being evacuated to pressures as low as 0.13×10^{-3} N/m² (10^{-6} torr). The radiant heater array is comprised of heater elements of silicon carbide resistance rods enshrouded by quartz tubes to eliminate the possibility of contamination. The heating elements are energized through a power controller. Feedback signals from the thermocouples on the test specimens or on control strips in the heater cavity control the power program. The heater elements are powered in banks of six so that each bank can be separately powered and controlled. This feature allowed the hot windward and the cold windward simulations to be conducted simultaneously.

A number of test specimens were instrumented with platinum-platinum rhodium surface thermocouples located at the center of each 0.1×0.2 m (4×8 inch) REI-Mullite tile. These specimens were used for controlling the heat input by using the surface thermocouple output in the controller feedback loop. These specimens were further instrumented with chromel-alumel thermocouples at the REI-Mullite mid-depth, REI-Mullite/PD-200 interface, PD200 mid-depth, and PD-200/aluminum interface to monitor in-depth temperature responses.

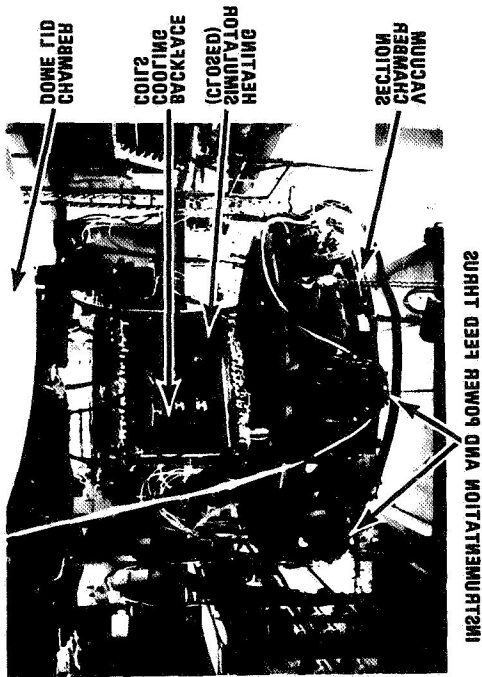
At discrete intervals in the test flow, specimens were subjected to the hot and cold conditions to be encountered during an orbital stay period. Test panels were subjected to 166° K (-160° F) prior to the start of the first, second, and eleventh re-entry heat cycles. The entry heating test was started with the panels at 194° K (-110° F).

For hot soak testing, two specimens were heated to 328° K ($+130^{\circ}$ F) at 1.3×10^{-3} N/m² (10^{-5} torr) for eight hours prior to the second entry heat cycle. The test panels were mounted back to back and wrapped in a rubber resistance heating blanket. This unit was then mounted in the vacuum chamber.

ИНИЦИАЦИОННОЕ ПОДГОТОВЛЕНИЕ



ИНИЦИАЦИОННОЕ ПОДГОТОВЛЕНИЕ



ИНИЦИАЦИОННОЕ ПОДГОТОВЛЕНИЕ

ИНИЦИАЦИОННОЕ ПОДГОТОВЛЕНИЕ

SPECIMEN NUMBER	ENTRY CYCLE				
	1	2	3 - 10	11 - 20	21 - 100
COLD FORWARD	X	X	X	X	X
	X	X	X	X	X
	X	X	X	X	X
	X	X	X	X	X
	X	X	X	X	X
	X	X	X	X	X
	X	X	X	X	X
	X	X	X	X	X
	X	X	X	X	X
	X	X	X	X	X
COLD REVERSE	X	X	X	X	X
	X	X	X	X	X
	X	X	X	X	X
	X	X	X	X	X
	X	X	X	X	X
	X	X	X	X	X
	X	X	X	X	X
	X	X	X	X	X
	X	X	X	X	X
	X	X	X	X	X

Figure 14

HOT WINDWARD ENTRY HEATING RESULTS

(Figure 15)

Hot windward specimens were tested through 100 entry simulation cycles at surface temperatures between 1590° K (2400° F) and 1644° K (2500° F). Temperature control problems were encountered on the first cycle resulting in a severe overtest requiring the replacement of two of the specimens. Modifications to the control system were made through cycle nine, after which power conditions were held constant. Upper and lower bounds of the thermocouple data show the stability and repeatability of REI-Mullite as a TPS for multicycle usage. The data spread from cycle to cycle; 60° K (110° F) for the REI-Mullite/PD-200 interface and 33° K (60° F) for the PD-200/aluminum interface is attributable to the variations in actual surface temperature achieved and the initial temperature of the specimens at the beginning of each cycle. In no case were the design limits of 616° K (650° F) for the PD-200 and 450° K (350° F) for the aluminum substrate exceeded.

NDE during the test program showed minor cracking of the sidewall coating occurred. After cycle 57, both tiles of one specimen developed surface cracks and then buckled, resulting in subsequent failure of the coating. On cycle 91, one of the two tiles on the second specimen developed surface cracks and buckled. The remaining tile was structurally sound throughout the 100 cycles.

HOT WINDWARD ENTRY HEATING RESULTS

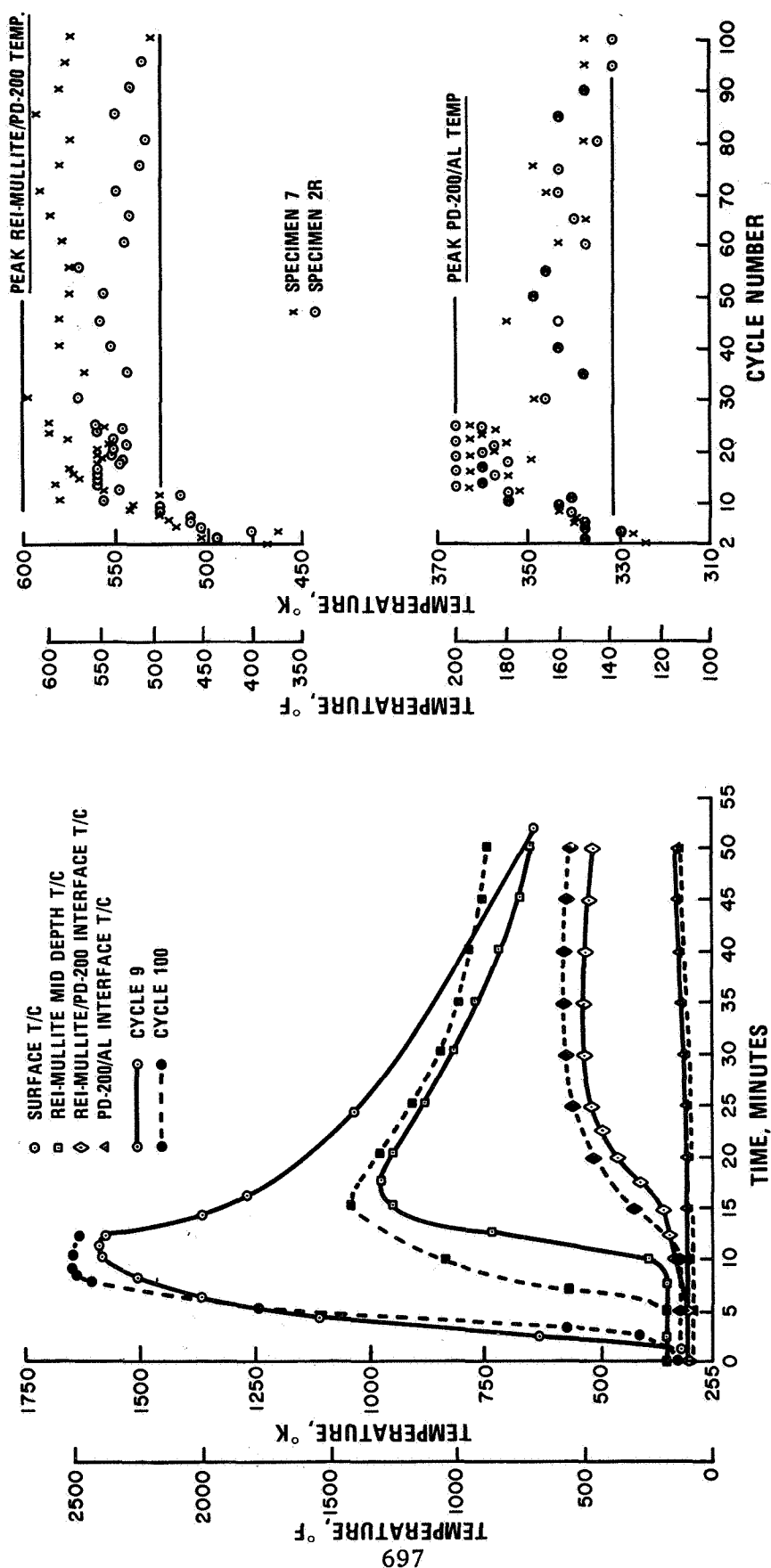


Figure 15

COLD WINDWARD ENTRY HEATING RESULTS

(Figure 16)

Cold windward specimens were tested through twenty-five entry simulation cycles at surface temperatures of 922° K (1200° F) and 978° K (1300° F). Modifications were made in the control cycle to raise the surface temperature to 978° K (1300° F) after cycle 7. Upper and lower bounds of the thermocouple data again show no change in performance of the REI-Mullite with re-entry heat cycling and that the design limits were not exceeded.

NDE during the test cycles again showed minor cracking of the sidewall coating.

Hot vacuum soaking to 328° K (130° F) at 1.3×10^{-3} N/m² (10^{-5} torr) and cold soaking to 166° K (-160° F) followed by entry heat from cold initial conditions of 194° K (-110° F) showed no structural changes in performance.

Coatings, except immediately adjacent to cracks, retained their waterproof characteristics throughout the one-hundred mission simulation.

COLD WINDWARD ENTRY HEATING RESULTS

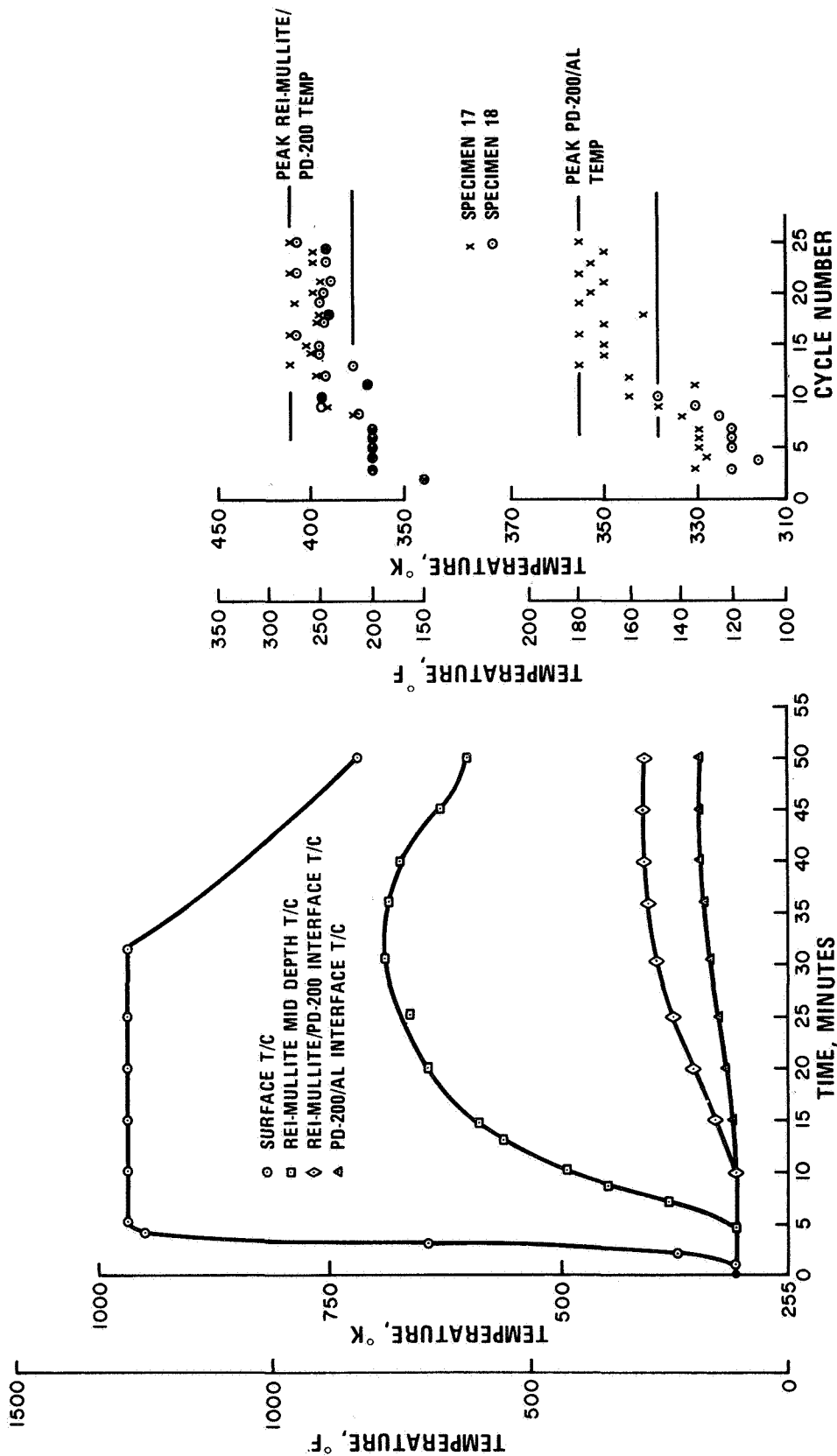


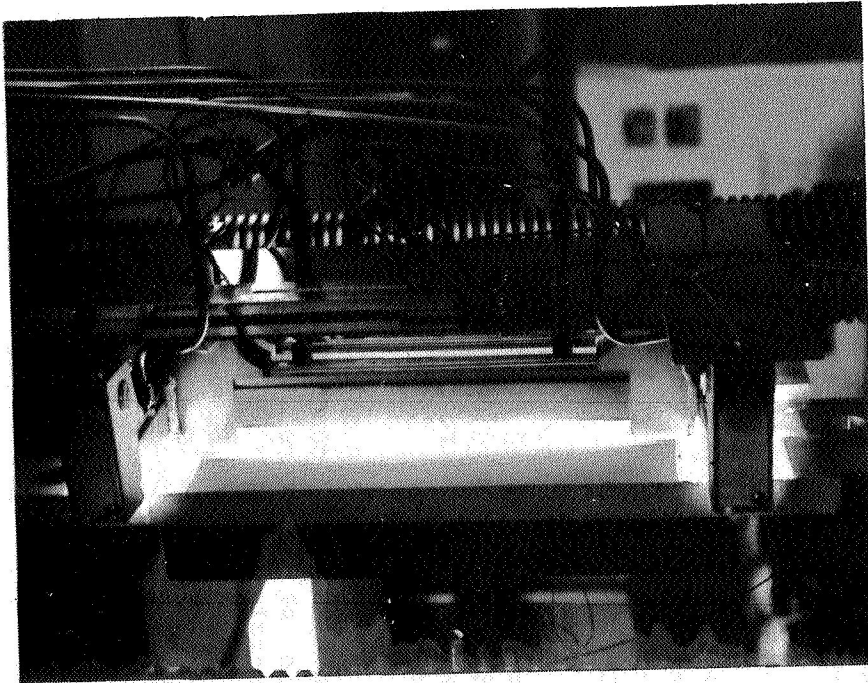
Figure 16

TENSILE LOAD TESTING

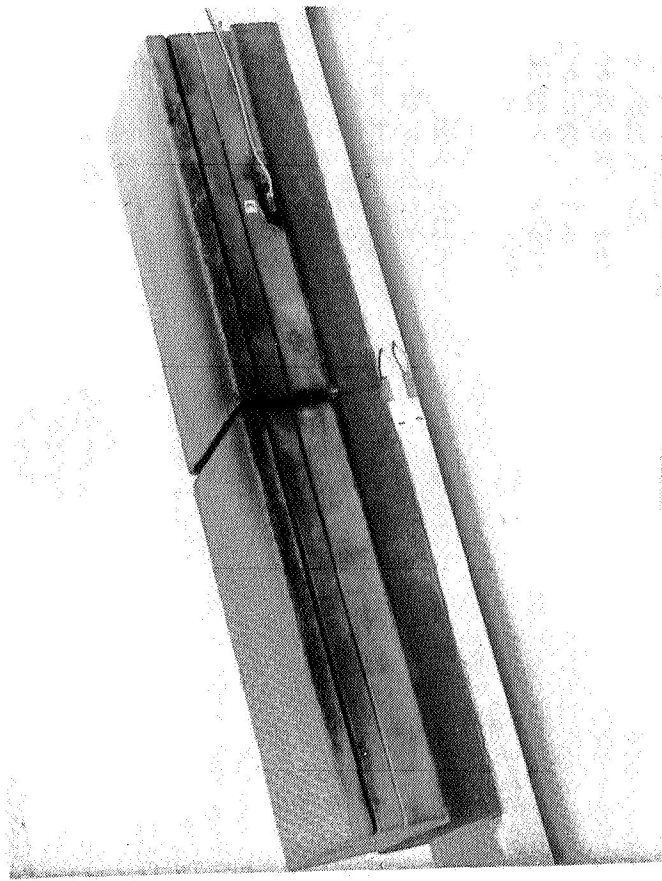
(Figure 17)

Tensile load tests were conducted to determine the ultimate load capability of the TPS for line loads at 450° K (350° F) after prior flight exposures to acoustics, entry heat, orbital conditions, and limit load conditions. This was found to be the worst case condition by prior analyses. The ultimate load was defined as the lowest of: (1) the load to delaminate coating or insulation; (2) load to produce normal cracks in coating or insulation; or (3) load that produces ultimate stress levels in the structure. The aluminum substrates were fabricated from 2024 T351 plate and had a calculated load capability of 199, 270 N (44,800 lb) at 450° K (350° F). Limit loads applied as part of the flight simulation cycles were two-thirds the ultimate load or 132,995 N (29,900 lb). Instrumentation consisted of chromel-alumel thermocouples to monitor the structure bondline temperature during test and strain gages on the coated tile and structure to determine the effectiveness of the PD-200 pad as a strain isolator.

TENSILE LOAD TESTING



VIEW OF SPECIMEN BACKFACE WITH QUARTZ HEATING LAMPS IN OPERATION



TYPICAL STRAIN GAGE INSTALLATION

Figure 17

TENSILE LOAD TEST RESULTS (Figure 18)

A summary of the loading data is shown on the figure. For the hot windward specimens, it was found that the ratio of strain developed in the coating to the strain applied to the structure ranged between 0.00311 and 0.00783 with an average value of 0.0053. Maximum coating strain measured at ultimate load conditions was 43×10^{-6} m/m (in./in.) clearly demonstrating the effectiveness of the PD-200 as a strain isolator.

NDE showed no damage initiated in any specimens due to the limit load cycles. In one case there was propagation of a side coating crack that had developed in prior thermal cycles. During ultimate load tests propagation of a sidewall coating crack from previous thermal cycles was noted. One specimen did develop sidewall coating cracks when ultimate load tested after 25 mission simulation cycles; however, these cracks were located away from peak stress regions and were probably initiated in prior cycles.

For the cold windward specimens, it was found that the strain ratio between the coating and structure ranged between 0.0105 and 0.0270 with an average of 0.019 or approximately four times that of the hot windward specimens. This is consistent with the reduction in pad thickness from the hot windward specimens to the cold windward specimens. Maximum measured coating strain was 164×10^{-6} m/m (in./in.).

NDE of the cold windward specimens showed one specimen to develop cracks in the side coating under ultimate load conditions. The strain gage output for the cold windward specimens showed erratic behavior at structure strain levels of approximately 4000×10^{-6} m/m (in./in.) which corresponds to approximately 80×10^{-6} m/m (in./in.) strain in the coating.

The tensile load test results showed (1) the limit and ultimate load capability of REI-Mullite bonded with PD-200 foam pads for tensile line loading is limited by substrate stress levels; (2) PD-200 foam pads effectively isolate REI from structural loads, reducing strain levels in the coating to less than two percent of the applied strain to the structure; and (3) prior exposure to up to 25 mission cycles of acoustics and re-entry gradients does not result in degradation of load capability of the TPS.

TENSILE LOAD TEST RESULTS

HOT WINDWARD	SPECIMEN NO.	PRIOR CYCLES	TENSILE LOAD NEWTONS (POUNDS)	AVERAGE MEASURED STRUCTURE STRAIN (10 ⁻⁶ m/m (IN/IN))	MEASURED COATING STRAIN (10 ⁻⁶ m/m (IN/IN))	ϵ COATING ϵ ALUMINUM	$\frac{\epsilon \text{ COATING}}{\epsilon \text{ ALUMINUM}} = 0.0053 \text{ AVG.}$
	1	AS FABRICATED	197,936 (44,500)	7,000	30	0.00569	
	2	AS FABRICATED	186,816 (42,000)	7,700	29	0.00603	
	3	1 ACOUSTIC 1 ENTRY	195,712 (44,000)	7,000	OUT	0.0045	
	4	1 ACOUSTIC 1 ENTRY	200,160 (45,000)	7,200	—	—	
	5	10 ACOUSTIC 10 ENTRY 1 LIMIT	195,712 (44,000)	7,500	23	0.00465	
	1R	9 ACOUSTIC 8 ENTRY	191,264 (43,000)	7,000	43	0.00783	
	7	25 ACOUSTIC 25 ENTRY 2 LIMIT	200,160 (45,000)	7,000	18	0.00311	
	2R	24 ACOUSTIC 23 ENTRY 1 LIMIT	191,264 (43,000)	6,900	—	—	
	13	AS FABRICATED	197,936 (44,500)	7,300	105	0.0198	
	14	AS FABRICATED	191,264 (43,000)	5,400	66	0.0105	
COLD WINDWARD	15	1 ACOUSTIC 1 ENTRY	182,368 (41,000)	4,800	89	0.0202	$\frac{\epsilon \text{ COATING}}{\epsilon \text{ ALUMINUM}} = 0.019 \text{ AVG.}$
	16	1 ACOUSTIC 1 ENTRY	195,712 (44,000)	7,600	46	0.0115	
	17	25 ACOUSTIC 25 ENTRY	193,488 (43,500)	7,400	129	0.0248	
	18	25 ACOUSTIC 25 ENTRY	186,816 (42,000)	6,300	164	0.0270	

Figure 18

NDE SUMMARY — STRUCTURES TEST PROGRAM

(Figure 19)

Non-destructive evaluation (NDE) was used to obtain characterization information on the quality of the REI-Mullite, coating, and foam pads, and to assess any damage or degradation that may have occurred after environmental exposure. The following techniques were employed during the program: X-Ray for cracking and attachment; microwave for moisture content; infrared for waterproofness; and visual examination. The following summary points are made with respect to the NDE performed:

● Coating Evaluation

1. Specimens tested to 1644° K (2500° F) show surface color changes from tan to light blue.
2. Surface coating cracks were found to occur after 57 entry heat cycles on two tiles and 91 cycles on one tile. One tile had no surface cracks after 100 cycles.
3. Coating is waterproof except at pinhole and crack locations.
4. Side coating cracks were observed after exposure to acoustic, entry heat, and tensile loading. Majority of side coating cracks resulted from entry heat tests.

● REI-Mullite Evaluation

1. No degradation of the REI-Mullite was observed.

● PD-200 Evaluation

1. No degradation of PD-200 was observed except as a result of the overtest condition experienced on entry heating cycle No. 1.
2. Only one specimen showed delamination of PD-200/aluminum bond.

NDE SUMMARY – STRUCTURES TEST PROGRAM

DESIGN CONFIGURATION	SPECIMEN NO.	AS FABRICATED CONDITION	AFTER 1 ACOUSTIC CYCLE	AFTER 1st ENTRY HEAT CYCLE	AFTER LIMIT LOAD	AFTER ACOUSTIC CYCLE NO. 10	AFTER ENTRY HEAT CYCLE NO. 10	AFTER LIMIT LOAD	AFTER ACOUSTIC CYCLE NO. 25	AFTER ENTRY HEAT CYCLE NO. 25	AFTER ULTIMATE LOAD	AFTER ENTRY HEAT CYCLE NO. 100
HOT WINDWARD	1	COATING CHIP				(N/A)					N/C	
	2	N/D		COATING CHIP							N/C	
	3	PINHOLES	N/C	SIDE COATING CRACKS							N/C	
	4	COATING CHIP	COATING CHIP	SIDE COATING CRACKS							N/C	
	5	PINHOLES	SIDE COATING CRACK	SIDE COATING CRACKS	N/C	SIDE COATING CRACK PROPAGATED	N/C		(N/A)		SIDE COATING CRACK PROPAGATED	
	6	N/D	COATING CHIP	CHARRED PD200 (REJECTED)								
	1R	COATING CHIP				N/C	SIDE COATING CRACK		(N/A)		N/C	
	7	N/D	N/C	N/C	N/C	SIDE COATING CRACK COATING CHIP	N/C		N/C	PINHOLES	SIDE COATING CRACK	SURFACE CRACK (CYCLE 91)
	8	SIDE COATING CRACK	N/C	CHARRED PD200 (REJECTED)							N/C	
	2R	N/D				N/C	SIDE COATING CRACK	SIDE COATING CRACK PROPAGATED	N/C	SIDE COATING CRACKS COATING CHIP		SURFACE CRACK (CYCLE 57)
COLD WINDWARD	13	PINHOLES					(N/A)				N/C	
	14	PINHOLES					(N/A)				SIDE COATING CRACKS	
	15	PINHOLES	N/C	SIDE COATING CRACK			(N/A)				N/C	
	16	N/D	N/C	SIDE COATING CRACK			(N/A)				N/C	
	17	PINHOLES	N/C	N/C			(N/A)		SIDE COATING CRACK BOND DELAMINATION	SIDE COATING CRACK	N/C	
	18	PINHOLES	SIDE COATING CRACK	SIDE COATING CRACK			(N/A)			SIDE COATING CRACK	N/C	

N/D – NO DEFECTS NOTED
N/C – NO CHANGE NOTED
N/A – NOT APPLICABLE

Figure 19

SUMMARY

(Figure 20)

A major element of GE's development of the Reusable External Insulation, REI-Mullite, for the Space Shuttle Orbiter is testing in simulated natural and induced environments. The test programs reported here, although a small part of the total number of tests performed, clearly demonstrate that REI-Mullite is capable of meeting all requirements for the orbiter TPS.

Tests conducted to evaluate the system's performance in the natural environments of salt spray, humidity, rain, vacuum, and cryogenic temperatures have shown the REI-Mullite to be completely compatible and that these environments have no adverse effects on subsequent mission performance. Rain erosion testing has indicated a damage threshold that must be accounted for in the final design.

Tests conducted to evaluate the performance of the REI-Mullite to the induced acoustic, re-entry, and structural load environments again have shown complete capability to fulfill mission environments. Although minor cracking of the sidewall coating was seen to occur throughout the induced environment test program, sidewall designs configured to provide increased flexibility have been successfully tested.

Additional materials development for both the REI-Mullite insulation and the SR-2 coating is continuing with testing similar to that discussed being used to evaluate the improvements.

SUMMARY

REI MULLITE CAPABILITY DEMONSTRATED FOR ALL TPS REQUIREMENTS

- NATURAL ENVIRONMENTS

- SALT SPRAY/HUMIDITY
 - NO DEGRADATION
- VACUUM
 - NO DEGRADATION
- CRYOGENIC TEMPERATURES
 - DEMONSTRATED 50 PERCENT SAFETY MARGIN
- RAIN
 - NO EROSION
 - IMPACT DAMAGE THRESHOLD REQUIRES PROPER DESIGN

- INDUCED ENVIRONMENTS

- ACOUSTICS
 - NO DEGRADATION
 - DEMONSTRATED 25 MISSION CAPABILITY FOR 163 dB
 - DEMONSTRATED THERMAL STABILITY TO 1644° K (2500°F) FOR 100 MISSIONS
- RE-ENTRY
 - DEMONSTRATED STRUCTURAL CAPABILITY TO 1644° K (2500°F) FOR 57 MISSIONS ON TWO TILES, 91 MISSIONS ON ONE TILE AND 100 MISSIONS ON ONE TILE.
 - SIDEWALL COATING CRACKING SOLUTION REQUIRES PROPER DESIGN
- STRUCTURE LOADS
 - PD-200 DECOUPLES AIRFRAME STRUCTURAL LOADS FROM REI-MULLITE TPS

REFERENCES

1. Final Report for Reusable Surface Insulation Thermal Protection System Development Program, GE-EYP-012, May 1972. NASA, MSC Contract No. NAS 9-12084. General Electric Co., Philadelphia, Pa.
2. Final Report on Evaluation of Nonmetallic Thermal Protection Materials for the Manned Space Shuttle, Volume V, June 1, 1972, NASA Contract NAS 9-10853, Battelle Memorial Institute, Columbus, Ohio.
3. Development of an External Insulation for the Space Shuttle Orbiter, NASA CR-112038, April 1972, General Electric Company, Philadelphia, Pa.
4. Rain Erosion Characteristics of Thermal Protection System Materials at Subsonic Velocities, AFML TR-72-145, August 1972, Textron Bell Aerospace Company.

**ENVIRONMENTAL COMPATIBILITY
OF THE
ALL-SILICA
RIGID SURFACE INSULATION**

S. J. Houston, J. A. De Runtz, and D. R. Elgin
LOCKHEED MISSILES & SPACE COMPANY, INC.

RESULTS OF DEVELOPMENT TESTING OF LMSC SILICA RSI (Figure 1)

Testing of the compatibility of the all-silica RSI with aspects of the orbiter environment other than reentry heating, has also been accomplished. These tests have included: a cyclic salt spray environment with specimen exposure to five simulated flight cycles each consisting of a 4-hr MIL STD salt fog exposure and simulation of a reentry heating cycle; a lost tile test, in which a tile in the center of a tile array was deliberately, destructively removed, and then the array was subjected to simulated reentry heating in a flow facility in an effort to evaluate the effect on adjacent tiles of the loss of a single tile; acoustic tests including a 15 minute exposure to 174 dB; cold soak tests including 5 minutes at 116°K (-250°F); effects of ultraviolet exposure on surface optical properties with up to about 5,800 equivalent sun hours; and a water absorption test with simulated ascent and reentry heating subsequent to water exposure.

The results of these tests in terms of influence on the Shuttle orbiter design are presented along with a description of test conditions and test specimens. In general, the results indicate compatibility of the all-silica RSI with the orbiter environment.

RESULTS OF DEVELOPMENT TESTING OF LMSC SILICA RSI

SIMULATED REENTRY TESTING

- TESTS BY LMSC, NASA/MSC, NASA/ARC
- MULTICYCLE – RADIANT AND CONVECTIVE
- ACCUMULATED TEST EXPOSURE TO DEMONSTRATE PERFORMANCE AND STABILITY

SPECIALIZED ENVIRONMENTAL TESTING

- LAUNCH CONDITIONS
- ORBIT CONDITIONS
- REENTRY – SPECIALIZED CONDITIONS

Figure 1

TEST SPECIMENS (Figure 2)

Specimens numbered 1 through 3 were used in the freeze/thaw and the salt fog tests described below:

Freeze/Thaw. These tests were performed to determine if the silica RSI would be affected by exposure to moisture followed by freezing and thawing. Specimens were exposed to moisture environments varying from 50 to 100 percent relative humidity for a minimum two-hour period and then a 255°K freeze temperature for a minimum of 8 hours. The specimens were then thawed in an ambient environment for a minimum of 8 hours. This cycle was repeated twice more, but with thaw temperatures of 534°K and 811°K (oven exposures). The specimens were weighed, measured, and visually inspected after each cycle. The average variations in weights and dimensions recorded were within the uncertainty/repeatability of the measurements.

Salt Fog. Concern for the effects of salt exposure on RSI materials has led to investigations regarding appropriate testing with a salt environment. LMSC has elected to use the MIL-STD-810B, Method 509, Procedure I. The 10 by 10 by 2.5-cm (4 by 4 by 1-in.) specimens were (1) subjected to four salt fog exposures of one hour duration; (2) weighed; (3) exposed to a radiant lamp simulation of the reentry heating pulse at 1 atmosphere pressure; and (4) weighed again. This procedure was followed for five cycles. Recorded weight changes were within the uncertainty of the measurement. These specimens were oversprayed with hydrophobic solution after the heating because this treatment was a part of the "baseline" concept in the early part of 1972 when this test was performed. The coating had some cosmetic changes (i.e., there was a somewhat mottled appearance to it), but there was no significant change in surface emittance.

Ascent depressurization tests were run using Specimens 4 through 9 and Specimen 12. The specimens were subjected to a moisture environment ranging from a 50- percent relative humidity to rain for a minimum of two hours and then exposed to a simulated ascent and reentry heating and pressure test. Since they were waterproof, these specimens did not absorb water in significant quantities. They survived this test without significant weight changes or degradation.

The remaining specimens were used in studies related to tile joint designs.

TEST SPECIMENS

SPECIMEN NO.	SPECIMEN TEST
1	FREEZE/THAW AND SALT FOG
2	FREEZE/THAW AND SALT FOG
3	FREEZE/THAW AND SALT FOG
4	ASCENT DEPRESSURIZATION
5	ASCENT DEPRESSURIZATION
6	ASCENT DEPRESSURIZATION
7	ASCENT DEPRESSURIZATION
8	ASCENT DEPRESSURIZATION
9	ASCENT DEPRESSURIZATION

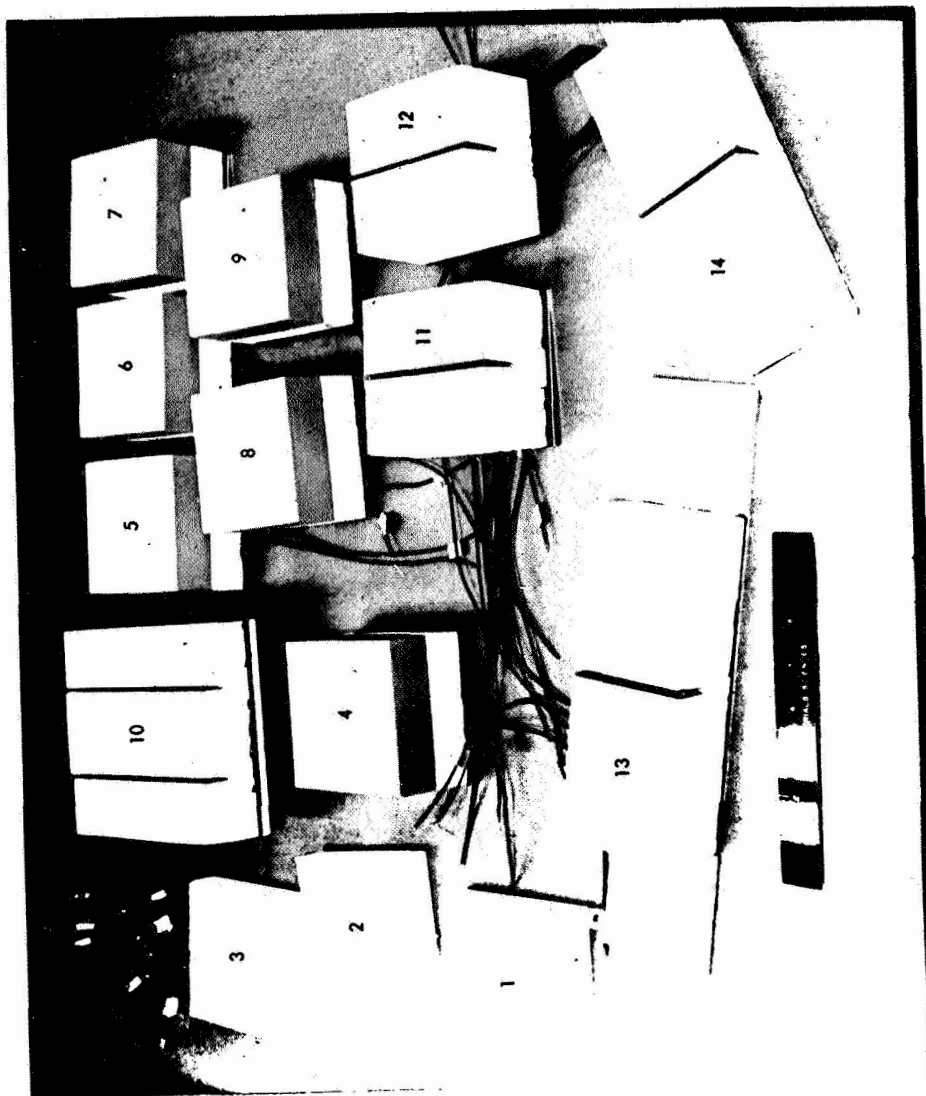


Figure 2

ACOUSTIC OVERSHOOT MODEL (Figure 3)

Acoustic testing has been performed on single and multiple all-silica RSI tile arrays with sound pressure levels of 160.7, 170, and 174.5 dB. A six-tile array was tested in the Ames Research Center 9 by 7 wind tunnel at the two lower levels and one-tile and two-tile specimens were tested in the LMSC progressive wave tube at the two higher levels. The six-tile array (2 tiles wide by 3 tiles long) suffered no apparent degradation after the 160.7-dB test, but after the 167.8-dB test, one tile had broken completely free; however, this is attributed to the fact that it was in contact with the adjacent downstream tile rather than having the required clearance. Further, it is noted that the other tile, which was symmetrically located in the stream and was not in contact with any adjacent tile, did not break loose. The specimens tested for 15 minutes in the progressive wave tube showed no failure of the basic all-silica RSI or its coating. However, in the two-tile sample the directly exposed FI-600 seal strip material disintegrated at 170 dB, while the seal strip material in the tile joint survived the 170-dB level but disintegrated at the 174.5-dB level. The conclusion from this testing is that the basic all-silica RSI can withstand acoustic sound pressure levels up to 174.5 dB. This appears to be well above the range of levels for which the orbiter TPS will be designed.

ACOUSTIC OVERSHOOT MODEL

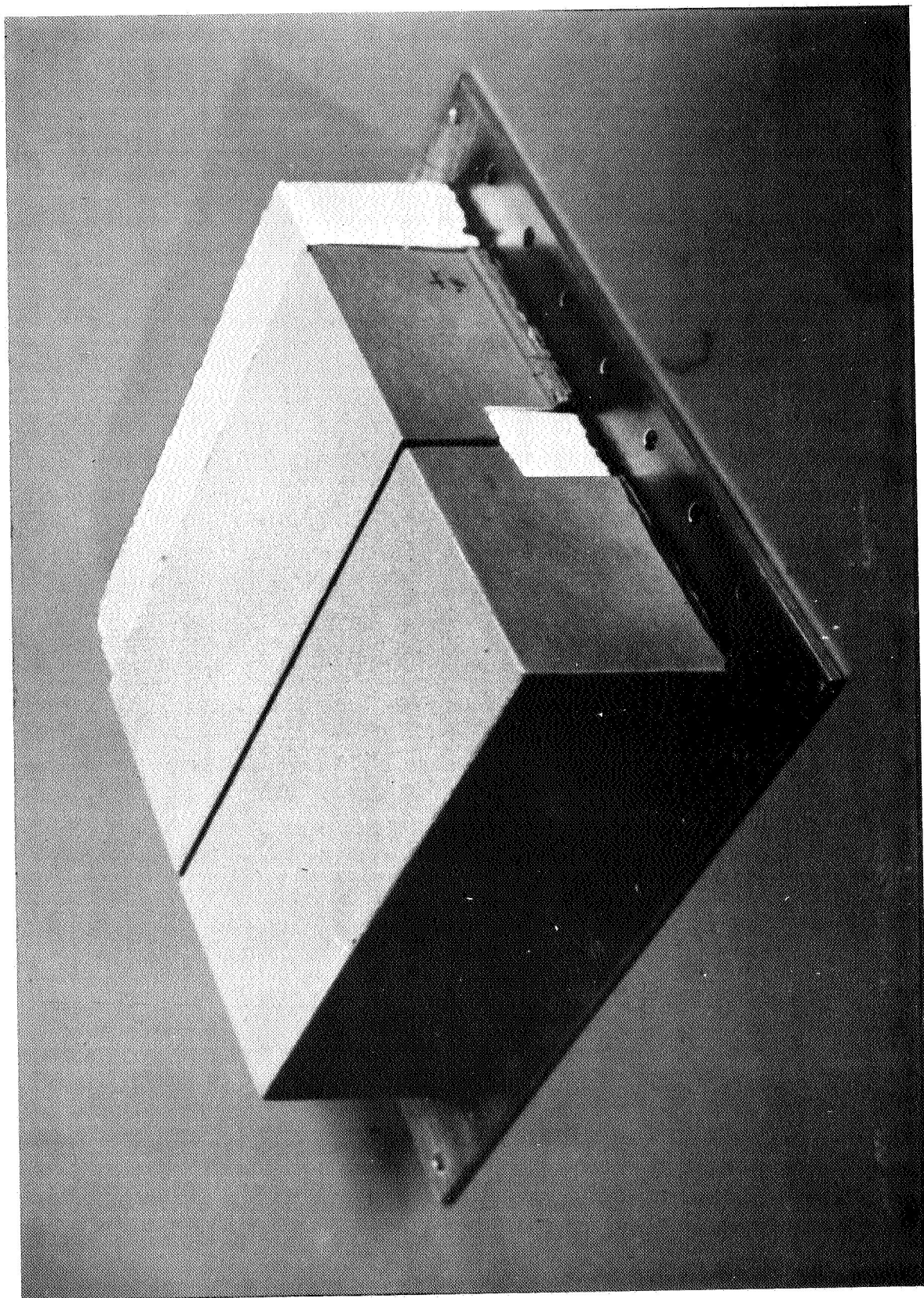


Figure 3

116° K (-250° F) COLD SOAK SPECIMEN (Figure 4)

The on-orbit cold soak condition of 116° K poses a severe test for the commonly used bonding agents because they undergo a glassy transition with a dramatic increase in modulus when temperatures drop below 170°K. As part of the investigation of attachment systems compatible with this environment, two 30.5 x 5 x 5 cm (12 by 2 by 2-in.) all-silica RSI tiles were bonded to aluminum plates, one using a foam pad 0.16 cm (0.063-in.) thick (RM RL-1973) bonded between the aluminum and the tile illustrated, and the other with a 0.025 cm (0.01-in.) thick Invar strip (to serve as a strain arrestor plate) bonded between the aluminum and the tile. These two specimens were chilled to 116° K and then returned to room temperature with no apparent damage. In addition, the aluminum base plates were loaded in tension to yield (at room temperature) with no apparent damage to the tiles or attachment systems.

116°K (-250°F) COLD SOAK SPECIMEN

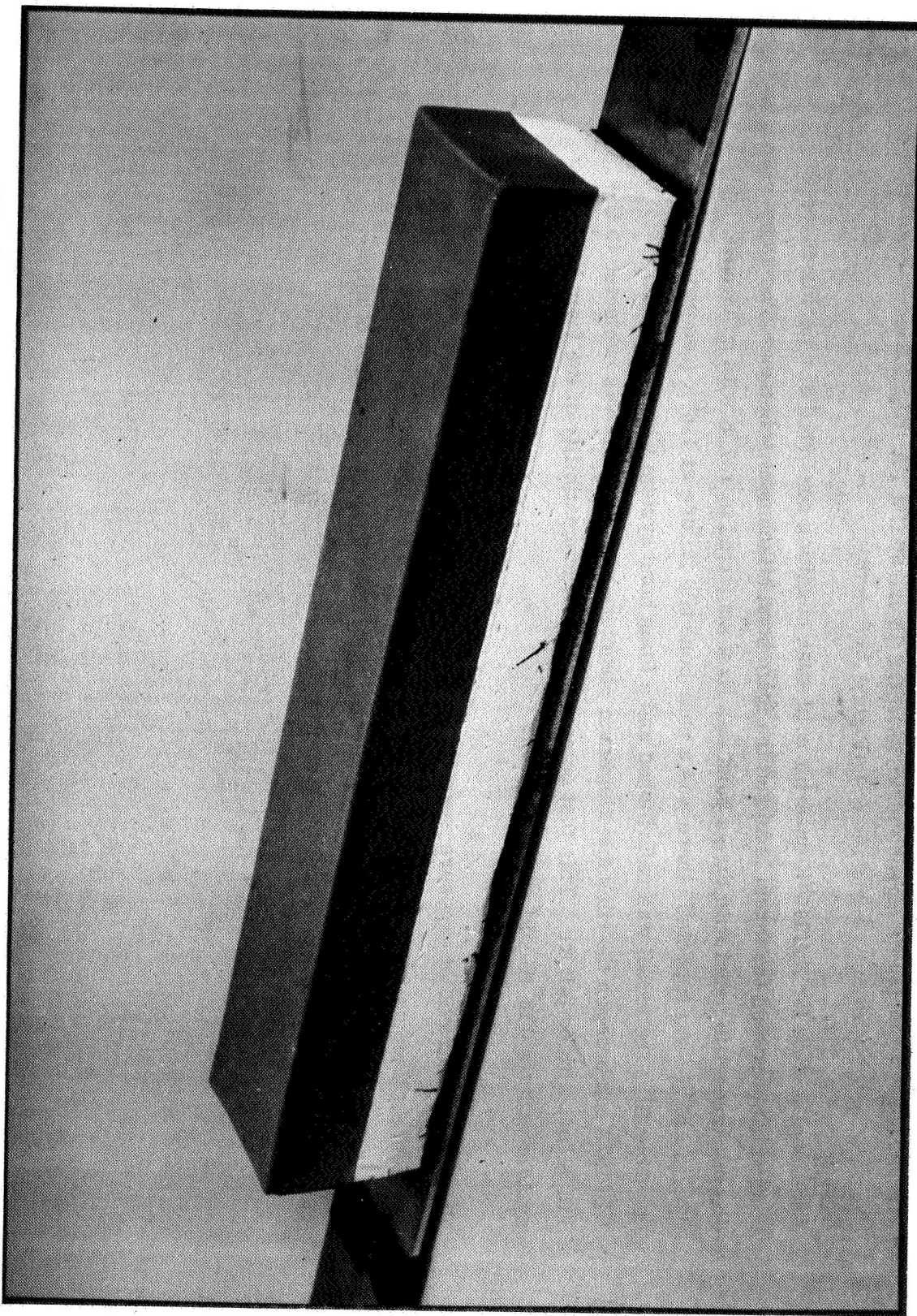


Figure 4

116° K (-250° F) TESTING OF 15 BY 60 CM PANEL
(Figure 5)

Additional testing for the 116°K on-orbit cold-soak condition consisted of a performance comparison between the direct bond and the foam bond attachment schemes. The 15 by 60 cm, three-tile panel with direct bond was first subjected to 137°K with no failure, and then to 116°K. As expected, there was a near bond tile failure at 116°K (see photo). Subsequently, the model was refurbished and a foam bond system with 2 mm thick RL-1973 pad between the tiles and aluminum structure was used. It was subjected to the 116°K test with no failure. This test demonstrates the compatibility of the foam bond system with the 116°K cold soak condition.

Vacuum and ultraviolet exposure were shown to have no effect on weight and coating emittance. Vacuum tests consisted of 30-day hard vacuum at room temperature and 394° K. Samples of the coating were subjected to 5700 equivalent sun hours of ultraviolet exposure with no degradation of emittance.

116°K (-250°F) TESTING OF 15 BY 60 CM PANEL

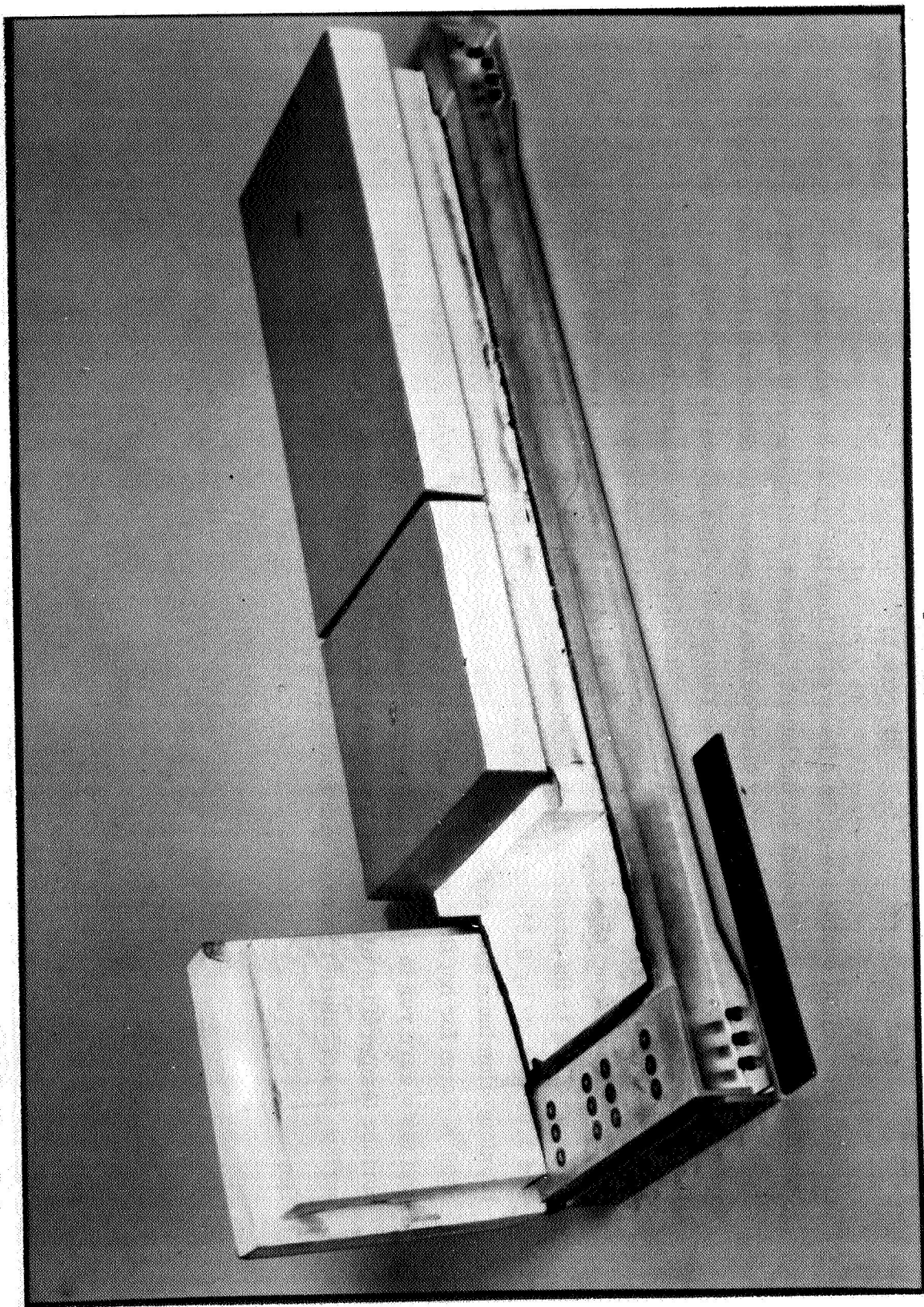


Figure 5

LOST TIME MODEL — PRETEST (Figure 6)

To obtain an initial evaluation of the effects of a "lost tile" in an RSI tile array (such as might occur due to bird impact during launch, collision during on-orbit docking, EVA accident, etc.), the nine-tile array pictured had the center tile deliberately removed to the point where about 1.9 cm thickness of tile remained. This specially prepared model was then placed in a model holder so that the surface of the array was inclined at 45 deg to the centerline of the exhaust of the hydrogen jet heater. The heater was controlled using a surface thermocouple located in the center tile of the upstream tile row for feedback, and controlling to the predicted flight surface temperature response for Area 2 perturbed. The 1.02 by 1.02 by 0.51 cm tiles were bonded with RTV-560 to a 38 by 38 by 2.5 cm titanium-aluminum honeycomb-sandwich. The hydrogen jet heater provides a 2500 to 3600°K flame for hot flow testing at heat rates up to $735 \times 10^4 \text{ W/m}^2$. Pretest calibration tests were run to determine flame conditions required to achieve peak LI-1500 surface temperature of 1535°K. The test consisted of a simulation of the reentry heating surface temperature response with feedback control.

LOST TILE MODEL — PRETEST

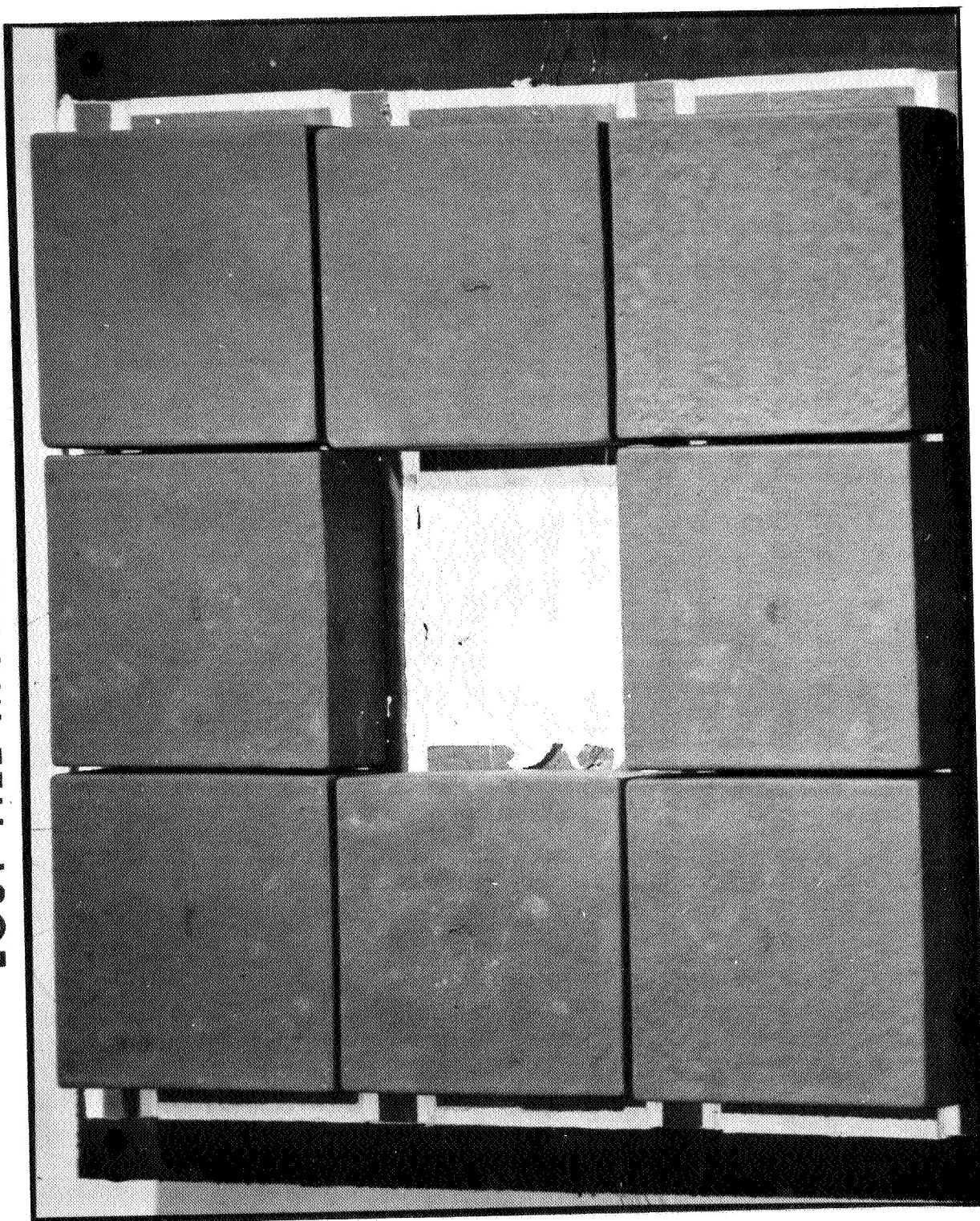


Figure 6

LOST TILE MODEL IN HOLDER — POST TEST
(Figure 7)

As indicated, the purpose of the test was the evaluation of the effects of accidental tile loss, and one of the qualitative conclusions drawn is that no progressive, catastrophic failure resulted. That is, no tiles came off or burned through, and the maximum temperature on the titanium portion of the structure was 700°K; this was within an acceptable, one time reentry survival bound. With this simulated accident, the adjacent tiles (particularly downstream) show degradation where the tile in the joint areas was overheated, and were this on a flight vehicle, refurbishment would be required. However, confidence in capability of this system was further enhanced when the specimen was subsequently utilized in tests (to obtain acoustic transmission data on the honeycomb structure) that included acoustic exposure to 147.5 dB, where no tiles fell off or showed any further degradation.

LOST TILE MODEL IN HOLDER - POST TEST

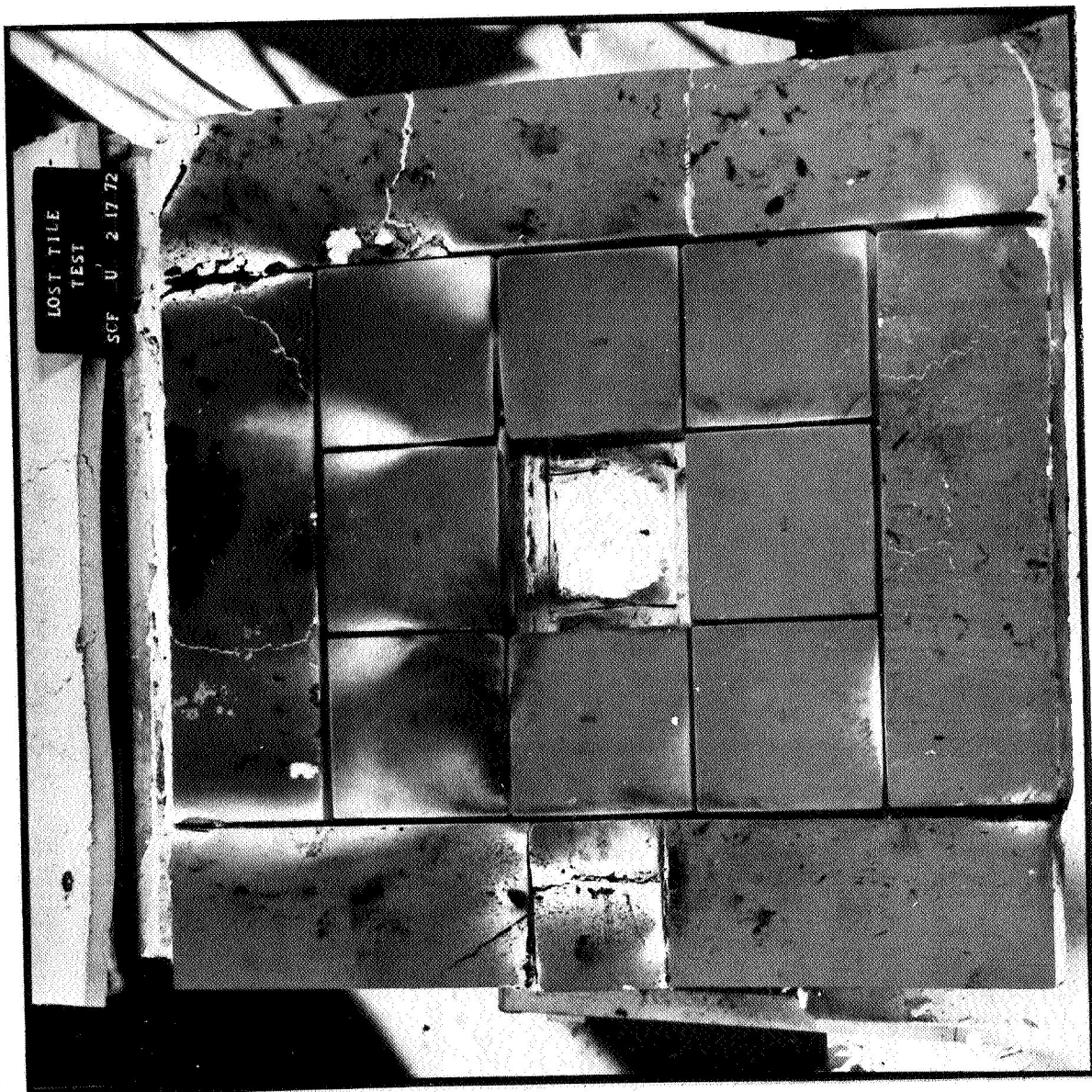


Figure 7

LI-1500/0042 COATING TEMPERATURE OVERSHOOT TEST
(Figure 8)

As part of the investigation of the capability of the all-silica RSI material, the specimen shown was subjected to a "temperature overshoot" environment that consisted of three radiation simulated reentry heating pulses up to a temperature of 1644° K (as used for the 100-cycle tests described in the paper entitled "Silica RSI Entry Simulation Tests," by R. P. Banas, et al., in Section 20 of these Proceedings) and then brought up to 1924° K surface temperature according to the curve shown. It should be noted that this test included 18 min above 1368° K, 16 min above 1535° K, and 15 min above 1644° K. Additionally, the heat rate required to produce the 1924° K surface temperature is larger than the heat rate for 1644° K by almost a factor of two and this represents a significant temperature overshoot. Although there is some surface slumping evident and such a tile would be replaced rather than reflowed, there was no catastrophic failure of the all-silica tile; thus it has been demonstrated that this system can tolerate significant excursions from the planned environment. Analysis of this hypothetical flight condition indicated that the structure temperature at the time equivalent to touchdown would be about 430° K with a maximum temperature around 485° K.

Arc-jet test run during December 1971 at Aerotherm further confirms the "foregoing nature" of the all-silica RSI. Samples were tested for five 30-min cycles at a calorimeter-measured heating rate in excess of $90.4 \times 10^4 \text{ W/m}^2$ (to be compared with the $24.8 \times 10^4 \text{ W/m}^2$ required to produce 1535° K surface temperature), and although there was distortion of the sample, this test demonstrated the ability of the all-silica system to provide one-time thermal overshoot protection to the structure.

LI-1500/0042 COATING TEMPERATURE OVERSHOOT TEST

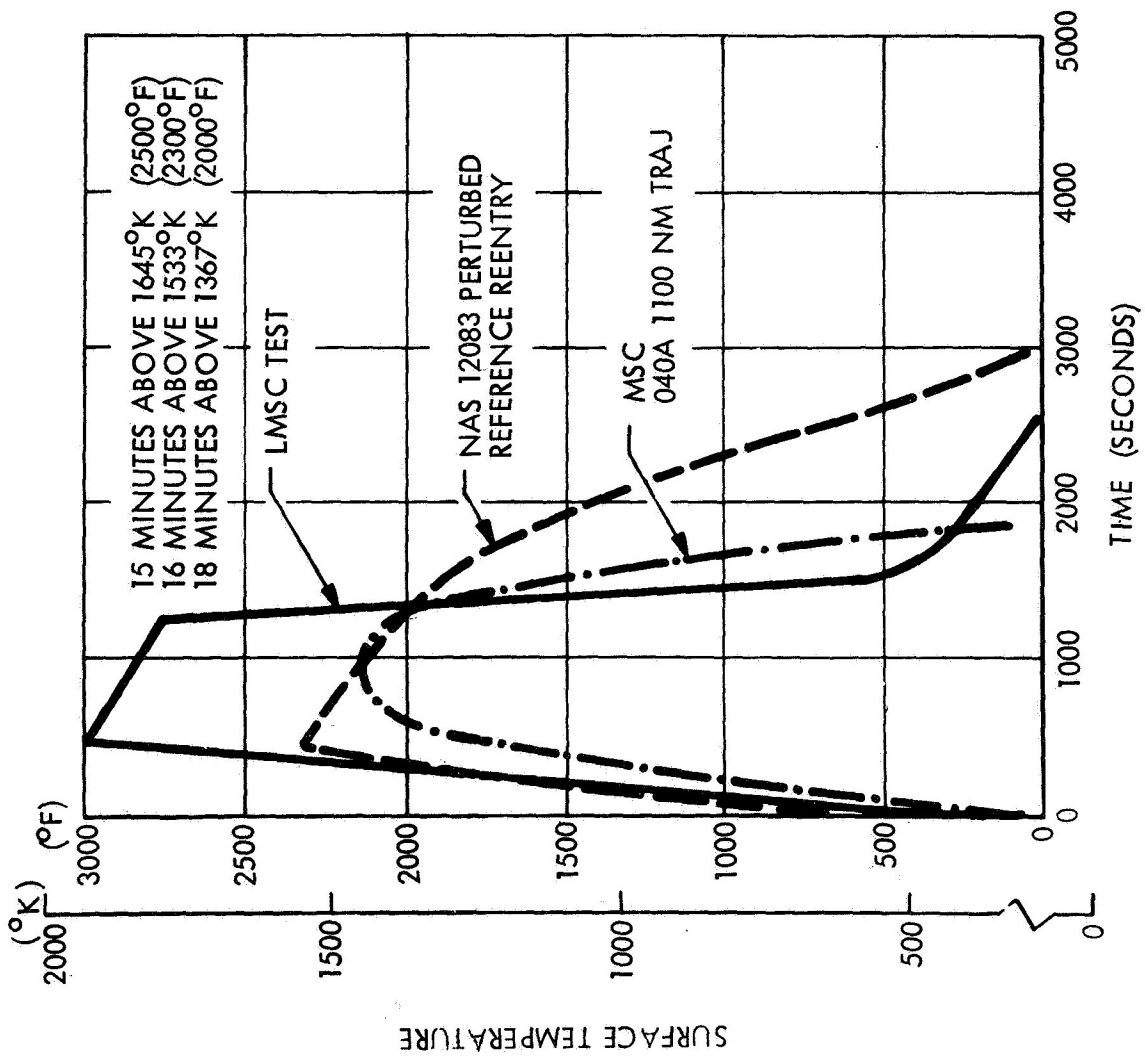


Figure 8

RAIN EROSION — 563 KM/HR (Figure 9)

Rain erosion test results, reported in Ref. 1 are shown in Figure 9. The 563 km/hr data presented show a variation in rain exposure effects for rain intensities from 0.635 cm/hr to 2.54 cm/hr and for 10 and 20 deg angle of attack. The data show that the all-silica RSI system is not affected at 10 deg angle of attack, while the other systems experience severe erosion in one-half hour. At 20 deg angle of attack it shows generally better performance (on the basis of the qualitative statements quoted from Ref. 1); however, an example of the superior performance of LI-1500 can be seen by looking at the quantitative data provided for the 2.54 cm/hr, 20-deg angle-of-attack condition, where the "one spot eroded" corresponds to a weight loss on the LI-1500 specimen of 55 milligrams in 5 min, while the HCF and REI suffered weight losses of 530 milligrams in 2.5 min, and 1695 milligrams in 2 min, respectively.

RAIN EROSION — 563 KM/HR

R.I. (RAIN INTENSITY) = .635 CM/HR

$\alpha = 10 \text{ DEG}$
 $\alpha = 20 \text{ DEG}$

LI-1500
HCF
REI

NOT
TESTED

SLIGHT IN 14 MIN
SLIGHT IN 5 MIN
SEVERE IN 7.5 MIN

R.I. = 1.27 CM/HR

$\alpha = 10 \text{ DEG}$
 $\alpha = 20 \text{ DEG}$

LI-1500
HCF
REI

NONE }
NONE } 5 MIN
NONE }

NONE IN 60 MIN
SEVERE IN 30 MIN
SEVERE IN 30 MIN

SLIGHT IN 2.5 MIN
SLIGHT IN 3.0 MIN
SLIGHT IN 2.5 MIN

SLIGHT IN 30 MIN
SLIGHT IN 4 MIN
SEVERE IN 4.5 MIN

R.I. = 2.54 CM/HR

$\alpha = 10 \text{ DEG}$
 $\alpha = 20 \text{ DEG}$

LI-1500
HCF
REI

NONE }
NONE } 5 MIN
NONE }

ONE SPOT ERODED IN 5 MIN
SLIGHT EROSION IN 2.5 MIN
SLIGHT EROSION IN 2.0 MIN

Figure 9

SUMMARY (Figure 10)

Testing to date has demonstrated the compatibility of the all-silica RSI system to a variety of Space Shuttle Orbiter environmental aspects for launch, on-orbit, and special reentry conditions.

Among the more important results are the success of the cold soak tests, which indicate the suitability of the foam/bond attachment system with an 2 mm thick foam pad for strain isolation, and the reentry temperature overshoot tests (to 1924° K), which show that this RSI system can tolerate considerable dispersion in reentry heating environment.

With continued development, more testing will be performed particularly with combined environments and improved simulation of the orbiter environment. However, the work to date has served to substantiate the LMSC choice of the all silica material.

SUMMARY

CAPABILITY OF ALL SILICA MATERIAL HAS BEEN DEMONSTRATED FOR:

LAUNCH PHASE

FREEZE THAW
SALT FOG
ACOUSTIC TESTS
ASCENT PRESSURE DROP

ON-ORBIT

STABILITY IN VACUUM
COLD SOAK

REENTRY/SPECIAL CONDITIONS

LOST TILE TEST
TEMPERATURE OVERSHOOT
RAIN EXPOSURE

Figure 10

REFERENCE

1. "Rain Erosion Characteristics of Thermal Protection System Materials At Subsonic Velocities," N. E. Wahl, Technical Report AFML-TR-72-145, August 1972.

SIMULATED METEOROID PENETRATION
OF REUSABLE SURFACE INSULATION

by

J.K. Lehman and H.E. Christensen

McDonnell Douglas Astronautics Company - East
St. Louis, Missouri

OVERVIEW

(Figure 1)

Meteoroid impact simulation tests of Reusable Surface Insulation (RSI) tiles were conducted at McDonnell Douglas Astrophysics Laboratory, El Segundo, California. Results of tests were used to determine penetration resistance of RSI attached to simulated Shuttle Structure. Probability of no meteoroid damage to a typical Shuttle Orbiter was determined. Specimens were plasma jet tested to determine effects of various size meteoroid cavities on thermal performance of RSI.

OVERVIEW

- METEOROID TESTS OF SIX RSI SPECIMENS
- PENETRATION RESISTANCE OF RSI
- PENETRATION RESISTANCE OF RSI PLUS STRUCTURE
- APPLICATION TO SHUTTLE
- THERMAL DEGRADATION OF IMPACTED RSI

Figure 1

RSI SPECIMENS FOR METEOROID TESTS

(Figure 2)

RSI tiles were bonded to aluminum skin panels representative of the Space Shuttle primary structure. Specimens consisted of a 20.3 cm x 20.3 cm x 0.081 cm (8.0" x 8.0" x 0.032") aluminum plate, a 15.2 cm x 15.2 cm x 0.64 cm (6.0" x 6.0" x 0.25") sponge pad, and a 15.2 cm x 15.2 cm (6.0" x 6.0") RSI tile. Thickness of tiles ranged from 1.90 cm (0.75") to 11.4 cm (4.5"). The RSI material used in these tests was 240 kg/m³ (15.0 lb/ft³) Hardened Compacted Fibers (HCF) produced by McDonnell Douglas Astronautics Company - East. Rasbestos Manhattan S105 sponge with a density of approximately 480 kg/m³ (30 lb/ft³) was used as the strain isolator. Spherical aluminum particles were propelled from a light gas gun at a velocity of about 7.3 km/sec (23,000 ft/sec).

RSI SPECIMENS FOR METEOROID TESTS

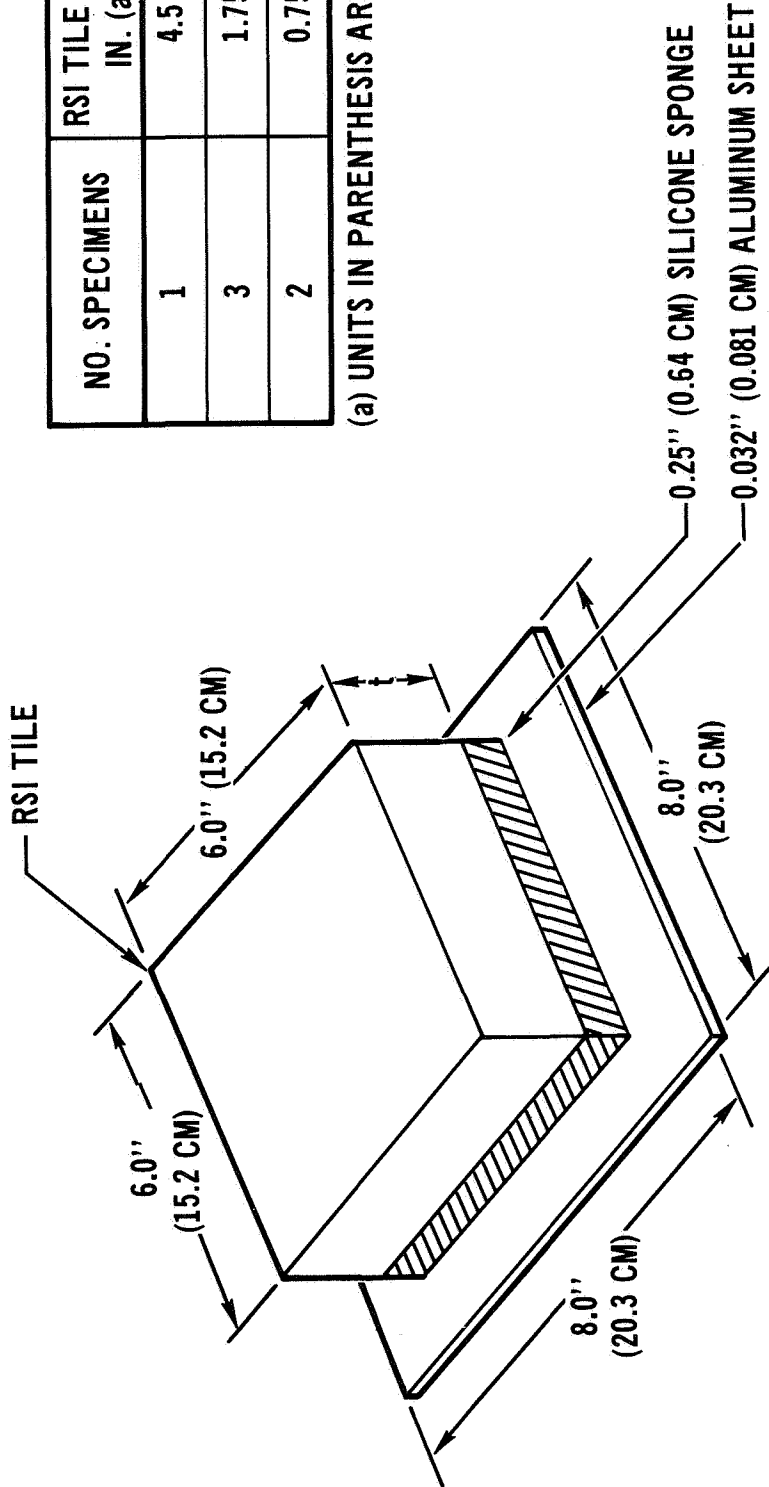


Figure 2

PREVIOUS POLYURETHANE FOAM TESTS

(Figure 3)

Results of previous meteoroid tests of polyurethane foam aided in developing empirical functions for predicting penetration resistance by assuming a similar penetration mechanism. Penetration depths into polyurethane foam for three different projectile masses are shown on this chart. Summers' equation for penetration into a semi-infinite solid was used as a basis for establishing an equation relating depth of penetration (t) into foam to projectile mass (m) and velocity (v). This equation is,

$$t = K m^{1/3} v^{2/3}$$

Constants K and X were determined from tests. Since velocity was not a test variable, the exponential value recommended by Summers was used.

PREVIOUS POLYURETHANE FOAM TESTS

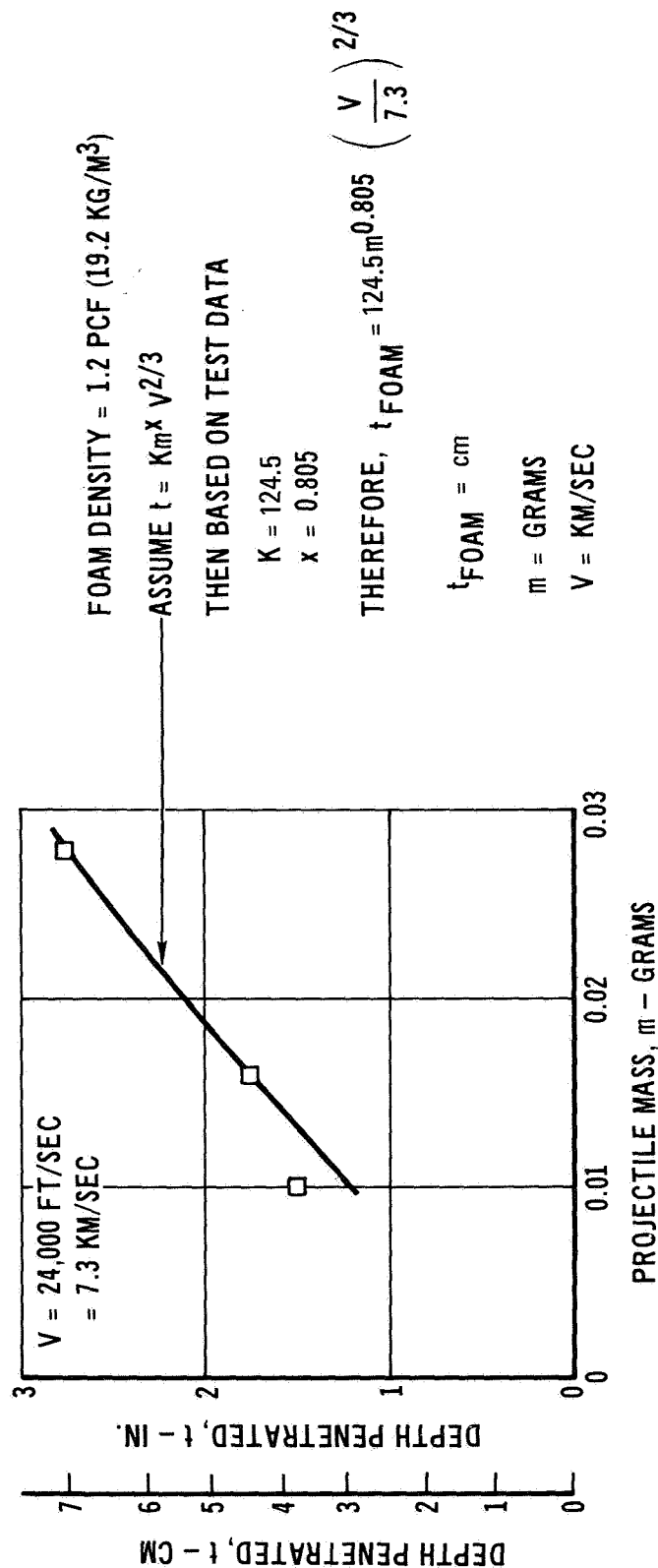


Figure 3

PRELIMINARY RSI ANALYSIS BASED ON FOAM TESTS

(Figure 4)

To obtain a penetration equation for RSI, it was assumed that the penetration mechanisms of RSI and foam are similar. This is reasonable because their densities are low relative to metallic materials. Therefore, it follows that the weight of RSI penetrated (ρ_{RSI}) (t_{RSI}) is some factor (ϕ) times the weight of foam penetrated (ρ_{FOAM}) (t_{FOAM}). Substitution of this equation into the empirical penetration equation for foam results in the penetration equation for RSI. The parameter ϕ was then obtained from tests.

PRELIMINARY RSI ANALYSIS BASED ON FOAM TESTS

$$(\rho_{RSI}) (t_{RSI}) = \phi (\rho_{FOAM}) (t_{FOAM})$$

t = THICKNESS PENETRATED BY GIVEN MASS AT GIVEN VELOCITY

ρ = MATERIAL DENSITY

$$\rho_{FOAM} = 0.0194 \text{ GRAM/CC (1.2 pcf)}$$

$$\rho_{RSI} = 0.2420 \text{ GRAM/CC (15 pcf)}$$

$$\text{THEREFORE } t_{RSI} = 9.98 \phi m^{0.805} \left(\frac{V}{7.3} \right)^{2/3}$$

$$t_{RSI} = \text{cm}$$

$$m = \text{GRAMS}$$

$$V = \text{Km/SEC}$$

Figure 4

PENETRATION RESISTANCE OF RSI

(Figure 5)

The first two data shots were used to establish the penetration resistance of RSI. Spherical aluminum particles were propelled from a light gas gun at a velocity of about 7.3 Km/sec (23,000 ft/sec). Two projectile diameters were used and depths of penetration are shown on this chart. Also shown is a plot of the empirical penetration equation for RSI using $\phi = 5$. Test results best fit this curve. The resulting penetration equation can then be used to calculate depth of penetration into RSI.

PENETRATION RESISTANCE OF RSI

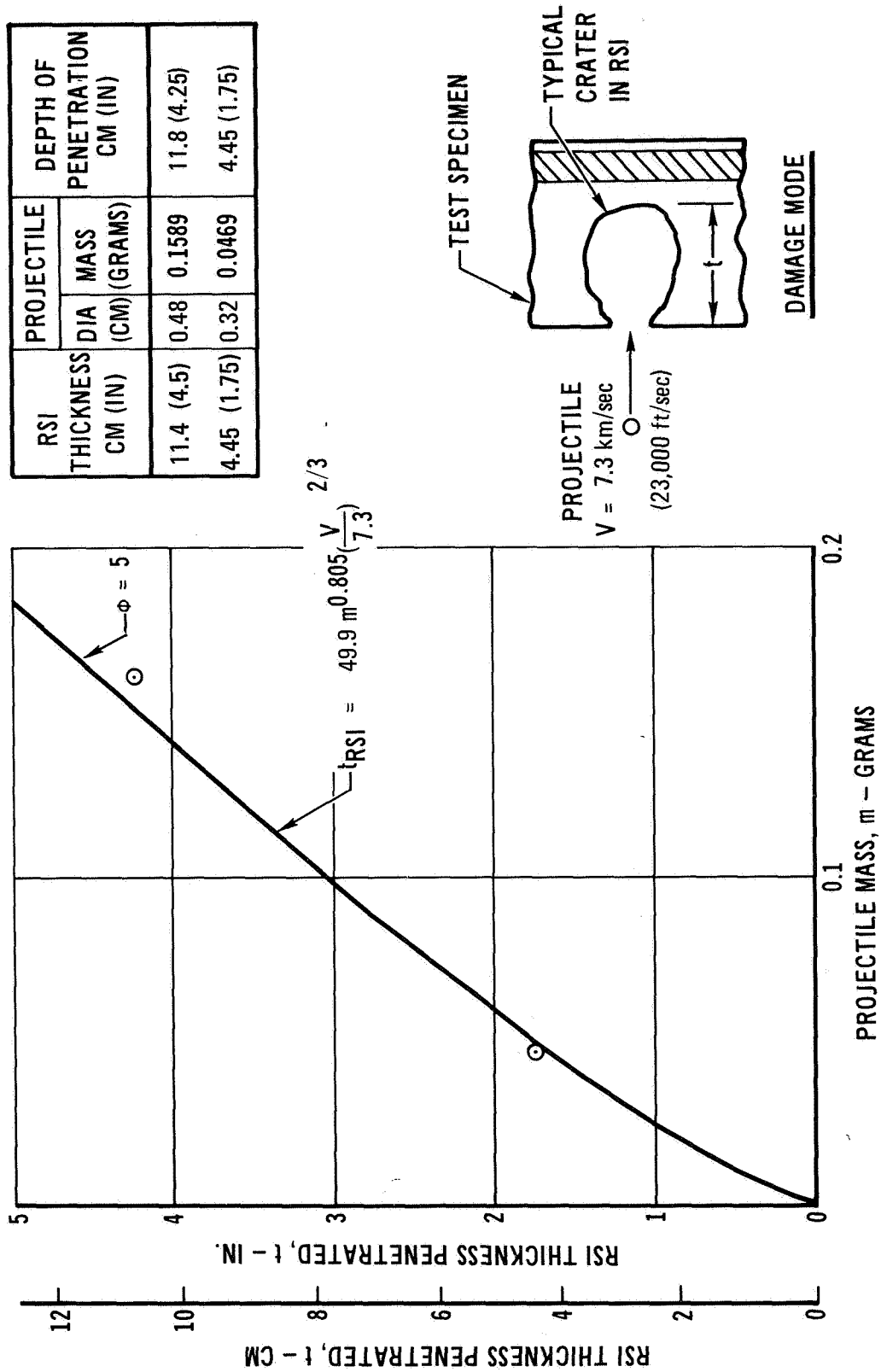


Figure 5

TYPICAL RSI DAMAGE DUE TO METEOROID IMPACT

(Figure 6)

Photos were taken of all specimens after testing to provide a permanent record of the degree of damage. This is a cutaway view of a 4.45 cm (1.75 inch) thick specimen showing typical simulated meteoroid damage. The projectile penetrated the full thickness of RSI in this test and created a large egg-shaped cavity.

TYPICAL RSI DAMAGE DUE TO METEOROID IMPACT

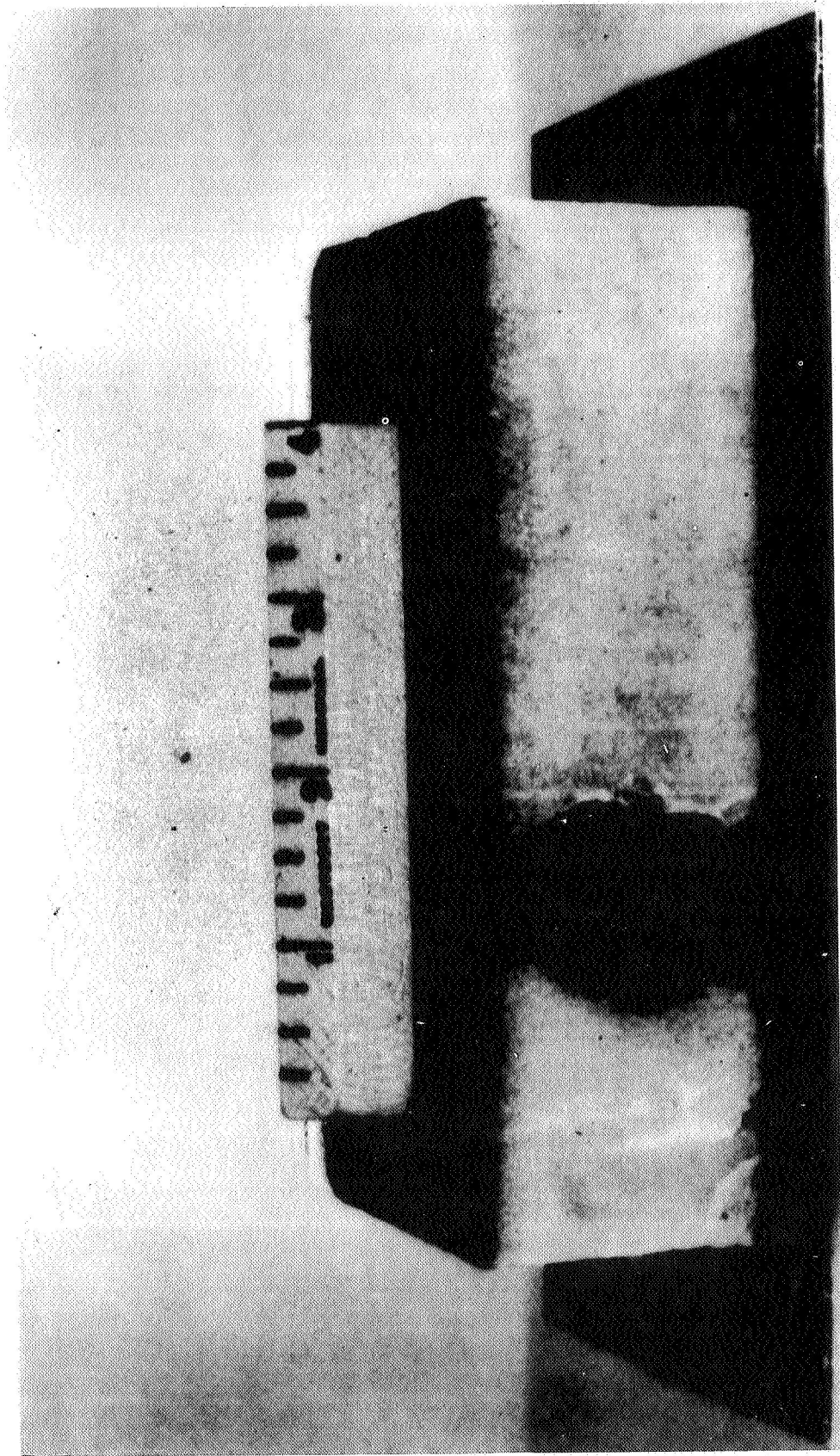


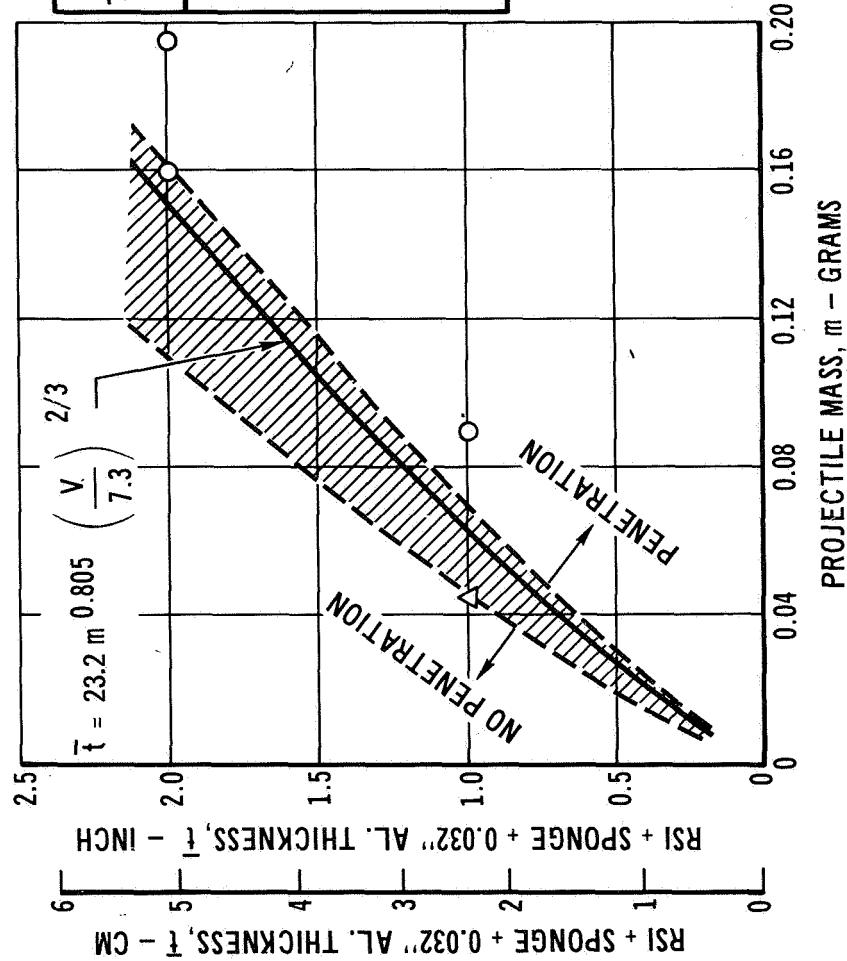
Figure 6

STRUCTURAL PENETRATION DATA

(Figure 7)

Four meteoroid shots were used to yield structural penetration data. Results of tests are shown on this chart. Three shots, denoted by circles, completely penetrated HCF, sponge, and aluminum panel. One projectile penetrated the HCF and sponge and made a large dent in the aluminum plate. A structural penetration equation was developed from these data based on the empirical equation developed for penetration into RSI only. The shaded area represents the region of uncertainty which could be reduced with further testing.

STRUCTURAL PENETRATION DATA



RSI* THICKNESS CM (IN)	PROJECTILE**		TEST RESULTS
	DIA (CM)	MASS (GRAMS)	
4.45 (1.75)	0.48	0.1593	JUST PENETRATED
● 4.45 (1.75)	0.52	0.1978	COMPLETE PENETRATION
1.90 (0.75)	0.32	0.0467	BIG DENT IN ALUMINUM SHEET
1.90 (0.75)	0.40	0.0919	COMPLETE PENETRATION

*TOTAL SPECIMEN THICKNESS IS RSI
THICKNESS + 0.64 cm (0.25")

SPONGE + 0.081 cm (0.032") AL.

** V = 7.3 km/sec (23,000 ft/sec)

Figure 7

RSI SPECIMEN METEOROID DAMAGE--COMPLETE PENETRATION

(Figure 8)

None of the RSI tiles failed catastrophically, but large, egg-shaped craters did result from meteoroid penetration. This chart shows the metallic side of a specimen that was completely penetrated. The petalled hole is typical of thin gage shielded structures.

RSI SPECIMEN METEOROID DAMAGE—COMPLETE PENETRATION



Figure 8

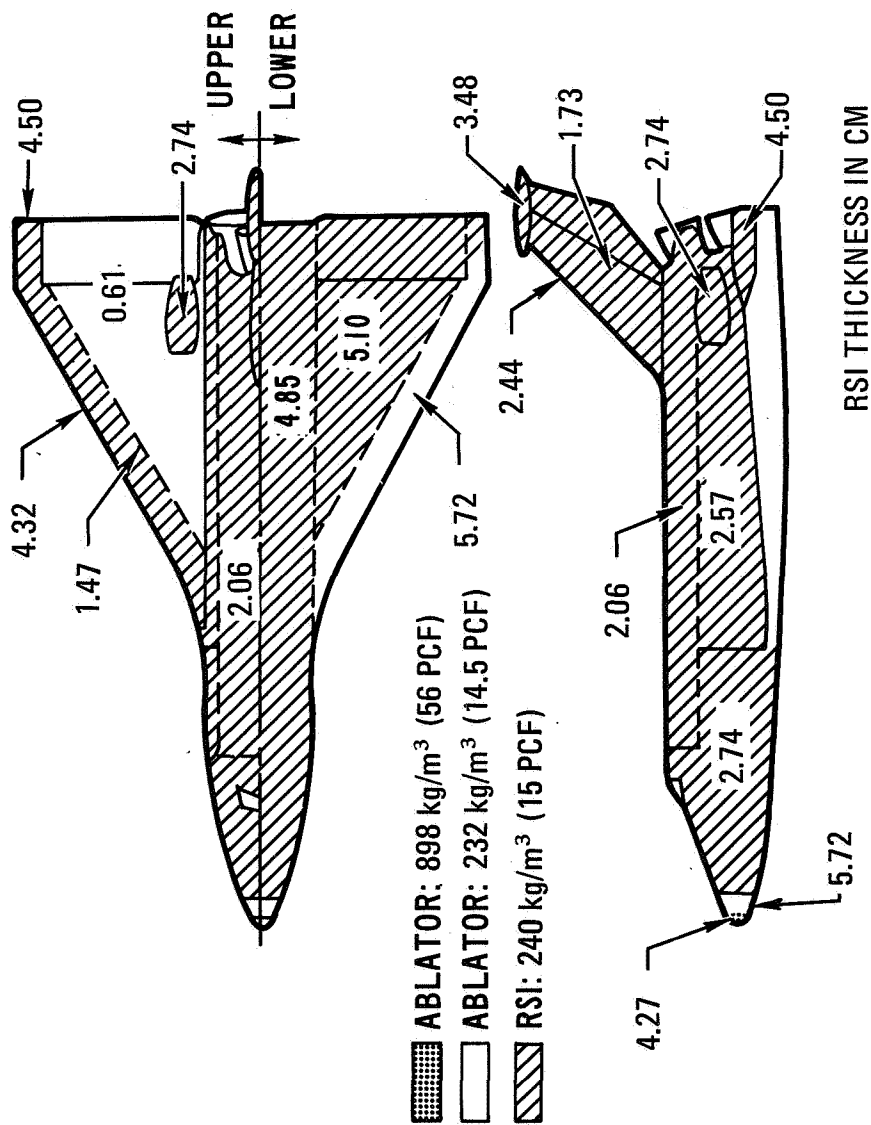
RSI SURFACE AREA COVERAGE

(Figure 9)

The penetration equations developed from tests were used to predict surface damage and to estimate probability of no penetration of the Shuttle Orbiter primary structure. Typical results are shown in figures 9 through 11.

For the Shuttle Orbiter configuration studied, RSI covers 77 percent of the surface area or about 890 m² (9600 ft²). For meteoroid analysis, the surface area was divided into three parts with different RSI thicknesses: 1.60 cm (0.63"), 2.41 cm (0.95"), and 4.90 cm (1.93").

RSI SURFACE AREA COVERAGE



AREA FT ² (a)	AVERAGE RSI THICKNESS IN. (b)
1400 (130)	0.63 (1.60)
4350 (404)	0.95 (2.41)
3880 (360)	1.93 (4.90)

(a) UNITS IN PARENTHESIS ARE M².
(b) UNITS IN PARENTHESIS ARE CM.

Figure 9

METEOROID ENVIRONMENT, MASS--FLUX MODEL

(Figure 10)

Environments for sporadic and stream meteoroids are summarized on this chart. Environments were taken from NASA TM X-53957. The seasonal factors are based on a seven day mission occurring during periods of peak sporadic and stream meteoroid activity. An orbital altitude of 370 Km (200 nm) was used to determine values for the defocusing factor and earth gravitational effects.

METEOROID ENVIRONMENT, MASS—FLUX MODEL

• SPORADIC METEORIODS

FOR $10^{-6} \leq m \leq 10^0$

$$\log N_{Sp} = -14.41 - 1.22 \log m + \log G_e + \log \left(\frac{1 + \sqrt{1 - 1/r^2}}{2} \right) + \log F_{\text{seasonal}}$$

N_{Sp} = NO. OF PARTICLES/ m^2 /SEC OF MASS m OR GREATER

m = MASS IN GRAMS

G_e = DEFOCUSING FACTOR = 0.976 (370 km ORBIT)

r = 1.06 (3.70 km ORBIT)

F_{seasonal} = 1.77 (7 DAY MISSION)

• STREAM METEORIODS

FOR $10^{-6} \leq m \leq 10^0$

$$\log N_{St} = -14.41 - \log m - 4.0 \log (V_{St}/20) + \log F$$

N_{St} = NO. OF PARTICLES/ m^2 /SEC OF MASS m OR GREATER

V_{St} = 40 Km/SEC

F = 6.0 (7 DAY MISSION)

REFERENCE: NASA TMX 53957

Figure 10

EFFECTS OF STRUCTURAL SKIN THICKNESS ON PENETRATION PROBABILITY

(Figure 11)

Probability of no structural penetration was determined for a seven day mission, assuming 77 percent of the shuttle covered with RSI and considering sporadic and stream meteoroids. For a 0.081 cm (0.032 inch) aluminum skin thickness the probability of no structural penetration is 0.99988. The probability of no penetration exceeding the thickness of RSI only was also calculated using the RSI penetration equation. A curve was drawn connecting the two points based on penetration probability analyses of other materials. Tests of other skin thicknesses are required to establish the correct relationship for RSI bonded to aluminum.

EFFECTS OF STRUCTURAL SKIN THICKNESS ON PENETRATION PROBABILITY

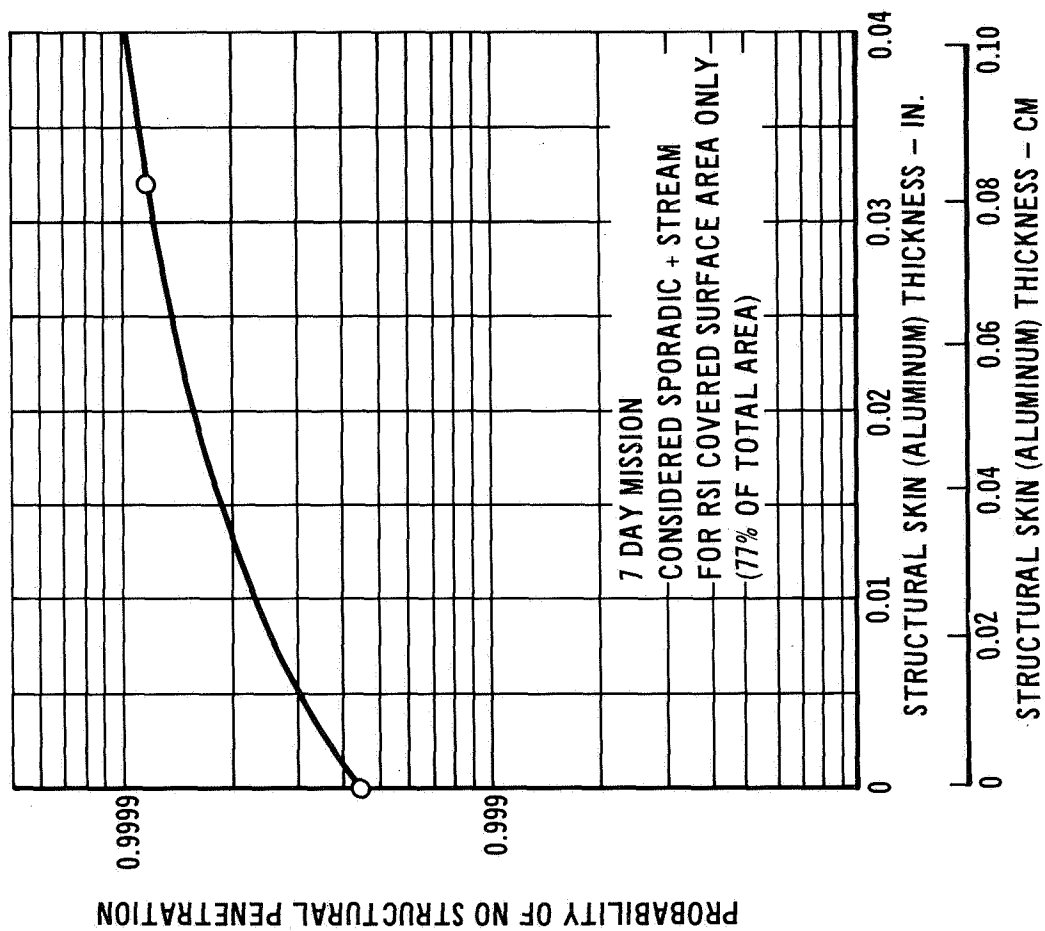


Figure 11

RSI SPECIMENS FOR THERMAL DEGRADATION TESTS
(PLASMA JET TESTS)

(Figure 12)

A RSI tile with simulated meteoroid cavities was tested in a plasma jet tunnel to determine the effects of cavity size on bondline heating. The heat pulse produced total heat and peak temperatures equivalent to a shuttle entry heating cycle. The same tile was tested four times with a successively larger cavity each test to obtain comparative data. The same heat pulse was used for each test except heating was terminated early if the bondline reached 423°K (300°F). Thermocouples were embedded in the tile to monitor temperatures during tests.

The test specimen was a 17.8 cm (7.0 inch) diameter by 5.08 cm (2.0 inch) thick RSI tile bonded with RTV 560 to a 0.64 cm (0.25 inch) thick sponge pad which was in turn bonded to a 0.25 cm (0.10 inch) thick titanium plate. The specimen was split along a diagonal to allow access for carving egg shaped cavities in the center of the tile. The specimen was bolted to support structure and was inclined at a 60° angle of attach to the air flow. The top surface of the specimen was coated with a high emittance coating. Thermocouples were located at several points through the thickness of the tile and at the RSI sponge bondline. Because of excessive electrical interference during tests with cavities in the RSI, only the thermocouples at the bondline functioned properly.

RSI SPECIMENS FOR THERMAL DEGRADATION TESTS (PLASMA JET TESTS)

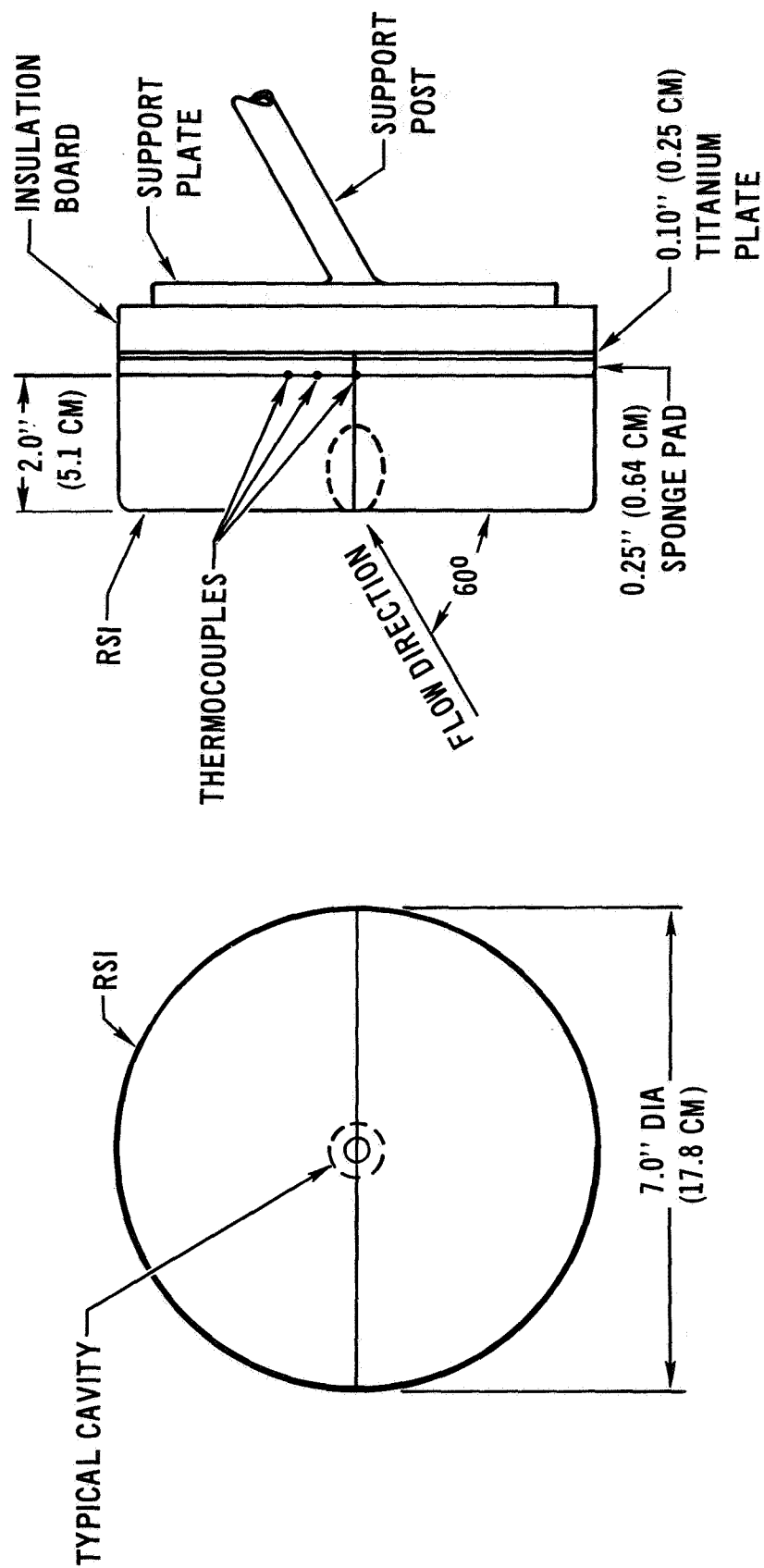


Figure 12

METEOROID CAVITY DIMENSIONS

(Figure 13)

Four tests were conducted; one with no cavity and three with successively larger egg-shaped cavities. For the four tests, cavity depths were respectively 0.0 cm, 1.93 cm (0.76 inch), 3.42 cm (1.35 inch), and 5.08 cm (2.0 inch). The 5.08 cm (2.0 inch) cavity completely penetrated the tile to the sponge. For tests 2, 3, and 4 the cavity proportions were approximately the same and the size of the entry hole was unchanged. Probable number of penetrations are indicated for each cavity size assuming seven day missions.

METEOROID CAVITY DIMENSIONS

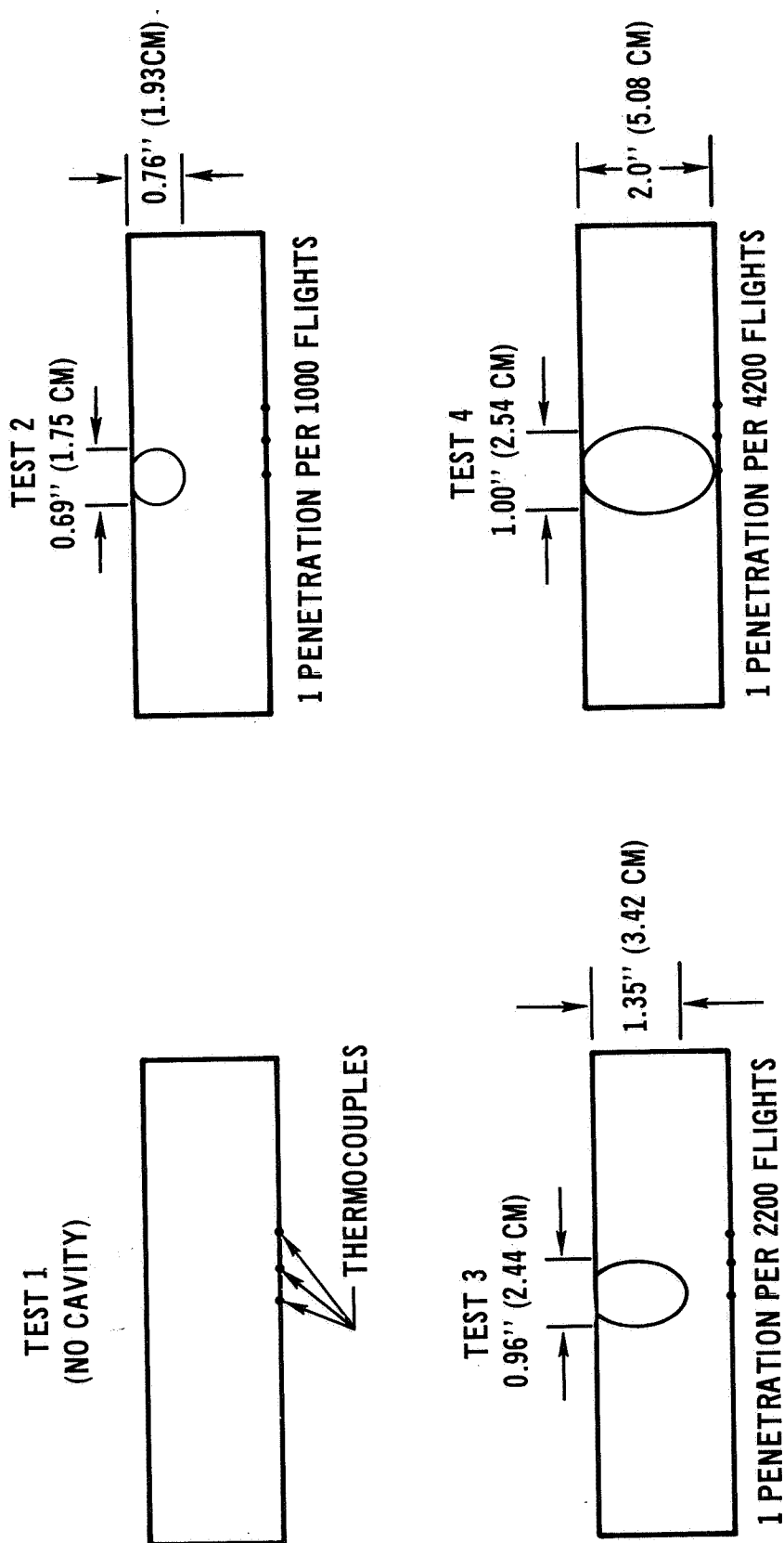


Figure 13

HEATING PULSE EQUIVALENT TO HEAT FROM 2000 KM (1100 MILE)

CROSS-RANGE ENTRY

(Figure 14)

The tile was subjected to a heat pulse equivalent to the total heat and peak temperature of a shuttle entry cycle, except heating was terminated early if the bondline temperature reached 420°K (300°F). The linear heating plan consisted of: (1) a tile surface temperature rise from ambient to 870°K (1100°F) in a few seconds as the tile was inserted into the 870°K (1100°F) heating stream; (2) a 150 second linear surface heat up to 1530°K (2300°F); (3) a 490 second constant surface heating at 1530°K (2300°F); (4) a 150 second linear surface cool down to 870°K (1100°F); and (5) removal of specimen and cool to ambient conditions. The entire heating pulse was 790 seconds duration. The actual heating pulse for the first test differed slightly from the plan as shown. For tests 3 and 4, the heating pulse was of shorter duration because the bondline temperature reached 420°K (300°F).

HEATING PULSE EQUIVALENT TO HEAT FROM 2000km (1100 MILE)

CROSS-RANGE ENTRY

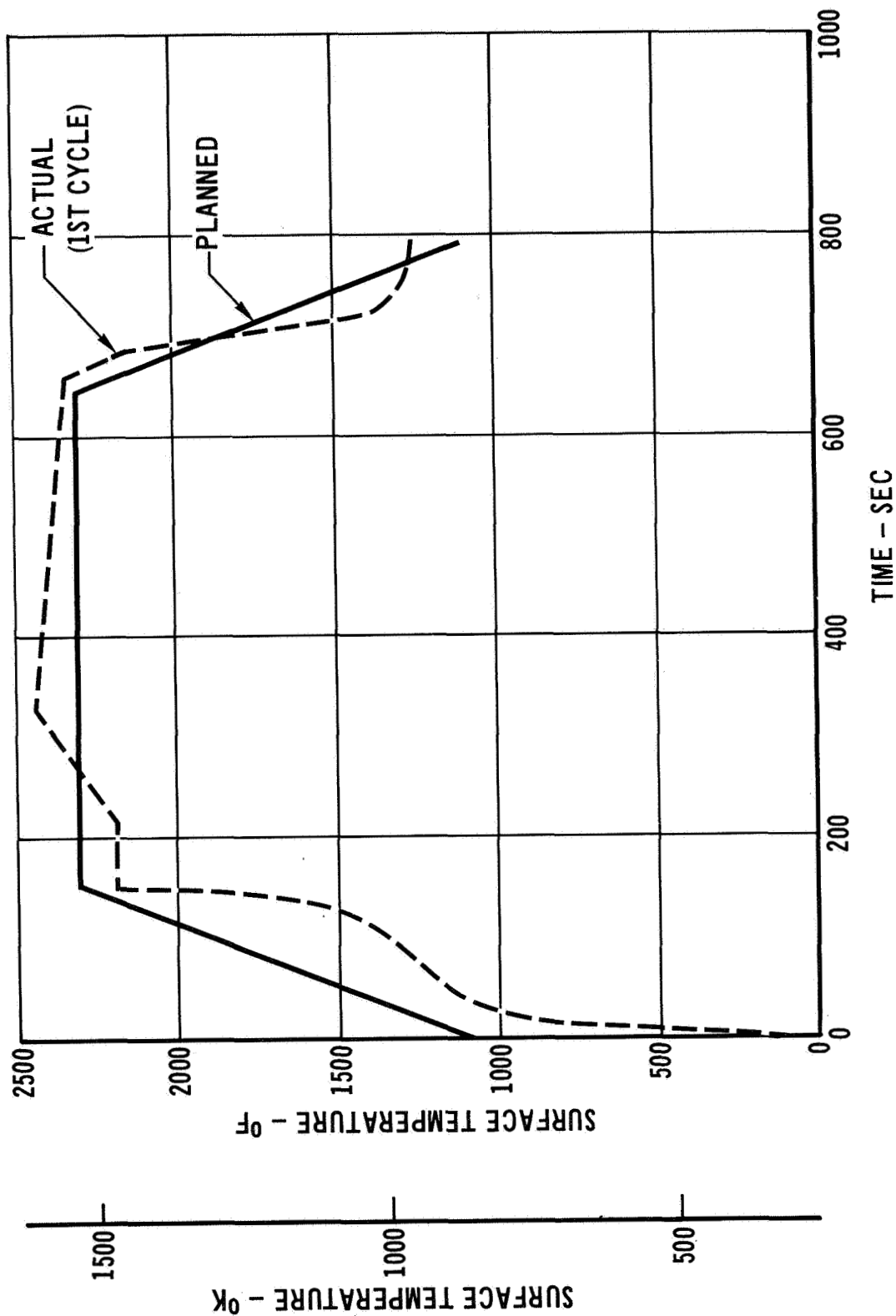


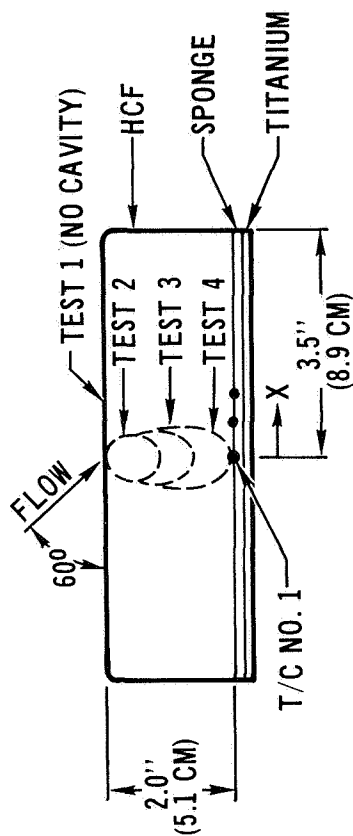
Figure 14

INFLUENCE OF CAVITY SIZE ON BONDLINE HEATING

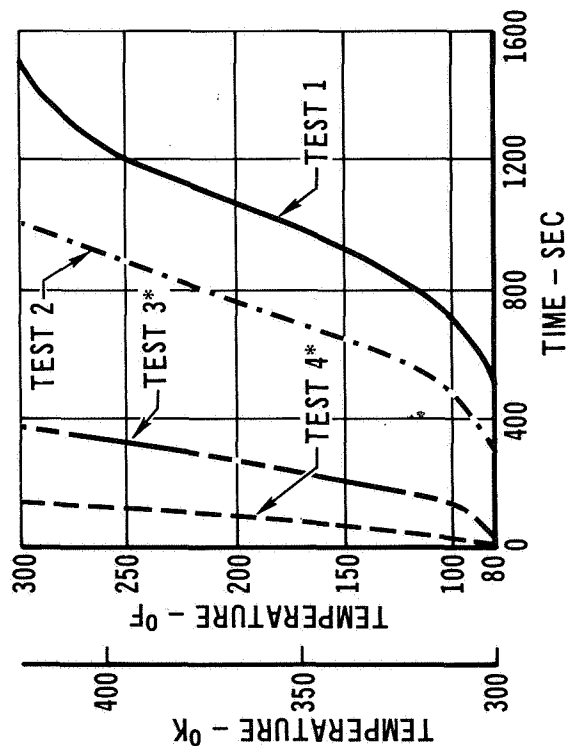
(Figure 15)

The presence of cavities in the tile did influence the bondline heating. Both the bondline temperature-time history and temperature distribution changed with changes in cavity size. With no cavity, the full 790 second heat pulse was input before a bondline temperature of 420°K (300°F) was reached and the bondline temperature distribution was approximately uniform. The 1.93 cm (0.76 inch) cavity was also exposed to the full heat pulse and the bondline reached a peak temperature of 460°K (370°F). Heating was stopped early for the 3.42 cm (1.35 inch) and 5.08 cm (2.0 inch) cavities to prevent overheating. For the 5.08 cm (2.0 inch) deep cavity a 420°K (300°F) bondline temperature was reached when only 135 seconds of the 790 second thermal pulse had been input. Also the tile bondline temperature dropped from 420°K (300°F) at the cavity centerline to ambient only 2.54 cm (1 inch) away after 135 seconds of heating. The two smaller cavities produced approximately proportional changes. A meteoroid penetration sufficient to reach the bondline on the shuttle orbiter would be expected once every 2500 seven day missions.

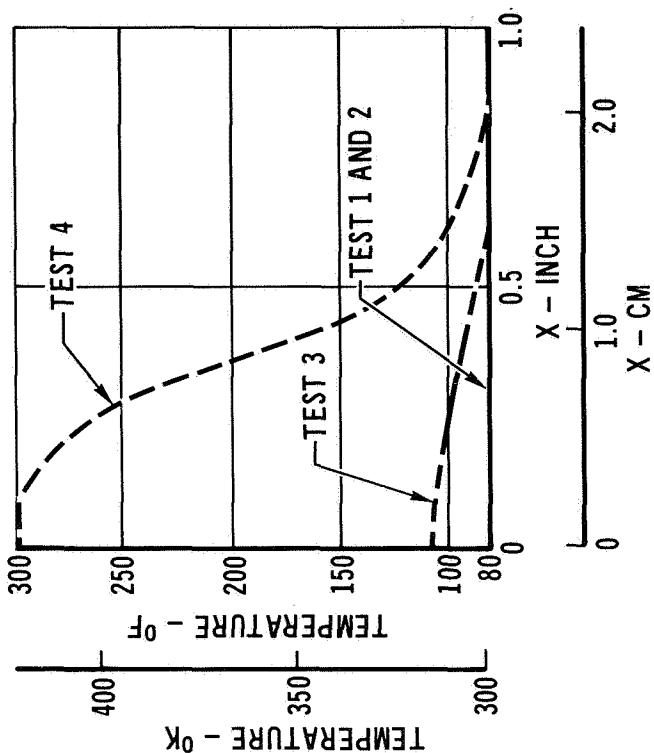
INFLUENCE OF CAVITY SIZE ON BONDLINE HEATING



BONDLINE TEMPERATURE VS TIME
(AT T/C NO. 1)



BONDLINE TEMPERATURE DISTRIBUTION
(TIME = 135 SEC)



*COOL DOWN INITIATED WHEN TEMPERATURE REACHED 420°K

Figure 15

FURTHER STUDIES REQUIRED

(Figure 16)

Recommended future studies are identified on this chart. They include determination of dependency of damage on projective velocity, investigations of penetration mechanics and effects of oblique impacts. Also, additional thermal performance tests are recommended for different cavity shapes which may be associated with coated RSI and to determine heat pulse duration which would cause structural damage.

FURTHER STUDIES REQUIRED

- PROJECTILE VELOCITY DEPENDENCY
- PENETRATION MECHANICS
 - RSI (COATED AND UNCOATED)
 - RSI/STRUCTURE
- OBLIQUE IMPACT EFFECTS
- THERMAL DEGRADATION OF IMPACTED RSI

Figure 16

EFFECTS OF SEA SALTS ON THE PHYSICAL CHARACTERISTICS
OF REUSABLE SURFACE INSULATION

By

Philip O. Ransone and Dennis L. Dicus
Langley Research Center

INTRODUCTION

(Figure 1)

The coatings on Reusable Surface Insulation (RSI) which are proposed for space shuttle are formulated of ceramic phases that can be modified by contamination with light metal salts contained in sea water. Since Cape Kennedy has been chosen as a base for space shuttle, it is important to determine if RSI coatings will be affected by exposure to the coastal atmosphere, which contains measurable quantities of sea salts.

Compositional changes of the glass in RSI coatings resulting from contamination with sea water salts are likely to modify melting temperature, melt viscosity, and thermal expansion. Changes in composition can influence the behavior of existing crystalline phases as well. In the silica glass system, contaminate particles can act as nucleation sites for devitrification. The resulting cristobalite phase can be destructive in a thermal cyclic environment because of the volume changes associated with polymorphic transformation of cristobalite. Since these coatings are designed to provide high emittance, the effect on emittance of changes in the surface characteristics due to melting and crystallization must be examined.

This paper reports partial results of a preliminary study in which coated specimens of RSI were exposed to sea salt and radiant heat cycles in the laboratory. The intent of this study was to demonstrate the necessity for testing these materials under realistic environmental conditions.

EFFECT OF SEA SALTS ON RSI
COATINGS DURING REENTRY HEATING

- MELTING TEMPERATURE AND MELT VISCOSITY LOWERED
- CRYSTALLINE PHASE CHANGES
- EXPANSION CHANGES, VOLUME AND THERMAL
- POSSIBLE EMITTANCE CHANGES DUE TO CHANGES IN
SURFACE CHARACTERISTICS

Figure 1

MATERIALS

(Figure 2)

Test specimens were cut to dimensions 3.2 cm square by 2.5 cm thick from large coated tiles of each material listed in this figure. One face of each specimen was coated.

The McDonnell Douglas (MDAC) material is coated with a base coat M5₂₃, a phosphate bonded chromium oxide diffusion barrier A, a borosilicate seal coat 7, and a P₇₀₀ emittance agent containing iron, cobalt, and chromium oxides. The insulation is mullite fiber with silica microspheres and silica binder.

The coating on the General Electric (GE) material is a kyanite/petalite multiphase glass composition with a nickel oxide emittance agent. The insulation is mullite fiber with Al₂O₃-SiO₂-B₂O₃ glass binder.

The coating on the Lockheed (LMSC) material is a borosilicate glass with a silicon carbide emittance agent dispersed in the glass. The insulation is silica fiber with colloidal silica binder.

The thickness of the coatings on all materials is nominally 0.038 cm. The GE and LMSC coatings

are considered current baseline, but the MDAC coating has been superseded by a newer version, MM_P Cr 7P₇₀₀.

MATERIALS

COMPANY	COATING DESIGNATION	INSULATION DESIGNATION
MDAC	M5 ₂₃ A7P ₇₀₀	MULLITE-HCF MOD III
GE	SR-2	REI MULLITE MOD I-A
LMSC	LI-0042	LI-1500

Figure 2

TEST PROCEDURE

(Figure 3)

This figure depicts the test procedure followed in this investigation. Specimens were alternately exposed to sea water fog and temperature cycles up to 50 times. Sea water was applied to specimens as an atomized spray. The weight of solids deposited per application was $0.05 - 0.08 \text{ mg/cm}^2$. Additional specimens were subjected to the same number of temperature cycles but without contamination. The temperature cycle used was a radiant heat simulation of short cross-range re-entry. The test cycle was 2700 sec reaching a maximum of 1530°K at 1700 sec but with a hold at 1140°K for most of the first 1550 sec. After completion of the cyclic heating and salt exposure, X-ray diffraction patterns were obtained for all specimens by scanning the coating surface at $2\theta = 2^\circ/\text{min}$ with Nickel filtered $\text{Cu K}\alpha$ radiation. Crystalline phases were identified by comparing d-spacings and intensities of the measured patterns with the ASTM powder diffraction file.

Spectral emittance of specimens was measured in the 1-15 μm range at temperatures of 800° , 1100° , and 1300°K using the method described by Kantsios et al. in Volume I of these Proceedings. Total normal emittance was calculated from these data by integrating over the wavelength. Specimens were then prepared for photographic documentation and destructive analyses.

TEST PROCEDURE

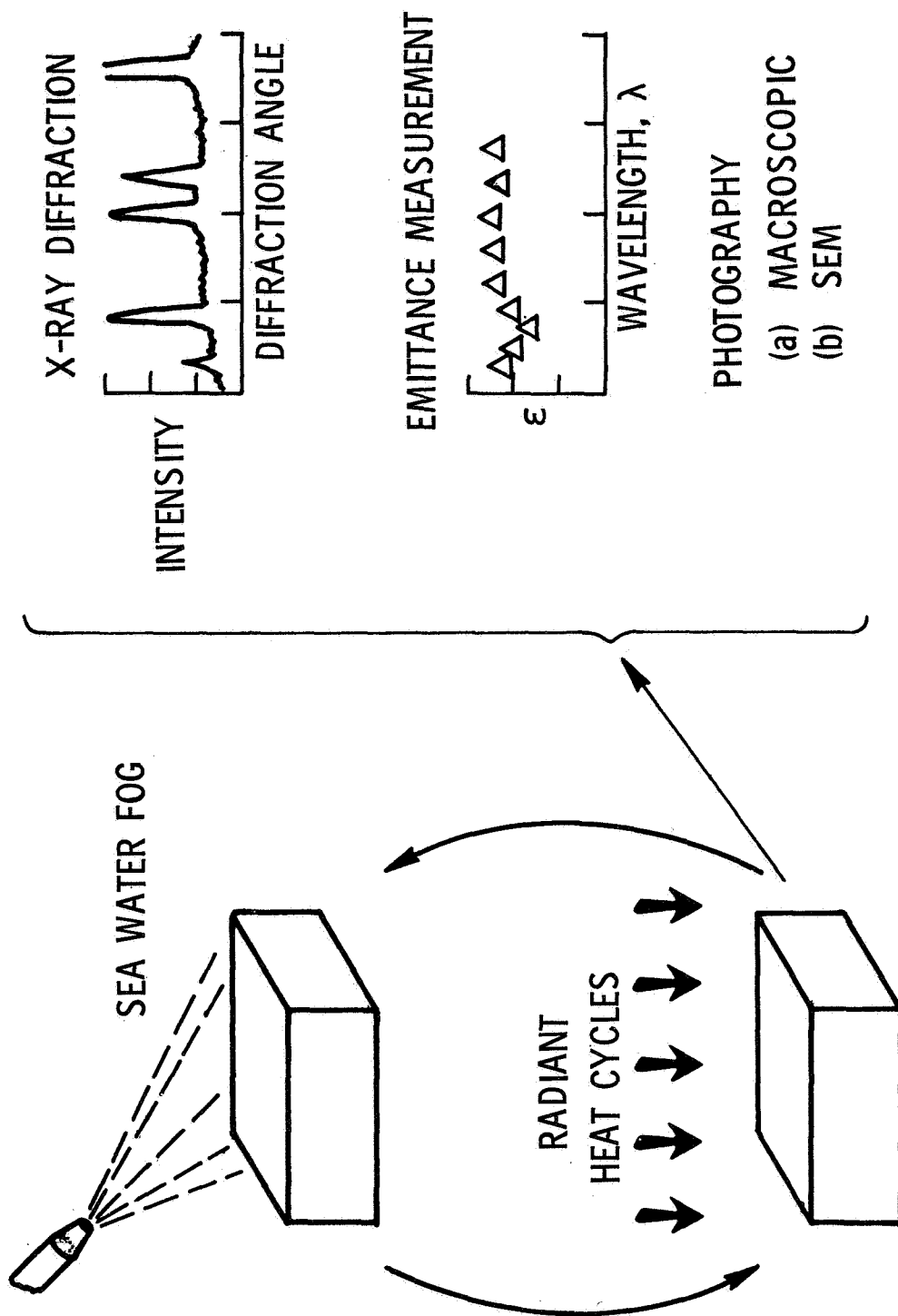


Figure 3

X-RAY DIFFRACTION PATTERNS OF M5₂₃A7P₇₀₀ COATING

(Figure 4)

This figure shows X-ray diffraction patterns for the MDAC coating in the as-received condition and after 50 thermal cycles with and without sea salt contamination. The contaminated specimen was sprayed with sea water before each of the 50 thermal cycles. Chromium oxide was the only crystalline phase identified in this coating. No new phases appeared after 50 cycles with or without contamination; however, there was some reduction in the amount of phase present as indicated by weakening of the diffraction lines.

X-RAY DIFFRACTION PATTERNS OF M5₂₃A7P₇₀₀ COATING

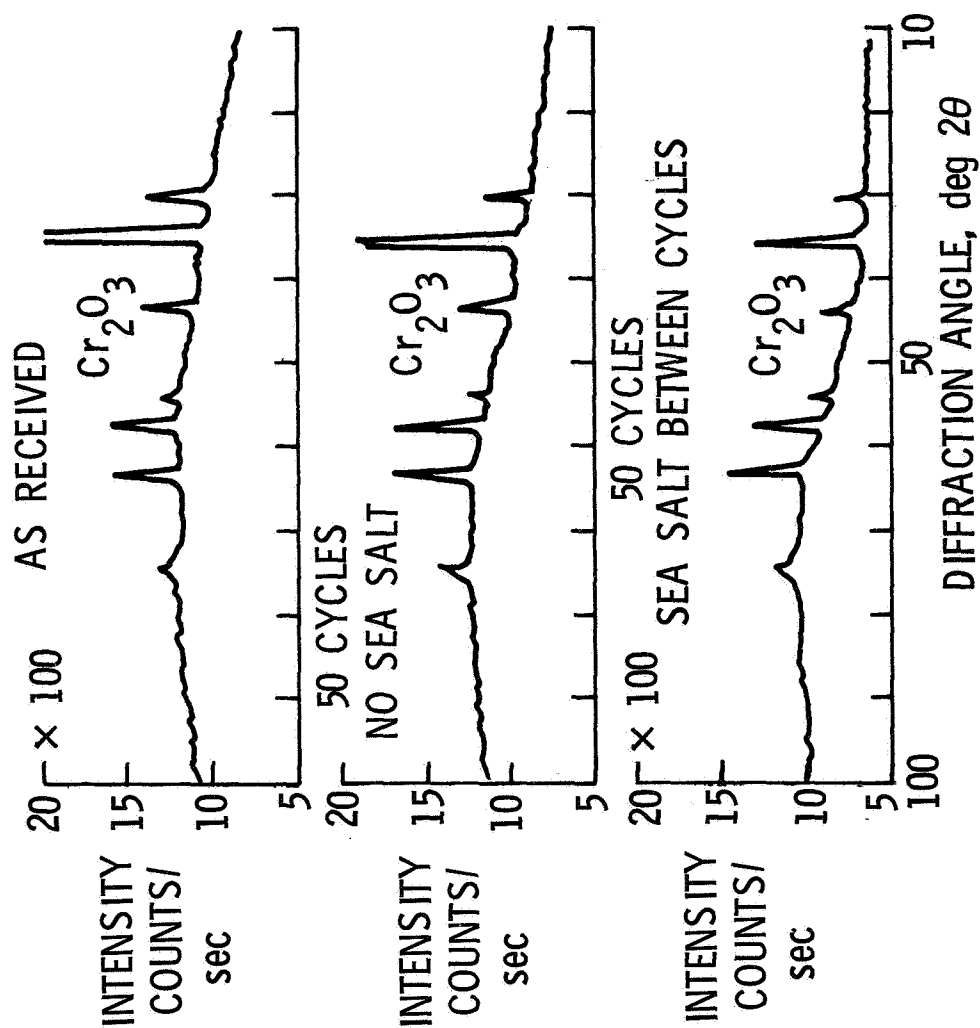


Figure 4

X-RAY DIFFRACTION PATTERN OF SR-2 COATING

As Received

(Figure 5)

This figure shows an X-ray diffraction pattern of the G.E. coating in the as-received condition. Three crystalline phases were tentatively identified in this coating. The strongest lines belong to the μ cordierite phase. Remaining lines agree closely with the lines of Iota alumina and nickel aluminate spinel.

X-RAY DIFFRACTION PATTERNS OF SR-2 COATING AS RECEIVED

- 1 Al_2O_3 (IOTA)
- 2 μ CORDIERITE
- 3 NICKEL ALUMINATE

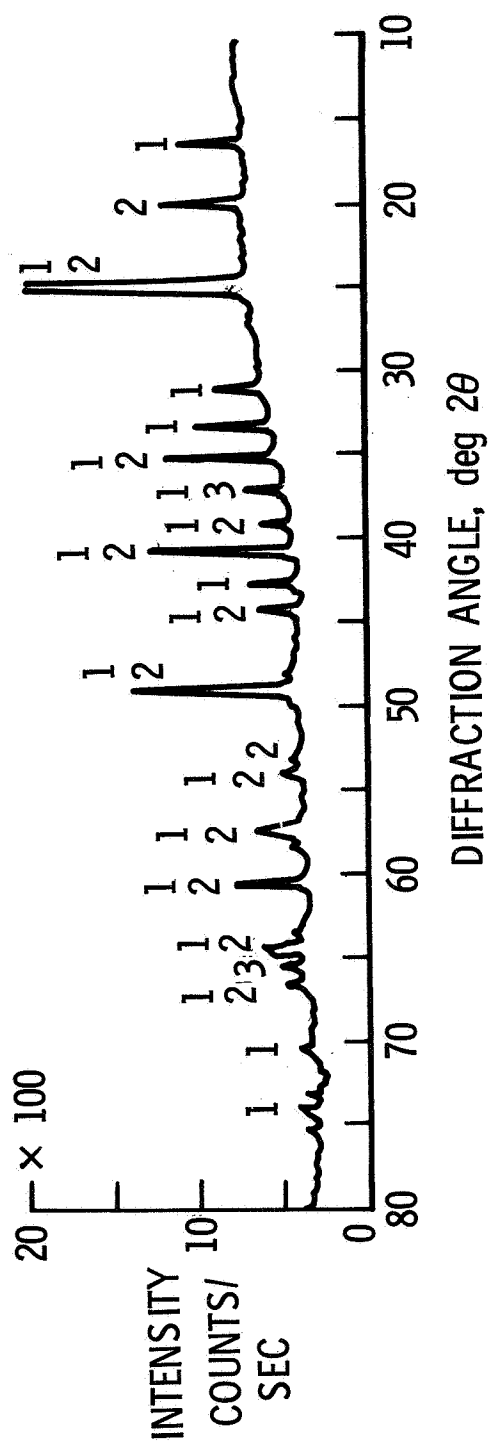


Figure 5

X-RAY DIFFRACTION PATTERNS OF SR-2 COATING

50 Thermal Cycles

(Figure 6)

Shown in this figure are X-ray diffraction patterns of contaminated and uncontaminated G.E. specimens after 50 thermal cycles. The contaminated specimen was sprayed with sea water before every cycle. When comparing the patterns in this figure to those of figure 5, it is seen that thermal cycles initiate a cristobalite phase and that contamination with salt inhibits initiation of the cristobalite phase. Contamination greatly accelerates the growth of the nickel aluminate phase but causes the cordierite and alumina phases to be dissolved.

X-RAY DIFFRACTION PATTERNS OF SR-2 COATING

50 THERMAL CYCLES

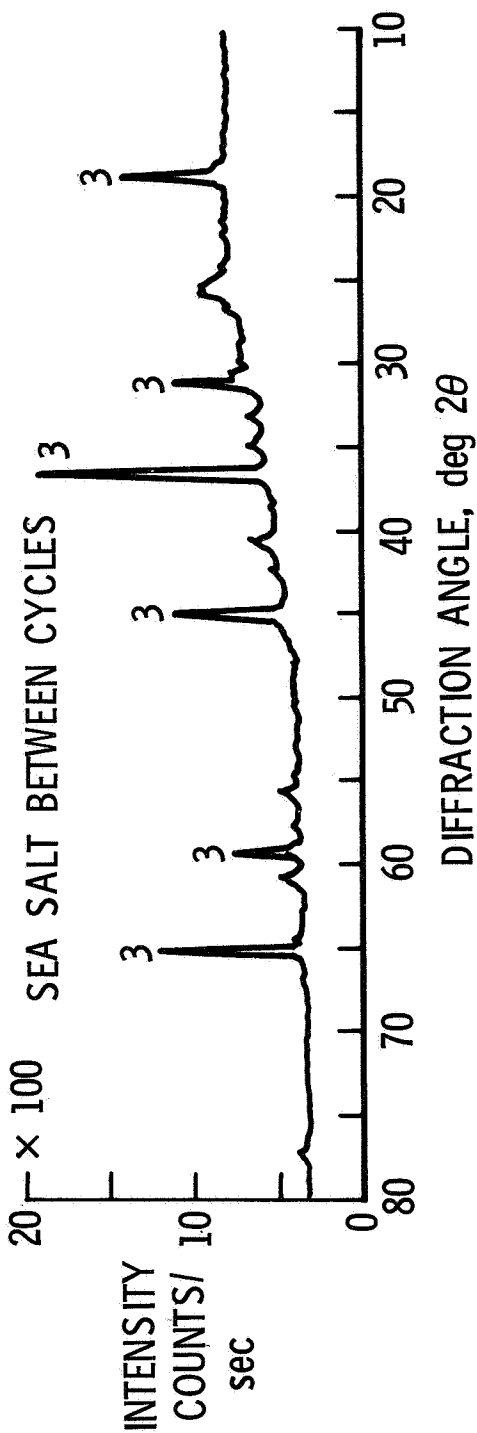
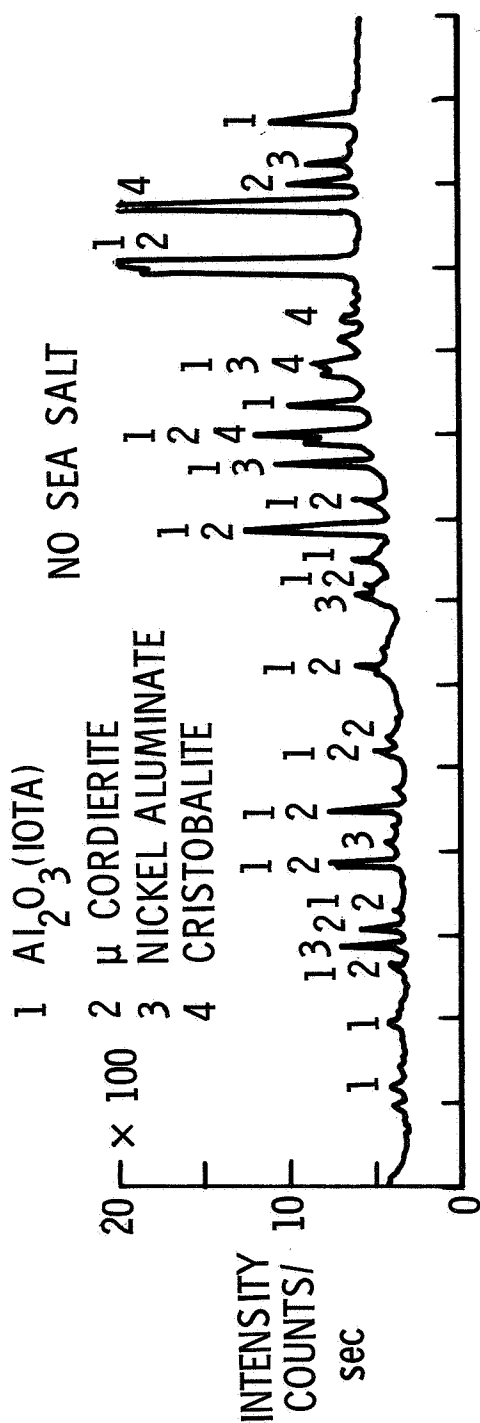


Figure 6

X-RAY DIFFRACTION PATTERNS OF LI-0042 COATING

As Received

(Figure 7)

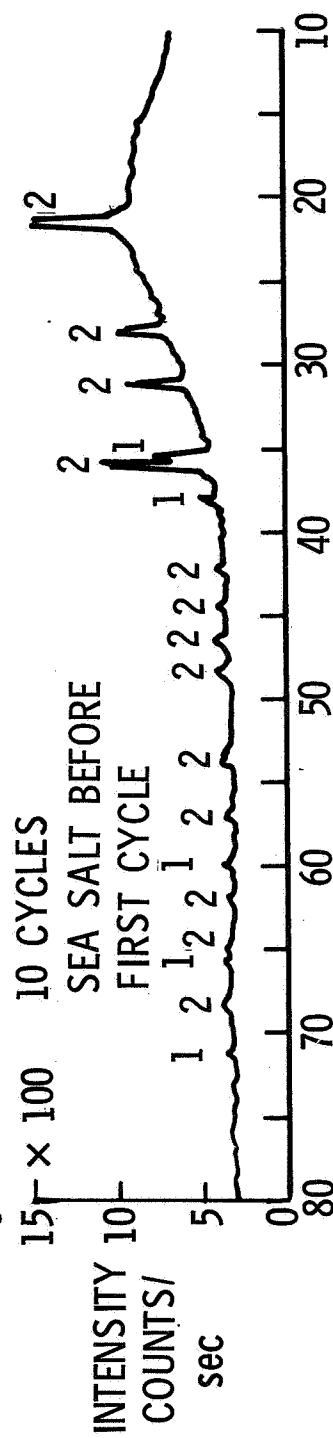
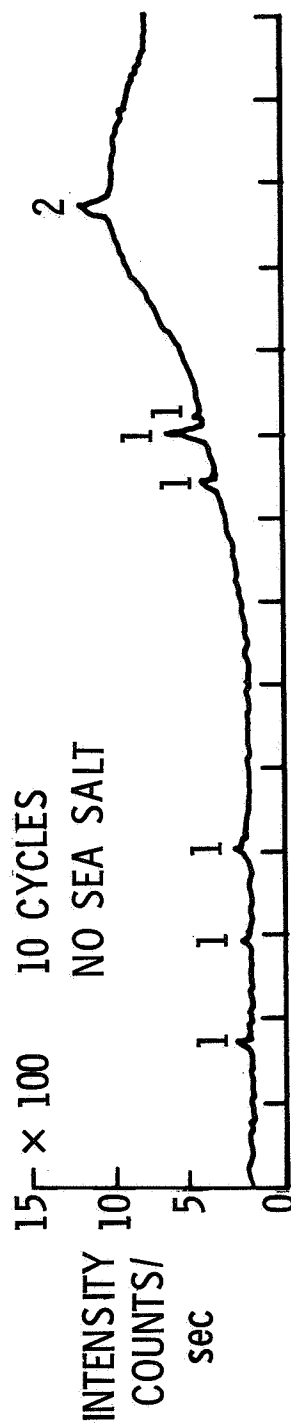
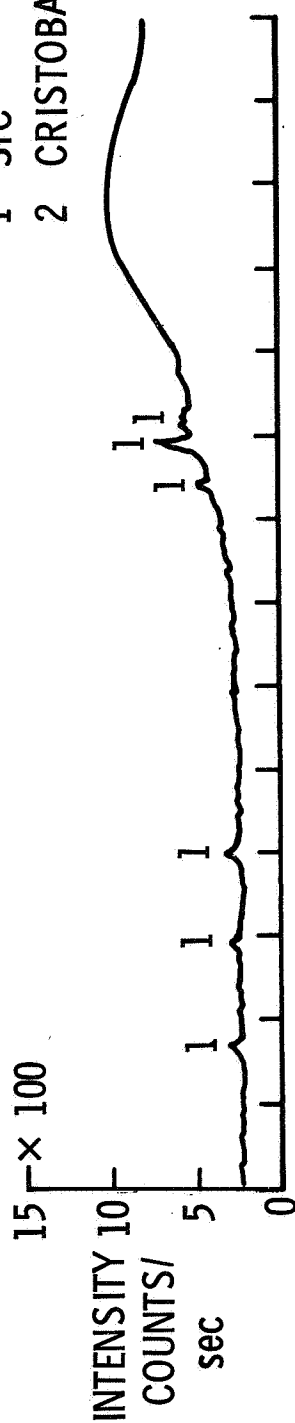
This figure shows X-ray diffraction patterns of the LMSC coating in the as-received condition and after 10 thermal cycles with and without contamination. The contaminated specimen was sprayed with sea water before the first cycle only. Silicon carbide was the only crystalline phase identified in the as-received coating. After 10 thermal cycles, the effect of contamination on cristobalite growth is apparent.

X-RAY DIFFRACTION PATTERNS OF LI-0042 COATING

AS RECEIVED

1 SiC

2 CRISTOBALITE



DIFFRACTION ANGLE, deg 2θ

Figure 7

X-RAY DIFFRACTION PATTERNS OF LI-0042 COATING

50 Thermal Cycles

(Figure 8)

The X-ray diffraction patterns shown in this figure are of the IMSC coating after 50 thermal cycles. No sea water was sprayed on the specimen that produced the first pattern. The specimens that produced the next two patterns were sprayed with one and four applications, respectively. These data show that there is a definite acceleration of devitrification associated with degree of sea salt contamination.

X-RAY DIFFRACTION PATTERNS OF LI-0042 COATING 50 THERMAL CYCLES

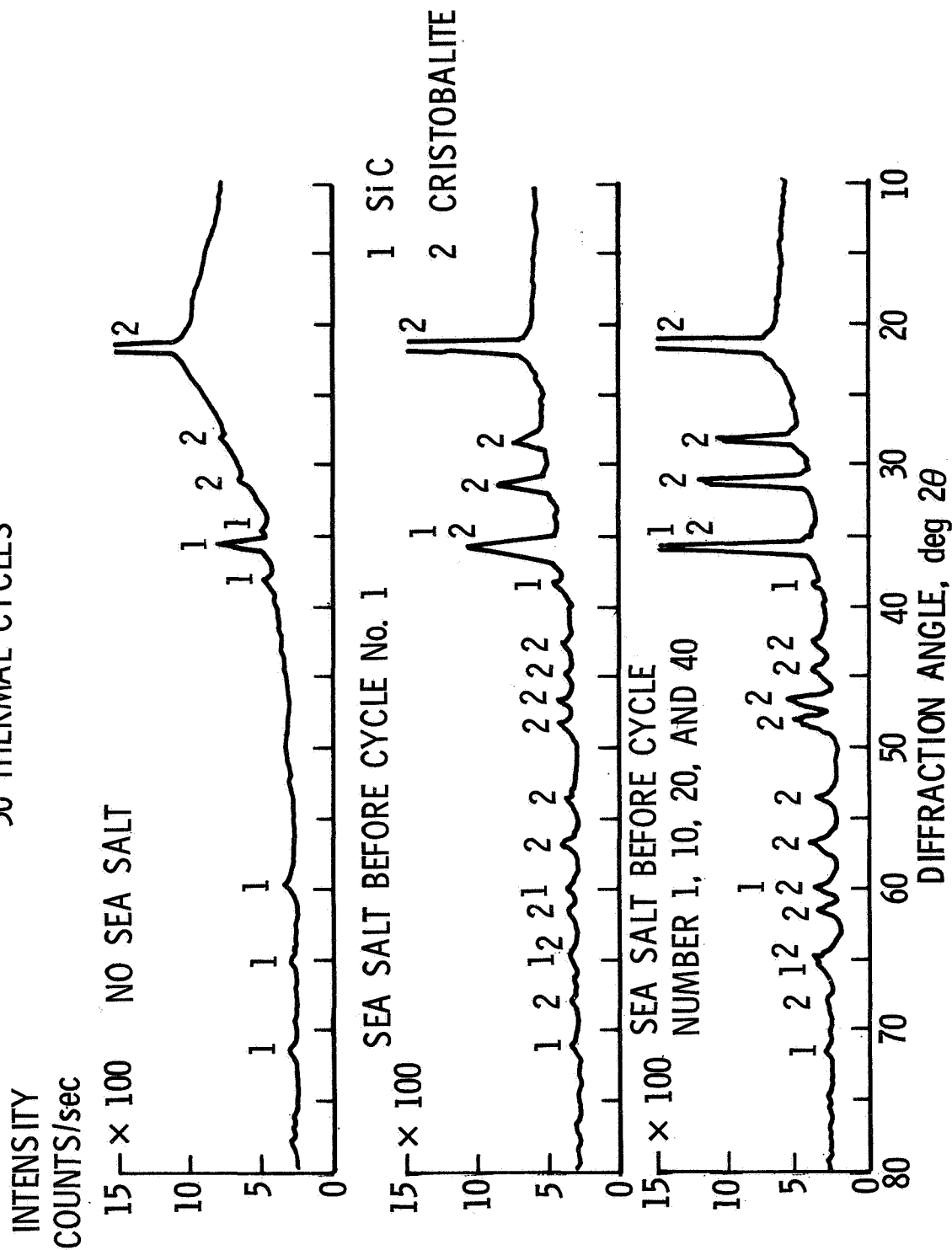


Figure 8

X-RAY DIFFRACTION PATTERNS OF LI-0042 COATING

20 Thermal Cycles + Sea Salt Between Cycles

(Figure 9)

The diffraction patterns shown in this figure were obtained to pinpoint the origin(s) of cristobalite formation in a IMSC specimen after contamination and thermal cycles. This was necessary because of suspicion that cristobalite was being detected in the insulation through cracks in the coating. The top pattern was obtained from a piece of coating that was removed from the specimen, mounted, and polished to remove traces of insulation from the backside. The resulting lines in the pattern must therefore belong to cristobalite originating in the coating. The lower pattern was obtained before removing the piece of coating from the specimen. This pattern shows stronger cristobalite lines which suggests that some cristobalite in the insulation is contributing to the intensities of the lines by means of X-rays passing through cracks in the coating. The existence of cracks in the coating is verified in the photograph of this test specimen shown in figure 10.

X-RAY DIFFRACTION PATTERNS OF LI-0042 COATING

20 THERMAL CYCLES + SEA SALT BETWEEN CYCLES

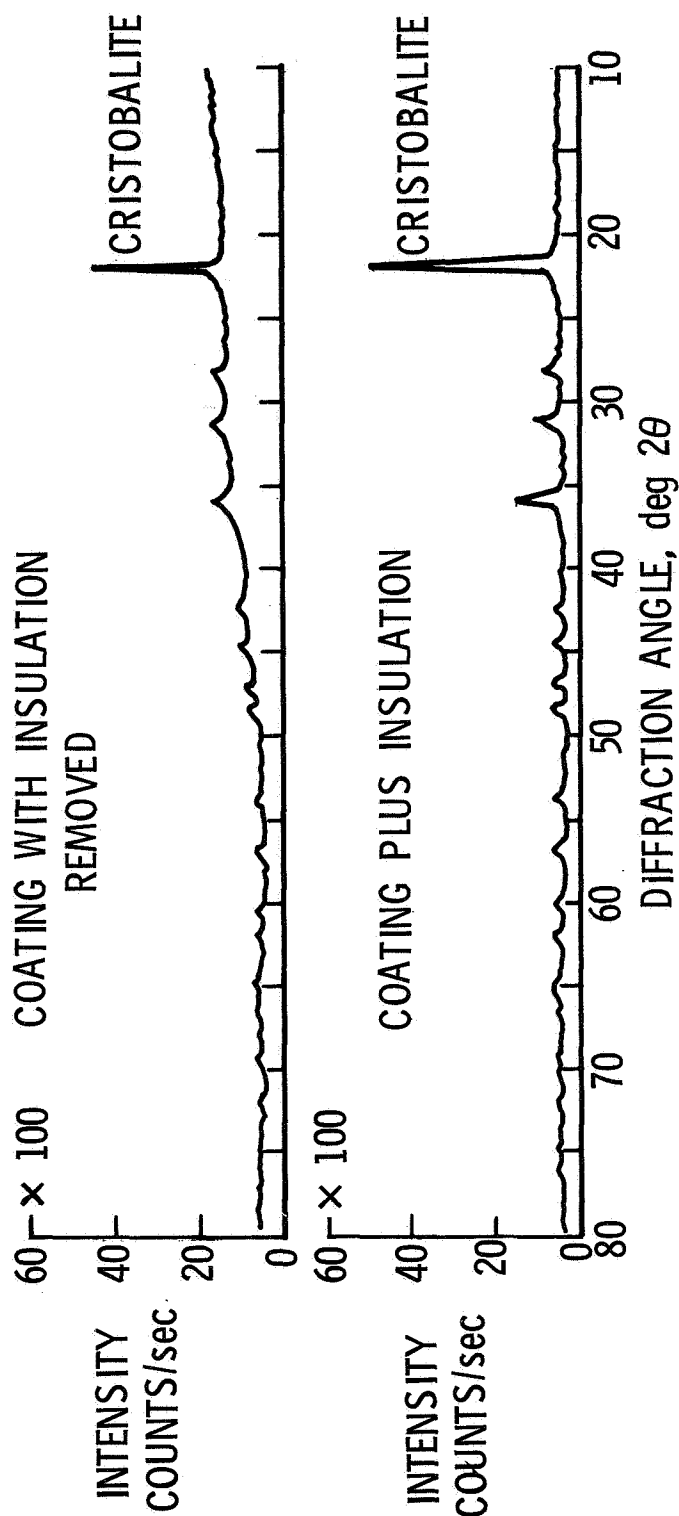


Figure 9

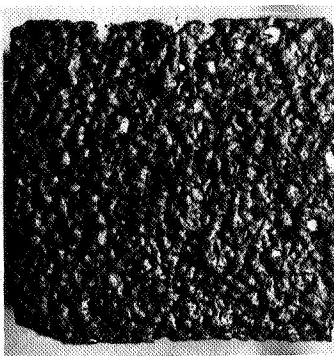
PHOTOGRAPHS OF THERMAL CYCLIC TESTS ON RSI SPECIMENS

(Figure 10)

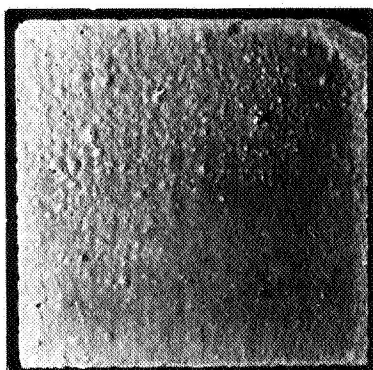
This figure shows photographs of tested and as-received specimens. Increased melting as a result of sea salt contamination is apparent in the MDAC and GE coatings. There is apparently no melting of the LMSC coating, but several cracks are visible in the 20 cycle specimen (same specimen discussed in figure 9). This specimen was one of three that were contaminated before each cycle. In all cases, the coating cracked. These specimens were not instrumented with thermocouples because they induced cracking in earlier 10 cycles tests. Cracking is thought to be associated with the polymorphic transformation of cristobalite during thermal cycling.

PHOTOGRAPHS OF THERMAL CYCLIC TESTS SPECIMENS

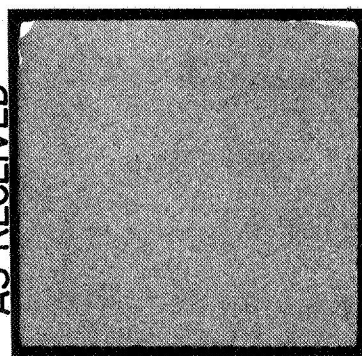
HCF



REI
MOD 1A;
SR2
COATING

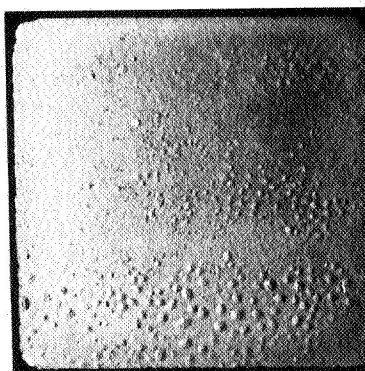


AS RECEIVED

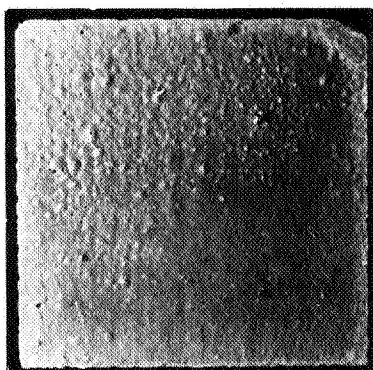


LI-1500;
0042
COATING

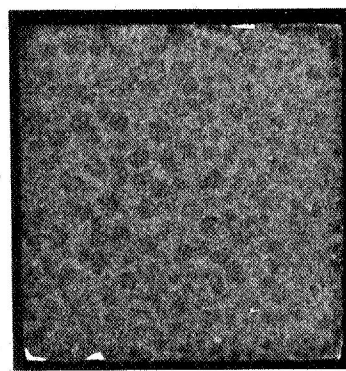
AFTER 10 CYCLES; NO SEA SALTS



AFTER 10 CYCLES; SEA SALTS



AFTER 10 CYCLES; SEA SALTS



AFTER 20 CYCLES; SEA SALTS

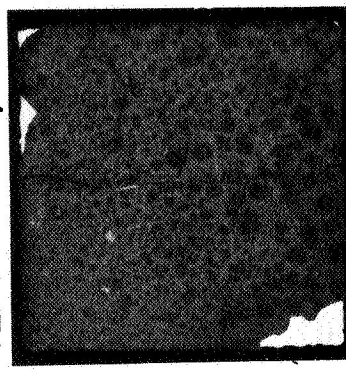


Figure 10

EFFECT OF SEA SALT AND THERMAL CYCLES ON EMITTANCE OF M5₂₃A7P₇₀₀ COATING

(Figure 11)

This figure shows total normal emittance versus temperature for MDAC specimens. The as-received data points are average values based on readings from three different specimens. The bars show the range of as-received values. The 50 cycle data are based on measurements from single specimens, thus making any accurate interpretation of the 50 cycle data difficult. The as-received data show a drop in emittance with increasing temperature. The 50 cycle data show little effect at the high temperature but possibly some decrease in emittance at the low temperature because of contamination. The reader is reminded that the contaminated specimen was exposed to salt before each cycle.

EFFECT OF SEA SALT AND THERMAL CYCLES ON EMITTANCE OF M523 A7P700 COATING

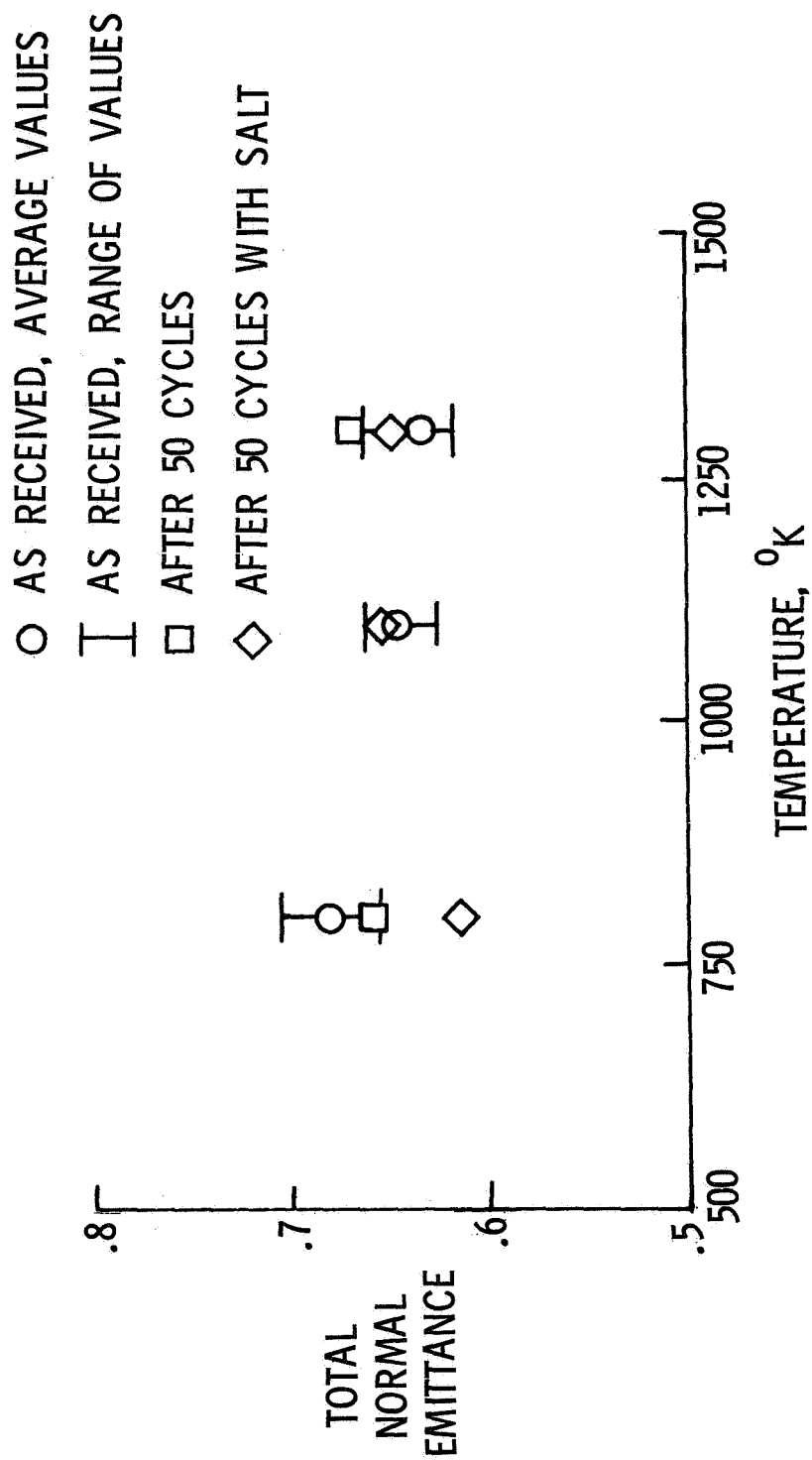


Figure 11

EFFECT OF SEA SALT AND THERMAL CYCLES ON EMITTANCE OF SR-2 COATING

(Figure 12)

This figure presents total normal emittance versus temperature data for the G.E. specimens. Again, the as-received data are based on measurements from three specimens and the 50 cycle data from single specimens. The as-received coating shows a drop in emittance with increasing temperature from a value higher than that of the MDAC coating to about an equal value ($\approx .65$). Thermal cycles and contamination show little effect on emittance at the high temperature, but there is a distinctive difference at the low temperature. In this case, contamination appears to have tempered the effect of thermal cycles. Again, the reader is reminded that the contaminated specimen was exposed before each cycle.

EFFECT OF SEA SALT AND THERMAL CYCLES ON EMITTANCE OF SR-2 COATING

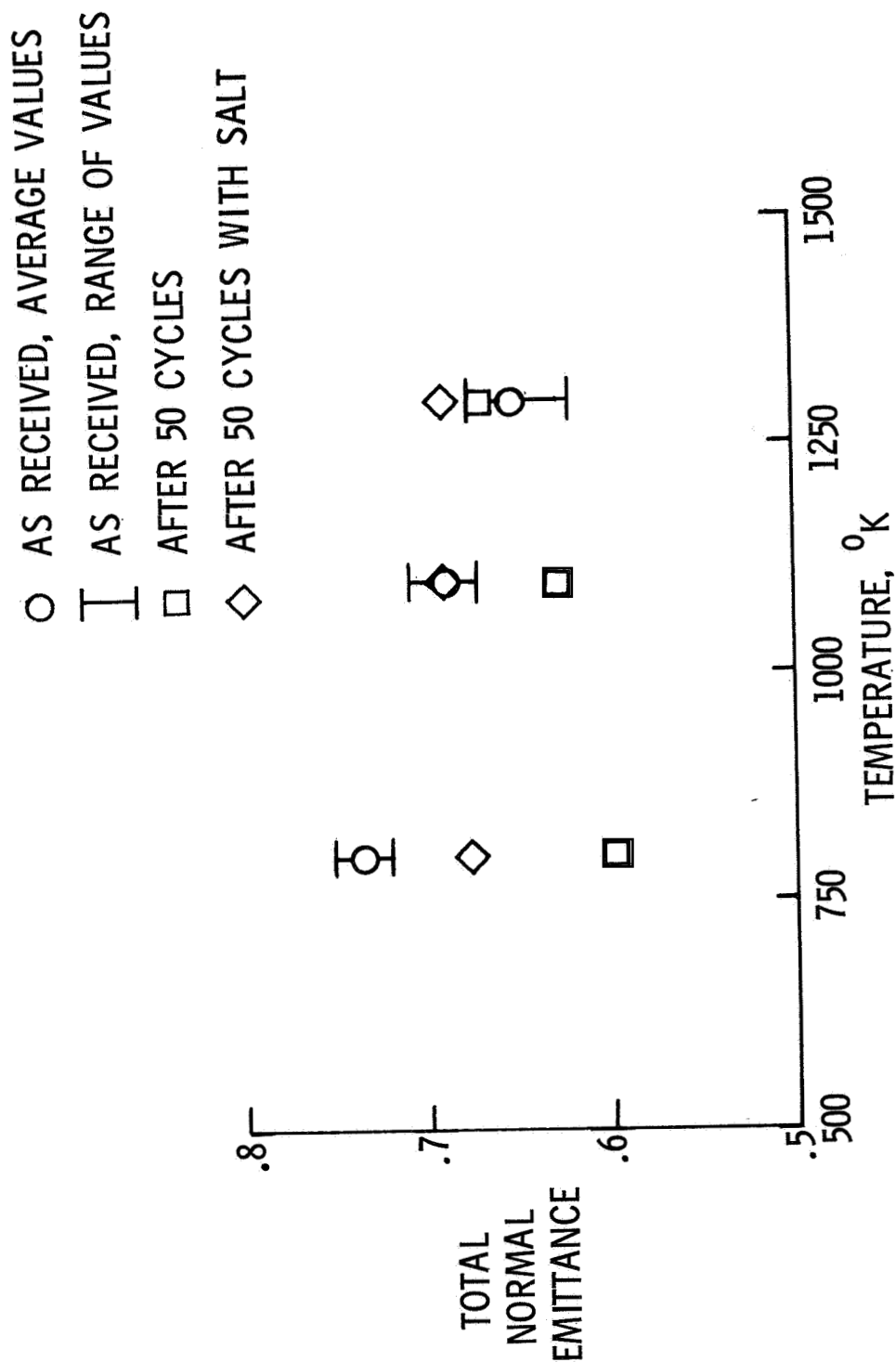


Figure 12

EFFECT OF SEA SALT AND THERMAL CYCLES ON EMITTANCE OF LI-0042 COATING

(Figure 13)

Total normal emittance versus temperature data are presented in this figure for IMSC specimens. The average as-received values are based on measurements from five specimens and the 50 cycle data from single specimens. Note the wider range of as-received values for the middle and lower temperatures. Emittance drops with temperature to a value of .63 or about equal to the other two materials at the high temperature. Thermal cycles appear to have some effect on emittance at the lower temperatures but, as with the other materials, show very little influence at the high temperature. In this case, contamination has shown no effect over the range of temperatures. It should be noted that the contaminated specimen was subjected to only four salt exposures where the other materials were exposed 50 times. Data could not be obtained from a 50 cycle specimen of the IMSC material after 50 salt exposures because of disintegration of the coating.

EFFECT OF SEA SALT AND THERMAL CYCLES ON EMITTANCE OF LI-OO42 COATING

- AS RECEIVED, AVERAGE VALUES
- ┌ AS RECEIVED, RANGE OF VALUES
- AFTER 50 CYCLES
- ◇ AFTER 50 CYCLES WITH SALT

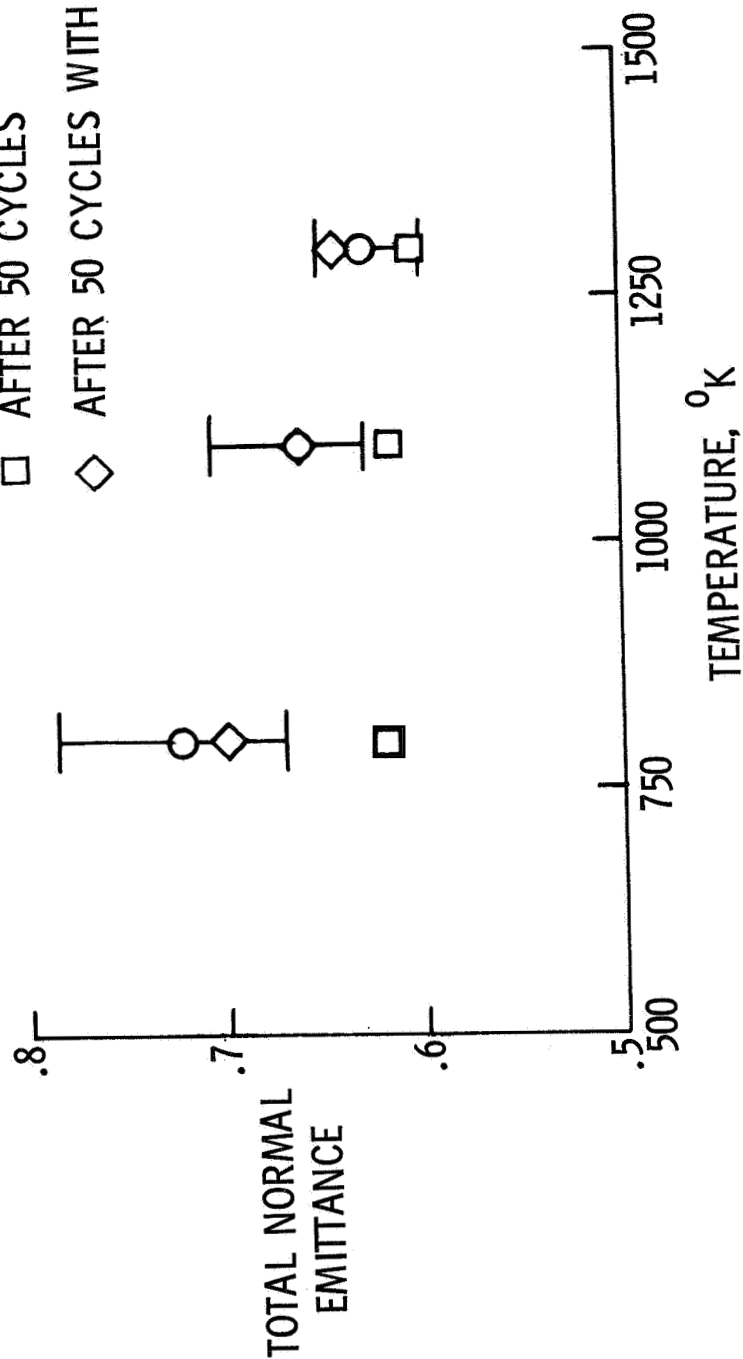


Figure 13

SUMMARY REMARKS

Results of this investigation show that sea salt contamination and thermal cycles cause significant changes in the morphology of the LMSC and GE coatings. Contamination causes increased melting of the GE and MDAC coatings. Sea salt contamination and thermal cycles do not have a significant effect on emittance of either coating at high temperatures (1300°K). At the lower temperatures there is apparently some effect on emittance but the evidence is inconclusive because of the absence of multiple tests.

STATUS

Emittance data, to date, have been obtained from a limited number of specimens because of a limited supply of material. More tests are needed on large numbers of specimens to conclusively determine the effects of thermal cycling and contamination on emittance.

Results of this investigation have led to the initiation of a joint program between Langley Research Center and Kennedy Space Center. In this program, coatings will be exposed to actual environmental conditions and realistic thermal testing.

CHARACTERIZATION OF RSI COATINGS

by

A.D. Miller, S.H. Garofalini, L.W. Smiser, and J.I. Mueller

Ceramic Engineering Division
University of Washington

INTRODUCTION

The Ceramic Engineering Division at the University of Washington has been involved since April 1, 1971, in study of RSI materials under contract NAS2-6541, administered by Ames Research Center. Studies of the coating systems used by the various suppliers were initiated in the fall of 1971.

The coating work was divided into two tasks: (1) to study the "as received" coatings with respect to their chemistry and morphology, and (2) to investigate the effect of thermal cycling upon the chemistry and morphology.

This presentation will outline the significant data and conclusions drawn from studies to date of coatings of three suppliers; General Electric, McDonnell Douglas, and Lockheed.

EXPERIMENTAL TECHNIQUES

Specimens of each of the RSI coatings tested were cut from panels provided by the suppliers in such a way as to leave the coating intact with respect to the tile. One specimen of each material was reserved, and two were subjected to thermal treatment; one with a maximum hot-face temperature of 1100°C (200°F) and the other 1250°C (2300°F). The cycling was conducted as follows. The specimen was placed in a window of a furnace with the coating face inward at a furnace temperature of 815°C (1500°F), the furnace temperature was rapidly (less than one minute) raised to the maximum temperature and held there for 15 minutes, then the furnace power was cut off. The furnace and specimen allowed to cool to 815°C, at which time the specimen was taken from the furnace to ambient air and another specimen put in its place and the cycle repeated. The cycling was normally done with pairs of specimens.

Specimens were then cut from the specimens for examination by X-ray diffraction, electron microprobe, SEM, optical microscope, and in some cases, for X-ray spectrographic analysis and porosity determinations. The details of sample preparation will not be discussed here; however, the general method for examination of coating cross-sections was to infiltrate the specimen with methyl methacrylate, polymerize to polymethylmethacrylate, section, and polish. The PMM was then removed by heating at 540°C (1000°F). In the cases of the MDAC MOD III coating, this treatment resulted in loss of the outer layer of the complex coating, but these effects were recognized and accounted for.

The porosity data reported were obtained by two methods, water absorption and mercury intrusion. The water absorption procedure was to immerse the coatings in boiling water for 24 hours and then to weigh them in air and suspended in water. From these data and the original weight of the specimen, the porosity that was filled during immersion was calculated. The mercury intrusion data were obtained using a mercury porosimeter capable of intruding mercury into a 15 nm pore.

In discussing these data it must be remembered that water can penetrate open porosity as small as 1.5 nm (15Å) while the mercury data only shows open porosity larger than 15 nm (150Å).

EXPERIMENTAL RESULTS

The results of these studies will be presented for each of the three contractors' materials. Since the time for presentation is rather limited, only the most significant data will be presented with comments as to its significance.

GE REI COATINGS--CRYSTALLINE SPECIES BY X-RAY DIFFRACTION

(Figure 1)

Figure 1 shows the results of the X-ray diffraction analyses of GE-REI materials in the as-received condition as well as after the cycling tests. There are two important factors to note here: (1) the rather dramatic increase in cristobalite in MOD I after the 1250°C cycling, and (2) the lack of this result in the MOD IA material.

GE REI Coatings

Crystalline Species by X-ray Diffraction

<u>Specimen</u>	<u>As-received</u>	<u>Cycled 10 times 1100°C (2000°F)</u>	<u>Cycled 10 times 1250°C (2300°F)</u>
Mod I	mullite, 5% cristobalite, nickel aluminate	no change	cristobalite increases to 15%
Mod 1A	same as above trace cristobalite	no change	no change

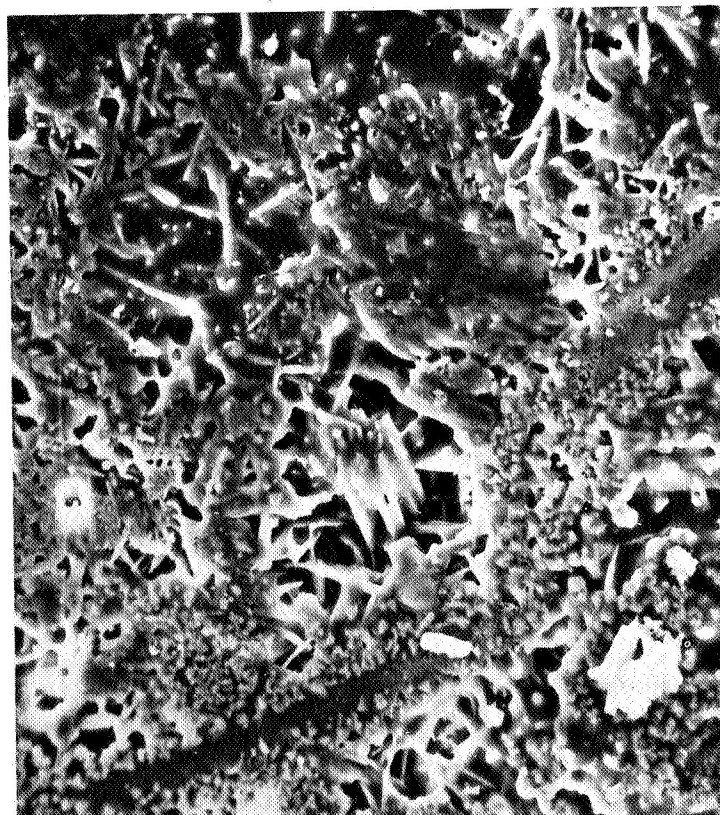
Figure 1

GE MOD I COATING AS RECEIVED--SEM VIEW OF SURFACE

(Figure 2)

Figure 2 shows the surface of the MOD I coating at two different magnifications. The coating appears porous in figure 2(a), but at the higher magnification (2(b)) it is seen that the crystals are well sealed by the glassy phase.

GE Mod I Coating
As Received
SEM View of Surface



20 μm
(a)



10 μm
(b)

Figure 2

GE MOD I COATING - AS RECEIVED
CROSS-SECTION OF COATING AND INTERFACE

(Figure 3)

Figure 3 shows a cross-section of the MOD I coating. It appears reasonably dense, with only occasional large porosity.

**GE Mod I Coating
As Received
Cross-section of Coating and Interface**



100 μm

Figure 3

GE MOD I COATING
10 CYCLES TO 1250°C (2300°F)
MACROPHOTOGRAPH SHOWING GREEN STAIN PENETRATION

(Figure 4)

Figure 4 shows the results of 10 cycles to a maximum temperature of 1250°C. A green-colored stain appears to penetrate the tile after the cycling test. X-ray spectroscopy of the stained region in tile showed only an increase in the silicon content. X-ray diffraction showed no additional phases. It is concluded that the glassy phase, with enough nickel to stain it green, penetrated the tile during the test. Similar tests on the MOD IA coating showed no sign of this behavior.

GE Mod I Coating
10 Cycles to 1250°C (2300°F)
Macro photograph Showing Green Stain Penetration

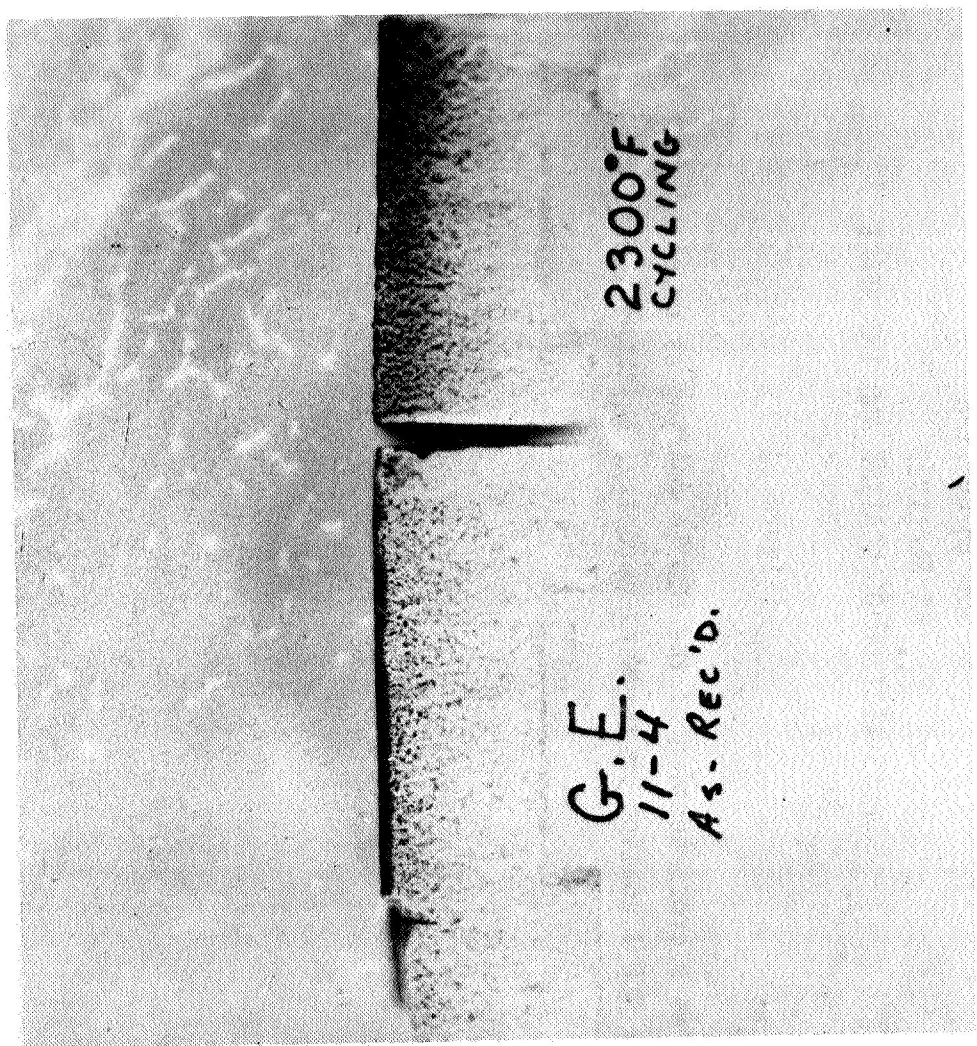


Figure 4

GE MOD IA COATING
AS RECEIVED
CROSS-SECTION OF COATING AND INTERFACE

(Figure 5)

Figure 5 shows a cross-section of the MOD IA coating as received from the supplier. It appears similar to the MOD I coating in terms of porosity, thickness, etc.

**GE Mod IA Coating
As Received
Cross-section of Coating and Interface**

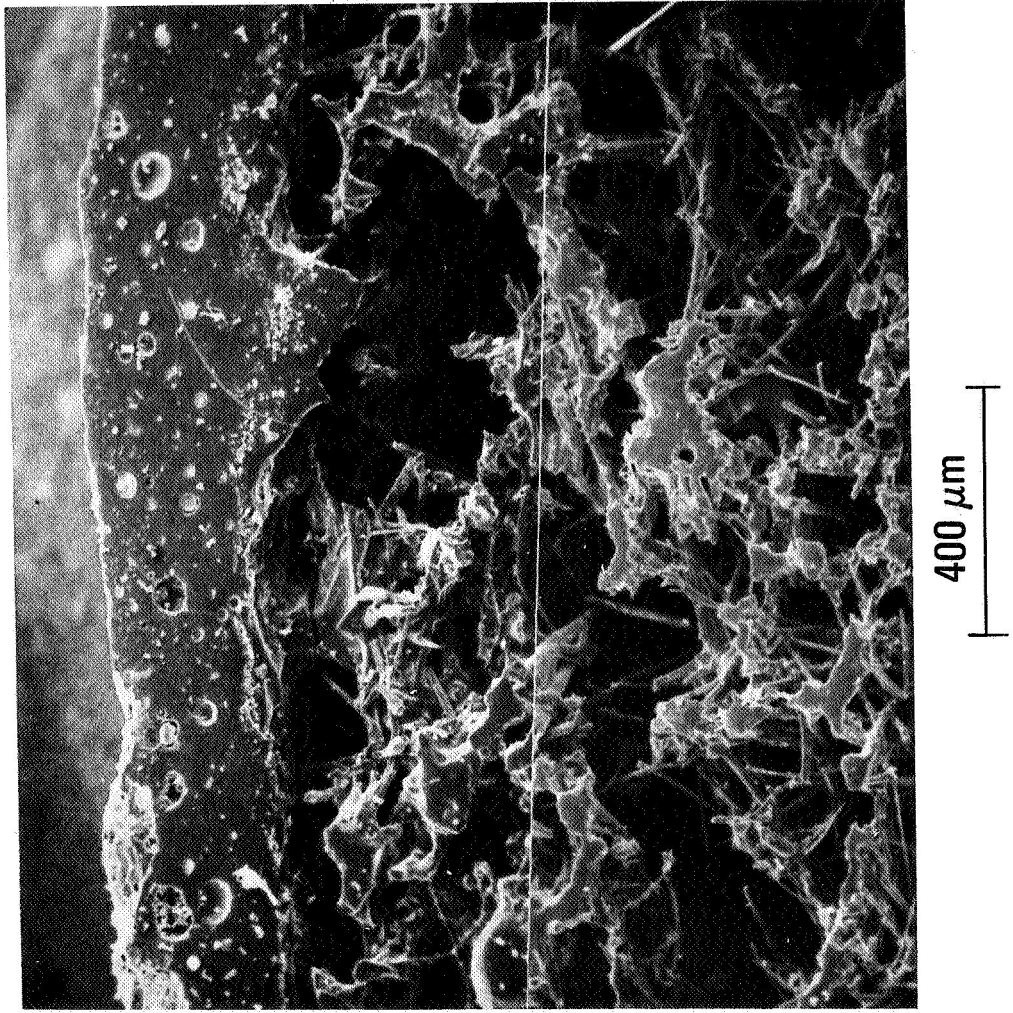


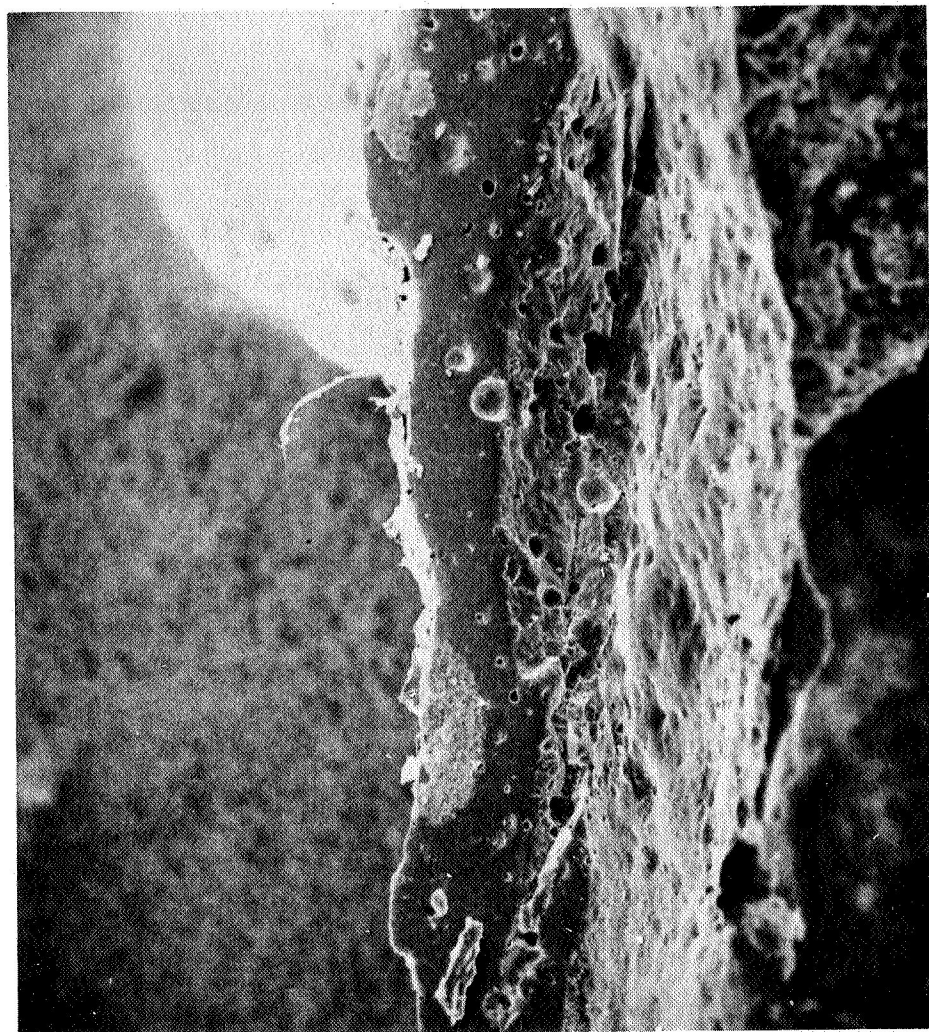
Figure 5

GE MOD IA COATING
10 CYCLES TO 1250°C (2300°F)

(Figure 6)

Figure 6 displays a cross-section of the MOD IA coating after 10 cycles to 1250°C. No significant changes are seen.

GE Mod IA Coating
10 Cycles to 1250°C (2300°F)
Cross-section of Coating and Interface



400 μm

Figure 6

POROSITY DATA
GE MOD IA COATING

(Figure 7)

Figure 7 summarizes the porosity data for MOD IA. These data are felt to be in error as much as five percent for the water method and two percent for the mercury method. The values shown indicate that the porosity is little affected by cycling to 1250°C and that the pores are mostly smaller than 15 nm.

Porosity Data GE Mod 1A Coating		
<u>Thermal Treatment</u>	<u>Porosity, % (H₂O method)</u>	<u>Porosity, % (Hg method)</u>
As received	19.4	4.3
10 cycles 1100°C	16.6	4.6
10 cycles 1250°C	18.2	4.5

Figure 7

GE REI
SIGNIFICANT CONCLUSIONS

(Figure 8)

This figure summarizes the most important results of the tests on REI coatings.

GE REI

SIGNIFICANT CONCLUSIONS

1. Mod I shows considerable increase in cristobalite in 1250°C cycling tests. Mod IA shows no change.
2. Mod I shows penetration of glassy phase into the tile in 1250°C cycling. Mod IA shows no change
3. Porosity remains essentially constant for Mod IA under 1100°C and 1250°C cycling. (10 cycles)

Figure 8

MDAC HCF COATINGS
CRYSTALLINE SPECIES BY X-RAY DIFFRACTION

(Figure 9)

Figure 9 is a summary of the crystalline phases determined by X-ray diffraction in McDonnell Douglas HCF coatings. The only changes noted after cycling was the slight increase in cristobalite in the MOD III coating after the 1250°C cycling.

MDAC HCF Coatings

Crystalline Species by X-ray Diffraction

<u>Specimen</u>	<u>As-received</u>	<u>10 Cycles to 1100°C (2000°F)</u>	<u>10 Cycles to 1250°C (2300°F)</u>
Phase I	Cristobalite, quartz, Cr ₂ O ₃	no data	no data
Mod I	Cristobalite, quartz, Cr ₂ O ₃ (Co,Fe,Cr)O _x	no change	no change
Mod III	Same as Mod I + AlPO ₄	no change	no new phases, slight cristo- balite increase

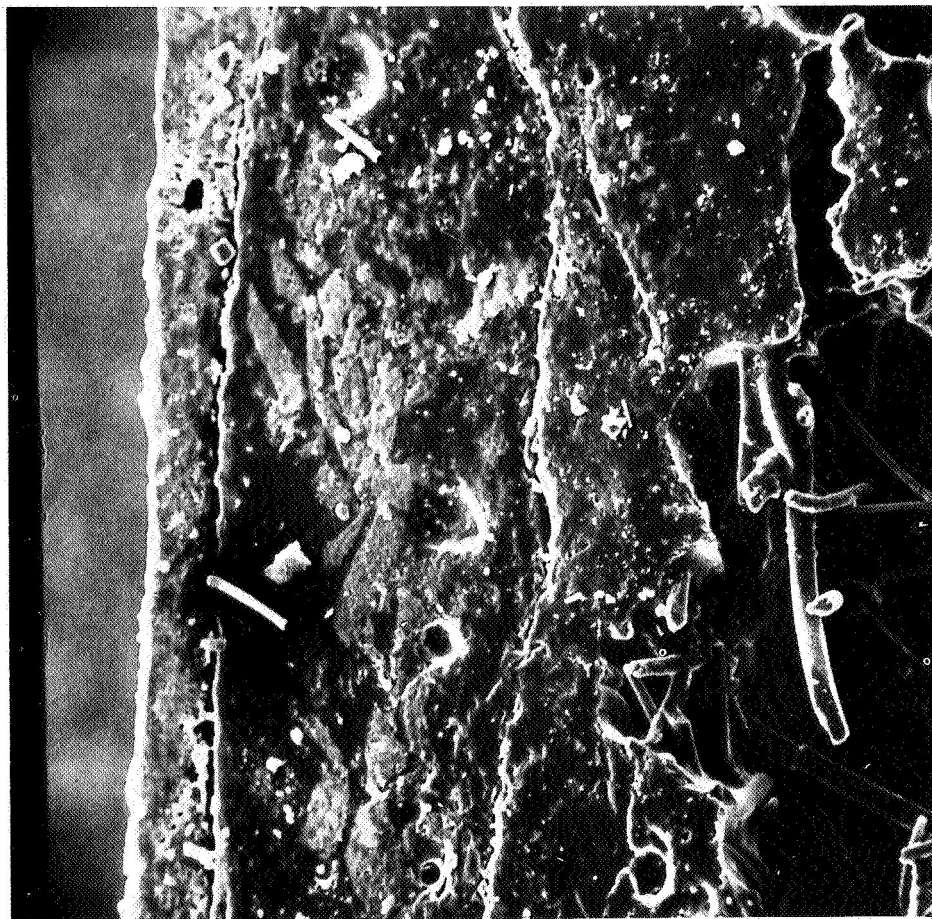
Figure 9

MDAC MOD I COATING
AS RECEIVED
CROSS-SECTION OF COATING AND INTERFACE

(Figure 10)

Figure 10 shows a cross-section of the MOD I coating as received from the supplier. The complex nature of the coating is evident. Electron microprobe analysis shows the coating contains chromium, cobalt, and iron in the outer layer and chromium only in the grains of the middle layer. It is concluded that the outer layer contains a complex (Co, Cr Fe) oxide while the middle layer contains chromium oxide. The inner layer appears glassy and contains little or none of the heavier metal ions.

MDAC Mod I Coating
As Received
Cross-section of Coating and Interface



100 μm

Figure 10

MDAC MOD I COATING
10 CYCLES TO 1250°C (2300°F)
CROSS-SECTION OF COATING

(Figure 11)

Figure 11 shows the results of cycling the MOD I coating ten times to 1250°C. There is a marked increase in porosity, the surface texture of the specimen becomes rougher and the color changed from black to dark gray.

MDAC Mod I Coating
10 Cycles to 1250°C (2300°F)
Cross-section of Coating



1 mm

Figure 11

MDAC MOD I COATING
10 CYCLES TO 1250°C (2300°F)
CROSS-SECTION OF COATING

(Figure 12)

This SEM photo shows, at higher magnification, a cross-section of the MOD I coating after 10 cycles to 1250°C. Note the small crystals between the outer layer and the middle layer (the reaction zone). These are newly nucleated crystalline species not seen in the as-received material. Electron microprobe scans show that cobalt and iron have migrated into and beyond the interfacial area between the two layers. Chromium does not appear to move under these conditions.

MDAC Mod I Coating
10 Cycles to 1250°C (2300°F)
Cross-section of Coating

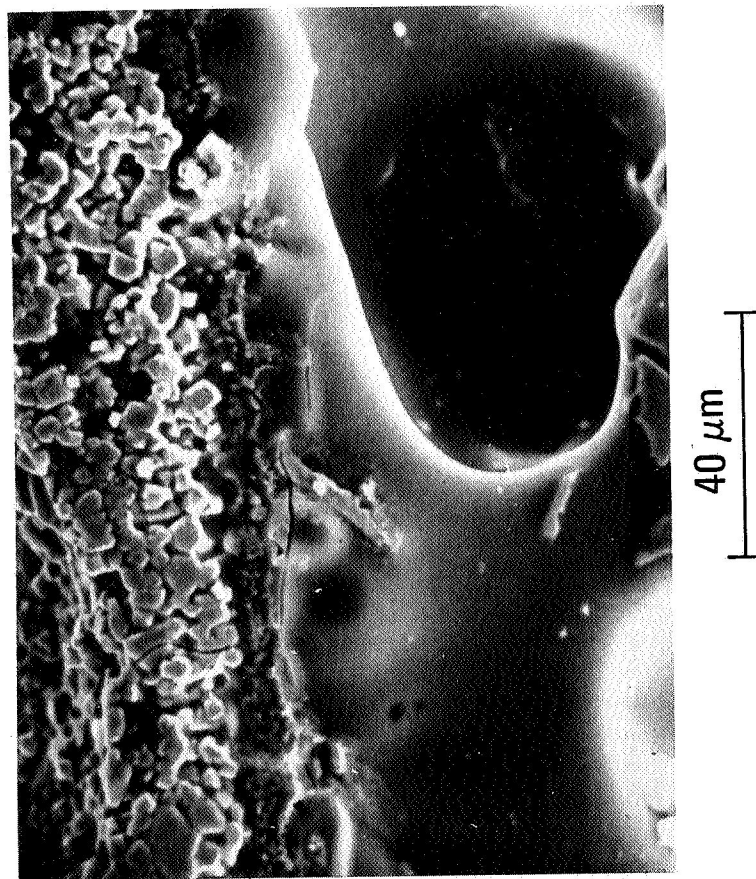


Figure 12

MDAC MOD III COATING
AS RECEIVED
CROSS-SECTION OF COATING

(Figure 13)

Figure 13 is a cross-section of the as-received MOD III coating. It appears similar to the MOD I except that the crystalline material (Cr_2O_3) is not so evident in the intermediate layer as in MOD I. Note that the top layer was spalled off during sample preparation.

MDAC Mod III Coating
As Received
Cross-section of Coating

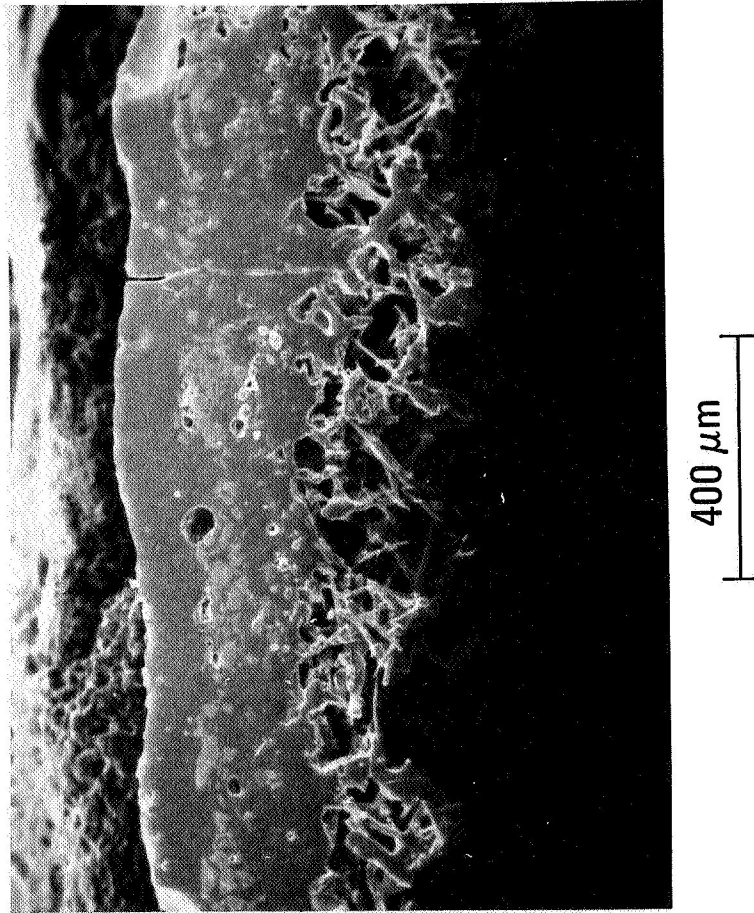


Figure 13

MDAC MOD III COATING
10 CYCLES TO 1250°C (2300°F)
CROSS-SECTION OF COATING

(Figure 14)

This figure shows the results of 10 cycles at 1250°C on the MOD III coating. Again the top layer was spalled off during sample preparation. The innermost layer shows a dramatic increase in porosity as compared with the previous figure. Suspecting that sample preparation might have had some effect on this result, we looked at fracture sections of the same specimen and found similar porosity. The microprobe analysis of this material, however, showed no migration of cobalt and iron as in MOD I.

MDAC Mod III Coating
10 Cycles to 1250°C (2300°F)
Cross-section of Coating

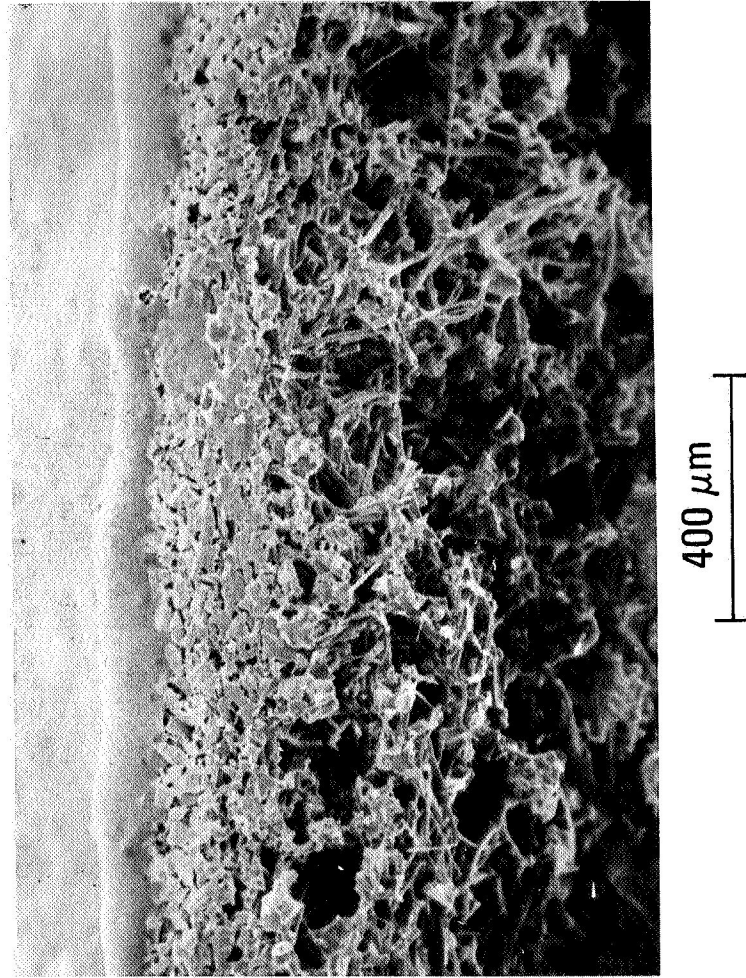


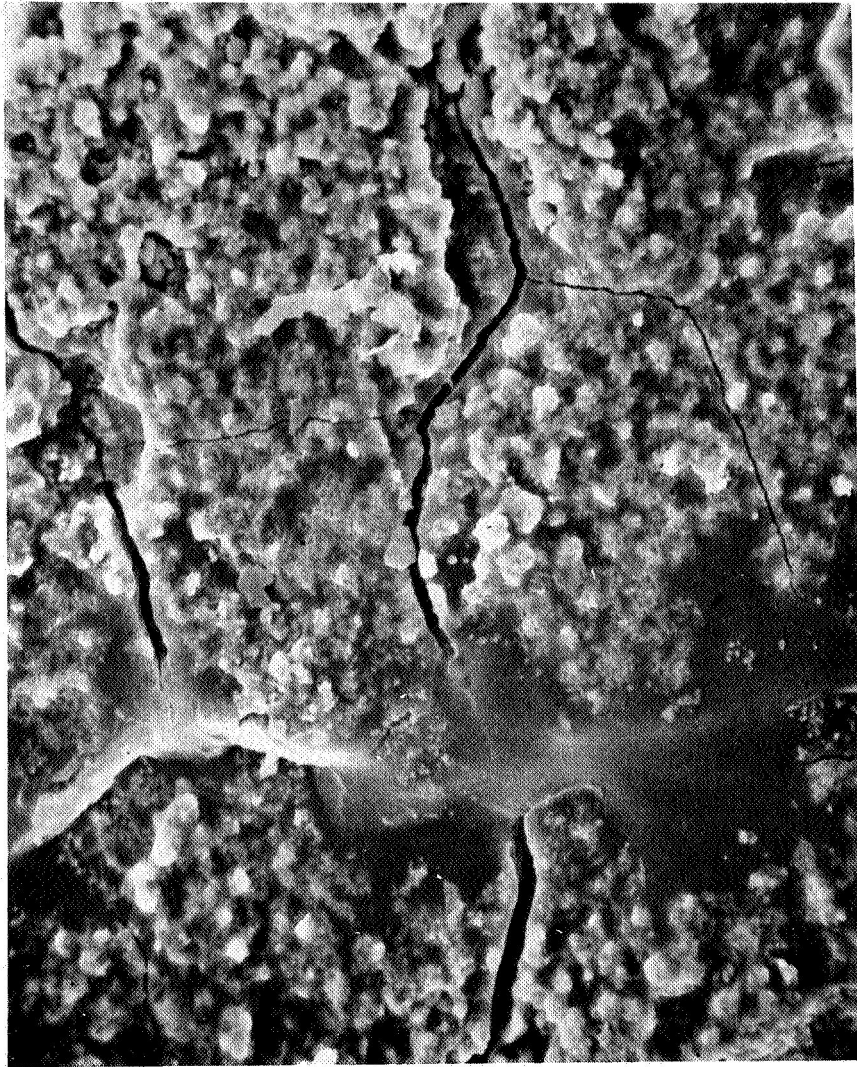
Figure 14

MDAC MOD III COATING
AS RECEIVED
REMNANT OF SURFACE LAYER

(Figure 15)

Figure 15 is a view of the surface of the MOD III coating as received from the vendor.
The cracking may be an artifact of sample preparation.

MDAC Mod III Coating
As Received
Remnant of Surface Layer



20 μm

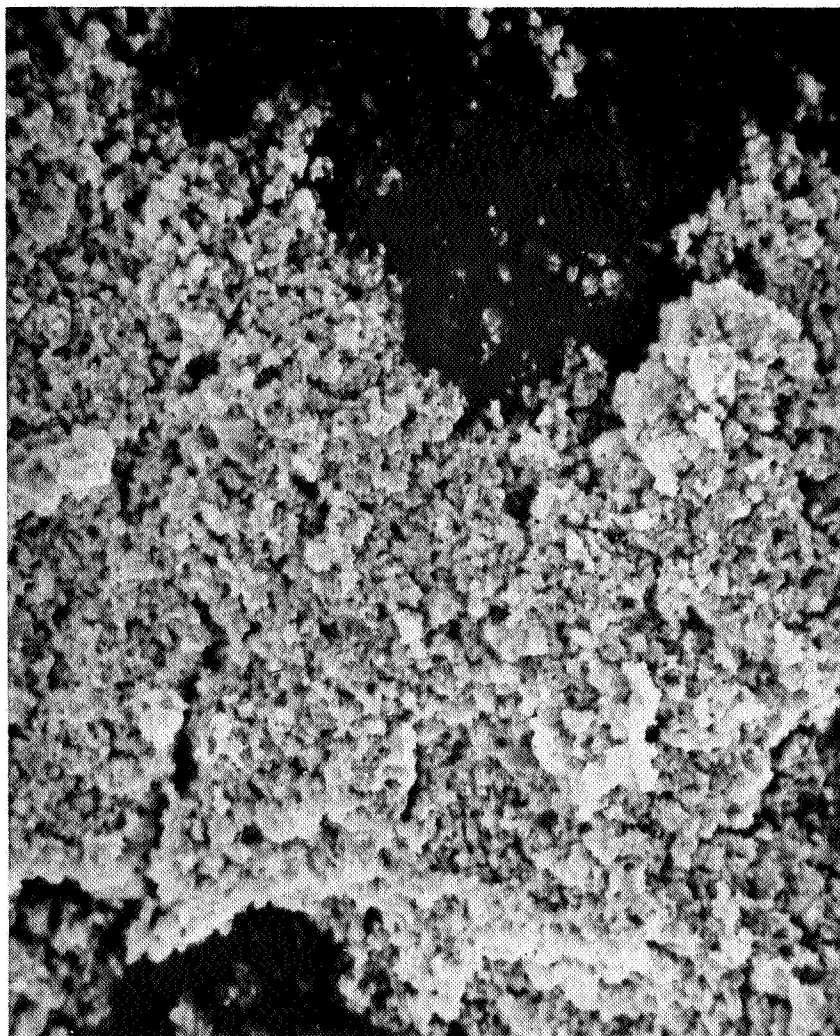
Figure 15

MDAC MOD III COATING
10 CYCLES TO 1250°C (2300°F)
REMNANT OF SURFACE LAYER

(Figure 16)

Figure 16 shows the coating surface after exposure to 10 cycles to 1250°C. It appears that much of the glassy phase present in the as-received material is absent here.

**MDAC Mod III Coating
10 Cycles to 1250°C (2300°F)
Remnant of Surface Layer**



20 μm

Figure 16

POROSITY DATA
MDAC MOD III COATING

(Figure 17)

This figure presents the porosity data for MOD III. The data would indicate that the total porosity remains essentially constant upon cycling, while the porosity larger than 15 nm decreases. These data are not consistent with the SEM studies. More work must be done.

Porosity Data
MDAC Mod III Coating

<u>Thermal Treatment</u>	<u>Porosity, % (H₂O method)</u>	<u>Porosity, % (Hg method)</u>
As received	25.4	21.1
10 cycles to 1100°C	24.3	18.1
10 cycles to 1250°C	28.0	15.5

Figure 17

MDAC HCF COATINGS
SIGNIFICANT CONCLUSIONS

(Figure 18)

This figure summarizes the important results of the work on MDAC HCF. Probably most important is the increased porosity upon cycling.

MDAC HCF Coatings

Significant Conclusions

1. Mod I shows migration of cobalt and iron with nucleation of new phase after 10 cycles to 1250°C.
2. Mod III shows no migration under same conditions as Mod I.
3. Both Mod I and Mod III show increased porosity after 10 cycles to 1250°C.
4. Water absorption and mercury intrusion porosity data inconsistent with SEM evidence.

Figure 18

LMSC LI-1500 COATINGS
CRYSTALLINE SPECIES BY X-RAY DIFFRACTION

(Figure 19)

Figure 19 summarizes the X-ray diffraction analysis of the LI-1500 coatings, LI-1525 and LI-1542.

LMSC L1-1500 Coatings

Crystalline Species by X-ray Diffraction

<u>Specimen</u>	<u>As received</u>	<u>10 cycles to 1100°C (2000°F)</u>	<u>10 cycles to 1250°C (2300°F)</u>
L1-1525	glass, Cr ₂ O ₃	~ 15% cristo- balite, Cr ₂ O ₃	~ 25% cristo- balite, Cr ₂ O ₃
L1-1542	alpha-SiC	SiC, ~3% cristobalite	SiC, ~8% cristobalite

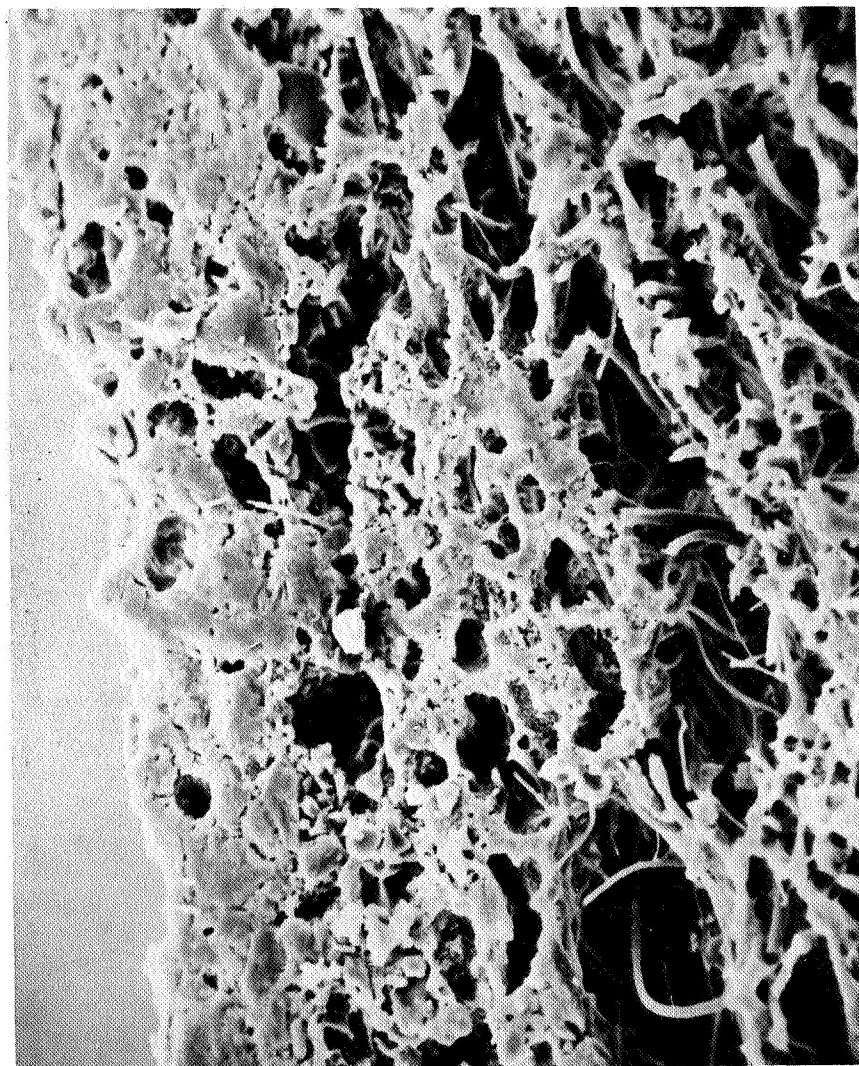
Figure 19

LMSC LI-1525 COATING
AS RECEIVED
CROSS-SECTION OF COATING AND INTERFACE

(Figure 20)

This figure shows a cross-section of the LI-1525 coating as received. Considerably porosity is evident, however, and good penetration into the transition zone is apparent.

LMSC LI-1525 Coating
As Received
Cross-section of Coating and Interface



100 μm

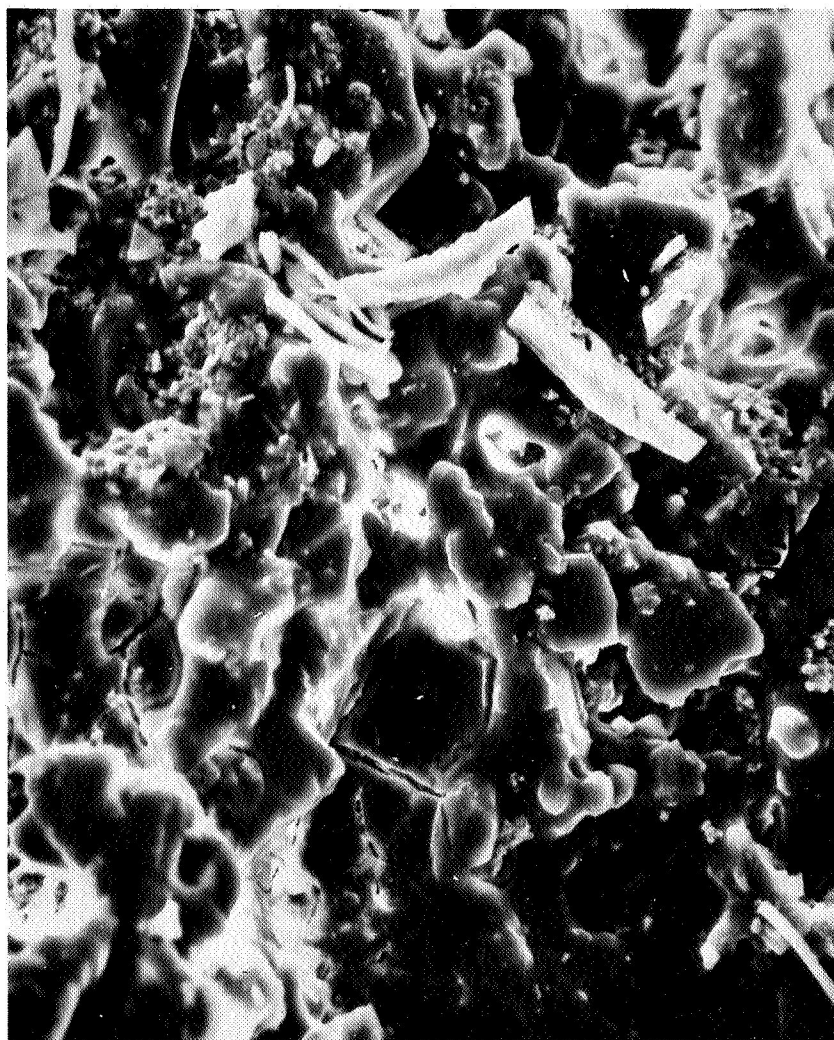
Figure 20

LMSC LI-1525 COATING
SURFACE OF AS-RECEIVED COATING

(Figure 21)

Figure 21 is a view of the LI-1525 surface. The surface appears well sealed by the glass phase.

LMSC LI-1525 Coating
Surface of As-received Coating



50 μm

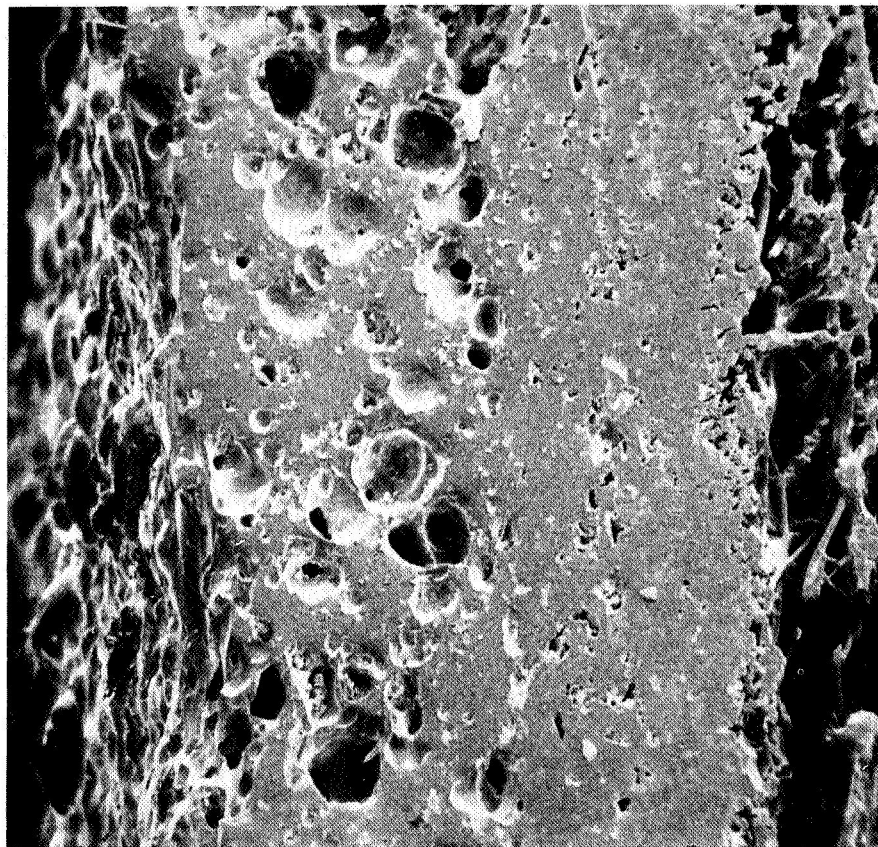
Figure 21

LMSC LI-1542 COATING
AS RECEIVED
CROSS-SECTION OF COATING AND INTERFACE

(Figure 22)

Figure 22 is a cross-section of the li_1542 coating as received. Note the high degree of porosity in the outer half of the coating.

**LMSC LI-1542 Coating
As Received
Cross-section of Coating and Interface**



100 μm

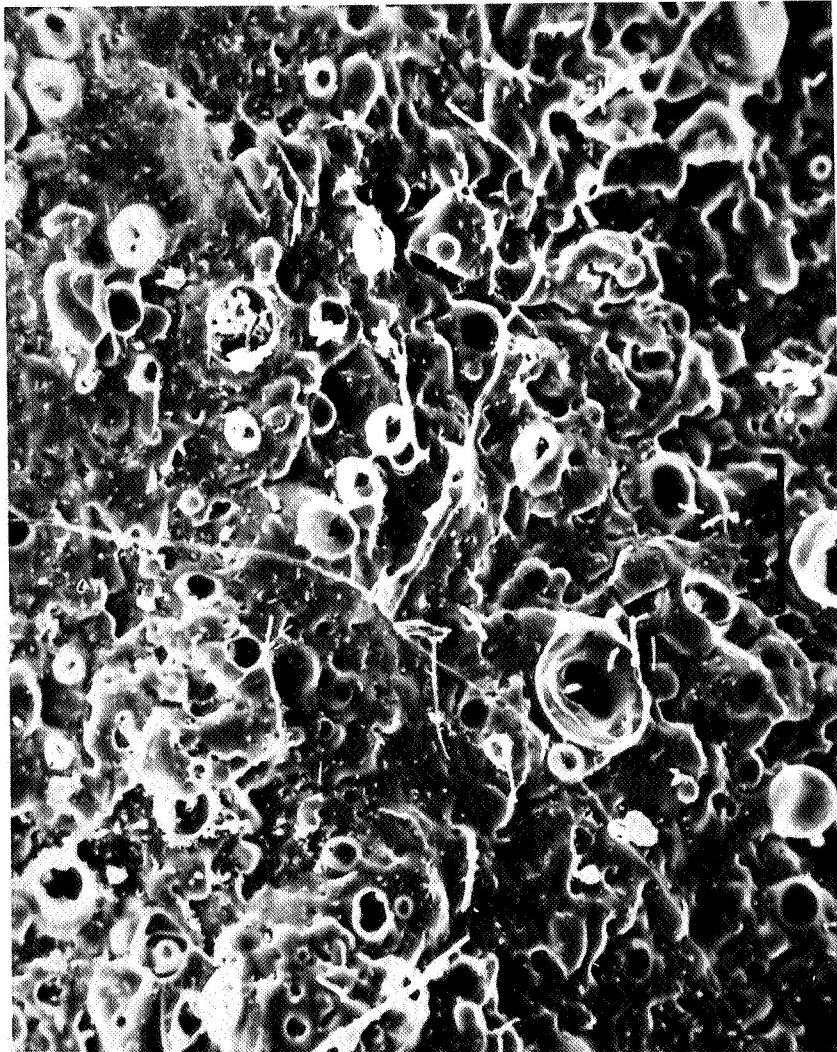
Figure 22

LMSC LI-1542 COATING
SURFACE OF AS-RECEIVED COATING

(Figure 23)

This SEM photo shows the surface texture of the LI-1542 coating; again the porosity is evident.

LMSC LI-1542 Coating
Surface of As-received Coating



100 μm

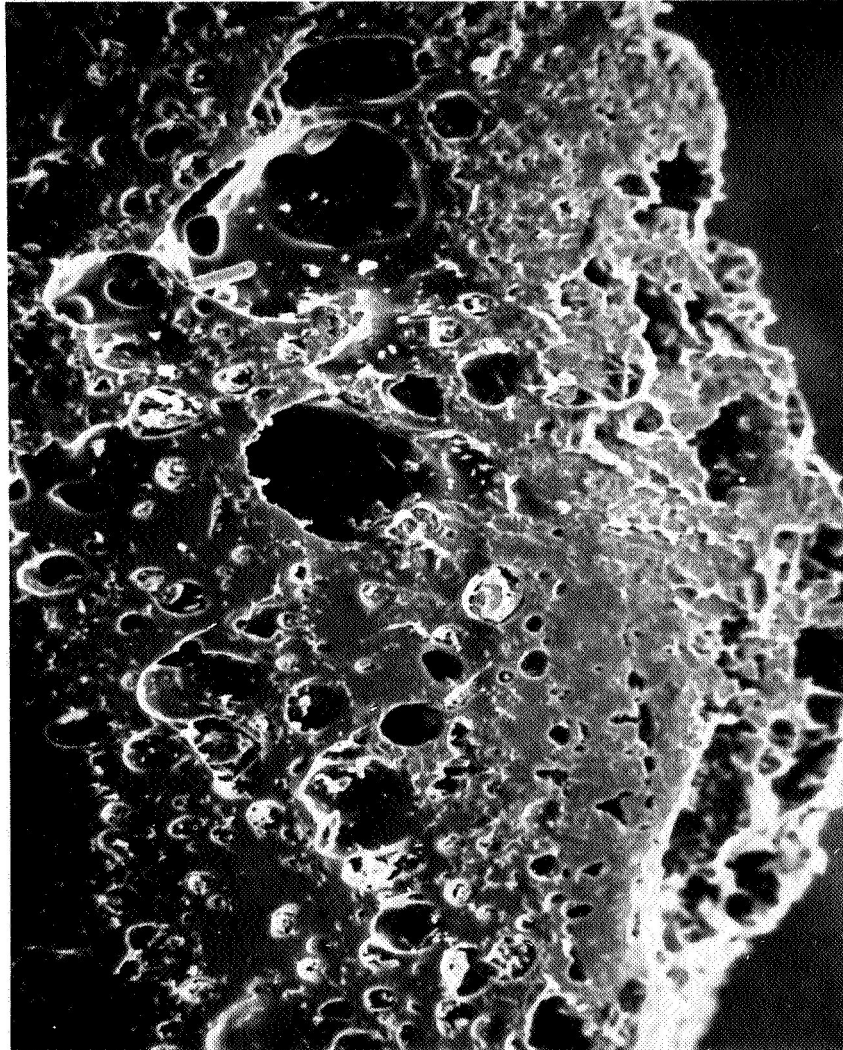
Figure 23

LMSC LI-1542 COATING
10 CYCLES TO 1250°C (2300°F)
CROSS-SECTION OF COATING

(Figure 24)

This cross-section of the LI-1542 coating shows the results produced by 10 cycles to 1250°C. Note the extreme growth of porosity in the outer layer.

LMSC LI-1542 Coating
10 Cycles to 1250°C
Cross-section of Coating



100 μm

Figure 24

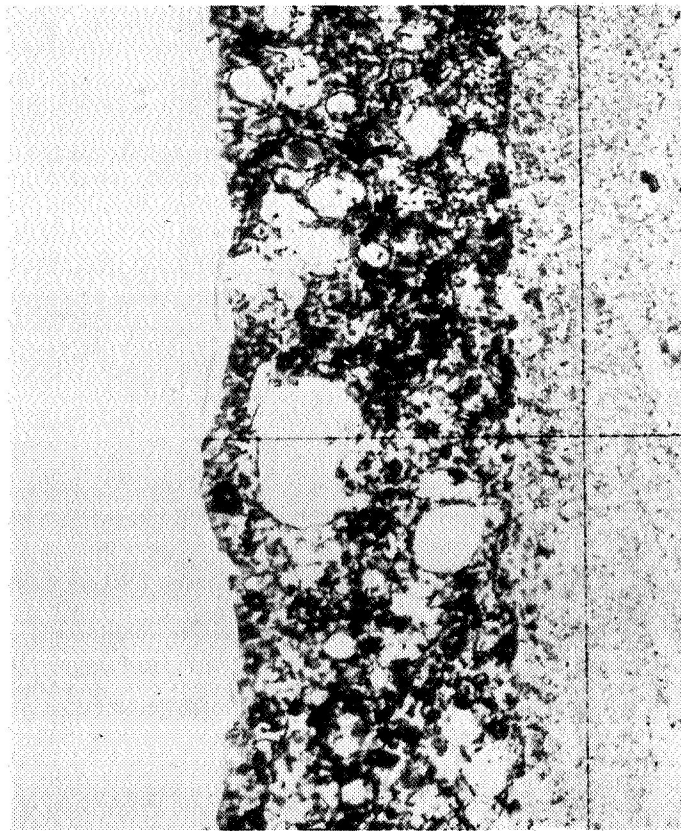
LMSC LI-1542 COATING
CROSS-SECTION, OPTICAL THIN-SECTION

(Figure 25)

Figure 25 shows a comparison of the 1250°C cycled LI-1542 coating with the as-received material. These optical thin sections show a growth of approximately 100 percent in the thickness of the coating as a result of cycling to 1250°C.

LMSC LI-1542 Coating
Cross-section, Optical Thin-section

As Received



10 Cycles to 1250°C



Figure 25

LMSC LI-1542 COATING
POROSITY DATA

(Figure 26)

These porosity data on LI-1542 coatings support the SEM and optical microscope data. After 1250°C cycling the porosity has increased approximately 100 percent. There is reasonably good agreement between the two methods indicating the porosity is all larger than 15 nm.

LMSC LI-1542 COATING

Porosity Data

<u>Thermal Treatment</u>	<u>Porosity, % (H₂O method)</u>	<u>Porosity, % (Hg method)</u>
As received	11.3	13.8
10 cycles, 1100°C	14.3	14.3
10 cycles, 1250°C	24.7	29.7

Figure 26

LMSC LI-1500 COATINGS
SIGNIFICANT CONCLUSIONS

(Figure 27)

The most important of the points summarized here is the large increase in porosity in the LI-1542 coatings.

LMSC L1-1500 Coatings

Significant Conclusions

1. L1-1525 shows a strong tendency to precipitate cristobalite during 10 cycles to 1250°C. L1-1542 much better in this respect.
2. Both L1-1525 and L1-1542 show considerable porosity in as-received condition.
3. 10 cycles to either 1100°C or 1250°C results in significant increase in porosity and dimensional instability for the L1-1542 coating.
4. Both mercury intrusion and water absorption porosity determinations support SEM data on porosity increase under cycling tests on L1-1542.

Figure 27

CONCLUSION

While these data are by no means complete, it is hoped that, together with results obtained by other investigators, they may help to provide the information necessary for a valid analysis of coatings for the various RSI materials.

CHEMICAL AND MORPHOLOGICAL CHANGES OF REUSABLE SURFACE INSULATION
COATINGS AS A FUNCTION OF CONVECTIVELY HEATED CYCLIC TESTING

by

D.B. Leiser, D.A. Stewart, and H.E. Goldstein
Ames Research Center
Moffett Field, California

ABSTRACT

The effects of convective heating upon reusable surface insulation coatings were studied utilizing scanning electron microscopy, X-ray fluorescence, and X-ray diffraction. Samples of coated LI-1542, HCF-MOD III and REI-MOD 1A were cycled in an arc plasma stream up to 15 times for 15 minutes per cycle at surface temperatures simulating those on the space shuttle vehicle in areas 2 and 2P as defined by the NASA-MSC.

The scanning electron microscope with an X-ray fluorescence analysis attachment was used to examine chemical and morphological changes in the insulation coating surfaces. The surfaces of REI-MOD 1A and HCF-MOD III coatings were roughened substantially by the convectively heated environment while the LI-1542 was significantly smoothed after testing. Most of the observed changes in morphology were almost complete within one cycle in REI-MOD 1A and LI-1542. The HCF-MOD III coating exhibited much more gradual changes. These gradual changes were due in part to the growth of an apparently new morphological phase out of the coating. Scanning electron microscopy also showed surface cracking of varying degrees in all of the coatings. The surface chemistry of the coatings as examined by X-ray fluorescence revealed that significant changes in composition were occurring during cycling, particularly within the HCF-MOD III coating, to a lesser extent within the REI-MOD 1A coating, while smaller changes in composition were observed in LI-1542. In order to evaluate the significance of the surface chemistry changes observed, scanning electron micrographs were taken of representative cross-sections of REI-MOD 1A and HCF-MOD III before and after testing, with concurrent analysis by X-ray fluorescence.

INTRODUCTION

This paper describes the results of a test program initiated to evaluate the response and stability in convective heating of reusable surface insulation (RSI). These data are required to define RSI's reusability during its proposed 100-mission lifetime as the thermal protection system on space shuttle. The paper describes the response of RSI to both convective and radiative heating environments in terms of the chemical changes in the coatings that occur. It also describes the morphological changes that occur during arc plasma testing. The testing methods and optical property variations after testing are described in another paper in this volume of the Proceedings entitled, "Cyclic Arc Plasma Tests of RSI Materials Using a Preheater," by D.A. Stewart.

The model configuration and analysis techniques are described first. Changes in coating morphology of HCF-MOD III, LI-1542, and REI-MOD 1A at two heating rates are then described followed by a discussion of the changes in surface chemistry that occur during these tests. Subsequently, the surface chemistry changes observed are compared to similar data obtained from radiantly heated coatings and the significance of the difference between the results are discussed. Finally, the changes in chemistry of the coatings in cross section before and after convectively heated cyclic testing are discussed and the significance of surface chemistry changes described.

RSI SAMPLES BEFORE AND AFTER ARC-PLASMA TESTING

(Figure 1)

The model configuration used in the investigation is shown in this figure. It consisted of nine, 40° reusable surface insulation (RSI) segments. The three RSI's studied, REI-MOD 1A mullite, HCF-MOD III mullite, and LI-1542 silica are shown in this figure before and after testing in the arc plasma environment. Each sample was subjected to a different number of convectively heated cyclic tests. Most of the results presented will be for a 340 kw/m² heating rate although some results at a 450 kw/m² heating rate are also presented. Comparisons will be shown of the results from convective heating with those of a radiantly heated test series at the same surface temperature and static pressure. The most obvious changes which occur in the coatings tested are changes in color. Other changes, some of which explain the color changes observed, are presented in the following figures.

The coatings studied have the following initial compositions:*

- (1) The LI-1542 coating designated as 0042, consists of a densified silica sublayer with a borosilicate glass sealer overlay. The borosilicate glass sealer is approximately 96% SiO₂, 3% B₂O₃ and 1% other oxides, and contains particulate silicon carbide as an emittance pigment.
- (2) The HCF-MOD III coating designated as M5₂3A7P700 is multilayered, having a dense mullite sublayer, a borosilicate chromium oxide intermediate layer acting as a diffusion barrier, and a high emittance top layer consisting of iron, cobalt, and chromium oxides (P700) bonded together with a potassium silicate glass.
- (3) The REI-MOD 1A coating designated as SR2/XSR2 is made up of a densified sublayer and an outer coating of kyanite/petalite in a glass matrix. Both layers have the same matrix composition, that is, Li₂O·Al₂O₃·SiO₂. Nickel oxide is added as an emittance pigment.

* A more complete description of each coating studied can be found in the final reports^{1,2,3} submitted by each contractor.

RSI SAMPLES BEFORE AND AFTER ARC-PLASMA TESTING

$$\dot{q}_{cw} = 340 \text{ kW/m}^2$$

$$H_{e0} = 10.4 \text{ MJ/kg}$$

$$P_s = 810 \text{ N/m}^2$$

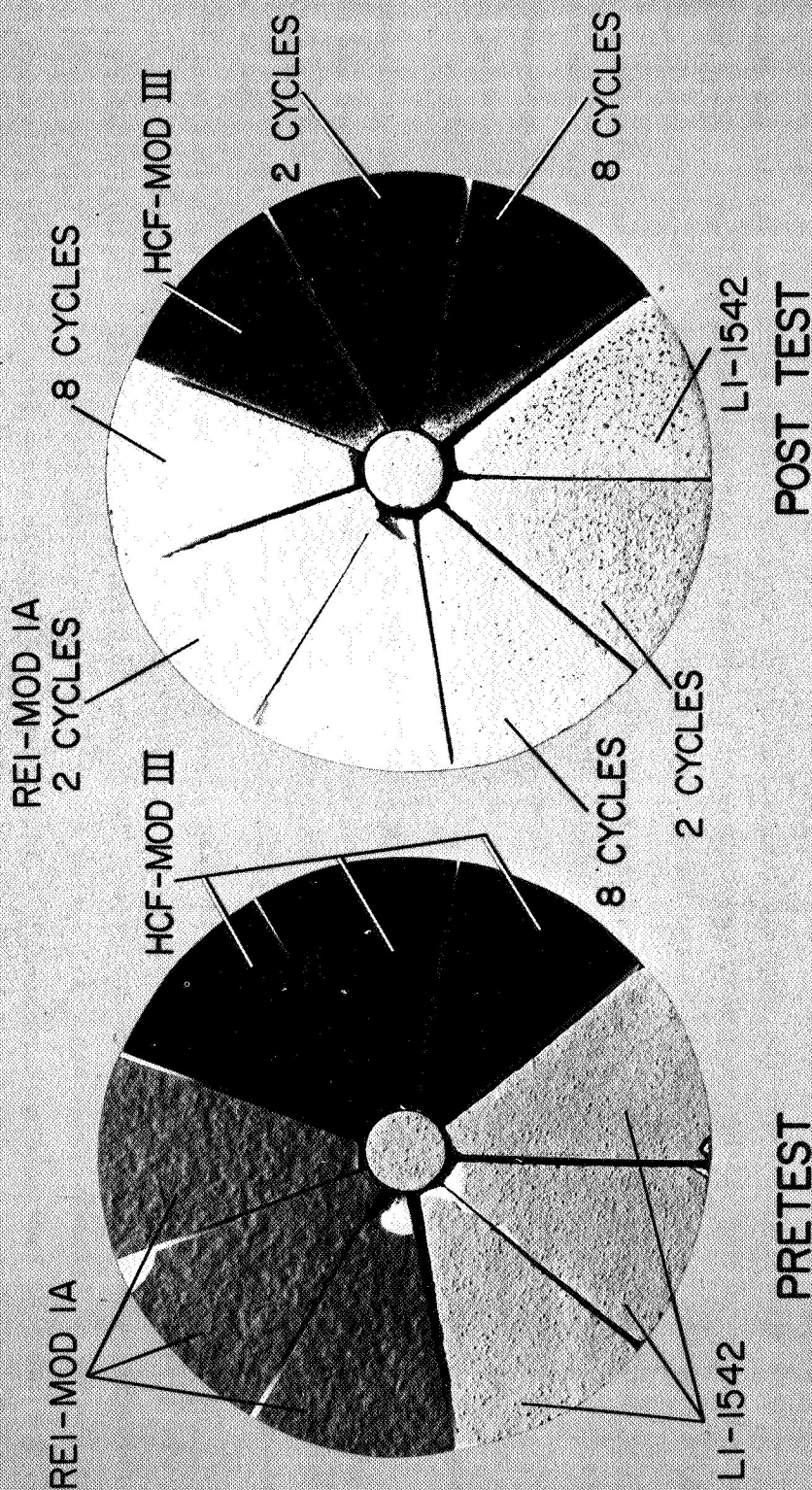


Figure 1

SCANNING ELECTRON MICROGRAPHS OF RSI COATINGS AS A FUNCTION OF CYCLIC ARC PLASMA TESTING

(Figure 2)

This figure illustrates the morphological structure of the three reusable surface insulation coatings before and after testing in the arc plasma environment at a convective heating rate of 340 kw/m^2 . Since each coating's reaction to the convectively heated cyclic testing was unique they will be discussed separately.

The LI-1542 coating, which exhibited the least change as a result of exposure to the environment, is transformed within one cycle from a very rough bubbled glass surface to a relatively smooth one with some small cavities. Subsequent cycling of this coating produced little effect except to cause a less glassy appearance of the coating. Because of this, no other scanning electron micrographs of this coating will be presented in subsequent figures.

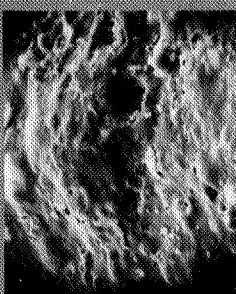
The REI-MOD 1A coating was affected significantly by the cyclic testing in the arc plasma environment. The coating transformed from a relatively smooth surface to a much rougher one with a foamy appearance and many attached and unattached lumps within one cycle. Continued cycling caused the surface to become smoother again by apparently flattening out the lumps present after the first test cycle.

The HCF-MOD III coating exhibited the most significant reaction to the convectively heated cyclic tests. It transformed from a relatively smooth particulate surface to a much rougher one with many new characteristic features evident within one cycle. These new features included a coral like morphological phase* and small areas of exposed glassy sublayer. After eight additional cycles, the coral grew in both diameter and height, but the area they covered decreased. In addition, a dendritic glass structure appeared between the coral and the significantly larger exposed glass sublayer.

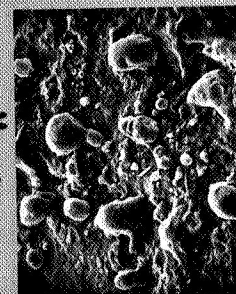
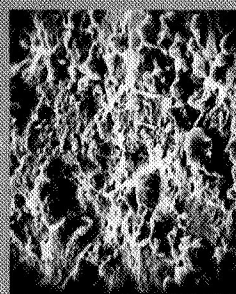
* Subsequent discussion of this phase will refer to it only as coral.

SCANNING ELECTRON MICROGRAPHS OF RSI COATINGS AS A FUNCTION OF CYCLIC ARC PLASMA TESTING

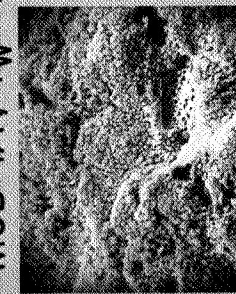
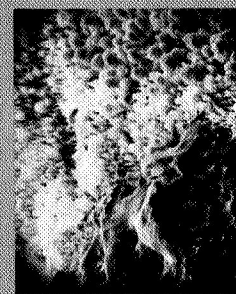
500 x, $\dot{q}_{cw} = 340 \text{ kw/m}^2$



(a) LI-1542, $T_w = 1422^\circ \text{K}$



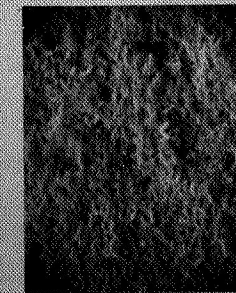
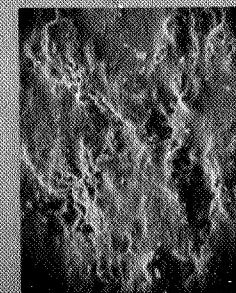
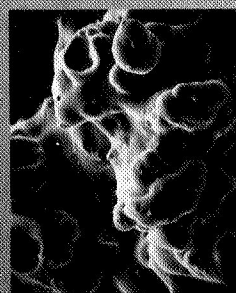
(b) REI-MOD IA, $T_w = 1450^\circ \text{K}$



9 CYCLES

1 CYCLE

(c) HCF-MOD III, $T_w = 1550^\circ \text{K}$



PRETEST

100 μ

Figure 2

(Figure 3)

This figure illustrates the morphological structure of the HCF-MOD III coating during the cyclic arc plasma tests. These tests were performed at heating rates of 340 kw/m² and 450 kw/m². The response of the HCF-MOD III coating to these heating rates differed only in the rate of transition from the initially smooth surface to the final result. At the lower heating rate the reaction proceeds very gradually after the initial transition. After one cycle it is multicroaked and very rough, and we see the newly formed coral phase, a cobalt iron oxide spinel. After one cycle the coral have a very loosely defined structure and cover a majority of the surface. The cracks and holes between the coral cover the remainder of the surface and expose the glassy sublayer below the surface layer. After three cycles the coral have grown significantly in both height and diameter and their overall structure is more clearly defined. In addition, the glassy areas exposed between the coral have expanded to cover a larger portion of the total surface of the coating. After six cycles the coral show continued growth in both height and diameter and the glassy areas have grown larger. The transition areas between the coral and the glassy areas have become more evident. The majority of the glassy areas appear less fluid, indicating an apparent loss of components of the original glass. At nine cycles the same trends have continued with the coral growing in height and slightly in diameter, and the glassy areas continuing to spread out and cover more of the total surface.

At the higher heating rate, 450 kw/m², the coating changes much more rapidly. After one cycle, for example, the coral have already grown to the same size as those produced after nine cycles at the lower heating rate. The glassy areas exposed between the coral have already begun covering a significant portion of the total surface. At three cycles, the glassy areas have become extensive and the coral have receded significantly. After six cycles the glassy areas are beginning to roughen up considerably while the coral are rapidly receding. At nine cycles the coral exist only in limited areas and the sublayer is extremely rough. This result indicates the reaction has proceeded much further at the higher heating rate than it did at the lower heating rate.

SCANNING ELECTRON MICROGRAPHS OF HCF-MOD III COATING AS A FUNCTION OF CYCLIC ARC PLASMA TESTING

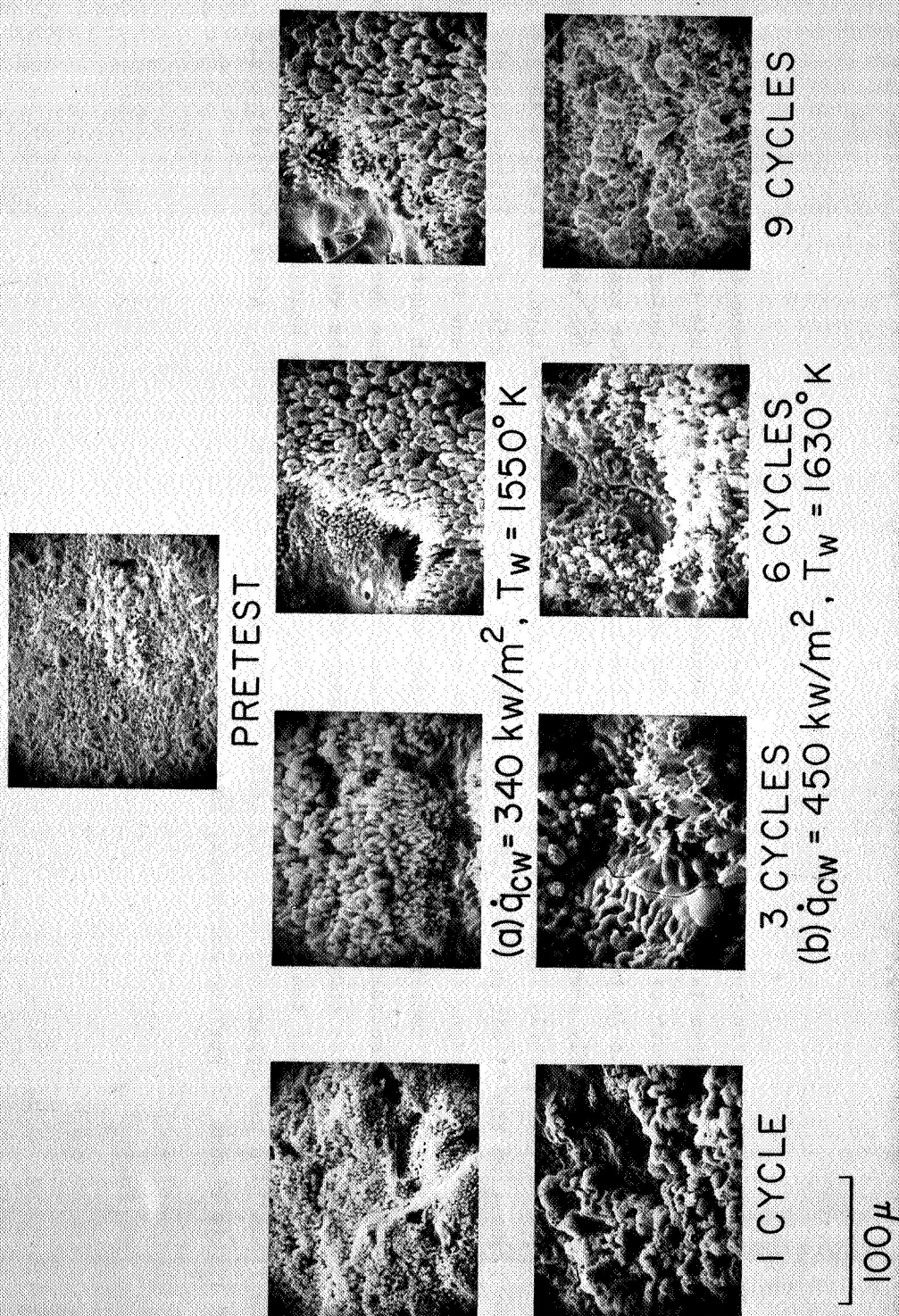


Figure 3

(Figure 4)

The morphological structure of the REI-MOD 1A coating as a function of convectively heated cyclic testing at the two heating rates is illustrated in this figure. The reaction of this coating to the cyclic testing was very similar at both of the heating rates. The end result appears morphologically equivalent. The only difference of note is in the initial stages at the lower heating rate. The transition from the initial surface is more clearly seen here than it is at the higher heating rate. The response of the coating at the lower heating rate clearly indicates that there are two steps to the transition. During the initial step of the transition the virgin surface, which is relatively smooth with some cubic crystallites visible, is transformed into a very rough, foamy surface that has apparently balled up in one cycle. This very rough surface becomes significantly smoother by apparently fusing and flattening out with continued cycling at the lower heating rate. The concentration of spherical particulates on the surface also decreases with continued cycling until after nine cycles they have completely disappeared. At this point the surface appears much like it does after one cycle of testing at the higher heating rate. At the higher heating rate the first step in the transition has apparently occurred prior to the end of the first cycle. After the first cycle of testing little change in surface morphology is evident.

SCANNING ELECTRON MICROGRAPHS OF REI-MOD IA COATING AS A FUNCTION OF CYCLIC ARC PLASMA TESTING

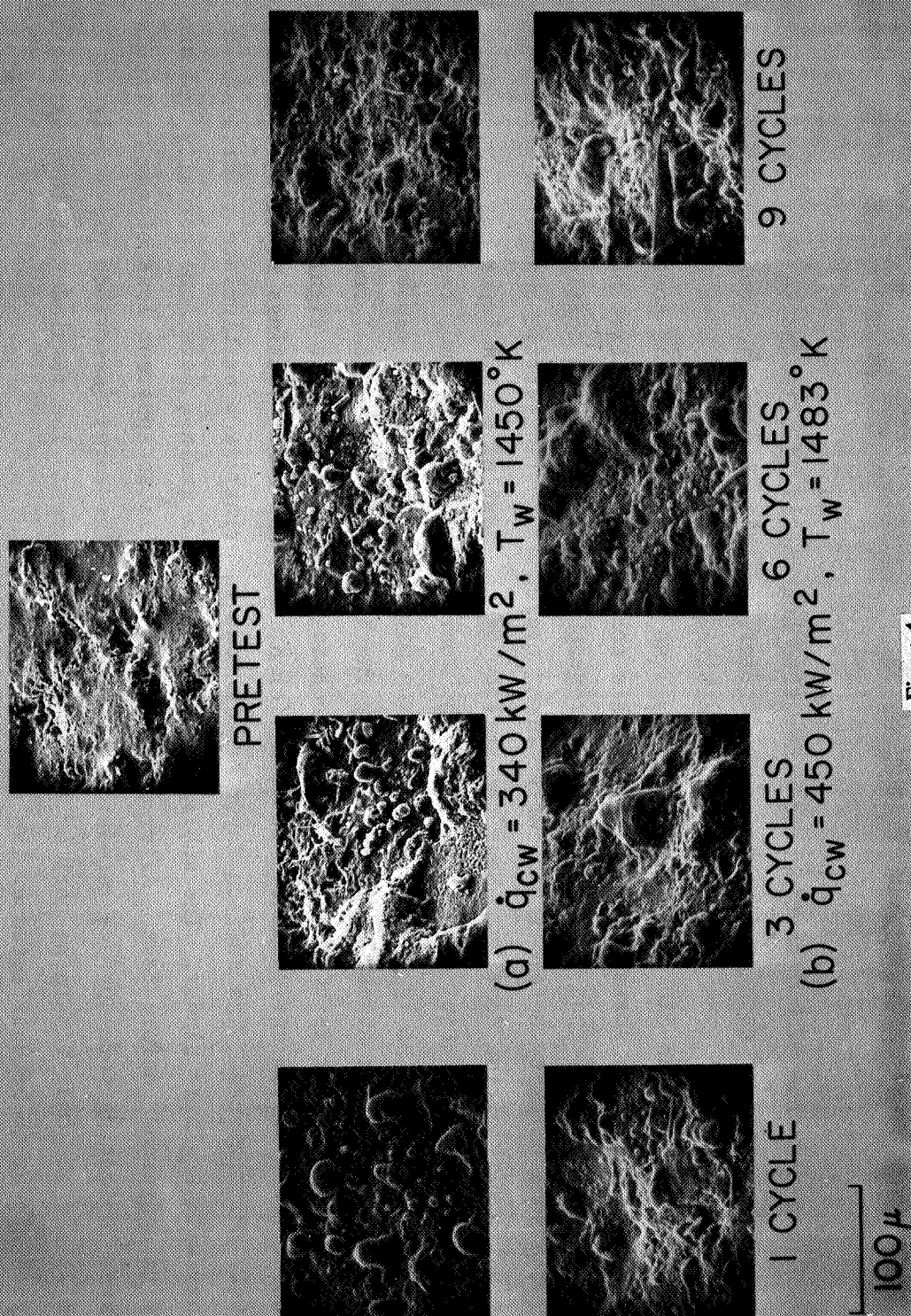


Figure 4

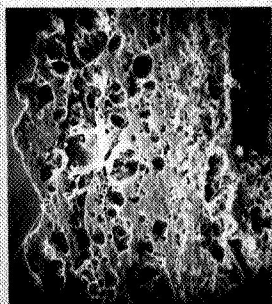
SCANNING ELECTRON MICROGRAPHS OF CROSS SECTION OF RSI COATINGS BEFORE AND AFTER ARC PLASMA TESTING
(Figure 5)

The response of RSI coatings to convective heating is illustrated in this figure, which shows cross sections of each coating before and after cyclic testing. Each coating's response to the environment was unique. The LI-1542 coating exhibited the most porosity both before and after eight cycles of testing at the 340 kw/m² heating rate, even though the amount of porosity had decreased with testing. The change in surface morphology of this coating during convective heating, noted previously, is also evident in the cross sectional photomicrographs. The REI-MOD 1A coating appears very uniformly dense with some porosity before test. After eight cycles of testing little change is evident except in the uniformity of the coating. Near the surface of the coating a thin layer has formed after test that appears to be different from the rest of the coating. This difference results in a lighter appearance of the coating in the scanning electron microscope and may be caused either by foaming, which makes the coating appear less dense, or by the loss of some elemental component, which makes it appear lighter after test. The HCF-MOD III coating exhibited the most significant response to the convectively heated environment. It is different from the other coatings studied, since it is obviously multilayered. The surface layer before test is primarily a particulate material held together with a glassy binder. The sublayers contain chromia grains, have some porosity and are glassy in appearance before test. After eight cycles there is an apparent loss of the particulate top layer indicating some surface recession has occurred. The coral (described previously in figure 2) are the only remaining part of that initial top layer. The remainder of the coating's sublayers appear to be unaffected by the environment.

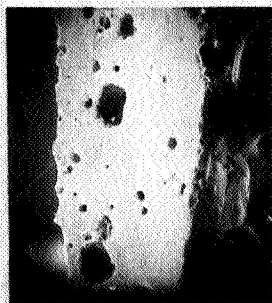
SCANNING ELECTRON MICROGRAPHS OF CROSS SECTION OF RSI COATINGS BEFORE AND AFTER ARC PLASMA TESTING

190 X

LI 1542



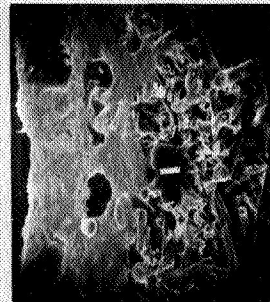
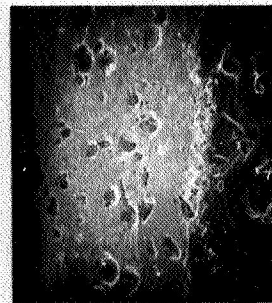
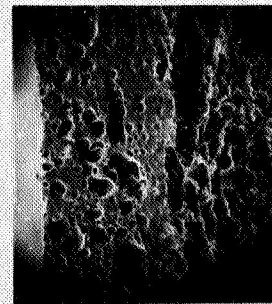
REI-1A



HCF-III



PRETEST



$T_w = 1422^\circ\text{K}$

$T_w = 1450^\circ\text{K}$

$T_w = 1550^\circ\text{K}$

$\overline{400\mu}$

8 CYCLES, $\dot{q}_{cw} = 340 \text{ KW/m}^2$

Figure 5

X-RAY FLUORESCENCE PATTERNS OF HCF-MOD III COATING

(Figure 6)

In order to obtain data on the chemical changes of the coatings studied as a function of cyclic arc plasma testing, an energy dispersive X-ray analysis (EDX) unit attached to the scanning electron microscope was used. This unit determines the elements present by X-ray fluorescence analyses. The elements are differentiated by the characteristic wavelengths or excitation voltages of the X-rays they emit when bombarded by electrons within the scanning electron microscope. The EDX unit was used in two different modes of operation. In the first mode, the location of an element present in oxide form in the coating could be established. The form of the data obtained in this mode was a dot pattern. This pattern was obtained by taking a photograph of an oscilloscope display which showed a white dot wherever X-rays of the correct excitation voltage were detected as the scanning electron microscope scanned across the surface. Subsequently, a scanning electron micrograph was taken of the same area from which the dot pattern was obtained to establish the location of the element. In the second mode, which will be described later, the EDX unit integrates all of the dot patterns to obtain a complete semi-quantitative X-ray fluorescence analysis.

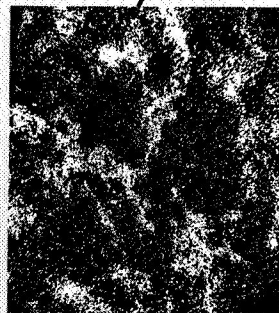
The photographs shown in figure 6 present some of the data obtained from the EDX unit in the first mode. It illustrates a scanning electron micrograph of the surface of the HCF-MOD III coating after nine cycles at the 340 kw/m² heating rate along with dot patterns for the elements of interest. It indicates that the elements on the surface of the HCF-MOD III coating are segregated with cobalt and iron being present in coralloid areas and silicon being the primary component of the phase in between. Chromium appears to be uniformly distributed. This type of analysis was used primarily for RSI coatings in cross section.

X-RAY FLUORESCENCE PATTERNS OF HCF-MOD III COATING

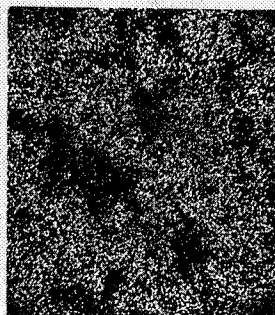
$\dot{q}_{cw} = 340 \text{ kW/m}^2$

9 CYCLES

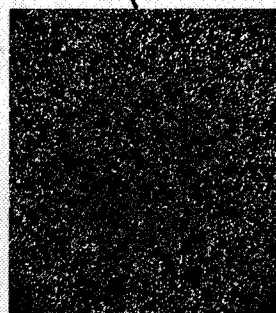
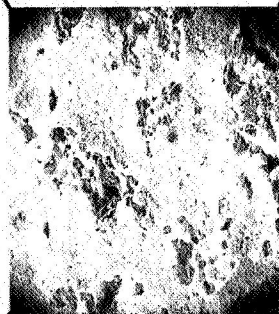
50 x



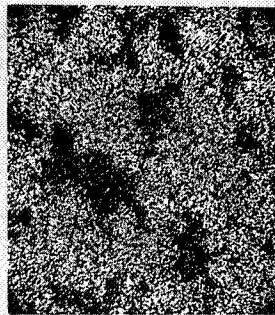
SILICON



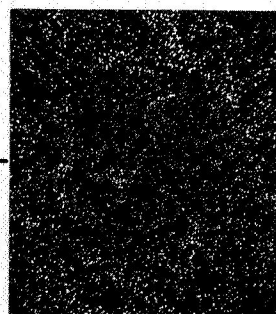
COBALT



CHROMIUM



IRON



POTASSIUM

1000 μ

Figure 6

SCHEMATIC OF DENSITOMETER EQUIPMENT

(Figure 7)

In the first mode of operation, the spatial distribution and relative amount of each element present in different layers of the coating were determined using a modified densitometer as schematically illustrated in figure 7. These data could then be used to determine if components of the coating were diffusing into the insulation itself or toward the surface of the coating with cyclic testing in the arc plasma environment. As the figure shows, a collimated beam of light is passed through a portion of a negative of the dot pattern of interest, and the intensity of the transmitted beam is measured with a photomultiplier tube. The dot pattern of interest is moved at a constant rate across the stationary 0.635 cm (1/4 inch) square beam so that a plot is produced of total intensity of the transmitted beam versus the distance traveled across the negative of the dot pattern. The optical system, which is unique to this equipment, diffuses and then concentrates the transmitted image of the square beam passed through the dot pattern. The output from the photomultiplier is a total intensity for the transmitted beam which represents the averaged or integrated dot density within the area of the negative the beam passed through. This plot obtained from the strip chart recorder is a semi-quantitative representation showing the location and concentration of the element of interest. This type of analysis for the elements present will be illustrated for cross sections of the HCF-MOD III and REI-MOD 1A coating before and after testing in the convectively heated environment. No patterns of the LI-1542 coatings will be presented since silicon is the only element detectable in it with this analytical technique.

SCHEMATIC OF DENSITOMETER EQUIPMENT

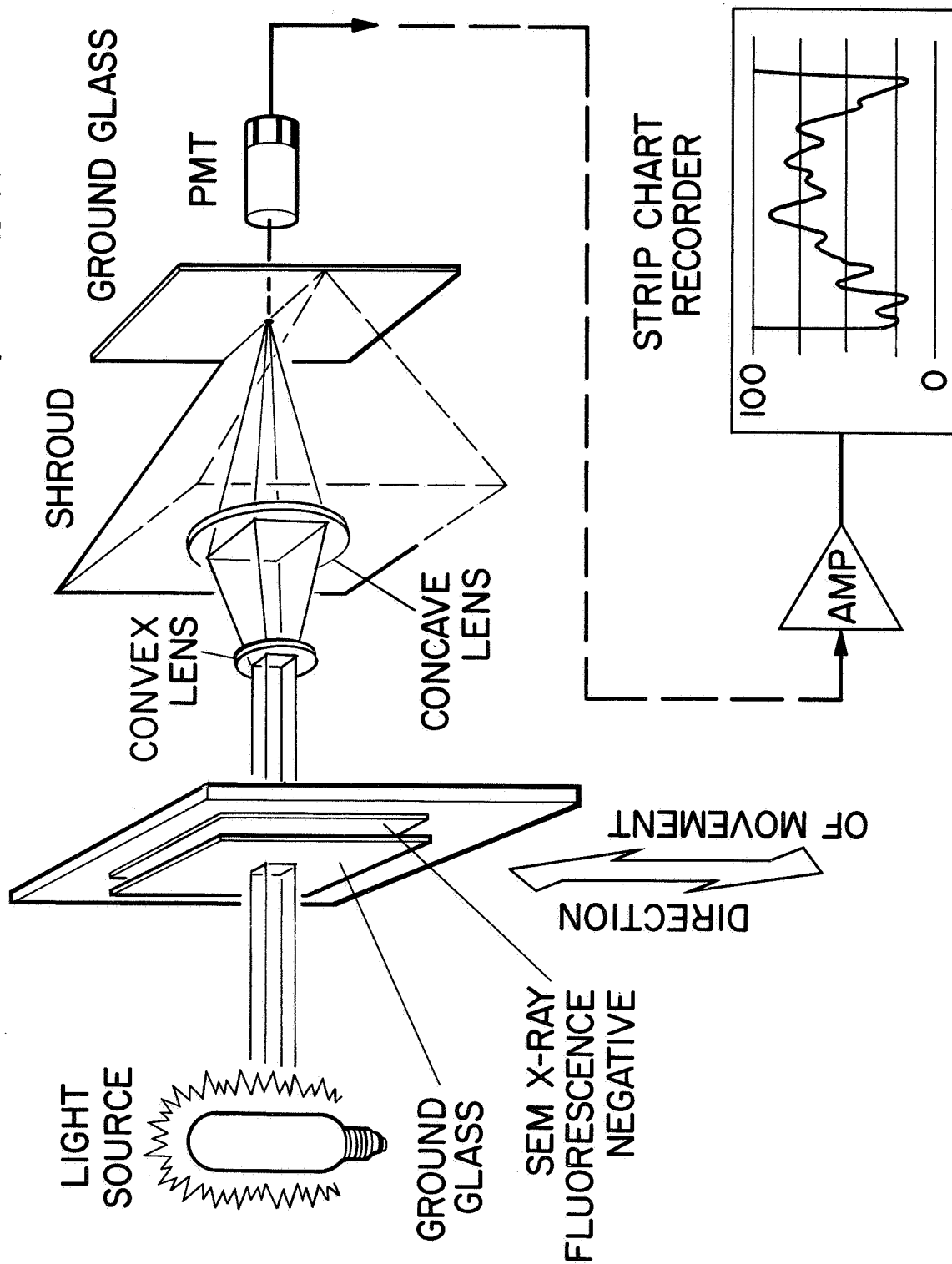


Figure 7

X-RAY FLUORESCENCE ANALYSIS OF HCF-MOD III COATING

(Figure 8)

This figure illustrates an X-ray fluorescence analysis of the HCF-MOD III coating before and after convectively heated cyclic testing utilizing the second mode of operation of the EDX unit. In this mode of operation the EDX unit counts all the X-rays detected and stores them according to their relative excitation voltages. This type of analysis results in a total average concentration on the surface of each element rather than the spatial distribution found with the first EDX mode. The data in this figure were obtained after counting for 40 seconds while the scanning electron microscope was scanning the surface of the HCF-MOD III coating. The peaks shown correspond to the excitation voltage of the elements identified in the pretest data. In the post test data the silicon (1.8 keV) and the iron (6.4 keV) peak intensity exceeded 10,000 counts and therefore are referred to the axis identified on the far right of the plot for their total peak intensity. These plots indicate that the surface chemistry of the HCF-MOD III coating is changing considerably with convectively heated cyclic testing. The relative concentration of silicon and iron have increased due to the depletion of potassium and chromium on the surface. The cobalt concentration appears relatively unaffected. These data also indicate the potential value of the EDX unit to determine surface chemistry changes with cyclic testing, although several limitations must be recognized before it can be used. These limitations are:

- (1) The chemical analysis obtained is from the materials lying within a half micron of the surface. This defines the meaning of surface.
- (2) The analysis is possible only for elements with an atomic number of 11 (Na) or more, primarily due to electronic noise.
- (3) The analysis is only semiquantitative.

X-RAY FLUORESCENCE ANALYSIS OF HCF - MOD III COATING

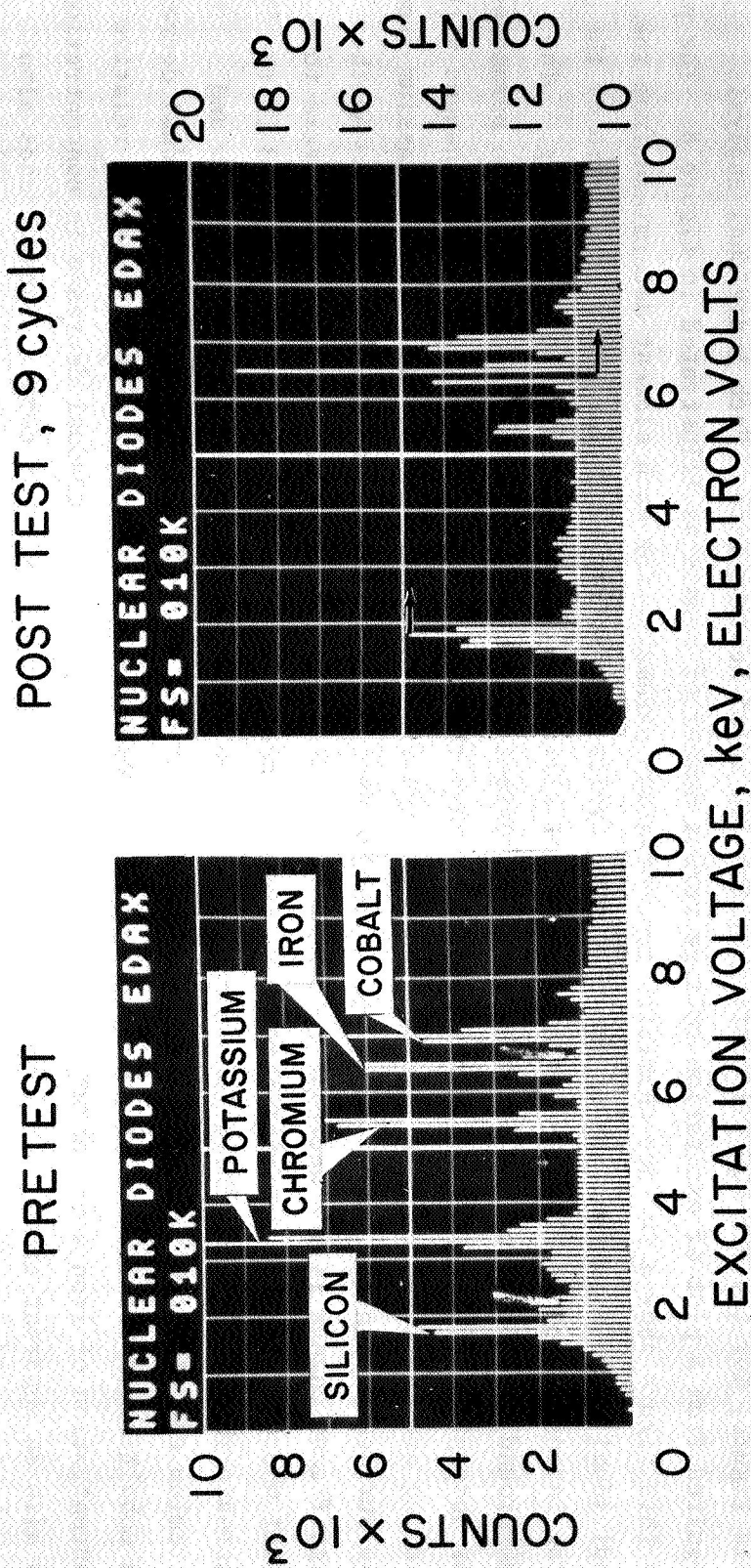


Figure 8

CHANGE IN SURFACE COATING CHEMISTRY AFTER ARC PLASMA TESTING HCF-MOD III

(Figure 9)

The change in surface coating chemistry during convectively heated cyclic testing is shown in this figure, for the HCF-MOD III coating at the 340 kw/m^2 heating rate. Each individual analysis resulted from a plot of excitation voltage versus number of counts as illustrated in figure 8. The plots in this figure show a surface chemistry concentration parameter for each element determined from the individual plots as a function of the number of cycles of testing. This parameter is a ratio of the peak intensity for an element examined to that of silicon in the same coating before testing. The background is subtracted out in each case. No correction has been made to the concentration parameter for absorption of X-rays by elements present within the surface under analysis. Several changes with cycling are indicated by this figure. The most significant change noted is the loss of potassium from the surface within one test. No change in the potassium concentration occurred thereafter. Another significant change is the decrease in concentration of chromium on the surface within one cycle to a point where it remains constant throughout the remainder of the tests. A third change noted is the increase in relative concentration of cobalt after one cycle caused by the loss of potassium and chromium coincident with the formation of coral, described in figure 2, followed by the gradual decrease in cobalt concentration, again coincident with the recession of the coral. The increase in relative concentration of iron after about three cycles, followed by its very gradual decrease in concentration, is also an apparent trend coincident with the formation and recession of coral. These trends also explain the optical property changes observed in this coating during cyclic testing reported in the paper by Stewart, presented at this symposium. The last change noted was the gradual increase in concentration of silicon due to the gradual depletion of all other elements with increasing cyclic exposure coincident with the apparent growth of glassy areas between the coral. When all these changes and trends are compared, one concludes that the more volatile oxides have decreased in concentration the fastest. Thus, the loss of potassium from the surface is the fastest followed in order by chromium, cobalt and iron. Silicon, being the most stable, actually appears to increase in concentration due to the depletion of the more volatile oxides.

CHANGE IN SURFACE COATING CHEMISTRY AFTER ARC PLASMA TESTING

HCF-MOD III

$\dot{q} = 340 \text{ kW/m}^2$

$H_{e0} = 10.7 \text{ MJ/kg}$

$P_s = 810 \text{ N/m}^2$

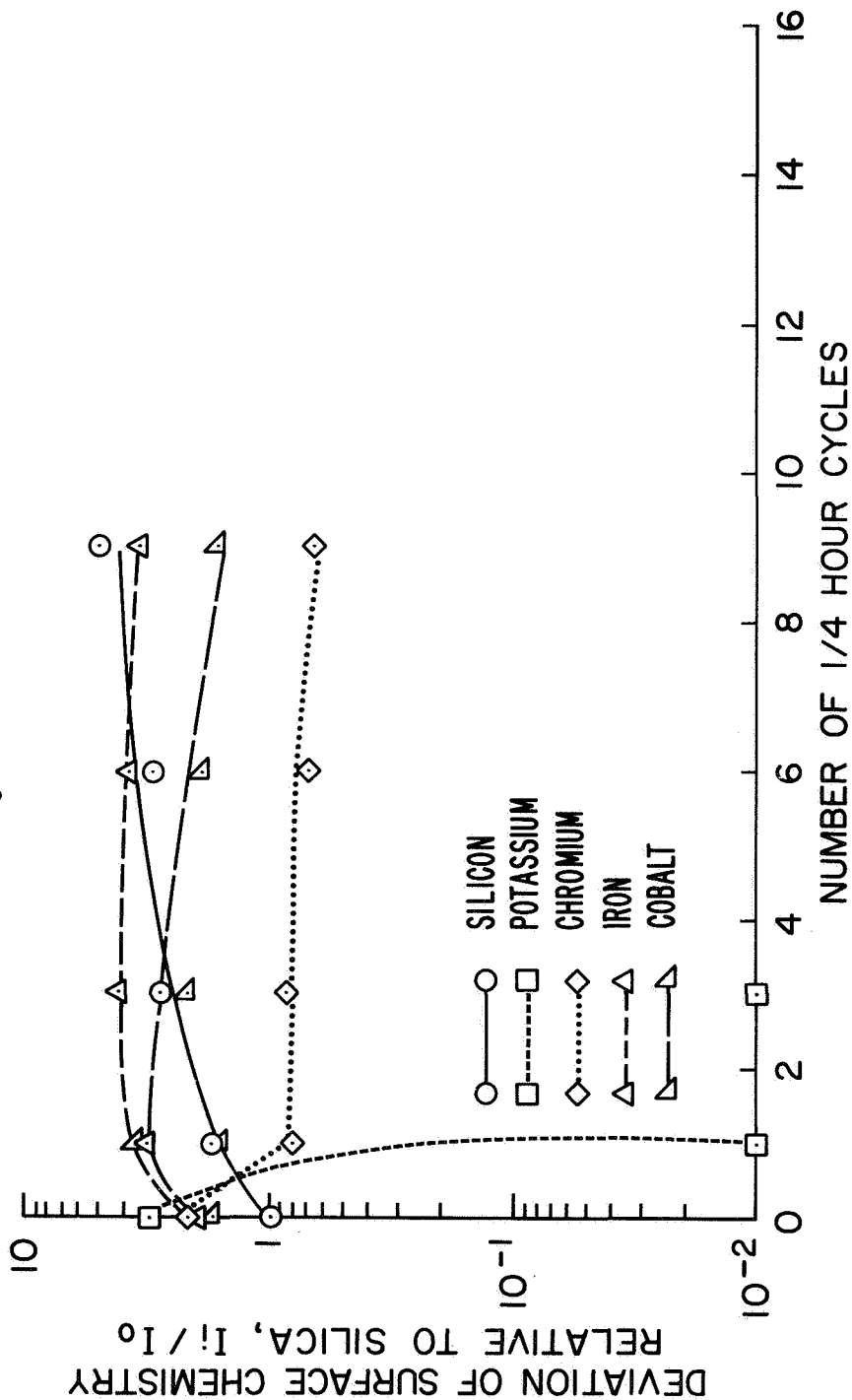


Figure 9

CHANGE IN SURFACE COATING CHEMISTRY AFTER ARC PLASMA TESTING
HCF-MOD III

(Figure 10)

The change in surface coating chemistry is shown in this figure for the HCF-MOD III coating at the 450 kw/m² heating rate. The changes and trends noted are similar to those noted at the lower heating rate for all of the elements except chromium, which is beginning to increase in relative concentration after about 15 cycles of testing at the higher heating rate. This increased chromium concentration may be the result of exposing chromia grains present within the sublayers of the HCF-MOD III coating. Figures 9 and 10 show that the response of the coating to the convectively heated environment is apparently equivalent in terms of surface chemistry at both heating rates, although the response is accelerated at the higher heating rate.

CHANGE IN SURFACE COATING CHEMISTRY AFTER ARC PLASMA TESTING HCF-MOD III

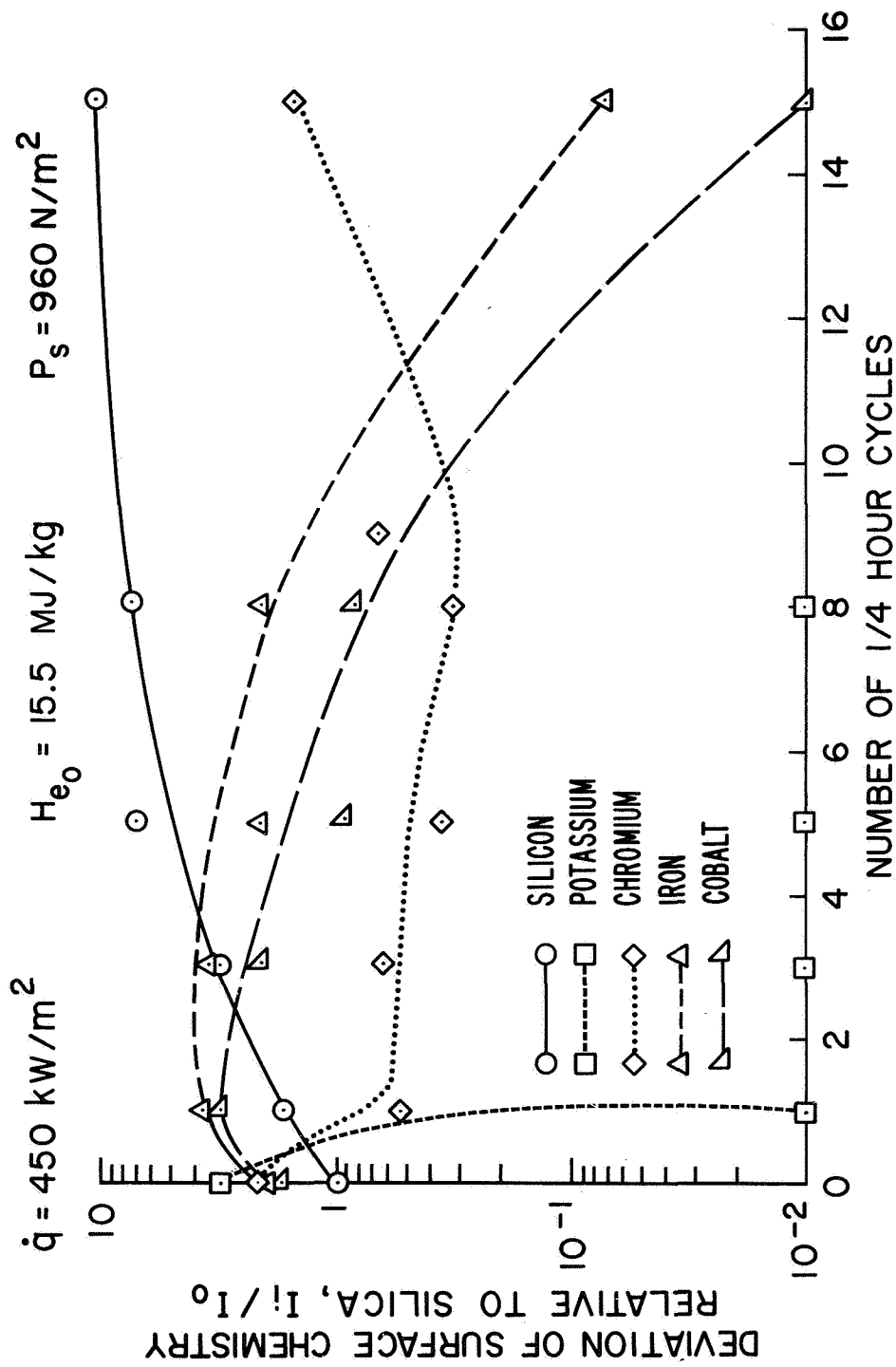


Figure 10

CHANGE IN SURFACE COATING CHEMISTRY AFTER RADIANT HEAT TESTING
HCF-MOD III

(Figure 11)

The change in surface coating chemistry which occurs as a function of radiantly heated cyclic tests at 1480°K for the HCF-MOD III coating is illustrated in this figure. The tests were conducted at a pressure of 810 N/m² (0.008 atm), which is equivalent to the surface pressure in the convectively heated cyclic tests. The results indicate several differences in surface chemistry between the radiatively heated cyclic testing behavior and the similar convective heating test results illustrated in figure 9. Specifically the potassium concentration drops an order of magnitude further during convective heating tests than it does during radiant tests, indicating a significant enhancement of its vaporization due to the boundary layer present during convective heating. The relative concentration of chromium appears to increase slightly in radiant heating whereas it decreases during convective heating, again indicating some reaction with the boundary layer is probably occurring. The cobalt and iron concentrations appear unaffected in radiant heating whereas they change significantly in convective heating concurrent with the formation of a coralloid phase described previously. The results shown in figures 9 and 11, therefore, indicate a significant difference in the HCF-MOD III coating's chemical response to the two environments.

CHANGE IN SURFACE COATING CHEMISTRY AFTER RADIANT HEAT TESTING

HCF - MOD III

$T_w \approx 1480^\circ \text{K}$ $P_s = 810 \text{ N/m}^2$

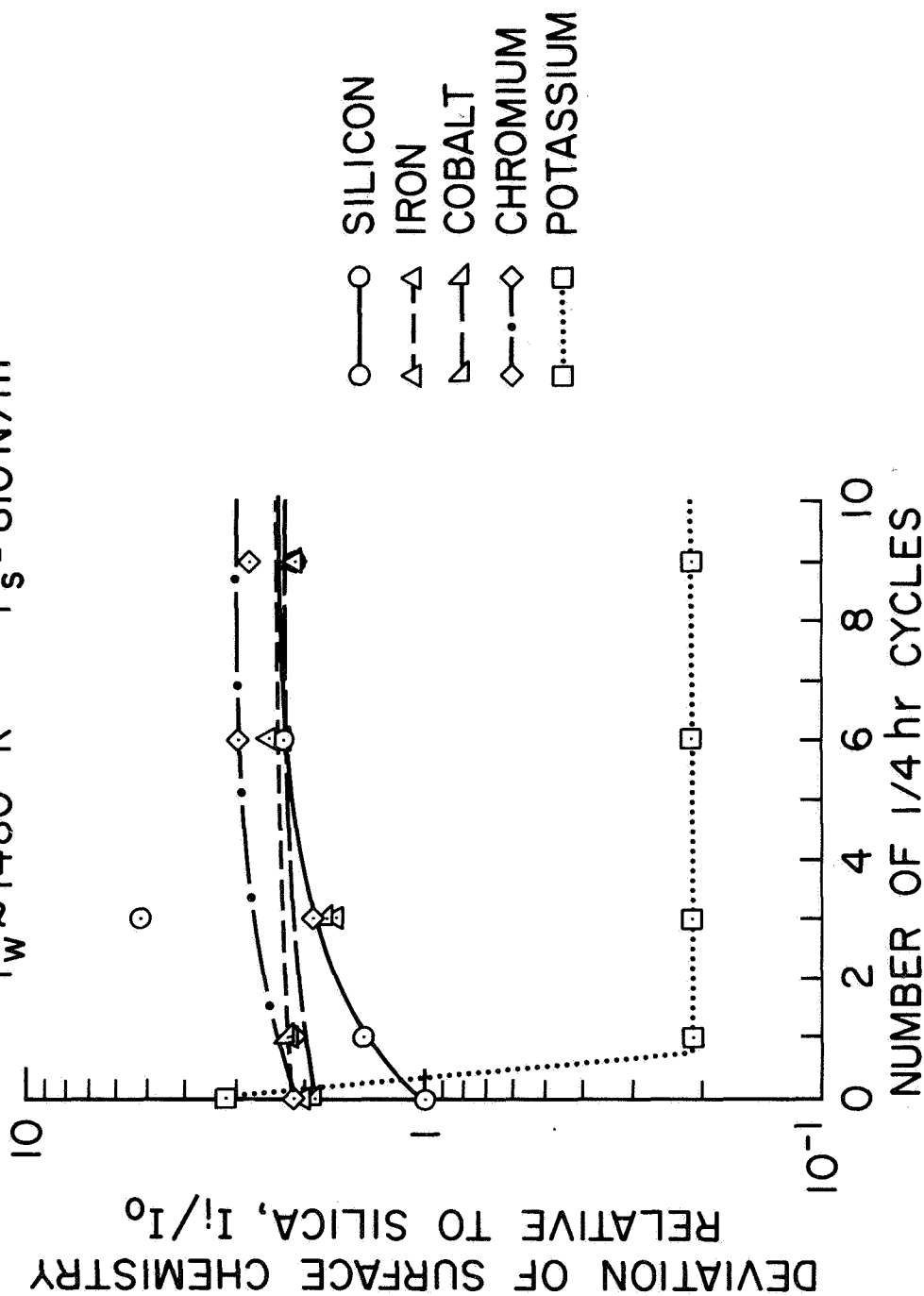


Figure 11

CHANGE IN SURFACE COATING CHEMISTRY AFTER ARC PLASMA TESTING

REI-MOD 1A

(Figure 12)

The change in surface coating chemistry during convectively heated cyclic testing of the REI-MOD 1A coating is illustrated in this figure for the 340 kw/m² heating rate. Several changes are indicated in this figure. The first change noted is the decrease in relative surface concentration of calcium, nickel, and iron. The decrease in nickel concentration on the surface is probably the cause of the change in coating color from greenish brown before test to grayish white after one cycle noted in figure 1. Another change noted is the increase in relative concentration of the aluminum and silicon, which are relatively nonvolatile oxides, after one cycle. This change is caused by the depletion of the other elements present initially including lithium, which could not be detected in this analysis. Little change in concentration of aluminum and silicon is noted thereafter with continued cycling. Another trend noted is the gradual increase in the relative concentration of titanium, which is another of the more stable oxides.

CHANGE IN SURFACE COATING CHEMISTRY AFTER ARC PLASMA TESTING

REI - MOD 1A

$\dot{q} = 340 \text{ kW/m}^2$

$H_{e0} = 10.7 \text{ MJ/kg}$

$P_s = 810 \text{ N/m}^2$

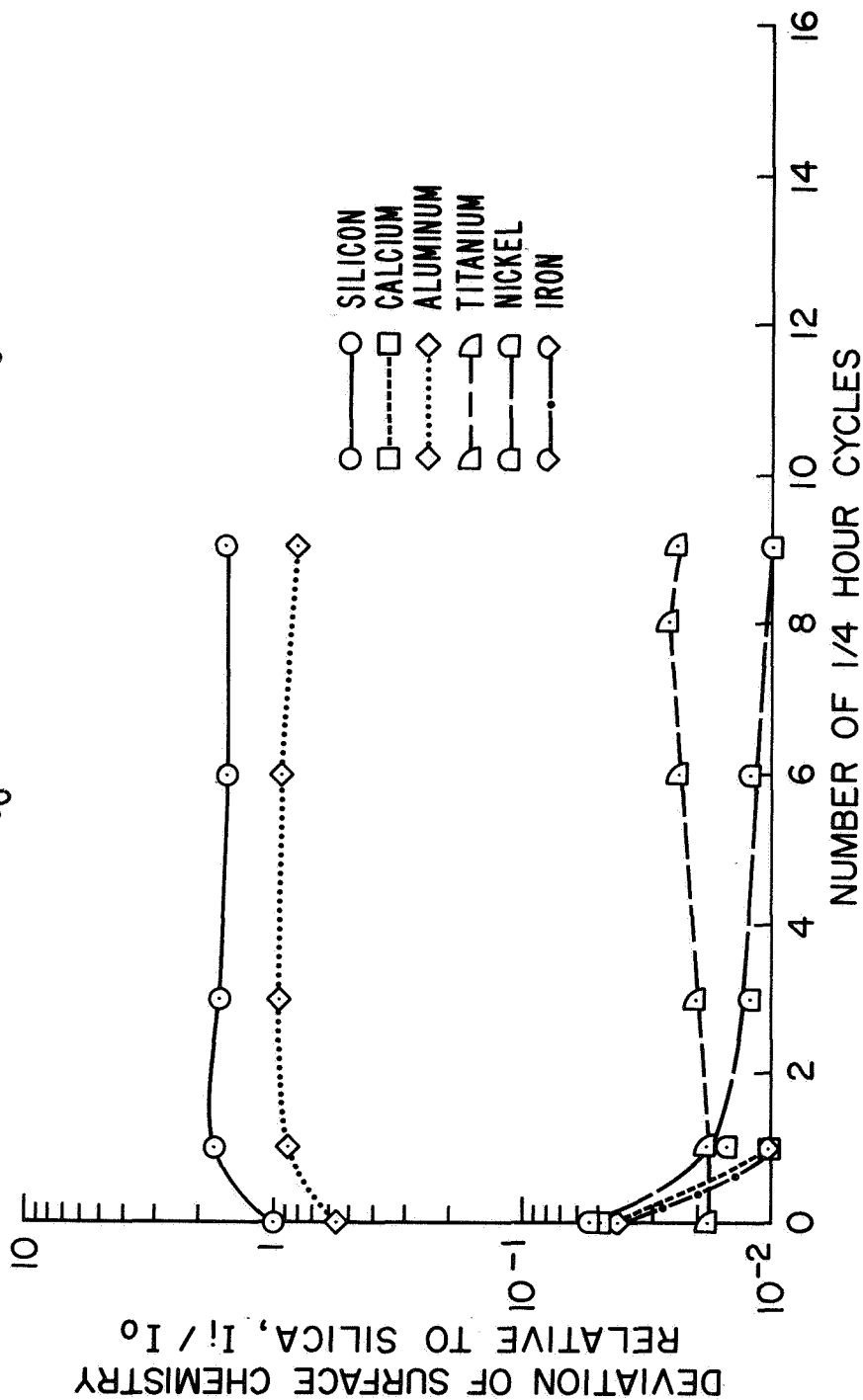


Figure 12

CHANGE IN SURFACE COATING CHEMISTRY AFTER ARC PLASMA TESTING

REI-MOD 1A

(Figure 13)

This figure illustrates the change in surface coating chemistry during convectively heated cyclic testing of the REI-MOD 1A coating at the 450 kw/m² heating rate. These results indicate that the changes at this heating rate are the same as those shown in the previous figure for this coating at the 340 kw/m². These changes also explain the optical property changes observed in the REI-MOD 1A coating as a function of cyclic convective heating tests reported in the paper by D.A. Stewart.

CHANGE IN SURFACE COATING CHEMISTRY AFTER ARC PLASMA TESTING

REI - MOD 1A

$\dot{q} = 450 \text{ kW/m}^2$

$H_{e0} = 15.5 \text{ MJ/kg}$

$P_s = 960 \text{ N/m}^2$

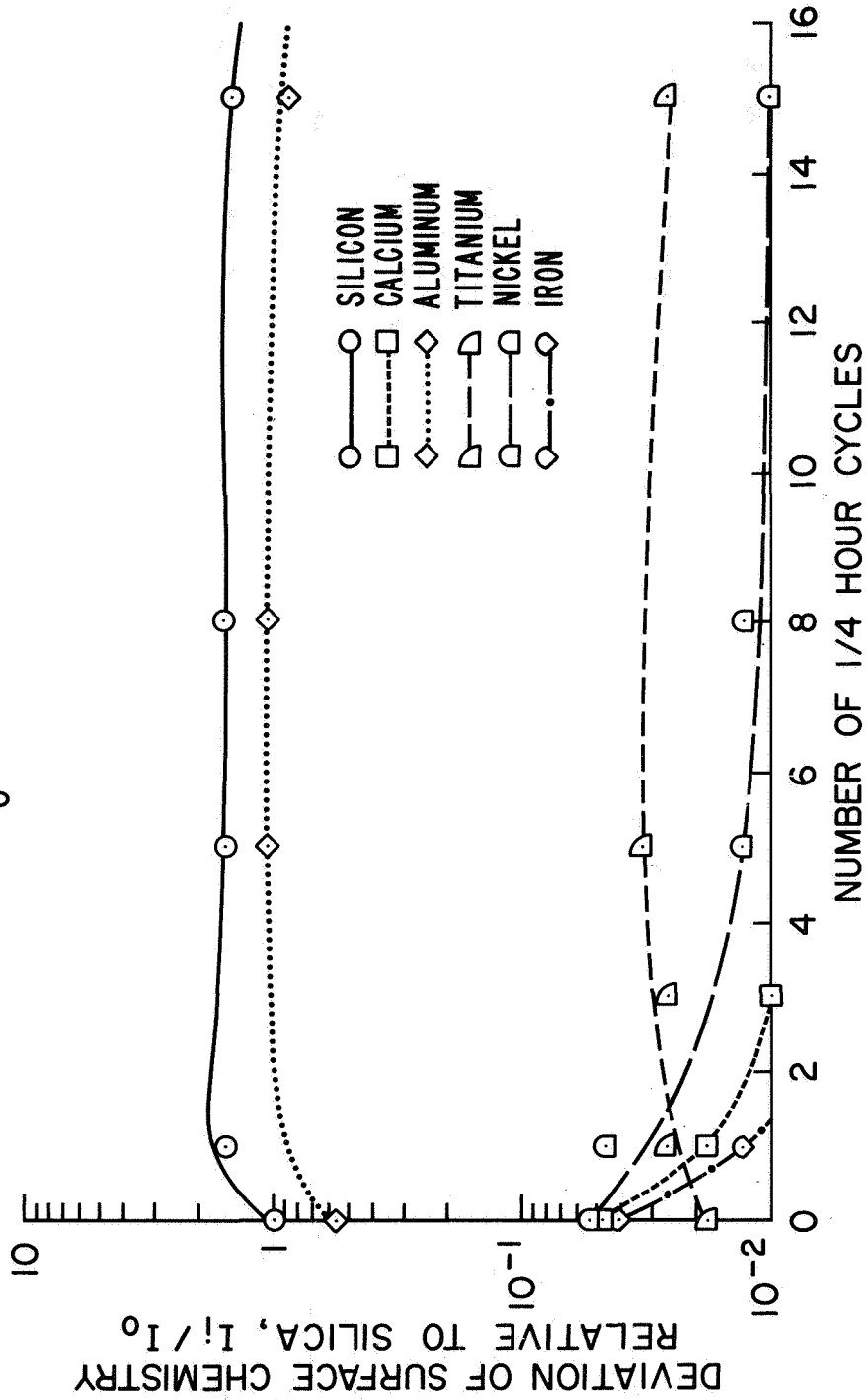


Figure 13

CHANGE IN SURFACE COATING CHEMISTRY AFTER RADIANT HEAT TESTING
REI-MOD 1A

(Figure 14)

This figure illustrates the changes in the surface chemistry that occur in the REI-MOD 1A coating as a function of radiantly heated cyclic tests at 1480°K. These tests were conducted at a pressure of 810 N/m² (0.008 atm), which was equivalent to the stagnation pressure in the convectively heated cyclic tests. The surface temperature achieved was about the same as that obtained at the 340 kw/m² heating rate during convective heating. The results indicate significant differences in surface chemistry behavior between the radiant heating tests and the convective heating tests illustrated in figure 12. Specifically, the relative concentration of nickel increases during radiantly heated cyclic tests while it decreases during convectively heated cyclic testing. This difference again indicates an interaction is occurring between the boundary layer present during convective heating and the REI-MOD 1A coating that does not occur in radiant heating. The increase in relative concentrations of nickel, aluminum, and silicon is again probably due to the loss of lithium from the coating, which is not detectable with this analytical technique. The concentrations of other minor constituents present in the coating that decrease during convective heating remain constant during the radiant heating tests.

CHANGE IN SURFACE COATING CHEMISTRY AFTER RADIANT HEAT TESTING

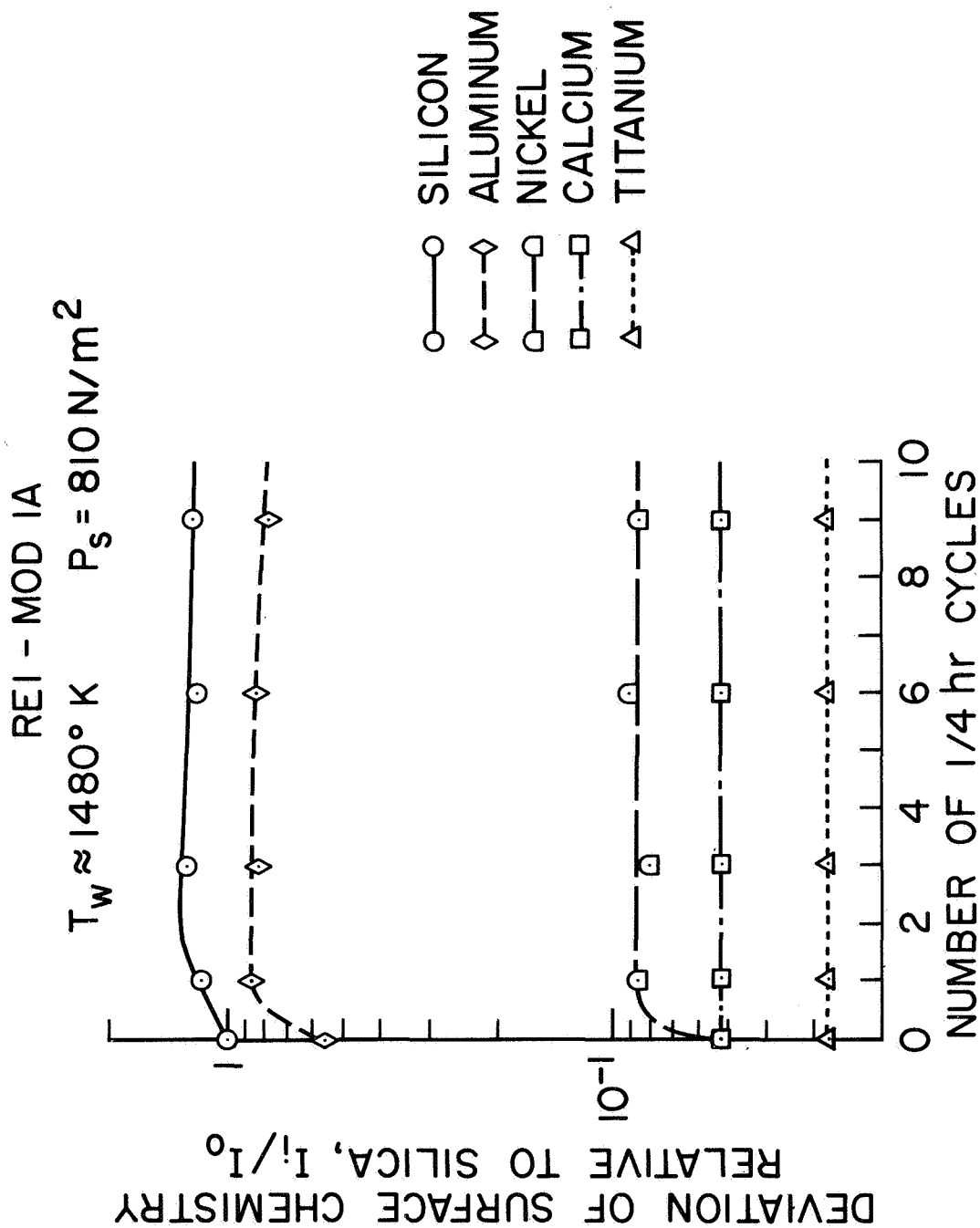


Figure 14

CHANGE IN SURFACE COATING CHEMISTRY AFTER ARC PLASMA TESTING

LI-1542

(Figure 15)

This figure illustrates the change in surface coating chemistry of the LI-1542 coating that occurs as a function of convectively heated cyclic testing, at the 340 kw/m² heating rate. The results indicate little change in chemical composition of the LI-1542 coating after one cyclic test. This result is partly due to the fact that this coating contains no elements other than silicon, carbon, oxygen, and boron in large enough concentrations to be significant, and, therefore, detectable. The increase in concentration observed after one cycle is probably the result of two factors. The first one is the change in the surface morphology (densification) of the coating itself, which occurred within one cycle. The second one is the loss of some of the minor constituents of the untested coating, primarily boron, which is undetectable with this particular analytical technique. A similar surface chemistry response was observed at the 450 kw/m² heating rate.

CHANGE IN SURFACE COATING CHEMISTRY AFTER ARC PLASMA TESTING

LI-1542

$$\dot{q} = 340 \text{ kW/m}^2 \quad H_{e0} = 10.7 \text{ MJ/kg} \quad P_s = 810 \text{ N/m}^2$$

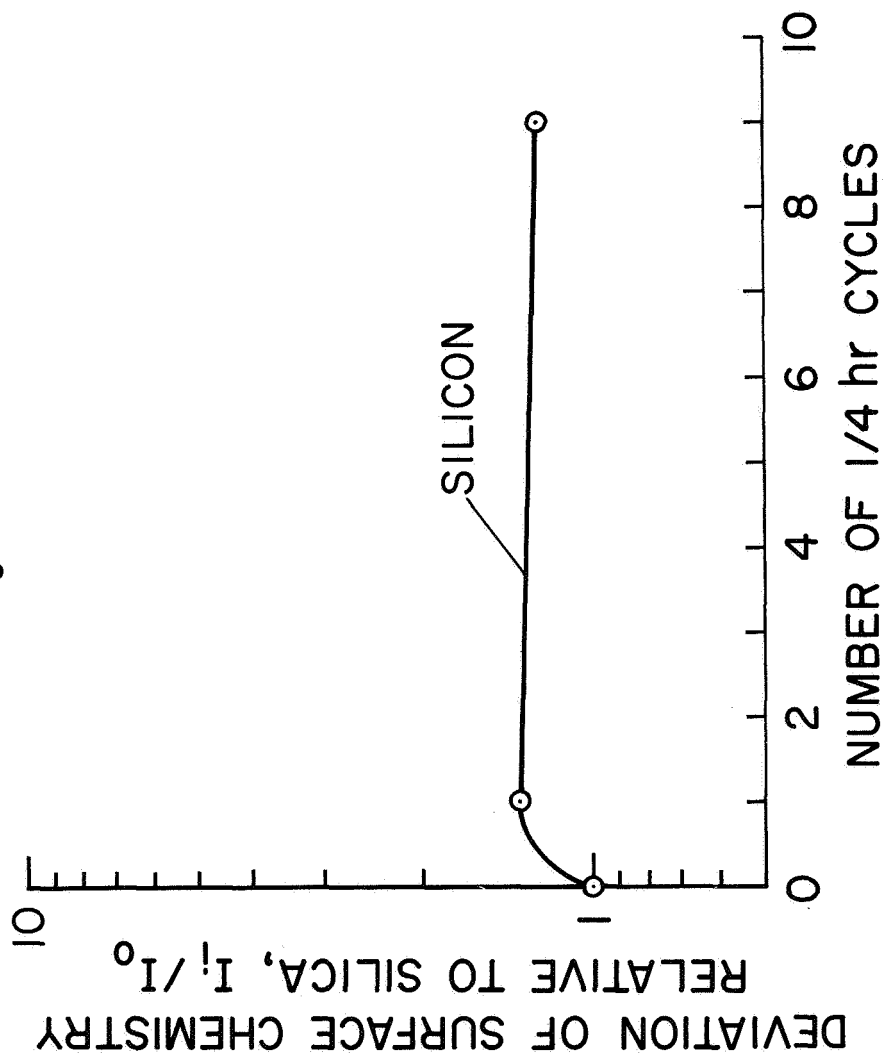


Figure 15

X-RAY FLUORESCENCE CHEMICAL ANALYSIS OF HCF-MOD III COATING

CROSS SECTION - PRETEST

(Figure 16)

This figure illustrates a chemical analysis of the HCF-MOD III coating in cross section before testing. It was obtained by the method described in figure 7. The analysis was taken through a strip 25 microns wide, which is illustrated by the white lines superimposed upon the scanning electron micrograph in the figure. These results are semiquantitative and uncorrected for absorption of X-rays, which will occur due to the elements present in the coating. The components of the individual layers of this coating are illustrated in this figure. The spatial response of the instrument is indicated by the shaded areas on the plots in the figure. The top layer is composed primarily of cobalt and iron with chromium and silicon also evident. Data for potassium, which is also present in the top layer, are not presented due to a sample preparation problem, which made the data unreliable. The intermediate layer is composed primarily of chromium and silicon. The bottom layer is primarily composed of aluminum and silicon.

X-RAY FLUORESCENCE CHEMICAL ANALYSIS OF HCF-MOD III COATING CROSS SECTION - PRETEST

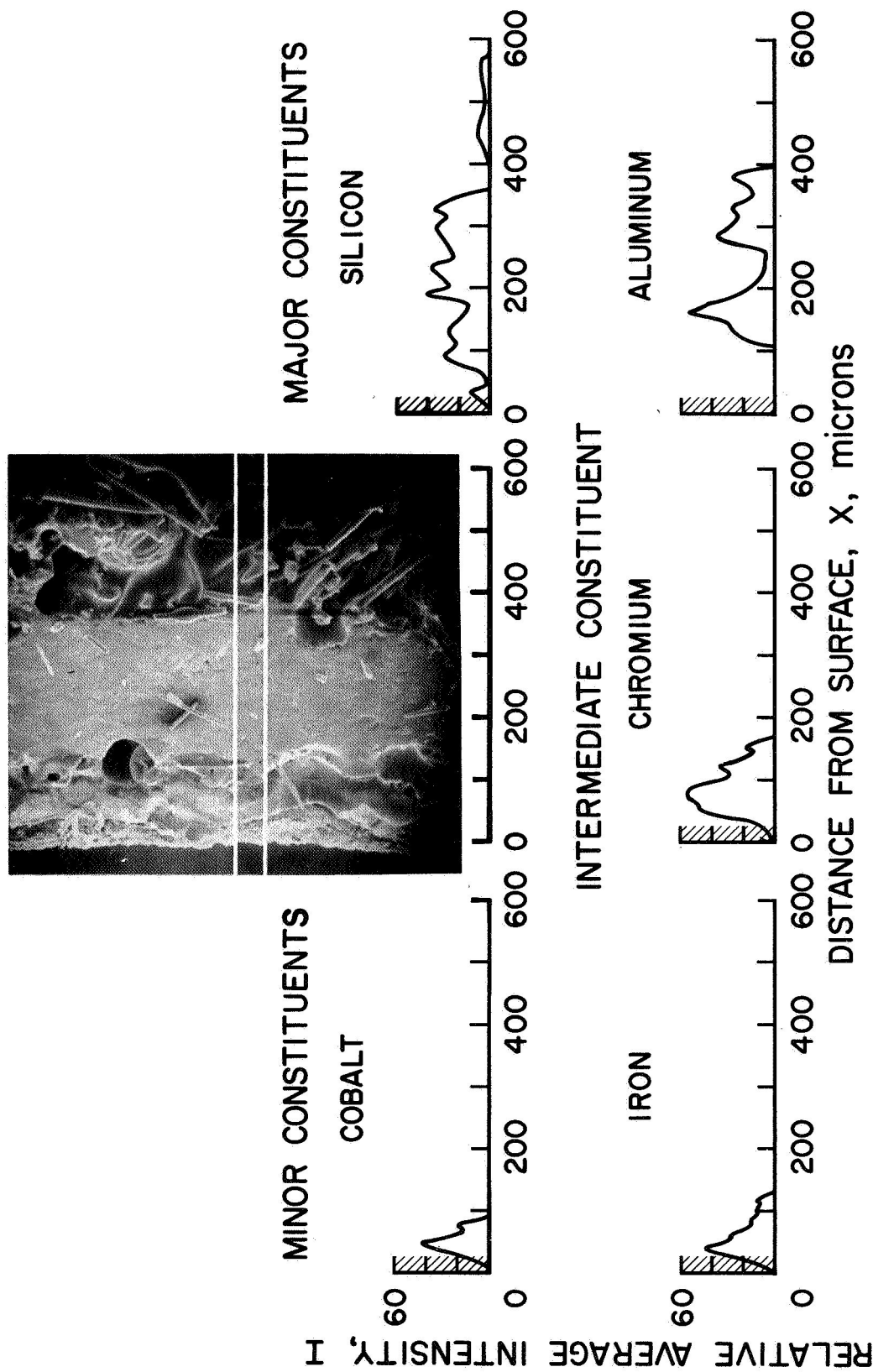


Figure 16

X-RAY FLUORESCENCE CHEMICAL ANALYSIS OF HCF-MOD III COATING
EXPOSED TO ARC PLASMA ENVIRONMENT AFTER 8 CYCLES

(Figure 17)

The analysis of the HCF-MOD III coating in cross section after eight cycles at the 340 kw/m² heating rate is illustrated in this figure. When this coating is compared to the pretest coating, figure 16, several changes are noted. The loss of cobalt and iron from the top layer coincident with the loss of the top coating is the most significant result. The appearance of chromium and aluminum closer to the surface is also indicative of the surface recession of the coating.

X-RAY FLUORESCENCE CHEMICAL ANALYSIS OF HCF-MOD III COATING EXPOSED TO ARC PLASMA ENVIRONMENT AFTER 8 CYCLES

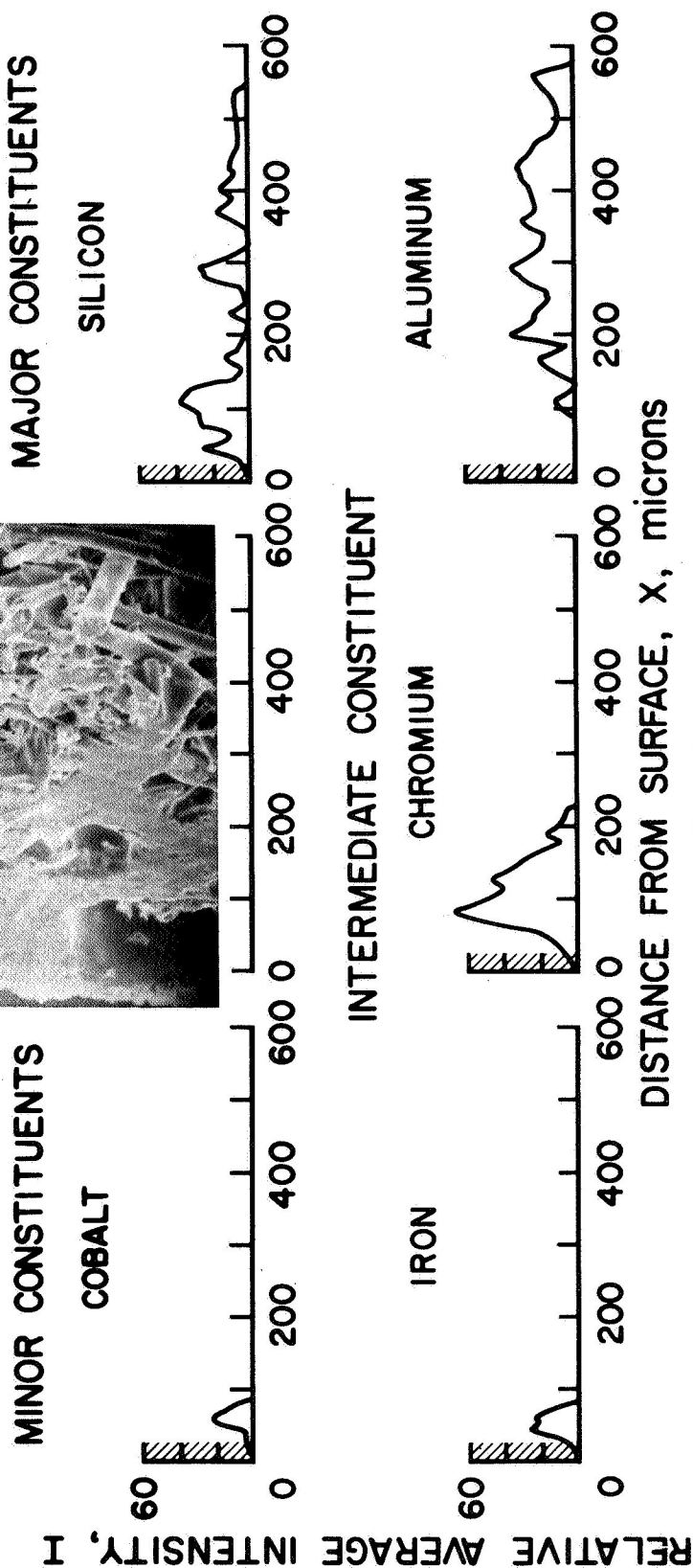
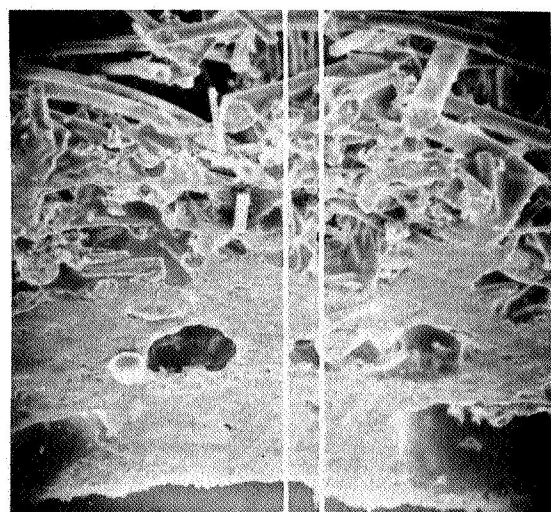


Figure 17

X-RAY FLUORESCENCE ANALYSIS OF CROSS SECTION OF REI-MOD 1A COATING
PRETEST

(Figure 18)

This figure illustrates the analysis of the REI-MOD 1A coating in cross section before testing. Although the results of this analysis indicate that the elements in the coating (nickel, titanium, aluminum, and silicon) are, in general, uniformly distributed, some areas of non-uniformity exist. Analysis for lithium, one of the major constituents of the coating, was not obtainable using this technique.

X-RAY FLUORESCENCE ANALYSIS OF CROSS SECTION OF REI-MOD IA COATING PRETEST

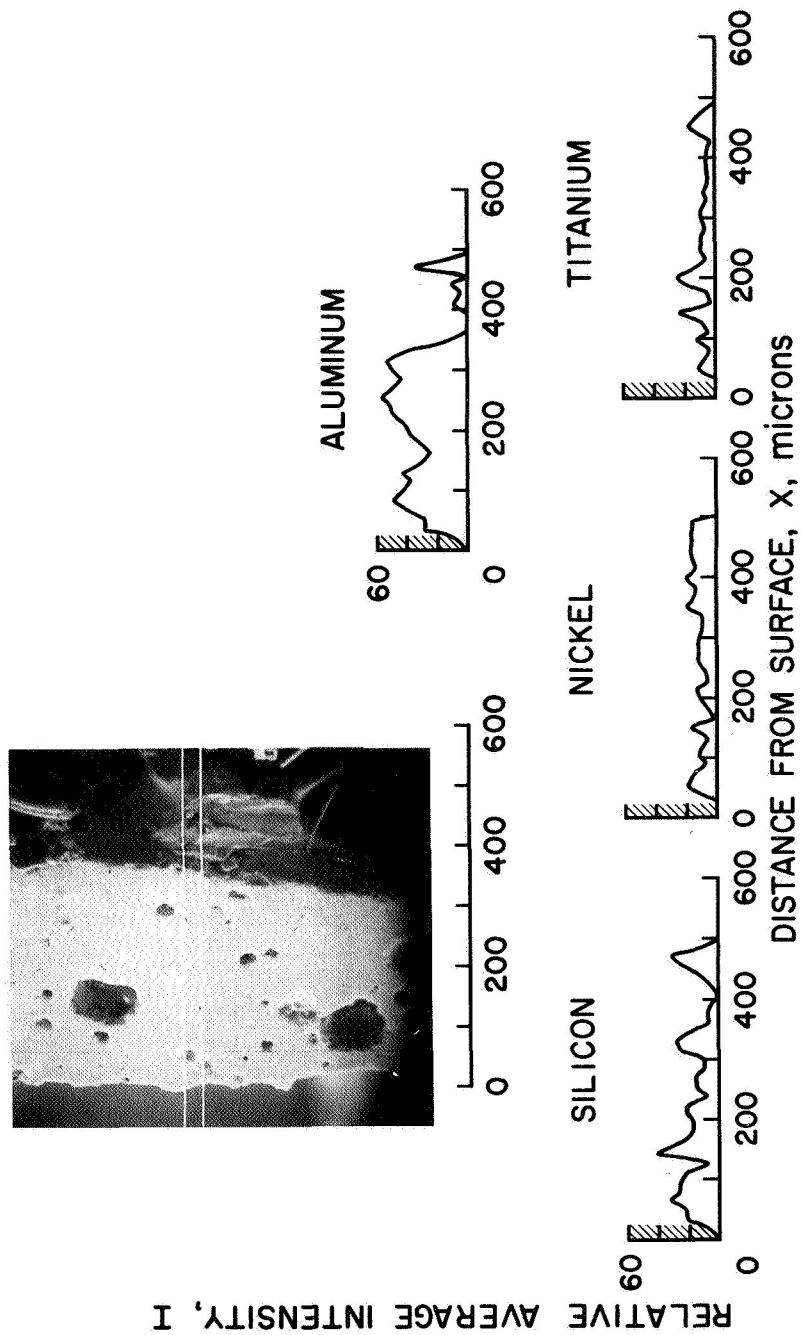


Figure 18

X-RAY FLUORESCENCE ANALYSIS OF CROSS SECTION OF REI-MOD 1A COATING
AFTER 8 CYCLES

(Figure 19)

An analysis of the REI-MOD 1A coating in cross section after eight cycles at the 340 kw/m^2 heating rate is illustrated in this figure. Little change in the location of components within the initially uniformly distributed coating is noted although it does appear that titanium is beginning to diffuse toward the surface. The difference between the top layer of the coating and the coating, in general, is still visible in the scanning electron microscope although no chemical difference can be found between the two layers utilizing this type of analytical technique. The change in appearance may be partly attributable to the loss of lithium from the coating, which cannot be detected with this technique, and to an increased foaming of the glass surface.

X-RAY FLUORESCENCE ANALYSIS OF CROSS SECTION OF REI-MOD 1A COATING AFTER 8 CYCLES

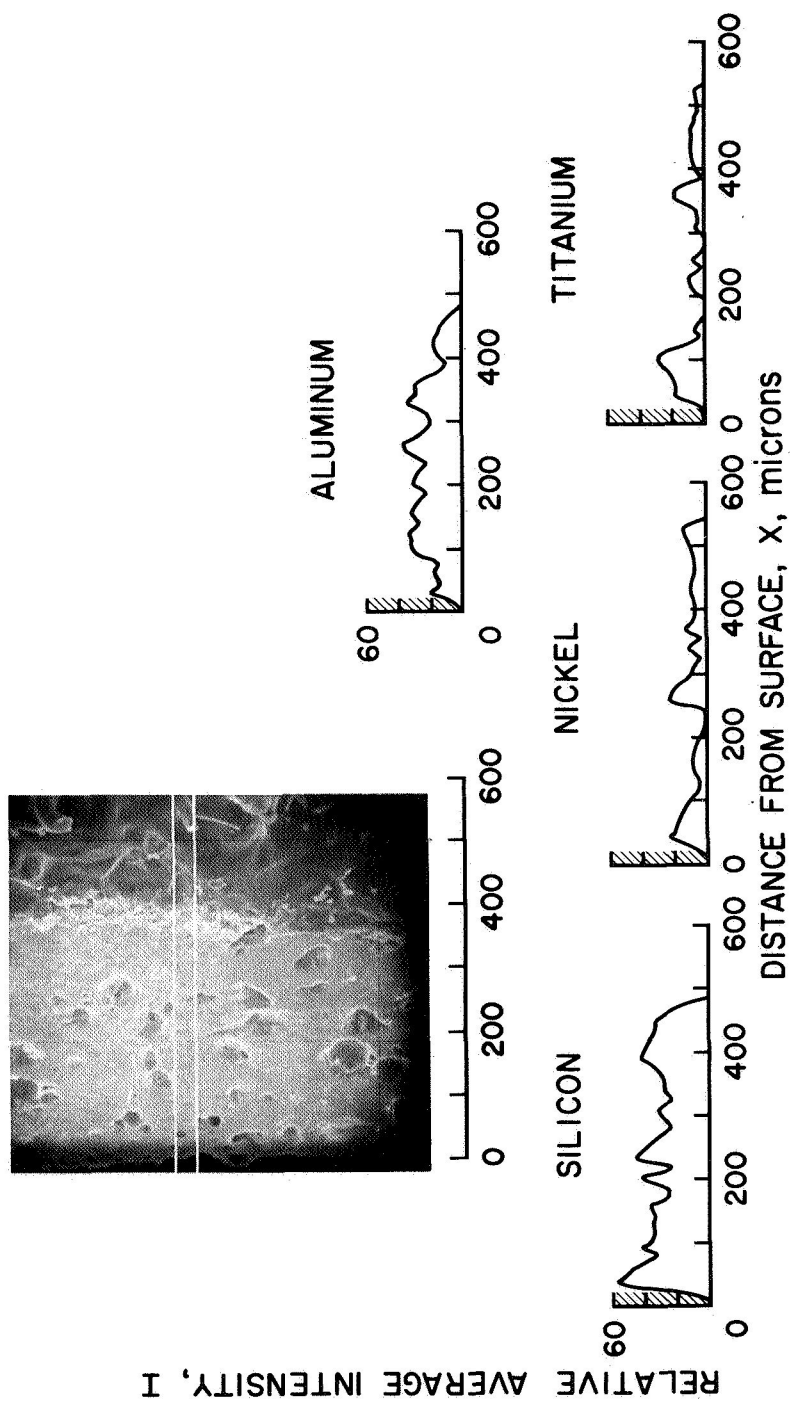


Figure 19

CONCLUSIONS

(Figure 20)

The response of RSI coatings to a convective heating environment has been described in terms of the morphological and surface chemistry changes that occur after cyclic testing. The loss of high vapor pressure molecular species to the convectively heated environment has been described for the HCF-MOD III and REI-MOD 1A coatings. The LI-1542 coating is also probably losing volatile species which are not detectable with the analytical techniques utilized but only to a limited extent. Each coating's reaction to the convectively heated environment was unique with the HCF-MOD III exhibiting the most significant response while the LI-1542 coating exhibited the least. The most significant result is that the response of RSI coatings to a radiant heating environment which is normally used to simulate the thermal history of space shuttle's reentry is chemically different from the coating's response to a convectively heated environment. This conclusion indicates, in particular, that the effect of convective heating on coatings must be evaluated in an arc plasma environment, rather than in a radiant heating environment.

CONCLUSIONS

- THE LOSS OF HIGH VAPOR PRESSURE MOLECULAR SPECIES TO THE CONVECTIVELY HEATED ENVIRONMENT IS OBSERVED IN HCF-MOD III COATING AND RESULTS IN A MEASURABLE AMOUNT OF SURFACE RECESSION.
- THE LOSS OF HIGH VAPOR PRESSURE MOLECULAR SPECIES TO THE CONVECTIVELY HEATED ENVIRONMENT IS OBSERVED ON THE REI-MOD IA SURFACE BUT NO MEASURABLE SURFACE RE-CESSION IS OBSERVED.
- THE HCF-MOD III COATING EXHIBITS THE MOST SIGNIFICANT CHEMICAL AND MORPHOLOGICAL CHANGES WHEN EXPOSED TO A CONVECTIVELY HEATED ENVIRONMENT.
- THE REI-MOD IA APPEARS TO FOAM IN RESPONSE TO THE CONVECTIVELY HEATED ENVIRONMENT.
- THE LI-1542 COATING EXHIBITS THE LEAST CHEMICAL AND MORPHOLOGICAL CHANGES WHEN EXPOSED TO A CONVECTIVELY HEATED ENVIRONMENT
- RSI COATING RESPONSE TO RADIANT HEATING IS DIFFERENT THAN TO CONVECTIVE HEATING.

REFERENCES

1. Tanzilli, R.A. (Ed.): Development of an External Ceramic Insulation for the Space Shuttle Orbiter. NASA-CR-112038, April 1972.
2. Buttram, R.D., Space Shuttle Thermal Protection System Development. Final Report, January 17, 1972, NAS9-12083.
3. Lehman, J.K., Rusert, E.L., Kummer, D.L. and Christensen, H.E.: Reusable Surface Insulation (RSI) Thermal Protection Development for Shuttle. Final Report, March 21, 1972, NAS9-12082.

REUSABLE SURFACE INSULATION THERMAL PROTECTION SYSTEMS
TEST EVALUATION STATUS

George Strouhal and Donald J. Tillian

NASA - Manned Spacecraft Center
Houston, Texas

INTRODUCTION

The economical development of a space shuttle depends on the development of low cost, light weight, reliable systems for the orbiter vehicle. One of the systems in the success of the space shuttle is the thermal protection system (TPS). The TPS must be designed to perform multiple missions and be capable of withstanding static and dynamic loads as well as the other environments induced by launch, orbit, entry, and ground handling. Several TPS materials and concepts have been proposed; the most promising from weight, cost, and design simplicity viewpoints utilizes reusable surface insulation (RSI) materials.

This paper discusses the design requirements used in the RSI technology development programs, and the results of recent test programs conducted at NASA-MSC in support of the RSI design developments. These test programs have provided information concerning the thermal/structural performance of candidate RSI materials and designs. The tests have also provided design development guidance and an insight into the necessary test programs and logic for TPS verification.

SUMMARY SCHEDULE OF RSI TECHNOLOGY DEVELOPMENTS

(Figure 1)

This figure illustrates the various phases of the RSI technology programs and the test programs conducted in support of the evolving RSI materials and design concepts. In early 1970, MSC initiated a screening program to evaluate these classes of materials for possible use on the space shuttle vehicle. Test evaluations on six candidate materials consisted primarily of arc jet screening and limited thermal and mechanical property tests. Based on the early arc jet evaluations, a decision was made to initiate a material development program (Phase I) on the silica LI-1500 and mullite MOD I materials with Lockheed and McDonnell-Douglas, respectively. This activity was expanded in the Phase II technology development program with three sources; Lockheed for a silica system (LI-1500), McDonnell-Douglas, and General Electric for mullite systems MOD III and MOD IA, respectively. The Phase II program emphasized design, development, and basic improvement of the RSI materials. During the Phase I and Phase II periods, extensive thermal/structural tests were conducted on prototype TPS panels with full-scale components. Preliminary property data were also generated to support design activities. The current technology program (Phase III) is a continuation of design development with the selected three RSI contractors and is concerned primarily with improving TPS attachment techniques, RSI material and coating improvement, and the gathering of design property data. McDonnell Douglas has concentrated on simplifying their coating process for HCF MOD III, while General Electric has been involved in a basic material process modification that has resulted in a mullite RSI MOD IB material with improved mechanical properties. Lockheed has continued with their basic silica material process and has concentrated on reducing bulk density, which has resulted in a LI-900 material with a bulk density of 144.18 kg/m³ (9 lb/ft³). During January 1973, one material system will be selected for the shuttle TPS from the three candidate RSI materials.

SUMMARY SCHEDULE OF RSI TECHNOLOGY DEVELOPMENTS

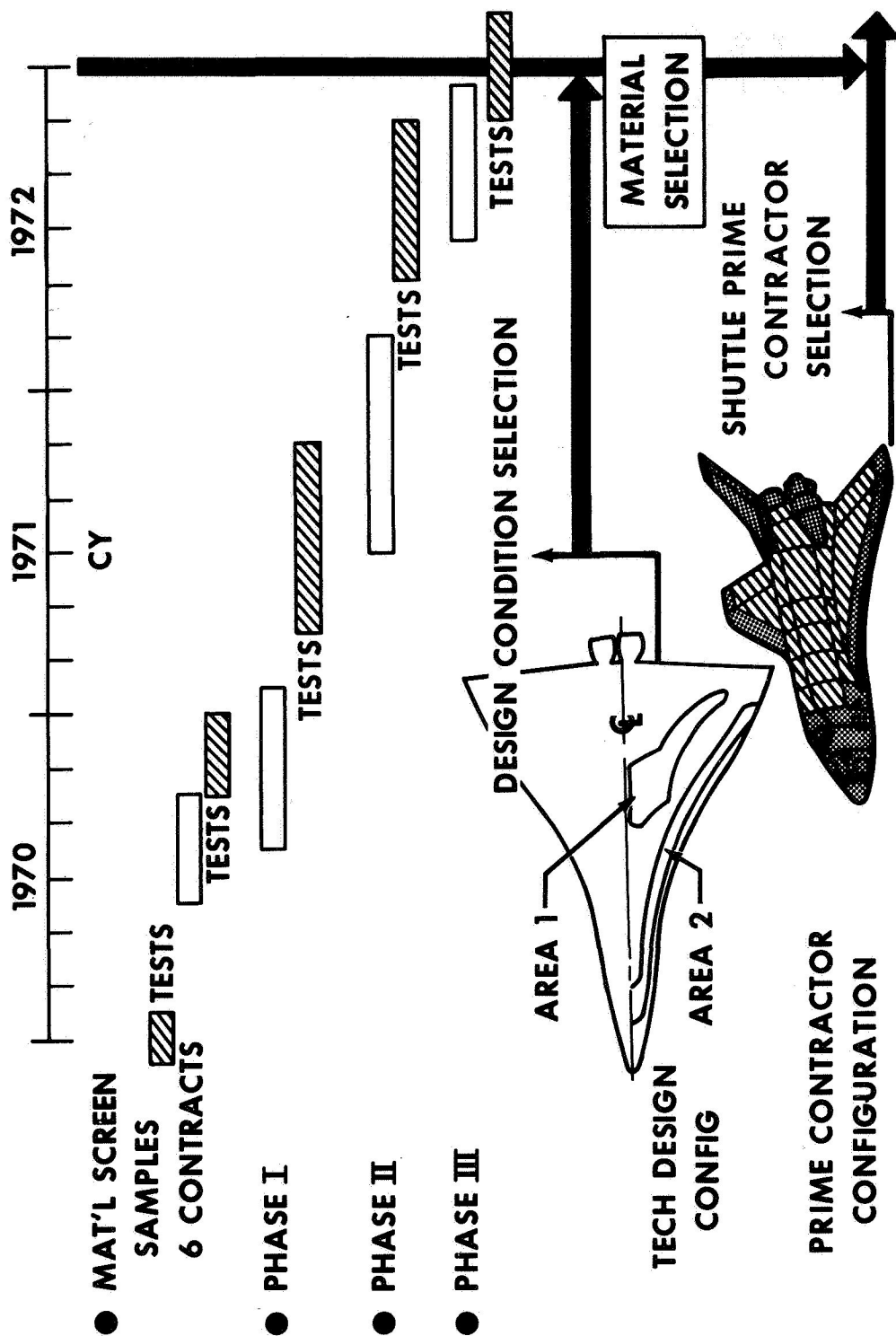


Figure 1

COMPARISON OF ENTRY HEATING HISTORIES

(Figure 2)

Reference heating rate histories to a 0.35 m (1 ft) radius sphere for the current North American baseline trajectory and the RSI technology baseline trajectory selected in the summer of 1971 are shown in this figure. It will be noted that the peak rates are similar for the two trajectories; the primary difference between the two is the shorter entry time of the current baseline trajectory.

COMPARISON OF ENTRY HEATING HISTORIES

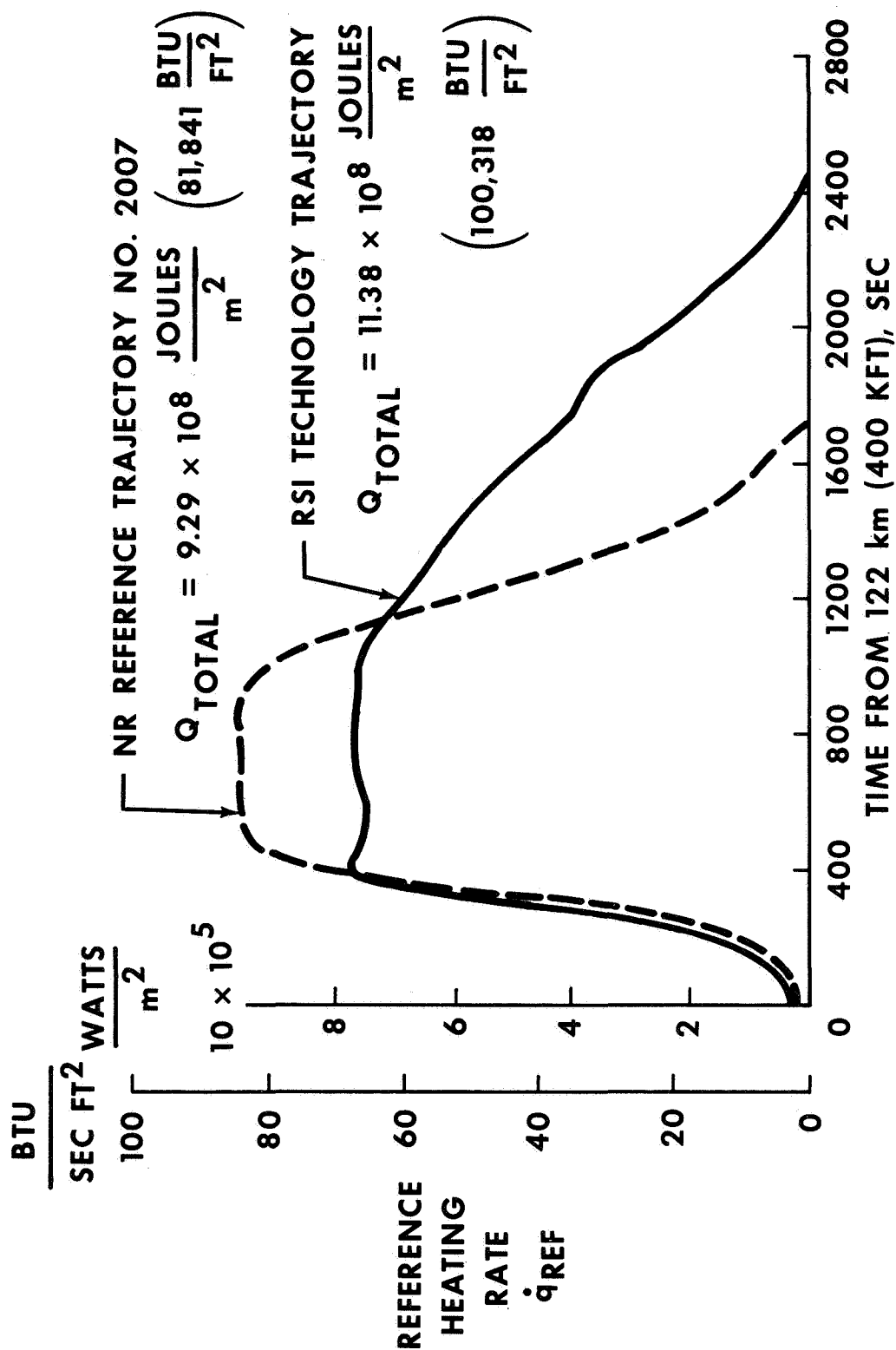


Figure 2

DISTRIBUTION OF PEAK SURFACE TEMPERATURE
RSI TECHNOLOGY BASELINE

(Figure 3)

Peak surface temperatures during entry were calculated for the reference heating rate trajectory shown in the previous figure and laminar heating rate distribution data obtained from wind tunnel tests. Isotherms for the vehicle lower surface are shown in this figure. Design requirements for prototype RSI panels were obtained by calculating heating environments and structural loads for two general locations on the vehicle lower surface. These locations are identified as Area 1 and 2 with boundaries as indicated. Area 1 experiences a peak temperature of 1035°K (1400°F) which is representative of the general acreage on the orbiter vehicle. The Area 2 panels were designed and thermally sized for a peak temperature of 1533°K (2300°F) with a capability for an overshoot test to 1643°K (2500°F).

Although 1476°K (2200°F) is more representative of Area 2 temperatures, 1533°K (2300°F) was selected for design. The combination of temperature with Area 2 loads is identified as an Area 2 perturbed (Area 2P) design.

DISTRIBUTION OF PEAK SURFACE TEMPERATURES
RSI TECHNOLOGY BASELINE

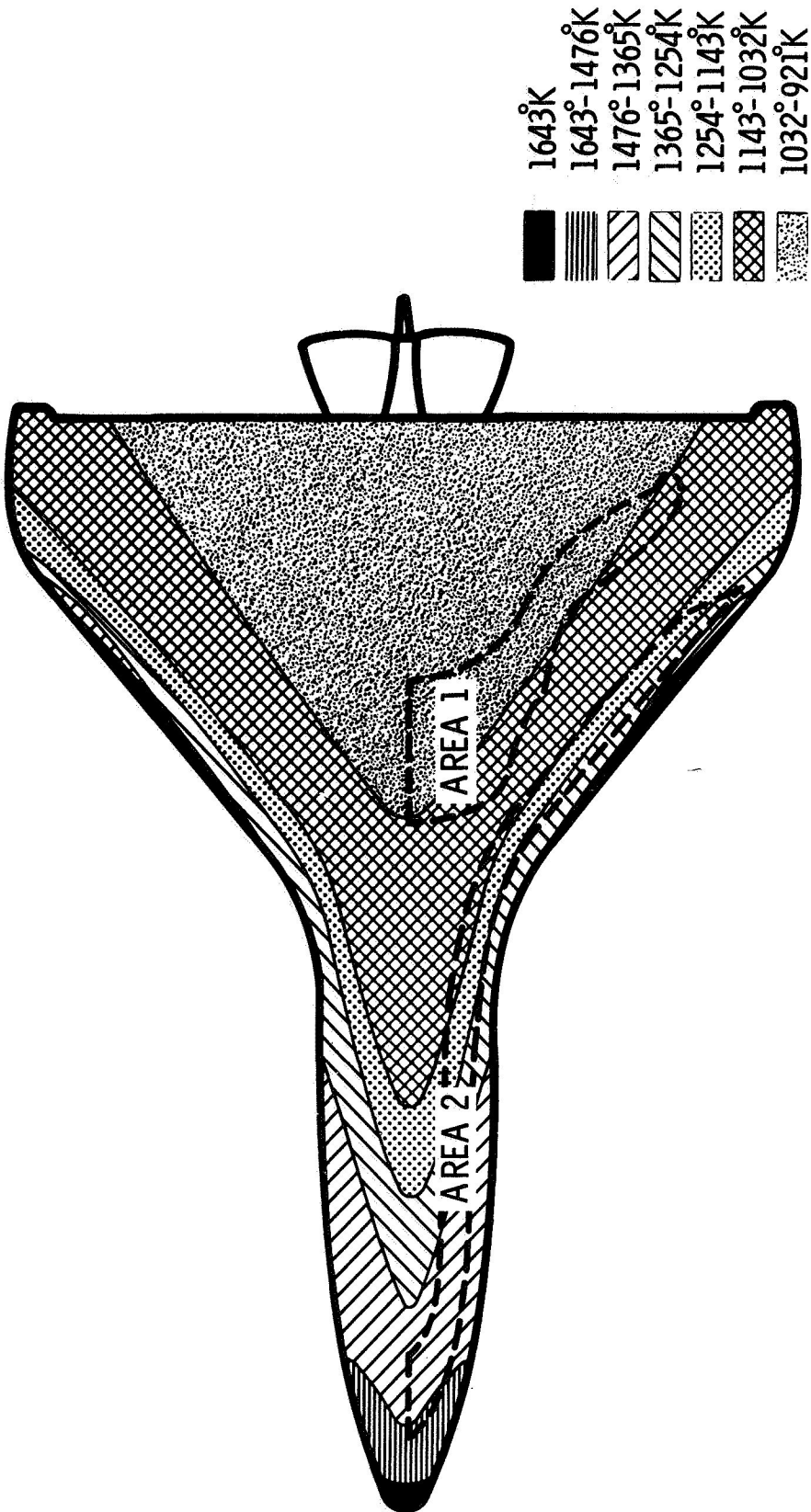


Figure 3

PEAK EQUILIBRIUM SURFACE TEMPERATURE/VEHICLE AREA DISTRIBUTION

(Figure 4)

Orbiter surface temperature distributions were calculated for each of the two reference entry trajectories shown previously and correlated as a function of area as shown in this figure. For any vehicle surface temperature selected on the abscissa, the ordinate value shows the percentage vehicle area at or above the selected temperature. Only a small percentage of the vehicle will be exposed to the peak temperature of 1533°K (2300°F) selected for Area 2P prototype TPS panel design. The temperature distribution for the NR reference trajectory is similar to that for the RSI technology trajectory shown.

PEAK EQUILIBRIUM SURFACE TEMPERATURE/ VEHICLE AREA DISTRIBUTION

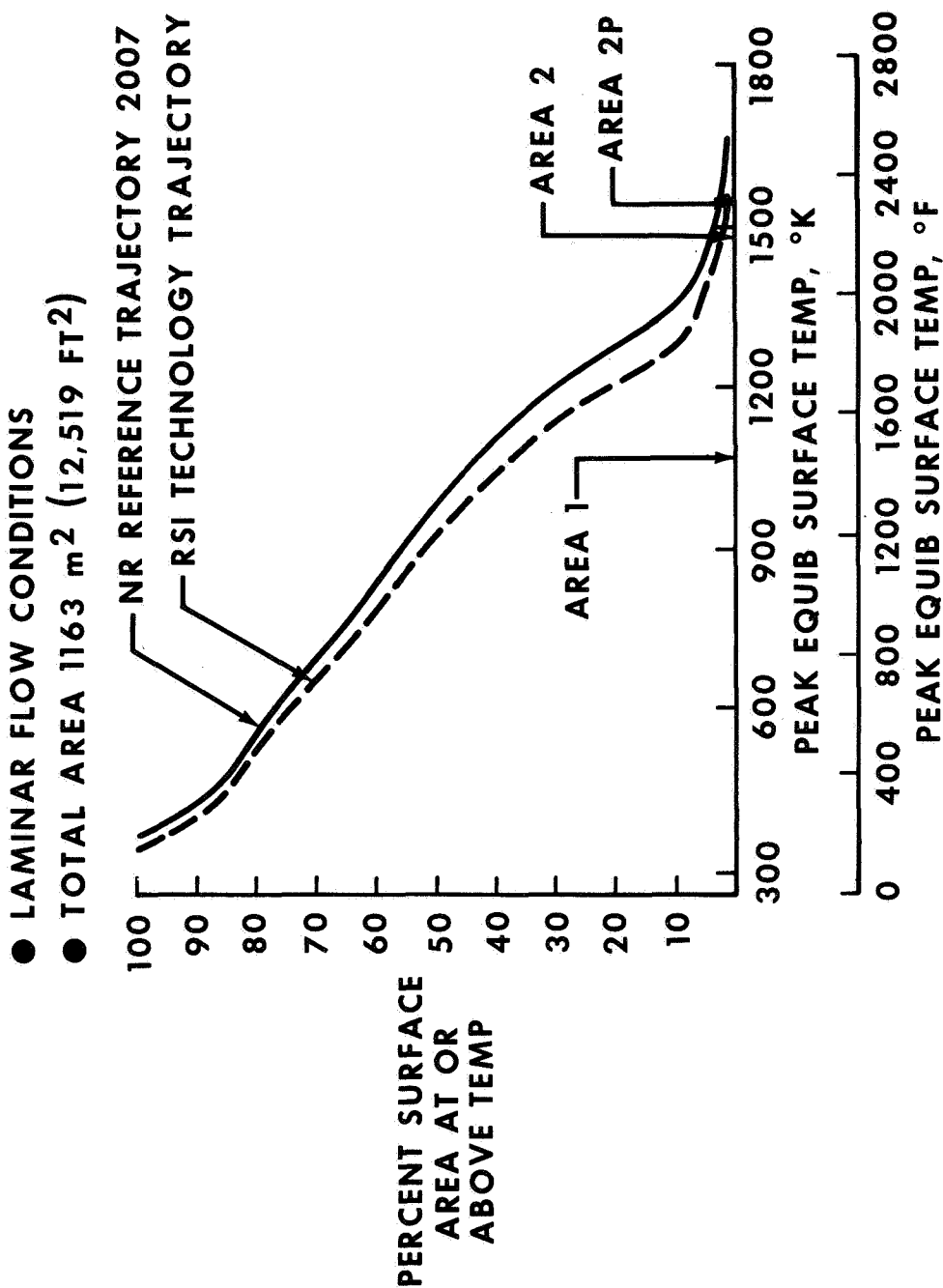


Figure 4

TEMPERATURE CHANGE RATE VERSUS EQUILIBRIUM SURFACE TEMPERATURE

(Figure 5)

In addition to peak temperature levels, one of the more critical environmental variables for the design of RSI thermal protection systems is the surface temperature change rate during entry. Surface temperature change rate is indicative of in-depth temperature gradients, which create thermal stress conditions within the thickness of RSI materials. Temperature change rate is plotted versus temperature for Area 2P for both the NR and RSI technology reference trajectories in this figure. For both trajectories, peak temperature change rates of $+3.3^{\circ}\text{K/sec}$ (6°F/sec) occur early in the entry phase (250 sec) at surface temperatures of 1050°K (1425°F). Thermal stress distribution surveys during entry tend to confirm that critical thermal stress occur at or around 250 seconds into the entry trajectory. After peak temperature levels of 1533°K (2300°F), temperature decrease rates are about one half of the temperature rise rates.

TEMPERATURE CHANGE RATE VERUS EQUILIBRIUM SURFACE TEMPERATURE

AREA 2P

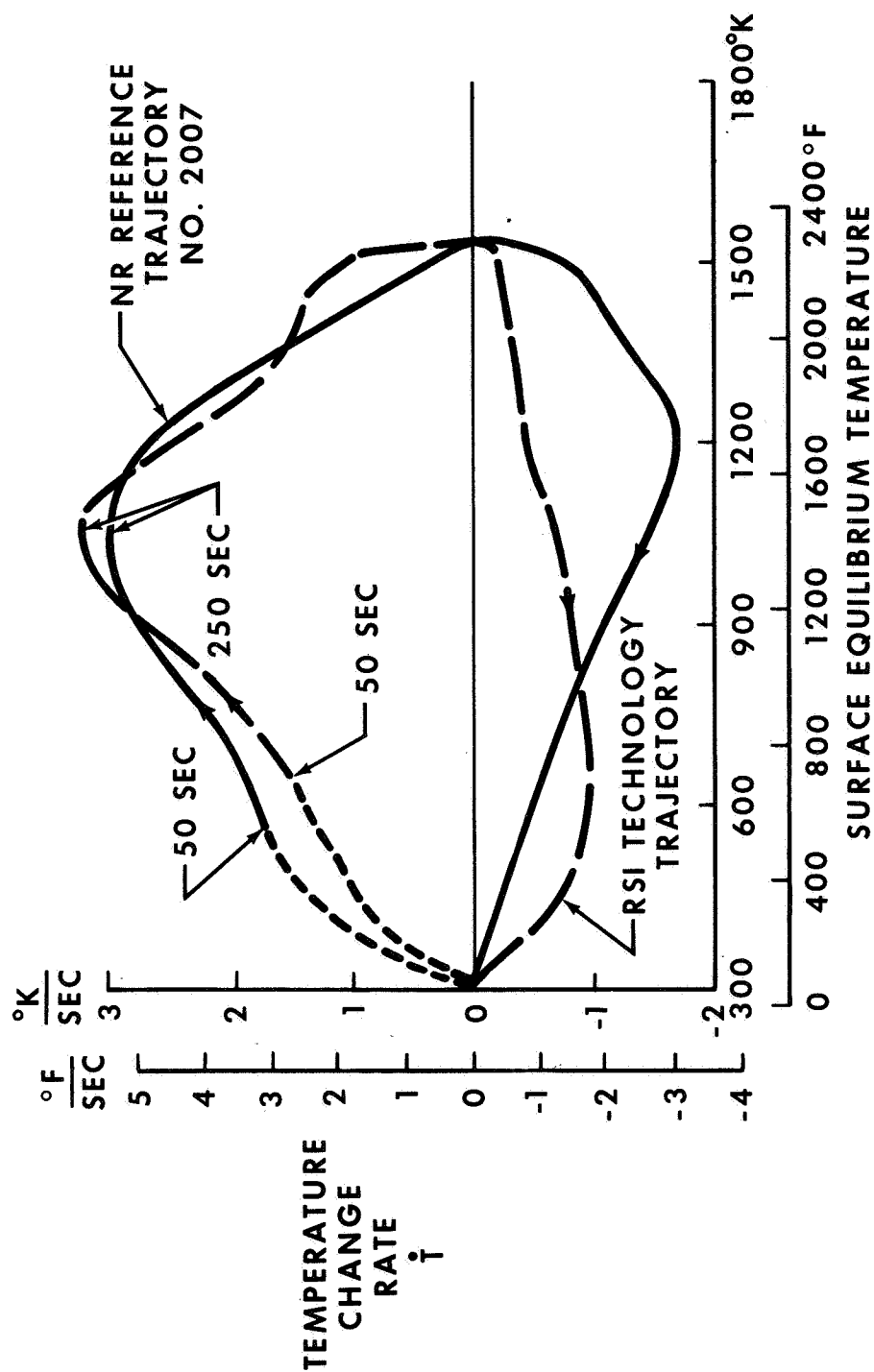


Figure 5

PRELIMINARY RSI MATERIAL PROPERTIES
USING SMALL SAMPLE STATISTICS

(Figure 6)

Available room temperature mechanical strength data have been analyzed statistically to obtain 90 percent exceedence values with 95 percent confidence levels using small sample statistics. Longitudinal and transverse direction tensile strengths and moduli for Phase II and III RSI materials are shown in this figure along with the number of sample data points used in the statistical analysis. Comparison indicates that the mullite materials have higher tensile strengths in the transverse direction than the silica materials. The scatter in properties appear to be higher for the silica materials than the mullite materials. It should be noted that the values shown represent as-received materials and do not contain data reflecting degradation effects of cyclic exposure to simulated entry environments.

PRELIMINARY RSI MATERIAL PROPERTIES USING SMALL SAMPLE STATISTICS

	GE MULLITE MOD 1A	GE MULLITE MOD 1B	LMSC SILICA LI-1500	LMSC SILICA LI-900	MDAC MULLITE MOD III
TENSILE STRENGTH $N/m^2 \times 10^{-5}$ LONGITUDINAL 90% EXCEEDENCE (PSI)	5.23 \pm 2.09 3.14 (45.7) [21]	10.1 \pm 2.03 8.07 (116.5) [39]	6.30 \pm 3.50 2.80 (40.6) [18]	3.49 \pm .77 2.72 (39.5) [10]	6.68 \pm 2.61 4.07 (59.1) [10]
TENSILE STRENGTH $N/m^2 \times 10^{-5}$ TRANSVERSE 90% EXCEEDENCE (PSI)	1.79 \pm .52 1.27 (18.4) [38]	2.27 \pm .67 1.60 (23.2) [35]	1.05 \pm .28 .77 (11.3) [11]	1.10 \pm .68 .42 (6.1) [10]	2.41 \pm .77 1.64 (23.9) [6]
TENSILE MODULUS $N/m^2 \times 10^{-5}$ LONGITUDINAL 90% NON-EXCEEDENCE (PSI $\times 10^{-3}$)	2900 \pm 970 3870 (56) [21]	3650 \pm 1240 4890 (71) [39]	5210 \pm 3100 8310 (120.6) [18]	1620 \pm 480 2100 (30.5) [10]	4340 \pm 2060 6400 (92.9) [10]
TENSILE MODULUS $N/m^2 / 10^{-5}$ TRANSVERSE 90% NON-EXCEEDENCE (PSI $\times 10^{-3}$)	621 \pm 145 766 (11.1) [38]	441 \pm 172 613 (8.9) [35]	565 \pm 248 813 (11.8) [11]	400 \pm 220 620 (9.0) [10]	117 \pm 65 182 (26.5) [6]
					NUMBER OF SAMPLES

Figure 6

THERMAL CONDUCTIVITY COMPARISONS

(Figure 7)

Thermal conductivities as a function of mean temperature at atmospheric pressure are shown in this figure for both silica and mullite RSI materials. Data measured by each of the RSI contractors are shown along with data measured by Battelle Memorial Institute (BMI) under contract to NASA-MSC. Some of the significant difference in conductivity values obtained by the different data sources can be attributed to measurement techniques. Despite these differences, the data shown as shaded areas for silica and mullite RSI still show that the conductivity of the silica is significantly lower than that of the mullite materials. Conductivity is dependent on pressure as well as temperature, and similar trends are exhibited at lower pressure on the order of $1.01 \times 10^3 \text{ N/m}^2$ (10^{-2} atm).

THERMAL CONDUCTIVITY COMPARISONS AT ATMOSPHERIC PRESSURE

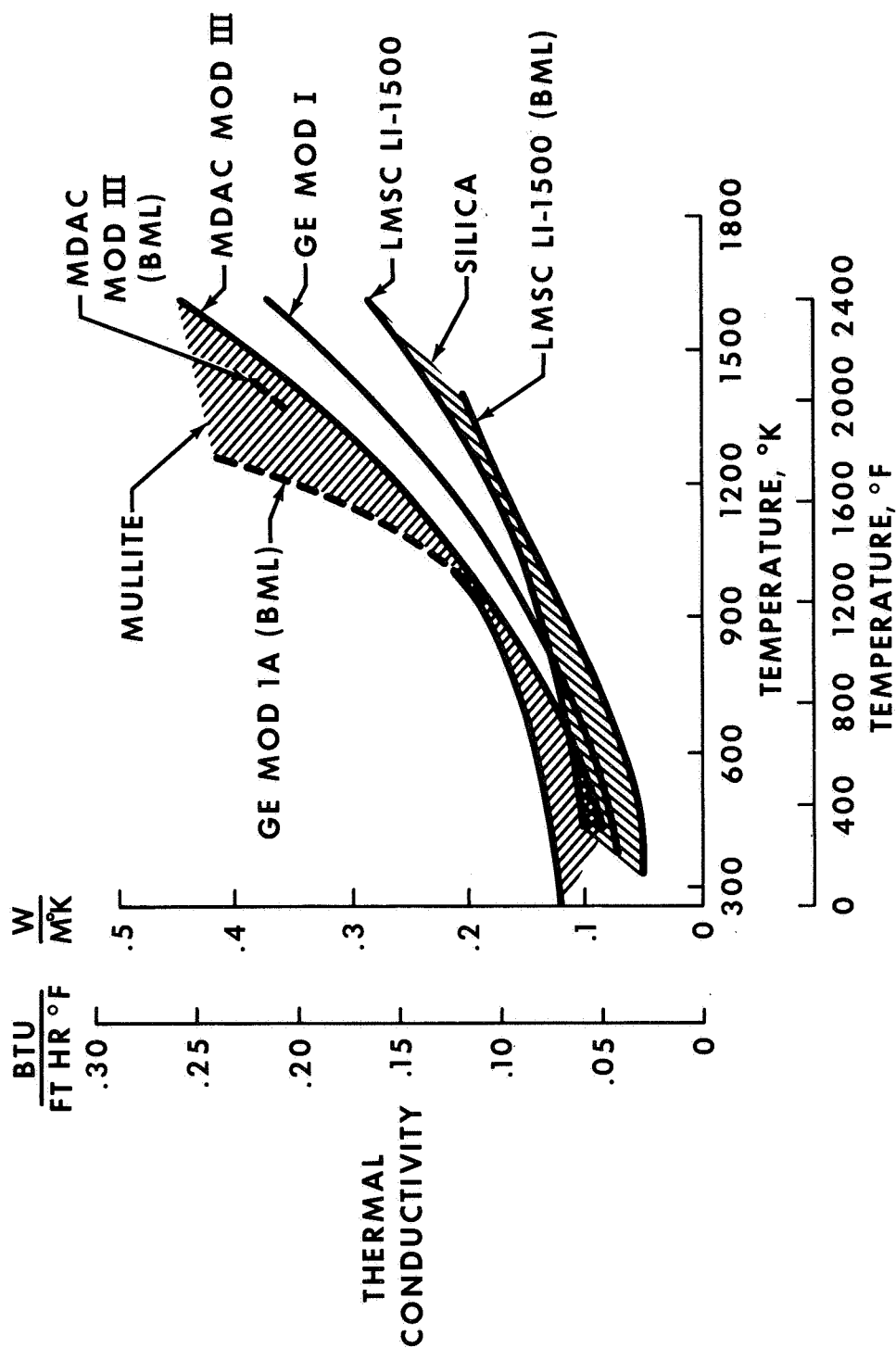


Figure 7

THERMAL CRACKING RESISTANCE

(Figure 8)

To provide some measure of resistance to cracking by thermal stresses during entry, a combination of thermal-mechanical properties as defined in this figure has been utilized to formulate a comparative cracking resistance index for the different materials. A high index value for a material is indicative of a greater resistance to cracking. Although this thermal cracking resistance index is neither dimensionless nor a fundamental property, it indicates how properties combine to influence the tendency of the RSI materials to crack under thermal stresses. Index values have been calculated for each of the RSI materials using average properties and type "B" properties (minimum strength, maximum modulus) at room temperature. Comparison of the indices for silica with those for mullite RSI shows that silica should be far less susceptible to thermal cracking than mullite.

THERMAL CRACKING RESISTANCE **IN-PLANE TENSION** **ROOM TEMPERATURE PROPERTIES**

PARAMETER	$\frac{^{\circ}\text{K}}{\rho C_p}$	$\frac{F_y}{E\alpha}$	$\frac{M^2}{\text{SEC}} \times 10^{-3}$	AVG PROPERTIES	TYPE B PROPERTIES
GE MULLITE (MOD IA)				15.6	7.1
GE MULLITE (MOD IB)				23.9	14.3
LMSC SILICA (LI-1500)				80.8	22.5
LMSC SILICA (LI-900)				241	144
MDAC MULLITE (MOD III)				17.1	9.8

Figure 8

PROTOTYPE TPS PANEL CONFIGURATIONS AND WEIGHT COMPARISONS FOR
AREA 2P, ALUMINUM STRUCTURE

(Figure 9)

This chart shows the total and component weights for the three designs for the Area 2P TPS AL panels delivered under the Phase II technology contracts. The weights of the aluminum primary structure are approximately the same even though the stiffeners on the structures were significantly different. The mullite TPS weights reflect the use of strain isolating foam bonds. This figure also shows the types of gap configurations selected by each contractor. The LMSC panel reflects a butt overlap with a filler strip, the MDAC panel--a straight butt joint, and the GE panel--a butt configuration with a roving fiber filler.

PROTOTYPE TPS PANEL CONFIGURATION AND WEIGHT COMPARISONS FOR AREA 2P, ALUMINUM STRUCTURE

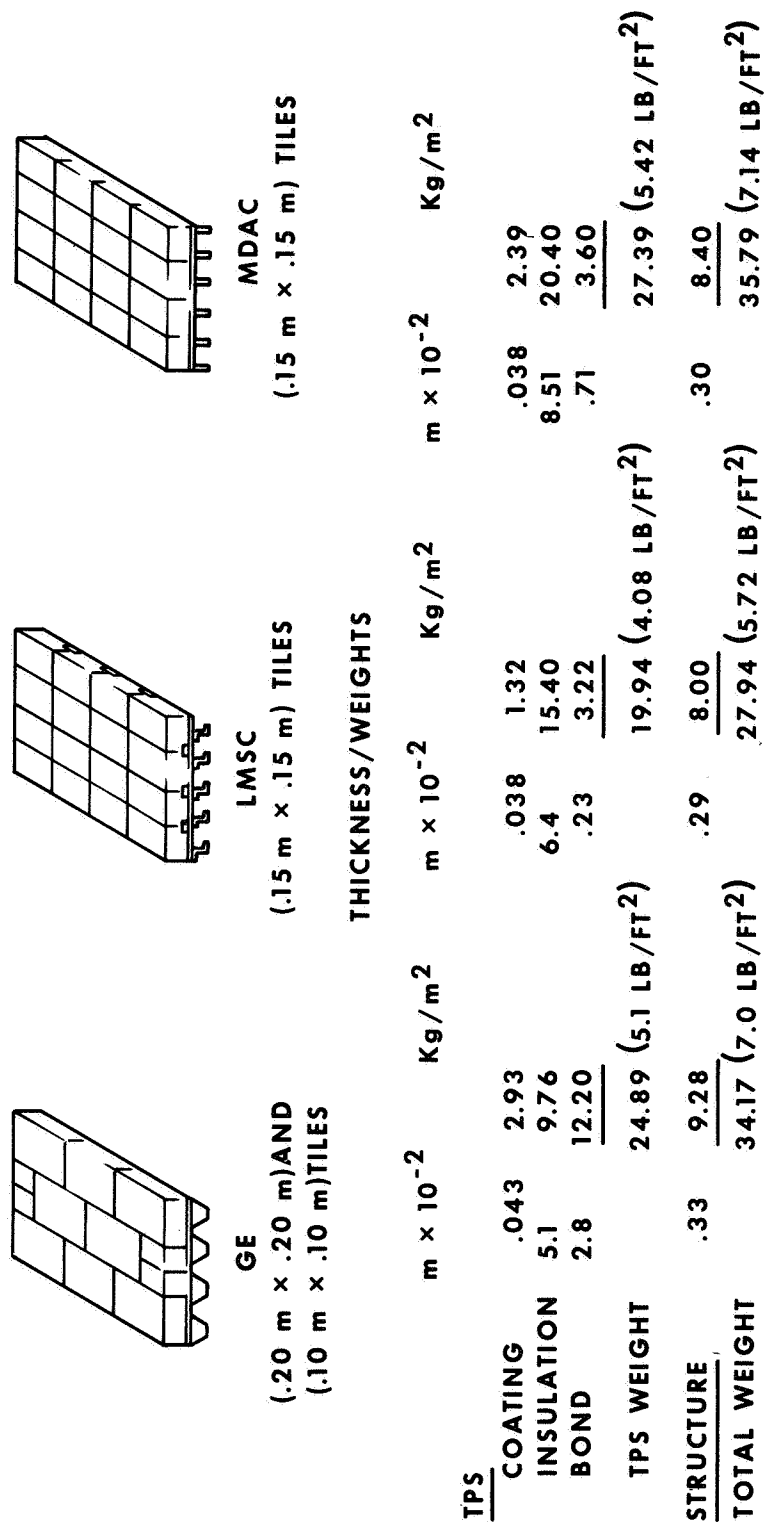


Figure 9

TESTING CONDITIONS AND TESTING SEQUENCE FOR RSI PROTOTYPE PANELS

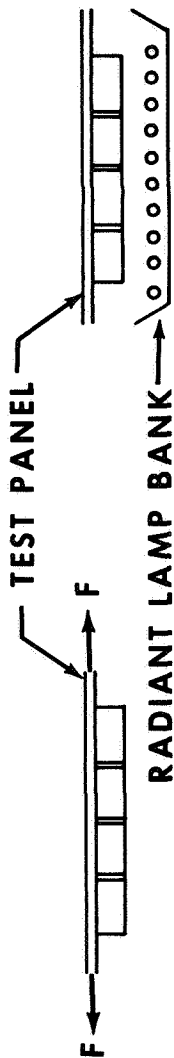
I. INITIAL EXPOSURE

(Figure 10)

The majority of the shuttle orbiter critical environments occur sequentially, and the tests performed reflect this sequence. The initial test consisted of tensile axial loading of the aluminum primary structure. Next, a thermal test was conducted at 1200°K (1700°F) with a room temperature start. The initial thermal test was performed at conditions substantially less than design to check out instrumentation, test procedures, and the interaction between the panel and the induced heating environment.

TEST CONDITIONS AND TESTING SEQUENCE FOR RSI PROTOTYPE PANELS

I INITIAL EXPOSURE



(a) AXIAL LOAD TEST AT ROOM TEMP (b) 1200°K (1700° F) TEST, NO LOAD

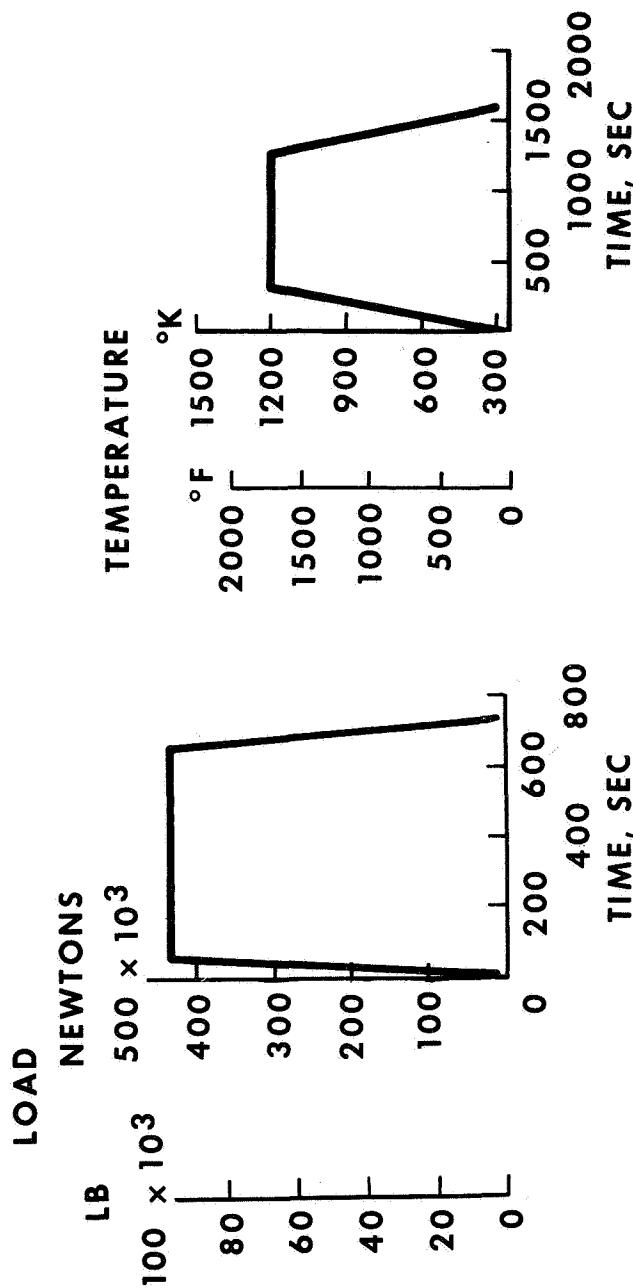


Figure 10

TESTING CONDITIONS AND TESTING SEQUENCE

II. FINAL EXPOSURES

(Figure 11 and Figure 12)

The next two figures show the subsequent multiple test environments selected for the RSI thermal structural test program. The sequential tests were conducted in multiples of five cyclic exposures consisting of thermal exposure at design temperature, 1533°K (2300°F), followed by load at atmospheric conditions and/or thermal exposure at design temperature under flight pressure conditions. Acoustic tests consisting of a single exposure for an equivalent test time of five missions followed the thermal tests. The thermal tests at atmospheric conditions were conducted at a cold start temperature of 172°K (-150°F) to permit simulation of full Area 2P heat pulse. Bondline temperatures were monitored during each test to prevent overtemperature of the structure, which was limited to 422°K (300°F) for the aluminum panels and 589°K (600°F) for the titanium panels. The tests were grouped in blocks of five exposures to minimize test article handling and minimize serial time including test preparation in the thermal and acoustic facilities. The atmospheric pressure thermal tests were conducted with standard quartz tube heaters; the reduced pressure tests were conducted in an evacuated chamber using graphite elements in combination with a columbium susceptor plate. The acoustic tests were conducted in a progressive wave tube operating at an overall 160 dB level.

TEST CONDITIONS AND TESTING SEQUENCE

II FINAL EXPOSURES (IN MULTIPLES OF FIVE CYCLES)



(a) 1533°K (2300° F) TEST AT ATMOSPHERIC CONDITIONS,
172°K (-150° F) START, PLUS LOAD

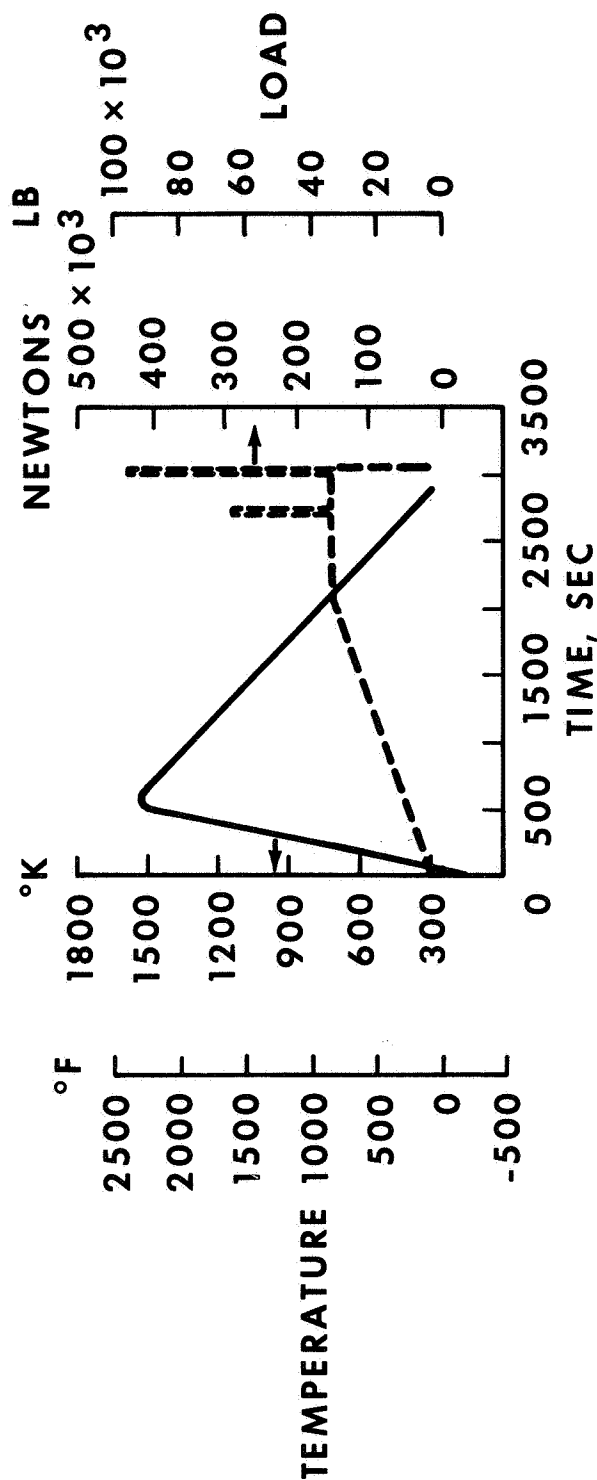
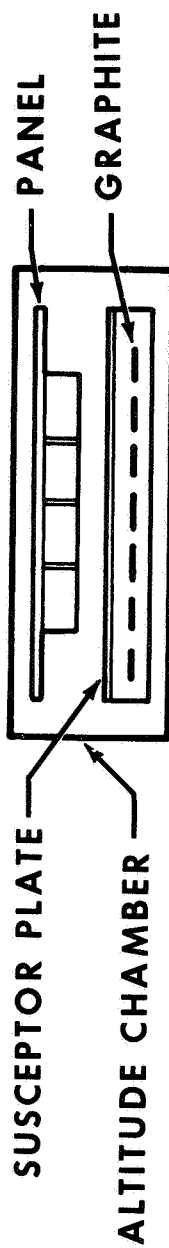


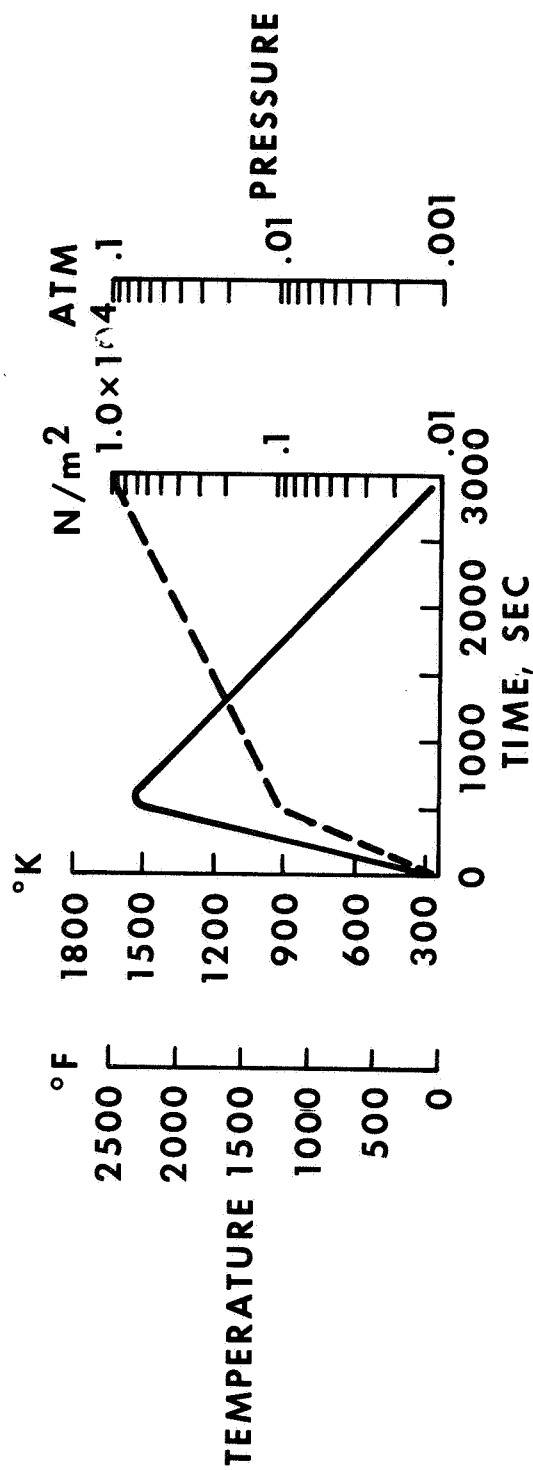
Figure 11

TEST CONDITIONS AND TESTING SEQUENCE

II FINAL EXPOSURES (IN MULTIPLES OF FIVE CYCLES)



(b) 1533°K (2300° F) TEST AT REDUCED PRESSURE, NO LOAD



(c) ACOUSTIC TEST AT ROOM TEMPERATURE x
FIFTEEN SECONDS AT 160 dB OASL

Figure 12

IN-DEPTH TEMPERATURE COMPARISONS

(Figure 13)

This figure illustrates typical thermal performance data obtained during thermal tests at atmospheric pressure. The predictions were obtained from a one-dimensional thermal model using the measured surface temperature as a driver and assuming an adiabatic structural backface. The comparisons between the test and analyses shown for the first 1000 seconds into the simulated entry profile indicate that silica possesses the lowest conductivity of the RSI materials, which tends to confirm the guarded hot plate data.

To achieve the correlation between test data and analysis shown for the mullite RSI, MOD I properties for the General Electric MOD IA material, and properties backed out from thermal tests at McDonnell-Douglas for the MOD III material were used.

IN-DEPTH TEMPERATURE COMPARISONS

- AREA 2P
 - 172°K (-150°F) INITIAL TEMPERATURE
- AT ATMOSPHERIC PRESSURE CONDITIONS

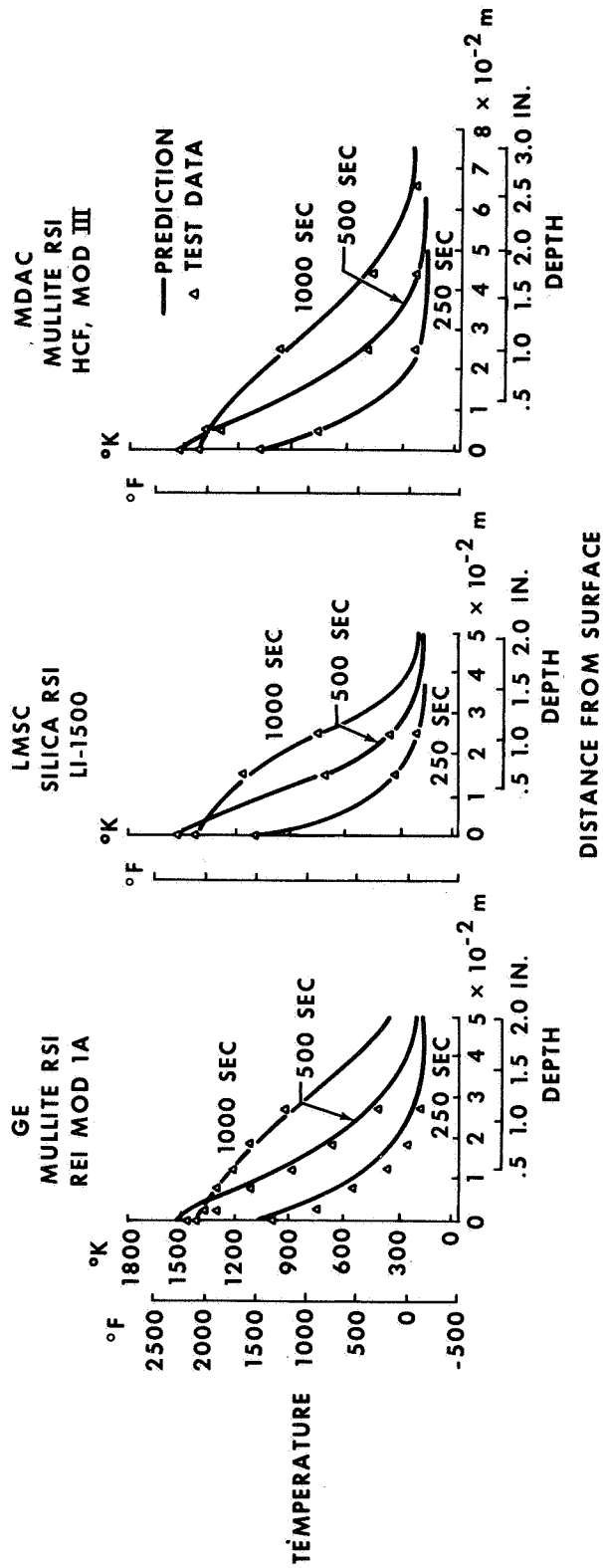


Figure 13

NONDESTRUCTIVE EVALUATION - GENERAL ELECTRIC AREA 2P ALUMINUM PANEL

(Figure 14)

This figure illustrates the RSI panel condition as received, after the axial load test, after five thermal exposures at 1533°K (2300°F) with 172°K (-150°F) start plus axial loading, and after the acoustic environment tests. Some pin holes were observed in several tiles in the as-received condition and after the axial load test. Cracking appeared in several of the RSI tiles after the initial 1200°K (1700°F) heating test. Upon completion of the 1533°K (2300°F) tests, one tile (which has instrumented with thermocouples identified as "tc" on the figure) was cracked extensively and seven other tiles exhibited cracks. The cracked tiles were apparently waterproof based on water drop tests performed in the vicinity of the cracks. During the design temperature tests 1533°K (2300°F) with the 172°K (-150°F) start, it was necessary to use an abbreviated heat pulse to limit temperatures at the RSI/foam bond interface to 533°K (500°F), confirming that the conductivity of the MOD IA material was closer to the MOD I thermal property measurements than to those measured on MOD IA. Subsequent acoustic testing of this panel fractured the instrumented tile; however, the remaining cracked tiles remained intact. Handling damage that occurred during testing is identified as "m" in the figure.

NONDESTRUCTIVE EVALUATION GENERAL ELECTRIC AREA 2P ALUMINUM PANEL

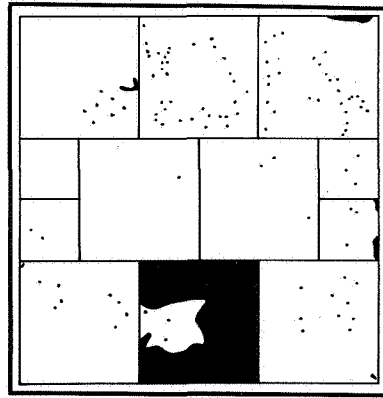
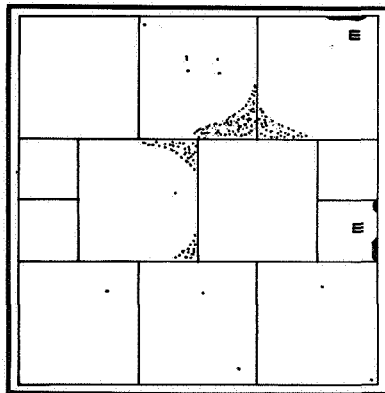
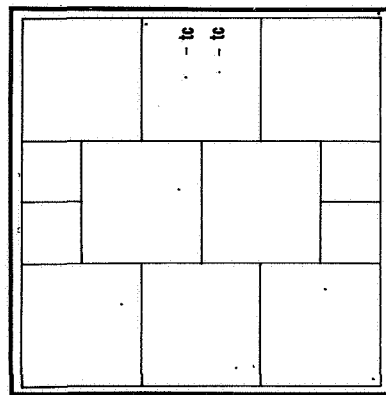


Figure 14

NONDESTRUCTIVE EVALUATION - LOCKHEED AREA 2P ALUMINUM PANEL

(Figure 15)

This figure illustrates the LMSC RSI panel condition as received, after the axial load test, after the thermal test at 1200°F (1700°F), and after initial exposures to 1533°K (2300°F). During the axial load test, excessive deflections occurred at the loaded ends plates of the substrate panel, which resulted in delamination of several tiles from the structure. Since the RSI tiles in the center of the panel were not damaged, the decision was made to acquire limited thermal performance data on this panel. The 1200°K (1700°F) thermal test was conducted and no cracks or anomalies were observed after the 1533°K (2300°F) tests, without load, cracks were observed on five tiles in the array. However, all the cracks appeared to initiate in regions of handling damage or from thermocouple instrumentation in the coating. The panel was then sent back to LMSC for modification of the end fittings. This test article has been returned to MSC and testing is currently in progress. Surface thermocouples and handling damage are identified in the figure as "tc" and "m", respectively.

NONDESTRUCTIVE EVALUATION LOCKHEED AREA 2P ALUMINUM PANEL

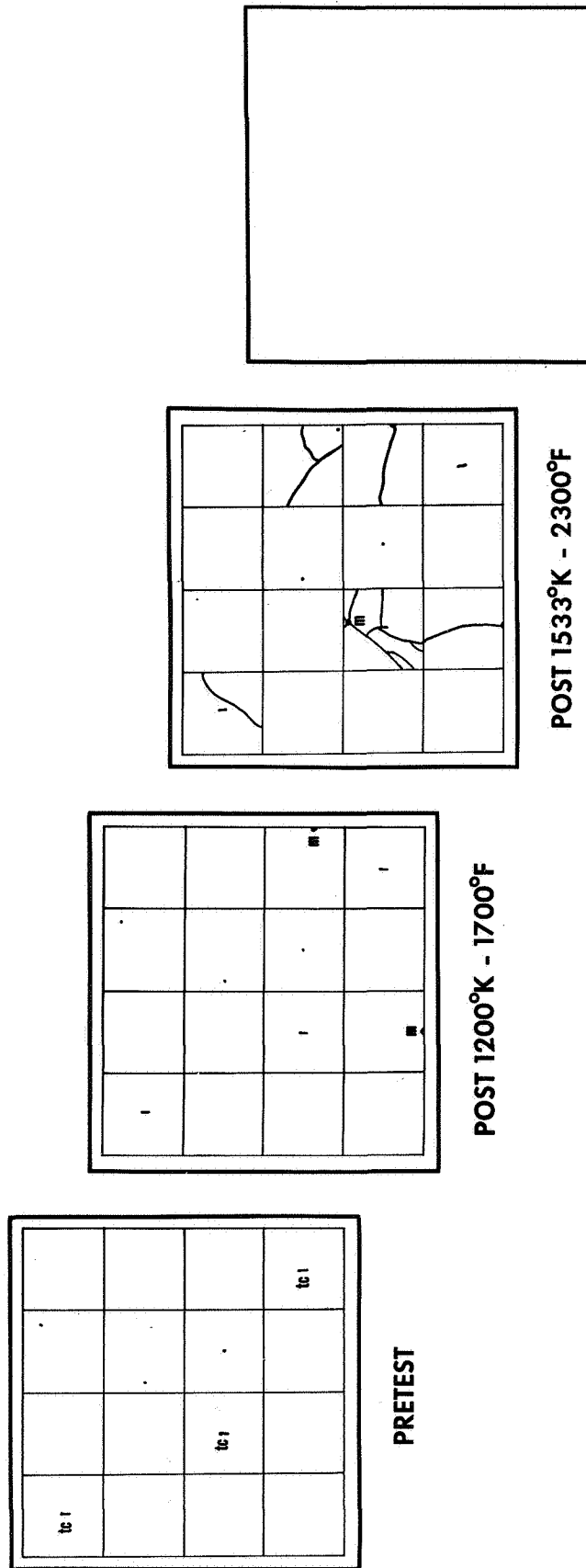


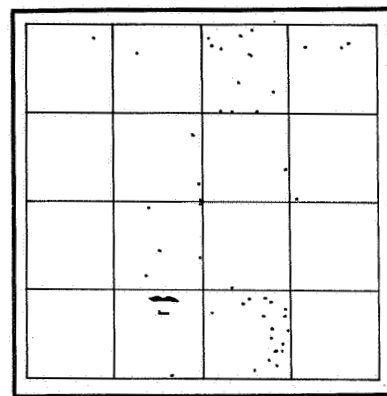
Figure 15

NONDESTRUCTIVE EVALUATION - MCDONNELL DOUGLAS AREA 2P ALUMINUM PANEL

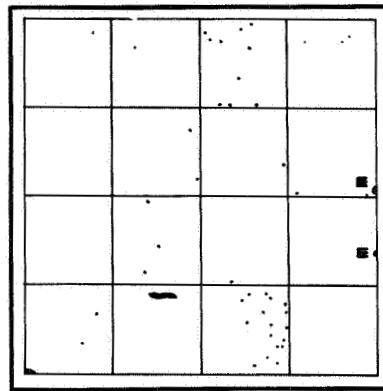
(Figure 16)

This figure shows the panel condition as received, after the axial load test, after the thermal test 1533°K (2300°F) started at 172°K (-150°F) plus axial loading, and after the acoustic tests. Pin holes were observed on several tiles in the as-received condition and after the axial load test. Cracking appeared in every MDAC RSI tile after the initial 1200°K (1700°F) heating test and became progressively worse as the testing continued. Cracking was quite severe on several of the tiles after the final thermal test [172°K (-150°F)] start and maximum design temperature 1533°K (2300°F), and the surface material appeared to have separated from the underlying tile. Subsequent acoustic testing fractured seven of the tiles along the most serious crack zones. These failures precluded further testing of this panel.

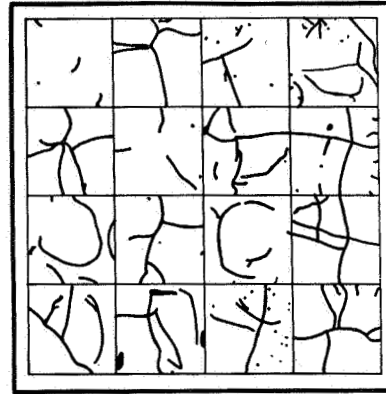
NONDESTRUCTIVE EVALUATION MC DONNELL-DOUGLAS AREA 2P ALUMINUM PANEL



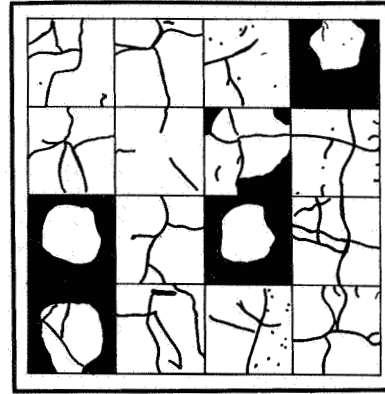
PRETEST



POST LOAD - 43,500 kg
96,000 lb



POST 1533°K - 2300°F



POST ACOUSTIC - 164 dB

Figure 16

NONDESTRUCTIVE EVALUATION - GENERAL ELECTRIC AREA 2P TITANIUM PANEL

(Figure 17)

During the testing period of the Phase II panels, the graphite heaters and vacuum test equipment became operational at MSC. This permitted radiant heat testing of some of the panels in a realistic simulated flight pressure environment. This figure illustrates the condition of the GE Area 2P titanium panel after completion of a series of acoustic-thermal exposures. The test panel was subjected to an initial acoustic exposure, and no cracks were observable after the test. Thermal testing was then initiated at temperatures of 1200°K (1700°F) and 1533°K (2300°F) at flight pressure conditions. One tile mounted on the barb attachment system (BAS) developed one large crack, and horizontal and vertical cracks were also evident along the sides of the tiles. During these thermal tests, it was necessary to reduce the total heat load (test time) to prevent overtemperature of the RSI/bond interface. The acoustic test performed after the thermal tests resulted in severe delamination and loss of the coating, which removed part of the insulation material from the cracked tile.

**NONDESTRUCTIVE EVALUATION
GENERAL ELECTRIC AREA 2P TITANIUM PANEL**

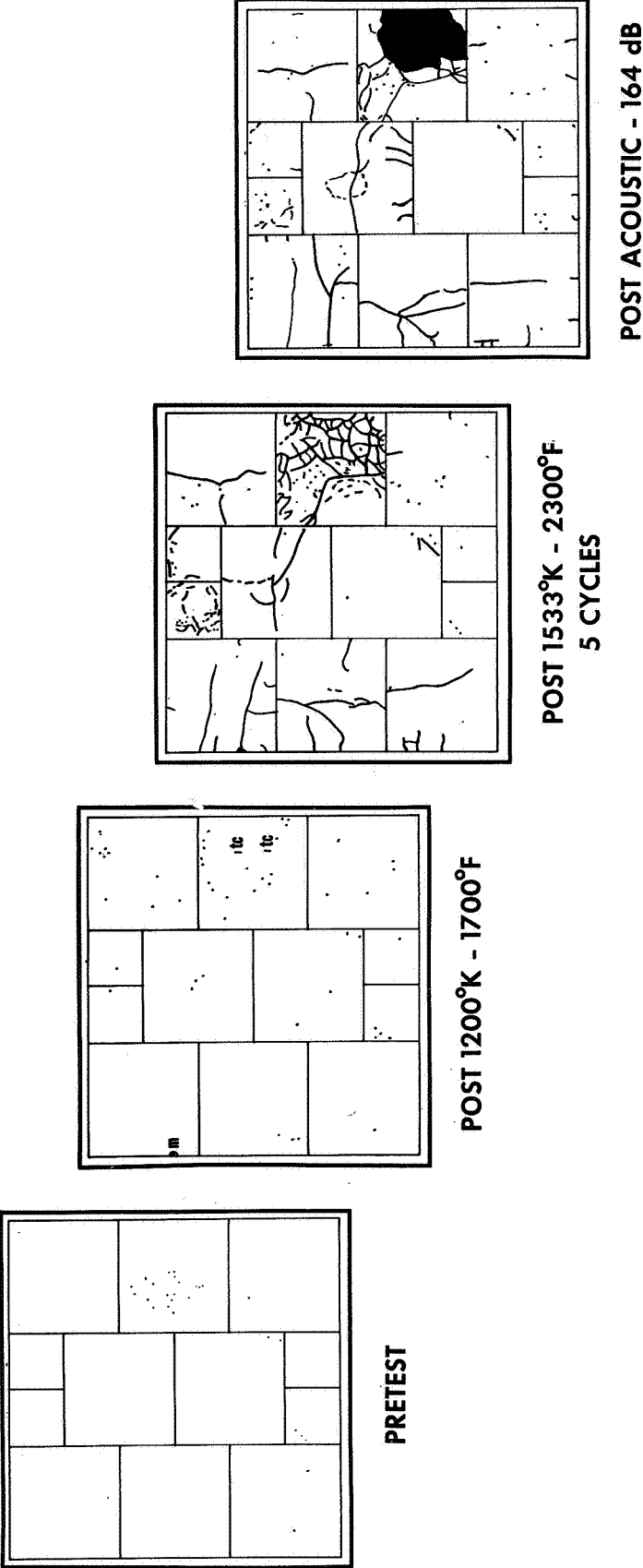


Figure 17

NONDESTRUCTIVE EVALUATION - LOCKHEED AREA 2P TITANIUM PANEL

(Figure 18)

This figure shows the condition of the LMSC Area 2P titanium panel after a series of acoustic thermal exposures. The panel in the as-received condition had several cracks, which tended to propagate during thermal tests at 1533°K (2300°F). Cracks also initiated and propagated from regions of surface thermocouple instrumentation. The panel was subjected to a total of five tests at the Area 2P design temperature level of 1533°K (2300°F) and at flight pressure conditions. The test article was also subjected to acoustic tests, which resulted in further crack formation. However, neither coating delamination nor catastrophic failure of the tiles occurred.

NONDESTRUCTIVE EVALUATION LOCKHEED AREA 2P TITANIUM PANEL

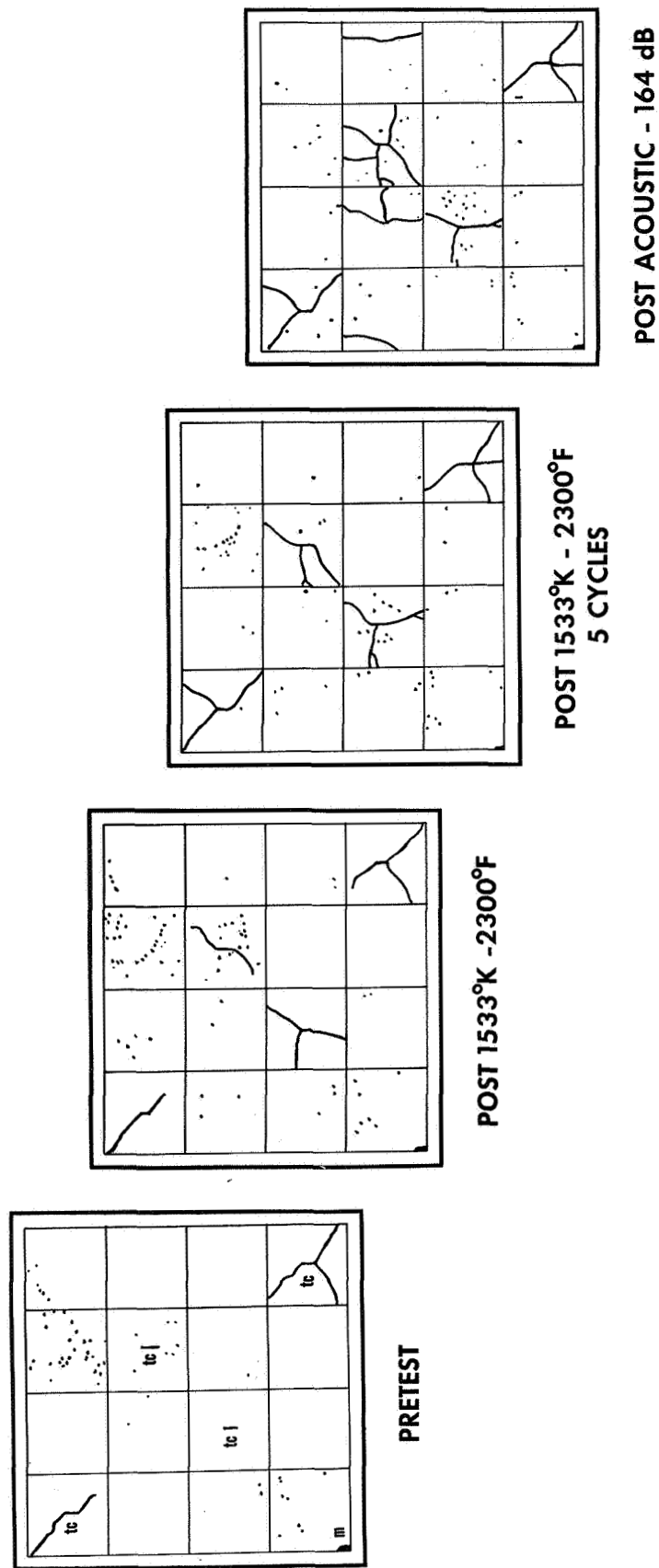


Figure 18

NONDESTRUCTIVE EVALUATION - MCDONNELL DOUGLAS AREA 2P TITANIUM PANEL

(Figure 19)

This figure shows the condition of the MDAC Area 2P titanium panel after a series of acoustic-thermal exposures. The test sequence for the MDAC Area 2P titanium panel was modified by performing the acoustic test initially followed by a 1200°K (1700°F) thermal test at reduced pressure. After the acoustic exposure, no cracks or anomalies were observed. The panel was then subjected to a reduced heat pulse at 1120°K (1558°F), and all 16 tiles cracked. All testing of the MDAC panels were suspended after these tests. This figure shows the panel condition after exposure to the various tests.

NONDESTRUCTIVE EVALUATION **MC DONNELL - DOUGLAS AREA 2P TITANIUM PANEL**

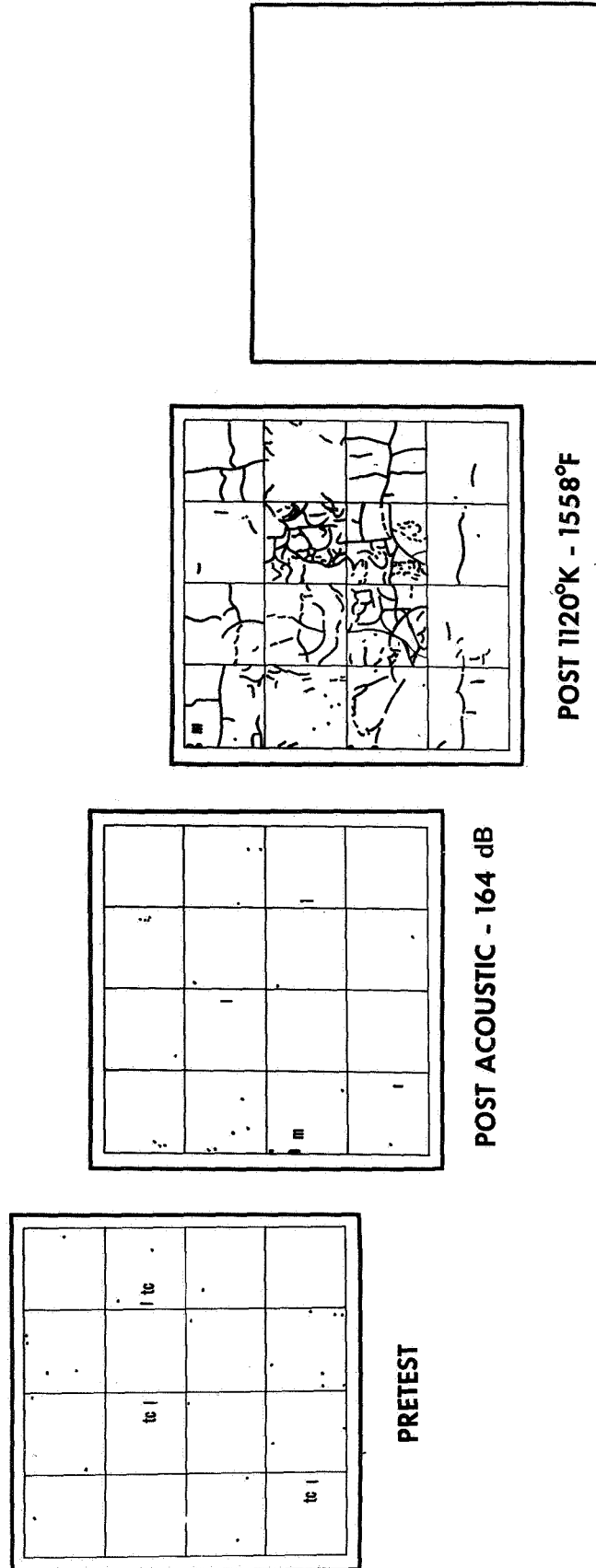


Figure 19

CONCLUDING REMARKS

- PROTOTYPE PANEL DESIGNS USING RSI TECHNOLOGY HEATING ENVIRONMENTS ARE REPRESENTATIVE OF CURRENT SHUTTLE BASELINE REQUIREMENTS
- FURTHER THERMAL CONDUCTIVITY EVALUATIONS OF RSI MATERIALS IN REPRESENTATIVE FLIGHT ENVIRONMENTS ARE REQUIRED. THERMAL CONDUCTIVITY OF MULLITE RSI IS HIGHER THAN SILICA RSI, BASED ON THERMAL RESPONSE DATA
- SURFACE THERMOCOUPLE INSTRUMENTATION AND LOCAL DAMAGED AREAS CREATE STRESS CONCENTRATORS AND CRACKS APPEAR TO INITIATE AND PROPAGATE FROM THESE REGIONS
- ACOUSTIC EXCITATION OF CRACKED SILICA TILES DO NOT LEAD TO CATASTROPHIC FAILURE SUCH AS SPALLATION OR TILE LOSS
- CRACKS IN THE MULLITE MATERIALS IDENTIFIED AFTER THERMAL EXPOSURE CAN LEAD TO FRACTURING OF THE COATING AND SURFACE INSULATION MATERIAL AFTER ACOUSTIC EXCITATION

NATIONAL AERONAUTICS AND SPACE ADMINISTRATION
WASHINGTON, D.C. 20546

OFFICIAL BUSINESS
PENALTY FOR PRIVATE USE \$300

SPECIAL FOURTH-CLASS RATE
BOOK

POSTAGE AND FEES PAID
NATIONAL AERONAUTICS AND
SPACE ADMINISTRATION
451



POSTMASTER: If Undeliverable (Section 154
Postal Manual) Do Not Return

"The aeronautical and space activities of the United States shall be conducted so as to contribute . . . to the expansion of human knowledge of phenomena in the atmosphere and space. The Administration shall provide for the widest practicable and appropriate dissemination of information concerning its activities and the results thereof."

—NATIONAL AERONAUTICS AND SPACE ACT OF 1958

NASA SCIENTIFIC AND TECHNICAL PUBLICATIONS

TECHNICAL REPORTS: Scientific and technical information considered important, complete, and a lasting contribution to existing knowledge.

TECHNICAL NOTES: Information less broad in scope but nevertheless of importance as a contribution to existing knowledge.

TECHNICAL MEMORANDUMS: Information receiving limited distribution because of preliminary data, security classification, or other reasons. Also includes conference proceedings with either limited or unlimited distribution.

CONTRACTOR REPORTS: Scientific and technical information generated under a NASA contract or grant and considered an important contribution to existing knowledge.

TECHNICAL TRANSLATIONS: Information published in a foreign language considered to merit NASA distribution in English.

SPECIAL PUBLICATIONS: Information derived from or of value to NASA activities. Publications include final reports of major projects, monographs, data compilations, handbooks, sourcebooks, and special bibliographies.

TECHNOLOGY UTILIZATION PUBLICATIONS: Information on technology used by NASA that may be of particular interest in commercial and other non-aerospace applications. Publications include Tech Briefs, Technology Utilization Reports and Technology Surveys.

Details on the availability of these publications may be obtained from:

SCIENTIFIC AND TECHNICAL INFORMATION OFFICE
NATIONAL AERONAUTICS AND SPACE ADMINISTRATION
Washington, D.C. 20546